# Abstracts of Papers

CONTENTS

§ *G*. General lectures

G·1. N. V. BELOV. *The crystal chemistry of silicates, Chapter 2.*

Chapter *A* was based on the work done 30 years ago by W. L. Bragg and his collaborators and dealt chiefly with the silicates of Mg, Al and their melanocratic substituents, mainly Fe in either of its stages of oxidation. The salient feature of chapter *A* was the close fit (commensurability after V. M. Goldschmidt) between the edge of an Mg- or Al-octahedron and that of a Si-tetrahedron, which allows these silicates to have relatively simple crystal structures, most of which are based on the closest packing of O(OH,F)-atoms. Large cations, such as Na, K, Ca, La etc., were considered in this chapter only as filling voids, i.e., gaps between components which for this chapter were more important.

In chapter *B*, where these large cations are predominant and play independent rôles, they are themselves octahedrally co-ordinated. The edges of these large octahedra are incommensurable, i.e., not similar in length to those of the Si-tetrahedra, and the ordinary way in which silica enters the structures of chapter *B* is as the diorthogroup Si_2O_7. The vertical edges of a trigonal prism, in which the group Si_2O_7 can be inscribed, adjust themselves well (are similar in length) to the edges of the large (Ca, Na, . . .)-octahedra and in this way the diorthogroups Si_2O_7 play in chapter *B* the same rôle as the orthogroups SiO_4 perform in chapter *A*.

The natural and synthetic Ca-hydrosilicates, which are so important in connection with cements, provide the largest number of examples with isolated groups Si_2O_7 and thus displaying the characteristic features of chapter *B*. Such examples are the structures of cuspidine $Ca_4[Si_2O_7]F_2$, tilleyite $Ca_5[Si_2O_7][CO_3]_2$, tricalciumsilicate hydrate, or TSH–$Ca_4[Si_2O_7](OH)_2 . 2 Ca[OH]_2$. In all these structures the Ca-octahedra which are directly linked (through common edges) with the Si_2O_7-groups alternate with Ca-octahedra which have no direct links to Si_2O_7-groups. This specific feature allows existence in these last octahedra of such cations as Zr, Mn and even Ti, all of which have ionic radii of intermediate size. A beautiful example is provided by the recently solved structure of the

<p align="center">Na–Ca–Mn–Zr–Ti-silicate–lovenite</p>

<p align="center">$CaNaMn(Fe)Zr(Ti)Si_2O_7OF$</p>
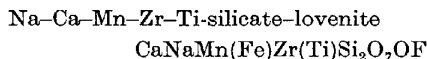
in which every 'coloured' cation alternates with the light one in common columns of octahedra. This structure—its geometrical pattern—repeats the structure of cuspidine as nearly as possible, but in lovenite there are two kinds of columns: In one of them alternating cations are Ca and Zr, and in the second Na and Mn(Fe). In cuspidine there are two F-atoms to which in lovenite correspond one F and one O. This O atom does not enter into the silicate radical, i.e., executes the same rôle as F.

Very similar in the structure of seydozerite

<p align="center">$Na_3Zr_3Ti_3Mn_2[Si_2O_7]_4O_4F_4$</p>
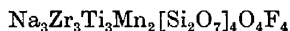
in which we have four kinds of columns corresponding to four Ca atoms in cuspidine: In two of them Zr-atoms alternate with Na, in the third kind the same Na alternates with Ti and in the last kind of column alternating cations are Na and Mn. Both in lovenite and in seydozerite the (neso) groups Si_2O_7 are compressed only between Na(Ca)-polyhedra. Seydozerite and cuspidine (lovenite) now head two mineralogical groups of seydozerite-rinkite and of cuspidine–wöhlerite, which one may call polymorphic as regards structures but not as regards individual compounds.

Silicate radicals analogous to the chains, double chains (or laths) of chapter *A* occur in chapter *B*, but instead of pyroxene chains with the formula $[Si_{1+1}O_6]_\infty$ we have pyroxenoid (wollastonite) chains with the formula $[Si_{2+1}O_9]_\infty$ and even $[Si_{2+1+2}O_{15}]_\infty$ (rhodonite). When we come to doubled chains or laths we find, instead of amphibole laths $[Si_4O_{11}]_\infty = [Si_{2+2}O_{11}]_\infty$ with hexagonal rings, a new type of xonotlite laths $[Si_6O_{17}]_\infty = [Si_{4+2}O_{17}]_\infty$ with octagonal rings. Such laths have recently been found not only in xonotlite but also in hillebrandite and perhaps are characteristic also for foshagite.

One is led to the conclusion that these octagonal rings are the most vital features of the hydrosilicates active in cement. At high temperatures ($\sim 750°$) all such Ca-hydrosilicates lose their activity, being dehydrated to give parallel oriented fibres of inactive wollastonite.

When the chains and (amphibolic) laths of chapter *A* condense to nets the only geometrically possible pattern is the well known one with hexagonal rings which occurs in talc, kaolin, micas and chlorites. But the same purely geometrical reasons do not permit the existence of nets with only octagonal rings. In chapter *B* octagonal rings must always alternate with tetragonal rings in the ratio 1:1 (apophyllite), with pentagonal rings in the ratio 1:2 (okenite), or with hexagonal and tetragonal rings in the ratio 3:1:1 (tobermorites). This last kind of net, the predominant details of which resemble those in xonotlite (with the xonotlite laths on two levels of this two-storied net) seems to be the most effective in giving cement properties.

G·2(i). N. F. MOTT. *The metallic bond and the Fermi surface.*

The lecture will deal with two themes, the concept of the chemical bond in metals, and the nature of localised or non-bonding states. On the former theme, theoretical chemists and metal physicists will agree that, if correlation (configurational interaction) is neglected, the correct way to describe the electrons in a metal is by the Slater determinant formed from the solutions ψ of the Hartree-Fock equation. These solutions are not directional and describe electrons shared between all atoms of the molecule or crystal. In most molecules, however, it seems certain that linear combinations of these functions ψ can be set up which do have the properties of a bond, are directional, and make contributions to the energy which to a first approximation are independent of each other; this has been examined by Lennard-Jones in his work on equivalent orbitals. I believe that this may be the

case in certain solids of low co-ordination number; I think it most unlikely that this applies in metals of high co-ordination number unless there is a strong admixture of d functions in the bonding electrons.

Both theory and much experimental evidence suggest that in most metals and alloys of co-ordination number 8 and 12 it is the atomic volume rather than the interatomic distance which remains constant to a first approximation when the co-ordination number changes; among transition metals iron and nickel are metals in this class, but not chromium. The evidence for this will be reviewed. It seems characteristic of the metallic bond that the energy of a metal atom in an alloy with structure of high co-ordination number depends to a first approximation only on the volume available to it and not on the nature of the atoms surrounding it.

On the second theme the lecture will emphasize the sharp physical differences between metals and non-metals, and in particular will stress that the Fermi surface in metals is a physical entity open to experimental investigation and not merely a theoretical concept. A discussion will then be given of the magnetic electrons in iron, following some of the ideas introduced by Mott & Stevens (*Phil. Mag.* (1957), **2**, 1364–1388). A question often discussed is whether these electrons are 'localised' or not. Now this may be treated as a qualitative matter; the wave-functions describing them may overlap to a greater or lesser extent, or they may be described by Bloch orbitals of more or less 'tight binding' type. It will be stressed that in addition one can ask a quantitative question about them; are they in states of which part of the Fermi surface is an upper limit? Or more simply, do they contribute to the conductivity? There is experimental evidence that they do not. The hypothesis used by Mott & Stevens (1957) that two $3d$ states with e_g symmetry are split off from the other three by the cubic crystal symmetry seems not to be compatible either with a recent determination of electron spin density by neutron diffraction (Weiss & Freeman, *J. Phys. Chem. Sol.* (1959), **10**, 147) or with calculations by Prof. Slater's school. Nevertheless the experimental evidence remains, and one has to ask under what conditions correlation can produce localised states in the sense used here.

G·2(ii). J. C. SLATER. *Quantum theory of electrons in metals.*

We consider the energy levels of a sample of metal, as a function of internuclear distance. This problem is similar to that of the energy levels of a diatomic molecule, such as H_2. The familiar results for H_2 are shown in Fig. 1. Here the curve marked $^1\Sigma_{g1}$ is the attractive Heitler–London state, the ground state. That marked $^3\Sigma_u$ is the Heitler–London repulsive state. These two states both go at infinite separation to the energy of two neutral hydrogen atoms; since each has an energy of -1 Rydberg, the energy goes to -2 Rydbergs. The two upper states, $^1\Sigma_u$ and $^1\Sigma_{g2}$, go to the state at infinite separation formed from one positive ion H^+, and one negative ion H^-, with energy of roughly -1 Rydberg.

The dotted curves marked H_{11} and H_{22} are derived from the molecular orbital approach. We can form two molecular orbitals from the hydrogen $1s$ states, one equal to the sum of the atomic orbitals, and corresponding to lower energy, and the other equal to the difference, therefore antisymmetric with respect to inversion in the

midpoint of the molecule. If we put both electrons in the lower molecular orbital, we get the energy H_{11}, and a wave function which is a singlet, and symmetric on inversion, indicated by the subscript g. If we put one in the lower, one in the upper, orbital, we get a singlet and a triplet, antisymmetric on inversion, indicated by the subscript u, and we have the two states $^1\Sigma_u$ and $^3\Sigma_u$, the triplet lying lower than the singlet. If we put both in the upper orbital, we have again a symmetric singlet, whose energy is H_{22}.
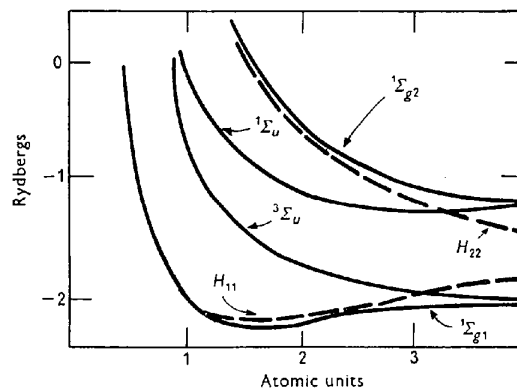

Fig. 1. Energy levels of the hydrogen molecule, as function of internuclear distance. States $^1\Sigma_{g1}$, $^3\Sigma_u$, $^1\Sigma_{g2}$ determined by solution of secular equation. Curves H_{11} and H_{22} represent molecular orbital approximation to states $^1\Sigma_{g1}$ and $^1\Sigma_{g2}$ respectively.

We see that the energies H_{11} and H_{22} form good approximations to the correct energies of the states $^1\Sigma_{g1}$ and $^1\Sigma_{g2}$ at the equilibrium internuclear distance, where $^1\Sigma_{g1}$ has its minimum, but that they become quite wrong at large distances, where they approach an energy which is the average of the energies of the states $^1\Sigma_{g1}$ and $^1\Sigma_{g2}$. We must make two linear combinations of them, solving a secular equation with two rows and columns, to get the correct states $^1\Sigma_{g1}$ and $^1\Sigma_{g2}$.

These facts regarding hydrogen are very familiar. Let us now see how they can be generalized when we go to metallic atoms rather than hydrogen, and when we put in contact not merely two atoms in a diatomic molecule, but more and more atoms so as to form a metallic crystal. The general situation for two monovalent atoms is similar to that for H_2. If now we add more and more monovalent atoms, the problem gets rapidly more complex. At infinite internuclear distance, if we have N atoms, the limiting energies of the states will correspond to N neutral atoms, or to $N-2$ neutral atoms, one positive ion, and one negative, or to $N-4$ neutral, two positive, two negative, and so on, to the limiting case where half are positive, half negative, none neutral. There will be $N/2$ such states of ionization, evenly spaced, and if we plot the energy per atom, the total energy separation between the two extremes of all neutral atoms, or half positive, half negative, will be the same as between the neutral and ionized limiting values in Fig. 1, modified to apply to a metal rather than hydrogen. In other words, this interval of energy, containing $N/2$ equally spaced levels, will be practically solidly filled with energy levels.

Similarly at the equilibrium distance, the whole range

of energies between the states $^1\Sigma_{g1}$ and $^1\Sigma_{g2}$ in Fig. 1 will be solidly filled with levels. The bottom will correspond to the ground state, and the energy difference between its minimum and the energy at infinite separation will be the heat of vaporization of the crystal. The top of the region of levels, corresponding to $^1\Sigma_{g2}$, will be that state of the metal in which the energy band arising from the atomic s states is half filled, as in the ground state, but in which the electrons occupy the top half of the band, rather than the bottom. If we take an energy band picture of an alkali metal, as in Fig. 2, considering only the energy band which would arise from the s electron, without mixing it up with the p and other states, then in the ground state we can imagine the bottom half to be filled, with an energy per atom for the whole crystal given approximately by the average energy of the bottom half of the band. Similarly for the top of the region of levels, corresponding to $^1\Sigma_{g2}$ in Fig. 1, the energy will be the average energy of the top half of the levels in Fig. 2. Since we know something about the energy bands in the alkali metals, we can deduce in this way the general nature of the diagram equivalent to Fig. 1, for such a metal. We may assume, as in H_2, that the energy band method forms an adequate approximation at distances around the equilibrium separation, but not at large distances. As a rough rule of thumb, we may say that the energy band method is probably satisfactory when it indicates an energy appreciably lower than the energy of the isolated atoms at infinite separation; that is, in Fig. 1, at distances where the curve H_{11} lies appreciably below the energy -2 Rydbergs.
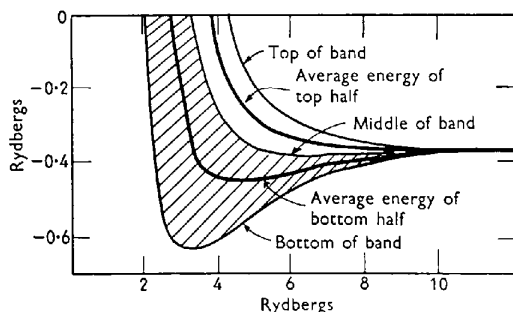

Fig. 2. Energy band of sodium metal arising from $3s$ electron. Shaded part, lower half of band, normally occupied by electrons. The average energy of the bottom half of the curve measures approximately the energy per atom of the crystal. Unshaded part, upper half of band, normally empty. If the upper half of the band were occupied, the bottom half empty, the average energy would represent approximately the energy per atom in a state corresponding to $^1\Sigma_{g2}$ in Fig. 1.

It would be very fine if we could carry through exactly some cases more complicated than H_2, more similar to real metals, and see how the diagrams similar to Fig. 1 worked out. Unfortunately, the complication very rapidly increases as the number of atoms goes up. For four hydrogens at the corners of a square, we find 28 states, instead of the four of Fig. 1. For six hydrogens at the corners of a regular hexagon, there are 267 states. For nine hydrogens, eight at the corners of a cube, and one at the center, there are 6635 states. This is the smallest

number of atoms for which, if we were working with a monovalent metal rather than hydrogen, the environment of the central atom would approach that actually found in a metallic crystal. This problem is beyond our present capacity to solve, but the hexagon, with 267 states, is not, and Mr Mattheiss, a student of Prof. Koster at M.I.T., is carrying it through. It will be very interesting, when this is completed, to observe the first steps encountered in filling up the diagram of Fig. 1 to produce essentially a continuum of levels.

Next we consider how these same arguments apply to other metals than monovalent ones, and in particular to the transition elements with their $3d$ electrons. Here the problem even of two atoms becomes unmanageable. For instance, in nickel, there are three configurations of the atom whose energy levels are very close to the ground state: $3d^84s^2$, $3d^94s$, and $3d^{10}$. Let us consider a diatomic Ni molecule, in which each of the atoms is found in one or another of these states, and compute the number of energy levels of the molecule which go to these states at infinite separation. We find that this number is 1008, a number to be compared with the two going to the ground state of unionized atoms in Fig. 1. No one has yet tried seriously to solve such a problem, though H. Kaplan (*Phys. Rev.* (1952), 85, 1038), following earlier work of J. H. Bartlett, Jr. (*Phys. Rev.* (1931), 37, 507) on p electrons, has studied the sign of the exchange integral, and has concluded that the ground state will be one in which the spins of the d electrons on the two atoms will be lined up parallel, as in ferromagnetism.

We may deduce some properties of the energy level diagram for Ni_2, however. Let us consider that it is to be in the $3d^94s$ state at infinite separation. The $4s$ orbitals are much more extended than the $3d's$, and consequently at relatively large distances, where only the $4s$ orbitals overlap, the energy levels will split much as in an alkali metal, or in H_2 as shown in Fig. 1. In place of the single level $^1\Sigma_{g1}$, however, we shall have a large number of almost identical levels coming from various orientations of the orbital and spin angular momenta of the d electrons in the two atoms. These will not affect the energy much until the d orbitals start to overlap; these levels will be almost degenerate with each other at large distances. At smaller distances, however, the levels will separate practically into a band. We may expect the same sort of thing to hold in other iron-group elements.

Instead of nickel let us consider iron, and instead of a diatomic molecule let us take a crystal. The question of interest is now, will the d electrons at the actual internuclear distance in a metal be close enough so that an energy band description is correct for them? A good many writers have doubted that this is the case. We cannot answer this question by calculations on individual molecular problems, because they have not been carried out, and we can see from the numbers already quoted that they would be almost impossibly difficult. However, we do have energy band calculations for iron, and we can use those to predict the energy levels, of the type given in Fig. 1, for iron, and can ask whether it is likely that the energy-band method is appropriate at the equilibrium distance.

In recent calculations at M.I.T., Dr J. H. Wood has studied very carefully the energy bands in iron, and finds that at the equilibrium distance the breadth of the $3d$ band is about 6 e.V. Let us ask what this means about

the corresponding extension of the levels of the whole crystal. We use an argument similar to that of Fig. 2. Iron has, according to the energy band theory, about 7·5 electrons in its d band, leaving the upper part of the band only half full, with electrons all of one spin, thereby explaining the ferromagnetism. This would correspond to the ground state. If now we transferred the electrons to the top part of the d band, leaving the vacancies at the bottom, we should have to move 2·5 electrons through an energy difference which would be a major part of the band width, perhaps 4 e.V. Thus we should have to do work of about 10 e.V. per atom. This would measure roughly the extension of the d levels in a diagram of the type of Fig. 1, in which we are giving the energy levels of the whole crystal.

This is great enough so that the energy band method should be applicable. It is furthermore great enough to indicate that the binding effect of the d electrons will be very considerable, as must be the case from the well-known fact that the heat of vaporization rises from the order of magnitude of 1 e.V. per atom in potassium to the order of 4 e.V. per atom in the middle of the iron group, dropping again as the $3d$ shell is drawn inside the atom. The energies derived from the band picture are of the right order of magnitude to lead to such values. Furthermore, the band picture explains why this binding effect of the $3d$ electrons should be greatest in the middle of the transition series: there the maximum number of electrons must be raised from the lower half of the energy band to the upper half, to go from the bottom to the top of the set of energy levels in the diagram of the type of Fig. 1, so that the extension of the energy levels will have its maximum value.

G·2(iii). L. PAULING. *The resonating-valence-bond theory of metals.*

The resonating-valence-bond theory of metals was developed during the period 1938 to 1948. It is an extension to metals and alloys of the chemical structure theory developed by chemists for organic and inorganic substances in general during the century from 1860 on. Some substances, such as propylene, can be represented satisfactorily by a single valence-bond structure; for this molecule the structure involves one arrangement of a carbon–carbon double bond, a carbon–carbon single bond, and six carbon–hydrogen single bonds. For other substances, such as benzene, more than one arrangement of the bonds is used.

The metals may be placed in the class of electron-deficient substances, together with the boranes, ferrocene and related substances, hexakaidekamethyltetraplatinum, and elementary boron. The characteristic feature of these substances is that some of the atoms have a larger number of stable valence orbitals than valence electrons. In general, some of the atoms of electron-deficient substances have a ligancy that is greater than the number of bond orbitals; there is some evidence that it is the atoms adjacent to an electron-deficient atom that are induced to increase their ligancy to a value greater than their orbital number. Chemical structures for electron-deficient substances can be found by assigning the electron-pair bonds (or one-electron bonds) to the available positions in all possible ways; that is, by writing all possible structures for the substance (with only one

arrangement of the nuclei), and then superimposing these structures, as in the general theory of chemical resonance. This theory accounts in a satisfactory way for observed interatomic distances and other structural features of electron-deficient substances.

Magnetic properties and observed bond lengths for metals have indicated that 0·72 orbital per atom in a metal (that is, about one orbital for each of three-quarters of the atoms) is to remain unused in the allocation of bonds. This orbital, called the metallic orbital, seems to be responsible for metallic properties, presumably in that it permits the unsynchronized resonance of valence bonds through a metal crystal, thus leading to electrical conductivity and other metallic properties. It is the metallic orbital that permits the classification of metals as electron-deficient substances.

The analysis of observed interatomic distances and saturation magnetic moments of transition metals in terms of the resonating-valence-bond theory, together with the proposal made by Zener about interaction between atomic electrons and bonding electrons, has led to the following description of metallic iron (L. Pauling, *Phys. Rev.* (1938), **54**, 899; *Proc. Nat. Acad. Sci. U.S.A.* (1953), **39**, 551). Two of the eight electrons of each iron atom occupy $3d$ orbitals, with parallel spins. These electrons, which may be called atomic electrons, do not participate in electrical conduction. The remaining six electrons are bonding (conduction) electrons. The orbitals that they occupy are hybrid orbitals, which, together with the metallic orbital, are made of the three remaining $3d$ orbitals, the $4s$ orbital, and the three $4p$ orbitals (with, of course, some contributions of less stable orbitals). The spin–spin interaction between the atomic electrons and the conduction electrons uncouples approximately 0·22 electrons in the conduction band per atom; it is this interaction that gives rise to ferromagnetism in this metal (Zener).

The iron atom in the metal may hence be described as being based upon the configuration $3d^5 4s 4p^2$, in the same way that the carbon atom in diamond is described as being based upon the configuration $2s 2p^3$. In each case this description represents only an approximation.

The description of the electronic structure of other metals is similar. For example, for nickel there are ten electrons outside of the argon shell. If the assumption is made that the metallic orbital, 0·72 per atom, must be preserved, there are only 8·28 orbitals available for occupancy by the ten electrons. Six of these orbitals are occupied by conduction electrons, as in iron. The remaining 2·28 orbitals contain 2·28 electrons with parallel spin and $4 - 2·28 = 1·72$ with antiparallel spin; the resultant magnetic moment of the atomic electrons is then 0·56. The saturation magnetic moment for nickel, 0·61, is due to this atomic moment plus the small moments of the uncoupled conduction electrons and the orbital contribution.

Two decades ago the electronic structure of iron was usually discussed on the basis of the band theory by stating that about 0·22 electron per atom had been promoted to the $4s$ conduction band, leaving a hole of 2·22 in the $3d$ shell; that is, that the configuration could be described as $3d^{7·78} 4s^{0·22}$. During recent years the description has been changed; for example, N. F. Mott & K. W. H. Stevens (*Phil. Mag.* (1957), **2**, 1364) describe metallic iron (body-centered) as having two $3d$ electrons

with parallel spin in non-conducting states, and the remaining six electrons, conduction electrons, occupying orbitals formed of $3d$, $4s$, $4p$, and higher functions, with about 0·2 uncoupling of electron spins by the Zener interaction. This description is essentially identical with that of the resonating-valence-bond theory. However, Mott & Stevens also say that the face-centered nickel crystal contains a mixture of ions $3d^9$ and $3d^{10}$ with 0·7 holes, and 0·7 electrons in the $4s$ orbital forming the conduction band. I feel that the striking gradual change in magnetic moments, interatomic distances, and other properties of the transition metals and their alloys with change in average atomic number provides strong support for the belief that the electronic structures are closely similar in such a sequence, rather than greatly different, and that the description provided by the resonating-valence-bond theory is a satisfactory one for nickel as well as for iron.

In interatomic compounds and other alloys there may be a transfer of electrons from atoms of one kind to those of another kind. This transfer is usually in the direction such as to neutralize the polarity of the bonds themselves that is correlated with the electronegativity difference of the atoms and such as to increase the number of bonding electrons. Alloys in which electron transfer occurs are often much denser, harder, and stronger than their components.

G·3. J. H. VAN VLECK. *Magnetic alignment.*

Alignment of the elementary magnets can be effected by one of three agencies (a) an applied magnetic field, (b) crystalline fields, (c) exchange forces. Mechanism (a) acting alone brings about a high degree of alignment only at very low temperatures, as in the region of adiabatic demagnetization, but can be studied at higher temperatures by means of susceptibility measurements. Although one thinks primarily of diffraction experiments as the source of information on how atoms are arranged in crystals, susceptibility measurements have sometimes been revealing in this regard in advance of good diffraction data. Process (b) is appreciable at ordinary temperatures only if the atom is not in an S state. The various orders of magnitudes of the crystalline potential in different types of atoms will be discussed. Magnetic resonance is the method par excellence for studying crystalline potentials, but cannot be employed in all cases. It is of course the cooperative alignment brought about by (c) that is so spectacularly studied by the method of neutron diffraction. Particularly interesting is the case of the rare earths, where the interplay of (b) and (c) is studied in recent diffraction experiments at Oak Ridge. The rôle of nuclear magnetic resonance in yielding information regarding forces in the solid state will be briefly discussed, including the most recent development, the Mossbauer effect.

G·4. M. F. PERUTZ. *The structure of crystalline proteins.*

Crystalline proteins cover a tremendous range of different sizes, from glucogen and insulin with a molecular weight of a few thousand to the smaller viruses with molecular weights of the order of millions. Most of them give beautiful X-ray diffraction patterns containing tens or even hundreds of thousands of reflexions which extend to spacings of the order of interatomic distances.

The phase angles of the reflexions can be determined by the method of multiple isomorphous replacement with heavy atoms, provided at least one of the heaviest atoms can be combined with a molecular weight unit not larger than about 50,000. In smaller proteins a single isomorphous replacement with a heavy atom, combined with measurements of anomalous scattering, may be enough to solve the structure.

The first three-dimensional Fourier synthesis of a protein was obtained by Kendrew and his collaborators in 1957. It gave a picture of myoglobin, a protein of mol.wt. 17,000, at a resolution of 6 Å, showing the position of the iron-containing pigment group and the general lay-out of the protein chains. Lately Kendrew and his collaborators have followed this up with a second Fourier synthesis at 2 Å resolution. This falls just short of resolving atoms, but nevertheless contains sufficient detail to solve most of the structure.

Perutz and others have now obtained a three-dimensional Fourier of haemoglobin at 5·5 Å resolution. This protein has a molecular weight of 67,000 and consists of 4 chains and four pigment groups. The chains, which have a configuration almost identical with myoglobin, form a tetrahedral array, and the pigment groups lie in separate pockets on the surface of the molecule.

Small viruses have a core of nucleic acid surrounded by a symmetrical array of small protein molecules all exactly alike. In rod-shaped viruses the nucleic acid forms a helical filament, around which protein sub-units are clustered in a helical array. In spherical viruses the configuration of the nucleic acid is still unknown, but the symmetry of the protein coat can be shown to conform to one of the cubic point groups. Poliomyelitis virus is the latest example of a particle of this kind.

G·5. B. K. VAINSHTEIN (with co-authors A. I. KITAIGORODSKY, J. M. RUMANOVA & Z. V. ZVONKOVA). *Theory and practice of direct methods of structure analysis.*

1. Review of the theory of sign determination. Three possible approaches to the phase determination of structure factors: consideration of the function of electron density, the determinants of the connections between structure factors, and statistical approach. The mutual connection of those approaches.

Exact equations between structure factors, derived from consideration of electron density. Sayre's equations, equations for the structure factors, belonging to the parallel planes of reciprocal lattice, and some others.

Theory of connections between structure factors. Harker–Kasper inequalities. Fundamental equation of connection—Gramm's determinant. Determinants of different power. Graphical representation of relations between structure factors.

Structure factors as chance values. Zachariasen–Cochran's statistical equations. Simple geometrical interpretation of this equation. The distribution function for structure factors. The Kitaigorodsky's product of structure factors and probability of its positive value. The Karle–Hauptman equations and Bertaut equations. The possibility of direct determination of phases in non-centrosymmetrical structures.

The additional conditions of phase determination. The

rôle of the symmetry and using of symmetry elements (the method of comparing). The arbitrarily chosen signs.

The connection between Patterson method and direct methods. The possibilities of phase determination of structure factors from the ideas of superposition method.

2. The practical routines of sign determination and examples of direct determinations of crystal structures. Reducing of F to the absolute scale. Realisation of the operation of convolution in sign determination. The routines of Rumanova and of Grant. The Karle–Hauptman procedure. The Woolfson's permutation method. The procedures, based on the use of modern computing techniques.

The examples of direct determinations (review of Russian works). The crystal structure investigations of silicates—epidote, xonotlite, datolite, gadolinite (which contain up to 80 atoms in the unit cell) by inequalities and statistical equalities. The investigations of zoisite, cuspidine, astrachanite by direct methods. The investigation of crystal structures of yeremeevite and lawsonite by means of Zachariasen's statistical method in combination with other methods.

The investigations of crystal structures of the realgar, of the complex compound—borontrifluoride with pyridine, of the diparatolylsulfide, of the 3,3'-diethylcarbocyane, of caprolactam by means of statistical equations with additional conditions. Some other examples of applications of direct methods.

§ 1(i). Apparatus for diffraction measurements

1(i)·1. A new diffractometer for diffraction studies.
By THOMAS C. FURNAS, JR., *Picker X-Ray Corporation, Cleveland, Ohio, U.S.A.*

This entirely new instrument for air or vacuum studies by X-ray or neutron diffraction or by X-ray spectrographic methods incorporates a variety of new features which open a broad new scope of experimental techniques to the investigator.

(1) It can be used with the diffraction plane either horizontal or vertical. Left and right handed versions facilitate the use of two diffractometers about one X-ray tube.

(2) It provides integral support of the X-ray tube so both tube and diffractometer may be moved without disturbing their critical alignment. A new ray-proof shutter, filter and collimator adaptor assembly combined with a simple alignment device and zero to ten degree take-off angle adjusting mechanism assures rapid alignment, optimum use of X-ray energy and safe operation with no leakage of direct or scattered X-rays around the tube.

(3) Its rugged main bearing has a $3\frac{3}{4}$ in. diameter through hole for easy access to the specimen, for attachment of large aperture vacuum pumps, for insertion of cryostat or heating implements, etc.

(4) It is available with special split worm wheels capable of absolute accuracies of the order of 0·0003°. The spring loaded interchangeable gear train has multiple shaft extensions for attachment of auxiliary devices in addition to the normal angle reading dials or counters. The

two-theta angle bisecting mechanism functions throughout a 360° range and allows independent 360° rotation (omega) of the specimen about the common axis.

(5) It is designed specifically for fully automatic remotely programmed operation in addition to the usual manual modes.

(6) It uses the new ACA Accepted Dovetail Track for mounting detector, collimator and specimen so these may be combined for photographic studies with a hitherto impossible precision, interchangeability, and freedom.

Paper to be submitted to the Review of Scientific Instruments for publication.

1(i)·2. An automatic X-ray diffractometer. By P. J. BROWN & J. B. FORSYTH, *Cavendish Laboratory, Cambridge, England.*

The instrument has been designed to eliminate the laborious hand setting of conventional single crystal X-ray diffractometers. It makes the collection of accurate intensity data by counter techniques comparable in speed and convenience with standard photographic methods.

The diffractometer is a two circle instrument and is used in the normal-beam geometry of reflection. The integrated intensity of reflection is measured by the oscillating crystal, stationary counter method. The crystal and counter positions for each reflection in a single layer are calculated from the lattice constants by the EDSAC II digital computer and a sequence of reflections is specified. The output tape from the computer is fed directly to the instrument, which then sets both crystal and detector to the correct positions. The background on either side of the crystal reflection and the integrated intensity of the reflection are measured. The results are punched on teleprinter tape in a form suitable for direct processing by the computer.

1(i)·3. Automatic single crystal diffractometers. By U. W. ARNDT, *Davy Faraday Research Laboratory, The Royal Institution, London, W. 1, England.*

Automatic single crystal X-ray diffractometers must provide the following facilities:

(1) Means for setting crystal and radiation detector for each Bragg reflexion in turn, either by an analogue device, which may be electrical or mechanical, or by a shaft-setting mechanism programmed by punched tape or cards.

(2) Means for measuring the reflexion and the diffuse background in the immediate neighbourhood.

(3) Means for recording the results of the measurements, preferably in a form suitable for direct processing by a computer.

(4) In addition ample facilities must be provided for checking the correct functioning of the automatic equipment.

Four separate diffractometers have either been completed or are approaching completion and their differing features will be used to illustrate possible solutions of the design problems involved in different circumstances.

Form of publication not yet decided.

1(i)·4. Appareil d'enregistrement numérique, entièrement automatique, des intensités des facteurs de structure sur bande imprimée. Par J. CLASTRE, *Laboratoire de Minéralogie et Rayons X, Université de Bordeaux, 20, Cours Pasteur, Bordeaux, France.*

L'application fructueuse des méthodes d'analyse de la fonction de Patterson, ou des méthodes de détermination des signes des facteurs de structure, exige une connaissance très précise des intensités diffractée par tous les plans *hkl* du cristal.

Nous avons étudié et fait réalisé, une installation entièrement automatique, commandée par bande perforée, et fournissant les intensités diffractées, en valeur numérique, sur bande imprimée.

Cette installation comporte 3 parties:

(1) Un goniomètre travaillant en équi-inclinaison, équipé de:

Un porte-cristal, pouvant tourner autour d'un axe fixe.

Un tube à Rayons X, avec compteur moniteur accouplé, pouvant se déplacer en équi-inclinaison.

Un compteur de mesure, pouvant tourner autour du cristal et se déplacer également en équi-inclinaison en synchronisme avec le tube à Rayons X.

(2) Une armoire de télécommande assurant le réglage automatique des 3 angles du goniomètre: cristal, compteur, équi-inclinaison, pour chacune des réflexion *hkl*.

Ce réglage est commandé par un lecteur de bande perforé (bande établie pour le cristal étudié).

(3) Une armoire de mesure comprenant:

Une alimentation des compteurs.

Un préamplificateur.

Une échelle de comptage.

Un traducteur numérique, donnant le nombre de coups reçus par le compteur de mesure, à des intervalles de temps définis par le compteur moniteur, éliminant ainsi les variations d'intensité des Rayons X incidents.

Un enregistreur de contrôle.

Une imprimante, commandée par le traducteur, inscrivant sur bande de papier les valeurs des intensités mesurées.

La bande perforée de commande étant placée dans le lecteur, le goniomètre se règle successivement sur chacun des réflexions *hkl*, sans interventions de l'opérateur.

Il est possible, grâce à cette installation de mesurer plusieurs fois les intensités, par exemple à des températures différentes, et d'étudier ainsi les modifications d'agitation thermique des cristaux, au voisinage de leur température de transition.

1(i)·5. Automatic single crystal diffractometry: II. Crystal orientation. By J. LADELL, N. SPIELBERG & K. LOWITZSCH, *Philips Laboratories, Irvington-on-Hudson, New York, U.S.A.*

Prior to the automatic registration of complete intensity data for structure determination using the linear reciprocal lattice tracking diffractometer (J. Ladell & K. Lowitzsch, *Acta Cryst.* (1960), **13**, 205), it is necessary to establish the reciprocal lattice parameters of the crystal being studied and orient the crystal about a suitable zone axis. Moreover, it is desirable that provisions be made for rapid preliminary investigation of an unknown crystal to establish the crystal class, space group and other pertinent symmetry properties using counter methods.

Although film techniques for this preliminary work are well known, optimum employment of the diffractometer as a precision instrument requires that such preliminary measurements be carried out in a manner compatible with the subsequent main task of the diffractometer and consistent with the angular precision available in the technique.

To accomplish these objectives a special crystal support goniometer (orienter) has been designed and constructed to be incorporated as an integral part of the unit. The angular deflections which can be provided by the support goniometer make it possible to bring to coincidence with the diffractometer axis any axis of an arbitrarily mounted crystal lying within a right circular cone of 130° apex.

Using the linear tracking features of the diffractometer, a small parallelepiped volume of reciprocal space is systematically scanned. By this means the previously unknown reciprocal cell dimensions and orientation is determined. This procedure permits the alignment and orientation of crystals by direct diffractometric methods obviating independent alignment by optical or X-ray film methods. The efficiency of this method depends upon instrumental and crystallographic parameters; an analysis of these parameters will be given.

Probably will be published in *Acta Cryst.*

1(i)·6. New continuous recording high and low temperature X-ray diffractometers. By YOSHIHIRO SHIMURA, *8 Kanda-Daidokoro-cho, Chiyoda-ku, Tokyo, Japan.*

High and low temperature X-ray diffractometers consist of four types which perform heating, cooling and recording automatically and continuously. The features of these four types are briefly described in the following.

(1) High temperature X-ray diffractometer.

Designed to operate with the specimen at temperature up to 1500 °C. in vacuum or gaseous atmosphere. Temperature scales are marked on the chart paper automatically.

(2) Low temperature X-ray diffractometer.

Designed to cover the temperature range of between 100 °C. and −190 °C. with the liquid nitrogen coolant. The automatic recording system is almost the same as that of high temperature X-ray diffractometer.

(3) X-ray diffractometer capable of automatic recording of temperature versus *d*-value.

There are two methods by means of this apparatus; one is so-called 'Single Peak Method' for measuring the temperature versus *d*-value curve of the single phase materials. The other is so-called 'Multi-Peak Method' for measuring the same curve of the multi-phase materials, and also is most suitable for the analysis of phase transition phenomena. Recording and temperature controlling are continuous and automatic.

(4) X-ray diffractometer capable of automatic recording of the thermal expansion coefficient curve.

The principle of this apparatus is based on the 'Single Peak Method'. Thermal expansion coefficient is recorded on the chart paper as a single line according to change of the temperature. X-axis corresponds to *d*-value (diffraction angle: 2θ), while Y-axis corresponds to temperature. Temperature controlling and recording are auto-

matic and continuous similar to the other apparatuses mentioned above.

Full account to be published in *J. Appl. Phys., Japan*.

1(i)·7. The use of standard X-ray goniometer GUR-3 as a neutron high resolution diffractometer. By R. P. Ozerow, *Karpov Institute of Physical Chemistry, Obucha 10, Moscow, USSR.*

The design of the neutron diffractometers is limited both by the necessity of high precision in determining the angle position and the stiffness of the spectrometer in supporting the heavy counter shielding on the long arm.

The standard X-ray equipment, the universal X-ray goniometer GUR–3 in particular, is of high precision in the determination of θ and 2θ angles, but does not possess the required stiffness. In order to use this goniometer as a neutron diffractometer for powder and single crystal investigation a special shielding covering the whole goniometer (with a cryostat for hydrogen and helium temperatures) had been designed. This shielding consists of a 30 cm. layer of water and can be moved on special rails. The small weight of the counter without the shielding permits to elongate the goniometer arm up to 1 m.

The use of the selsin systems having no backlash permits the remote control of the diffractometer without reducing the precision. An auxiliary automatic device enables a point to point recording of the diffraction patterns.

The investigation being now in progress confirms the possibility of utilizing this equipment for the study of of powder and single crystal samples with a relatively high resolution.

The results of this work will be published in *Kristallographia*.

1(i)·8. X-ray diffraction by substances at high pressures.* By J. S. Kasper, *General Electric Research Laboratory, Schenectady, N.Y., U.S.A.*

The increased activity of high pressure research makes all the more desirable structural information at high pressures. This is particularly the case for reversible phase transformations. Since the usual high pressure apparatus is so massive as to preclude X-ray diffraction measurements, we have developed a technique, first employed by Lawson and co-workers (A. W. Lawson & A. N. Riley, *Rev. Sci. Instrum.* (1949), **20**, 763; A. W. Lawson & T. Tang, *Rev. Sci. Instrum.* (1950), **21**, 815; J. C. Jamieson, *Ninth Annual Report to ONR on High Pressure Research.*—Inst. for the Study of Metals, Univ. of Chicago (July 1955–July 1956)), utilizing a single crystal diamond cell as the pressure chamber.

With diamonds of 2 to $2\frac{1}{2}$ carats, pressure up to 35,000 atmospheres have been attained on substances contained in a cylindrical hole, through the diamond, of about 0·015 inch diameter. X-ray diffraction data are obtained with Mo $K\alpha$ radiation.

A study has been made of various alkali halides which transform from NaCl to CsCl structures. Also, a variety

---

* This research was supported in whole or in part by the United States Air Force under Contract No. AF 33(616)–5995, monitored by the Materials Laboratory, Wright Air Development Center, Wright–Patterson Air Force Base, Ohio.

of substances, such as graphite, have been investigated where no structural transformations occur but where lattice parameter changes can be ascertained.

The emphasis of the work, however, has been on Bi and its alloys. With special techniques, to be described, a successful recording has been made of the diffraction pattern of the transformed Bi structure beyond 25,000 atmospheres. Also, it has been ascertained that an intermetallic compound, BiSn, is formed by pressure from the immiscible elements, and its diffraction pattern has been obtained.

Full account probably to appear in *J. Appl. Phys.*

1(i)·9. Die Böhmit-Entwässerung verfolgt mit einer neuen Röntgen-Heizkamera. Von H.-U. Lenné, *Ammoniaklaboratorium der Badischen Anilin- & Sodafabrik AG, Ludwigshafen am Rhein, Deutschland.*

Zur kontinuierlichen Verfolgung von Umwandlungsvorgängen, Strukturänderungen u.a. stand für Röntgenbeugungsuntersuchungen kein der bei der Elektronenbeugung bewährten Boettcher-Kassette vergleichbares Instrument zur Verfügung. Die Seemann–Heizkamera und deren Weiterentwicklung bei Unicam erlaubt Röntgenaufnahmen nur bei diskreten Temperaturen. Endter entwickelte 1956 eine kontinuierlich registrierende Röntgen–Heizkamera nach dem Debye–Scherrer-Prinzip, während wir bei unserer Entwicklung 1958 die Vorteile der streng - monochromatischen und fokussierenden Guinier–Seemann–Bohlin-Kamera mitberücksichtigten: Das vom Quarzkristall kommende Primärstrahlenbündel durchsetzt den Heizkopf (Widerstandsheizung) aus Platin, der gleichzeitig Blende und Halter für das ebene Präparat ist. Er ist umgeben von einem Kühlmantel, der die Öffnungen für Präparateinführung, Primärstrahl und evtl. Schutzgasfüllung und den Schlitz (3,5 oder 7 mm. Breite) enthält, hinter dem der Film senkrecht zum Fokussierungskreis kontinuierlich aufwärts bewegt wird (5 oder 10 mm./Stunde). Hinter dem herausziehbaren Primärstrahlfänger befindet sich nochmals eine sehr enge Blende, so dass am Ort des Winkels O Zeit- oder Temperaturmarken belichtet werden können. In der jetzigen Ausführung erreichen wir mindestens 1200 °C. im Präparat.

Mit dieser Kamera untersuchten wir die Entwässerung des Böhmits (AlOOH) in durchkristallisierter Form, wie man ihn z.B. durch hydrothermale Behandlung im Autoklaven erhält. Dieser Böhmit gibt bei etwa 480 °C. sein Wasser fast vollständig ab und wandelt sich um in das γ-Al$_2$O$_3$, welches bei etwa 800 °C. in das δ-Al$_2$O$_3$ und bei noch höheren Temperaturen in θ und α-Al$_2$O$_3$ übergeht. Day und Hill indizieren das γ-Al$_2$O$_3$ noch kubisch (Spinell-Typ) und das δ-Al$_2$O$_3$ tetragonal und stellen bereits fest, dass der Übergang kontinuierlich sei. Unsere Untersuchung zeigt folgendes: Das primäre Entwässerungsprodukt des Böhmits besitzt ein tetragonales Gitter mit $a = 7,86$ und $c = 8,02$ Å. Diese Gitterkonstanten ändern sich ineversibel und etwa linear mit der Temperaturerhöhung, wobei a zunimmt bis 8,02 Å und c abnimmt bis 7,66 Å bei etwa 1000 °C.

Bei etwa 700 °C. werden die beiden Gitterkonstanten einander gleich, so dass ein pseudokubisches Gitter mit $a = 7,95$ Å entsteht. In diesem Gitter sind die Ebenenscharen (222) ausserordentlich stabil: Erstens ergeben sie

Tabelle 1. *Gitterkonstanten von δ-Al$_2$O$_3$*

°C.	a	c	$d_{(222)} \cdot \sqrt{(12)}$
500	7,86$_4$ Å	8,01$_6$ Å	7,93$_5$ Å
700	7,94$_8$	7,94$_8$	7,95$_3$
900	8,00$_8$	7,87$_6$	7,97$_0$
1000	8,02$_4$	7,86$_4$	7,97$_6$

die bei weitem schärfste Interferenz im Vergleich zu allen anderen; zweitens ändert sich deren Netzebenen-abstand mit der Temperatur fast überhaupt nicht (von 2,29 Å bei 500 °C. auf 2,30 Å bei 1000 °C.). Da angenommen werden darf, dass der Ausdehnungskoeffizient nicht so klein ist wie er sich hieraus errechnen würde, so folgt daraus eine zunehmende Verdichtung des δ-Al$_2$O$_3$, was im Einklang mit der Verschärfung der Interferenzen mit zunehmender Temperatur steht. Würde man diese Ebenenschar als (222) eines Spinell-Typs indizieren, ergäben sich die kubischen Achsen zu 7,94 bzw. 7,98 Å, liegen also in jedem Fall zwischen den tetragonalen a- und c-Werten und teilen deren Differenz etwa im richtigen Verhältnis 1:2.

Aus dieser Untersuchung folgt, dass es keinen Grund gibt zwischen γ- und δ-Al$_2$O$_3$ zu unterscheiden: Das Entwässerungsprodukt des Böhmite ist tetragonales δ-Al$_2$O$_3$, dessen Achsenverhältnis irreversibel temperaturabhängig ist, so dass die Angaben der höchsten erreichten Temperatur als Index sinnvoll und notwendig erscheint.

Auf die sehr umfangreiche Literatur über die Entwässerung der Aluminiumhydroxyde kann hier nicht eingegangen werden.

Ausführliche Mitteilungen sind für die *Z. Kristallogr.* vorgesehen.

1(i)·10. Optimum dimensions of collimators for neutron crystal spectrometers and diffractometers. By P. SZABÓ, *Central Research Institute for Physics, Budapest* 114, *Hungary.*

A calculation method is shown for determining the optimum dimensions of primary collimators of given collimating power for neutron diffractometers and crystal spectrometers. Exact expressions of closed form consisting of elementary functions are given for the calculation of transmitted intensity. The numerical evaluation of these expressions being rather lengthy and laborious, approximate formulae are derived too and it is shown that in cases of practical interest the use of these latter and more convenient ones is quite sufficient.

We examined further the effect that is exercised by the total reflection developing at the walls of primary collimators used in neutron diffractometers and crystal spectrometers on the optimum dimensions of such collimators. The formulae for computation of the intensity transmitted by a single total reflection are given. It is shown that as to the intensity thus transmitted (similarly to the case of direct transmission treated above) there is an optimum in the dimensions of the collimator which in cases of practical interest is found to be the same as that determined for direct transmission.

The first part of this paper was published: *Nuclear Instruments and Methods* (1959), 6, 184.

The second part is accepted for publication at the *Nuclear Instruments and Methods.*

1(i)·11. An oscillating crystal monochromator. By E. H. WIEBENGA, E. KEULEN & G. C. VERSCHOOR, *Laboratorium voor algemene chemie, anorganische chemie en kristalchemie der Rijksuniversiteit Groningen, The Netherlands.*

Reflection intensities can only be measured accurately if strictly monochromatic radiation is used or if the measurements are corrected for the presence of white radiation (see for instance W. Cochran, *Acta Cryst.* (1950), 3, 273). The first method is preferable in principle, but requires the use of a crystal monochromator, by which the X-ray intensity is reduced appreciably.

A further problem connected with the use of a crystal monochromator is that of obtaining a sufficiently homogeneous beam around the crystal to be measured. This difficulty was overcome by mounting the monochromator crystal on a slide, which was moved back and forth uniformly several times per second by means of a rotating cam. The direction of oscillation was parallel to the characteristic X-rays to be reflected by the monochromator crystal, the amplitude of the oscillation was in our case (LiF, reflection 200, Mo-radiation) 1·5 mm. These oscillations of the monochromator crystal cause mere displacements of the monochromatic beam of 0·5 mm. to each side. The effect of moving the monochromatic beam is that its inhomogeneous intensity distribution is integrated in points lying in and near the crystal to be measured. Since the beam had a height of approximately 0·5 mm. and was moved ±0·5 mm., an intensity plateau of about 0·5 mm. appeared. In this plateau the intensity variations were less than 2%.

Connected with the gain of homogeneity is, however, a further loss of intensity by about 50% and a loss of monochromatisation. In our case the calculated maximum deviation from the characteristic wavelength is ±1% without oscillation of the beam, and ±2·5% when oscillating the beam.

1(i)·12. X-ray diffractometer for the study of highly radioactive materials. By J. ADAM, R. CAUSER & D. A. DUNKASON, *United Kingdom Atomic Energy Authority, Atomic Energy Research Establishment, Harwell, Didcot, Berks., England.*

It is well known that diffraction patterns with a very low background can be obtained from highly radioactive materials when the diffracted beam is monochromatised by reflection from a crystal. Photographs will be shown of a diffractometer used at A.E.R.E., Harwell for work on fissile materials after irradiation in a nuclear reactor. The instrument is enclosed in a dry-box behind a lead wall and all operations are performed with remote handling tools.

When the diffracted beam is monochromatised excellent quality diffraction patterns can be obtained even if the examined materials fluoresce in the primary X-ray beam. Thus copper radiation may be used for work on materials containing iron.

Paper will be submitted to *J. Sci. Instrum.*

1(i)·13. Charts for two-parameter lattices. By MARTIN ČERNOHORSKÝ, *Czechoslovak Academy of Sciences, Laboratory for the Study of Metals, Brno, Czechoslovakia.*

Construction. The individual steps in constructing new charts for tetragonal and hexagonal lattices are shown.

Similarly as in the Bjurström's charts only straight lines are used. According to this feature and to the simplicity of the preparation of the scales (wave-lengths, lattice parameters, Bragg angles) the construction is very easy.

Synthesis of powder photographs. The distribution of lines for the respective type of the lattice with the given parameters and for the chosen wave-length can be determined. The results appear on a linear scale of Bragg angles. Thus a complete scheme of the powder photograph is obtained.

Analysis of powder photographs. Indexing of lines and determining of lattice parameters is possible without film measuring. Simple auxiliary charts for finding out the lines of the type $hk0$ and $00l$ help to make the procedure easy.

Examples of derived application. Determining last lines, determining appropriate wave-length, information for working with internal standards.

Reference. The complete set of the charts in size great enough for convenient use is to be published in a special issue of Acta Academiae Čechoslovenicae Basis Brunensis (can be obtained from the Publishing House of the Czechoslovak Academy of Sciences, Prague, Czechoslovakia). The detailed description of the construction as well as of the application will be given there in English.

Note. It is intended to display the charts with explanatory texts at the Exhibition.

§ 1(ii). Techniques and methods for diffraction measurements

1(ii)·1. A routine method for correcting for extinction errors in crystal analysis. By S. CHANDRA-SEKHAR & D. C. PHILLIPS, *Davy Faraday Research Laboratory, The Royal Institution, London, W. 1, England.*

S. Chandrasekhar's (*Acta Cryst.* (1956), 9, 954; (1960), in press) method for estimating extinction in small single crystals has been adapted for routine use in crystal structure analysis. The method involves the measurement of the variation in the integrated intensity of a reflexion with rotation of the plane of polarization of the incident X-ray beam. A simple apparatus for rotating the plane of polarization of the X-ray beam has been constructed and used in the measurement of reflexions from a number of crystals. Results will be presented and the applicability of the method discussed.

To be published in *Acta Cryst.*

1(ii)·2. Single crystal intensity measurements by means of the automatic linear diffractometer. By U. W. ARNDT & D. C. PHILLIPS, *Davy Faraday Research Laboratory, The Royal Institution, London, W. 1, England.*

The Linear Diffractometer (U. W. Arndt & D. C. Phillips, International Union of Crystallography Conference, Stockholm, 1959) measures automatically the intensities of all the reflexions in a reciprocal lattice level and records them, together with the appropriate hkl indices, both in plain language and on punched tape ready for immediate transfer to a computer. The instrument generates and applies its own settings for both

crystal and counter, given only the reciprocal lattice dimensions of the crystal under investigation. It is being used in the collection of complete intensity data from protein crystals. The method of operation will be described and details will be given of the speed and accuracy of measurement which have been attained.

To be published in *Acta Cryst.*

1(ii)·3. Quantitative method for determination of fibre texture in wires. By V. SYNEČEK, *Institute of Technical Physics of the Czechoslovak Academy of Sciences, Prague, Czechoslovakia.*

An X-ray diffraction method is described for the quantitative determination of the fibre texture in cylindrical specimens (wires), which does not require specimen preparation. The integrated intensity is measured from a certain atomic plane in the direction parallel to the plane determined by the axis of the wire and by the direct beam for different orientations of the axis of the wire. These measurements can be carried out in practice using a counter diffractometer or Weissenberg goniometer. The pole figure is determined from the dependence of the diffracted intensity on the orientation of the wire after correcting the intensities for the absorption. The geometric arrangement enables the absorption factor to be calculated analytically. The method is applied to the texture determination of a drawn copper wire using Weissenberg goniometer.

To be published in *Czech. J. Phys.*

1(ii)·4. The determination of the preferred orientation in a metal sheet. By. I. H. HARDWICH, *Research Department, A.E.I. (Manchester) Ltd., Trafford Park, Manchester, 17, England.*

The measurement of the preferred orientation in a metal sheet using an X-ray diffractometer with a scintillation counter detector is described.

May be offered to the *Brit. J. Appl. Phys.*

1(ii)·5. Ein lochstreifengesteuertes Zählrohrspektrometer für Einkristalle. Von W. HOPPE & E. BERKL, *Abteilung für Röntgenstrukturforschung am Max-Planck-Institut für Eiweiss- und Lederforschung, München 2, Deutschland.*

Die Geometrie des Goniometers erlaubt die vollständige Vermessung aller Reflexe des reziproken Gitters mit einer einzigen Kristalljustierung. Damit können auch Messungen der anomalen Streuung ohne Änderung der Kristallorientierung vorgenommen werden. Die Eingabe der Winkelwerte erfolgt über einen Lochstreifen; die Werte werden als Komplementwerte in die beiden zwei elektronischen Zähler eingegeben, die auch (in der Quarzuhr und im Impulszähler) für die Messungen selbst verwendet werden. Der Antrieb der Winkeleinstellung erfolgt durch Impulsmotore, wobei Lichtimpulse solange gezählt werden, bis die Zähler aufgefüllt werden. Die gleichzeitige Zählung in beiden Zählern bewirkt eine hohe Sicherheit und eine ständige Prüfung der elektronischen Zähler (über Koinzidenzschaltungen). Die Messung selbst erfolgt in Scintillationszählern nach der Abtastmethode;

das Gerät bestimmt automatisch seinen Messbereich. Die Ausgabe der Resultate erfolgt auf Lochstreifen.

Probably will be published in Z. angew. Phys.

1(ii)·6. Fourier- and anisotropic temperature factor-programmes for various computers (IBM 650 and 704, Siemens 2002). By R. Hildebrand & Th. Hahn, *Mineralogisches Institut der Universität, Frankfurt am Main, Deutschland.*

General three-dimensional Fourier-programmes have been written for the IBM 704 and the new computer Siemens 2002. They are applicable to any symmetry. The number and positions of the two-dimensional sections as well as the step-width within the sections may be chosen. It is possible to calculate specified parts of the sections. Only structure factors with $F \neq 0$ need be put in.

A short description of the Siemens-computer will be given. The computation times and efficiency of these programmes and of similar calculations on the IBM 650 are discussed.

Programmes for the calculation of isotropic and anisotropic temperature factors for the IBM 650 are described and an extension of Sayre's IBM 704 least-squares programme XR2 to anisotropic temperature factors is given. Some experiences gained in the refinement of hexagonal crystals, particularly with respect to off-diagonal terms, are discussed.

It is intended to publish the results in *Zeitschrift für Kristallographie* and *Neues Jahrbuch für Mineralogie, Monatshefte.*

1(ii)·7. Some supplementary crystallographic programmes for the IBM 704 computer. By John A. Sliter & J. Lawrence Katz, *Physics Department, Rensselaer Polytechnic Institute, Troy, N.Y., U.S.A.*

Some programmes have been written as supplements to the usual Fourier, structure factor and least-squares calculations now available for the IBM 704 computer.

The first programme is a modification and extension of R. G. Treuting's programme (Abstract of Paper at Cornell University, A.C.A. meeting, July 1959) to compute electron density summations on any general inclined plane through the unit cell. This is available for all crystal systems and is suitable for an 8K memory.

Second is a peak search programme for three dimensional Fourier sums. This programme searches for the true maximum of the Fourier sum, within a pre-determined accuracy, in the neighbourhood of the highest gridpoint. Since all reflections must be kept in core memory a 32K memory is recommended.

The third programme determines the maxima of peaks on two-dimensional summations. It makes use of the elliptic paraboloid approximation of J. Ladell & J. L. Katz (*Acta Cryst.* (1954), **7**, 460). A 4K memory is sufficient for this programme.

The application and utilization of these programmes in crystal structure analysis will be discussed.

1(ii)·8. Planning of optimum and generalized S.F. programs for medium size computers. By F. R. Ahmed, *Division of Pure Physics, National Research Council, Ottawa 2, Canada.*

Generalized crystallographic programs which are capable of computation in any space group have been prepared in this laboratory first for a large computer (Ferranti Mark II with over 15,000 words memory) and then for a medium size computer (IBM 650 with drum storage capacity of only 2,000 words); they have been employed successfully for the past few years. An account of the principles employed in programming for the large computer have been reported by F. R. Ahmed & W. H Barnes (*Acta Cryst.* (1958), **11**, 669). The same basic principles, with only minor changes, have been followed in the preparation of most of the programs for the medium size computer. However, a new scheme has been introduced in planning the structure factor program for the IBM 650 in order to enable the machine to compute the geometric part of the structure factor according to the mathematical form requiring the least number of arithmetical operations. This optimum scheme for performing the computation has proved to be practical and worthwhile for medium size computers without any loss in the generality of the program.

The program is built up of a number of blocks of instructions, and each block performs one simple operation. There are as many of these blocks as would be required by the most complicated S.F. expression. The subroutines corresponding to the parts of the flow diagram which are common to all space groups are permanently joined together, while those for the variable parts of the flow diagram are assembled by arranging as many of the available blocks as are required in the order appropriate to the S.F. expression. This assembly is easily performed according to a short list of variable instruction cards which govern the flow of the computation and the data.

To be published in *Acta Cryst.*

1(ii)·9. Some comments on the theory of least squares and the testing of statistical hypotheses.* By Walter C. Hamilton, *Chemistry Department, Brookhaven National Laboratory, Upton, L.I., N.Y., U.S.A.*

The refinement of crystal structures by least-squares methods is becoming more and more commonplace; unfortunately, the wealth of information obtained in such refinements is often incompletely or sometimes incorrectly used. The following points will be discussed:

(1) It is often incorrectly stated that an assumption of a normal distribution function for the observational errors is necessary for certain results of the least-squares theory to be valid. The theory of least squares depends in no way on the use of a normal distribution function, and, in particular, it can be shown that the mean value of the weighted sum of squares of the residuals is equal to the number of degrees of freedom and that the matrix

---

* Research performed under the auspices of the U. S. Atomic Energy Commission.

of the normal equations provides an unbiased estimate of the variance-covariance matrix of the parameters for any distribution with finite second moments.

(2) The difference between marginal standard deviations and conditional standard deviations will be discussed; in particular, a wider use of Hotelling's T^2 statistic for multivariate distributions is urged.

(3) The various 'R factors' and their distributions will be discussed. For example, we might ask if an R factor of 0·05 is more significant than one of 0·10 for a particular structure determination. (Frequently, it is not.)

(4) Finally, some of the points discussed above will be illustrated by a correct determination of a best least-squares plane.

Amplified portions of this paper have been or will be submitted to *Acta Cryst.*

1(ii)·10. An improved method and computed tables for accurate determination of axial ratio and lattice spacings of close-packed hexagonal metals and alloys. By T. B. MASSALSKI & H. W. KING, *Mellon Institute, Pittsburgh 13, Pennsylvania, U.S.A.*

Withdrawn.

1(ii)·11. New methods for determination of small-angle intensity distribution from measured intensities. By V. SYNEČEK & M. ŠIMERSKÁ, *Institute of Technical Physics of Czechoslovak Academy of Sciences, Prague, Czechoslovakia.*

A method of the small-angle intensity measurement has been developed in which the integrated scattered intensity is measured along the lines parallel to the trace of the direct beam of arbitrary intensity distribution and of negligible width. The obtained intensity distribution $E(x)$ is identical with the intensity distribution $J(x)$ measured by the usual technique in the points on the equator line by using the infinite direct beam of uniform intensity (will be published in *Acta Cryst.* (1960)). The radial intensity distribution $I(x)$ can be derived therefore from $E(x)$ by the exact expression derived by Guinier & Fournet. To evaluate this expression it is necessary to carry out the integration of a set of curves constructed from $E'(x)/x$ on a deformed scale. A rapid graphical method of plotting these curves is described and its accuracy is proved on an example. It is further shown that $I(x)$ can be determined in principle directly from the analogous curves constructed from $E(x)$.

The exact derivation of the unsmeared diffraction pattern in a general case of a non-radial intensity distribution can be done from the same intensity measurements carried out for different orientations of the sample obtained by turning it about an axis parallel to the direct beam propagation.

To be published in *Czech. J. Phys.* and in *Acta Cryst.*

1(ii)·12. Coherent diffraction intensities from distorted crystals. By J. M. COWLEY, *Division of Chemical Physics, Chemical Research Laboratories, C.S.I.R.O., Melbourne, Australia.*

By taking into account the geometry of a diffraction instrument we may calculate the coherence function which specifies to what extent portions of a sample in a plane perpendicular to the beam direction must be considered as diffracting coherently. Usually the half width of this coherence function, which we call the 'coherence range', is of the order of 1/10 to 1 μ for practical X-ray and electron diffraction experiments.

In calculating the diffraction intensities from bent or otherwise distorted crystals for which appreciable bending takes place within the coherence range it is incorrect to make the usual assumption that intensities from areas of different orientation can be added incoherently. For each coherent region within which the deviation from periodicity is not too great, the contribution to the total intensity is given by the Fourier transform of the product of the Patterson function for that region and the coherence function.

When a crystal is elastically bent, planes of atoms perpendicular to the beam become compressed or expanded. If two layers of atoms with the same unit cell but different amounts of bending are projected in the beam direction it is seen that the projection of an atom in one layer is displaced from the projection of a corresponding atom in the other layer by an amount and direction which varies over the coherence range. Diffraction from the two layers must therefore be considered partially incoherent. Hence the effect of a combination of coherence in directions perpendicular to the beam and a bending of the crystal is to introduce incoherence between layers of atoms separated in the beam direction.

This concept has been used to explain successfully a number of experimental observations including:

(1) Anomalies in line profiles in X-ray diffraction patterns of metahalloysite obtained by Brindley & Robinson (*Min. Mag.* (1948), **28**, 393).

(2) The frequent occurrence of hexagonally symmetric, single-crystal, electron diffraction spot patterns obtained by Dr A. Goswami and the author from monoclinic clay minerals.

(3) The apparent high degree of disorder present in layer lattice crystals for which single crystal electron diffraction structure analyses have been made.

Probably will be published in *Acta Cryst.*

1(ii)·13. Multiple X-ray diffraction effects in diamond-type lattices. By H. COLE & F. W. CHAMBERS, *IBM Research Laboratory, Poughkeepsie, N.Y., U.S.A.*

Each time a new experimenter starts a diffraction study using single crystals having a diamond-type lattice, he 'rediscovers' the multiple diffraction (Renninger) effects at the 'forbidden' diffraction positions. In order

to ease the path for later discoverers, simple charts have been prepared which predict, and index, the pattern to be observed upon rotation around the diffraction vector, as a function of a/λ, for several 'forbidden' reflections. These effects occur, of course, when two, or more, reciprocal lattice points are on the sphere of reflection simultaneously, but are most easily observed if one of the reflections is very weak. The use of this effect as a sensitive tool for measuring the lattice parameter in Ge, Si, and GaAs will be shown, and the effects of various imperfections upon the patterns observed will be discussed. The existence of the weak, but true, 222 reflections in these systems will be commented upon.

Would be submitted to *Acta Cryst.*

1(ii)·14. Present status of precision lattice parameter determination by counter diffractometry.* By W. PARRISH & J. LADELL, *Philips Laboratories, Irvington-on-Hudson, N.Y., U.S.A.*

The diffractometer gives promise of becoming an ideal instrument for the accurate determination of lattice parameters. To realize the complete potential of this technique, painstaking attention must be given to numerous factors in the instrumentation and methodology. A summary will be presented of the factors that have been solved and those requiring further study to achieve accuracies well beyond 0·01% which appears to be the present limit of agreement in film methods (W. Parrish, *Acta Cryst.* (1960), **13**, in press). Recent advances in precision instrumentation and automatic data collection and processing have made it possible to record the line profile and to measure certain features to an accuracy of 0·001° (2θ). For example line profiles are now recorded using a fixed-time step-scanning method. The angle and intensity data are automatically coded and punched into paper tape directly as the data are accumulated at the X-ray unit. The tape is then fed to a small electronic digital computer programmed to compute the centroid within a few minutes of time using the 90% cut method (J. Ladell, W. Parrish & J. Taylor, *Acta Cryst.* (1959), **12**, 253, 561, 567). Thus the principle experimental and computational difficulties have been overcome.

It will be shown that various commonly used measures of the reflection angles such as the mode, bisectors-of-chords, etc., with the same or different wavelengths do not lead to a unique value of the lattice parameter. This results from a type of systematic error which has its origin in the interaction or folding of the intrinsic diffraction profile, the aberrational functions and the spectral line profiles, and is not eliminated by the use of extrapolation procedures. The centroid method can now be used to account for the distortions arising from the aberrations and the diffraction process, thereby removing these systematic errors. However, one of the most important remaining problems is the lack of knowledge of the full intrinsic spectral distribution. Work is in progress in collaboration with the X-ray spectroscopists to acquire a further understanding of this

_____

problem. Some of the theoretical difficulties in obtaining the necessary spectral data will be discussed.

Probably will be published in *Acta Cryst.*

1(ii)·15. The precision measurement of lattice parameters. By A. FRANKS, *National Physical Laboratory, Teddington, Middx, England.*

The National Physical Laboratory is participating in the project sponsored by the International Union of Crystallography, to determine the accuracy with which lattice parameters can be measured.

The first objective of this work was to produce a camera in which the instrumental and systematic errors are reduced to a minimum and in which a high precision in the measurement of line position can be achieved. A back reflection focusing camera offers one of the best means of reducing or eliminating systematic errors and a camera has been designed and constructed according to metrological principles so that the diffraction angles can be measured to an accuracy of a few seconds of arc. The error in the lattice constant, resulting from this limitation in the precision of angular measurement is about 1 part in 10^6, which is less than the effect of such factors as the uncertainty of the X-ray wavelength. Errors due to uneven film shrinkage have been eliminated or very much reduced and the form of the specimen is such that the horizontal and vertical divergence of the beam do not cause any line shift. The specimen is accurately positioned with an optical indicator and its temperature is controlled to 0·05 °C. The X-ray source is a demountable semi-microfocus tube and the radiation is monochromatized by reflection from a ground and bent quartz crystal.

Probably will be published in *Brit. J. Appl. Phys.*

1(ii)·16. Experimental factors affecting the accuracy of single-crystal intensity measurements by counter methods. By LEROY E. ALEXANDER & GORDON S. SMITH, *Mellon Institute, Pittsburgh 13, Pennsylvania, U.S.A.*

When a small stationary crystal is irradiated by a broad X-ray source, diffraction occurs simultaneously from the entire crystal. The intensity profile of the diffracted ray is the convolution of the crystal size, mosaicity, and spectral dispersion functions. The area under this 'stationary' profile we shall designate I_H. When the crystal rotates through its angular range of Bragg reflection, this 'stationary' diffraction profile scans the source, kinetically generating a somewhat broadened and smoothed image of the source profile. The area under this 'kinetic' profile is a measure of the integrated reflection intensity, I_A.

Theory and experiment both demonstrate that as θ increases, the ratio I_A/I_H is at first constant and equal to $(I_A/I_H)_0$, then begins to increase at intermediate Bragg angles where, due to heightened spectral dispersion, the degree of overlap of the α_1 and α_2 source images has become small. At still larger θ's the ratio $(I_A/I_H)/(I_A/I_H)_0$ continues to increase to approximately 1·5 for complete resolution of the α_1 profile, and finally a further increase is observed due to dispersion within the α_1 profile itself. The particular form of the curve of I_A/I_H versus θ has

a marked dependence upon the experimental conditions, being principally a function of the 'take-off' angle, radiation employed, crystal size, and crystal mosaicity. Therefore, to exclude errors arising from spectral dispersion it is recommended that I_A rather than I_H measurements be employed, with the possible exception of the region of constant I_A/I_H at the lower Bragg angles.

A semiquantitative treatment will be given of the geometrical and other experimental factors determining the diffraction profiles and affecting the reliability of their measurement. The predictions will be compared with experimental results for crystals of four compounds obtained with an Eulerian cradle apparatus and proportional counter.

The full account of this work is likely to appear in *Acta Cryst.* or *Rev. Sci. Instrum.*

1(ii)·17. **The accuracy of measurement of the intensity of X-ray reflections by photographic methods.** By J. W. JEFFERY & K. M. ROSE, *Birkbeck College, Crystallography Laboratory, London, W.C. 1, England.*

Photometry of spots on an integrating Weissenberg film has been chosen, after trials of other methods, as the best photographic method of measuring intensities.

With considerable care it is possible to confine the sources of error effectively to: (i) absorption in the crystal; (ii) the film and its development; (iii) non-uniformity of film background. The latter is mainly caused by variation along the Laue streak for low-angle reflections. For this reason Cu $K\alpha$ radiation was chosen as more suitable than Mo $K\alpha$ for measuring intensities photographically.

Up to a maximum density of 1·2 the standard deviation of errors due to the film and its development can be reduced below 1% of this maximum.

To minimize absorption errors spherical crystals of Whitlockite

$$\text{Ca}_3(\text{PO}_4)_2 \quad (\mu = 274 \text{ for Cu } K\alpha)$$

and

$$\text{Co[Hg(CNS)}_4] \quad (\mu = 480)$$
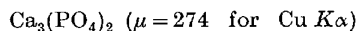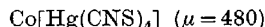
were ground to a diameter of about 0·2 mm. The exact size and a measure of the imperfections were obtained by photomicrography.

Both crystals were of high symmetry so that a satisfactory test of the accuracy achieved was obtained by comparison of symmetry equivalent reflections. Whitlockite ($R\bar{3}c$) gave 10 sets of 16 equivalent reflections on the same film and Co[Hg(CNS)$_4$] ($I\bar{4}$) a larger number of sets of 5 or 6 reflections.

Errors due to small irregularities of shape were shown theoretically to be proportional to the intensity of reflection and the absorption coefficient. The results for the two spherical crystals were in agreement with the theory and, by extrapolation, showed that for a similar near-spherical crystal of $\mu = 10$, crystal errors should be negligible compared with film errors. For such a crystal the standard deviation of symmetry equivalent reflections should be less than 1% of the maximum intensity measured. Highly symmetrical organic crystals are being used to check this conclusion and the results will be reported to the Congress.

The main paper will be submitted to *Acta Cryst.*

A description of the photometer and its performance will be submitted to *J. Sci. Instrum.*

1(ii)·18. **Atomic scattering factors for Na⁺, Ne and F⁻ from poly-detor wave functions.** By B. DAWSON, *Division of Chemical Physics, C.S.I.R.O., Chemical Research Laboratories, Melbourne, Australia.*

Bernal & Boys' (*Phil. Trans.* (1952), A, **245**, 139) poly-determinantal calculations for Na⁺, Ne and F⁻ yield atomic wave functions with total energies significantly lower than those from Hartree–Fock calculations, the experimental, poly-detor and Hartree–Fock energies (in Hartree units) being: for Na⁺, $-162\cdot126$, $-161\cdot8784$, $-161\cdot8$; for Ne, $-129\cdot03$, $-128\cdot6920$, $-128\cdot5431$; for F⁻, $-99\cdot9374$, $-99\cdot5279$, $-99\cdot4591$. Atomic scattering factors for the poly-detor functions have been evaluated analytically to assess the influence on Hartree–Fock f-curves of correlation effects not considered in the self-consistent field method with exchange. The f-curves of Na⁺ and Ne obtained from the two methods are in good agreement, but those of F⁻ differ. The differences are related to the different values of $\overline{r^2}$, the mean-square atomic radius, given by the poly-detor and Hartree–Fock radial charge densities, with the poly-detor result providing a theoretical molar diamagnetic susceptibility in closer agreement with the experimental (solid-state) value than is the Hartree–Fock result.

The Hartree–Fock and poly-detor charge distributions for F⁻ are considered in terms of Krug, Witte & Wölfel's (*Z. Phys. Chem.* (1955), **4**, 36) experimental data for LiF.

To be published in *Acta Cryst.*

1(ii)·19. **Experimental atomic scattering factors and anomalous dispersion corrections for Th, U, and Pu.*** By R. B. ROOF, JR., *Los Alamos Scientific Laboratory, University of California, Los Alamos, New Mexico, U.S.A.*

Experimental atomic scattering factors have been determined for Th, U, and Pu with Mo $K\alpha$, Cu $K\alpha$, Fe $K\alpha$, and Cr $K\alpha$ X-radiations. The Thomas–Fermi–Dirac scattering curves were used as a theoretical basis, and the difference between the experimental and *TFD* curves was taken as a measure of the anomalous dispersion correction.

As a result of determining the scattering factors for Th, U, and Pu from experimental samples of ThO$_2$, UO$_2$, and PuO$_2$, the scattering factor for oxygen was also determined. The experimentally derived scattering curve for oxygen is in good agreement with the theoretical scattering curve for oxygen according to McWeeney.

Calculated values for $\Delta f'$ and $\Delta f''$, the real and imaginary portions of the anomalous dispersion correction are compared with experimental values for these quantities. Agreement can be described as semi-quantitative since the experimental terms are of the same order of magnitude and have the same signs as those indicated by theory.

To be submitted for publication to *Acta Cryst.*

---

* Work done under the auspices of the United States Atomic Energy Commission.

1(ii)·20. On the electron distributions in diamond and silicon at different temperatures. By S. Göttlicher, H. Witte & E. Wölfel, Eduard-Zintl-Institut, Technische Hochschule Darmstadt, Darmstadt, Deutschland

Intensity measurements on powder samples and single crystals of diamond and silicon at different temperatures show that the bonding mechanism in these lattices causes two effects:

(1) The measured structure factors $f_{exp.}$ 111 and 331 are higher, whereas $f_{exp.}$ 311 and 400 are lower compared with the theoretical ones ($f_{theor.}$) as calculated with electron distribution according to Hartree. The deviations are in the range of 0·1–0·2 (per atom) whereas the experimental errors are in the range of 0·01 (for diamond) and 0·03 (for silicon).

(2) The 'forbidden' reflection 222, which has the same order of magnitude as the deviations mentioned above.

For 222 the phase problem can be solved and three-dimensional electron distributions $\varrho(xxz)$ for the plane xxz have been calculated using $f_{exp.}$ at different temperatures. Further, difference Fourier synthesis with ($f_{exp.}-f_{theor.}$) as coefficients have been calculated. From difference synthesis the displacements of the bonding electrons compared with Hartree-distributions will be discussed. They can be described by additional charge distributions between nearest neighbours. To get a better idea of the electron distribution in diamond, the model according to Ewald–Hönl calculations was used for comparison. It can be shown that the axial-symmetrical charge between neighbouring atoms contains 0·42 electrons, whereas the radial symmetrical torso of the atoms contains 2 K- and 3·16 L-electrons. The electron distributions of these different parts will be discussed at various temperatures.

1(ii)·21. Variation of extinction with X-ray wavelength. By J. J. DeMarco & R. J. Weiss, Materials Research Laboratory, Ordnance Materials Research Office, Watertown, Massachusetts, U.S.A.

A study of the effect of extinction as a function of X-ray wavelength has been made on copper and iron powders by comparing the ratio of the integrated intensities of the first Bragg reflection from unannealed samples to that from annealed samples.

Unannealed and annealed compressed samples in the form of briquets were made from 5 micron size carbonyl iron powder, 400 mesh pure iron filings and 5 micron size copper powder. The samples were annealed in vacuum for one hr., the iron briquets at 850 °C. and the copper at 700 °C.

Measurements were made at seven wavelengths, Ag $K\alpha$, Mo $K\alpha$, Cu $K\beta$, Cu $K\alpha$, Ni $K\alpha$, Co $K\alpha$ and Cr $K\alpha$ on an X-ray diffractometer with a scintillation detector.

The observed ratios and the corresponding wavelengths are:

λ (Å)		Cu (5μ)	Fe (5μ)	Fe (400 mesh)
Cr $K\alpha$	(2·291)	1·47	3·64	2·22
Co $K\alpha$	(1·791)	1·37	3·19	1·83
Ni $K\alpha$	(1·659)	1·30	1·54	1·47
Cu $K\alpha$	(1·542)	1·26	1·61	1·49
Cu $K\beta$	(1·392)	1·22	1·93	1·72
Mo $K\alpha$	(0·710)	1·16	1·92	1·34
Ag $K\alpha$	(0·561)	1·10	1·57	1·25

The observed data could not be fitted to any of the standard primary or secondary extinction corrections, although the primary extinction correction (W. H. Zachariasen, Theory of X-ray Diffraction in Crystals (1945), eq. 3·167. New York: Wiley) $A/\tanh A$ fitted quite well in regions where the absorption is not high.

1(ii)·22. Experimental determination of atomic scattering factors. By Boris W. Batterman, Bell Telephone Laboratories, Incorporated, Murray Hill, New Jersey and David R. Chipman & J. J. DeMarco, Ordnance Materials Research Office, Watertown, Massachusetts, U.S.A.

Accurate intensity measurements of low order Bragg reflections can give important information on the outer electron configuration of elements in the solid state. It is our opinion that such measurements cannot be made with single crystals because extinction effects cannot be reliably eliminated. Measurements of powder specimens, in addition to extinction, have other sources of error, viz. surface roughness absorption and preferred orientation. However, it is possible by independent checks to show if all these known sources of error are negligible. Extinction can be eliminated by using cold worked powders with particle sizes the order of several microns. Preferred orientation can be checked by comparing the intensities of different orders as a function of amount of compression of a powder briquet. Surface roughness can be checked by comparing the fluorescence scattering at low angles from the powder specimens with that from a highly polished piece of the same material. Although there is no reliable way of correcting for any of these effects if present, one can accurately ascertain their absence.

Since primary beams are too intense to count directly, powder measurements are usually reported relative to a standard scatterer for which the theoretical scattering factors are assumed accurate. We have used two techniques to measure primary beam intensities in order to present powder intensities on an absolute basis. In the first method the primary beam is attenuated by a set of judiciously selected absorbers whose individual attenuation factors can be measured directly. The second method employs Bragg reflection from a highly perfect crystal as an attenuator. The reflecting power of the crystal is separately measured with a double crystal spectrometer. The narrow reflecting range of the crystal allows in effect a measurement of the primary beam in a series of small countable steps. These techniques have been applied to measurements on iron, copper and aluminum powders.

The results of these measurements will be submitted for publication in the Phys. Rev.

1(ii)·23. Measurement of the X-ray atomic scattering factors of iron, copper, and aluminum. By David R. Chipman & John J. DeMarco, Ordnance Materials Research Office, Watertown, Mass., and Boris W. Batterman, Bell Telephone Laboratories, Incorporated, Murray Hill, New Jersey, U.S.A.

Measurements of the scattering factors of iron and copper were recently reported (R. J. Weiss & J. J. DeMarco, Rev. Mod. Phys. (1958), 30, 59; B. W. Batter-

man, *Phys. Rev.* (1959), **116**, 81; Y. Komura, Y. Tomiie & R. Nathans, *Phys. Rev. Letters* (1959), **3**, 268) in the literature in an attempt to provide some information on the distribution of $3d$ electrons in the metallic states of these elements. Since the reported measurements were not consistent with one another, we have attempted to repeat these measurements choosing experimental parameters to minimize the corrections in reducing the experimental X-ray intensities to atomic scattering factors. Samples were made from iron, copper, and aluminum powders having particle sizes in the range of 5–10 microns. For each material, about six samples were pressed using pressures varying from one just sufficient to form a compact, to one strong enough to cause marked flowing of the metal. Following procedures outlined earlier (B. W. Batterman, D. R. Chipman & J. J. DeMarco (Abstract, this meeting)), extensive tests were then made to discover which, if any, samples showed negligible effects of surface roughness, preferred orientation, and extinction. The integrated intensities of the first six to eight reflections of each of the selected samples were then measured with monochromatic Mo $K\alpha$ radiation. The relative intensities of the lowest order iron, copper, and aluminum reflections gave ratios of experimental atomic scattering factors in good agreement with values calculated for the free atom and confirm the experimental ratio of iron to copper previously measured (B. W. Batterman, *Phys. Rev.* (1959), **116**, 81) with monochromatic Fe $K\alpha$ radiation. However, an absolute standardization of the X-ray intensity is necessary to unambiguously define the electron distribution in any single element. We are therefore reducing the measured relative intensities of iron, copper, and aluminum to absolute values. The results of two independent methods of standardization will be presented.

These data will be submitted for publication in the *Phys. Rev.*

§ 2. Recent progress in structure determination

2·1. Application of a direct sign-determining method based upon Fourier series to mellitic acid. By A. Bezjak, *Department for Structural and Inorganic Chemistry, Institute Rudjer Bošković, Zagreb, Yugoslavia.*

The direct sign-determining method based upon Fourier series has been described by the author (A. Bezjak, *Acta Cryst.* (1959), **12**, 765) and now applied to the projections (100) and (001) in the determination of the structure of mellitic acid. ·

A preliminary report on crystallographic and X-ray measurements on mellitic acid as well as the general feature of the structure will be published shortly by A. Bezjak & D. Grdenić (*Nature*, in press).

Of the functions proposed it was necessary and possible to use $G(H, \xi)$, $G(H_1, \xi)$ for one-dimensional case and $G_{cc}(H, H_1, \xi)$ and $G_{css}(H, H, H_1, \xi)$ for two-dimensional case, where H refers to 010 and H_1 to $h00$ or $00l$.

The above functions are one-dimensional Fourier series which, under a chosen h or l, connected the unitary structure factors $U(hk0)$ with $U(h00)$, and $U(0kl)$ with $U(00l)$ through all k.

The unitary structure factors were obtained by correct-

ing the experimental $F(hk0)$ and $F(0kl)$ with temperature factor and by dividing them with $\overset{N}{\underset{1}{\sum}} f_i$. By introducing $U(hk0)$ and $U(0kl)$ into the corresponding G-functions and by varying their signs the necessary conditions for the functions $G(H, \xi) = 0$, $G_{cc}(H, H_1, \xi) = 0$ and

$$G_{css}(H, H, H_1, \xi) = 0$$

within an interval $\xi_{\min.} \leq \xi \leq \frac{1}{4}$ were found. The value $\xi_{\min.}$ was about 0·150.

In most cases the functions depended upon three to four (five at most) unitary structure factors and it was therefore necessary to calculate at most 32 variations of one-dimensional Fourier series for each function.

According to theory the set of signs satisfying the above mentioned conditions could be considered correct.

The functions for two-dimensional cases did not give the signs directly but only the connections of the signs S_{hk0} to S_{h00}, and S_{0kl} to S_{00l}.

Functions $G(H_1, \xi)$ connected $U(h00)$ through all h, and $U(00l)$ through all l, as well as their signs. In this way the signs of the moduli of the structure factor related to the projections (100) and (001) were definitely determined.

Of 44 observed $I(hk0)$ 41 signs of the corresponding $F(hk0)$ and of 61 $I(0kl)$ 56 signs $F(0kl)$ were determined.

With those signs electronic densities on (100) and (001) were calculated. The structure factors calculated from the coordinates obtained from the electronic density maps did not change in signs obtained by means of the method described.

The application of this method for the three-dimensional solution of the structure of mellitic acid is in progress.

The full-length account is likely to be published in *Acta Cryst.*

2·2. Application of probability methods to N-benzyl dihydronicotinamide. By I. L. Karle, *U.S. Naval Research Laboratory, Washington 25, D.C., U.S.A.*

The configuration of the dihydronicotine ring is of considerable interest in the coenzyme dihydrodiphosphopyridine nucleotide (DPNH). Therefore the structure of a simpler analogue, N-benzyl dihydronicotinamide, $C_6H_5CH_2(C_5H_5N)CONH_2$, has been studied. The crystal is monoclinic with

$$a = 11·98, \quad b = 5·82, \quad c = 20·82, \quad \beta = 129·4°, \quad Z = 4;$$

space group $P2_1/c$. The crystals were very fine yellow needles and grew along the b axis. Accordingly, three-dimensional data with Cu radiation were obtained only along the b axis. The F_c^2 were corrected for vibrational motion and placed on an absolute scale by means of a K curve. E values were then obtained from the corrected F_o^2.

The determination of initial phases using Σ_1 (H. Hauptman & J. Karle, *Solution of the Phase Problem I.* (1953). A.C.A. Monograph) was somewhat hampered by the fact that the maximum k index was four in the data collected. To facilitate the phase determination, some of the newer phase determining relationships derived on the basis of an algebraic analysis were employed. After several initial

phases were well established, the phases of all the other structure factors with large E values were obtained directly from the Σ_2 relation.

The molecules lie near the 200 and 102 planes. The dihydronicotine ring is nearly planar and the $CONH_2$ group attached to it is in the same plane. The benzene ring is twisted considerably out of the plane containing the dihydronicotine ring.

To be published in *Acta Cryst.*

2·3. The systematic application of sign relations to 3-dimensional data. By D. F. Grant, R. Hine & J. P. G. Richards, *Viriamu Jones Laboratory, University College, Cardiff, Wales.*

The method of Grant, Howells & Rogers (*Acta Cryst.* (1957), **10**, 489) for the application of sign relations to the plane groups *pgg*, *pmg*, *p4g* has been extended to certain centrosymmetric space groups. A programme for the Ferranti 'Pegasus' computer has been devised to determine the products for each reflexion considered and also to search and record 'coincidences', i.e. the occurrence of the product $S(A)S(B)$ in relation with several terms $S(C_1)$, $S(C_2)$ etc. The choice of arbitrary signs, the correlation of the signs from the coincidences and the iterative process leading to a single set of signs are as described previously.

The application of this method to the structures of anisic acid and 2,6-dinitro-*p*-toluic acid (both in the space group $P2_1/c$) is described. The effect of changing the lower limit of $|U|$ for the terms considered is discussed in relation to the numbers of products and coincidences recorded, the numbers of signs obtained and the time involved.

It is hoped to publish a full account in *Acta Cryst.*

2·4. The use of three-dimensional Fourier transforms in structure determinations. By H. P. Stadler, *King's College, Newcastle upon Tyne, 1, England.*

The fitting of Fourier transforms of flat molecules to central sections of the reciprocal lattice is now a well established aid in the determination of crystal structures.

The extension of the transform to upper layers of the r.l. was first discussed by P. A. Kenyon & C. A. Taylor (*Acta Cryst.* (1953), **6**, 745) and can lead to a great deal of additional information:

(1) the inclination of the molecules,
(2) the vector distance between origins of different molecules,
(3) the signs of structure factors to be used in generalized projections.

For purposes of (1) and (2) above, consideration of the 'origin peaks' of the transforms is particularly rewarding and has been used in the determination of the structures of pyranthrone, dibenzanthrone and iso-dibenzanthrone, each of which contains two independent molecules in the unit cell.

Generalized projections with signs determined from the transform fit of the flat part of the molecule have been used in the elucidation of the structure of the pyranthrone–sulphuric acid complex.

A full length account is likely to go to *Acta Cryst.*

2·5. Ordre logarithmique des densités de probabilité. Par E. F. Bertaut, *Laboratoire d'Electrostatique et de Physique du Métal, Institut Fourier, Grenoble, France.*

Si $P(A_1, A_2, \ldots, A_m)dA_1 \ldots dA_m$ est la probabilité pour que les facteurs de structure normalisés E_k soient compris entre A_k et $A_k + dA_k$ ($k = 1, \ldots, m$), l'auteur a établi antérieurement que la probabilité conditionnelle $P^+(A_1)$ que A_1 soit positif, $|A_k|$ ($k = 1, \ldots, m$) étant connus, est

$$P^+(A_1) = \tfrac{1}{2} + \tfrac{1}{2}P_i(A_1)/P_p(A_1) .$$

Ici $P_i(A_1)$ et $P_p(A_1)$ désignent respectivement la partie impaire et la partie paire en A_1 de la densité de probabilité $P(A_1, \ldots, A_m)$.

Klug a récemment attiré l'attention sur la nécessité d'ordonner judicieusement les termes de la densité de probabilité $P(A_1, \ldots, A_m)$ en fonction de puissances N^{-k} (N = nombre total d'atomes).

On montre qu'il est beaucoup plus avantageux d'ordonner

$$L(A_1, \ldots, A_m) = \log P(A_1, \ldots, A_m) .$$

On obtient les résultats suivants (1) à (5):

(1) $L(A_1, \ldots, A_m)$ peut s'ordonner de telle sorte qu'à un poly-nôme de degré k soit associé un ordre de grandeur ε^{k-2} ($\varepsilon = N^{-\frac{1}{2}}$). (Cela n'est pas possible avec $P(A_1, \ldots, A_m)$).

(2) $\qquad P(A_1, \ldots, A_m) = \exp\left(L(A_1, \ldots, A_m)\right)$

sera toujours une fonction définie positive.

(3) La probabilité $P^+(A_1)$ pour que A_1 soit positif prend la forme

$$P^+(A_1) = \tfrac{1}{2} + \tfrac{1}{2} \operatorname{th} L_i$$

où L_i est la partie impaire en A_1 de $L(A_1, \ldots, A_m)$. La partie paire L_p n'intervient pas.

(4) On considère une *chaîne statistique*, c'est-à-dire un ensemble de triples produits, reliés par des conditions de phase. La probabilité pour qu'un triple produit soit positif, dépend alors non seulement de la valeur absolue du triple produit, mais *aussi* des facteurs de structure faisant partie de la chaîne statistique.

(5) On développe un critère simple permettant de choisir dans les procédures combinatoires (Douglas & Cochran), parmi plusieurs jeux de signes probables le jeu de signes le plus probable.

Publication in *Acta Cryst.*

2·6. Procedures for phase determination. By J. Karle, *U.S. Naval Research Laboratory, Washington 25, D.C., U.S.A.*

Detailed procedures for the direct determination of phase have been derived for all the space groups. These procedures consist of a description of methods based on the theory of the seminvariants for making proper specifications of phase for the purpose of defining the origin and additional specifications, e.g. for choosing an enantiomorph, when appropriate. They describe how the specified phases are to be used in combination with seminvariants (special linear combinations of phases) obtained from phase determining formulas, to ultimately provide a set of phases from which a structure may be calculated.

It is to be emphasized that these procedures are general for the direct determination of phase and are not dependent upon the particular nature of the phase determining formulas in their present stage of development. The procedures will therefore maintain their validity as phase determining formulas continue to be developed and improved. Judging from our present experience it appears that phase determination will involve similar calculations for the different space groups, with the main difference one of interpretation facilitated by a knowledge of seminvariant theory as contained in the detailed procedures.

Typical procedures for centrosymmetric and non-centrosymmetric space groups will be illustrated.

To be published in *Acta Cryst.*

2·7. On the renormalization of structure factors.
By HERBERT HAUPTMAN, *U.S. Naval Research Laboratory, Washington 25, D.C., U.S.A.*

In procedures for the direct determination of phase from observed intensities it is convenient to employ the normalized structure factors E having the property that $\langle |E|^2 \rangle_K = 1$, where the average is taken over all vectors K in reciprocal space. In case a certain kind of rational dependence of atomic coordinates is present, a condition which is revealed by significant deviations from unity of the averages of $|E|^2$ taken over selected subsets of vectors in reciprocal space, the usual procedures must be modified. One way of doing this is to renormalize the $|E|^2$'s in such a way that their averages, even over the troublesome subsets of reciprocal space, are restored to unity.

To be published in *Acta Cryst.*

2·8. Exploitation par les inégalités classiques de certaines connaissances géométriques de la structure. Par GÉRARD VON ELLER, *Laboratoire de l'I.R.Ch.A. 12, quai Henri IV, Paris (IV°), France.*

On remplace la structure d'atomes par une structure de sphères homogènes de densité ϱ_0 et de rayon R variable suivant les besoins. Il devient ainsi possible d'exploiter par inégalités:

(*a*) Le maximum de densité, en donnant à R une valeur inférieure au rayon de van der Waals R_0.

(*b*) La distance interatomique minimale, en donnant à R une valeur égale au plus petit R_0: les sphères ne s'interpénètrent pas et le maximum de densité n'excède jamais celui d'une seule sphère.

(*c*) Le plus petit triangle formé par les centres de trois atomes voisins, en donnant aux R des valeurs telles que $\varrho_x \leq 2\varrho_0$.

On peut évidemment tenir compte de figure plus complexes et améliorer le rendement en choisissant des ellipsoïdes à la place des sphères, ou en utilisant des sphères multiples à plusieurs rayons liés à des densités différentes. Si l'on opère en projection, les sphères sont remplacées par des 'jetons'.

2·9. Cinemasummation as a new method of optical two-dimensional Fourier syntheses. By V. I. VLASENKO & G. S. ZHDANOV, *Inst. for Phys.-Chem. Research, Moscow, Obukha 10, U.S.S.R.*

Cinemasummation like a cinematograph based on the same principles of using the inertia of visual sense. In order to make Fourier syntheses it is enough to show successively for the observer, the series of pictures, each of them is the two-dimensional sine wave. The important condition of this summation is the great frequency of change this pictures. The summary visualization is the image of electron density function.

The cycle repetition of this process gives the stable semitone image, where the maximums of electron density are represented by light spots. During such cinemasummation it is possible to investigate the optical image and even to make some measuring.

For cinemasummation it is necessary to prepare a full complex of different pictures of sine waves on film, they are termed masks. The masks, which are similar of well known Huggins masks, are selected according to the data of the X-ray experiment.

These masks are inserted in special nests of a devise and it is switched on. As the result of it, all masks are projected successfully a simple screen (without any afterglow) and after a few seconds on this screen appears the image.

'Cinemasummator' allows to change the signs of any structure factors, and to make a new synthesis after it, not later than fourty seconds, thus it is possible to test different signs at the first steps of structure determination.

This new method differs greatly from the well known method of photosummation which has been used by Huggins or M. M. Woolfson. In 'cinemasummator' the summation of light rays, during projecting of masks, follows the linear dependence, therefore we may except a greater accuracy of this new method.

'Cinemasummator' allows to summarize simultaneously about 100–200 harmoniques.

It is possible to produce the masks for this devise with the indexes h and k from -30 to $+30$.

2·10. Recent developments in optical-transform methods. A survey paper presented by C. A. TAYLOR incorporating work by G. HARBURN, B. ROBINSON & F. A. UNDERWOOD, *Physics Department, College of Science and Technology, Manchester 1, England.*

The paper will describe the three main experimental lines which are being followed at the moment.

The first is concerned with the preparation and use of three-dimensional optical transforms. By a simple process involving the passage of circularly polarized light through mica plates it is possible to produce a continuously variable phase change. The z-coordinates of a structure whose x- and y-coordinates are already represented by the positions of holes in a mask may then be incorporated, for a given level l in reciprocal space, by adjustment of the phase of the light passing through the holes. Sections with any l value—including non-integral values—of the three-dimensional transform may then be observed. The ease with which three-dimensional transforms can be studied in this way has led to some interesting ideas, and to some techniques which may prove useful in certain kinds of structure problems.

The second development is based on an optical diffractometer that has been adapted to produce, by means of photomultipliers, a graph of the variation in intensity across a central line of a transform. This is being used at the moment in the general study of fibre problems. If the mask representing the structure under investiga-

tion is rotated continuously between the lenses of the diffractometer, the intensity distribution along the central line corresponds to the intensity distribution along the central line of an X-ray fibre diagram; although the planes of the two diffraction patterns are not the same, they intersect in this common line.

The third investigation is concerned with the application of the convolution principle, and refers particularly to the crystal structure of klockmanite (CuSe). This structure is hexagonal and has a pseudo unit cell with $a = 3.95$, $c = 17.25$ Å. There are, however, extra reflexions which at first suggested a true a-dimension of 51.4 Å ($= 13 \times 3.95$ Å). Progress has been made in interpreting the diffraction patterns, partly in terms of a twin hypothesis which now suggests a true a-dimension of 19.66 Å ($= \sqrt{(13)} \times 3.95$ Å), and some interesting illustrations of transform and convolution theory have emerged.

2·11. Some suggestions for new experimental approaches in X-ray diffraction. By C. A. TAYLOR, *Physics Department, College of Science and Technology, Manchester* 1, *England.*

For some time we have been using optical methods to assist in the solution of X-ray diffraction problems, and have claimed as one of their principal advantages that they emphasize the physics of the diffraction process. It is the purpose of the present communication to suggest that the parallel study of optical and X-ray diffraction should perhaps be extended to include the experimental arrangements for obtaining the patterns as well as their interpretation.

We have recently been studying the optics of the diffractometer in an attempt to obtain better patterns, and our attention has been drawn to the influence of the coherence of illumination. A study of the parallel problem of the coherence of radiation in X-ray diffraction is now suggested.

It has already been shown that it is possible, under certain conditions, to prepare an optical transform of one 'molecule' from a mask representing a regular array of 'molecules' (i.e. a two-dimensional representation of a crystal) by modifying the coherence of the illumination. Although the X-ray problem with a three-dimensional crystal is much more difficult it would seem to be possible, in principle at least, to obtain some information about the transform between reciprocal lattice points by a comparable alteration in the coherence of the X-ray beam.

The normal dimensions of apparatus used in X-ray diffraction are such that any effects due to incoherence would not be observed; their observation would involve the design of special tubes and possibly special cameras.

No experimental work has yet been done, but it is felt that one of the functions of a conference should be to discuss tentative ideas of this kind.

2·12. Some experiments with three-dimensional Patterson superpositions. By J. KRAUT, *Biochemistry Department, University of Washington, Seattle* 5, *Washington, U.S.A.*

A systematic exploration of the practical capabilities of the vector coincidence method has been undertaken with the aid of computer programs designed to convert three-dimensional Patterson maps into reduced maps by superposition methods. A series of compounds of increasing difficulty have been studied:

2-amino-ethyl phosphate, $P2_1/c$,
$$a = 9.03, \quad b = 7.74, \quad c = 8.87, \quad \beta = 102° 27';$$

adenylic acid, $P2_1$,
$$a = 12.77, \quad b = 11.82, \quad c = 4.88, \quad \beta = 92° 19';$$

myoinositol, $P2_1/c$,
$$a = 6.64, \quad b = 12.09, \quad c = 19.69, \quad \beta = 105° 49';$$

androsterone, $P2_1$,
$$a = 9.56, \quad b = 7.90, \quad c = 11.78, \quad \beta = 111° 22'.$$

As a result of the experience acquired on these compounds some conclusions are suggested concerning the rôles of molecular size, heavy atoms, symmetry and homometric structures in applying the method. In general terms, it appears that this is a powerful tool, potentially capable of solving structures of the complexity of those mentioned in a virtually routine manner, but that its fullest utilization requires the development of rapid procedures for visualizing three-dimensional reduced maps and for abstracting therefrom sterically acceptable configurations.

Full account likely to be published in *Acta Cryst.*

2·13. Crystal structure determination by the 'convolution molecule method'. By W. HOPPE, G. WILL, R. RAUCH & K. ANZENHOFER, *Abteilung für Röntgenstrukturforschung am Max-Planck-Institut für Eiweiss- und Lederforschung, München* 2, *Deutschland.*

The convolution molecule method (W. Hoppe, *Acta Cryst.* (1957), **10**, 750; W. Hoppe, *Z. Elektrochem.* (1957), **61**, 1076) for the interpretation of Patterson functions is a counterpart of the image-seeking methods and at the same time the equivalent of the Fourier transform method in the direct space. While the image-seeking methods try to unscramble the Patterson structure into the 'images' of the structure itself, the convolution molecule method unscrambles the Patterson structure into the 'convolution molecules' (convolution products of the molecule in the structure). A knowledge of some features of the molecular structure is therefore essential for a useful application of this method (as in the Fourier transform method). The method is especially suited for the determination of the translational parameters of the molecule, because translations of molecules will be translated into translations of the convolution molecules.

The application of this method will be demonstrated on several structure determinations of organic crystals. Of special interest are the exclusion of 'nearly homometric solutions' (tetramethyl-naphthaline) and the symmetry relations of convolution molecules (demonstrated in the structure determination of tetrachlorine-ketonaphthaline).

In a recent paper (*Z. Kristallogr.* (1959), **112**, 414) C. A. Beevers & H. W. Ehrlich have discussed some principles of the interpretation of Patterson structures. Apart from the remarks concerning the 'vector convergence method' it can be shown that these principles are based on an application of the convolution molecule method in a more qualitative and empirical way.

To be published in *Z. Kristallogr.*

2·14. Structure analytical methods for disordered crystals. By K. DORNBERGER-SCHIFF in collaboration with P. SEDLACEK & O. JARCHOW, *Deutsche Akademie der Wissenschaften zu Berlin, Institut für Strukturforschung, Berlin-Adlershof, Deutschland.*

The theory of OD-structures (see *Acta Cryst.* (1956) and a recent paper submitted to *Acta*) has been applied to the analysis of two disordered structures, to that of strontium metavanadate ($Sr(VO_3)_2 . 4 H_2O$) which shows one-dimensional disorder (in collaboration with P. Sedlacek) and to that of sodium tetrametaphosphate $Na_2H_2P_4O_{12}$ showing two-dimensional disorder (in collaboration with O. Jarchow).

The groupoid family of $Sr(VO_3)_2$ as deduced from the distribution of sharp points and diffuse rods in reciprocal space and the systematic absences, shown in Fig. 1 is either

$$P\ 1\ (c)\ 1 \qquad \text{or} \qquad P\ m\ (c)\ 2_1$$
$$\{2_{\frac{1}{2}}\ (1)\ n_{\frac{1}{2},2}\} \qquad \{2_{\frac{1}{2}}\ (2_2)\ n_{\frac{1}{2},2}\}$$

(see Fig. 2).

The higher symmetrical groupoid family seems to apply to the heavy atoms only.

Fairly sharp maxima on the diffuse rods show that the structure may, as a first approximation, be thought of as a micro-twinned structure. It turns out that modified generalized Patterson projections P_+^c and P_-^s calculated with the $F_{Hkl}^2 + F_{\bar{H}kl}^2$ and the $F_{Hkl}^2 - F_{\bar{H}kl}^2$ as coefficients, respectively, for $H = 2n + 1$ (Figs. 3 and 4) have a meaning relevant to the structure and are easier to interpret than an ordinary Patterson projection. These projections contain easily recognizable maxima corresponding to interatomic Sr–Sr-vectors and prove beyond doubt, that the V-atoms lie on an ordered sublattice corresponding to the reciprocal lattice produced by the sharp points only. The refinement of the structure is still in progress. The results so far obtained are in agreement with the results of F. Hanic (private communication) on the ordered projection of the structure.

For the *sodium tetrametaphosphate* investigated the partial operations were also deduced from the distribution of sharp points and diffuse sheets in reciprocal space which had already been described by J. W. Gryder, G. Donnay & H. M. Ondik (*Acta Cryst.* (1958), **11**, 38) as 'form II'. From the sharp $(hk0)$-reflections an ordered electron-density projection was obtained by triple product methods (see Fig. in abstract on sodium tetrametaphosphate). This projection is equally compatible with rings of 4 tetrahedra and with chains containing 4
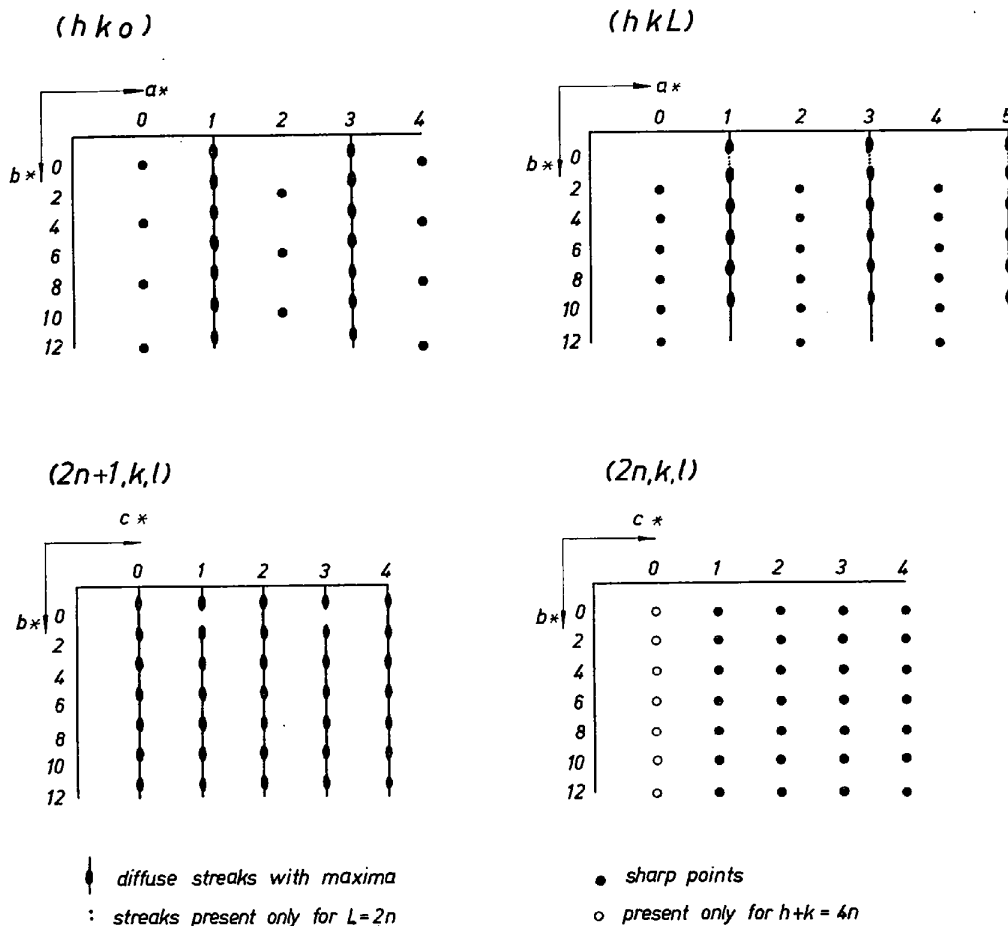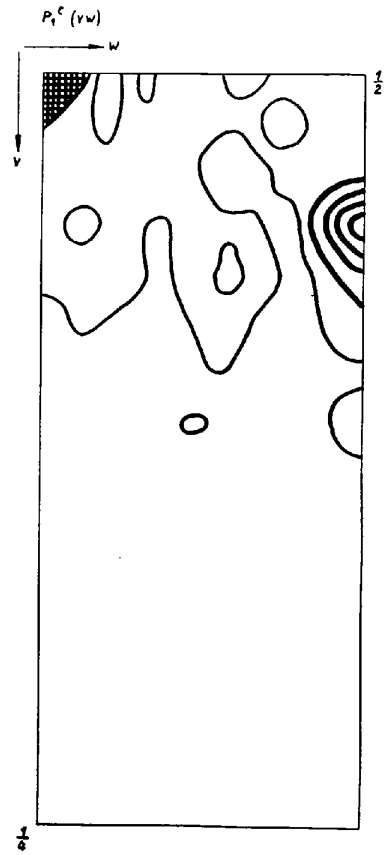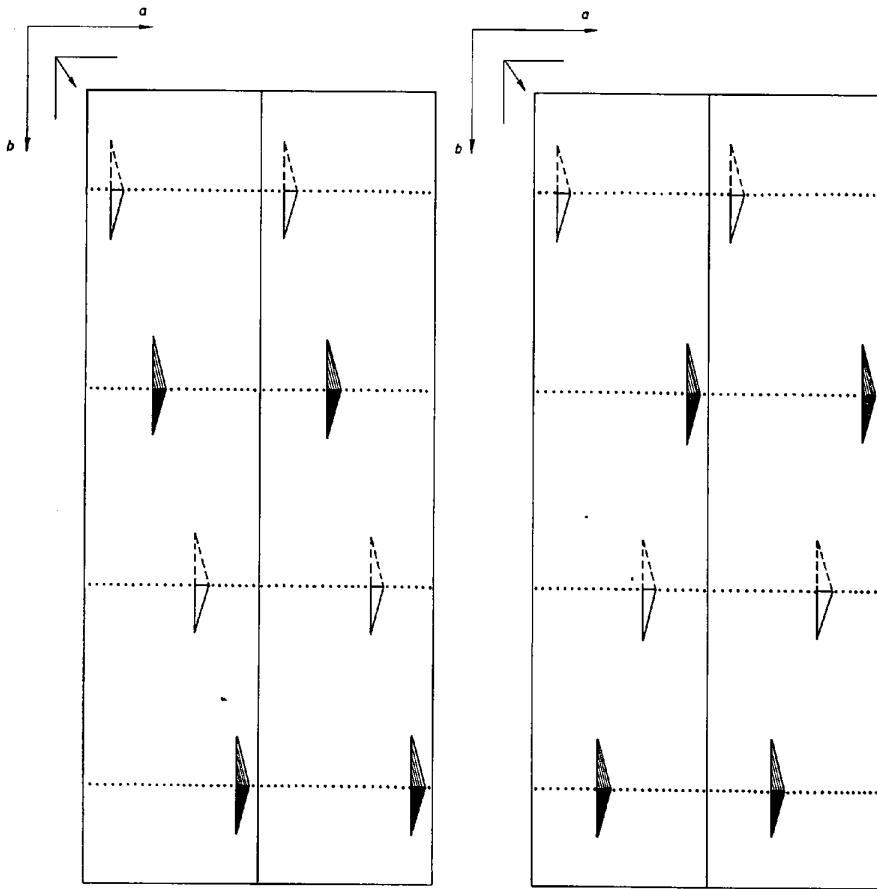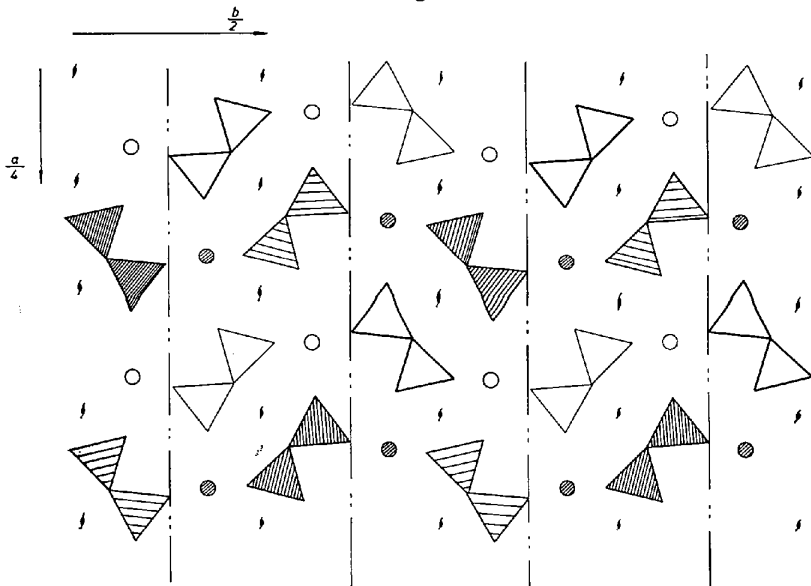

Fig. 1.

Fig. 2.

Fig. 3.

Fig. 4.

Fig. 5.
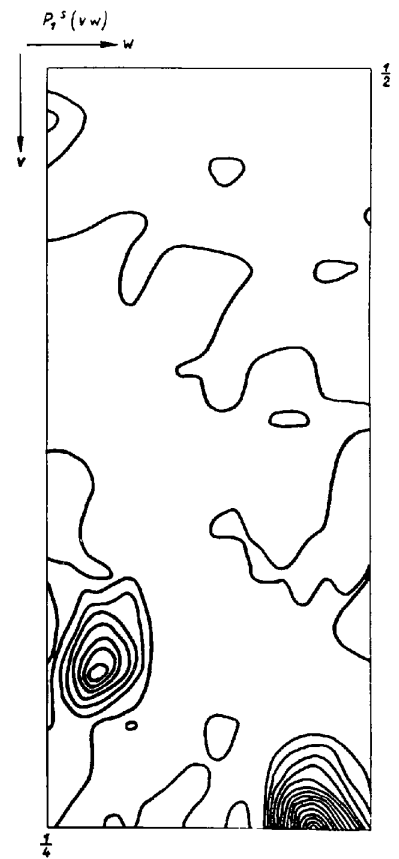
tetrahedra per repeat, but not with the interpretation of the structure as an ultraphosphate, as suggested by J. W. Gryder, G. Donnay & H. M. Ondik (1958). The sharp reflections $(h, k, 2n)$ are not sufficient to distinguish between these two possibilities. However, structure factor calculations for the $(\xi, \eta, 2n+1)$ may again be based on coordinates of equivalent positions, deduced from the OD-groupoid family, if the crystal is assumed to approximate to a micro-twin. One of the possible twin individuals compatible with the observed positions of maxima in reciprocal space is shown schematically in Fig. 5. Structure factor calculations based on this kind of twinning and atomic parameters deduced from the $(h, k, 2n)$, are being carried out for the maxima on the diffuse sheets. The results are to be given; so far they seem to point undubitably towards the existence of rings and against chains.

With these two examples we believe to have begun to collect experience in the proper use of the intensities of maxima on diffuse streaks (or sheets), for the solution of crystal structures. It will be shown how such an analysis has to be based on OD-groupoid theory, if mistakes are to be avoided.

2·15. Some experiences with sharpened Patterson syntheses. By S. ABRAHAMSSON & E. N. MASLEN, Chemical Crystallography Laboratory, Oxford, England.

Highly sharpened Patterson syntheses are required for the recognition of vectors due to pairs of a fairly heavy atom in structures containing large molecules like cephalosporin C ($C_{16}H_{20}O_8N_3SNa$).

Analysis of Patterson peak shapes for different modification functions shows that, in the 3-dimensional case, a very high weight can be given to outer terms without introducing serious diffraction ripples. The resolution of the Patterson synthesis and the relative height of the heavy atom peaks is thereby considerably enhanced in comparison with using less extreme modification functions.

Patterson syntheses calculated with the highest weight on the outer terms do not show any disturbing features but give easily recognizable S–S vectors.

2·16. Fourier methods applicable to structures containing more than 1000 atoms. By D. M. BLOW & MICHAEL G. ROSSMANN, Medical Research Council Unit for Molecular Biology, Cavendish Laboratory, Cambridge, England.

The unit cell of a protein crystal is so large that a huge number of reflexions would need to be measured before atoms could be fully resolved, and in any case the X-ray pattern usually becomes too weak to measure beyond about 2 Å. Unconventional Fourier methods are therefore called for. These make use of the very efficient averaging of unwanted contributions to a Fourier synthesis, brought about by the large number of terms. Thus, in a synthesis for locating a heavy atom used in isomorphous replacement, the height of the heavy atom peak increases approximately as the number of terms, n, while, the r.m.s. background, if random, increases as $\sqrt{n}$. In consequence, the inclusion of a sufficiently large number of terms makes it possible to use a synthesis with large background contributions. We will give ex-

amples of Fourier syntheses in which each individual term contains large errors, but by choosing appropriate weighting their effect on the summation can be minimized.

The first example shows the use of anomalous dispersion data from a single compound to determine the positions of its anomalous scatterers. A Fourier series with $(|F(hkl)| - |F(\bar{h}\bar{k}\bar{l})|)^2$, for some mercury derivatives of haemoglobin, revealed both the mercury atoms and the iron atoms of the haem groups.

The second example shows how an approximate solution of a non-centrosymmetric crystal structure can be obtained by isomorphous replacement, using only one pair of isomorphous compounds. In this case a phase ambiguity arises for each reflexion and it is generally thought that at least three members of an isomorphous series are required to resolve this. If, however, the array of replacing heavy atoms is non-centrosymmetric and if sufficient contrast is available in the true structure when seen at the same resolution, a recognizable structure may be obtained even if only two compounds are available. This idea has been tested with data from haemoglobin and myoglobin.

We plan to publish detailed accounts of this work in Acta Cryst.

2·17. The use of a Monte Carlo method for obtaining trial and error structures.* By V. VAND, A. NIGGLI† & R. PEPINSKY, Crystal Research Laboratory, The Pennsylvania State University, University Park, Pa., U.S.A.

An IBM 704 program has been written in which the absolute values of a limited set of structure factors serve as an input. A convenient set is 64 strongest structure factors. The program then internally emits random sets of co-ordinates of a predetermined number of atoms, and refines these in a small number of cycles, using a method of optimum shift. This method operates on one structure factor at a time, and shifts atoms according to the derivative of the structure factor. The method is not identical with that of least-squares, and has the advantage of being faster for refinement of a small number of reflections. The program then considers the disagreement factor of a structure so obtained. If this is lower than a certain limit, the co-ordinates and calculated structure factors are written down via magnetic tape. The limit itself is automatically movable, so that, in the long run, a predetermined number of trial structures is printed out. The most promising of these then can serve as a starting point for further refinement by least-squares methods.

2·18. Direkte Methode zur Strukturanalyse bei Polarisation und anomaler Dispersion. Von R. HOSEMANN, Fritz-Haber-Institut der Max-Planck-Gesellschaft, Berlin-Dahlem, Deutschland.

Die Auswertung der Integralintensitäten von Kristallreflexen führt über Faltungsintegrale in vielen interessanten Fällen zu direkten Informationen über die mittlere Elektronendichteverteilung in den einzelnen Atomen bzw. Ionen. Auf diese Weise konnte z. B. die von

Fajans, Joos (1925) vorausgesagte Deformation von Na^+ und Cl^- in Kochsalz bei Raumtemperatur direkt errechnet werden. Bei anomaler Dispersion tritt neben der Strukturgrösse $\varrho(x)$ der ungestörten Elektronendichteverteilung noch eine weitere Strukturgrösse $a(x) \exp[i\delta(x)]$ auf, die die Amplitudenvergrösserung (Faktor a) und die Phasenverschiebung δ gegenüber dem Fall der normalen Dispersion kennzeichnet. Währenddem in der quantenmechanischen Behandlung der Impuls der schwingenden Elektronen in einen Hamiltonoperator des gestörten und des ungestörten Anteils additiv zerlegt wird, ist nun die Atomformamplitude durch das Faltungsprodukt aus ungestörter Atomformamplitude und der Transformierten von $a \exp[i\delta]$ gegeben und liefert über Faltungsintegrale direkte Informationen über diese Einzelgrössen. Unterscheidet man wie in der quantenmechanischen Behandlung zwischen 'Dispersionselektronen' und praktisch ungebundenen Elektronen und nimmt hierfür die aus spektroskopischen Messungen errechneten Werte, setzt man ferner für a und δ die aus der Dispersionstheorie von Kallmann–Mark und Compton folgende Werte ein, so ergibt sich sowohl für die anomale Atomformamplitude als auch für den Brechungsquotienten und den wahren Absorptionskoeffizienten eine mit den experimentellen Ergebnissen im Gebiet der Röntgenstrahlung ausgezeichnete Übereinstimmung. Die Diskrepanzen mit den quantenmechanischen Ergebnissen von Hönl, Eisenlohr und Müller werden diskutiert. R. Hosemann u. G. Schoknecht, *Z. Nat. Forsch.* **12a**, 932 (1957). G. Schoknecht, *Z. Nat. Forsch.* **12a**, 983 (1957). R. Hosemann, *Acta Cryst.* **13**, 794.

Ausführliche Veröffentlichung ist vorgesehen in *Phys. Rev.*

2·19. The optimal shift method for refinement of crystal structures.* By A. NIGGLI,† V. VAND & R. PEPINSKY, *Crystal Research Laboratory, The Pennsylvania State University, University Park, Pa., U.S.A.*

The usual methods of refinement—e.g., least-squares—are adequate for overdetermined problems with more equations than unknowns. In the first steps of refinement or in choosing trial structures, however, it may be desirable to include only a smaller set of structure factors (e.g., with known phases or with strong intensities).

In the trial-and-error method, the shifting of atoms to obtain agreement between a few $|F_c|$ and $|F_o|$ values was accomplished by intuition or with the aid of Bragg–Lipson diagrams. The 'optimal shift method' has been devised in order that this task can be done by computers. In the case of centro-symmetry, the analytical expression for optimal shifts perpendicular to the planes H is

$$\Delta x_j = \sum_H \{ \Delta F_H (\partial F_H / \partial x_j) / \sum_i (\partial F_H / \partial x_i)^2 \}.$$

Tests have shown that the optimal shift method converges much faster than other refinement methods, if the number of structure factors included is smaller than the number of parameters.

Full-length account likely to be published in *Acta Cryst.*

---

§ 3. Minerals (including clay minerals)

3·1. The crystal structure of bikitaite, $LiAlSi_2O_6 \cdot H_2O$. By DANIEL E. APPLEMAN, *U.S. Geological Survey, Washington 25, D.C., U.S.A.*

As part of a program now in progress at the U.S. Geological Survey to investigate the system Li_2O–Al_2O_3–SiO_2, W. C. Phinney has carried out studies on the dehydration and stability range of the naturally-occurring hydrous lithium aluminosilicate bikitaite. The crystal-structure investigation of this zeolitic mineral has been undertaken in an attempt to explain various problems arising from these studies; especially the limited stability and stepwise dehydration.

Bikitaite, $LiAlSi_2O_6 \cdot H_2O$, was first described by C. S. Hurlbut, Jr., (*Amer. Min.* (1957), **42**, 792) from an occurrence in lithium-rich pegmatites at Bikita, Southern Rhodesia. The present study, which confirms Hurlbut's crystallographic data, was carried out on material from the type locality obtained through the U.S. National Museum. Powder diffractometer and single-crystal measurements yield the following crystallographic data: monoclinic $P2_1$,

$$a = 8{\cdot}611, \ b = 4{\cdot}960, \ c = 7{\cdot}610 \text{ Å}$$

(all $\pm 0{\cdot}2\%$), $\beta = 114° \ 26' \pm 5'$; the crystals are piezoelectric.

The crystal structure of bikitaite was solved by successive applications of the Buerger minimum-function procedure to the b-axis projection. Refinement has been carried out by Fourier and least-squares techniques on a digital computer. The structure consists of endless zigzag chains of silicate tetrahedra extending parallel to [010]. Three crystallographically non-equivalent kinds of silicate chains are linked laterally to form a three-dimensional network, containing one large channel and several smaller channels, also parallel to [010], in which Li ions and water molecules are located. Distribution of Al and Si in the structure is being studied by difference syntheses and least-squares methods.

To be published in *Acta Cryst.*

3·2. Methods for determining Al in tetrahedral and octahedral coordination with respect to oxygen. By G. W. BRINDLEY, H. A. McKINSTRY & V. STUBIČAN, *The Pennsylvania State University, University Park, Pa., U.S.A.*

Methods of determining Al–O coordination and the proportions of Al^{IV} and Al^{VI} in systems not suitable for accurate crystal structure analysis are considered.

(1) *Acid dissolution of layer silicates*

It has been shown that acid dissolution curves for a chlorite and for many montmorillonites distinguish quantitatively the more readily soluble Al^{VI} from the less soluble Al^{IV}. Extensive measurements on other minerals (G. W. Brindley & Vanden Heuvel) show that the method probably is applicable only to swelling structures which permit acid attack on the entire structure.

(2) *Al $K\alpha$ wavelength measurements*

Al^{IV} and Al^{VI} ions coordinated to oxygen show a small but measurable difference in the emission wavelength.

The method has provided clear evidence that Al ions in metakaolin have 4-fold coordination, a result previously known only by inference. A similar application to 'meta-gibbsite' suggests mainly 6-fold coordination. The method is useful only where one type of coordination predominates.

(3) Infra-red measurements (by V. Stubičan)

In clay minerals $Al^{VI}-O$ gives an infra-red vibration with strong absorption at about 535 cm.$^{-1}$. Absence of this band with metakaolin indicates absence of 6-fold coordination. With beidellite and pyrophyllite (heated between 600–1000 °C.) the presence of this band suggests that 6-fold coordination persists. It is not possible to assign any separate band to $Al^{IV}-O$ vibrations, but the amount of Al^{IV} can be estimated from its disturbing effect on Si–O neighbours. For example, in saponites the amount of Al^{IV} is determined from changes of the Si–O band at 670 cm.$^{-1}$. In chlorites, the distribution of Al between 4-fold and 6-fold coordination can be quantitatively correlated with changes of absorption frequencies in the region 550–800 cm.$^{-1}$.

Items (1) and (2): Publication channel is still uncertain. Item (2) *may* go to *J. Amer. Ceram. Soc.*
Item (3) will be published in *Amer. Min.* and in *Z. Anorg. Chem.*

3·3. The crystal structure of yoderite, a new aluminium silicate showing weak subsidiary X-ray reflections. By S. G. Fleet, *Crystallographic Laboratory, Cavendish Laboratory, Cambridge, England.*

Yoderite is a hydrous magnesium iron aluminosilicate discovered in Tanganyika by D. McKie in 1956. The approximate empirical formula is

$$(Mg_{2\cdot0}Ca_{0\cdot2}(Fe''Fe''')_{0\cdot5}Al_{5\cdot3})Si_4O_{17\cdot6}OH_{2\cdot4}.$$
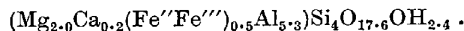
The structure is monoclinic, with space group $P2_1/m$ and cell dimension

$$a = 8\cdot035 \pm 0\cdot003, \quad b = 5\cdot805 \pm 0\cdot003, \quad c = 7\cdot346 \pm 0\cdot003 \text{ Å},$$
$$\beta = 105° 38' \pm 4'.$$

There are weak subsidiary maxima in layers perpendicular to x with unitary structure factors $\leq 0\cdot03$ (McKie, *Miner. Mag.* Dec. 1959). The average structure has been deduced from the intensities of X-ray reflections, ignoring the weak subsidiary maxime, and refined by two-dimensional Fourier methods. Chains of XO_6 octahedra sharing edges run parallel to the screw diad axis, linked by isolated SiO_4 tetrahedra and XO_5 trigonal bipyramids with X sites mainly occupied by aluminium and magnesium cations. The packing of oxygen atoms resembles (but is not identical with) that in kyanite with which the mineral forms intergrowths. The weak reflections can be indexed using an A-face-centred unit cell twenty-four times the size of the average cell which now becomes a subcell. They are due to variations of atomic coordinates between the subcells consequent on ordering of cations in the six and five fold cation sites. The true structure has been refined with the help of Fourier techniques, in particular by the use of difference maps showing the difference between the average and the true structure.

To be published in *Acta Cryst.*

3·4. The structure of anorthite. By C. J .E. Kempster, H. D. Megaw & E. W. Radoslovich, *Cavendish Laboratory, Cambridge, England.*

Anorthite, $CaAl_2Si_2O_8$, has an ordered structure with 8 formula units in the unit cell, which is built up from 4 albitoid subcells. The structure was derived in two stages from trial coordinates given by the albite structure: in the first stage, reflections with $h+k$ even (l even or odd) were considered, giving the 'base-centred approximation', and in the second stage those with $h+k$ odd, which were systematically weaker, were included to give the true primitive lattice. At each stage the signs of the systematically weak reflections were first found by supposing them due to Ca contributions only, and then corrected during refinement by inclusion of the other atoms (effectively a heavy-atom technique). No assumptions were made about (Si, Al) distribution; in the later stages, these atoms were distinguished by their size, the standard deviation of the mean tetrahedral bond length being about 0·012 Å.

It is found that Si and Al alternate, each O atom having one Si and one Al neighbour. The order is perfect, within the limits of experimental error, which are fairly narrow. There are differences of coordinates of all atoms between the four subcells, most marked for Ca; three Ca's have 7 neighbours in the range 2·3 to 2·8 Å, while the fourth has 6 only.

Geometrical differences between subcells related by a body-centring translation cannot be attributed to difference of (Si, Al) occupation, and are in fact larger than between subcells with different (Si, Al) occupation. They must be explained as a mechanism of reducing strain in the (Si, Al)–O framework, and attention is called to their importance. The conspicuous difference of sites for Ca in the four subcells follows as a consequence. Since these atoms make the largest contributions to the difference intensities they provide sensitive indicators of the subcell differences without being physically important in relation to their cause.

Probably will be published in *Acta Cryst.*

3·5. The crystal structure of harmotome. By R. Sadanaga, F. Marumo & Y. Takéuchi, *Mineralogical Institute, Faculty of Science, University of Tokyo, Hongo, Tokyo, Japan.*

The crystal structure of harmotome has been determined. There is one chemical unit of $Ba_2Al_4Si_{12}O_{32}12H_2O$ in the unit cell of symmetry $P2_1$, with

$$a = 9\cdot87, \quad b = 14\cdot14, \quad c = 8\cdot72 \text{ Å}; \quad \beta = 55° 10'.$$

The crystal is pseudorhombic; upon transformations: $a' = a$, $b' = b$ and $c' = 2c - a$, the new β angle becomes as nearly 90° as 89° 37'. The atomic positions in the a-axis projection were determined from the Patterson projection along the direction with the aid of the minimum function method. The b-axis projection of the Patterson function produced no definite conclusion owing to serious overlappings of peaks. A Patterson function consisting of higher order terms only was then calculated to enhance the contribution of the cations. The information obtained from this function and the pseudosymmetry made it possible to determine the positions of the Ba atoms in

the projection, and the framework of the structure was derived from minimum functions. The refinement was started on the basis of space group $P2_1/m$ since the statistical test of the diffracted X-ray intensities suggested a nearly centrosymmetric arrangement of atoms, and the small deviations from it were taken into consideration at the final stage.

The structure is based upon a three-dimensional alumino–silicate frame-work composed of four- and eight-membered rings of Si(Al)–O tetrahedra, and bears close resemblance to the feldspar structures. Through the frame-work, channels run along [100] and [010], water molecules and metal atoms being situated in them. Barium is surrounded by six oxygen atoms and four water molecules. The cruciform twinning characteristic of the crystal is satisfactorily explained by the structure.

To be published in *Acta Cryst.*

3·6. Studies on pyroxene, amphibole, zeolite and feldspar minerals at the Department of Mineralogy, Pennsylvania State University. By W. L. BROWN, J. H. FANG, G. V. GIBBS, R. N. LEWIS, J. V. SMITH & W. TAUBENECK, *Mineral Sciences Bldg., Pennsylvania State University, University Park, Pa., U.S.A.*

(1) *Pyroxenes* (WLB, JVS). Using a new furnace attachment on a precession camera, single crystals of natural rhombic enstatite have been converted rapidly to proto-enstatite between 1100 and 1300 °C. On holding at 900 °C. for several weeks, the proto-enstatite transforms into disordered forms of enstatite, transitional between proto and rhombic enstatite. Similar D-enstatites have been found in a meteorite and in synthetic enstatites. Preliminary studies have been made on hypersthene crystals heated in sealed silica tubes up to 1300 °C. Data for a new mineral from pyroxene-bearing rocks is reported

(monoclinic $a = 8·02$, $b = 4·97$, $c = 6·34$ Å; $\beta = 107°\ 40'$).

(2) *Amphiboles* (WLB, GVG, RNL.JVS). A single crystal and powder X-ray diffraction survey has revealed that most amphiboles are single phases. The existence of cummingtonite–hornblendes 'perthites' described by Asklund has been confirmed. Hydrothermal treatment up to 800 °C. has not yet homogenized the intergrowths. Amphiboles can be typed from powder diffraction patterns, but it is doubtful whether the chemical composition can be estimated with much accuracy from these patterns.

(3) *Zeolites* (JHF, JVS, W.T.). Studies of chabazite and other minerals have been made to obtain information on the adsorption and ion-exchange properties. The Si, Al–O framework in dehydrated chabazite differs in position by up to 1 Å from that in the hydrated zeolite showing that it is unwise to use data for the frame-work for hydrated zeolites in physico chemical calculations of adsorption in dehydrated zeolites. The two Ca atoms of dehydrated Ca-chabazite occur 1/3 each in 3 sites and probably 1/12 each in 12 sites. In hydrated chabazites the Ca atoms also are statistically arranged, though in a different pattern. The water molecules are not in rigorously fixed positions. Data on dehydrated K-chabazite, hydrated Na-chabazite and Cl_2–Ca-chabazite will also be presented.

A new zeolite mineral has been found to occur with heulandite in granite rocks from Oregon. It is orthorhombic, pseudo-tetragonal. with $a = 17·8$, $b = 18·2$, $c = 13·6$ Å. space group $F222$, $Fmm2$ or $Fmmm$. Although the cell dimensions are related to both thomsonite and analcite, there appears to be no similarity in the intensities of the X-ray reflections.

(4) *Feldspars* (JVS). Recent values for Si, Al–O distances are discussed in terms of Smith's 1954 relation. The distance Al–O $1·80 \pm 0·016$ Å in zungite is consistent with the predicted value of $1·78 \pm 0·02$ Å. Several recent values of Si–O greater than $1·60$ are disturbing and suggest that the Si, Al–O distances depend on factors other than Si, Al content.

The influence of order–disorder, strain and local charge balance on the stability of feldspars is discussed. It is concluded that substitution of ions introduces changes in the ionic and covalent forces that cannot be estimated in terms of present knowledge. The entropy changes brought about by order–disorder are thought to be more important than local charge balance in determining the stable crystal structure. Local charge balance is thought to be important in determining the Al, Si ordering when the Al/Si ratio is near 1, but to be of much less importance when the Al/Si ratio is 1/3.

Publications plans not known for sure, but probably *Amer. Min.* for items (1) and (2), *Acta Cryst.* or *J. Amer. Chem. Soc.* for (3), and *Z. Kristallogr.* for (4).

3·7. A refinement of the dickite structure and some remarks on polymorphism in kaolin minerals. By R. E. NEWNHAM, *Cavendish Laboratory, Cambridge University, and Laboratory for Insulation Research, Massachusetts Institute of Technology, Mass., U.S.A.*

The crystal structure of the clay mineral dickite $(Al_2Si_2H_4O_9)$ has been refined to a greater accuracy than that reported in an earlier analysis (R. E. Newnham & G. W. Brindley, *Acta Cryst.* (1956), 9, 759). The refinement was carried out with zero-layer intensity data collected about [100] and [110] using Mo $K\alpha$ radiation. The coordinates obtained after ten cycles of $(F_o - F_c)$ difference syntheses gave an R-factor of 7·5% for 420 observed reflections. Improved lattice parameters,

$$a = 5·150 \pm 0·001,\quad b = 8·940 \pm 0·001,\quad c = 14·424 \pm 0·002\ \text{Å};$$
$$\beta = 96°\ 44' \pm 1',$$

were determined from single crystal diffraction spectra near $\theta = 90°$ by graphical extrapolation. The dickite structure shows several significant distortions from the geometry of the idealized kaolin layer, including deformation and rotation of the silica tetrahedra. The most striking features of the octahedral layer are the extremely short shared edges of 2·37 Å. Although the analysis was not sufficiently accurate to position the hydrogen atoms with certainty, a model is proposed which is consistent with the infra-red absorption spectra. The stacking sequences of kaolin layer minerals have been considered with reference to the structural features observed in dickite. There are 36 ways of superposing two kaolin layers commensurate with the O–H $\cdots$ O interlayer bonds found in kaolinite, dickite and nacrite. Many of these possibilities are at variance with the lowered sym-

metry of the individual layers, while others violate Pauling's rules.

To be published in *Miner. Mag.*

3·8. Thermal transitions in some calcium silicate hydrates. By E. J. McIver, *Crystallographic Laboratory, Cavendish Laboratory, Cambridge, England.*

The structures of Bultfonteinite, $Ca_4Si_2O_{10}F_2E_6$, with space group $P\bar{1}$, and of Afwillite, $Ca_3Si_2O_{10}H_6$, with space group Cc, have strongly marked pseudo symmetries of $P2_1/c$ and Cm (with halved c axis) respectively. With the exception of certain hydrogen atoms, all other atoms can be made to satisfy the higher symmetry by means of small displacements. High temperature single crystal studies show, that prior to dehydration, both minerals change to the high symmetry forms, at approximately 400 and 200 °C. respectively. An explanation is offered, based on the behaviour of the calcium–oxygen coordination polyhedron and their relation to the hydrogen bonds. The relevance of these phase changes to the subsequent dehydration reactions is discussed.

To be published in the *Miner. Mag.*

3·9. Crystallographic studies of some phase transformations in minerals. By M. C. Ball, L. S. Dent Glasser, A. G. Freeman, J. A. Gard, F. P. Glasser, A. W. Nicol & H. F. W. Taylor, *Department of Chemistry, University of Aberdeen, Scotland.*

Single crystal studies have been made of some reactions of silicate and other oxygen-containing minerals. These include hydrothermal and dehydration processes and thermal transitions, and provide new examples of oriented transformations, in which a single crystal of a starting material gives a single crystal or preferred orientation aggregate of a product.

(1) *Hydrated calcium silicates.*—Hydrothermal and dry heating of afwillite $(Ca_3(HSiO_4)_2 . 2H_2O)$ under various conditions yields phase Z (of D.M.Roy; $9CaO . 6SiO_2 . H_2O$), xonotlite $(Ca_6Si_6O_{17}(OH)_2)$, γ-Ca_2SiO_4, and other products. Treatment with water at about 380 °C. and 200 bars gives first phase Z, as an unstable intermediate product, followed by xonotlite as an apparently stable product. From X-ray study of these oriented transformations, together with electron diffraction evidence, the unit cell or pseudocell of phase Z has been determined.

(2) *Amphiboles and pyroxenes.*—Dehydration of tremolite $(Ca_2Mg_5(Si_8O_{22})(OH)_2)$ on dry heating to give the corresponding pyroxene occurs by an oriented mechanism. This is compared with the mechanisms previously suggested for the dehydration processes of xonotlite (Dent & Taylor, 1956) and foshagite $(Ca_4Si_3O_9(OH)_2)$; Gard & Taylor, 1958), which occur under similar conditions.

(3) *Calcium silicates containing other ions.*—Hydrothermal reaction of tilleyite $(Ca_5(Si_2O_7)(CO_3)_2)$ with water at 500 °C. and 700 bars gives xonotlite with partial preservation of orientation. Examples of fully oriented transformations without change of composition are provided by the thermal transitions of rhodonite $(Mn_4Ca(SiO_3)_5)$ and johannsenite $(CaMn(SiO_3)_2)$ to wollastonite solid solutions at about 1200 °C.

(4) *Hydroxides.* — Dehydration of fibrous brucite $(Mg(OH)_2)$, either on dry heating or hydrothermally to give MgO, proceeds through intermediate formation of a spinel-like phase. A new hypothesis is proposed for the reaction mechanism, which may apply also to the dehydration processes of gibbsite and other layer-type hydroxides.

The mechanisms of these processes are discussed.

Different parts of the work will be submitted for publication in *Acta Cryst.*, *Amer. Min.*, and *Miner. Mag.*

3·10. The crystal chemistry of the amphiboles and pyroxenes. By E. J. W. Whittaker, *Ferodo Ltd., Chapel-on-le-Frith, Stockport, England.*

The amphiboles constitute a group of minerals having a complex system of substitution relationships. For example in certain ranges of composition iron may substitute completely for magnesium leading to a complete range of solid solution between tremolite and actinolite, whereas in other ranges of composition the same substitution leads to a change of symmetry from orthorhombic to monoclinic as between anthophyllite and cummingtonite. The range of composition of the orthorhombic amphiboles is very restricted whereas that of the monoclinic amphiboles is very wide, and the latter show a range of β angles. Several amphibole structures have now been determined and it has been found that the detailed structure of the silicate chain is approximately the same in all of them. The present paper shows how the differences between the different amphibole species may be accounted for on the basis of rigid amphibole chains whose packing is determined by the radii of the metal ions. The effects of the ionic radii are different for the ions occupying three different kinds of site in the structure. The theory accounts quantitatively for the range of composition of the orthorhombic amphiboles and for the β angles of the monoclinic ones and predicts various new relationships which might be investigated by synthetic work.

The same phenomena are shown to be reflected in the crystal chemistry of the pyroxenes, although here the effects of ionic size are much less rigidly defined. It is suggested that this is due to the greater flexibility of the single silicate chain in pyroxenes as compared with the double chain in amphiboles, a suggestion which is in line with such structural knowledge of the pyroxenes as is available.

3·11. X-ray study of the thermal decomposition of thaumasite. By M. Font-Altaba, *Rocafort, 111, Barcelona, Spain.*

The study of thermal decomposition of thaumasite begins with the obtention of the d.t.a. curve and its interpretation. Two peaks appear, one very strong endothermic at 206 °C., and another exothermic of an intensity seven times less at 709 °C. The first corresponds to an endothermic chemical reaction of 1st order as the loss of crystallization water; the second is due to a consolidation or inversion of a phase. In order to know the nature of this transformation, an X-ray study of the mineral is carried out after having been submitted to a temperature between 200 and 1000 °C. The end product is

formed by two phases, $CaSO_4$ and $\beta\text{-}Ca_2SiO_4$, whose formation was to be foreseen taking into account the chemical composition of the thaumasite. The endothermic peak at 709 °C. is due to the crystallization of the $\beta\text{-}Ca_2SiO_4$.

To be published in *Miner. Mag.*

3·12. Study of ranquilite, a calcium uranyl silicate.

By M. Jiménez de Abeledo, María Rodríguez de Benyacar & Ernesto E. Galloni, *Comision Nacional de Energia Atomica, Avda, Libertador Gral San Martin 8250, Buenos Aires, Argentina.*

A yellow fluorescent mineral appearing in very small amounts in samples of gypsum from the Ranquil-Có area (Mendoza, Argentina) is studied. X-ray powder pattern data showed it to be a new mineral; it was named ranquilite, from the locality of its occurrence. According to chemical analyses, probable formula is:

$$1\cdot5 \text{ CaO} . 2 \text{ UO}_3 . 5 \text{ SiO}_2 . 12 \text{ H}_2\text{O} .$$
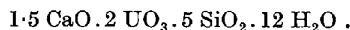
Dehydration and rehydration studies showed that two 'hydrates' are present in our samples of ranquilite, and allowed us to select the lines belonging to each 'hydrate' on the X-ray powder patterns. From selected area electron diffraction patterns, values for a_0 and b_0 were obtained. A value for c_0 was obtained assuming that the lines that shift during dehydration represent $00l$ reflections.

All the lines in the pattern for the form rich in water could be indexed assuming rhombic symmetry with dimensions:

$$a_0 = 17\cdot64, \quad b_0 = 14\cdot28, \quad c_0 = 18\cdot4 \text{ Å} .$$

Study is being continued on ranquilite, as well as on a green variety occurring in significant amounts in new samples of the material from Ranquil-Có.

To be published in *Amer. Min.*

3·13. Structural investigations on sulfosalts from the Lengenbach, Binn Valley, Switzerland.

By W. Nowacki, Y. Iitaka & H. Bürki, *Bern, Sahlistr. 6, Switzerland.*

(1) *The pseudostructure of scleroclase (Y.I.)*

Oscillation, Weissenberg and precession photographs showed two kinds of spots: 'strong' and 'weak' ones. The intensities of the 'strong' spots have an orthorhombic symmetry, but the missing spectra yield a monoclinic symmetry of the pseudo-cell with

$$a' = 19\cdot62, \quad b' = 7\cdot89, \quad c' = 4\cdot19 \text{ Å}, \quad \beta' = 90°,$$

$C_{2h}^5\text{-}P2_1/n$, $Z = 4$. $PbAs_2S_4$ ($d = 5\cdot05$). The intensity distribution of the 'weak' spots is monoclinic, stronger in the high angle region and probably varying in different specimens. The 'weak' spots may be caused by periodic shifts from the mean atomic positions, so that the true structure is a superposition of a pseudo-structure and a modulation (of the displacive type). The true cell has the periods

$$a = 3 \times 19\cdot62 = 58\cdot9, \quad b = 7\cdot89, \quad c = 11 \times 4\cdot19 = 46\cdot1 \text{ Å},$$
$$\beta = \beta' = 90°.$$

A Patterson projection $(hk0)$ gave the position of the heavy Pb-atoms of the pseudo-structure, which yielded the signs for a Fourier, which was refined by difference Fouriers to show at the end all As- and S-positions $(R = 26\%)$. In the $(h0l)$-projection the z-coordinates were fixed by the orthorhombic intensity distribution as $0, \frac{1}{4}, \frac{2}{4}, \frac{3}{4}$ and crystal chemical considerations gave a plausible arrangement for which the R-value dropped from 29% to 15·8% when individual temperature factors for each atom (As = 7·4, S = 4·5 Å²) and an anisotropic one for lead ($\|a$ 6·7, $\|c$ 3·6 Å²) were introduced. The 'weak' spots and these high factors (B = 4·5 Å² for $(hk0)$ projection) indicate the presence of some kind of superstructure and disorder. The difference Fourier maps show still a large anisotropy also for As and S.

The atomic coordinates are:

	x'	y'	z'
Pb	0·1947	0·0849	0·2500
As_1	0·1290	0·5030	0·7500
As_2	0·0040	0·8020	0·2500
S_1	0·2210	0·3630	0·7500
S_2	0·1680	0·6810	0·2500
S_3	0·0780	0·9750	0·7500
S_4	0·0480	0·3410	0·2500

The coordination is:

$$Pb = 2\cdot80(S_2) + 3\cdot08(2S_1) + 3\cdot19(2S_1) + 3\cdot22(2S_3)$$
$$+ 3\cdot23(S_2) + 3\cdot52(S_4) = 8 + 1,$$
$$As_1 = 2\cdot12(S_1) + 2\cdot63(2S_2) + 2\cdot92(2S_4) = 3 + 2,$$
$$As_2 = 2\cdot38(S_3) + 2\cdot59(2S_4) + 2\cdot89 \text{ A } (2S_3) = 3 + 2.$$

The coordination of the Pb-atoms is similar to that in $PbCl_2$ and $PbBr_2$. The structure show layer like regions of Pb- and S-atoms $\|$ (100), separated by regions of As- and S-atoms (good cleavage $\|$ (100)). There are $(AsS_2)n$-chains $\|$ c; because of the modulation in the true structure it is probable that they do not extend infinitely, but are broken into pieces of—up to present—unknown length.

(2) *Lengenbachite (Y.I.)*

Oscillation, Weissenberg, precession and Laue photographs yielded the data:

$$a = 35\cdot1_3, \quad b = 11\cdot5_2, \quad c = 36\cdot9_0 \text{ Å}, \quad \beta = 92°\cdot6,$$

space group $C_{2h}^2\text{-}P2_1/m$.

(3) *Fibrous sulfosalt (H. B.)*

In the Lengenbach dolomite fine needles of a grey, sometimes reddish sulfosalt occur [see Fig. 16 in W. Nowacki, *Die Neuerschliessung der Mineralfundstelle Lengenbach* (Binnatal, Kt. Wallis). *Mitt. Natf. Ges.*, Bern (N.F.), (1960) **18**, 35–43]. These needles consist of two (or one and two) species: an orthorhombic [with $a = 8\cdot38$, $b = 2 \times 25\cdot61$, $c = 7\cdot89$Å, space groups $C_{2v}^{11}\text{-}Cmm2$, $C_{2v}^{14}\text{-}Cm2m\text{-}C2mm$, $D_2^6\text{-}C222$, $D_{2h}^{19}\text{-}Cmmm$; the spots with $h = $ odd are weaker than those with $h = $ even and somewhat diffuse] and two monoclinic [with $a = 8\cdot38$, $b = 25\cdot61$, $c = 7\cdot89$ Å, $\beta = 90°25'$, space groups $C_s^1\text{-}Pm$, $C_2^1\text{-}P2$, $C_{2h}^1\text{-}P2/m$, $C_2^2\text{-}P2_1$, $C_{2h}^2\text{-}P2_1/m$ (hkl and $h0l$ all present, $0k0$ coinciding with spots of the orthorhombic species)] (needle axis $\| a$). The whole mass of a needle is distributed

about equally over the three species. Each species only shows *one* orientation within a given crystal. The cells of the two monoclinic species are symmetrical to a plane $\perp$ to the needle axis. The structure of the two monoclinic species may be either identical or enantiomorphous. The lattice constants show a striking similarity with those of rathite ($a = 8 \cdot 43$, $b = 25 \cdot 80$, $c = 7 \cdot 91$ Å, $\beta = 90° \pm 15'$, C_2^2-$P2_1$) and of dufrenoysite ($a = 8 \cdot 41$, $b = 25 \cdot 85$, $c = 7 \cdot 88$, $\beta = 90°\ 30'$, C_{2h}^2-$P2_1/m$).

To be published in *Acta Cryst.* or *Z. Kristallogr.*

3·14. The crystal structure of cahnite, $Ca_2BAsO_4(OH)_4$.
By CHARLES T. PREWITT & M. J. BUERGER, *Massachusetts Institute of Technology, Mass., U.S.A.*

Cahnite is one of the few crystals which had been assigned to crystal class $\bar{4}$. A precession study showed that its diffraction symbol is $4/mI$-/-, which contains space groups $I4$, $I\bar{4}$, and $I4/m$. Because of the known $\bar{4}$ morphology, it must be assigned to space group $I\bar{4}$, which it then shares with only one other mineral, nagyagite. The unit cell, whose dimensions are $a = 7 \cdot 11$ Å, $c = 6 \cdot 20$ Å, contains two formula weights of

$$Ca_2BAsO_4(OH)_4 .$$
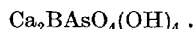
The structure was studied with the aid of intensity measurements made with a single-crystal diffractometer. Patterson syntheses were first made for projections along the c, a, and [110] directions. The atomic numbers of the atoms are in the ratio As : Ca : O : B $= 33 : 20 : 8 : 5$, so that the Patterson peaks are dominated by the atom pairs containing arsenic as one member of the pair. Since there are only two arsenic atoms in a body-centered cell, one As can be arbitrarily assigned to the origin. Then the major peaks of the Patterson syntheses are at locations of atoms in the structure. The structure, determined approximately in this manner, was refined by two-dimensional difference maps, and later by least-squares using all hkl reflections recordable with Cu $K\alpha$ radiation. The coordinates of the final structure are:

Atom	Equipoint	x	y	z
Ca_I	$2b$	0	0	$\frac{1}{2}$
Ca_{II}	$2d$	0	$\frac{1}{2}$	$\frac{1}{4}$
B	$2c$	0	$\frac{1}{2}$	$\frac{3}{4}$
As	$2a$	0	0	0
O_I	$8g$	0·177	0·051	0·167
O_{II}	$8g$	0·340	0·055	0·613

These coordinates determine a structure in which As is tetrahedrally surrounded by O_I at a distance of $1 \cdot 67$ Å, B is tetrahedrally surrounded by O_{II} at a distance of $1 \cdot 47$ Å. The calcium atoms are each surrounded by 8 oxygen atoms at about $2 \cdot 45$ Å.

To be published in *Z. Kristallogr.*

3·15. Crystal structures of the Cu_9S_5-Cu_5FeS_4 series.
By N. MORIMOTO* & G. KULLERUD, *Geophysical Laboratory, Carnegie Institution of Washington, Washington 8, D.C., U.S.A.*

Complete solid solution exists, above approximately

---

* Present address: Department of Mineralogy, University of Tokyo, Tokyo, Japan.

350 °C., between Cu_5FeS_4 (bornite composition) and Cu_9S_5 (digenite composition). In order to elucidate the relationship between crystal structures on the one hand and composition and temperature on the other, 'single' crystals of 10 different compositions between Cu_5FeS_4 and Cu_9S_5 were synthesized above 350 °C. The quenched products were examined by the precession and Weissenberg methods.

Characteristic features observed on the synthetic materials are:

(1) *Superstructure phenomena.*—Crystals of all compositions have super cells built from variants of a unit, which is a cube with cell edges, a, ranging from 5·47 Å for Cu_5FeS_4 to 5·54 Å for Cu_9S_5. The edges of the supercells are multiples, t, of the edge of the cube. t ranges from 2 for Cu_5FeS_4 through 3 and 4 for intermediate compositions to 5 and 6 for Cu_9S_5.

(2) *Extinction rules.*—Only the reflections of

$$(2 . t . m \pm L,\ 2 . t . n \pm L,\ L)$$

were observed when the lengths of the unit-cell edges were $a . t$ Å. These extinctions were explained by assumption of twinning of the fundamental rhombohedral cells, which have $1/(4t^2)$ of the apparent supercell volume, $(a . t)^3$ Å^3.

The crystal structure of Cu_5FeS_4 was determined on the basis of the fundamental rhombohedral cell with $a_r = 6 \cdot 71$ Å, $\alpha = 33°\ 32'$ and the space group, $R\bar{3}m$. There is one $(Cu, Fe)_3S_2$ in the unit cell. The discrepancy factor R is 0·206 for the final structure. This structure is interpreted as the layer-structure parallel to (111). Sulfur layers lie between two kinds of metal layers, for one of which all positions are filled and for the other, only a half of the positions is filled. The crystal structures of other compositions with different cell edges, including Cu_9S_5, are explained by the different stacking order of partly filled metal layers keeping the sulfur layers constant for the whole series.

3·16. Polymorphism of Ag_2Te. By ALFRED J. FRUEH, JR., *Department of Geological Sciences, McGill University, Montreal 2, P.Q., Canada.*

Three polymorphs of Ag_2Te exist between room temperature and the melting point. They are, in the order of increasing temperature: monoclinic, face-centered cubic, and body-centered cubic. The transformation temperature between the face-centered cubic and the body-centered cubic forms increases with a slight stoichiometric excess of Ag. Three polymorphs of Ag_2S have been listed, in order of increasing temperature, as monoclinic, body-centered cubic, and face-centered cubic. The transformation temperature between the body-centered cubic and the face-centered cubic forms decreases with a slight stoichiometric excess of Ag. A structural explanation is sought for the increase in the stability range of the face-centered cubic structure with stoichiometric excess of Ag in both these compounds.

Likely to be published in *Amer. Min.*

3·17. Electron microscope transmission studies of ceramic materials. By A. KELLY & G. K. WILLIAMSON, *University of Cambridge, Department of Metallurgy, Cambridge, England.*

Electron Microscope transmission studies have been made of ceramic materials such as graphite, boron nitride and magnesium oxide. The specimens can be prepared by cleavage or chemical thinning and dislocations and other defects observed in exactly the same way as for metals. In the case of magnesium oxide dislocations associated with cracks have been studied and also the mode of cross slip of screw dislocations. In the case of the layer structures values of the stacking fault energy can be deduced by measurements of the curvature of dislocations at extended nodes. The values are very low in graphite being less than 1 erg/cm.^{2}. The ease with which the layer structure may be sheared parallel to the basal planes is to be interpreted in terms of the width of the dislocations rather than in terms of weak van der Waals bonding between the layers.

To be published in *J. Amer. Ceram. Soc.*

3·18. Zur Kenntnis der metamikten Minerale der Euxenit-Familie. By H. SEIFERT & B. BECK, reported by H. SEIFERT, *Mineralog.-Petrologisches Institut der Universität, Münster/Westf., Deutschland.*

At the second International Congress of the Union (Stockholm 1951) one of us reported about successful recrystallization of powders of the metamict minerals of the euxenite family, among them of classical localities, by heating them in an electrical furnace at 900 °C.– 950 °C. He got X-ray powder diagrams of a wholly uniform type. These could be interpreted apparently orthorhombic in analogy to the columbite crystals. This was naturally connected with uncertainty because of richness of the interferences. Euxenite, aeschynite, polycrase and blomstrandine, they all gave very similar lattice constants, but not an axial ratio very satisfactorily conformable with the medium morphological axial ratio of the literature. Various non systematic oscillations of intensity might plausibly be interpreted by strong chemical differences within the formula AB_2O_6.

These investigations were taken up. It was established with further material like Berman (1950) that powder diagrams of the recrystallized specimens were variable in dependence of the temperature and the time of heating. Therefore it is the question if at all the original structure of the minerals is reached by this process. Surely there are localities which give the same diagrams at a low or high temperature of heating—as an example the euxenite from Moss. It seems to be more frequent that this is not the case.

A second considerable result of the experiments by *synthesis* is the following: On the base of mixtures of the oxides Y_2O_3, TiO_2 and Nb_2O_5 in the ratio 1:1:1, i.e. for a compound $y[NbTiO_6]$, we got diagrams which were found to be in an excellent harmony with those of recrystallized specimens of the same minerals as above on one side, but now heated at high temperatures in air, to those of the euxenite from Mattawan/Canada (and the aeschynite of Hitterö/Norway), treated by us and by Berman (1955) in the same manner at the other side.

The latter mineral was already examined by Arnott (1950) and structurally interpreted in a manner that there existed a good harmony with the morphological axial ratio. Thus we can now agree with this proposal. Arnott, too, got diagrams with much more interferences for Mattawan at a lower temperature and shorter time of exposure. It must therefore be examined if such diagrams are ever homogeneous or not.

A general view of series of other syntheses is to be joined. We hope to report, too, about new hydrothermal syntheses which are now in progress and aim to get single crystals for further investigation of the mineral group in the aspect of crystal structure and geochemistry.

In recent days, however. we were succesful in producing single crystals of the compound YTiNbO$_6$ and the Euxenite of Mattawan by melting the mixture of oxides resp. the metamikt material and cooling slowly.

We found the following lattice constants and space groups:

Synthetical YTiNbO$_6$	Euxenite Mattawan
$a_0 = 5{\cdot}59 \pm 0{\cdot}03$ Å	$a_0 = 5{\cdot}59 \pm 0{\cdot}03$ Å
$b_0 = 14{\cdot}65 \pm 0{\cdot}07$	$b_0 = 14{\cdot}62 \pm 0{\cdot}07$
$c_0 = 5{\cdot}22 \pm 0{\cdot}03$	$c_0 = 5{\cdot}23 \pm 0{\cdot}01$
$D_{2h}^{14} = Pcan$	$D_{2h}^{14} = Pcan$

These results are in good agreement with those of R. I. Arnott obtained by measurement of powder-diagrams from an Euxenite of Mattawan too.

Probably will be published in *Geochimica Acta.*

3·19. The crystal structure of kettnerite (BiO)(CaF)CO$_3$. By V. SYNEČEK & L. ŽÁK, *Institute of Technical Physics, Czechoslovak Academy of Sciences, Prague and Dept. of Mineralogy, Charles University, Prague, Czechoslovakia.*

The orthorhombic unit cell of kettnerite with $a = b = 5{\cdot}36$, $c = 13{\cdot}59$ Å contains four molecules. The structure was studied from the ordinary and generalized Patterson projections on (010). Tetragonal layers (Ca, 2F, Ca) and (Bi, 2O, Bi) parallel to the basal face were found. The spatial arrangement of these layers corresponds to the symmetry of the space group $P4/nmm$. These layers alternate in the [001] direction being interleaved by single CO$_3$ layers. Both the biaxial character of the mineral and the uncertainty concerning the rotation of the CO$_3$ groups indicate a lower symmetry. The highest possible symmetry is that of *Cmma*. The structure is related to that of the type X_1 found by Sillén *et al.* for several bismuth oxyhalides and especially to that of bismutite.

To be published in *Czech. J. Phys.*

3·20. The 'Edge Effect' in crystals of gangue minerals from Derbyshire and elsewhere. By G. MUELLER, *University of Concepcion, Chile.*

It was found that certain fluorite, calcite, quartz and barite crystals from Derbyshire show remarkably well defined distribution patterns of discrete enclosures of haematite, pyrite, etc., or diffused colouration, in relation

to the edges. 'Positive edge effect' consists of concentration of the foreign matter on all or occasionally some edges or edge loci only, whereas 'negative edge effect' is the corresponding reverse structure. Preferential deposition of impurities on certain types of faces or corners has been observed also, but these structures are rare. It was found that in case of calcite and quartz sprinkled with haematite, the edge effect is most pronounced on crystals overhanging from the ceilings of vugs, and it is absent on horizontally situated ones, indicating a process of actual attraction towards the edges of the colloidal Fe_2O_3 particles from the solution which in turn becomes obliterated through gravitationally settled substance. The structures, which are relatively common in Derbyshire gangues, have been found to be extremely rare and ill-developed in minerals from other localities. It is believed by the author that the well known cross of carbonaceous inclusions in certain andalustes, which was investigated from Chilean specimens, is also a positive edge effect, and not the result of subsequent filling in of a sceletal crystal with less pure matter, as explained previously.

It is suggested that the structures are produced through charges developing on the growing edges, which repel or attract equally or oppositely charged colloidal particles, respectively. In order that the low intensity electrostatic charges should sufficiently accumulate, the screening effect of carbonaceous emulsions collecting on the surface of the crystals is necessary, and in this connection it is significant to note, that the veins of Derbyshire are exceptionally rich in bitumens, further that the cross appears in andalusites only within rather pronouncedly carbonaceous schists.

3·21. Interrelations between coloration, absorption spectra and radioactivities of fluorites from diverse localities. By G. MUELLER, W. RECKE & R. VERA-MEGE, University of Concepcion, Chile.

A total of 60 fluorite specimens originating from all the major localities of the globe were determined for U-equivalent of radioactivity up to ± 1 p.p.m. accuracies, through β and γ counts. It has been found that the radioactivity increases from $1-3$ p.p.m. U-equivalent for colourless, finely ground powders to around 100 p.p.m. with the darkening of the blue-purple coloration. The curves constructed between radioactivity and certain characteristic wavelength of the absorption spectra clearly indicate the quantitative or quasiquantitative nature of this relation.

The coloration is explained through gradual accumulation of Ca-colloids, through development of lattice imperfections, within the CaF_2 lattice as a result of bombardment by radioactive projectiles, and for this reason, as anticipated, very dark fluorites also contain detectable free F_2. The steel blue coloration provoked through X-rays or intensive radioactive radiation is less stable than the natural one. This fact can be explained through the cumulative effect throughout a geological time-scale, of low intensity irradiation during which relatively larger sized colloidal particles of Ca can condense here and there, due to chance co-incidences. This applies particularly to purple coloration, which is the most termostable, and presumably represents maximum grain size. The close succession of sharply defined purple, blue and colorless zones in certain crystals seems to indicate

coloration due to α-activity, further that only some types of fluorites with presumed imperfections in the lattice are adapted to accomodate the larger sized calcium colloids, which constitute stable coloration. It seems from microscopic and chemical studies of coloured haloes surrounding bitumen inclusions, that in certain specimens at least, the U and minor Th is carried into the lattice through finely divided carbonaceous substances, of aromatic, that is 'uranophyl' chemical constitution, but that the latter are not the primary causes of the coloration.

3·22. The crystal structure of eosphorite. By A. W. HANSON, Division of Pure Physics, National Research Council, Ottawa, Canada.

The crystal structure of eosphorite,

$$AlPO_4 . (Mn,Fe)(OH)_2 . H_2O ,$$
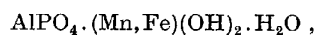
is described with reference to the pseudo-orthorhombic space group Bbam with $a = 10.52$, $b = 13.60$, $c = 6.97$ Å, $Z = 8$. The structure was determined by inspection of some Patterson sections, and refined with the aid of three-dimensional differential syntheses. In the structure described there are two parallel sets of infinite chains, one composed of $(Mn,Fe)O_4(OH)_2$ octahedra sharing opposite O–O edges, and the other of $AlO_2(OH)_2(H_2O)_2$ octahedra sharing opposite H_2O corners. These chains alternate, sharing OH corners to form a set of parallel sheets held together by phosphorus ions in tetrahedral coordination of oxygen ions.

A complete account is in Acta Cryst. (1960). **13**, 384.

§ 4. Metals and alloys

4·1. Considerations regarding Vegard's law. By F. M. D'HEURLE, A. S. NOWICK & D. P. SERAPHIM, IBM Research Center, Yorktown Heights, New York, U.S.A.

The lattice spacing of solid solutions can be expressed as a statistical average of bond lengths, d_{AA}, d_{AB}, and d_{BB}, characteristic of AA, AB and BB bonds, respectively. Changes of lattice spacings with composition depend upon the relative values of the bond lengths and the variation of the lengths with composition.

For a limited range of composition, as in terminal solid solutions, it can be assumed that the three bond lengths are independent of composition. Under this assumption the deviation from Vegard's law is expressed as

$$2[d_{AB} - (d_{AA} + d_{BB})]/d_{AA} .$$

The three characteristic bond lengths can be calculated from the experimentally determined dependence of the lattice parameter on composition. The values of d_{BB} obtained in this way for A-rich solid solutions are compared with the equivalent values obtained from the lattice of pure B.

In addition, the magnitude of the Zener anelastic effect in solid solutions, which is due to the reorientation of solute-atom pairs, is shown to depend on the deviation from Vegard's law as defined above. Experimental data presently available confirm this prediction.

To be submitted to Acta Metallurg.

4·2. The lattice spacings of close-packed hexagonal intermediate phases based on noble metals. By T. B. MASSALSKI & H. W. KING, Mellon Institute, Pittsburgh 13, Pennsylvania, U.S.A.

Withdrawn.

4·3. Closest packing of spheres with a subsidiary condition in alloys. By K. SCHUBERT, Max Planck Institut für Metallforschung, Stuttgart, Deutschland.

It is well known that in alloys between transition metals at an average number of 4 to 6 outer electrons per atom the cubic body centered structure ($A2$) is observed (K. Schubert, Z. Naturforschung (1956), 11a, 999). Another structure found in transition metal alloys is the sigma phase structure of βU; it has been pointed out (D. S. Bloom & N. J. Grant, Trans. AIME (1953), 197, 88) that phases with this structure are found with an outer electron concentration of 6·7. The structure first found with 'βW' or $W_3O(A15)$ which is similar to that of βU has till now found only with 75 at.% of a transition metal having itself a modification if cubic body centered structure. A further statistical evaluation of structural knowledge shows (K. Schubert, Z. Naturforschung (1956), 11a, 999) that at higher and at lower electron concentrations hexagonal or cubic close packed structures are found. By this fact the question arises whether the structures of W, 'βW', βU can be considered as packings which are closest with a subsidiary condition. If one prescribes the atomic distances in one crystal plane it may be that the following layers are congruent and the problem of the density of the structure is solved by a one-dimensional movement of the following layers. The $A2$ structure (cell edges a_1, a_2, a_3) is of such a kind: if one prescribes the atomic distances in the $a_1 \times a_2$ plane in the manner of this structure the following planes are congruent and give in the case of highest density the $A2$ structure. Of a similar character is the $A15$ structure. The cause of the atomic distances may be sought in a spacial correlation of the outer electrons.

4·4. Bonding in complex transition-group intermetallic compounds*. By DAVID P. SHOEMAKER & CLARA B. SHOEMAKER, Department of Chemistry, Massachusetts Institute of Technology, Cambridge, Massachusetts, U.S.A.

Several related complex intermetallic compounds of transition-group elements have been examined from the point of view of interatomic distances and coordination. Within these the coordination polyhedra are restricted to four types, with coordination numbers 12, 14, 15, and 16 (J. S. Kasper, Theory of Alloy Phases, Amer. Soc. of Metals Symposium (1956), p. 264). Each of these polyhedra contains twelve 5-fold vertices; the remaining vertices are 6-fold.

For the sigma (G. Bergman & D. P. Shoemaker, Acta Cryst. (1954), 7, 438), P, (D. P. Shoemaker, C. B. Shoemaker & F. C. Wilson, Acta Cryst. (1957), 10, 1), and R phases (Y. Komura, W. G. Sly & D. P. Shoemaker, Acta Cryst. (1960), 13, in press), a quantitative treatment of interatomic distances has been carried out. For each of these, when a 5-fold radius and a 6-fold radius is assigned to each polyhedron on the basis of least-squares, the radius sums agree remarkably well with the actual distances, the mean deviations for the respective phases being 0·039, 0·036, and 0·057 Å. This we take to imply that the effective local field symmetry at each atom is very nearly that of the idealized polyhedron. From this some inferences can be drawn regarding the nature of the bonds; for example, since p and d orbital degeneracy is not removed in a field of icosahedral symmetry, no directed (spd) bonds should be formed by the atoms with coordination 12. It is attractive to assume, but by no means established, that in these atoms the d shell principally concerned is filled, by electron transfer if necessary, and that the 6-fold bonds are more or less localized and with considerable d character.

To further substantiate present indications of site occupancies in ternary P and R phases, procedures have been developed for supplementing X-ray ordering parameters with neutron powder data, even in cases with incomplete resolution. The calculations have been programmed for the IBM 704 computer.

Full-length account to be submitted to Acta Metallurg.

4·5. The atomic arrangement of some iron-poor aluminium silicon phases. By PER SPIEGELBERG, Metallografiska Institutet, Stockholm Ö, Sweden.

A description is given of the atomic arrangement of some iron-poor aluminium silicon phases, that have been studied by direct methods.

Due to the similarity of the atomic scattering factor for aluminium and silicon, a hypothesis concerning the bonds and the distribution of the valence electrons had to be used for an interpretation of the complete structure. A hypothesis, that seems to fit well with X-ray results, also seems to indicate an explanation of the apparent valence-electron absorption by transition–metal atoms in aluminium-rich alloys.

To be published in Acta Cryst.

4·6. Sur la nature des liaisons dans les composés I-V. Par J. P. SUCHET, Centre National de la Recherche Scientifique, Laboratoire de Bellevue (S & O), Paris, France.

Les travaux de H. Krebs (Z. Anorg. Chem. (1955), 278, 82; Acta Cryst. (1956); 9, 95; Z. Elektrochem. (1957), 61, 925) ont montré que les forces de liaison homopolaires étaient plus répandues dans les cristaux minéraux qu'il ne l'était admis autrefois et E. Mooser & W. B. Pearson (J. Electronics (1956), 1, 629; J. Chem. Phys. (1957), 26, 893) ont avancé que c'était là une condition essentielle à l'existence d'un ensemble de propriétés liées au caractère 'semiconducteur' et présentées notamment par le germanium, l'antimoniure d'indium, etc. ...

J. P. Suchet (*J. Phys. Chem. Solids* (1959), **12**, 74) a remarqué enfin qu'une partie seulement des atomes pouvait former un réseau covalent, les autres formant un réseau ionique interstitiel, et que des translocations électroniques pouvaient intervenir entre les premiers et les seconds (réseaux compensés).

Les composés binaires unissant les éléments des colonnes I (alcalins) et V de la classification périodique présentent à cet égard un grand intérêt, le caractère semiconducteur ayant été récemment reconnu ou confirmé dans Li_3Bi, Cs_3Sb, Na_3Sb, K_3Sb et $NaSb$. Les cas de Li_3Bi (structure DO_3) et de Cs_3Sb (structure B32) ont déjà été étudiés et la considération de réseaux partiels covalents $[Li_2Bi]^-$ et $[CsSb]^{2-}$ ayant respectivement les structures C1 et B3 s'y impose. L'auteur examine ici les composés du type Na_3As (structure DO_{18}) et propose un schéma de liaisons comportant un réseau partiel hexagonal $[NaAs]$ à structure B12 et des 'molécules' interstitielles Na_2 dont la position exacte dans la maille dépend d'un paramètre u. Il aborde ensuite les composés LiAs et NaSb, dont la structure révèle l'existence d'une chaine spiralée covalente, et propose de considérer les réseaux compensés $[As]^-Li^+$ et $[Sb]^-Na^+$ où $[As]^-$ et $[Sb]^-$ auraient une structure analogue à A8.

L'existence de réseaux partiels tels que $[Li_2Bi]^-$ dans la structure C1 permet de compléter pour les alcalins les rayons tétraédriques r_{IV} calculés par Pauling. Les augmentations Δr_{IV} de ces rayons lorsqu'on passe d'un élément au suivant dans la colonne I (alcalins) et dans la colonne V de la classification sont comparés avec les augmentations correspondantes Δr_{III} déduites de l'étude des longueurs de liaison dans les réseaux partiels $[I\ V]$ de la structure DO_{18}. Une table de rayons r_{III} similaires à ceux du graphite et du bore est alors construite en supposant que $r_{III}/r_{IV} = \Delta r_{III}/\Delta r_{IV}$. Ces rayons atomiques s'accordent avec une notation covalente pure

$$Na^{2-} > Na^- > Na \quad \text{et} \quad As > As^+ > As^{2+}.$$
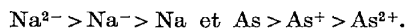
Ils interviennent en outre dans les inégalités fixant les domaines de stabilité des structures DO_3, DO_{18} et B32.

To be published in *Acta Cryst.*

4·7. Guinier–Preston zones in an aluminium–silver alloy. By E. J. FREISE, A. KELLY & R. B. NICHOLSON, *University of Cambridge, Department of Metallurgy, Cambridge, England.*

X-ray small angle scattering measurements and electron microscope transmission studies have been carried out on the same specimen of an aluminium–silver alloy quenched and aged at 125 °C. The X-ray measurements alone can yield unambiguously only such quantities as the probability of finding a silver atom at a given distance from another silver atom averaged over all silver atoms. In conjunction with electron microscope observations, however, a precise model of the microstructure of the alloy can be set up and the size, spacing and composition of the Guinier–Preston zones deduced. It is concluded from the measurements that there are 2×10^{17} clusters per c.c. with diameters varying between 20 and 60 Å. The average composition of these clusters is greater than 90 % silver. Only $\sim$ 10 % of the alloy undergoes this segregation.

To be published in *Acta Metallurg.*

4·8. X-ray small angle scattering from Guinier–Preston zones in deformed aluminium-silver single crystals. By S. SATO & A. KELLY, *Department of Metallurgy, Northwestern University, Evanston, Illinois, U.S.A.*

Aluminium–silver single crystals containing 6 at.% silver, which have been aged at room temperature, contain spherical clusters of atoms, rich in silver. After deformation of these crystals the X-ray small angle scattering is no longer spherically symmetric and measurements are reported here of the asymmetry observed after various amounts of deformation in tension. Similar experiments on polycrystals have been reported by Jan (*J. Appl. Phys.* (1955), **26**, 1291) but the use of single crystals in the present work permits a much more detailed analysis of the results. The asymmetry can be interpreted in terms of the average plastic shear which the clusters have undergone and values of this quantity can be found from the measurements. The average plastic shear of the clusters is shown to be the same as that to which the crystals as a whole has been subjected. Hence large numbers of dislocations pass through the clusters.

Evidence has also been found of a change in the average cluster size after deformation which is attributed to accelerated ageing due to deformation.

To be published in *Acta Metallurg.*

4·9. On the formation of G-P zones in some aluminum alloys. By A. LUTTS & H. LAMBOT, *Centre National de Recherches Metallurgiques, Abbaye du Val Benoit, Liege, Belgium.*

Single crystals of high-purity aluminum-base alloys (Al–0·7% Mg_2Si, Al–1·0%, Mg_2Ge and Al–1·4% Mg_2Ge) have been studied by a crystal monochromated X-ray technique. The pre-precipitation stage of these alloys has been investigated in detail during isothermal ageing at 135, 150 and 200 °C.

Diffuse X-ray scattering observed during the early ageing period shows that the needle-shaped G.-P. zones are probably formed in at least two steps. When first detected these segregates do not seem to possess any internal periodicity whatever. X-ray scattering effects are also observed which seem to indicate that these primitive zones possess a high vacancy concentration.

The second part of the process is associated with the establishment of a linear periodicity along the segregate axis which lies parallel to one of the matrix cube directions. The periodicity is identical to that of the matrix —9·04 Å—along these directions. During this stage, the vacancy concentration of the primitive zones seems to abruptly decrease.

Microhardness measurements of single crystals speimens of these alloys isothermally aged at the same temperatures reveal that the G.-P. zones are only hardening agent.

Probably will be published in *Acta Metallurg.*

4·10. The primary extinction of matrix reflections of an Al-Cu solid solution. By KAREL TOMAN, *Institute of Technical Physics, Czechoslovak Academy of Sciences, Prague, Czechoslovakia.*

The influence of the formation of different decomposition products on the primary extinction of the matrix

reflection (200) is studied during the ageing of the Al–Cu (4 wt.%) solid solution. The quenched Al–Cu crystals exhibit a large primary extinction, which is not substantially lowered by the formation of Guinier–Preston zones. The primary extinction is, on the contrary, largely reduced by the formation of θ'' precipitate and to even a greater extent by the θ' precipitate. The reduction of the primary extinction does not depend in this case on the volume of the precipitate only, but also on its thickness and size. The discussion of this effects based on the model of the mosaic blocks with partly coherent precipitate is attempted.

It seems, that the formation of new atomic sites and of incoherent boundaries which accompanies the precipitation, influences much more the primary extinction than a great change in the distribution of copper atoms among the sites of the solid solution. This occurs in the G.-P. zones' formation.

The integrated intensity (200) of the matrix and the intensity of diffraction effects on the decomposition products has been measured with the double crystal spectrometer adapted for work at elevated temperatures.

To be published in *Czechosl. Journ. Phys.*

4·11. Precipitation in Al–4% Cu alloy. By G. Thomas, *Metallurgy Department, University of Cambridge and the Department of Mineral Technology, University of California, U.S.A.* & M. J. Whelan, *Cavendish Laboratory, Cambridge, England.*

A high temperature stage fitted to the Siemens Elmiskop 1 electron microscope has been used to study directly the formation of precipitates in thin foils prepared from quenched and aged bulk specimens of Al–4% Cu alloy. Angular precipitates about 500 Å in diameter were observed to form in a few sec. at 250 to 300 °C. Much of the initial precipitation is probably a surface effect. On raising the temperature the precipitates coarsened and eventually went into solution at about 500 °C. The effects observed have been recorded on 16 mm. ciné film. The measured rates enable an estimate of the diffusion coefficient of Cu in Al to be made.

To be published in *Phil. Mag.*

4·12. Crystallography of alloy steels. By H. Hughes & K. W. Andrews, *The United Steel Companies Limited, Research & Development Department, Swinden Laboratories, Moorgate, Rotherham, Yorkshire, England.*

The crystallographic interest provided by alloy steels derives, not from the matrix which has either a body-centred cubic or a face-centred cubic lattice, but chiefly from the numerous other constituents which occur in the form of small particles often leading to greatly improved strength and sometimes embrittlement. These particles are studied by X-ray diffraction after separation by electrolytic or other means, or by electron microscopy and diffraction. These constituents include carbides, nitrides, borides, silicides, sigma, chi and several other intermetallic phases. The authors have recently shown the importance of interstitial carbides and nitrides having a close-packed hexagonal arrangement of metal and reported crystallographic data (*J. Iron and Steel Inst.*, November 1959). This work has enabled the interpreta-

tion of hardening or delayed softening in new materials as a result of coherency between the two lattices. Solid solution phases in this series are frequently found and are analogous to the interstitial cubic phases.

Certain steels with the face-centred lattice can harden by the formation of a coherent precipitate of the ordered face-centred lattice based on the formula Ni_3Al. Analogously, hardening of the body-centred lattice by the ordered body-centred phase based on NiAl has also been established. Precipitation of NiAl in the face-centred lattice is also possible. Restricted solid solutions between Ni_3Al (cubic), Ni_3Ti (hexagonal) and Ni_3Fe (cubic), with their respective crystal lattices may form in face-centred iron-base alloys in the same manner as they precipitate in nickel-base alloys.

Other constituents include silicides which appear to be analogous to carbides such as $M_{23}C_6$ and M_6C, and boride solid solution phases based on the borides Fe_2B (orthorhombic) and M_3B_2 (tetragonal).

To be submitted to *J. Iron & Steel Institute.*

4·13. Structural features of new phases with the cementite and related structures. By Bertil Aronsson, Stig Rundqvist & Erik Stenberg, *Institute of Chemistry, University of Uppsala, Uppsala, Sweden.*

In addition to the earlier reported phases with the cementite structure, Mn_3C, Fe_3C, Co_3C and $NiAl_3$, recent investigations at this Institute have shown that Co_3B, Ni_3B, Pd_3B and Pd_3Si also possess the cementite structure.

The atomic positions in Ni_3B, Pd_3B and Pd_3Si have been determined from single crystal data. The environment of the non-metal in these phases and in Fe_3C is described and discussed. We have also studied the conditions for isomorphous substitution of the non-metals in some cementite phases.

The structures of Re_3B, Ru_7B_3(Th_7Fe_3-type) and Pd_5B_2 have also been investigated and their similarities to the cementite structure are pointed out.

Is likely to be published in *Acta Metallurg.*

4·14. Etude des carbures du type $M_{23}C_6$ dans divers aciers et alliages austénitiques. Par J. Philibert, G. Henry & J. Plateau, *IRSID, Saint Germain en Laye (S. et O.), France.*

On a examiné par microscopie et diffraction électroniques des carbures précipitant dans divers aciers et alliages austénitiques contenant du nickel et du chrome.

Les carbures précipités dans une lame métallique mince ont été extraits par dissolution dans le brome et recueillis sur un film de carbone préalablement déposé à la surface de la lame. De telles préparations permettent d'effectuer des diagrammes Debye–Scherrer et des analyses à la microsonde de Castaing.

On a étudié l'évolution de la composition chimique des carbures en fonction de la durée et de la température de précipitation et en fonction de la composition des alliages. La teneur en nickel du carbure varie peu avec la teneur en nickel de l'alliage. Par contre, le rapport [Cr]/[Fe] dans le carbure croit avec la valeur de ce même rapport dans l'alliage.

4·15. Röntgenographischer Nachweis einer Über-struktur in Neusilber-Legierungen. Von D. Bia-las, R. Hosemann, A. Kussmann, F. Motzkus & H. Wollenberger, *Fritz-Haber-Institut der Max-Planck-Gesellschaft, Berlin–Dahlem und Physikalisch Technische Bundesanstalt, Berlin – Charlottenburg, Deutschland.*

In einer kalorimetrischen Untersuchung der Ordnungs-vorgänge im α-Mischkristallgebiet des Systems Cu–Ni–Zn konnten A. Kussmann und H. Wollenberger zeigen, dass die im Temperaturverlauf der wahren spezifischen Wärme getemperter Legierungen zwischen 200 und 500 °C. auftretende endotherme Wärmetönung ihrem Betrage nach von den Randgebieten des Systems zur Mitte hin zunimmt und in der Nähe der Zusammensetzung Cu_2NiZn ein Maximum hat. Diese Tatsache sowie die inzwischen ermittelte Abhängigkeit der wahren spezifischen Wärme von Anlassbehandlungen liessen vermuten, dass hier eine atomare Fernordnung vorliegt. Mit Hilfe einer hoch-auflösenden Streukammer nach Guinier–Jagodzinski mit einem Johansson-Kristall, E. G. Hofmann und H. Jagod-zinski, *Z. Metalk.* 9, 601 (1955), wurde neben den Reflexen des flächenzentrierten Gitters bei Proben, die innerhalb 500 Std. von 400 auf 200 °C. abgekühlt wurden, sämtliche Reflexe eines einfach primitiven Gitters nachgewiesen. D. Bialas, R. Hosemann, A. Kussmann, F. Motzkus u. H. Wollenberger, *Naturwiss.* 4, 81 (1960). Ihre Intensität beträgt bei Benutzung von Cu $K\alpha_1$-Strahlung, also unter Ausnutzung der anomalen Dispersion etwa 0,1% der Hauptlinien. Bei einer Anlasstemperatur von nur 180 °C. konnten nur noch einige der Überstrukturlinien, allerdings weit schwächer, nachgewiesen werden. Sie waren gegenüber dem erstgenannten Fall nachweisbar verbreitert und beweisen damit, dass die Fernordnung gestörter war. Aus ihrer Linienbreite wurde ein Durch-messer der Fernordnungsbereiche von etwa 100 Å er-rechnet. Die Struktur der Gitterzelle und die Änderung der Gitterkonstanten in Abhängigkeit vom Ordnungs-zustand werden diskutiert.

Ausführliche Veröffentlichung ist vorgesehen in *Acta Metallurg.*

4·16. X-ray investigations of the dissolution of oxy-gen in cold rolled niobium sheets and the forma-tion of ordered solid solutions. By N. Norman, *Central Institute for Industrial Research, Blindern, Oslo, Norway.*

As part of a research programme on the high tempera-ture behaviour of niobium extensive X-ray diffraction measurements have been carried out on cold rolled niobium sheets oxidized at temperatures from 150 to 1000 °C. and at pressures ranging from 760 to 10^{-2} torr. Depending on the pressure oxides, mainly pentoxide, were formed at temperatures above about 400 °C. whereas no oxide could be detected on sheets oxidized below this temperature even after 6 days. Measurements on sheets kept at 300–450 °C. showed a rapid decrease and a broadening of the niobium lines during the first minutes of oxidation, followed by a shift in the position of the lines towards lower angles and a gradual decrease in line width, the integrated intensity of a peak remaining constant as long as no oxide was formed on the surface of the metal. Such line broadenings and peak shifts due

to the dissolution of oxygen in the body centered cubic niobium lattice were registered even at 200 °C. The amount of dissolved oxygen determined from gravimetric measurements and the maximum increase in the cubic parameter were considerably larger than previously re-ported. At temperatures below 400 °C., irrespective of the oxygen pressure, peaks adjacent to and at the low angle side of the main niobium peaks could frequently be detected. Within experimental errors, the position of these lines was constant indicating the existence of a definite Nb–O phase. Sheets oxidized at 400–500 °C. in oxygen of pressures from 100 torr. and downwards also gave extra lines. In this case the lines could be indexed on the basis of a superlattice with at least two of the axes twice or six times the cubic axis of niobium, showing the presence of another ordered Nb–O phase.

Likely to be published in *J. Inst. Met.*

4·17. Studies of the structural properties of Au–Mn alloys. By S. G. Humble, *Physics Department, The Royal Institute of Technology, Stockholm, Sweden.*

Alloys in the composition range 0–75 at.% Mn have been investigated in different states of order. The X-ray equipment used consisted of powder cameras of conven-tional type, an X-ray monochromatic camera and a Weissenberg goniometer camera (for the study of the complicated structure of Au_3Mn).

The results to be reported concern primarily the atomic arrangements and lattice dimensions of the disordered and ordered structures of the system, and secondly the existence conditions for phases of the compositions Au_3Mn, Au_2Mn, AuMn and $AuMn_3$ occurring in that system.

The paper will appear in *Arkiv för Fysik.*

4·18. The structure of the sigma-phase Nb_2Al. By P. J. Brown & J. B. Forsyth, *Cavendish Laboratory, Cambridge, England.*

The sigma-phase structure reported by C.R.McKinsey & G. M. Faulring (*Acta Cryst.* (1959), **12**, 701) for the intermetallic phase Nb_2Al, has been confirmed by making single crystal measurements. Weissenberg data have been collected for two projections and the structural para-meters have been refined. There is evidence for virtually complete ordering of the aluminium atoms on the twelve-coordinated sites of the sigma-phase structure; the niobium atoms have been shown to occupy the more highly coordinated positions.

The occurrence of a sigma-phase between niobium and aluminium is unexpected, and the relationship of this structure to other sigma-phases will be discussed.

4·19. X-ray and metallographic studies of refractory alloy systems.* By A. Taylor (*Westinghouse Electric Corp.*), N. J. Grant (*M.I.T.*), J. Wulff (*M.I.T.*) & A. & R. Kaufmann & E. J. Rapperport (*Nuclear Metals Inc.*), *U.S.A.*

Thermal equilibrium diagrams and X-ray data are presented for the refractory alloy systems Mo–Hf, Re–Hf,

W–Os, Ta–Ru, Ta–Os, W–Ru, Ta–Re, Nb–Re and Mo–Hf–Re, the data having been obtained using materials of the highest available purity. Among the wide variety of structural types found among the intermediate phases in these systems are cubic and hexagonal structures of the Laves type, and sigma-phase structures. Martensitic transformations from the high temperature body-centered cubic structure to the low temperature hexagonal close-packed modification have been found to occur in certain Hf-rich primary solid solutions. The difficulties encountered in the preparation, melting point determination and heat treatment of such easily oxidizable high-melting point alloys will be discussed, along with the problems associated with producing satisfactory samples for X-ray examination.

4·20. Crystallographic data on the Ag–Sr system.
By L. D. CALVERT & CYNTHIA KNIGHT, *Division of Applied Chemistry, National Research Council, Ottawa, Ontario, Canada.*

The intermetallic compounds in the Ag–Sr system are being investigated to explore the similarities between the Ag–Ca and Ag–Sr systems. The first phase isolated appears to be orthorhombic with

$$a = 9\cdot7, \quad b = 16\cdot6, \quad c = 7\cdot7 \text{ Å}$$

and is very similar to the phase Ag_2Ca. The other phases in the system will be investigated by single crystal methods and also by powder photographs.

Likely to be published in *Canad. J. Chem.*

4·21. MX_2 compounds of thorium and the polymorphism of thorium disilicide. By ALLAN BROWN, *Crystal Analysis Group, Research Laboratories, The General Electric Co. Ltd., Wembley, Middx., England.*

An investigation has been made of compounds of thorium with the following elements; copper, silver, gold, nickel, zinc, cadmium, mercury, aluminium, gallium, indium, silicon, germanium, tin and lead. The crystal structures of these compounds have been examined by X-ray diffraction techniques and most phases with the composition MX_2 have been found to have one of two related structures. These are the C32 (AlB_2)-type and the $C_c(\alpha\text{-ThSi}_2)$-type.

Consideration of these phases has suggested that the formation of ThX_2 compounds with these two structures is influenced by the atomic radius r and the valency e of the X atom. When the product r^3e^2 is below 19·7 compounds with the C32 structure are obtained. $ThGa_2$ and $ThGe_2$ have the C_c structure and their values of r^3e^2 lie between 19·7 and 32·2. The value of this product for $ThSi_2$ is 19·7 and this compound crystallizes in two polymorphic forms with the above structures. A mechanism has been suggested to explain the observed polymorphic transformation.

Further investigation has shown that where r^3e^2 is greater than or equal to 19·7 defect C32-type structures can exist with the approximate composition Th_3X_5. In each of these defect compounds, the axial ratio c/a for the hexagonal structure cell is greater than unity. In the stoichiometric C32 compounds the value for c/a is less than unity.

It is hoped to extend this investigation to include the known MX_2 compounds of uranium, plutonium, cerium and related actinide and lanthanide elements and hence to formulate a more general rule for the occurrence of these compounds.

It is intended to submit this paper for publication in *The Journal of Nuclear Materials.*

4·22. Atomic structure of some compounds of bismuth and antimony. By N. N. ZHURAVLEV, G. S. ZHDANOV & R. N. KUZMIN, *Physical Faculty, Moscow State University, Moscow B-234 USSR.*

No abstract provided.

4·23. The pre-precipitation state in aluminium-zinc alloys. By VOLKMAR GEROLD, *Max-Planck-Institut für Metallforschung, Stuttgart N, Deutschland.*

Withdrawn.

§ 5. Inorganic structures

5·1. Compounds containing chromium in different valency states a perovskite $Ca_4(Fe,Cr)_4O_{11}$ and an apatite $Ca_5(CrO_4)_3OH$. By W. JOHNSON, *X-ray-Department, the United Steel Companies Limited, Research & Development Department, Swinden Laboratories, Moorgate, Rotherham, England.*

The substitution of Cr^{3+} for Fe^{3+} in dicalcium ferrite $Ca_2Fe_2O_5$ is possible up to about 10%, beyond which point oxidation begins to occur in air and the ferrite transforms to a perovskite structure. The perovskite is orthorhombic and isomorphous with $GdFeO_3$ with

$$a = 5\cdot42, \quad b = 5\cdot49, \quad c = 7\cdot48 \text{ Å} .$$

From powder patterns the transformation appears to take place by the alteration of the space group of dicalcium ferrite from *Pcmn* to *Icma* by small atomic movements and the subsequent inclusion of oxygen atoms in the hole left in the structure to give a non-stoichiometric perovskite structure again belonging to the *Pbnm* space group.

With the above axes the following relations hold:

perovskite $a \equiv$ dicalcium ferrite c,
perovskite $b \equiv$ dicalcium ferrite a,
perovskite $c \equiv \frac{1}{2}$ dicalcium ferrite b.

The equivalence of mixtures of tri- and hexavalent chromium (and trivalent iron) to an intermediate valency of four gives the analogy with the perovskite $CaTiO_3$. This is further exemplified in a chromium containing apatite $Ca_5(CrO_4)_3OH$ which contains Cr^{3+} and Cr^{6+} in the ratio of 1:2 and hence equivalent to pentavalent phosphorus in the isomorphous hydroxyapatite $Ca_5(PO_4)_3OH$. The chromium apatite has $a = 9\cdot67, c = 7\cdot01$ Å.

A note will appear shortly in the *Mineralogical Magazine* and it is hoped to submit further information to *Acta Cryst.*

5·2. Die Kristallstruktur des Strontiumgermanats $Sr_3Ge_3O_9$. Von WALTRAUD HILMER, *Institut für Anorganische Chemie, Deutsche Akademie der Wissenschaften, Berlin-Adlershof, Deutschland.*

Withdrawn.

5·3. The crystal structure of Ba_2TiO_4.* By J. A. BLAND, I.C.I. Ltd., Akers Research Laboratories, The Frythe, Welwyn, Herts, England.

The crystal structure of Ba_2TiO_4 has been determined with moderate accuracy. The space group is $P2_1/n$ and the cell dimensions are:

$$a_0 = 6·12 \pm 0·03, \quad b_0 = 7·70 \pm 0·03, \quad c_0 = 10·50 \pm 0·03 \text{ Å},$$
$$\beta = 93° 8' \pm 10'.$$

There are four molecules per unit cell. The atomic coordinates were found by means of two-dimensional F_o and $F_o - F_c$ syntheses. The structure is of the β-K_2SO_4 type and is closely related to β-Ca_2SiO_4. The environment of the titanium atom is unusual; it is approximately tetrahedral and the structure is considered as an arrangement of discrete TiO_4 groups and barium atoms. The relationship between Ba_2TiO_4 and ferroelectric $BaTiO_3$ is discussed.

To be published in Acta Cryst.

5·4. Structure et propriétés magnétiques des ortho-vanadates $V_2O_5,3MO$ (M=Mg, Co, Ni). Par E. F. BERTAUT, A. DURIF & R. PAUTHENET, Laboratoire d'Electrostatique et de Physique du Métal, Institut Fourier, Grenoble, France.

La structure a été déduite par la méthode statistique. On montre, contrairement à une opinion répandue, que les triples produits ont des poids différents dépendant de la symétrie du groupe.

Les orthovanadates cristallisent dans le groupe d'espace orthorhombique $Abam$-(D_{2h}^{18}). La structure peut être décrite par un enchaînement de tétraèdres VO_4 isolés et d'octaèdres MO_6. Malgré la présence de 2 sous-réseaux différemment occupés ($4M$ en $4a$; $8M$ en $8c$) les orthovanadates de Co et de Ni ne sont pas ferrimagnétiques comme le sont les ferrites spinelles. On montre que la raison réside dans la structure.

To be published in Acta Cryst.

5·5. Pyrochlores de terres rares. Par E. F. BERTAUT & M. C. MONTMORY, Laboratoire d'Electrostatique et de Physique du Métal, Institut Fourier, Grenoble, France.

Nous avons réalisé la synthèse de pyrochlores de formule $A_2B_2O_7$ où A est un ion trivalent de terre rare Pr, Nd, Sm, Eu; Gd, Tb, Dy, Ho, Er, Tm, Yb, Lu et B un ion tétravalent ou tétravalent en moyenne et dont l'oxyde BO_2 cristallise dans le type rutile ou dans un type apparenté.

Des séries isomorphes ont été préparées avec B = Ti, Hf, Rn et Ir, mais aussi avec B = $Sb_{0,5}Fe_{0,5}$, $Sb_{0,5}Cr_{0,5}$; $Sb_{0,5}Rh_{0,5}$ et $Sb_{0,5}Al_{0,5}$, $Sb^{5+}Fe^{3+}O_4$ cristallisant dans une structure du type rutile.

Les mesures des paramètres illustrent bien la contraction des lanthanides. Les propriétés magnétiques des composés sont discutées.

Publication planned in Bull. Soc. Franç. Minér.

5·6. Composés rhomboédriques $MLiO_2$ (M=métal de transition). Par E. F. BERTAUT & J. DULAC, Laboratoire d'Electrostatique et de Physique du Métal, Institut Fourier, Grenoble, France.

On sait que $LiNiO_2$ (W. D. Johnston, R. R. Heikes & D. Sestrich, Phys. Chem. Sol. (1959), 7, 1) et $LiCoO_2$ sont isomorphes et appartiennent au groupe $R\bar{3}m(D_{3d}^5)$. Ces structures dérivent de la structure de NaCl par un ordre des cations $ABAB\ldots$ et une déformation selon la diagonale du cube.

Nous avons préparé $LiCrO_2$ et $LiRhO_2$ par réaction directe du carbonate de lithium sur l'oxyde de métal de transition. Ces composés rhomboédriques, isomorphes de $LiNiO_2$ et $LiCoO_2$, ne constituent qu'un cas particulier d'un isomorphisme plus général. En effet, la substitution $Rh^{3+} \rightleftarrows Cr^{3+}$ conserve généralement la structure. On en donne quelques exemples.

Publication planned in Bull. Soc. Franç. Minér.

5·7. Déformations dans les pérovskites contenant des terres rares. Par E. F. BERTAUT & F. FORRAT, Centre d'Etudes Nucléaires, Chemin des Marturs, Grenoble, France.

Les paramètres a, b, c des pérovskites contenant des terres rares sont représentées en fonction des distances métal–oxygène moyennes relatives aux ions 'terre rare'. L'allure des courbes montre:

que la déformation est directionnelle,
que l'évolution de la déformation en fonction de la contraction des lanthanides n'est pas linéaire.

Le premier fait est attribué à la polarisation de l'ion terre rare, le second à un effet géométrique.

Publication prévue dans le Bull. Soc. Franç. Minér.

5·8. Erbium manganite—a new ABO_3 structure. By H. L. YAKEL, Metallurgy Division, W. C. KOEHLER, Physics Division, Oak Ridge National Laboratory,* Oak Ridge, Tennessee, U.S.A. and E. F. BERTAUT & E. F. FORRAT, Institut Fourier, Universite de Grenoble, Grenoble, France.

Sesquioxides of erbium, lutecium, and yttrium combine with Mn_2O_3 to form mixed oxide compounds with ABO_3 stoichiometry. These compounds crystallize in a novel structural arrangement which is not simply related to known ABO_3 structure types. The unit of structure is hexagonal, space group $P6_3cm$. Lattice parameters for $ErMnO_3$ and $LuMnO_3$ are

$$a_0 = 6·1150, c_0 = 11·411 \text{ Å, and } a_0 = 6·0428, c_0 = 11·369 \text{ Å},$$

respectively.

The structure of these compounds was determined by an analysis of X-ray diffraction data obtained from a single crystal of $LuMnO_3$. A unique feature of this structure is a five-fold coordination of oxygen atoms about each manganese atom.

It was observed that, depending on conditions of formation, yttrium manganite could crystallize either in the

---

* Carried out at Department of Mines and Technical Surveys, Ottawa, Canada.

67*

* Operated for the U.S. Atomic Energy Commission by the Union Carbide Corporation.

form reported here or in a perovskite structure. On the other hand, high-temperature X-ray diffraction experiments indicated that the hexagonal structure of $ErMnO_3$ was stable at least up to 1000 °C.

The paper will probably be submitted to *Acta Cryst.*

5·9. Sur quelques antimoniates spinelles. Par J. Du-LAC & A. DURIF-VARAMBON, *Laboratoire d'Electrostatique et de Physique du Métal, Institut Fourier, Grenoble, France.*

Synthèse et étude cristallographique de quelques antimoniates isotypes des spinelles.

La formule générale de ces composés $Sb^V Fe^{III} M_4^{II} O_8$ avec $M = Co$, Ni... dérive des titanates spinelles par le schéma de substitution:

$$2\,Ti \rightleftarrows Sb^V + Fe^{III}.$$
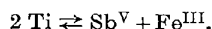
5·10. Sur deux nouveaux composés du type grenat. Par A. DURIF-VARAMBON & G. MAUPIN, *Laboratoire d'Electrostatique et de Physique du Métal, Institut Fourier, Grenoble, France.*

Synthèse et étude cristallographique de deux nouveaux germanates isotypes des grenats:

$$Ge_3 M_2 Ca Na_2 O_{12} \text{ avec } M = Ti \text{ ou } Sn.$$
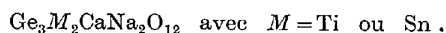
Le schéma de substitution utilisé montre que la totalité des sites octoédriques peut être occupée par du Titane ou de l'Etain.

5·11. Surstructure antimoine-fer dans un composé du type perowskite. Par A. DURIF, *Laboratoire d'Electrostatique et de Physique du Métal, Institut Fourier, Grenoble, France.*

Etude cristallographique d'un composé du type $A^V B^{III} Sb_2 O_6$ mise en évidence d'un ordre des ions A et B sur les sites octaédriques. — La maille élémentaire de perowskite doit être doublée.

5·12. Über Kristallstruktur und Kristallchemie des $Ag_2Si_2O_5$. Von F. LIEBAU, F. WODTCKE & H. BUNGE, *Institut für Anorganische Chemie der DAdW, Berlin-Adlershof, Deutschland.*

Silberphyllosilikat $Ag_2Si_2O_5$ entsteht durch Behandlung von α-$Na_2Si_2O_5$ mit geschmolzenem $AgNO_3$ bei 280 °C. durch Austausch der Na^+- gegen Ag^+-Ionen. Dabei erfolgt die Wanderung der Kationen durch kanalförmige Hohlräume, welche die Struktur des α-$Na_2Si_2O_5$ parallel [001] durchziehen, so dass sich Einkristalle des Natrium-silikats in $Ag_2Si_2O_5$-Einkristalle umwandeln. Beide Silikate erweisen sich auf Grund der Lage und Intensitäten von Einkristallreflexen als isotyp:

α-$Na_2Si_2O_5$:

$a = 6·43$, $b = 15·46$, $c = 4·91$ Å, $Z = 4$;
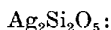
$Ag_2Si_2O_5$:

$a = 6·55$, $b = 15·66$, $c = 4·91$ Å, $Z = 4$.

Sie enthalten stark gefaltete [Si_2O_5]-Zweierschichten parallel (010). $Ag_2Si_2O_5$ lässt sich schon bei Zimmertempera-

tur mit Wasserstoffgas, innerhalb 5 Tagen, praktisch vollständig unter Bildung von metallischem Silber reduzieren. Der Mechanismus dieser Reduktion lässt sich ohne Schwierigkeiten aus der Struktur des Silbersilikats verstehen.

Das metallische Silber scheidet sich gut orientiert in Bezug auf die kristallographischen Achsen des ursprünglichen $Ag_2Si_2O_5$-Kristalls aus. Röntgenographisch waren zwei verschiedene Orientierungen feststellbar, die aus der Tabelle zu ersehen sind.

$Ag_2Si_2O_5$	Ag	Differenz in % bezogen auf $Ag_2Si_2O_5$
1. Orientierung		
[001] = 4,91 Å	[211[= 2 × 5,003 Å	+ 1,8
[100] = 6,55	[110] = 5,778	− 11,8
$F = 32,2$ Å^2	$F = 28,9$ Å^2	− 10,2
2. Orientierung		
[001] = 4,91 Å	[110] = 5,778 Å	+ 17,7
[100] = 6,55	[211] = 2 × 5,003	− 23,7
$F = 32,2$ Å^2	$F = 28,9$ Å^2	− 10,2

Bei beiden liegen die (111)-Flächen der Silberkristallite parallel zu den [Si_2O_5]-Schichten des ursprünglichen Silbersilikatkristalls. Die 1. Orientierung ist die energetisch günstigere und bei niedrigen Reduktionstemperaturen stark bevorzugt. Bei etwa 300 °C. sind beide Orientierungen ungefähr gleich häufig. Die Silberkristallite sind anscheinend dünne Plättchen nach (111). Diese bevorzugte Ausbildung der (111)-Fläche des Silbers ist wahrscheinlich der Grund für die hohe katalytische Wirksamkeit solcher Präparate, die ausgezeichnete Trägerkatalysatoren für die Dehydrierung organischer Verbindungen sind. Die bei der Reduktion gebildete $H_2Si_2O_5$ ist röntgenamorph.

Publikation ist in *Z. Elektrochem.* vorgesehen.

5·13. Zur Kristallstruktur des wasserhaltigen Bariumsilikats $BaSiO_3 \cdot 5,3\,H_2O$. Von E. HÖHNE, *Deutsche Akademie der Wissenschaften zu Berlin, Institut für Strukturforschung, Berlin-Adlershof, Deutschland.*

Für das Bariumsilikat $BaSiO_3 \cdot 5,3\,H_2O$ sind nach den beobachteten Auslöschungen nur die beiden orthorhombischen Raumgruppen $P2_1cn$ und $Pmcn$ möglich. Gitterkonstanten:

$$a = 8{,}43,\ b = 12{,}96,\ c = 15{,}01\ \text{Å},$$

8 Formeleinheiten/Elementarzelle.

Gewöhnliche und verallgemeinerte Pattersonprojektionen $P_0(u, w)$, $P_0(v, w)$, $P_1(v, w)$ und $P_2(v, w)$ ergaben eindeutig die Ba-Parameter. Die zentrosymmetrische Raumgruppe konnte ausgeschlossen werden. Allerdings liegen die 8 Ba-Atome für sich zentrosymmetrisch, und zwar beide zur asymmetrischen Einheit gehörenden Ba-Atome nahezu auf der n-Gleitspiegelebene. Dadurch tragen sie fast ausschliesslich zu den $F(hkl)$-Werten mit $h + k = 2n$ bei. Ein erster Strukturvorschlag wurde mittels einer Minimumfunktion aus einer Patterson-projektion $P_0^{h=2n+1}(v, w)$, die nur mit den Koeffizienten mit $k = 2n + 1$ berechnet wurde, erhalten.

Anhand einer Reihe von verallgemeinerten Projektionen wird der Strukturvorschlag diskutiert. Schon jetzt

kann eindeutig festgestellt werden, dass die Substanz ein Orthosilikat ist. Dabei werden die Tetraeder zum Teil von OH-Gruppen gebildet.

5·14. The crystal structure of huntite, $Mg_3Ca(CO_3)_4$.

By D. L. GRAF & W. F. BRADLEY, *Illinois State Geological Survey, Urbana, Illinois, U.S.A.*

Huntite is an ordered rhombohedral double-carbonate, based, like the simple compositions, on a deformation of the NaCl face-centered cube. Its ordering, in R32, affords a true structural unit in the shape of the familiar cleavage rhomb, with $a = 6.06$ Å and $\beta = 102°\ 55'$. With Ca at origins, 3 Mg are disposed about face centers, one CO_3 is unique at the body center, and 3 CO_3 are disposed about edge centers.

Although huntite is available only as powder (of about 1 micron particle size), and involves seven variable parameters, the precision with which pertinent bond lengths are known from the simpler carbonates permits a moderately accurate evaluation of the structure.

When atom parameters are taken as:

Ca in	(a)	0, 0, 0
Mg in	(d)	$x = 0.541$
C_I in	(b)	$\frac{1}{2}, \frac{1}{2}, \frac{1}{2}$
C_{II} in	(e)	$x = -0.039$
O_I in	(e)	$x = 0.365$
O_{II} in	(e)	$x = 0.096$

and O_{III} in (f), $x = -0.033$, $y = 0.180$, $z = 0.371$, C–O bonds are 1.28 Å; Mg are octahedrally surrounded by 6 O at 2.10 Å, each octahedron distorted by two shared edges of 2.56 Å, with 10 other edges from 2.86 to 3.30 Å; and Ca are coordinated in a trigonal prism of base edge 3.32 Å and height 2.70 Å.

Calculated F-values depart no more than 50% from those reduced from the powder diffractogram, and the average departure is under 20%.

To be submitted to *Acta Cryst.*

5·15. On the crystal structure of a basic aluminum selenate.

By GEORG JOHANSSON, *Gates and Crellin Laboratories of Chemistry, California Institute of Technology, Pasadena, California, U.S.A. and Department of Inorganic Chemistry, Royal Institute of Technology, Stockholm 70, Sweden.*

A basic aluminum selenate,

$$Na_2O . 13\ Al_2O_3 . 8\ SeO_3 . 74\ H_2O ,$$
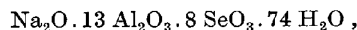
can be obtained in the form of tetrahedral crystals if sodium selenate is added to an aluminum chloride solution that has been hydrolyzed by the addition of about 2·5 equivalents of alkali. The structure was thought to be of interest since it might give some information about the polynuclear complexes that seem to exist in hydrolyzed aluminum salt solutions (C. Brosset, G. Biedermann & L. G. Sillén, *Acta Chem. Scand.* (1954), 8, 1917; H. W. Kohlschütter & P. Hantelmann, *Z. Anorg. Chem.* (1941), 248, 319). The crystals are cubic ($a_0 = 18.0$ Å), space group $T_d^2–F\overline{4}3m$, with two formula weights in the unit cell. The structure has been solved from the three-dimensional Patterson function and refined by means of three-dimensional Fourier maps. The reliability

index at the present stage of the refinement is 0·11 for the 245 reflections observed with Cu K-radiation. The structure is built up from discrete $Al_{13}O_{40}$ groups, each containing 12 AlO_6 octahedra sharing edges and with a four-coordinated aluminum atom in the center of the group. These large complexes are not directly connected but are joined by hydrogen bonds to the selenate groups. If the hydrogen atoms are located from the positions of the hydrogen bonds and from Pauling's rule for the sum of the electrostatic bond strengths, then the formula for the discrete aluminum oxygen complexes seems to be $[Al_{13}O_4(OH)_{24}(H_2O)_{12}]^{7+}$. Preliminary work on the tetragonal crystals of

$$6\ (NH_4)_2SO_4 . 11\ Al_2O_3 . 6\ SO_3 . xH_2O \quad (x = ca.\ 72)$$
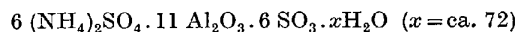
and on the monoclinic crystals of

$$13\ Al_2O_3 . 6\ SO_3 . xH_2O \quad (x = ca.\ 79) ,$$
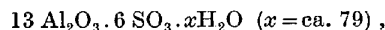
which can be obtained from the same hydrolyzed aluminum chloride solutions as the basic selenate, seems to indicate that the same kind of aluminum–oxygen complexes are present in these structures.

5·16. Die Strukturen der Kurrol'schen Salze $(AgPO_3)_x$ und $(NaPO_3)_x$.

Von K. H. JOST, *Institut f. Anorganische Chemie, Deutsche Akademie der Wissenschaften, Berlin-Adlershof, Deutschland.*

Silberpolyphosphat $(AgPO_3)_x$ mit den Gitterkonstanten

$$a = 11,85, \quad b = 6,06, \quad c = 7,31\ \text{Å}, \quad \beta = 93,5°$$

und die Form A des Kurrol'schen Natriumsalzes $(NaPO_3)_x$ mit den Gitterkonstanten

$$a = 12,12, \quad b = 6,20, \quad c = 6,99\ \text{Å}, \quad \beta = 92°$$

kristallisieren isotyp in der Raumgruppe $P2_1/n$. Sie enthalten spiralig um die 2_1-Achsen gewundene PO_4-Tetraederketten mit 4 Tetraedern pro Windung. Beide Strukturen wurden mit direkten Methoden bestimmt (Methode von Bertaut, kombiniert mit Tripelprodukten).

Die Arbeiten werden voraussichtlich in *Acta Cryst.* verföfentlicht.

5·17. The structure of ammonium bromate.*

By ANTONIO SANTORO, *Comitato Nazionale per le Ricerche Nucleari, Rome, Italy* and STANLEY SIEGEL, *Argonne National Laboratory, Lemont, Illinois, U.S.A.*

NH_4BrO_3 is rhombohedral with space group $R\overline{3}m$. The unit cell, of dimensions

$$a = 4.477 \pm 0.002\ \text{kX.} \quad \text{and} \quad \alpha = 87.61° \pm 0.07°,$$

contains one molecule with bromine and nitrogen atoms in x, x, x, and oxygen atoms in x, x, z; x, z, x; and z, x, x.

Crystals developed with a needle axis normal to $(1\overline{1}0)$ and Weissenberg data were collected about this axis. Although the crystal contains no center of symmetry, a Fourier synthesis was carried out using phases com-

---

* Based on work performed under the auspices of the U. S. Atomic Energy Commission.

puted from the bromine contribution. This is possible since the bromine atom may be chosen at the origin. The oxygen positions appeared in the projection along with a set of peaks centro-symmetrically located relative to the first. Either of these configurations may be chosen if hydrogen positions are not specified. The oxygen positions were refined by a least-squares method. Final coordinates, with N in 0, 0, 0, are: Br in $\frac{1}{2}, \frac{1}{2}, \frac{1}{2}$ and $x = 0.559$ and $z = 0.139$ for oxygen. The bond distances are: $O-O = 2.61$, $Br-O = 1.64$, $N-3O = 2.88$ and $N-6O = 3.19$ Å. The height of bromine above the oxygen plane is 0.66 Å. All errors are ± 0.02 Å.

Probably will be published in *J. Amer. Chem. Soc.*

5·18. On the linking of Archimedean square anti-prisms in basic salts of tetravalent metal ions.
By BENGT AURIVILLIUS & GEORG LUNDGREN, *Institute of Inorganic and Physical Chemistry, University, Stockholm; Research Institute of National Defence, Dept 1, Sundbyberg and Department of Inorganic Chemistry, Royal Institute of Technology, Stockholm, Sweden.*

In investigations on the crystal structures of basic salts of tetrapositive metal ions (G. Lundgren, *Svensk Kem. Tidskr.* (1959), **71**, 200), it was found that the co-ordination $Me-O$ is eightfold in the shape of a more or less distorted square Archimedean antiprism and that each pair of neighbouring metal atoms is joined by a double $OH^-(O^{2-})$ bridge. In this way, infinite chains are formed. One way of describing the metal–oxygen arrangement is to consider the spatial arrangement as consisting of Archimedean antiprisms sharing edges. It was found that two ways of linking the polyhedra to each other existed in these structures. From purely geometrical considerations, a total number of eight arrangements could be predicted, assuming such bridges and only two antiprisms in the repeat unit. The geometry of these arrangements will be discussed.

Furthermore, in some salts isolated, polynuclear $Me-OH(O)$ ions are found (G. Lundgren, *Svensk Kem. Tidskr.* (1959), **71**, 200; A. Clearfield & P. A. Vaughan, *Acta Cryst.* (1956), **9**, 555). They can be described as consisting of polyhedra condensed in a similar way. The arrangements of these groups will also be discussed.

A full report will be published in *Acta Chem. Scand.*

5·19. Unit cell and space-group determination of tetra- and di-calcium aluminate hydrates. By E. ARUJA, *Building Research Station, Garston, Watford, Hertfordshire, England.*

These hydrates and their polymorphic forms have been reported by M. H. Roberts (*J. Appl. Chem.* (1957), **7**, 543–546). The unit cell and space-group determination of the following will now be reported (characteristic basal spacings in brackets):

Tetra-calcium aluminate hydrates.—Two 19 H_2O-hydrates–two polytypes (10·7 Å); two 13 H_2O-hydrates–two polymorphs (8·2 and 7·9 Å); one 11 H_2O-hydrate (7·4 Å) and one 7 H_2O-hydrate (7·4 Å).

Di-calcium aluminate hydrates.—Three 8 H_2O-hydrates–two polytypes (10·7 Å) and another polymorph (10·4 Å); one 7·5 H_2O-hydrate (10·6 Å), one 5 H_2O-hydrate (8·7 Å), and one 4 H_2O-hydrate (7·4 Å).

Solid solution seems to take place between some di- and tetra-calcium aluminates. The effect of carbonation will also be discussed.

Single crystals of poor stability of only two of the hydrates have been obtained; powder photographs often show small amounts of impurities. The unit cells determined are hexagonal with rather long c axis (from 22 to 64 Å). Single crystal photographs show streaks in the c^* direction.

To be published probably in *Acta Cryst.*

5·20. Structures des deux formes allotropiques de CdSO₄. Par JEAN COING-BOYAT, *Attaché de Recherches au C.N.R.S., Laboratoire d'Electrostatique et de Physique du Métal, Institut Fourier, Grenoble, France.*

Le sulfate de Cadmium anhydre présente deux formes cristallographiques suivant la température à laquelle il a été porté; l'une α est stable immédiatement au-dessus de la température de dessication complète de

$$CdSO_4 . H_2O;$$
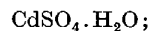
l'autre β stable au-dessus de 800 °C. environ et que l'on peut tremper.

Ces deux formes sont orthorhombiques; α appartient au groupe d'espace $Pmnm(D_{2h}^{13})$; β qui est isomorphe des sulfates anhydres de Ni, Co–II (forme basses températures) Fe–II et Mn–II, est du type $CrVO_4$ et appartient au groupe D_{2h}^{17}–$Cmcm$.

A paraître dans le *Bull. Soc. Franç. Minér.*

5·21. The crystal structure of CaB₃O₅(OH). By JOAN R. CLARK & C. L. CHRIST, *U.S. Geological Survey, Washington 25, D.C., U.S.A.*

In a preliminary survey of the system $CaO-B_2O_3-H_2O$ at elevated temperatures and pressures, being carried out at the *U.S. Geological Survey* by Brian J. Skinner, several new compounds have been found, not all of which have yet been characterized. In particular, when inyoite, $CaB_3O_3(OH)_5 . 4 H_2O$, was subjected to 2000 bars H_2O pressure at 400 °C. for several days, two new ortho-rhombic compounds were formed.

The crystal structure of one of these compounds has been solved, and from the structure the formula
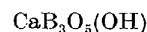
$$CaB_3O_5(OH)$$

is deduced, showing the compound to be a member of the series $2 CaO . 3 B_2O_3 . xH_2O$ with $x = 1$. The crystals are piezoelectric, orthorhombic, $Pbn2_1-C_{2v}^9$, $a = 6.97_2$, $b = 13.47$, $c = 4.39_1$ Å (all $\pm 0.3\%$), density (calc.) 2.72_9 g.cm.⁻³, with cell contents 4 [CaB₃O₅(OH)]. The habit is sword-like, with elongated [001], terminal {111}, and prism forms {110}, {120}, and {010}.

The structure of CaB₃O₅(OH) is closely related to the structures previously found by us for the other known members of the 2:3:x series:

colemanite, $CaB_3O_4(OH)_3 . H_2O$ (2:3:5);
meyerhofferite, $CaB_3O_3(OH)_5 . H_2O$ (2:3:7);
a synthetic, $CaB_3O_3(OH)_5 . 2 H_2O$ (2:3:9);
and
inyoite, $CaB_3O_3(OH)_5 . 4 H_2O$ (2:3:13).

All of these crystals contain a six-membered boron-oxygen ring formed from two tetrahedra and a triangle linked at corners. In meyerhofferite, the 2:3:9 synthetic, and inyoite, these rings exist as insular groups of composition $[B_3O_3(OH)_5]^{-2}$; in colemanite the rings link to produce infinite chains of composition $[B_3O_4(OH)_3]_n^{-2n}$ that may be considered as polymerization products resulting from the splitting out of water between successive insular $[B_3O_3(OH)_5]^{-2}$ groups. In $CaB_3O_5(OH)$ there are infinite sheets corresponding to the polymerization of adjacent infinite chains of the kind found in colemanite. These sheets are held together in the crystal through Ca–O and hydrogen bonding.

The crystal structure of the second compound is under study; its chemical formula is still unknown. It is ortho-rhombic, $Pccn–D_{2h}^{10}$, $a = 8.37_5$, $b = 13.86$, $c = 5.01_5$ Å (all $\pm 0.3\%$).

Full-length account to be submitted to Acta Cryst.

5·22. Square pyramid coordination in polyvanadate complexes. By Howard T. Evans, Jr., U.S. Geological Survey, Washington 25, D.C., U.S.A.

Many crystal structure determinations of quinquevalent vanadium–oxygen compounds in recent years have established three characteristic types of oxygen coordination about the vanadium atom. One is tetrahedral, as found in the orthovanadates, and in the alkali metavanadates such as KVO_3. A second is trigonal bipyramidal as found in $KVO_3.H_2O$. A third is also fivefold, square pyramidal in shape. This last is especially characteristic of complexes formed under acid conditions, and is commonly involved in corner or edge sharing with neighboring polyhedra to form chains, sheets or network structures. In the square pyramid, the apical V–O distance, designated A, is usually short, 1.52–1.68 Å; the four basal distances designated B, are longer, 1.75–2.00 Å. Often a sixth oxygen approaches at the base, opposite A, at a greater distance, designated C, 2.20–3.50 Å.

Two new crystal structure refinements by least-squares on the IBM 704 have added to our knowledge of these bonds: $K_3V_5O_{14}$ and CsV_3O_8. As previously reported (Byström and Evans, Acta Chem. Scand. (1959), 13, 377), $K_3V_5O_{14}$ (space group $P31m$) contains both square pyramids and tetrahedrons linked into a sheet structure. The square pyramid has the dimensions

$$A = 1.60, \quad B = 1.85 \text{ and } 1.97 \text{ Å (all } \pm 0.02).$$

In an adjacent sheet, a sixth oxygen gives $C = 3.39$ Å. CsV_3O_8 is monoclinic, space group $P2_1/m$, with

$$a = 8.20, \ b = 8.55, \ c = 5.00 \text{ Å}, \ \beta = 95° \, 35',$$

and a cell content of 2 formulas. The R factor for the $(hk0)$ and $(h0l)$ data together is 8.5%. CsV_3O_8 has a complex sheet structure made up of two types of square pyramid. Two thirds of the vanadium is of one type which has

$$A = 1.52, \ B = 1.99, \ 1.96, \ 1.85, \ 1.76, \text{ and } C = 2.90 \text{ Å }.$$

One third is of the second type which has

$$A = 1.65, \ B = 1.91, \ 1.85, \text{ and } C = 2.22 \text{ Å (all } \pm 0.02 \text{ Å}).$$

Comparison of these data with those of other compounds ($Li_4V_6O_{16}$, V_2O_5, $K_2(UO_2)_2V_2O_8$, etc.) shows a wide variation in A, B and C. The bond character is evidently very sensitive to the crystal field. It will be shown that a useful estimate of bond number may be made from the bond length D_n by use of Pauling's empirical relation:

$$D_n - D_1 = -2k \log n,$$

where n is the bond number, D_1 is the length of a single bond, 1.81 Å and $k = 0.39$.

5·23. On the crystal structure of $Th(OH)_2SeO_4$. By Gunilla Bergström & Georg Lundgren, Research Institute of National Defence, Dept 4, Solna 8 and Department of Inorganic Chemistry, Royal Institute of Technology, Stockholm 70, Sweden.

By means of recent investigations (G. Lundgren, Svensk Kem. Tidskr. (1959), 71, 200) on the crystal structures of basic salts of tetravalent cations, it was found that the metal ions in

$$Th(OH)_2CrO_4H_2O, \ Th(OH)_2SO_4, \text{ and } U(OH)_2SO_4$$

are arranged in zigzag rows within which they are joined by double bridges of hydroxide ions. Other more complicated Me–OH(O) complexes were found in

$$U_6O_4(OH)_4(SO_4)_6, \ Ce_6O_4(OH)_4(SO_4)_6, \text{ and } CeOSO_4H_2O.$$
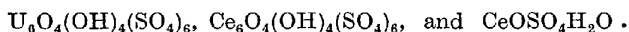
In all these crystals, the metal–oxygen coordination is eightfold in the shape of a square Archimedean antiprism and the Me–OH(O) arrangement can be considered as built up of such antiprisms sharing edges in different ways. The Me–OH(O) complexes are related to the fluorite structure, from which for instance the

$$[Th(OH)_2^{2+}]_n$$
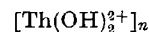
chains in $Th(OH)_2SO_4$ can be cut out.

The structure of $Th(OH)_2SeO_4$ is, however, quite different from that of $Th(OH)_2SO_4$. The metal ions in it are also arranged in zigzag rows but the angles Th–Th–Th are 125° as compared with 99° in $Th(OH)_2SO_4$. The thorium atoms are joined by double bridges of OH⁻ ions as in $Th(OH)_2SO_4$ but two consecutive bridges form nearly right angles to each other. The coordination Th–O is again eightfold. A detailed description of the structure and its relation to the fluorite structure will be given.

A full report will be published in Acta Chem. Scand.

5·24. The crystal structure of anhydrous sodium thiosulphate. By E. Sándor & L. Csordás, Department of Physics, L. Eötvös University, Budapest, Hungary.

Strongly deliquescent crystals of anhydrous sodium thiosulphate ($Na_2S_2O_3$) were grown from aqueous solution in a thermostat set at 93 °C. The density of the crystals measured by flotation was $d = 2.345 \pm 0.001$ g.cm.⁻³. Weissenberg photographs were taken with the multiple-film method around all three crystallographic axes. Altogether six layers were recorded containing 353 independent reflexions. The integrated intensities of the reflexions were first measured with an AMG micro-densitometer, then corrected for Lorentz and polarization

factor and placed to an absolute scale by the statistical method of Wilson. The space group from statistical absences was found to be $P2_1/a$ with four formula units in the unit cell. The unit cell parameters are:

$$a = 6\cdot50 \pm 0\cdot05, \quad b = 8\cdot12 \pm 0\cdot01, \quad c = 8\cdot52 \pm 0\cdot02 \text{ Å},$$
$$\beta = 95° \ 4' \pm 16'.$$

Attempts to solve the structure from two Harker sections of the Patterson function remained unsuccessful, because of multiple chance coincidences in the y-coordinates of the atoms. The one-dimensional Harker section $(\frac{1}{2}, v, 0)$ showed only three peaks, and of the five peaks appearing in the two-dimensional Harker section $(u, \frac{1}{2}, w)$ only three were genuine Harker peaks. Finally the structure was determined by direct methods using the Harker-Kasper inequalities and the equations derived by Karle-Hauptmann, Sayre and Zachariasen. Accepting only those signs for which the probability calculated from the formula of Cochran & Woolfson exceeded 0·9, altogether 219 signs were determined, which all turned out to be right in the final analysis. The initial structure has been further refined by computing successive two-dimensional and later three-dimensional $(F_o - F_c)$ syntheses. The final value of the R-factor was 15·0%.

In the S_2O_3 thiosulphate group one S and the three O atoms are arranged tetrahedrally around the other S atom. The S–S distance is 2·01 Å, and the mean S–O distance 1·46 ± 0·05 Å. The mean S–S–O and O–S–O angles are 108·5° ± 1·5' and 110·5° ± 1·5° respectively. These results are in good agreement with the results of Taylor & Beevers (1952), who derived a somewhat distorted tetrahedral arrangement for the S_2O_3 group in $Na_2S_2O_3.5 H_2O$, and are at variance with the results of Brunt (1946), who concluded that the S_2O_3 group in $(NH_4)_2S_2O_3$, $MgS_2O_3.6 H_2O$ and $NiS_2O_3.6 H_2O$ was essentially planar.

To be published in *Acta Cryst.*

5·25. Zur Struktur des Dinatrium-dihydrogen-Tetrametaphosphat $Na_2H_2P_4O_{12}$. Von O. JARCHOW & K. DORNBERGER-SCHIFF, *Deutsche Akademie der Wissenschaften zu Berlin, Institut für Strukturforschung, Berlin-Adlershof, Deutschland.*

Die Untersuchung wurde an Einkristallmaterial durchgeführt, das uns freundlicherweise von Fr. Dr Winkler, Institut für anorganische Chemie der DAdW zur Verfügung gestellt wurde und das als Hauptbestandteil bei der Darstellung nach dem von E. J. Griffith (*J. Amer. Chem. Soc.* (1956), **78**, 3867) beschriebenen Verfahren auftrat. 'Gitterkonstanten' und Verteilung von diffusen Ebenen und scharfen Reflexen lassen erkennen, dass es sich um die von J. W. Gryder, G. Donnay & H. M. Ondik (*Acta Cryst.* (1958), **11**, 38) als 'II' bezeichnete Substanz handelt. In dieser Arbeit kommen die Autoren zu dem Schluss, dass diese Struktur kein Natriumtetrametaphosphat der Formel $Na_2H_2P_4O_{12}$ sei, sondern ein Ultraphosphat der Formel $Na_3P_1O_{12}$.

Die Phasen der $(hk0)$-Reflexe wurden mit Tripelproduktmethoden bestimmt, und diese Projektion anschliessend verfeinert (Fig. 1). Schon diese Projektion lässt auf die Richtigkeit der ursprünglich vorgeschlagenen Formel schliessen. Strukturfaktorberechnungen der für die scharfen $(hk, 2n)$-Reflexe und die Maxima auf den
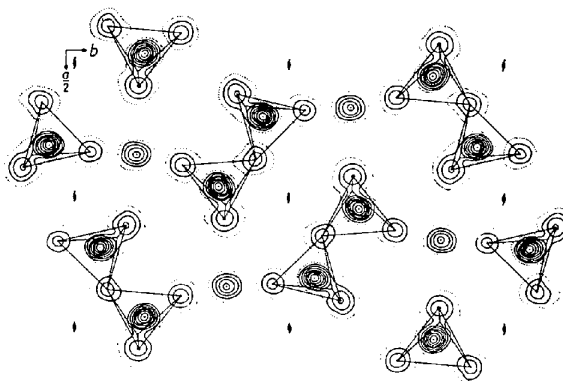
Fig. 1.

diffusen Ebenen lassen das Princip der Struktur erkennen (siehe Beitrag in Sektion 2).

5·26. On the structure of strontium metavanadate $Sr(VO_3)_2 \cdot 4H_2O$. By P. SEDLACEK & K. DORNBERGER-SCHIFF, *Deutsche Akademie der Wissenschaften zu Berlin, Institut für Strukturforschung, Berlin-Adlershof, Deutschland.*

Using methods described in section (2) the outline of the structure has been determined. There are chains of $(VO_3)_x$ somewhat similar to the chains found by C. L. Christ, J. R. Clark & H. T. Evans, Jr., *Acta Cryst.* (1954), **7**, 801) in $KVO_3.H_2O$.

These chains form an ordered lattice into which Sr and possibly H_2O are placed in a disordered way. The details of the structure will be given.

5·27. Die Struktur der Perjodsäure H_5JO_6. Von O. JARCHOW & K. DORNBERGER-SCHIFF, *Deutsche Akademie der Wissenschaften zu Berlin, Institut für Strukturforschung, Berlin-Adlershof, Deutschland.*

Withdrawn.

5·28. Zur Struktur des Natrium-Kupfer-Perjodats $-Na_4H_3Cu(JO_6)_24H_2O$. Von S. BÄHR, *Deutsche Akademie der Wissenschaften zu Berlin, Institut für Strukturforschung, Berlin-Adlershof, Deutschland.*

Withdrawn.

5·29. Crystal structure of ammonium chloride dithionate. By L. RIVOIR & Miss. P. GUARDABRAZOS, *Consejo Superior de Investigaciones Científicas, Instituto de Física 'Alonso de Santa Cruz'. Seccisn de 'Estructuras Cristalinas', Serrano 119, Madrid, Spain.*

The crystal structure of ammonium chloride dithionate has been determined using single-crystal X-ray diffraction technique. The unit cell is orthorhombic, with

$$a = 1\cdot46, \quad b = 12\cdot65, \quad c = 6\cdot08 \text{ Å}.$$

There are four molecules per unit cell.—The space group is *Pbcm*.

A detailed crystal-structure analysis by means of two-dimensional Fourier and difference syntheses of the electron density projected perpendicular to the a and c axes is given.

The interatomic distances of the dithionate ion are:

$$S-S = 2 \cdot 16; \quad S-O = 1 \cdot 44; \quad O-O = 2 \cdot 44; \quad S-S-O = 104°.$$

The N–O distance varies from $-2 \cdot 72$ up to $3 \cdot 19$ Å. Each Cl^- ion is surrounded by six NH_4^+ ions at distance $Cl-N = 3 \cdot 04$ Å.

Probably will be published in *Acta Cryst.*

5·30. Occurrence of the π phase among chalkogenides. By OSVALD KNOP, *Department of Chemical Engineering, Nova Scotia Technical College, Halifax, N.S., Canada.*

π phases are face-centred cubic compounds of the structure type $D8_9$ and corresponding to the ideal formula M_9X_8, with or without this stoichiometry. They seem to be restricted to the sulphides and selenides of the lower transition elements. Until recently only two such phases were known, Co_9S_8 and π(Fe, Ni, S), the latter occurring also as the mineral pentlandite. Bøhm *et al.* (*Acta Chem. Scand.* (1955), **9**, 1510) reported the phase π(Co, Se), and the existence of an isotypic compound Fe_9S_8 has recently been claimed by Meyer *et al.* (*Corrosion* (1958), **14**, 69). The homogeneous ternary phase π(Fe, Co, Ni, S) has now been shown to exist over an appreciable range of compositions in the section Fe_9S_8–Co_9S_8–Ni_9S_8 of the quaternary system Fe–Co–Ni–S. The stoichiometry of this phase with respect to the metal-to-sulphur ratio has been investigated.

Homogeneous π phases Co_3MS_8 can be ordered by segregating the cobalt atoms into tetrahedral and the M atoms into octahedral sites in a manner reminiscent of ferrites, the ratio of the numbers of the two types of sites ideally occupied being 8:1. This possibility has been investigated for Co_8NiS_8 by neutron diffraction. In fourteen other Co_8MS_8 samples the stability limits of the corresponding π phases and the possibility of ordering have been studied by X-ray diffraction. General features of the π phase and its relationship to similar phases are discussed.

A full account of this work will appear in the *Canad. J. Chem.*

5·31. MX_2 layer structures. By. F. JELLINEK, *Laboratorium voor anorganische chemie, Rijksuniversiteit Groningen, the Netherlands.*

A number of MX_2 layer structures can be based on close packings of X atoms, with M inserted in octahedral holes. If all M atoms are to be equivalent, only four structures of this kind are possible with the following atomic sequences:

C6 -type (trigonal):	$bAc \dots$
C27-type (hexagonal):	$aCb \, aBc \dots$
C19-type (rhombohedral):	$bAc \, aCb \, cBa \dots$
... (rhombohedral):	$bAc \, bAc \, aCb \, aCb \, cBa \, cBa \dots$

(Here a or A denotes atoms in 0, 0, z: b or B in $\frac{1}{3}$, $\frac{2}{3}$, z; c or C in $\frac{2}{3}$, $\frac{1}{3}$, z; a, b, c stand for X atoms, A, B, C for M.)

In the ideal case, i.e. when each X is equidistant from its $12X$ neighbours, c/a is a multiple of $\sqrt{\frac{8}{3}} = 1 \cdot 6330$, and

the M–X distances are $\sqrt{\frac{1}{2}} = 0 \cdot 7071$ times the distances X–X.

In a similar way four MX_2 layer structures can be constructed, in which the environment of M is trigonal prismatic, while the stacking of MX_2 slabs corresponds to close packing. The atomic sequences for these structures are:

(α)	(hexagonal):	$bAb \, cAc \dots$
(β)	(hexagonal):	$bCb \, cBc \dots$
(γ)	(rhombohedral):	$bAb \, aCa \, cBc \dots$
(δ)	(rhombohedral):	$bAb \, cAc \, aCa \, bCb \, cBc \, aBa \dots$

The metal sequences, therefore, are the same as in the types with M in octahedral sites. If each X is equidistant from its $10X$ neighbours, the distances M–X are $\sqrt{\frac{7}{12}} = 0 \cdot 7638$ times the distances X–X, and c/a is a multiple of $1 + \sqrt{\frac{2}{3}} = 1 \cdot 8165$.

Structure (β) is the C7-type of Strukturbericht, structures (α) and (γ) have recently been found in the system Nb–S (F. Jellinek, G. Brauer & H. Müller, *Nature, Lond.* (1960), **185**, 376). In NbS_2 generally some stacking disorder in the c direction is observed; this is prevented by the insertion of additional M atoms in part of the octahedral holes between the slabs. Results of a preliminary study of the system Ta–S suggest that structures and phase relationships are analogous to those in Nb–S.

5·32. Interstitial solutions of oxygen and nitrogen in α-titanium and α-zirconium. By BO HOLMBERG, *Institute of Inorganic and Physical Chemistry, University of Stockholm, Stockholm, Sweden.*

Studies of the extended ranges of solubility of small non-metals in α-titanium and α-zirconium have revealed the existence of various degrees of order.

To be published in *Acta Chem. Scand.*

5·33. On the ordered, defective NaCl-type structure of $VO_{1·27}$. By SVEN WESTMAN, *Institutet för oorganisk och fysikalisk kemi, Stockholms Högskola, Stockholm Va, Sweden.*

A phase analysis of the vanadium–oxygen system has revealed the existence of a tetragonal phase of approximate composition $VO_{1·27}$, stable below 900 °C.

The following cell dimensions have been obtained from Guinier photographs:

$$a = b = 16 \cdot 623 \text{ Å} = 4.4 \cdot 156 \text{ Å},$$
$$c = 16 \cdot 515 \text{ Å} = 4.4 \cdot 129 \text{ Å}.$$

The diffraction symmetry is pseudo-cubic, with reflexions $h00(h \neq 4n)$ missing. It is evident from single crystal, as well as powder data, that the crystal structure is a superstructure of a slightly deformed VO (NaCl type) structure.

The observed density of the phase indicates that the vanadium lattice is only partly occupied. The vacancies should, on the above evidence, be ordered, and the number per unit cell, a multiple of four. If the cell content is assumed to be $V_{204}O_{256}$, observed and calculated values of density and composition agree rather well:

Obs.	Calc.
$d = 5\cdot269$ g.cm.$^{-3}$	$d = 5\cdot272$ g.cm.$^{-3}$
$VO_{1\cdot27}$	$VO_{1\cdot26}$

Several tentative structure models have been proposed, which give a fair general correspondence between observed and calculated structure factors. The convergence of these models is being investigated.

To be published in *Acta Chem. Scand.*

5·34. The TiO_2-phase explored by the lattice constant and density method. By M. E. STRAUMANIS, T. EJIMA & W. J. JAMES, *Departments of Metallurgical and Chemical Engineering of the University of Missouri, School of Mines and Metallurgy, Rolla, Missouri, U.S.A.*

Samples of TiO_2 of various colours (bluish black to yellowish white) were obtained by heating TiO_2 at 1400 °C. under oxygen of increasing pressure. At that temperature the dissociation pressure is about 2/3 atm. (in oxygen). It was found that the homogeneity region of the phase extends from $TiO_{1\cdot989}$ to about $TiO_{2\cdot006}$. The composition of the samples was determined from lattice parameter and density measurements. The latter showed further that TiO_2 of stoichiometric composition has a sound lattice with $n' = 1\cdot9999 \pm 0\cdot0009$ molecules per unit cell. The structure of the grayish and deeper coloured samples is imperfect, caused by missing oxygen ions (up to 0·02 ions per unit cell or 0·5% of all oxygen positions are vacant at the left phase border). The imperfection of the yellowish white preparations on the right side of the phase is due to atoms of excess oxygen located in interstitial positions (up to 0·006 atoms per unit cell or 0·3%).

The lattice constants of the tetragonal TiO-phase varied only slightly with increasing oxygen content (a increased and c decreased). The constants of stoichiometric TiO_2 were obtained by extrapolation: $a_{25} = 4\cdot5937_4$ and $c_{25} = 2\cdot9619_7$ (precision: $\pm 0\cdot00005$ Å); $c/a = 0\cdot6447_8$; $v_{25} = 62\cdot505 \pm 0\cdot004$ Å^3; the expansion coefficients between 10 and 60 °C. were $\alpha_a = 6\cdot9 \times 10^{-6}$ and $\alpha_c = 9\cdot9 \times 10^{-6}$ along the a- and c-axes respectively. The macroscopic density of TiO_2 was: $d_{25} = 4\cdot2438 \pm 0\cdot0005$ g.cm.$^{-3}$. The density of the preparations increased with increasing oxygen content; their expansion coefficients were within the limits of error independent of composition.

The article will be submitted to *Acta Cryst.* for publication.

5·35. The crystal structure of V_3O_5. By STIG ÅSBRINK, *Institute of Inorganic and Physical Chemistry, University of Stockholm, Stockholm, Sweden.*

The crystal structure of V_3O_5 is related to the corundum structure as well as to the structure of orthorhombic ReO_2. All three structures have the oxygen atoms in a hexagonal close-packed arrangement. In V_3O_5, the octahedral interstices are partially filled with vanadium atoms in such a way that the VO_6 octahedra form infinite chains of two types. One type is composed of pairs of octahedra—each pair is formed by two octahedra sharing a face, these double-octahedra being then coupled together by sharing edges. These chains are separated by single octahedra which share corners in such a way as to form the other type of chain which runs parallel to the former type. The chains are united by sharing edges and corners of octahedra.

The chains of double octahedra are similar to those existing in the corundum structure while the chains of single octahedra are similar to those in orthorhombic ReO_2.

A few phases isomorphous with V_3O_5 have been prepared, *viz.* V_2TiO_5 and Cr_2TiO_5, the latter of which, however, was never obtained in a pure state.

The full-length account is likely to be published in *Acta Cryst.*

5·36. New crystal structures in the system calcium oxide—iron oxide. By P. B. BRAUN, *Philips Research Laboratories, Eindhoven, The Netherlands.*

A group of three mutually related structures has been solved in the system calcium oxide–iron oxide. These new structures are hexagonal with large c/a ratios. For one of these a complete three-dimensional Patterson and Fourier method has been used to solve the structure, followed by a three-dimensional least-squares refinement.

Once this structure being known the other two could be solved in a straight forward way.

The relation between these new structures and the hexagonal structures in the barium oxide–iron oxide system will be discussed in the light of the differences in ionic radius between Ca and Ba giving rise to structurally new layers.

This abstract is meant to be a provisional one. It has been kept somewhat cryptic for reasons of patent policy. It will be replaced in due time by a more descriptive one.

Meant to be published as paper in *Acta Cryst.*

5·37. Crystallographic data of tin(II) compounds. By JOHN D. DONALDSON, *Department of Chemistry, The University, Old Aberdeen, Scotland.*

The unit cell and X-ray powder data of a number of crystalline tin(II) compounds (including hydroxide, sulphate, hydrated chloride, an explosive basic nitrate and other basic salts) are given. The use of these data, and of high temperature transformations, in determining the composition of some of the materials is discussed. Preliminary work on the structure of anhydrous tin(II) sulphate indicates that it is not isomorphous with the sulphates of barium, strontium and lead, in spite of a similarity in unit-cell dimensions.

These data are likely to be included in a series of papers on the individual materials in *J. Chem. Soc.* The structural work will be submitted to *Acta Cryst.*

5·38. The crystal structure of niobium dioxide. By BENGT-OLOV MARINDER, *Institute of Inorganic and Physical Chemistry, University of Stockholm, Stockholm, Sweden.*

The crystal structure of niobium dioxide has been determined. The structure is of a deformed rutile type. A noticeable feature is the occurrence of metal–metal atom doublets. In this respect the structure resembles that of molybdenum dioxide. The tilt of the doublets is however different.

A full-length account will be published in *Acta Chem. Scand.*

5·39. On the structures of Cs-Mn(II)-chlorides. By PALLE ANDERSEN,* *The Chemical Laboratory B, Technical University of Denmark, Copenhagen, Denmark.* Withdrawn.

5·40. On the structures of solid solutions. By PALLE ANDERSEN,* *The Chemical Laboratory B, Technical University of Denmark, Copenhagen, Denmark.* Withdrawn.

5·41. Structures of sulfur-selenium mixtures. By Y. M. DE HAAN & M. P. VISSER, *Laboratorium voor technische Fysica van de Technische Hogeschool, Delft, The Netherlands.*

Previous investigations on sulfur and selenium were extended to mixtures of these elements. Mixed structures were obtained in different ways, that will be described. Most mixed structures of sulfur and selenium are built up from δ-atomic ring molecules in essentially the same way as the pure elements. These ring modifications are all soluble in CS_2. At all mixing ratios chain modifications may also occur. They are of the same kind as found with the pure elements, but the great strength of extended pure sulfur fibres is not retained in the mixed structures. Several new structures were found, but not fully analysed.

A full-length account of this study will be published in *Physica.*

5·42. Transition metal hydroxides. By Y. M. DE HAAN, *Massachusetts Institute of Technology, Laboratory for Insulation Research, Cambridge, Massachusetts, U.S.A.*

An investigation of the structures of divalent Ni, Co, and Mn hydroxides is being carried out by X-ray and

* Present address: The Royal Dental College, Vennelyst Boulevard, Århus, Denmark.

neutron-diffraction techniques to elucidate the magnetic properties of these materials and the nature of the hydroxyl ion and its environment. The structure analyses will be supplemented by studies of the infrared vibrational spectra and low-temperature magnetic susceptibilities.

5·43. Mixed oxides of titanium and vanadium. By CLAES NORDMARK, *Inst. of Inorganic and Physical Chemistry, University of Stockholm, Stockholm VA, Sweden.*

A phase analysis of the system Ti–V–O in the monoxide region is being carried out in order to elucidate the influence of the Ti–V ratio on the ordered and disordered phases previously found in the monoxides of titanium and vanadium.

Mixed oxides of the compositions

$$Ti_mV_{10-m}O_n \quad (m=1\text{-}9 \text{ and } n=6\text{-}13)$$
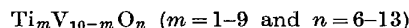
were prepared by arc-melting and heat-treated at 800 and 1000 °C. followed by quenching. The arc-melted and heat-treated samples have been analyzed by means of their X-ray powder patterns.

In the system Ti_2O_3–V_2O_3 the variation of the unit-cell parameters with the composition has been studied.

The full-length account is likely to be published in *Acta Chem. Scand.*

5·44. The crystal structure of β-Ga$_2$O$_3$. By S. GELLER, *Bell Telephone Laboratories, Incorporated, Murray Hill, New Jersey, U.S.A.*

The crystal structure of β-Ga$_2$O$_3$ has been determined from single crystal three-dimensional X-ray diffraction data. The monoclinic crystal has cell dimensions

$$a = 12\cdot23 \pm 0\cdot02, \quad b = 3\cdot04 \pm 0\cdot01, \quad c = 5\cdot80 \pm 0\cdot01 \text{ Å},$$
$$\beta = 103\cdot7 \pm 0\cdot3°$$

as originally reported by J. A. Kohn, G. Katz & J. D. Broder (*Amer. Min.* (1957), **42**, 398). There are 4Ga$_2$O$_3$ in the unit cell. The most probable space group to which the crystal belongs is C_{2h}^3–$C2/m$; the atoms are in five sets of special positions 4(i): (0, 0, 0; $\frac{1}{2}$, $\frac{1}{2}$, 0) $\pm$ (x, 0, z). There are two kinds of coordination for Ga^{3+} ions in this structure, namely tetrahedral and octahedral. Average distances are: tetrahedral Ga–O, 1·83 Å; octahedral Ga–O, 2·00 Å; tetrahedron edge O–O, 3·02 Å; and octahedron edge O–O, 2·84 Å. Because of the reduced coordination of half of the metal ions, the density of β-Ga$_2$O$_3$ is substantially lower than that of α-Ga$_2$O$_3$ which has the α-corundum structure. Also the closest approach of two Ga^{3+} ions in β-Ga$_2$O$_3$, 3·04 Å, is considerably larger than the closest approach of metal ions in the sesquioxides with α-corundum type structure and, in agreement with the results of the thermal studies (L. M. Foster & H. C. Stumpf, *J. Amer. Chem. Soc.* (1951), **73**, 1590), the β-phase appears to be the structurally more stable one.

The average Ga–O distances in the structure seem to account for the fact that although the Ga^{3+} ion is substantially larger than the Al^{3+} ion, its quantitative preference for tetrahedrally coordinated sites when substituted for Fe^{3+} ion in the iron garnets is very nearly the same as that of the Al^{3+} ion.

The structure accounts for a recent result obtained by M. Peter & A. L. Schawlow (*Bull. Amer. Phys. Soc.* (1960), in press) from paramagnetic resonance measurements on Cr^{3+} ion doped β-Ga_2O_3, namely that the Cr^{3+} ion substitutes for the Ga^{3+} ions in a single set of equivalent octahedral sites.

The magnetic aspects of the β-Ga_2O_3 structure are discussed and it is shown that a possible Fe_2O_3 isomorph could be expected to be at least antiferromagnetic with a Néel temperature of about 700 °K. Furthermore, a knowledge of the β-Ga_2O_3 structure and of the nature of site preferences of the Ga^{3+} and Fe^{3+} ions in the garnets lead to a prediction regarding the structure of the ferrimagnetic crystals of formula $Ga_{2-x}Fe_xO_3$ recently discovered by J. P. Remeika (*J. Appl. Phys.* (1960), **31** in press).

Manuscript to be submitted to *J. Chem. Phys.*

5·45. The structure of β-ZnOHCl. By HANS-ERIK FORSBERG, *Department of Inorganic Chemistry, The Royal Institute of Technology, Stockholm 70, Sweden; Institut für anorganische, analytische und physikalische Chemie, Institut für Mineralogie und Petrographie, Universität, Bern, Switzerland.*

The structure of β-ZnOHCl is of interest in connection with the study of the structures of the oxidehalides of bivalent metals (W. Feitknecht, H. R. Oswald & H.-E. Forsberg, *Chimia* (1959), **13**, 113) since β-ZnOHCl is one of the few substances of this class of salts of which it is possible to prepare single crystals large enough for X-ray investigations. The preparation of β-ZnOHCl was carried out using ZnO and $ZnCl_2$.

From rotation and Weissenberg photographs taken around the three crystal axes, it was concluded that the crystals are orthorhombic ($a = 5·86$, $b = 6·58$, $c = 11·33$ Å, $V = 436·9$ Å^3, $Z = 8$). The reflections systematically absent are in agreement with the centrosymmetric space group *Pcab* (*International Tables for X-ray Crystallography*, Kynoch Press, Birmingham, 1952, Vol. I, p. 150). The following parameters of the atoms were determined from Patterson and Fourier projections along [010], [100] and [001]:

8 Zn in 8(c) with $x \approx 0·25$, $y = 0·131$, $z = 0$
8 O in 8(c) with $x \approx 0·59$, $y = 0·126$, $z = 0·429$
8 Cl in 8(c) with $x \approx 0·58$, $y = 0·107$, $z = 0·143$
8(c), $\pm(x, y, z)$, $\pm(\frac{1}{2} - x, \frac{1}{2} + y, \bar{z})$,
$\pm(\frac{1}{2} + x, \bar{y}, \frac{1}{2} - z)$, $\pm(\bar{x}, \frac{1}{2} - y, \frac{1}{2} + z)$.

As has been predicted by W. Feitknecht (*Fortschr. der chem. Forschg.* (1953), **2**, 670), the structure of β-ZnOHCl is similar to the structure of $Mg(OH)_2$ (C_6-type) if half of the hydroxide ions are replaced by chlorine ions. Thus, the zinc atoms form pseudohexagonal layers separated by an ordered layer of oxygen and chlorine atoms. Each

zinc atom is surrounded by three oxygen and three chlorine atoms so that a coordination Zn-6X in the shape of an octahedron is obtained.

A full report will be published in *Acta Cryst.*

5·46. Mischkristallbildungen zwischen Verbindungen mit der mittleren Elektronenkonfiguration s^2p^3. Von H. KREBS & D. KALLEN, *Chemisches Institut der Universität Bonn, Bonn, Deutschland.*

In Analogie zu den in diamantähnlichen Gittern kristallizierenden isoelektronischen Verbindungen gibt es eine in steinsalzähnlichen Gittern auftretende isoelektronische Verbindungsreihe. Als Beispiele seien genannt: rhombischer schwarzer Phosphor, rhomboedrisches Arsen, rhomboedrisches GeTe und kubisches PbS. Die Verwandtschaft des Gitteraufbaues wird nachgewiesen durch weitgehende isotype und heterotype Mischkristallbildung. Die Gitterstrukturen, die elektrischen Eigenschaften (Halbleiter bzw. Metall) und die Mischkristallbildungen sind deutbar durch die Möglichkeit eines kontinuierlichen, nicht gequantelten Überganges der Valenzelektronen vom reinen p-Typ in solche mit s-Hybridisierung.

The paper will be published in the *Z. anorg. Chem.*

5·47. Complexes of antimony trichloride with aromatic hydrocarbons. By R. HULME & J. T. SZYMANSKI, *Chemistry Dept., Kings College, London, W.C. 2, England.*

X-ray examination has shown the real existence of crystalline compounds of antimony trichloride with benzene, p-xylene, mesitylene and naphthalene. A single crystal of the naphthalene compound was obtained from a 3 : 2 molecular ratio melt of antimony trichloride and naphthalene, the crystals being washed free from adhering mother liquor by warm pet. ether. Oscillation and Weissenberg photographs lead to a monoclinic cell

$$a = 9·12, \quad b = 9·13, \quad c = 11·68 \text{ Å}, \quad \beta = 122° 0',$$

space group $P2_1/c$ (C_{2h}^5).

From the (0kl) Patterson synthesis it can be deduced that there are four antimony trichloride molecules in the unit cell. This has been confirmed by the first (0kl) electron-density synthesis where antimony and chlorine atoms are resolved. Sufficient space now remains for up to two molecules of naphthalene, and space group requirements indicate that there must be at least two molecules lying around one or other of the four alternative two-fold positions. The *ideal* formula is thus

$$2 \text{ SbCl}_3 . \text{C}_{10}\text{H}_8 .$$
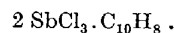
Analytical results have often diverged from this ideal composition. This may imply a genuine naphthalene deficiency statistically distributed throughout the whole structure, or, less likely, a surface deficiency due to washing. The density observed for the batch of crystals

from which one was chosen for photography was about 2·25 g.cm.$^{-3}$. This corresponds to the composition $SbCl_3.(C_{10}H_8)_{0.36}$ made up of alternating antimony trichloride and naphthalene layers.

Ultimate publication *Acta Cryst.*

5·48. The crystal structure of some dithiocarbamates of the univalent coinage metals. By R. HESSE, *Institute of Chemistry, University of Uppsala, Uppsala, Sweden.*

The univalent dialkyl dithio carbamate complexes of the coinage metals, copper, silver and gold are polymeric in solutions of different organic solvents. Their crystal structures are also built up of polymeric molecules, in the center of which the metal atoms form aggregates with short metal–metal distances. These distances are of the same order of magnitude as those in the metallic elements. The center of the $[(C_2H_5)_2NCS_2Cu]_4$ complex is a slightly distorted Cu_4-tetrahedron. In $[(C_2H_5)_2NCS_2Ag]_6$ there is a somewhat S-shaped Ag_6-chain and in $[(nC_3H_7)_2NCS_2Au]_2$ there is a central Au_2-pair. The short metal–metal distances may indicate the existence of binding forces between the metal atoms.

The full length account is likely to be published in *Acta Chem. Scand.*

5·49. The crystal structure of *bis*-N-methylsalicylaldiminato-copper. By E. C. LINGAFELTER, B. MOROSIN & G. L. SIMMONS, *Department of Chemistry, University of Washington, Seattle 5, Washington, U.S.A.*

The cell dimensions and space group of *bis*-N-methylsalicylaldiminato-copper were first reported by Stackelberg (*Z. anorg. Chem.* (1947), **253**, 136). We have confirmed his results and have completed the determination of the structure. The cell, of dimensions

$$a_0 = 24·71, \quad b_0 = 9·25, \quad c_0 = 6·66 \text{ Å}$$

contains 4 molecules and the space group is *Ibam*.

The crystal structure is quite similar to that reported for *bis*-dimethylglyoximato-nickel by L. E. Godycki & R. E. Rundle (*Acta Cryst.* (1953), **6**, 487), and consists of columns of planar molecules. The molecular planes are parallel to [001] and the copper atoms form chains along the C axis with a Cu–Cu separation of 3·33 Å, slightly greater than the Ni–Ni separation of 3·25 Å in *bis*-dimethylglyoximato-nickel.

Thus it appears that this type of molecular packing is not restricted to nickel, but may be formed by either nickel or copper if the molecules are sufficiently near to exact planarity. Both *bis*-N-methylsalicylaldiminato-nickel (Frasson *et al.*, *J. Phys. Chem.* (1959), **63**, 1908) and *bis*-dimethylglyoximato-copper (Frasson *et al.*, *J. Inorg. and Nucl. Chem.* (1958), **8**, 452) show considerable distortion from planarity, which accounts for their failure to form the columnar arrangement with metal–metal interactions. On the other hand, the failure of *bis*-salicylaldiminato-nickel (J. M. Stewart & E. C. Lingafelter, *Acta Cryst.* (1959), **12**, 842) and *bis*-salicylaldoximato-nickel (L. L. Merritt, C. Guare & A. E. Lessor,

Acta Cryst. (1956), **9**, 253) to form the columnar structure even though they are planar within a few hundredths of an Ångström unit, is probably due to the poorer overall packing of the columnar structure for these molecules. This is indicated by two observations:

(1) The molecular volume of *bis*-N-methylsalicylaldiminato-copper is 381 Å^3, while that of *bis*-N-methylsalicylaldiminato-nickel is 347 Å^3;

(2) *bis*-N-methylsalicylaldiminato-copper is reported by Stackelberg to also crystallize in another, non-columnar form with a molecular volume of 373 Å^3.

To be published in *Acta Cryst.*

5·50. The crystal and molecular structure of 2,2′,2″-triamino-triethyl-amine-Ni(II)-di-thiocyanate. By SVEND ERIK RASMUSSEN, *Chemical Institute, University of Aarhus, Aarhus, Denmark.*

The crystal structure of 2,2′,2″-triamino-triethylamine-Ni(II)-di-thiocyanate (Nitren(SCN)$_2$) was determined from its three-dimensional Patterson function. Superposition methods were applied using both the nickel atom and the two sulphur atoms as searcher atoms. The structure was refined by a least-squares analysis, employing three-dimensional data.

The crystal is built up from Nitren(SCN)$_?$ units. The four nitrogen atoms from the amine and the two nitrogen atoms from the thiocyanate groups form a distorted octahedron around the nickel atom. The thiocyanate groups being in *cis* positions. A full account is given of axial lengths, atomic coordinates, temperature factors, bond lengths and bond angles, and reliability index.

5·51. The structure of $Al_2Br_6.C_6H_6$. By J. H. TAYLOR & S. C. WALLWORK, *Dept. of Chemistry, The University, Nottingham, England.*

The structure of the complex between aluminium bromide and benzene, of composition $Al_2Br_6.C_6H_6$, has been determined from single crystal X-ray photographs. The complex is very readily attacked by atmospheric moisture so vacuum techniques were used in the preparation of the crystals and in transferring them to pyrex capillary tubes. The crystals were sealed inside the capillaries with a drop of mother liquor to prevent the decomposition which takes place in the absence of benzene. Weissenberg $h0l$ and $0kl$ intensity data were corrected for absorption and used in the determination and refinement of the structure by Patterson, Fourier and least-squares techniques. The crystals are triclinic, space group $P\bar{1}$, with

$$a = 6·85, \quad b = 6·91, \quad c = 9·00 \text{ Å},$$
$$\alpha = 104·6°, \quad \beta = 103·1°, \quad \gamma = 90·0°.$$

Uncertainty about the composition was resolved partly by comparing the cell volume with the approximate volumes of the component molecules and partly by the successfull refinement of the structure. It has been shown that the aluminium bromide is present as Al_2Br_6 molecules and that besides the one Al_2Br_6 molecule per unit cell there is only sufficient space for one benzene mole-

cule. Small peaks showing in the spaces in difference Fourier $(F_o - F_{Al_2Br_6})$ projections are consistent with a benzene molecule in a satisfactory position and orientation. It seems to be parallel to, and held between discontinuous layers of approximately close-packed bromine atoms. The complex is therefore best regarded as being of the lattice type but it is possible that some charge transfer between bromine atoms and benzene molecules is contributing to the intermolecular forces.

The full account will probably be published in *J. Chem. Soc.*

5·52. A 5-co-ordinated zinc complex, monoaquo bis-acetylacetone zinc. By E. L. LIPPERT & MARY R. TRUTER, *School of Chemistry, The University, Leeds 2, England.*

The compound, $Zn(CH_3.CO.CH.CO.CH_3)_2.H_2O$ crystallises in monoclinic needles,

$$a = 10·91, \quad b = 5·517, \quad c = 10·46 \text{ Å}, \quad \beta = 93·6°,$$

with two formula units per unit cell. The space group, $P2_1$, could only be established by determination of the structure. Three-dimensional analysis shows that the zinc atom is five-co-ordinated, with the bonds arranged in a trigonal bipyramid. The water molecule and one oxygen atom from each acetylacetone group lie in the equatorial plane, the bond lengths are

$$Zn-H_2O = 2·02 \pm 0·03 \text{ Å} \quad \text{and} \quad Zn-O = 1·96 \pm 0·02 \text{ Å}.$$

The other oxygen atoms of the chelating acetylacetone groups form the apices of the bipyramid and the Zn–O length is $2·11 \pm 0·02$ Å.

To be submitted to *J. Chem. Soc.*

5·53. The crystal structure of cerium (IV) acetylacetonate. By B. MATKOVIĆ, *Department for Structural and Inorganic Chemistry, Institute Rudjer Bošković, Zagreb, Yugoslavia.*

It has recently been established that the coordination polyhedron for the thorium atom in thorium(IV) acetylacetonate is an Archimedean antiprism (D. Grdenić & B. Matković, *Nature, Lond.* (1958), **182**, 465). Subsequently it was shown that the crystals of cerium(IV) and uranium(IV) acetylacetonate are isomorphous with the α-modification of thorium acetylacetonate (D. Grdenić & B. Matković, *Acta Cryst.* (1959), **12**, 817). In the same paper it was reported that $Ce(C_5H_7O_2)_4$ is monoclinic $P2_1/C$,

$$a = 11·70, \quad b = 12·64, \quad c = 16·93 \text{ Å}, \quad \beta = 112° 15', \quad Z = 4.$$

Further investigation was carried out on the cerium compound because the central atom has a considerably lower atomic number than thorium or uranium atoms, which enables a better resolution of light atom positions in the electron density projection. In order to facilitate the absorption correction the specimen was made cylindrical by grinding. Multiple-film Weissenberg photographs were taken from cylindrical specimens with Cu $K\alpha$ radiation. The relative intensities $h0l$ and $0kl$ reflexions were determined from the optical densities measured by means of a microdensitometer. The positions

of the atoms were determined from (010) and (100) Fourier projections.

The work on a more exact determination of the co-ordinates of all light atoms as well as an improvement of the reliability index is now in progress. A three-dimensional Fourier synthesis is anticipated.

The full length account is likely to be published in *Acta Cryst.*

5·54. The crystal structure of di-p-chlorodiphenyl-tellurium diiodide.* By GEORGE Y. CHAO & J. D. McCULLOUGH, *Department of Chemistry, University of California at Los Angeles, Los Angeles 24, California, U.S.A.*

Previous studies on compounds of the type R_2SeCl_2, R_2SeBr_2, R_2TeCl_2 and R_2TeBr_2 have shown that molecules of these substances contain nearly linear $X-Se-X$ and $X-Te-X$ bonding (G. D. Christofferson, R. A. Sparks & J. D. McCullough, *Acta Cryst.* (1958), **11**, 782). By contrast, the iodine complexes of 1,4-diselenane and 1,4-dithiane have been found to contain nearly linear Se–I–I and S–I–I bonding (J. D. McCullough, G. Y. Chao & D. E. Zuccaro, *Acta Cryst.* (1959), **12**, 815). No complete structural study of a compound of the type R_2TeI_2 has as yet appeared in the literature. Of the several compounds of this type available for study, preliminary investigations indicated di-p-chlorodiphenyltellurium to be the most promising.

Crystals of $(p\text{-}ClC_6H_4)_2TeI_2$ display triclinic holohedral symmetry. Sets of Weissenberg and precession camera photographs were prepared by use of Mo radiation on crystals about 0·10 to 0·15 mm. in thickness. These indicated the following cell dimensions:

a	$=$	$9·751 \pm 0·006$ Å	α^*	$= 62° 35' \pm 03'$
b	$=$	$10·682 \pm 0·006$ Å	β^*	$= 79° 45' \pm 05'$
c	$=$	$9·531 \pm 0·006$ Å	γ^*	$= 61° 59' \pm 03'$
α	$=$	$115° 42' \pm 05'$		
β	$=$	$92° 48' \pm 05'$	V	$= 788·8$ (Å)^3
γ	$=$	$116° 21' \pm 05'$		

The observed density is approximately 2·5 g.cm.$^{-3}$ while that calculated from the X-ray data is 2·529 g.cm.$^{-3}$ for $Z = 2$. The space group is assumed to be $P\bar{1}$ with two non-centrosymmetric molecules per unit cell.

With the aid of Patterson and electron-density summations on (001), (100) and (010), the heavy atom positions were found to be:

Atom	x	y	z
H_1	0·779	−0·062	−0·087
H_2	0·798	−0·010	0.239
H_3	0·809	0·035	0.569

These positions indicate the following interatomic distances and bond angle:

$$H_1-H_2 = 2·96 \text{ Å}, \quad H_2-H_3 = 2·89 \text{ Å} \quad \text{and}$$

$$\angle \ H_1-H_2-H_3 = 173° 40'.$$

At this stage, the chlorine positions are somewhat

ambiguous. Because of this and the similarity in the atomic scattering factors for Te and I, it is still impossible to decide with certainty between the I–Te–I and Te–I–I configurations. A three-dimensional study is in progress which should not only locate the chlorine but also the carbon atoms, thus revealing the complete structure.

Completed study to be submitted to *Acta Cryst.*

5·55. The crystal structure of Cu-N-N-di-*n*-propyl-dithiocarbammate. By GIORGIO PEYRONEL & ANNA PIGNEDOLI, *Istituto di Chimica Generale dell' Università, Modena, Italy*

The complex Cu-N-N-di-*n*-propyldithiocarbammate

$$Cu \left[\begin{matrix} S \\ \ \\ S \end{matrix} \!\!\! >\!\! C\!-\!N = (n\text{-}C_3H_7)_2 \right]_2$$
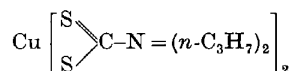
crystallizes in the $P2_1/a(C_{2h}^5)$ space group with four molecules in the elementary cell. By Patterson and Buerger syntheses, Sayre's equality, Fourier f_o, f_c and $f_o - f_c$ syntheses, this structure has been determined and refined.

The CuS_4 group is not planar; the coordination of copper(II) in this complex will be discussed in relation to the different types of coordination of Cu(II) in other complexes.

The full-length account will be published in *Acta Cryst.*

5·56. On the structure of the AgSCN-P(*n*-propyl)₃. By CARLO PANATTONI & EDOARDO FRASSON, *Centro di Strutturistica Chimica del C.N.R., Padova, Italy.*

The crystals of this complex belong to the monoclinic system with the following lattice constants:

$$a = 6·32, \ b = 14·00, \ c = 18·24 \text{ Å}, \ \beta = 114°, \ Z = 4;$$
$$\text{space group } P2_1/c \ .$$

The structure determined with the two-dimensional Fourier technique appears to be similar under certain respect to that of AgSCN determined by I. Lindqvist (*Acta Cryst.* (1957), **10**, 29) where a chain

$$\ldots\text{–AgSCN–AgSCN–}\ldots$$
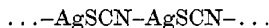
is formed through Ag–N bonds.

The distance between two Ag-atoms bonded through a SCN-group is about the same in both structures. Also in this compound the Ag-atom exhibits tetrahedral coordination; but, in the AgSCN this is achieved through an intramolecular Ag–S bond, an Ag–N and two Ag–S intermolecular bonds; in the phosphyne-derivate the 4-fold coordination is achieved through intramolecular Ag–S and Ag–P bonds and intermolecular Ag–N and Ag–S bonds.

It follows that the molecular chains present in the AgSCN are bonded one to the other giving rise to a compact structure involving the whole crystal. In this complex the only extra-chain intermolecular bond Ag–S gives rise to a coupling of the chains.

This note will be sent to the *Le Ricerca Scientifica* for extensive publication.

5·57. The structural chemistry of cupric compounds. By J. A. J. JARVIS & A. F. WELLS, *Research Department, I.C.I. Ltd., Dyestuffs Division, Manchester, 9, England.*

The structure of three compounds of divalent copper with organic molecules have been determined.

Copper(II) *bis* (*benzene azo-β-naphthol*)

The monoclinic unit cell has dimensions:

$$a = 17·34, \ b = 3·90, \ c = 17·46 \text{ Å}, \ \beta = 96·9°.$$

The space group is $P2_1/n$ and the cell contains 2 Cu (at symmetry centres) and four molecules of $C_{16}H_{11}N_2O$. The structure was determined from the intensities of 1780 *hkl* reflexions by least-squares refinement on 'Pegasus'; $R = 16·0\%$.

The copper atoms have square planar coordination, with two oxygen atoms at 1·93 Å and two nitrogen atoms at 2·01 Å. The next nearest neighbours are oxygen atoms of two adjacent molecules (Cu–O = 3·00 Å) completing a distorted octahedral coordination group. The structure shows that only one nitrogen atom of each azo group is bonded to the metal atom.

Copper(II) 1:2:4-*triazole dichloride*

The monoclinic unit cell has dimensions:

$$a = 6·81, \ b = 11·39, \ c = 7·13 \text{ Å}, \ \beta = 97·0°.$$

The space group is $I2/a$ and there are $4 \text{ CuCl}_2.\text{C}_2\text{H}_3\text{N}_3$ in the unit cell. The structure was refined on 'Pegasus' using 520 *hkl* reflexions; $R = 10·3\%$.

In this structure Cu(II) has a distorted octahedral coordination group,

$$\text{Cu–2 Cl, } 2·34, \text{ Cu–2 N, } 1·98, \text{ Cu–2 Cl, } 2·78 \text{ Å}.$$

The structural unit is an infinite chain of the type:
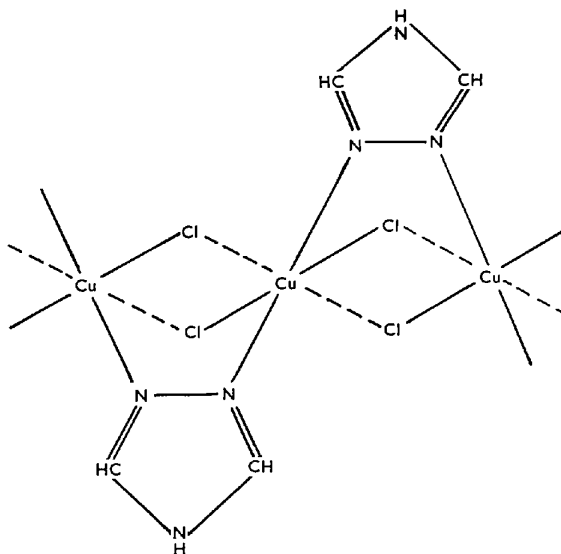
which is a new variant, for a compound MX_2R, of the MX_2R_2 chain found in crystals of compounds such as $CuCl_2.2 H_2O$, $CuCl_2(pyr)_2$, $MnCl_2(pyr)_2$ etc.

Copper(II) *imidazole*

One polymorph of this compound has cell dimensions:

$$a = 11\cdot75, \quad b = 14\cdot07, \quad c = 8\cdot77 \text{ Å}, \quad \beta = 97\cdot2°.$$

The space group is $I2/c$ and the cell content is

$$8 \text{ Cu}(\text{C}_3\text{H}_3\text{N}_2)_2 .$$

The structure was derived by least-squares refinement on 'Pegasus' using 1448 hkl reflexions; $R = 11\cdot5\%$.

There are two types of crystallographically non-equivalent Cu atom. Each is bonded to four nitrogen atoms of different imidazole molecules so that the whole assembly forms a three-dimensional network of Cu atoms linked by imidazole molecules. The coordination around one type of Cu(II) atom is square planar and around the others flattened tetrahedral.

To be submitted to *Acta Cryst.*

5·58. The crystal structure of the compound of aniline with an ammonia nickel cyanide complex.
By J. H. RAYNER, *Rothamsted Experimental Station, Harpenden, Herts, England.*

X-ray examination of single crystals of the compound $\text{Ni(CN)}_2.\text{NH}_3. \text{C}_6\text{H}_5\text{NH}_2$ showed that if slight disorder, shown by streaks on the films, were ignored the dimensions of the tetragonal cell which explained all the sharp spots were

$$a = b = 7\cdot23 \pm 0\cdot02, \quad c = 9\cdot25 \pm 0\cdot05 \text{ Å} .$$

The structure was similar to that of the corresponding benzene compound which has a similar unit cell but c shorter by $1\cdot0$ Å. The aniline molecules have their C–N bonds perpendicular to flat parallel sheets, consisting of Ni atoms linked in square array by CN groups. The aromatic molecules are trapped upright between the sheets, and are also in contact with the NH_3 groups which project one on each side of alternate Ni atoms. The best fit to the $0kl$ data is given by a structure in which all the aniline molecules have their CN bonds pointing in the same direction. This is consistent with the polar 4 fold axis shown in the face development of some crystals. It is, however, suggested that the disorder consists of groups of layers with aniline molecules with CN bonds in one direction alternating with groups of layers with CN bonds in the opposite direction.

Crystals of the compound $\text{Ni(CN)}_2.\text{C}_5\text{H}_5\text{N}$ large enough for single crystal examination were grown from a nickel cyanide ammonia solution and pyridine vapour. It is suggested that the structure is based on the same nickel cyanide sheets with pyridine replacing ammonia and the sheets displaced from vertical superposition to accommodate the aromatic rings.

To be submitted to *J. Chem. Soc.*

5·59. Structures and nature of bonding of $\text{C}_5\text{H}_5\text{Co}$ $(\text{CH}_3\text{C}_2\text{CH}_3)_2\text{CO}$ and $\text{Mn}_2(\text{CO})_{10}$. By L. F. DAHL & D. L. SMITH, *Department of Chemistry, University of Wisconsin, Wisconsin, U.S.A.*

$\text{C}_5\text{H}_5\text{Co}(\text{CH}_3\text{C}_2\text{CH}_3)_2\text{CO}$ is monoclinic with cell parameters:

$$a = 8\cdot18, \quad b = 13\cdot37, \quad c = 11\cdot02 \text{ Å}, \quad \beta = 91° \ 44'.$$

Density (g.cm.$^{-3}$), calc. 1·43, obs. 1·46 with $Z = 4$. The probable space group is $P2_1/n$. Single crystal intensity data involving over 1000 independent reflections have been obtained photographically with Mo $K\alpha$ radiation.

Patterson and three-dimensional Fourier syntheses were used to determine the atomic positions. Three-dimensional refinement of the structure by least squares has been carried out and to date the discrepancy factor $R_1 = 8\cdot6\%$.

$\text{C}_5\text{H}_5\text{Co}(\text{CH}_3\text{C}_2\text{CH}_3)_2\text{CO}$ can be described as a sandwich complex in which the cobalt lies between a cyclopentadienyl radical and a tetramethyl-cyclopentadienone ring. Details of the refined structure will be presented including bond lengths and angles; the nature of bonding will be discussed.

A three-dimensional least-squares refinement of

$$\text{Mn}_2(\text{CO})_{10}$$
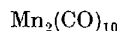
(L. F. Dahl, E. Ishishi & R. E. Rundle, *J. Chem. Phys.* (1957), **26**, 1750) has been carried out. Details of the molecular and crystal structure will be presented.

To be published either in *J. Amer. Chem. Soc.* or *Acta Cryst.*

5·60. Structures of the Cu- and Ni-methyl-ethyl-glyoxime. By EDOARDO FRASSON & CARLO PANATTONI, *Centro di Strutturistica Chimica del Consiglio Nazionale delle Ricerche, Padova, Italy.*

During a systematic investigation of the metal-complexes of the glyoximes, a singular case of pseudo-isomorphism has been encountered on the complexes Cu- and Ni-methyl-ethyl-glyoximes. The phaenomenon is all the more interesting if we consider that the examination of the structures of the Cu- and Ni-dimethyl-glyoximes (E. Frasson, R. Bardi & S. Bezzi, *Acta Cryst.* (1959), **12**, 201; L. E. Godycki & R. E. Rundle, *Acta Cryst.* (1953), **6**, 487) has revealed very noticeable structural differences between the two similar complexes.

The unit cell of the Cu-methyl-ethyl-glyoxime has a volume twice that of the Ni-methyl-ethyl-glyoxime. This is due to the doubling of the lengths of the parameter a in this structure with all the other cell constants fairly unchanged.

The metal atoms are in both cases along the x direction at 0,0 and at $\frac{1}{2}, \frac{1}{2}$ of y and z. The molecules are parallel one to another and almost parallel to the plane (100) of the structure. In the Ni-methyl-ethyl-glyoxime the metal-atoms are at the origin of the cell and on the other equivalent position of the space group $P2_1/c$. In the Cu-methyl-ethyl-glyoxime, couples of molecules are localized around the origin of the cell and the other equivalent positions of the space group $P2_1/n$.

In other words the molecular impact in the two structures can be summarized as follows. In the Ni-methyl-ethyl-glyoxime the molecules are along the x direction of the cell at regular intervals of 3·32 Å. In the Cu-methyl-ethyl-glyoxime the molecules are again along the x direction but the intervals between overlying molecules are alternatively about 3·0 and 3·6 Å. In both cases the

inclination of the molecules in respect to the axis a is so that if we conduct a straight line, normal to the molecular plane, passing through the Me-atom, we meet over and under two oxygen atoms belonging to two adjacent molecules.

The comparison between the sterical situation of the two complexes is very interesting. In fact we can suppose that the above cited differences are due to the different coordination caracteristics of the two metal-atoms with formation of a chain in the case of the Ni-complex and of a dimer in the case of the Cu-complex, although the Me–O distances are very large. These distances (3·32 Å in the Ni-complex and 3·00 Å in the Cu-complex) considered independently from the particular steric situation are such to create perplexity.

This note will be sent to *Acta Cryst.* for extensive publication.

5·61. The structure of the iron carbonyl phenylacetylene complex $Fe_2C_{30}H_{18}O_6$. By G. S. D. KING, *European Research Associates s. a., Bruxelles 18, Belgium.*

The iron carbonyl phenylacetylene complex

$$Fe_2(CO)_6(C_6H_5C_2H)_3$$
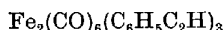
prepared by Hübel & Braye (*J. Inorg. Nucl. Chem.* (1959), **10**, 250) crystallizes with four molecules per unit cell in space group $P2_1/n$ with

$$a = 11·963 \pm 0·003, \ b = 20·442 \pm 0·005 \,,$$
$$c = 10·326 \pm 0·003 \text{ Å}, \ \beta = 93° \ 24' \pm 5' .$$

The positions of the iron atoms were found from the sharpened Patterson function. Twenty six of the light atoms were located by use of minimum function and the remainder were found from two successive Fourier syntheses.

The three phenylacetylene residues and one carbonyl group form a seven-membered carbon chain with phenyl groups at the 1, 3 and 6 positions and the carbonyl group in the 5 position. This chain is linked at each end and at the middle to one of the iron atoms to give two fused five-membered rings with an iron and a carbon atom in common. This iron atom is also bonded to three carbonyl groups and is octahedrally coordinated. The second iron atom is linked to the remaining two carbonyl groups and to the C_1–C_2, C_5–C_6 and C_6–C_7 bonds of the organic system.

To be submitted to *Acta Cryst.*

5·62. Zur Struktur des $HgCl_2$-Kollidins-2 [$HgCl_2$. NC_9H_9]. Von SIEGFRIED KULPE, *Deutsche Akademie der Wissenschaften zu Berlin, Berlin–Adlershof, Institut für Strukturforschung, Deutschland.*
Withdrawn.

AC 13 — 68

5·63. Structural study of the high-pressure polymorphs of ice. By W. BARCLAY KAMB & SANKAR K. DATTA, *California Institute of Technology, Pasadena, California, U.S.A.*

X-ray structural study of the high-pressure forms of ice is in progress. Powder data have been obtained for ice II, ice III, and ice VI, and single crystal data for ice III. Published powder data (MacFarlan, 1936) for ice II agree reasonably with our powder data for ice III; the published data for ice III do not correspond either to Ice II, III, or VI. Ice III is tetragonal,

$$a = 6·75, \ c = 6·79 \text{ Å} \,,$$

space group probably $P4_12_1$. The ice II powder data are accounted for by a cubic cell having $a = 11·25$ Å. No analysis has yet been made of the ice VI data. The methods of preparing and studying the high-pressure ice samples, and of identifying the phases, will be discussed, and the structural results for ice III presented.

To be published in *Acta Cryst.*

5·64. Polyhedral clathrate 'Ice' structures in some high hydrates.* By G. A. JEFFREY, D. FEIL & R. K. McMULLAN, *The Crystallography Laboratory, The University of Pittsburgh, Pittsburgh 13, Pa., U.S.A.*

The crystal structures have been determined for two members of a series of hydrated salts containing tetra and tri alkyl organic ions, (R. K. McMullan & G. A. Jeffrey, *J. Chem. Phys.* (1959), **31**, 1231), *viz.*,

$$(n\text{-}C_4H_9)_3S^+.F^-.20 \text{ H}_2O, \text{ m.p. } 5 \text{ °C., and}$$
$$(i\text{-}C_5H_{11})_4N^+.F^-.38 \text{ H}_2O, \text{ m.p. } 31 \text{ °C.}$$
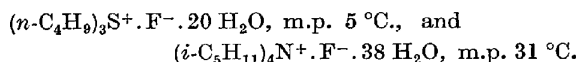
In both these structures the basic framework consists of hydrogen-bonded water molecules linked in the form of pentagonal dodecahedra, such as have been postulated to exist in water, by Pauling (*Nature of the Chemical Bond*, 3rd ed., p. 473), and in the gas hydrates, by W. F. Claussen (*J. Chem. Phys.* (1951), **19**, 259) and by M. V. Stackelberg & H. R. Muller (*J. Chem. Phys.* (1951), **19**, 1319), and was found in chlorine hydrate by L. Pauling & R. E. Marsh (*Proc. Nat. Acad. Sci.* (1952), **38**, 112).

The structure of the tri n-butyl sulphonium fluoride hydrate is cubic with $a = 12·34$ Å, $Pm3n$, $Z = 2$. It is very closely related to the structure of $6 \text{ Cl}_2 . 46 \text{ H}_2O$, in which the pentagonal dodecahedra are linked together through corners into a pseudo body-centered arrangement. The alkyl groups occupy the tetrakaidecahedral voids in the 'ice' structure in a statistically disordered arrangement.

The tetra i-amyl ammonium fluoride hydrate is orthorhombic with

$$a = 12·08, \ b = 21·61, \ c = 12·82 \text{ Å}, \ Pbmm, \ Z = 2 .$$

In this structure the pentagonal dodecahedra share faces to form infinite columns in the a direction. These columns are linked by hydrogen-bonded water molecules to form other dodecahedra and larger voids in which lie the alkyl groups.

Several examples of polymorphism have been observed, which appear to correspond to the variety of different ways in which the basic pentagonal dodecahedral units can be associated to form these clathrate-type structures.

5·65. The crystal structure of hydrogen peroxide dihydrate. By IVAR OLOVSSON & DAVID H. TEMPLETON, *Department of Chemistry, University of California, Berkeley* 4, *California, U.S.A.*

The crystal structure of hydrogen peroxide dihydrate, $H_2O_2 . 2 H_2O$, has been determined from single crystal X-ray data. Exposures at -70 and -190 °C. indicate the same structure. The crystals are monoclinic (space group $C2/c$) with four molecules in a unit cell of dimensions

$$a = 9·400, \quad b = 9·479, \quad c = 4·51 \text{ Å}, \quad \beta = 121·33°$$

at -190 °C. Oxygen atoms of the peroxide are at 0·9925, 0·1809, 0·0785, etc., and oxygen atoms of water are at 0·2980, 0·0822, 0·2850, etc. The structure contains planar chains of water molecules connected by hydrogen bonds of 2·74 Å. The chains are cross-linked by the hydrogen peroxide molecules into a three-dimensional network by hydrogen bonds of 2·76 and 2·69 Å. Peaks in a difference synthesis suggest the positions of the hydrogen atoms in these bonds, and indicate slight displacements from the lines joining the oxygen atoms. These positions correspond to a dihedral angle of about 130°, in the hydrogen peroxide molecule, between the planes defined by the peroxide link and the hydrogen atoms.

To be published in *Acta Chem. Scand.*

5·66. The crystal structure of perchloric acid monohydrate at -80 °C. By C. E. NORDMAN, *Department of Chemistry, University of Michigan, Ann Arbor, Michigan, U.S.A.*

Perchloric acid monohydrate (hydronium perchlorate) undergoes a phase transition at about -30 °C. (R. C. Taylor & G. L. Vidale, *J. Amer. Chem. Soc.* (1956), **78**, 5999). The form stable above this temperature apparently has a disorder in the orientation of the hydronium ions (F. S. Lee & G. B. Carpenter, *J. Phys. Chem.* (1959), **63**, 279; H. G. Smith & H. A. Levy, Abstracts, ACA Annual Meeting, Ithaca, N.Y. (1959)).

Single crystals of the low temperature modification prepared by recrystallization from an excess of anhydrous perchloric acid at dry ice temperature were sealed in capillaries and mounted while being kept below the transition temperature, as the crystals were found to shatter in the transition.

The low temperature modification is monoclinic, space group $P2_1/n$, with the cell parameters

$$a = 7·54, \quad b = 9·37, \quad c = 5·36 \text{ Å}, \quad \beta = 97·7°.$$

The structure determination was based on 820 observed intensities collected on the precession camera using standard low temperature techniques. Isotropic least-squares refinement of chlorine and oxygen parameters to $R = 0·105$, and anisotropic refinement to $R = 0·075$, has established the arrangement of these atoms. The four Cl–O distances in the tetrahedral perchlorate ions are in the range 1·44–1·47 Å, corrected for the error due

to angular motion. The hydronium oxygen is surrounded, in pyramidal fashion, by three perchlorate oxygens at distances between 2·63 and 2·71 Å. These three perchlorate oxygens, which are presumably hydrogen bonded to the hydronium ion, form a roughly equilateral triangle. Three-dimensional difference Fourier syntheses are being evaluated in an effort to locate the hydrogen atoms directly.

The gross relationship to the orthorhombic room temperature structure is indicated by the rough similarity in lattice parameters. The detailed relationship of the two modifications and the nature of the transition will be discussed.

5·67. The crystal structure of $B_{10}H_{12}[S(CH_3)_2]_2$.* By DONALD E. SANDS & ALLAN ZALKIN, *University of California, Ernest O. Lawrence Radiation Laboratory, Livermore, California, U.S.A.*

$B_{10}H_{12}[S(CH_3)_2]_2$, a derivative of decaborane, forms monoclinic crystals with

$$a = 11·79, \quad b = 10·79, \quad c = 12·74 \text{ Å}, \quad \beta = 95° \, 07',$$

space group $P2_1/c$, $Z = 4$. The intensities of 992 reflections, of which 333 were unobserved, were measured visually on Cu $K\alpha$ multiple-film equi-inclination Weissenberg exposures. The sulfur atoms were located by analysis of the three-dimensional Patterson function. All boron and carbon atoms were obtained from Fourier sections calculated using the signs given by the sulfur atoms. Least-squares refinement of these parameters, excluding hydrogen, resulted in a reliability factor of 17%.

As in the case of $B_{10}H_{12}(CH_3CN)_2$ (J. van der Maas Reddy & W. N. Lipscomb, *J. Chem. Phys.* (1959), **31**, 610) the boron configuration of the decaborane molecule is essentially unchanged in this derivative. The substituent groups are attached to the 6, 9 positions of the decaborane skeleton, with the boron-sulfur distance close to that expected for a single bond (1·92 Å).

5·68. The crystal structure of a nickel boride related to tetragonal boron. By B. F. DECKER & J. S. KASPER, *General Electric Research Laboratory, Schenectady, N.Y., U.S.A.*

It is found that a reaction of boron with nickel occurs at 80,000 atmospheres and 1600 °C. to yield a 'boride' containing approximately 4 at.% nickel. Good needle-like single crystals are produced and these are being studied by single crystal X-ray methods. The noteworthy feature is that while the boron framework is essentially the same as that reported for tetragonal boron (J. L. Hoard, R. E. Hughes & D. E. Sands, *J. Amer. Chem. Soc.* (1958), **80**, 4507), the Ni atoms form bonds to boron atoms and seem to be essential in stabilizing the structure. Similar conditions of pressure and temperature with pure boron do not result in the production of tetragonal boron.

Unlike the situation with tetragonal boron (Hoard *et al.* (1958)) the crystals with Ni show no evidence of appreciable disorders or of variability in lattice parameters. The

---

experimental density is 2·60 g.cm.$^{-3}$, corresponding to 50 B and somewhat less than 2 Ni per unit cell:

$$a_0 = 8·986 \pm 0·006, \quad c_0 = 5·078 \pm 0·003 \text{ Å};$$

space group $P4_2/nnm$. The boron parameters are being refined from hhl data obtained with a G.E. single crystal orienter, but are close to those reported in (1).

The Ni atoms occur in positions 2(a). Their coordination consists of 8 boron atoms at 2·20 and 6 at 2·53 Å. The former distance is sufficiently close to the sum of the radii of metallic Ni and of B to suggest definite bonding of the kind found in lower borides. In view of these results it appears appropriate to consider whether tetragonal boron is in fact a stable phase of boron or a variant of a boride.

Full account to appear in *Acta Cryst.*

5·69. Crystal structure of β-iodine monochloride. By G. B. CARPENTER & STEPHANIE M. RICHARDS, *Metcalf Research Laboratory, Brown University, Providence 12, Rhode Island, U.S.A.*

Single-crystal diffraction patterns of β-ICl show it to be monoclinic, space group $P2_1/c$,

$$a = 8·88, \quad b = 8·40, \quad c = 7·57 \text{ Å}, \quad \beta = 91·3°.$$

There are 8 molecules per cell. The structure is being determined by Patterson syntheses. It will be compared with that of α-ICl (K. H. Boswijk, J. van der Heide, A. Vos & E. H. Wiebenga, *Acta Cryst.* (1956), **9**, 274). The two forms differ less than 10° in melting point and have the same space group but the cell dimensions are not related in any obvious way.

Likely to be submitted to *Acta Cryst.*

5·70. The crystal structure of Hg$_2$O$_2$NaI. By KARIN AURIVILLIUS, *Institute of Inorganic and Physical Chemistry, University, Stockholm, Sweden.*

The crystal structure of Hg$_2$O$_2$NaI has been studied by X-ray (single crystal) and neutron (powder) diffraction methods. The Laue symmetry is $6/mmm$. The space group is $P6_222(P6_422)$. Every sodium atom in the structure is surrounded by four oxygen atoms and four iodine atoms, forming a deformed Archimedean square antiprism. These coordination polyhedra share their base planes to form infinite chains running along the c axis of the unit cell. The mercury and oxygen atoms form infinite planar chains –Hg–O–Hg–O– lying in the ab plane. The Hg–O distance is 2·03 Å and the angles O–Hg–O and Hg–O–Hg are 179° and 109° respectively. The chains are thus analogous to those in orthorhombic mercury(II)oxide. This atomic arrangement suggests that the bond between Hg and O within the chains is mainly homopolar. Similar building principles exist in the structures of the hexagonal mercury(II)oxide and the hexagonal mercury(II)sulphide.

The positions of the mercury and iodine atoms are derived from three-dimensional X-ray data. Geometrical considerations gave thus three possible alternatives for the positions of the light atoms. The neutron powder data made possible a clear decision between these arrangements.

A full report will be published in *Acta Chem. Scand.*

5·71. The crystal structure of mercury oxycyanide. By S. ŠĆAVNIČAR, *Mineralogical and Petrological Institute, Zagreb, Yugoslavia.*

The application of the methods of X-ray crystal analysis has shown that the molecular structure of mercury oxycyanide, HgO.Hg(CN)$_2$, should be interpreted by the formula (NCHg)$_2$O.

The crystals, obtained from the aqueous solution, are orthorhombic with

$$a = 18·93, \quad b = 7·09, \quad c = 3·90 \text{ Å} .$$

The cell contains 4 formula units of HgO.Hg(CN)$_2$. From two space groups $Pnam$-D_{2h}^{16} and $Pna2_1$-C_{2v}^9, consistent with extinctions, the holohedric one seems probable. It is supported by the morphology of crystals and by the complete correspondence of the intensities for $hk0$ and $hk2$ pairs of reflections.

The x and y parameters of all atoms—as determined from $(x, y, 0)$ Patterson synthesis, as well as from electron-density projection along [001] and $(F_o - F_{c\,\text{Hg}})$-synthesis—are:

	x	y	z
Hg$_\text{I}$	$-0·022_5$	$0·199_0$	$\frac{1}{4}$
Hg$_\text{II}$	$0·152_5$	$0·128_6$	$\frac{1}{4}$
O	$0·057$	$0·007$	$\frac{1}{4}$
C$_\text{I}$	$0·071$	$0·535$	$\frac{3}{4}$
N$_\text{I}$	$0·102$	$0·390$	$\frac{3}{4}$
C$_\text{II}$	$0·243$	0.255	$\frac{1}{4}$
N$_\text{II}$	$0·296$	$0·344$	$\frac{1}{4}$

The z parameters result from the symmetry of *Pnam*, taking also into account crystallochemical requirements.

A reliability factor $R(hk0) = 0·10$ was obtained.

The crystal structure of mercury oxycyanide is built up from N$_\text{I}$≡C$_\text{I}$–Hg$_\text{I}$–O–Hg$_\text{II}$–C$_\text{II}$≡N$_\text{II}$ molecules, which occupy the positions in the symmetry planes parallel to (001). The bond lengths within the molecule are:

N$_\text{I}$–C$_\text{I}$ = 1·18, C$_\text{I}$–Hg$_\text{I}$ = 2·10, Hg$_\text{I}$–O = 2·03,

O–Hg$_\text{II}$ = 2·00, Hg$_\text{II}$–C$_\text{II}$ = 1·94 and C$_\text{II}$–N$_\text{II}$ = 1·18 Å.

The angles are:

C$_\text{I}$–Hg$_\text{I}$–O = 158°, Hg$_\text{I}$–O–Hg$_\text{II}$ = 112° and

O–Hg$_\text{II}$–C$_\text{II}$ = 180°.

(NCHg)$_2$O molecules, related by two-fold screw axis [001] at 000, are arranged in an infinite column (parallel to c axis—needle axis of crystal) through the pairs of Hg$_\text{I}$–O approaches, which amount to 2·53 Å; in this way the resulting polyhedron around Hg$_\text{I}$ is a distorted tetrahedron.

The distances of Hg$_\text{II}$ atom to two crystallographically equivalent N$_\text{I}$ atoms as well as to two such N$_\text{II}$ atoms from the molecules of neighbouring columns are 2·86 and 2·97 Å, respectively. These four nitrogen atoms, lying in a plane normal to O–Hg$_\text{II}$–C$_\text{II}$ line, complete the octahedral co-ordination of Hg$_\text{II}$.

The values of all other intermolecular distances tally well with the sums of van der Waals radii.

The full-length account is likely to be offered to a chemical journal.

5·72. The crystal structures of tetrathiazylfluoride (NSF)₄ and trithiazylchloride (NSCl)₃. By G. A. WIEGERS, *Laboratorium voor algemene chemie, anorganische chemie en kristalchemie der Rijksuniversiteit Groningen, The Netherlands.*

Crystals of (NSF)₄ were obtained from Prof. O. Glemser (University of Göttingen) who had already determined the cell dimensions and space group (O. Glemser, H. Schröder & H. Haeseler, *Z. anorg. Chem.* (1955), **279**, 28).

The crystals are tetragonal, space group $P\bar{4}2_1c$. The cell dimensions are $a = 9\cdot22$, $c = 4\cdot30$ Å: per cell two molecules (NSF)₄ at special positions with symmetry $\bar{4}$.

The atomic coordinates were obtained by trial and error, use being made of the information from the Patterson projections. After refinement with successive difference Fourier syntheses of the projections and trial and error with the $hk2$ reflexions, the disagreement indices amounted to 0·07, 0·09 and 0·06 for the $hk0$, $h0l$ and $hk2$ reflexions respectively.

The molecule consists of a puckered eight membered ring of alternating nitrogen and sulfur atoms. The fluorine atoms, which are linked to the sulfur atoms, are situated such as to give the most compact molecule. The lengths of the crystallographically non-equivalent S–N bonds are 1·65 and 1·55 Å with e.s.d. of 0·02 Å, indicating alternating single and double bonds in the eight membered ring. The S–F bond length is 1·64 Å. The values of the valence angles N–S–N, S–N–S, F–S–N and F–S =N are 112°, 123°, 91° and 106° respectively.

Trithiazylchloride (NSCl)₃ is monoclinic, space group $P2_1$ or $P2_1/m$. The cell dimensions are:

$$a = 5\cdot53, \; b = 11\cdot2, \; c = 6\cdot12 \text{ Å}, \; \beta = 99\cdot4°;$$

two molecules (NSCl)₃ per unit cell.

The approximate structures was determined from the sharpened Patterson syntheses of the [001] and [100] projections. Accurate atomic coordinates cannot be obtained from the projections due to the overlap and the anisotropic thermal movement of the molecules.

The molecule consists of a six membered ring of alternating sulfur and nitrogen atoms. In the present stage of refinement it is not certain whether the ring is completely planar. The chlorine atoms are linked to the sulfur atoms and lie at the same side of the six membered ring. The S–Cl bonds make angles of approximately 100° with the plane of the sulfur atoms.

The full account is likely to be published in *Acta Cryst.*

5·73. Molecular structure of (PCF₃)₅. By CAROL SPENCER & WILLIAM N. LIPSCOMB, *Harvard University, Cambridge 38, Massachusetts, U.S.A.*

Visual estimates of 2078 reflections obtained with Cu $K\alpha$ and Mo $K\alpha$ radiation from a single crystal of (PCF₃)₅ (m.p. −33 °C.) at −100 °C. indicated four molecules in a unit cell having symmetry $P2_1/n$ and parameters

$$a = 9\cdot87, \; b = 9\cdot78, \; c = 16\cdot67 \text{ Å}, \; \beta = 103° \; 0'.$$

The P₅ ring is highly distorted by the mutual steric interaction of the CF₂ groups (one on each P), and by one interesting non-bonding F · · · P distance of 3·04 Å,

shorter than the van der Waals distance of 3·25 Å and shorter than any other F · · · P contact between atoms not bonded through C.

Average distances are

$$\text{P–P} = 2\cdot224 \pm 0\cdot007, \; \text{P–C} = 1\cdot91 \pm 0\cdot02,$$
$$\text{C–F} = 1\cdot35 \pm 0\cdot03 \text{ Å} .$$

The P–P–P angles vary from 94·6 to 107·5°($\pm 0\cdot4°$). The structure was determined by location of the P₅ ring in the Patterson function, and by successive Fourier and least-squares refinement of the three-dimensional data on the IBM 704. Agreement factors of

$$R = ||F_o| - |F_c||/\Sigma|F_o| = 0\cdot18 \text{ and}$$
$$r = \Sigma w||F_o|^2 - |F_c|^2|^2/\Sigma w|F_o|^4 = 0\cdot14$$

do not include the anisotropic thermal motions of the P₅ ring along approximately the x direction, and the torsional oscillation of CF₃ about the P–C bonds.

We wish to thank Prof. A. B. Burg for the sample, and to acknowledge support by the Office of Naval Research.

The full paper will be submitted to *Acta Cryst.*

5·74. Crystal structure of tetrameric phosphonitrilic octadimethylamide. By G. J. BULLEN, *Birkbeck College Crystallography Laboratory, London W.C. 1. England.*

Molecular structures already proposed for tetrameric phosphonitrilic compounds include (i) a 'boat' form, symmetry $\bar{4}$, for P₄N₄Cl₈ (I, $R = R'$ = Cl) which is tetragonal (Ketelaar & de Vries, *Rec. Trav. Chim.* (1939), **58**, 1081), (ii) a centrosymmetrical 'chair' form for P₄N₄F₈ (I, $R = R'$ = F), monoclinic (Paddock & Searle, *Advances in Inorganic Chemistry and Radiochemistry* (1959), Vol. 1, p. 368). The octadimethylamide

$$(\text{I}, \, R = R' = \text{N(CH}_3)_2)$$
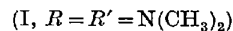
is tetragonal, $a = 13\cdot00$, $c = 8\cdot59$ Å, 2 molecules per unit cell, systematic absences of X-ray reflexions indicating space groups $I4$, $I\bar{4}$ or $I4/m$. $I\bar{4}$ and molecular symmetry $\bar{4}$ is chosen as most probable because molecular symmetries 4 and $4/m$ are inconsistent with the view of the molecule in [001] projection. Solution of the structure by Patterson methods with Fourier and least-squares refinement has shown that the molecule has a 'boat' form which is more distorted than that of P₄N₄Cl₈. The distance of each P atom from the 'mean plane' of the ring is about 0·15 Å as compared with 0·5 Å in the chloride. Eight-membered rings have sufficient freedom to allow 'boats' of considerably different shapes while retaining $\bar{4}$ symmetry and similar bond lengths and angles. The intensity data do not seem to accord with a disordered structure of the type suggested for P₄N₄(CH₃)₈ (I, $R = R'$ = CH₃) (Searle, *Proc. Chem. Soc.* (1959), p. 7)

$$
\begin{array}{ccc}
R'RP & -N= & PRR' \\
\parallel & & | \\
N & & N \\
| & & \parallel \\
R'RP & =N- & PRR'
\end{array}
$$

(I)
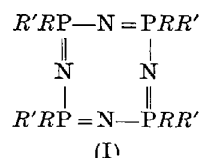
Crystals of the octaamide (I, $R = R' = NH_2$) and of $P_4N_4(C_6H_5)_4(NHCH_3)_4$ (I, $R = C_6H_5$, $R' = NHCH_3$) have also been examined. They are triclinic but pseudo-tetragonal. It seems likely that the requirements of intermolecular hydrogen bonding prevent exact tetragonal packing of the molecules. We may thus expect only those structures where cohesion is conferred solely by van der Waals forces to be tetragonal.

A full account is likely to be published in *Acta Cryst.*

5·75. The rôle of 3d orbitals in π-bonds between Si, P, S or Cl and O or N. By D.W. J. CRUICKSHANK, *School of Chemistry, The University, Leeds, 2, England.*

The single system of π-orbitals in planar aromatic molecules is well known. Evidence will be presented for a double system of π-orbitals in silicates, phosphates and sulphates, which also extend throughout the molecules. In XO_4^{n-} two strong π-bonding molecular orbitals are formed with $X3d_{x^2-y^2}$ and $3d_{z^2}$ orbitals and the appropriate oxygen $2p$ orbitals. Thus the S-O bond in SO_4^{2-} is reduced from a single bond length of 1·69 to 1·49 Å. In ethyl sulphate (Truter, 1959) the ester oxygen still shares in one π-orbital, which explains its intermediate S-O value of 1·60 Å. Because the other π-orbital is shared with only three oxygens, their S-O lengths contract to 1·46 Å. A very short X-O bond, e.g. 1·39 Å in P_4O_{10}, occurs when the other three oxygens of a tetrahedron link to further tetrahedra, and when the X-O-X angles are near 120°. However, when X-O-X is linear, as in one Si_2O_7, the central X-O bonds share fully in both π-electron systems.

These ideas will be extended to interpret the structures of many silicates, phosphates, phosphoramides, sulphamides, etc. In ions with OH groups, the bonds are intermediate in length between those for the ion without the proton and for the ion with R in place of H, apparently due to hydrogen bond formation.

During the interpretation new crystallographic results will be reported for $K_2S_2O_7$ (H. Lynton & Mary R. Truter), $Se_2Si_2O_7$ (with H. Lynton) and $(NO_2)ClO_4$ (with M. R. Truter & G. A. Jeffrey). Significant refinements of P_2O_5 (Form III) (with Caroline H. MacGillavry), $KHSO_4$, $NaPO_3NH_3$, $NaP_2O_7 \cdot 10 H_2O$ and other relevant structures will also be reported.

The π-orbital theory will be submitted probably to a chemical journal; the new structures and refinements to *Acta Cryst.*

A-B in molecules and crystals, in the main, depends on two factors: (1) of the electronegativities differences Δx and (2) of the potentials of the nucleises z^*/r (where z^* is the effective nuclear charge and r is the covalent radius of the atom A). In the formula $\Delta d = \beta \Delta x$ for a calculation of the difference of the experimental and calculated (by the sum of the covalent radii) bond lengths we have obtained the values of the coefficients $\beta = 0·06$ (I row of elements of the periodic system)

$$0·10(II), \quad 0·16(III), \quad 0·11(V) \text{ and } 0·14(VII).$$

We have suggested a method which permits to predict the σ-valent bond lengths with an accuracy of röntgen structural experiments to within $\pm 0·01$–$0·02$ Å or permits to determine the quantitative value of the electronegativities differences of atoms according to the crystal chemical data.

As to the character of a change of the bond lengths, the crystal structures A_xB_y are divided into the groups depending on the type of the external electrons of the atom A:

> the s–p electronic bonds
> the f-electrons
> the d-electrons

For the s–p bonds of the metals the regularities of the change of the bond lengths for any ligands are defined by the leaps of the potentials of metal nucleis z^*/r. In the transition metals (with the unfilled d-orbitals) the bond lengths depends on the action of the ligands field and are changed according to the splitting of the degenerative d-levels into the d_e- and d_y-levels.

We have learned that the lone pair electrons of the nitrogen, sulfur and oxygen atoms take part in the formation of the π-bonds in the following crystal structures (thiocyanates, 2-mercaptobenzothiazole thiourea, dichlorobisthioureazinc, tetramethylthiourea, diethyldithio carbomate sodium, cyanamide, 2-5 diphenyl thiodiazole, p-thiocyanato aniline, di-p-tolyldisulphide, caprolactam). —The greatest changes of the bond lengths are conditioned by the participation of the free electrons of the nitrogen and sulfur atoms in π-interaction and are observed in the $\rangle N$-$C_1 = S$ group with the conjugated N-C and C = S bonds. We have drawn up a diagram of the dependence of the C-N, C = N and C-S, C = S bond lengths. We have established that the π-interaction of the N-C and C = S bonds is mutually increased for coplanar bonds of the nitrogen atom and mutually diminished for the pyramidal bonds of the nitrogen atom. The change of the π-bond strength depends on the s–p electronic state of the σ-bond.

The papers are published in the Journals: *Crystallographica, Structural Chemistry* and *Problems of Physical Chemistry.*

5·76. The crystal chemical data on the nature of σ- and π-bonds. By Z. V. ZVONKOVA, N. S. IVANOVA, V. P. GLUSHKOVA, J. TASHPULATOV, I. V. ISAKOV, O V. KOLNINOV, L. G. VORONCOVA & E. J. KOIRANSKAY, *Institute for Phys.-Chem. Research, Karpova, Obukha 10, Moscow, Russia.*

We have established that the σ-valent bond lengths

5·77. New crystal and molecular structure determinations of charge transfer compounds. By O. HASSEL, *Chemistry Department, University of Oslo, Blindern, Norway.*

Withdrawn.

§ 6. Organic structures

6·1. The crystal structure of DL-aspartic acid hydrochloride. By B. DAWSON, *Division of Chemical Physics, C.S.I.R.O., Chemical Research Laboratories, Melbourne, Australia.*

Approximate x- and z-parameters of DL-aspartic acid hydrochloride

$$COOHCHNH_2CH_2COOH.HCl$$
$$1\ 1\ 2\quad 2\qquad 3\quad 4\ 3\ 4$$

$(P2_1/a,\ a=11\cdot12,\ b=6\cdot32,\ c=11\cdot29\ \text{Å},$
$\beta=120°\ 30'\ (\pm0\cdot5\%),\ Z=4)$

were obtained from the b-axis Patterson projection and refined by F_0 and (F_0-F_c) $(h0l)$ syntheses. Early refinement (1953–4), using McWeeny's f-curves for C, O and N and James and Brindley's $f(\text{Cl}^-)$ from the Hartree calculation neglecting exchange, showed anisotropic thermal motion in all atoms, and the x-, z-determinations proceeded with two anisotropic temperature factors, one for chlorine and the other for the molecule. Subsequent difference maps showed not only peaks near reasonable H positions, but also evidence of inadequacies in the $f(\text{Cl}^-)$-curve. Least-squares treatment for possible f-curve errors $(\varDelta f)$ gave negligible changes for C and O, but for Cl⁻ yielded a curve in close agreement with that obtained later from the Hartree–Fock calculation with exchange. For N, the $\varDelta f$-values suggested the probable presence of N^{+1}, which was consistent with the detection of three hydrogen peaks about this atom. Succeeding refinements employed an $f(\text{N}^{+1})$ curve and Hartree–Fock curves for C, O and Cl⁻. Present x- and z-coordinates of all atoms give $R(h0l)$ (omitting terms with $F_0=0$) = 0·057, and 0·045 and 0·086 (with and without H respectively) for $0<\sin\theta\leq0\cdot6$, when a general molecular temperature factor is used; with individual anisotropic temperature factors, the corresponding R-values are 0·047, 0·037 and 0·085.

Refinement of y-parameters has proceeded by $(0kl)$ difference and least-squares analysis and by $(1kl)$, $(h1l)$ and $(h3l)$ generalized projections. The $R(0kl)$ and $R(h1l)$ are 0·065 and 0·057, and R-values for $0<\sin\theta\leq0\cdot6$ show sensitivity to H similar to that of $R(h0l)$ above. Further y-refinement is contemplated to improve the determination of the central (C_2–C_3) bond whose present length is 1·47 Å. The other bond lengths are

C_1–C_2=1·54, C_3–C_4=1·52, C_1–O_1=1·22, C_1–O_2=1·32, C_4–O_3=1·34, C_4–O_4=1·21, C_2–N=1·51 Å.

The location of H from $(h0l)$, $(0kl)$ and $(h1l)$ difference projections yields average C–H, N–H and O–H distances of 0·95, 0·89 and 0·78 Å respectively.

To be published in *Acta Cryst.*

6·2. The crystal structure of the potassium salt of o-nitrophenol hemihydrate. By J. P. G. RICHARDS, *Viriamu Jones Laboratory, University College, Cardiff, Great Britain.*

The potassium salt of o-nitrophenol crystallizes in space group $C2/c$ with 8 molecules of

$$C_6H_4.NO_2.OK.\tfrac{1}{2}H_2O$$

in the unit cell of dimensions

$a=24\cdot8,\ b=5\cdot13,\ c=11\cdot9\ \text{Å},\ \beta=105\cdot0°.$

The structure has been solved by the heavy-atom method and has been refined by Fourier and least-squares syntheses using the $(h0l)$, $(h1l)$ and $(hk0)$ data.

The structure is made up of double layers. The forces between adjacent double layers are entirely van der Waals in character whilst a complex system of hydrogen bonds and electrostatic contacts operate within each double layer to hold the structure together. Each potassium ion is coordinated by seven oxygen atoms, six occurring in three different residues and one from the water. The distances vary between 2·68 and 2·94 Å; no symmetry is apparent in the system. Pairs of residues are linked together through water molecules on diad axes by hydrogen bonds involving the phenolic oxygens in such a manner that the system of hydrogen bonds and electrostatic contacts about each water is roughly tetrahedral. The residue is strictly planar, giving rise to a short non-bonded intramolecular distance; the possible stereochemical implications of this are discussed.

To be published in *Acta Cryst.*

6·3. The crystal structure of barbituric acid dihydrate and some related compounds.* By SUBRATA GHOSE, G. A. JEFFREY, B. M. CRAVEN & J. O. WARWICKER, *The Crystallography Laboratory, The University of Pittsburgh, U.S.A. and The Chemistry Department, The University of Leeds, England.*

Barbituric acid dihydrate, $C_4H_4N_2O_3.2\,H_2O$ is orthorhombic with

$$a=12\cdot74,\ b=6\cdot24,\ c=8\cdot89\ \text{Å},\ Z=4,\ Pnma.$$

It has a very compact layer structure in which both the barbituric acid and the water molecules lie in the mirror planes. The acid molecule is in the tri-keto form. The hydrogen-bond coordination of the water molecules is unusual in that it is approximately trigonal planar. The structure was refined by three-dimensional Fourier techniques and isotropic least squares to $R=0\cdot14$ and thereafter by anisotropic least squares.

Violuric acid monohydrate, $C_4H_3N_3O_3.H_2O$, has a similar layer structure with the molecules in the mirror planes of $A2_1am$ with

$$a=7\cdot57,\ b=14\cdot41,\ c=6\cdot23\ \text{Å},\ Z=4\ .$$

The preliminary crystal data have also been determined for ammonium barbiturate, $P2_1/n$,

$$a=10\cdot74,\ b=3\cdot85,\ c=14\cdot39\ \text{Å},\ \beta=96\cdot4°,\ Z=4;$$

sodium violurate, monohydrate, $P2_1/c$,

$$a=3\cdot97,\ b=18\cdot89,\ c=9\cdot75,\ \beta=94\cdot4°,\ Z=4;$$

5·5′ dimethyl barbituric acid, $P1$ or $P\bar{1}$,

$$a=11\cdot84,\ b=6\cdot52,\ c=5\cdot71\ ,$$
$$\alpha=118°,\ \beta=95\cdot5°,\ \gamma=118°,\ Z=2;$$

5·5′ diethyl barbituric acid, trigonal form, $R\bar{3}$,

$$a=27\cdot12,\ c=6\cdot83\ \text{Å},\ Z=18;$$

orthorhombic form, $Pmma$, $P2_1ma$ or $Pm2a$,

$$a=12\cdot80,\ b=22\cdot20,\ c=6\cdot89\ \text{Å};$$

(for monoclinic form, see Giacomello *et al.*, *Ann di Chim.* (1959), **49**, 825);

5·5′ ethyl phenyl barbituric acid monohydrate, *Pcab*,

$$a = 10·89, \quad b = 30·93, \quad c = 7·19, \quad Z = 8 .$$

6·4. Organic crystal structures determined at Osaka University. By ISAMU NITTA, *Department of Chemistry, Faculty of Science, Osaka University, Nakanoshima, Osaka, Japan.*

Triethylenediamine

The crystal of triethylenediamine, one of the typical cage molecules with high symmetry, belongs to the hexagonal system. Two molecules are in a unit cell with the dimensions of $a = 6·20$ and $c = 9·58$ Å, the space group being $P6_3/m$. The N $\cdots$ N axis of the molecule, which has the symmetry D_{3h}, is oriented along the c axis. The N–C–C–N linkage has a *cis* configuration. The position of hydrogen atoms has also been determined (Y. Tomiie, T. Wada & I. Nitta, to be published in *Bull. Chem. Soc., Japan*).

Acrylic acid at −70 °C.

The crystal structure has been determined at -70 ± 3 °C. The orthorhombic unit cell with the dimensions of

$$a = 11·68, \quad b = 10·06, \quad c = 6·38 \text{ Å}$$

contains eight molecules, the space group being *Ibam*. The molecules lie on the planes $z = 0$ and $\frac{1}{2}$. Pairs of molecules are linked by hydrogen bonds into centrosymmetric dimers. The bond lengths determined from a bounded projection on (001) are C=O 1·24, C–O 1·33, C–C 1·47, C=C 1·34 and OH $\cdots$ O 2·65 Å. (Y. Chatani, Y. Sakata & I. Nitta, to be published in *Acta Cryst.*).

α,ω-Diphenyl-octatetra-yne and α,ω-diphenyl-decapenta-yne

The structure of the α-modification of α,ω-diphenyl-octatetrayne, of which the unit-cell dimensions and space group were reported in *Acta Cryst.* (1959), **12**, 347, was determined at +30 °C. and −110 °C. The molecules are arranged side by side, all the molecular axes being oriented nearly parallel. The bond distances found are:

$$C_1'–C_1 = 1·32, \quad C_1–C_2 = 1·22, \quad C_2–C_3 = 1·36, \quad C_3–C_4 = 1·19,$$

$$C_4–Ph = 1·41 \text{ Å}$$

$$(Ph'–C_4' \equiv C_3'–C_2' \equiv C_1'–C_1 \equiv C_2–C_3 \equiv C_4–Ph) .$$

The carbon chain is slightly distorted from a linear structure. The thermal expansion is largest along the a axis, while sensibly small along the c axis. Torsional oscillation of the phenyl groups was concluded. The crystal structure of α,ω-diphenyl-decapentayne, determined at room temperature and at −130 °C., is not *isostructural* with the octatetrayne. Here, too, the carbon chain is not strictly linear, though to a less extent (T. Watanabé, N. Masaki & H. Mitsuda, to be published in *Acta Cryst.*).

6·5. The crystal structure of 6-methyl 2-thio uracil. By G. S. PARRY & (Miss) F. STRACHAN, *Department of Structural and Inorganic Chemistry, The University, Leeds, 2, England.*

6-methyl 2-thio uracil, a drug which depresses the activity of the thyroid gland, crystallizes in the monoclinic system with cell dimensions

$$a = 13·05, \quad b = 14·49, \quad c = 4·44 \text{ Å}, \quad \beta = 132·5°.$$

The unit cell contains four molecules in the space group $P2_1/a$. As the 00*l* reflexions were observed to be very strong and as (001) was a perfect cleavage, a layer structure was suggested with all molecules centred on $z \approx 0$ and this was confirmed by the subsequent 2-dimensional analysis.

The well resolved c-axis projection was solved by locating the sulphur atom by Patterson methods and subsequently searching for a structure showing a reasonable arrangement of NH $\cdots$ O hydrogen bonds within the molecular layers. The projection was refined by Fourier methods including difference syntheses. The molecular inclination to the plane (001) was estimated from an electron-density projection based on the phase relation $s(h0l) = s(h00)$. This relation was found to be completely accurate as the z parameters were very small ($< 0·15$ Å in the final analysis). Approximate z parameters based on this molecular tilt were refined by trial considering only

$$F(0kl)_{k \text{ odd}} (\approx 8\pi l \sum_j f_j z_j \sin 2\pi k y_j) .$$

Allowance for anisotropic thermal motion of the molecules was made by assuming different temperature factors parallel and perpendicular to the molecular layers. Final values were estimated to be $B_{||} = 3·6$, $B_{\perp} = 5·9$ Å^{-2}.

Within the pyrimidine ring, the final bond lengths (using chemical numbering) were:

$$N_1C_2 = 1·30, \quad C_2N_3 = 1·33, \quad N_3C_4 = 1·43, \quad C_6N_1 = 1·41 \text{ Å},$$

$$C_4C_5 = 1·41, \quad C_5C_6 = 1·30 \text{ Å};$$

and for the bonds external to the ring:

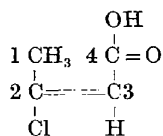$$C_2S = 1·73, \quad C_4O = 1·17, \quad C_6CH = 1·45 \text{ Å} .$$

Only one intermolecular NH $\cdots$ O hydrogen bond is formed. Its length is 2·80 Å and it links the molecules into chains parallel to the a-axis. These hydrogen bonds are not of themselves sufficient to account for the formation of well defined molecular layers and it is of interest therefore that two NH $\cdots$ S contacts of 3·48 Å and related by a centre of symmetry occur between molecules in neighbouring chains. It is thought that these contacts may represent weak hydrogen bonds.

A detailed account of this work will be submitted for publication in *Acta Cryst.*

6·6. Crystal and molecular structure of β-chlorocrotonic acid. By MARIO MAMMI, C. GARBUGLIO & E. FRASSON, *Laboratorio Ricerche Sicedison S.p.A., Bollate, Milano, Italy.*

β-Chlorocrotonic acid, *cis* form, crystallizes out in fine monoclinic needles, space group $P2_1/c$ with four molecules in the unit cell of the following dimensions

$$a = 4·92, \quad b = 8·80, \quad c = 12·81 \text{ Å}, \quad \beta = 94° \ 46'.$$

$$\begin{array}{cc} & \text{OH} \\ & | \\ 1\ \text{CH}_3 & 4\ \text{C}=\text{O} \\ | & | \\ 2\ \text{C}\!=\!\!=\!\!=\!\text{C3} \\ | & | \\ \text{Cl} & \text{H} \end{array}$$

Due to the high vapour pressure of the acid we have worked with mono-crystals of cylindrical form obtained from the melt in the sealed Lindeman capillary. The choice of axis of crystals in the cylindrical form was computed adopting Buerger's method of cell reduction. The structure analysis was carried out on the levels $0KL$ and $H0L$ with the aid of Fourier syntheses and difference syntheses with the thermic isotropic correction for each atom. The value of R, the usual discrepancy factor, was $0\cdot15$ for reflexions $0KL$ and $0\cdot16$ for $H0L$.

Asymmetric hydrogen bond of normal length ($2\cdot64$ Å) determines the formation of dimers. Atoms of each dimer are on the plane and this is in the agreement with the partial character of double bond between C_3–C_4 ($1\cdot44$ Å).

The above work may appear in *Acta Cryst.*

6·7. A refinement of the crystal structure of ammonium oxalate hydrate at 30 °K. By JOHN H. ROBERTSON, *School of Chemistry, The University, Leeds 2, England.*

This investigation was chosen because of the interest attaching to the shape of the oxalate ion, which in this particular crystal is twisted instead of having the expected planar configuration. The structure of the crystal was first elucidated by Hendricks & Jefferson (1936) and was later refined, at room temperature, by Jeffrey & Parry (1952) who, however, used two 2-dimensional projections only. The angle of twist is about 28° at room temperature. The work to be described is a refinement based on 3-dimensional data and aims at establishing the exact conformation of the ion at a temperature at which thermal motion is largely eliminated. The collection of data has been carried out by Weissenberg and oscillation photography, with the crystal at about 30 °K. cooled by a stream of hydrogen from a gas-flow cryostat.

6·8. The crystal and molecular structure of alloxan and alloxantin. By CHATAR SINGH, *Cavendish Laboratory, Cambridge, England.*

Alloxan monohydrate, $C_4H_4N_2O_5$, crystallizes in the triclinic space group $P\bar{1}$ with two molecules per unit cell. The dimensions of the cell are:

$$a = 5\cdot764,\ \ b = 6\cdot758,\ \ c = 8\cdot141\ \text{Å},$$
$$\alpha = 75°\ 7',\ \ \beta = 82°\ 25',\ \ \gamma = 66°\ 53'.$$

The structure has been determined by direct methods using the equation relating the signs of three unitary structure factors, $S(h')S(h+h') \approx S(h)$. Unitary structure factors of the b-axis projection were used in a programme developed by Dr Cochran for EDSAC II to obtain probable sets of signs, one of which proved to be correct. The structure has been refined by two-dimensional difference Fourier syntheses using visually estimated intensities for all the three axial-projections. The R-factor for the cb- and c-axis is 8% and for the a-axis is 12%. The results show no unusual features in the

C–C, C–N, and C–O bond lengths of the pyrimidine ring but the interesting feature of the compound is the existence of two hydroxyl groups attached to $C_{(5)}$. A system of hydrogen bonds link the molecules together, the lengths of which range from $2\cdot7$ Å, to $2\cdot9$ Å.

Work is now in progress on more accurate measurement of the X-ray intensities of the a- and c-axis projections for the accurate determination of the electron density and the location of the hydrogens. The results of this work should be available before the Congres.

Alloxantin dihydrate, $C_8H_6N_4O_8$, $2H_2O$, crystallizes in the triclinic space group $P\bar{1}$ with one molecule per unit cell; the dimensions of which are:

$$a = 6\cdot691,\ \ b = 6\cdot864,\ \ c = 7\cdot284\ \text{Å},$$
$$\alpha = 67°\ 19',\ \ \beta = 84°\ 10',\ \ \gamma = 71°\ 10'.$$

The structure has been determined by solving the b-axis projection by direct methods using sign relations. The refinement has been done by two-dimensional difference Fourier syntheses on the planes (100), (010), (001) and (01$\bar{1}$). The R-factor for plane (010) is 5%, including the hydrogens, 11% for (100) and (001) and 8% for (01$\bar{1}$). The results show that the structure conforms with the pinacol formula and not the hemiacetal formula sometimes given. The bond length show no departures from the normal. The water molecules are linked by a system of hydrogen bonds to the parent molecules.

To appear in *Acta Cryst.*

6·9. The crystal structures of some benzene derivatives. By G. FERGUSON, A. T. McPHAIL & G. A. SIM, *Chemistry Dept., The University, Glasgow, W.2, Scotland.*

The crystal structures of a number of substituted benzoic acids, nitro-benzenes and anilines have been determined. Some interesting intra-molecular steric effects have been found.

To be submitted to *Acta Cryst.*

6·10. The crystal structure of mellitic acid, (benzene hexacarboxylic acid). By S. F. DARLOW, *College of Science and Technology, Manchester 1, England.*

Mellitic acid (benzene hexacarboxylic acid, $C_6(COOH)_6$) is orthorhombic, space group $Pccn$, with

$$a = 8\cdot14,\ \ b = 16\cdot50,\ \ c = 19\cdot05\ \text{Å}.$$

The structure consists of layers perpendicular to the a axis. Each layer is formed by molecules in approximately hexagonal array, linked through the carboxyl groups by the hydrogen bonds. The carboxyl groups hydrogen bonded together are not coplanar. The molecules are in two crystallographically independent sets and the differences between them, mainly in the tilts of the carboxyl groups to the benzene rings, are quite large. These last two features of the structure are necessary in order to keep the layers close together, and the structure is an interesting example of the effect of packing considerations on the relative orientation of groups within a molecule, and on the hydrogen bonding between molecules.

This paper will appear in full in *Acta Cryst.*

6·11. The crystal and molecular structure of 2-amino-3-methylbenzoic acid. By GEORGE M. BROWN* & RICHARD E. MARSH, *California Institute of Technology, Pasadena, California, U.S.A.*

Data:

$$a = 11·48, \ b = 4·044, \ c = 15·79 \ \text{Å}, \ \beta = 91° \ 18'$$

(subject to slight revision); $P2_1/c$, $Z = 4$; nearly 1600 Cu $K\alpha$ intensities. After solution from the [010] Patterson synthesis and 2-D refinement, y parameters were found by trial, and coordinates and anisotropic thermal parameters of the heavy atoms were refined in eighteen 3-D least-squares cycles (diagonal). Hydrogen coordinates from 3-D difference maps were included in the structure factor calculations after cycle eight, but not optimized. Refinement ended with two least-squares adjustments of hydrogen coordinates only. $R = 0·057$. E.s.d. of atomic coordinates: 0·0011 to 0·0018 Å for heavy atoms; about 0·03 Å for hydrogens.

The molecules form centrosymmetric dimers by hydrogen bonding through the carboxyl groups (O–H $\cdots$ O distance 2·645 Å). The ring atoms are almost exactly coplanar; the others show slight deviations from the best ring plane. The molecular symmetry overall, including hydrogen atoms, is approximately m. Bond lengths and angles:

C_1–C_2, 1·415; C_2–C_3, 1·420; C_3–C_4, 1·380; C_4–C_5, 1·395; C_5–C_6, 1·371; C_6–C_1, 1·407; C_1–C_7, 1·464; C_2–N, 1·367; C_3–C_8, 1·502; C_7–O_1, 1·319; C_7–O_2, 1·233; $O_2 \cdots$ N (non-bonded), 2·705; N $\cdots C_8$ (non-bonded), 2·829; average C–H, 1·00; average N–H, 0·90; O_1–H, 0·93 Å; C_1–C_2–C_3, 118·8°; C_2–C_3–C_4, 119·2°; C_3–C_4–C_5, 122·3°; C_4–C_5–C_6, 118·8°; C_5–C_6–C_1, 121·3°; C_6–C_1–C_2, 119·6°; C_6–C_1–C_7, 118·9°; C_7–C_1–C_2, 121·5°; C_1–C_2–N, 122·4°; C_3–C_2–N, 118·8°; C_2–C_3–C_8, 119·9°; C_4–C_3–C_8, 120·9°; C_1–C_7–O_1, 114·7°; C_1–C_7–O_2, 124·5°; O_1–C_7–O_2, 120·8°.

A second set of data (different observer) from the same films was treated independently and used in two heavy-atom least-squares cycles. For these data: $R = 0·076$; e.s.d. of coordinates average just slightly higher. Between the two sets of data some serious discrepancies appear among large, low-angle reflections. The bond lengths from the second set, however, differ from those above only by an average of 0·002 Å and a maximum of 0·005 Å. The differences in angles are correspondingly small.

To be published in *Acta Cryst.*

6·12. The crystal structure of nitranilic acid hexahydrate. By E. KROGH ANDERSEN, *Chemical Laboratory, Royal Veterinary and Agricultural College, Copenhagen, Denmark.*

Nitranilic acid (2,5-dihydroxy-3,5-dinitroquinone) hexahydrate crystallizes in the monoclinic system. The space group is $P2_1/c$, with two molecules in the unit cell. The

* Present address: Chemistry Division, Oak Ridge National Laboratory, Post Office Box X, Oak Ridge, Tennessee, U. S. A.

structure has been determined from projections and details of the molecular geometry has been obtained.

6·13. Investigations of some benzoquinone-monoximes (nitrosophenols) and their derivatives. By C. ROMERS, E. FISCHMANN, A. J. H. UMANS & E. HAVINGA, *The University of Leiden, Organic Chemistry Department, The Netherlands.*

Recently a study has been made of the structural and chemical features of several quinone-monoxime (nitrosophenol) derivatives. Spectro-photometry, synthetical work and X-ray diffraction methods were the main tools of investigation.

(1) 2-Chloro-5-methyl-p-benzoquinone-4-oxime exists in two stable forms, yellow crystals (α) and white fibres (β). In the α-form the NOH group is *syn* with respect to the Cl atom while hydrogen bonds (2·70 Å) which connect the CO group of one molecule with the NOH group of the next molecule act as links in infinite chains. The β-form consists of helical chains of hydrogen-bonded molecules with the NOH groups *anti* with respect to the Cl atoms. The β-form—not the α-form—was found to give a blue coloured product with iodine: the channel within the helix seems sufficiently wide to contain iodine molecules.

(2) 2-Chloro-p-benzoquinone-4-oxime acetate is found in two forms. In the stable α-form the NOCOCH$_3$ group is *syn* with respect to the Cl atom and in the unstable β-form these two groups are in *anti*-configuration.

(3) 5-Alkoxy-o-benzoquinone-2-oximes occur in two different forms, α and β, in which the α-form is usually the stable one.

α-5-(2'-Chloroethoxy-)-o-benzoquinone-2-oxime has an oxime structure with, again, intermolecular hydrogen bonds between CO and NOH groups, which are in *anti*-configuration. The Cl–C_2H$_4$–O group is in *gauche* conformation.

β-5-(2'-Chloroethoxy)-o-benzoquinone-2-oxime and the corresponding n-propoxy compound, however, do not have intermolecular hydrogen bonds in their crystals, but presumably have an intramolecular bond between the CO(H) and NO(H) group of the same molecule. These CO(H) and NO(H) groups are in *syn*-configuration. The R–C_2H$_4$–O group, again, has a *gauche*-conformation. The bond distances as well as the striking pleochroism of these layer-packed molecules show that these β-forms are nitrosophenol compounds.

6·14. The crystal structures of some acid salts, and some apparently symmetrical hydrogen bonds. By J. C. SPEAKMAN, *Chemistry Department, The University, Glasgow, Scotland.*

Many monocarboxylic acids, HX, form crystalline acid salts with formulae such as MHX_2. About a dozen such compounds have now been studied by X-ray diffraction. The proposed paper would briefly summarize earlier results and briefly describe some recent analyses. The salts recently studied include sodium hydrogen diacetate (a preliminary account of whose structure is in *Proc. Chem. Soc.*, 1959, p. 316), potassium hydrogen di-p-nitro-

benzoate, and some acid salts of the halogeno-benzoic acids, of glycollic acid, and possibly of some others.

The acid salts studied fall into two categories: *Type B* yields an infra-red spectrum which approximates to a superposition of the spectra of the free acid (HX) and its salt (M^+X^-); and in their crystals HX and X^- are separately distinguishable. *Type A* gives a different, and anomalous, spectrum; and in their crystals HX and X^- are not distinguishable, being related by some crystallographic symmetry element and joined by a hydrogen bond that is—at least formally—symmetrical. This unusual kind of hydrogen bonding is presumably connected with the spectral anomaly.

If a hydrogen bond is to be strictly symmetrical, with its proton oscillating in a single potential-well at the mid-point between the oxygen atoms, it must be very short, with O $\cdots$ O perhaps $< 2 \cdot 4_5$ Å. Although the hydrogen bonds in the acid salts of type B so far studied are uniformly 'short' (i.e. $< 2 \cdot 6_5$ Å), they are not generally short enough (nor have they been accurately enough measured) to satisfy this severe condition for symmetry. Therefore their apparent symmetry could be merely statistical. But the bond in sodium hydrogen diacetate has been more accurately measured, in a three-dimensional analysis, it proves to be very short, and it may possibly be genuinely symmetrical.

6·15. The crystal structure of sodium formaldehyde bisulphite. By J. H. RAYNER, *Rothamsted Experimental Station, Harpenden, Herts, England.*

Sodium formaldehyde bisulphite, recrystallized from methanol, has the composition NaHSO₃.HCHO and decomposes in damp air to the hemihydrate. Crystals coated in cedar wood oil showed no signs of progressive decomposition and the powder photograph of a ground crystal showed the anhydrous compound. The single crystal X-ray diffraction pattern showed streaks parallel to c^* due to a partially disordered structure. The structure can be imagined to be based on an ideally disordered cell with

$$a = 5 \cdot 15, \quad b = 6 \cdot 45, \quad c = 12 \cdot 8 \text{ Å}$$

and space group *Pcmn* containing 8 half molecules, one statistical half molecule forming the asymmetric unit. The $h0l$ and $0kl$ zones were free from streaks and correspond to projections which are the same for the ideally ordered and ideally disordered structures. Satisfactory electron-density maps were obtained for these zones and the two interpenetrating 'molecules' of the disordered structure could be separated on stereochemical grounds and the structure of the formaldehyde bisulphite ion shown to be $(SO_3.CH_2.OH)^-$. The ions are linked in 2_1 spirals parallel to b by hydrogen bonds from OH to an O attached to S. In the disordered structure spirals going 'up' and 'down' b interlock so that their sulphur atoms coincide. It is suggested that in the ideally ordered structure, to which the structure observed tends, spirals adjacent to one another in the a direction go in opposite directions along b. The layers parallel to (001) formed by these spirals are interleaved with sodium ions and the layers can be superposed in two ways differing in the direction of the spirals to give an ordered orthogonal cell with

$$a = 10 \cdot 3, \quad b = 6 \cdot 45, \quad c = 25 \cdot 6 \text{ Å}$$

but with only monoclinic symmetry $B1\ 2_1/a\ 1$ corresponding to primitive cells with

$$a = 10 \cdot 3, \quad b = 6 \cdot 45, \quad c = 13 \cdot 8 \text{ Å}, \quad \beta = 68 \cdot 1° \text{ and } 111 \cdot 9°.$$

To be submitted for publication in *Acta Cryst.*

6·16. Crystal data of some new organic compounds. By M. FONT-ALTABA, *Rocafort, 111, Barcelona, Spain.*

The crystal data of a series of compounds derivating from the 5-nitro-2-furoilacetic acid are determined. The powder diagram of these compounds are obtained by a quadruple camera of focalization of the type Guinier–De Wolff, and are wholly interpreted. The lattice constants and the space group are deduced from the Weissenberg diagrams. The X-ray data are completed with the optical and micromorphological study.

To be published in *Acta Cryst.*

6·17. The structure of calycanthine. By T. A. HAMOR & J. MONTEATH ROBERTSON, AND IN PART H. N. SHRIVASTAVA & J. V. SILVERTON, *Chemistry Department, The University, Glasgow W. 2, Scotland.*

The structure of the alkaloid calycanthine $C_{22}H_{26}N_4$ has been determined by means of a 3-dimensional X-ray analysis of the dihydrobromide dihydrate

$$C_{22}H_{28}N_4Br_2 . 2 H_2O .$$

The crystals are orthorhombic,

$$a = 9 \cdot 61, \quad b = 14 \cdot 13, \quad c = 16 \cdot 97 \text{ Å} ,$$

space group $P2_12_12_1$ with four molecules per unit cell. The positions of the bromine atoms were found from the sharpened Patterson synthesis and the Fourier synthesis based on the heavy atom phases enabled 15 of the 28 light atoms (C, N and O) to be placed. In succeeding Fourier syntheses the remaining atoms could be placed and their coordinates refined. Further refinement by least-squares using anisotropic temperature factors has reduced the discrepancy over the 2111 observed planes to about 11%.

A preliminary account of this work has been published in *Proc. Chem. Soc.*, 1960, pages 78–80.

6·18. The structure of dl-alphaprodine hydrochloride, and the absolute configuration of codeine hydrobromide dihydrate. By G. KARTHA,* F. R. AHMED & W.H. BARNES, *Pure Physics Division, National Research Council, Ottawa, Canada.*

The structure of dl-alphaprodine hydrochloride

(dl-α-1:3-dimethyl-4-phenyl-4-propionoxy piperidine)

has been determined by the isomorphous replacement method with the aid of data for the hydrobromide. It has been refined by three-dimensional Fourier and differential syntheses. The stereochemical configuration found for the alphaprodine molecule agrees with that of one of four

---

* National Research Council Postdoctorate Fellow, now at Rosewell Park Memorial Institute, Buffalo, N.Y., U.S.A.

possible isomers and confirms that proposed by Reckett and co-workers (*Chem. & Ind.* (1959), **19**) on conformational and other grounds. The piperidine ring has the chair form with the phenyl ring equatorial and the propionoxy chain axial, the methyl group on C(3) is *trans* to the phenyl ring on C(4). The phenyl ring is definitely planar.

The structure of codeine hydrobromide dihydrate ($C_{18}H_{21}O_3N$. HBr . 2 H_2O), previously determined in this laboratory from two-dimensional projections, has been refined by four cycles of differential syntheses, including correction for finite summation, with the use of a complete set (Cu radiation) of three-dimensional intensity data. For determination of the absolute configuration of the codeine molecule, the intensities $I(hkl)$ and $I(h\bar{k}l)$ have been remeasured more accurately on a Geiger-counter spectrogoniometer for over 100 low-order reflections. The corresponding structure factors have been calculated for the refined structure, with the hydrogen atoms assumed to be in their theoretical positions, and have been corrected for the anisotropic vibration and anomalous scattering of the bromine atom. The differences in the calculated structure factors for twenty-five (hkl) and $(h\bar{k}l)$ reflections agree in direction and approximate magnitude with those observed, thus uniquely establishing the absolute configuration.

A paper on 'The Crystal and Molecular Structure of dl-Alphaprodine Hydrochloride' is in Press, *Acta Cryst.*, 1960; a paper on the refinement of the structure of codeine hydrobromide dihydrate and the absolute configuration of the codeine molecule probably will be submitted to the same journal.

6·19. Die Strukturanalyse von Phyllochlorinester.
Von W. Hoppe & G. Will, *Abteilung für Röntgenstrukturforschung am Max–Planck-Institut für Eiweiss- und Lederforschung, München 2, Deutshland.*

Phyllochlorinester, $C_{33}H_{38}N_4O_2$,
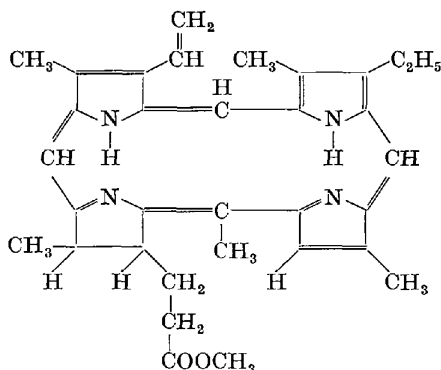
ist ein Chlorophyllderivat, in welchem im wesentlichen der für die Kristallisation ungünstige und sterisch uninteressante Phytolrest abgespalten ist (unter Erhalt der sterischen Konfiguration des porphyrinähnlichen Ringes mit seinen beiden asymmetrischen C-Atomen). Die Strukturaufklärung dieses schweratomfreien Kristalls ermöglichte eine Erprobung der von uns entwickelten neuen Methoden (diffuse Streuung, Faltmolekülmethode) an

einem komplizierten Problem: Der Kristall ist azentrisch und enthält 39 leichte Atome in der asymmetrischen Einheit; er ist die atomreichste azentrische Leichtatomstruktur, die bisher gelöst wurde.

Phyllochlorinester kristallisiert monoklin C_2^2–$P2_1$,

$$a = 12,23, \quad b = 14,82, \quad c = 7,87 \text{ Å}, \quad \beta = 94° 59',$$
$$D = 1,20_6, \quad Z = 2 .$$

Aufnahmen der diffusen Streuung um [010] und um die Normale der Molekülebene (eine irrationale Richtung im Kristall), (W. Hoppe, *Z. Kristallogr.* (1957), **108**, 335), gestatteten durch Vergleich mit der gerechneten Fouriertransformierten des Porphyrinringes die Ermittlung der Lage der Porphyrinringebenen (mit einer Neigung gegen (001) von 28°) sowie die Orientierung der Ringe in ihrer Ebene.

Pattersonprojektionen auf (010) und (001) bestätigten die Ergebnisse der diffusen Streuung und gestatteten darüber hinaus durch Anwendung der Faltmolekülmethode (W. Hoppe, *Z. Elektrochem.* (1957), **61**, 1076) in der Projektion auf (001) eine weitere Kontrolle der Orientierung der Moleküle. Mit Hilfe der gemischtindizierten Faltmoleküle konnten schliesslich auch die Translationsparameter eindeutig ermittelt werden.

Durch Fouriersynthesen in den Projektionen auf (010) und (001) wurden diese Strukturvorschläge geprüft, wobei anfangs (bes. in (001)) der aus den obigen Untersuchungen in seiner Lage und Orientierung bekannte Porphyrinring zur Berechnung der Phasen herangezogen wurde und somit die Aufgabe eines Schweratoms übernahm. In sukzessiven Fouriersynthesen wurden die Koordinaten des Ringes verbessert und die am Ring unmittelbar angreifenden Seitenkettenatome festgelegt. Zur Fortführung der Strukturuntersuchung wurden dreidimensionale Fouriersynthesen gerechnet. Auch hier wurde in der ersten Synthese der Ring als 'Schweratom' in die Rechnung eingegeben und in üblicher Weise in sukzessiven Synthesen die weiteren Atome der Seitenketten lokalisiert.

To be published in *Acta Cryst.* or *Z. Kristallogr.*

6·20. On the structure of 'samandarin' an alkaloid containing an oxazolidine system. By G. Weitz & E. Wölfel, *Eduard–Zintl-Institut, Technische Hochschule Darmstadt, Darmstadt, Deutschland.*

Samandarin ($C_{19}H_{31}O_2N$) is the main alkaloid in the poison of the salamander. Its structure is of interest because it is the only alkaloid so far known in animals. The investigation of the structure by chemical and spectroscopical methods has been carried out by C. Schöpf and collaborators. From this work it was probable, that it has a sterine-type structure containing an oxazolidine system. The HCl, HBr and HJ-salts were found to be most suitable for X-ray work. They crystallize with 1 methanol. (Space group $P2_1$ with 2 molecules in the unit cell.) There are different modifications and it turned out to be difficult to grow the metastable monoclinic modification. After a short time the monoclinic crystals become triclinic. The position of the heavy atom has been derived from a Patterson projection of the HJ-salt. Taking the same position for the Br⁻, the signs for the Fourier projection were derived. The first projection showed 19 maxima. The isotypic replacement

technique did not lead to straightforward results although the structures of the 3 salts seemed to be isotypic.

After 7 cycles plausible x and z parameters of all C-, N- and O-atoms were derived of HBr. Several difference Fouriers have been calculated to improve the atomic positions.

A similar treatment has been undertaken with the HJ which showed slightly different atomic position. With suitable thermal parameters of the different atoms a reliability factor of ≈ 0.25 was reached. With the help of the x and z coordinates a three-dimensional model of the molecule was constructed. By shifting the molecule against the heavy atom optimal mutual positions were found where the best agreement between observed and calculated structure factors was reached. With the atomic position (except of methanol) the phases were determined and a three-dimensional Fourier synthesis was calculated on the IBM 650 which confirmed our model and showed the methanol y-positions approximately. Further Fourier synthesis and refinement procedures on the IBM 650 and the IBM 704 are planed. We hope to have the refinement completed to a certain until the Cambridge meeting.

6·21. The structure of menthyl trimethylammonium iodide. By E. J. GABE & D. F. GRANT, *Viriamu Jones Laboratory, University College, Cardiff, Wales.*

Menthyl trimethylammonium iodide ($C_{13}H_{28}NI$) crystallizes in the space group $P2_12_12_1$ with

$$a = 8.4, \quad b = 12.4, \quad c = 15.0 \text{ Å}, \quad Z = 4, \quad \mu = 178 \text{ cm.}^{-1}.$$

Two-dimensional methods were used to locate the iodine atom, but were unsuccessful in solving the structure.

Three-dimensional data were collected with a spherical crystal and absorption corrections applied. These data were used to calculate a three-dimensional Fourier map, the phases used being those of the iodine atom alone. A vector-convergence map was also calculated from a three-dimensional sharpened Patterson. The positions of five of the fourteen light atoms were found by comparing these two maps, and a second Fourier was calculated with the phases of these five atoms and the iodine atom. Successive calculations of this kind ultimately yielded the structure and refinement along these lines is proceeding. The R_0 value is 15% at present.

At the moment it appears that the six-membered ring is boat-shaped though badly buckled, and the three substituents, the trimethylammonium, isopropyl and methyl groups, are equatorial. The configuration adopted is such that the three carbons of the trimethylammonium group are approximately equidistant from the iodine ion at about 4·2 Å.

Full account will appear in *Acta Cryst.*

6·22. The crystal structure of α_1-bromopicrotoxinin. By B. M. CRAVEN, *Crystallography Laboratory, University of Pittsburgh, Penna, U.S.A.*

α_1-Bromopicrotoxinin ($C_{15}H_{15}O_6Br$) is one of a number of halogen substituted derivatives of picrotoxinin, whose crystal data have previously been reported (B. M. Craven, *Acta Cryst.* (1959), **12**, 254).

The present compound is orthorhombic $P2_12_12_1$,

$$a = 13.40, \quad b = 11.60, \quad c = 8.86 \text{ Å}, \quad Z = 4 .$$

A three-dimensional crystal structure analysis has been carried out using the heavy atom method of phase determination. The lighter atoms were all revealed in the initial Fourier synthesis and their positions refined by two successive Fourier cycles. Subsequent refinement was by three cycles of differential synthesis and finally by the method of least-squares, with anisotropic thermal parameters for the bromine atom only.

The molecular structure and stereochemistry obtained (I) completely confirm the brilliant deductions by Conroy (*J. Amer. Chem. Soc.* **79**, 1726) which were based on degradation studies and were later supported by conformational analysis.
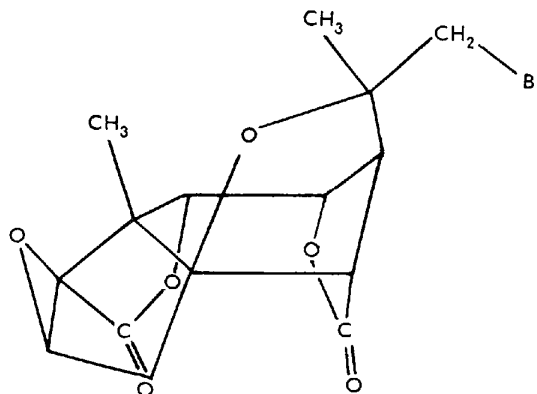
To be submitted to *Acta Cryst.*

6·23. Cevine hydroiodide, $C_{27}H_{43}NO_8 \cdot HI$. By W. T. EELES, *Viriamu Jones Laboratory, University College, Cardiff, Wales.*

Cevine is a veratrum alkaloid which has been the subject of extensive chemical studies. It was suggested by W. A. Jacobs & S. W. Pelletier (*J. Org. Chem.* (1953), **18**, 765) that the skeleton of the molecule is a fused ring system consisting of one pentacyclic ring and five hexacyclic rings. Subsequently the way in which this skeleton could accommodate three methyl groups, seven hydroxyl groups and one etheric oxygen was propounded by D. H. R. Barton, O. Jaeger, V. Prelog & R. B. Woodward (*Experientia* (1954), **X, 3**, 81). An X-ray determination of the crystal structure of the hydroiodide is in progress and has reached a degree of refinement sufficient to constitute confirmation of the formula given in D. H. R. Barton, O. Jaeger, V. Prelog & R. B. Woodward, *Experientia* (1954), **X, 3**, 81.

Subsequent publication likely to be in *Acta Cryst.*

6·24. Structural studies of derivatives of natural products. By S. ARNOTT, A. W. DAVIE, G. FERGUSON, C. J. FRITCHIE, G. H. McCALLUM, J. M. ROBERTSON, G. A. SIM & D. G. WATSON, *Chemistry Department, The University, Glasgow W. 2, Scotland.*

The crystal structures of a number of derivatives of natural products have been elucidated by means of three-dimensional Patterson and electron-density syntheses.

In the case of serine-O-phosphate the molecule has the zwitterionic structure usual with amino acids, but with the negative pole on the phosphoric, rather than the carboxylic group. Connecting the molecules there is an interesting complex of hydrogen bonds, one of which is rather short (2·47 Å).

By the determination of the crystal structure of epilimonol iodoacetate, limonin, $C_{26}H_{30}O_8$, the bitter principle of citrus fruits, has been shown to be a highly oxygenated triterpenoid related to euphol. The analysis was complicated by the presence of two independent molecules in the asymmetric unit, necessitating the location of 76 atoms other than hydrogen.

The stereochemistry of 2-chloro-2-nitroso-10-bromocamphane has been determined. The chlorine atom is found to be in a cis-configuration with respect to the bridge.

6·25. The crystal structure of carotol. By ALLAN LÍNEK, Institute of Technical Physics, Czech. Acad. Sci., Praha, Czechoslovakia.

The behaviour of carotol was in contradiction with the generally accepted chemical formula. We tried parallel with chemical investigations, to revise this formula by X-ray crystal structure methods.

The diffraction data were received of a bromine derivative of carotol. The Br atoms were located from Patterson projections and electron-density projections into the basal planes were obtained after a number of trial experiments.

The bromine derivate of carotol crystallizes in orthorhombic system. The space group is $P2_12_12_1$ and there are 4 molecules in the unit cell. The lattice parameters are

$$a = 6·37, \quad c = 10·71, \quad b = 23·49 \text{ Å}.$$

The chemical formula derived from crystal structure data differs substantially from the chemical formula so far used.

To be published in Czech. Journ. Phys.

6·26. Crystal data of retamine and its chloride and bromide. By M. FONT-ALTABA & L. MIRAVITLLES, Av. José Antonio, 758, Barcelona, Spain.

A complete study of the crystallographic properties of retamine and its chloride and bromide is carried out. The powder diagram of these compounds is obtained by a quadruple camera of focalization of the type Guinier-De Wolff, and are wholly interpretated. The lattice constants and the space group are deduced from the Weissenberg diagrams. The X-ray data are completed with the optical and micromorphological study.

To be published in Acta Cryst.

6·27. Structures of medium-sized aliphatic ring compounds. By EFFI HUBER-BUSER, R. F. BRYAN, J. D. DUNITZ, H. C. MEZ & H. M. M. SHEAPER, Laboratorium für organische Chemie, Eidg. Technische Hochschule, Zürich, Switzerland.

The determination of the structures of the medium-sized alkanes, $C_nH_{2n}(n, 7\text{--}12)$ and of their derivatives is necessary for the interpretation of the characteristic chemical reactions and thermochemical properties of these compounds. Although various physical methods have hitherto been applied to the problem, the multitude of possible solutions is so great (even assuming all C–C bond lengths and C–C–C angles to be fixed) that definite structural information is obtainable only from X-ray analysis of single crystals.

We have begun a series of such studies. Since the hydrocarbons themselves have low melting points and tend to form disordered structures in the solid state, we have examined a large number of salts of amine-derivatives and of cyclopolymethylene-imines. Most of these were unsuitable for more detailed investigation but we have succeeded in establishing the structures of the following compounds, (i) cyclododecane (12-ring), (ii) 1,6-trans diaminocyclodecane 2 HCl (10 ring), (iii) cyclononylamine HBr (9-ring), (iv) azacyclooctane HBr (8-ring). The results may be summarized as follows:

I. No significant deviations from normal single-bond distances have been observed.

II. The C–C–C valency angles tend to be somewhat greater than tetrahedral.

III. The individual molecular conformations have been obtained. Here they are given in terms of torsion angles (in degrees) about successive bonds for each cycle (together with the approximate point symmetry):

12-ring $\quad +163 \quad -70 \quad -67 \quad +155 \quad -68 \quad -69 \quad +161 \quad -69$
$\quad\quad\quad -68 \quad +155 \quad -67 \quad -70 \ (422),$

10-ring $\quad +156 \quad -60 \quad -60 \quad +64 \quad +57 \quad -156 \quad +60 \quad +60$
$\quad\quad\quad -64 \quad -57 \ (2/m),$

9-ring $\quad -73 \quad -65 \quad +67 \quad +48 \quad -94 \quad +86 \quad -104 \quad +43$
$\quad\quad\quad +84 \quad -61 \quad -81 \quad +78 \quad +45 \quad -95 \quad +95 \quad -104$
$\quad\quad\quad +26 \quad +90$ (two independent molecules (1)),

8-ring $\quad$ all about 90, alternatively $+$ and $-$
$\quad\quad\quad$ (nearly regular crown, $\bar{8}2m$).

IV. The hydrogen positions can be inferred from the observed ring skeletons, assuming the four bonds from each carbon atom to have $2/m(C_{2v})$ symmetry with an appropriate choice of H–C–H angle. It is found that in the 10- and 9-rings (which possess the highest thermochemical strain energies) non-bonded $H \cdots H$ distances of about 1·8 Å must occur. In the 12- and 8-rings, however, where the strain is smaller, the shortest $H \cdots H$ distances are greater than 2·0 Å. It is seen that the torsion angles tend to be close to either 60° (syn-skew) or 180° (anti-planar) except in the 8-ring where impossibly short $H \cdots H$ distances would be produced by an all syn-skew arrangement.

Full length accounts in Helv. Chim. Acta. Some parts will probably be published before the date of the Congress.

6·28. X-ray analysis of some transition-metal complexes with unsaturated hydrocarbons. By J. D. DUNITZ, H. C. MEZ, O. S. MILLS, P. PAULING & H. M. M. SHEARER, Laboratorium für organische Chemie, Eidg. Technische Hochschule, Zürich, Switzerland.

(1) Cycloheptatriene-molybdenum-tricarbonyl,

is monoclinic, $\quad C_7H_8Mo(CO)_3,$

$$a = 13·42, \quad b = 7·14, \quad c = 12·28 \text{ Å}, \quad \beta = 122·25°,$$

space group $P2_1/a$, $Z = 4$. An approximate structure,

derived by the heavy-atom method, has been refined by difference syntheses and least-squares analysis to an R value of 0·06. An interesting feature of the refinement is that in spite of the presence of the molybdenum atom, the hydrogen contributions to the electron density and to the structure factors are discernable. The molecule possesses an approximate symmetry plane passing through the Mo, the CH_2 group of the ring, and one of the CO groups, the three carbonyls being arranged symmetrically on the opposite side of the metal atom to the ring (Mo–C, 1·95 to 1·98 Å, C–O, 1·15 to 1·19 Å). In the 7-membered ring the pattern of single and double bonds is clearly established from the observed C–C distances. The CH_2 group deviates markedly (0·7 Å) from the mean plane of the other six atoms which are only roughly equidistant (2·31 to 2·46 Å) from the metal atom.

2. Crystals of the tetramethylcyclobutadiene-nickel dichloride complex, $C_8H_{12}NiCl_2$, obtained from benzene solution contain solvent of crystallization but are stable for several days when enclosed in glass tubes. The monoclinic crystals have

$$a = 12·72, \quad b = 11·94, \quad c = 8·13 \text{ Å}, \quad \beta = 103·0°,$$

space-group $P2_1/a$, and contain 4 molecules of complex plus 2 molecules of benzene in the unit cell. The approximate structure was derived by standard methods and refined by least-squares analysis to an R factor of about 0·07. The molecule, as it exists in the crystal, is a dimer, $C_8H_{12}Ni_2Cl_4C_8H_{12}$. Each Ni atom has, on one side, the four atoms of the cyclobutadiene ring (Ni–C, 2·01 to 2·05 Å), and on the other side 3 Cl neighbours, two shared with the second Ni to form a 4-membered ring (Ni–Cl, 2·35 Å) and one unshared (Ni–Cl, 2·26 Å). The cyclobutadiene ring (C–C, 1·41 to 1·47 Å) is planar but the methyl groups (C–CH_3, 1·48 to 1·53 Å) are displaced outwards (i.e. away from the Ni atom) by 0·15 to 0·20 Å, probably as a result of steric interference with the Cl atoms. The benzene rings lie between, and approximately parallel to, pairs of C_8H_{12} groups belonging to different molecules and undergo a strong rotational disorder in their own planes. The bond distances in the complex are discussed.

Full length accounts in *Helv. Chim. Acta.*

6·29. The crystal and molecular structure of $Fe(CO)_3(C_6H_5C_2C_6H_5)_2$. By R. P. DODGE & V. SCHOMAKER, *Union Carbide Research Institute, Tuxedo, New York, U.S.A.*

A series of iron carbonyl acetylene derivatives has recently been synthesized (W. Hübel, E. H. Braye, A. Clauss, E. Weiss, U. Krüerke, D. A. Brown, G. S. D. King & C. Hoogzand, *J. Inorg. Nucl. Chem.* (1959), 9, 204; G. N. Schrauzer, *J. Amer. Chem. Soc.* (1959), 81, 5307). Among these compounds a yellow crystalline substance having the formula $Fe(Co)_3(C_6H_5C_2C_6H_5)_2$ was chosen for a structure determination by X-ray diffraction. This compound is of interest because of the possibility that it is in fact tetraphenylcyclobutadiene stabilized by complex formation (H. C. Longuet-Higgins & L. E. Orgel, *J. Chem.Soc.* (1956), p. 1969; D. A. Brown, *J. Inorg. Nucl. Chem.* (1959), 10, 39).

The crystals, kindly supplied by European Research Associates, are monoclinic with

$$a_0 = 8·93, \quad b_0 = 18·73, \quad c_0 = 14·10 \text{ Å}, \quad \beta = 92·6°,$$

four molecules per cell, and extinctions corresponding to space group $P2_1/c$. Diffraction data were obtained by the stationary crystal–stationary counter technique (T. C. Furnas, Jr., *Single Crystal Orienter Instruction Manual*, p. 81) using a General Electric XRD-5 spectrometer equipped with single crystal orienter and scintillation counter. A total of 2306 reflections were measured with a Mo $K\alpha$ source. Special precautions were taken to insure that intensities measured at the rate of 500 per day would maintain good accuracy.

The three-dimensional Patterson function clearly indicated the correct Fe–Fe vectors in the unit cell. A three-dimensional superposition was based on the Fe position and the minimum function was plotted. All but two carbon atoms were located with good accuracy. The structure determination was completed by use of electron-density Fouriers and least squares. The structure is pictured in Fig. 1.
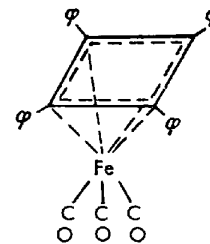

Fig. 1

Publication to appear in *Acta Cryst.*

6·30. The crystal and molecular structures of [3·3] paracyclophane and related substances.* By P. K. GANTZEL, C. L. COULTER & K. N. TRUEBLOOD, *Department of Chemistry, University of California, Los Angeles 24, California, U.S.A.*

The paracyclophanes are molecules in which two benzene rings are joined in the *para* position by bridges of methylene groups so as to form one large ring. The general formula is thus $(CH_2)_m(C_6H_4)_2(CH_2)_n$. The structures of the [2·2]-compound ($m = n = 2$) and the corresponding *meta* derivative were determined by C. J. Brown (*J. Chem. Soc.* (1953), p. 3265, 3278) and have been further refined by us. Lonsdale & Milledge have independently refined the structure of [2·2] paracyclophane using new data (private communication). We have previously reported (American Crystallographic Association Meeting, Ithaca, July 1959) the structure of the di-olefin of [2·2] paracyclophane.

The structure of [3·3] paracyclophane has now been determined. This compound forms crystals of space group $P2_1/n$, with

$$a = 9·715 \pm 0·01, \quad b = 8·138 \pm 0·01, \quad c = 8·524 \pm 0·01 \text{ Å},$$
$$\beta = 90·69 \pm 0·03°, \quad Z = 2.$$

Because the molecules are necessarily centrosymmetric and are of approximately known shape, only two vectors are needed to locate eight of the nine carbon atoms in the asymmetric unit. Ten peaks from a sharpened three-dimensional Patterson were used to obtain the directions of these two vectors. An observed Fourier map revealed the position of the ninth carbon atom. After least-squares refinement, a difference synthesis indicated reasonable positions for all hydrogens. If the fifteen strongest intensities are omitted, R is 8·2%.
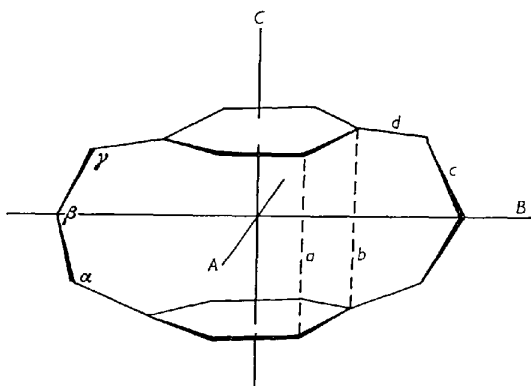
The intramolecular non-bonded distances between the rings are (a) 3·29 and (b) 3·13 Å. The benzene rings are displaced parallel to one another (in directions A and B), are folded slightly about an axis parallel to the long direction of the molecule (B), and are bowed 6·4° at each end. The average values of the angles within the aromatic rings are 116·8 ± 0·4° at the atoms to which the methylene bridges are joined and 121·3 ± 0·4° at the other four atoms. Before corrections for thermal vibration, the average aromatic C–C bond distance is 1·386 ± 0·004 Å, the average single bond distances are 1·506 (bond d) and 1·530 ± 0·005 Å (bond c). The bond angles in the bridges are: α, 113·5; β, 117·2; and γ, 115·8. The corresponding dihedral angles are 65° and 70°.

A detailed comparison is made of the geometries of these different molecules, and in particular of the distortions in both the aromatic rings and the aliphatic bridges.

To be submitted to Acta Cryst.

6·31. The crystal structure of 4,4′-bipyridyl-dihydrobromide.
By B. Mestvedt, Institutt for teoretisk Kjemi, Norges Tekniske Høgskole, Trondheim, Norway.

During the last ten years the Oslo school has carried out electron diffraction studies of a number of molecules consisting of equal conjugated rings connected by C–C bridges, e.g. biphenyl, bithienyl, bipyridyl. These determinations of the steric conditions of the molecules in the gaseous state showed that some freedom of rotation around the C–C bridge usually exists. The mean orientations of the rings deviate from coplanarity.

The aim now was to investigate the steric conditions for the same and similar molecules in the crystalline state. As a part of this work the determination of the crystal structure of some bipyridyls' salts is carried out, including the crystal and molecular structure of 4,4′-bipyridyl-dihydro-bromide.

The structure of 2,2′-bipyridyl is already solved by L. Merrit et al., and shows the planarity of this molecule.

For 4,4′-bipyridyl-dihydrobromide following data are given: Space group $P\bar{1}$.

The unit cell contains 1 molecule.

To show the centrosymmetry of the crystal the method for intensity distribution of A. J. C. Wilson, modified by G. A. Sim for crystals containing heavy atoms, was used.

The structure has been solved by means of electron-density projections and least-squares refinements.

To be published in Acta Chem. Scand.

6·32. The structure of strontium caprylate hydrate.
By E. Stanley, Physics Department, College of Science and Technology, Manchester 1, England.

Strontium caprylate hydrate crystallizes from aqueous solution in the form of very fragile plates. All crystals examined were twins. The unit cell is triclinic with

$$a = 4·7, \ b = 8·0, \ c = 25·8 \ \text{Å}, \ \alpha = 94°, \ \beta = 91°, \ \gamma = 100°,$$

two molecules per unit cell. The space group has been assumed to be $P\bar{1}$.

The position of the strontium atom was determined from Patterson syntheses of the [100] and [010] projections. Both projections have been refined by Fourier and difference methods to $R = 0·16$. The |100| projection has apparent, non-crystallographic, symmetry about the lines perpendicular to the b-axis through $\frac{1}{4}$, 0 and $\frac{3}{4}$, 0. The [010] projection has apparent symmetry pgm ($\beta^* = 90$).

The strontium and oxygen atoms form a crumpled two-dimensional pattern of ionic bonding in (001) plane with the hydrocarbon chains perpendicular to this plane. The hydrocarbon chains appear to be vibrating, perpendicular to their own planes, about the carboxylic group which is more or less stationary.

6·33. The crystal structures of n-pentane, n-hexane, n-heptane, and n-octane.
By N. Norman & H. Mathisen, Central Institute for Industrial Research, Blindern, Oslo, Norway.

The crystal structures of the four normal hydrocarbons n-pentane, n-hexane, n-heptane, and n-octane have been determined using single crystal X-ray techniques. The single crystals were grown in thin capillaries of boron–lithium glass and maintained at temperatures well below their melting points during the exposures. The materials used were of high purity, ranging from 99·63 ± 0·18 to 99·88 ± 0·06%. Rotation and equi-inclination Weissenberg diagrams about the a-axis were obtained. The reciprocal parameters b^*, c^*, and α^* were determined from (0kl) Debye–Scherrer patterns by the method of least squares. The crystal data are (N = number of C-atoms in the molecule; n = number of molecules in the unit-cell).

N	Space group	n	a	b	c	α	β	γ
5	$Pbc2_1$	4	4.10	9.04	14.70	90°	90°	90°
6	$P\bar{1}$	1	4.19	4.75	8.62	97.0°	85.6°	105.0°
7	$P1$	2	4.18	4.75	20.16	93.1°	94.9°	106.2°
8	$P\bar{1}$	1	4.16	4.75	11.00	94.8°	84.5°	105.1°

The crystal structures have been solved by two-dimensional Patterson, electron density and generalized projections and refined by means of two-dimensional difference syntheses and the method of least squares. The structures of both n-pentane and n-heptane are principally different from the structures of the higher odd numbered members of the n-hydrocarbon series, whereas crystals of n-hexane and n-octane are isostructural with for instance n-octadecane and n-eicosane.

Likely to be published in Acta Cryst.

6·34. Refinement of the stucture of hexamethylene-bispropionamide (HMBPA). By L. H. JENSEN, *Department of Anatomy, University of Washington, Seattle 5, Washington, U.S.A.*

The structure of HMBPA (*Acta Cryst.* (1957), **10**, 528) has been refined from three-dimensional X-ray diffraction data in an investigation of the short C–C bonds in the chain of the molecule.

Unidimensionally integrated photometric Weissenberg data were collected from a single cylindrical crystal 0·15 mm. in diameter. The cylinder axis was *b* and data complete through the level with $k = 4$ were collected.

Calculation of the observed structure factors with an overall isotropic temperature factor and coordinates from the projections resulted in a reliability index, R, of 19·3%. Three refinement cycles including individual atom anisotropic thermal parameters reduced R to 9·4%.

The direction of maximum thermal motion is in a plane perpendicular to the axis of the molecule and for most of the atoms makes an angle of about 8° with (010). If the thermal anisotropy is interpreted in terms of molecular oscillation about an axis in the plane of the molecule, the short C–C bonds in the chain are accounted for.

A difference map at the present stage of refinement indicates appreciable positive electron density running down the backbone of the chain, and it is apparent that it cannot be accounted for on the basis of an exponential temperature factor. It is probably due in part, at least, to bonding electrons.

The full length paper will be submitted to *Acta Cryst.*

6·35. Some recent structure determinations of long-chain compounds. By S. ABRAHAMSSON, S. ALEBY, G. LARSSON, K. LARSSON, I. RYDERSTEDT-NAHRING-BAUER & E. VON SYDOW, *Institute of Chemistry, University of Uppsala, Sweden.*

At present work is in progress on unsaturated fatty acids, branched-chain fatty acids, alcohols, simple esters and glycerides.

Oleic acid crystallizes from acetone at −14 °C. at least in two polymorphic modifications. The structure of one of these has been determined to consist of V-shaped molecules. The bending takes place at the double bond and the angle between the two chain parts is 109°. The side packing of these parts deviates from earlier known chain arrangements.

Ethyl stearate exists in two modifications. The β-form has the chain axes tilted towards the end group planes and has a structure closely related to the earlier determined structure of methyl stearate except that no dimerization occurs. The carbon chains pack in the common orthorhombic way (0⊥).

The racemic *l*-monoglycerides show five crystal forms. Two of these, β_1 and β_2, have common structural features. The molecules of the β_2-form are tilted towards the end group planes and are parallel in monomolecular layers. Adjacent layers have opposite tilt of the chain axes. This is also the case in the β_1-form, but here the layers are two molecules thick. The β_1-form has the same chain packing as the β_2-form.

The optically active *l*-monoglycerides exist in four

polymorphic forms. Crystallization from solvents gives rise to two stable modifications, both with the orthorhombic chain packing 0⊥.

6·36. Structure and thermal vibration of the *p*-dichlorobenzene at room temperature. By CARLO PANATTONI, EDOARDO FRASSON, CARMINE GARBUGLIO & SILVIO BEZZI, *Centro di Strutturistica Chimica del C.N.R. and Istituto di chimica organica dell' Universita', Padova, Italy.*

The structure of the monoclinic form of *p*-dichloro-benzene at room temperature has been determined with the same crystals, the same experimental and refinement technique which has been used for the determination of the structure at −140 °C. (E. Frasson, C. Carbuglio & S. Bezzi, *Acta Cryst.* (1959), **12**, 126).

This work has confirmed the geometrical regularity of the benzene ring which has been noted by U. Croatto, S. Bezzi & E. Bua (*Acta Cryst.* (1952), **5**, 825). On the contrary in the triclinic form studied by J. Housty & J. Clastre (*Acta Cryst.* (1958), **10**, 695) the hexagon is very distorted and the molecule is not planar.

In the three recent determinations of the structure of this compound the molecule of *p*-dichloro-benzene appears to have anisotropic oscillations. The directions of maximum vibration in the two determinations on the monoclinic form are very different. At −140 °C. the molecule vibrates around an axis which crosses the molecular centre and the two bonds C–C of the benzene ring parallel to the direction Cl–Cl. At room temperature the molecule vibrates around an axis perpendicular to the molecular plane. This last vibration type has been noted also in the triclinic structure. Such vibration facilitates the transfer of the molecule from the packing which is caracteristic of the monoclinic form to the packing caracteristic of the triclinic form or vice versa.

This note will be sent to the *Gazz. Chim. Ital.* for extensive publication.

6·37. The crystal and molecular structures of some overcrowded halogenated compounds. By G. GAFNER & F. H. HERBSTEIN, *National Physical Research Laboratory, South African Council for Scientific and Industrial Research, Pretoria, South Africa.*

A systematic study is being made of molecules in which the overcrowded atoms are halogens in order to obtain information about the molecular shapes and the interactions among the various halogen atoms. Data have been obtained for nine different crystals (β- and γ-1:2-4:5-tetrabromobenzene; 1:1 molecular compound of 1:2-4:5-tetrabromobenzene and hexabromobenzene; 1:4:5:8-tetrachloronaphthalene; octachloronaphthalene; hexabromobenzene; chloranil; α- and β-1:2-4:5-tetrachlorobenzene) (G. Gafner & F. H. Herbstein, *Acta Cryst.* (1960), in the press). The structures of the first four crystals have been determined.

The crystal structure of β-1:2-4:5-tetrabromobenzene (the polymorph stable at room temperature) has been determined by a three-dimensional least-squares analysis, using separate but isotropic temperature factors for

individual C and Br atoms (G. Gafner & F. H. Herbstein, *Acta Cryst.* (1960), in the press). The molecules are planar to within the accuracy of the measurements; the distance between adjacent bromine atoms is $3 \cdot 377 \pm 0 \cdot 004$ Å, an increase of $\sim 0 \cdot 08$ Å over that in the hypothetical regular molecule. An approximate calculation has been made, using published van der Waals functions, of the conformations expected for 1:2-4:5-tetrahalogenated benzenes. A general survey of available results for polychlorinated and polybrominated benzenes leads to the conclusion that these molecules are planar in the solid state but the situation in the fluid states is still uncertain. The molecular arrangement and twinning in β-1:2-4:5-tetrabromobenzene is discussed. γ-1:2-4:5-tetrabromobenzene (stable above 46 °C.) has a crystal structure closely related to that of the β-polymorph.

The structure of 1:4:5:8-tetrachloronaphthalene has been solved using the three-dimensional Patterson function, and is being refined by three-dimensional least-squares methods. The molecule has symmetry C_2-2 and is considerably distorted from a regular and planar model. The distance between adjacent chlorine atoms is increased to $\sim 3 \cdot 0$ Å, compared to $2 \cdot 4$ Å for the regular model. This increase is accomplished by bending the C–Cl bonds up and down out of the mean molecular plane and also splaying them apart. Deviations from planarity are also apparent in the aromatic ring system.

The 1:1 molecular compound of hexabromobenzene and 1:2-4:5-tetrabromobenzene was found as small amounts of a separate crystalline phase in a commercial sample of the latter compound. Its composition was determined by a combination of infra-red and crystallographic techniques and its structure has been worked out by Patterson and Fourier methods. Crystals of the molecular compound exposed to the air at room temperature lose tetrabromobenzene over a period of a few weeks, leaving behind a pseudo-single crystal of hexabromobenzene having a definite orientation relationship to the original compound.

Part of this work has been accepted for publication in *Acta Cryst.* and the rest will probably be submitted to the same journal.

6·38. The crystal and molecular structures of two isomeric methyl-1:2-benzanthraquinones. By R. P. FERRIER & J. IBALL, *Chemistry Department, Queen's College, Dundee, Scotland.*

Three-dimensional methods have been used in determining the structure of 5-methyl- and 2′-methyl-1:2-benzanthraquinones. The unit cells are respectively, orthorhombic ($P2_1/nb$; $a = 14 \cdot 13$, $b = 23 \cdot 27$, $c = 3 \cdot 94$ Å) and monoclinic ($P2_1$; $a = 20 \cdot 67$, $b = 4 \cdot 06$, $c = 7 \cdot 77$ Å, $\beta = 90 \cdot 8°$). The structures were determined by a combination of optical transforms, trial-and-error and Patterson synthesis. In the refinement, two-dimensional Fourier synthesis was followed by two dimensional least-squares and then by three dimensional least-squares and three-dimensional difference Fourier synthesis. The bond lengths show some unexpected variations and overcrowding within the molecules results in them not being planar.

It is hoped to publish the full account in *Acta Cryst.*

## 6·39. Structure du violurate dihydraté de potassium.
Par HUGUES GILLIER, *Laboratoire de Chimie Cristallographique, Paris, 5°, France.*

Withdrawn.

6·40. Structure de colorants indigoides. Par HÉLÈNE VON ELLER-PANDRAUD, *Laboratoire de Chimie Cristallographique, Paris 5°, France.*

(1) *Structure de l'indirubine*

La structure de l'indirubine, déterminée par essais et erreur, a été précisée par le calcul de projections de densité électronique, de séries différence bidimensionnelles et de projections généralisées. Un raffinement tridimensionnel par la méthode des moindres carrés selon la programmation XR2 sur IBM 704 a fourni les coordonnées atomiques définitives. L'erreur maximale sur les positions
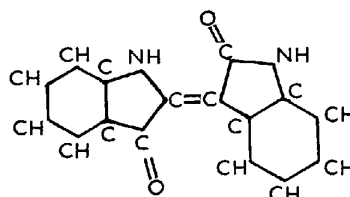
atomiques est inférieure à 0,02 Å. On a pu mettre en évidence la légère configuration en V de la molécule, l'agitation thermique croissante à partir de la liaison médiane éthylénique vers les extrémités des deux demi-molécules, le raccourcissement des liaisons entre chacun des atomes d'azote et les deux atomes de carbone voisins, l'existence de liaisons hydrogène intra- et inter moléculaires. Les premières renforcent la stabilité de la forme moléculaire trans; les secondes associent les molécules en chains parallèles à l'axe *a*, direction d'allongement des cristaux.

(2) *Structure de l'isoindigo*

L'isoindigo cristallise dans le système monoclinique, groupe spatial $C2/m$. La molécule, en position spéciale dans le plan miroir de la maille, est en configuration *trans*. La structure élucidée par essais et erreur, a été
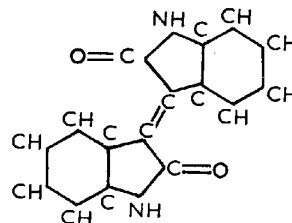

précisée par le calcul de sections de densité électronique et de séries différence. Les distances intra-moléculaires présentent de grandes analogies avec celles de l'indigo, de l'isatine et de l'indirubine. Les liaisons hydrogène qui s'établissent entre atomes d'oxygène cétoniques et groupes

imines autour des centres d'inversion jouent un rôle important dans l'édification du cristal.

6·41. Structure d'un composé rouge de formule indeterminée: probablement une dehydropyrolidone. Par ODETTE LEFEBVRE-SOUBEYRAN & CÉCILE STORA, *Laboratoire de Chimie Cristallographique, Paris, 5°, France.*

Mademoiselle Chauvelier ayant découvert un isomère rouge $C_{23}H_{17}ON$ de la phénylimino-1, pentène-2, hydroxy-3, diphényl-1-5, yne-4 produit d'addition d'aniline et de bisphénétinylcétone sans que les procédés chimiques habituels puissent lui permettre de déterminer laquelle des trois formules qu'elle proposait correspondait à la réalité, nous avons entrepris de déterminer la structure de ce composé afin d'éssayer d'apporter quelques éclaircissements sur sa configuration moléculaire.

Parmi les trois composés: p. iodé, p. bromé et sans atome mourd, seul le dérivé p. bromé (obtenu à partir de la p. bromaniline) rhomboèdrique noncentré ($R3c$) avec 6 molécules par maille, nous a permis de résoudre une projection $x0y$ parallèle au plan moléculaire. D'après cette projection, nous serions très probablement en présence d'une déhydropyrolidone comportant un cycle pentagonal ferméqui pourrait expliqué la coloration intense du composé, sa formule exacte étant: phényl-5, p. bromophényl-1, benzylidine-2, déhydro-4-5, pyrolidone-3, soit

CH——C⁼O
C_6H_5—C⟍N⟋C =CH—C_6H_5
|
C_6H_4Br
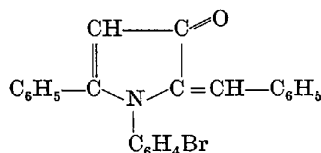
Naturellement ces conclusions ne seront définitives que lorsque la cote des différents atomes sera connue.

Les atomes de brome sont deux à deux superposés dans les plans de symétrie avec glissement, les molécules se répartissant de part et d'autre de ces plans. Les atomes d'azote et d'oxygène sont également superposés. Les différents phényles sont plus ou moins inclinés autour de leur grand axe lié au reste de la molécule par une de ses extrémités et sétué lui-même approximativement dans le plan de la molécule. Les distances interatomiques en ce qui concerne le pentagone, le grand axe des phényles, le brome, seraient aux erreurs de calcul près, en assez bon accord avec les distances de liaison données par Pauling.

6·42 X-ray investigation of some halogen derivatives of benzene and anthraquinone.

»Рентгеноструктурное исследование некоторых галоидопроизводных бензола и антрахинона«. *Г. А. Гольдер, Г. С. Жданов, Л. А. Четкина, В. П. Глушкова Institute for Phys.-Chem. Research. Karpova. Obukha 10, Moscow. Russia.*

Характер взаимодействия NO_2 – и OH групп, связанных с бензольным или антрахиноновым циклами с атомами галоидов, присоединенных к тем же циклам, а также с самими циклами, в значительном мере зависит от размеров присоединенных атомов галоидов и их расположения относительно указанных групп.

На примере Br и Cl производных парадинитробензола

показано, что деформация валентных углов связи $C-NO_2$ значительно слабее деформации угла связи C–Гал. Углы поворота нитрогрупп относительно бензольного кольца увеличиваются с увеличением радиуса атома галоида в орто–положениях.

Характер взаимодействия OH–группы антрахинона сильно зависит от радиуса атома галоида в 1,5 положениях. Сохранение копланарности с антраценооым ядром при присоединении атомов F в 1,5 положения обуславливает сильное их взаимодействие. Выход из плоскости атомов галоидов Br и Cl /последний случай исследован другими авторами/ приводит к значительному ослаблению или полному выключению взаимодействия их с OH–группой.

Статьи будут опубликованы в журнале »Кристаллография«.

6·43. Thermochromism in dixanthylene. By S. C. NYBURG & J. F. D. MILLS, *Department of Chemistry, University College of North Staffs., Keele, Staffordshire, England.*

Dixanthylene(I) changes colour from yellow to blue when the solid

(I)
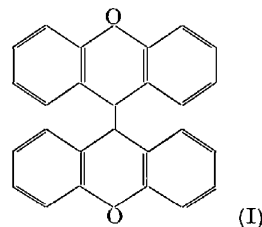
is heated, irradiated or compressed. (The solutions also change colour when heated or irradiated.) The crystal structures of the yellow and blue solid forms have been analyzed and the cause of the colour change revealed.

To be published in *J. Chem. Soc.*

6·44. Crystal-structure studies of polynuclear hydrocarbons. By J. TROTTER, *Chemistry Department, The University, Glasgow, W. 2, Scotland.*

X-ray investigations of the crystal and molecular structures of polynuclear hydrocarbons exhibiting asymmetric annellation effects are in progress.

Crystals of 1,2:7,8-dibenzocoronene are monoclinic, with four molecules in a unit cell of dimensions

$$a = 22·83, \quad b = 5·22, \quad c = 15·77 \text{ Å}, \quad \beta = 103·9°,$$

space group $C2/c$. The structure has been determined from normal and generalized projections along the b-axis. Details of the molecular geometry and dimensions and of the intermolecular separations have been obtained.

Crystals of 2,3:4,5:6,7:8,9:10,11:12,1-hexabenzocoronene are monoclinic, with two molecules in a unit cell of dimensions

$$a = 18·42, \quad b = 5·11, \quad c = 12·86 \text{ Å}, \quad \beta = 112·5°,$$

space group $P2_1/a$. The structure has been determined from normal and generalized projections along the b-axis, and details of the molecular dimensions and intermolecular separations have been obtained.

To be published in *J. Chem. Soc.*

6·45. A study of the structure of cyclo-octadecanonaene near 90 °K. By JUDITH BREGMAN& DOV RABINOVICH, *Department of X-Ray Crystallography, Weizmann Institute of Science, Rehovoth, Israel.*

The crystallographic constants of the recently prepared cyclo-octadecanonaene, $C_{18}H_{18}$ (F. Sondheimer & R. Wolofsky, *Tetrahedron, Letters* (1959), No. 3, p. 3–6) have been measured near 90 °K.

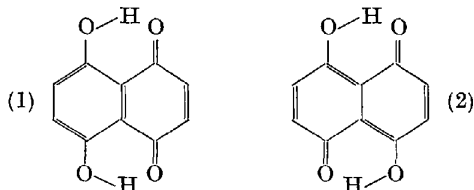$$a = 14·89, \quad b = 4·83, \quad c = 10·23 \text{ Å}, \quad \beta = 111·6°, \quad n = 2.$$

The space group is $P2_1/a$, indicating a molecular center of symmetry, whose presence would preclude an alternation of bond lengths around the carbon ring. Whether the center is real, or apparent due to a packing disorder, cannot be determined at this stage. Room temperature photographs of the $h0l$ zone do not extend beyond $\sin \theta \sim 0·5$; low temperature (90 °K.) data were obtained out to the limit of the copper reflecting sphere. No change in symmetry of the $h0l$ zone was observed on cooling. Refinement of the low-temperature structure is now in progress.

The close similarity of this structure to that of coronene (J. M. Robertson & J. G. White, *J. Chem. Soc.* (1945), p. 607) will be discussed.

Possible journal for publication: *Acta Cryst.*

6·46. Structures des trois formes cristallines de la naphtazarine. Par Madame CLAUDINE PASCARD-BILLY,[*] *Laboratoire de l'I.R.CH.A, sous la direction de Monsieur MERING.*

Les chimistes ont donné à la naphtazarine la formule suivante: 5–8 dihydroxy 1–4 naphtoquinone (1).

(1)   (2)

L'étude structurale des trois formes cristallines de ce composé conduit cependant à admettre la possibilité d'une formule centrée.

Les trois formes cristallines A, B et C, sont monocliniques, et appartiennent au groupe spatial centré $P2_1/c$. Dans tous les cas, les molécules se placent aux centres de symétrie de la maille. En admettant que la centrosymétrie n'est qu'approchée, un essai de raffinement a été fait dans le cas du groupe Pc; cet essai n'a pas abouti. Par contre, il a été possible de raffiner les structures A et B sur des projections équatoriales, dans l'hypothèse du groupe spatial $P2_1/c$, et d'obtenir les positions des atomes avec une précision de 0,02 Å.

Les conclusions qu'on peut tirer de cette étude sont les suivantes: Il est hors de doute que les rayons X donnent une image centrosymétrique de la molécule. Les distances $C=O$ et $C–OH$ sont toutes deux égales à 1,30 Å,

---

[*] Actuellement au laboratoire de Chimie Cristallographique, 1 rue Victor Cousin, direction: Mademoiselle Stora.

mais le raffinement ayant été poussé assez loin, l'auteur ne pense pas que cela puisse être le résultat statistique d'un empilement de molécules non-centrées. De plus, il a été observé une nette différence de densité électronique entre les oxygènes carbonyls et oxydriles. L'auteur suggère l'existence, dans le cristal, d'une molécule centrée, la 4–8 dihydroxy 1–5 naphtoquinone (2).

6·47. The crystal structure of juglone (5-hydroxy-1,4-naphthoquinone). By O. BORGEN, *Institutt for teoretisk Kjemi, Norges Tekniske Høgskole, Trondheim, Norway.*

In the course of an investigation of α-hydroxy-substituted quinones, the structure of juglone has been studied.

The unit cell of the crystals was found to be monoclinic with space group $P2_1/c$, containing two formula units, each of which must have a centre of symmetry. As this is incompatible with the composition of the molecule, the structure is disordered.

A number of diffuse reflections were observed, indicating that the unit cell corresponding to an ordered structure would be twice as large as that of the disordered structure, and have the space group $P2_1/n$.

Similarities of the $0kl$ Weissenberg-film of juglone with that of naphthazarin whose structure has been studied earlier, suggested a trial structure for the disordered case. A number of models have been fitted to the observed intensity data by the least-squares method for comparison.

Likely to be published in *Acta Chem. Scand.*

6·48. Molecular deformation in the overcrowded 1,12-dimethyl 3:4-benzophenanthrene. By F. L. HIRSHFELD & G. M. J. SCHMIDT, *Weizmann Institute of Science, Rehovoth, Israel.*

A partial three-dimensional analysis of the crystal structure of 1,12-dimethyl 3:4-benzophenanthrene at boiling-nitrogen temperature has revealed the molecular shape with an estimated standard deviation averaging 0·005 Å in carbon coordinates and about 0·1 Å in hydrogen coordinates. The methyl carbon atoms are 3·254 Å apart across a crystallographic twofold symmetry axis but each is only 3·047 Å from the opposite substituted carbon atom. Two equivalent methyl hydrogen atoms make contact at 2·0 Å across the twofold axis. The orientation of the methyl groups is such as to maximize the carbon–hydrogen contact distances. Deformation due to overcrowding is distributed throughout the molecular skeleton. Several C–C bond lengths differ by as much as 0·02 Å from values predicted by molecular-orbital calculations of a planar model of 3:4-benzophenanthrene (Berthier, Coulson, Greenwood & Pullman, *C. R. Acad. Sci., Paris* (1948), **226**, 1906) but the relation, if there be any, between these discrepancies and the mode of deformation is not obvious. Anisotropic thermal analysis indicates that the molecule as a whole vibrates fairly isotropically, with an amplitude of about 0·1 Å in every direction, while librating about an axis approximately normal to the mean molecular plane, with an amplitude of 0·04 radian.

The molecular dimensions differ greatly from those reported for the unsubstituted 3:4-benzophenanthrene (Herbstein & Schmidt, *J. Chem. Soc.* (1954), p. 3302). The latter structure is currently being refined from full three-dimensional room-temperature data.

It is hoped that descriptions of both structures will be ready later this year to be submitted for publication in *J. Chem. Soc.*

6·49. Crystal structures and photochemistry of some organic nitrocompounds. By PH. COPPENS & G.M.J. SCHMIDT, *Weizmann Institute of Science, Rehovoth, Israel.*

The crystal structures of two modifications of *p*-nitrophenol and of *o*-nitrobenzaldehyde have been determined as part of a research programme outlined previously (Schmidt, *Acta* (1957), **10**, 793).

The structures of α-*p*-nitrophenol and *o*-nitrobenzaldehyde were obtained from partial three-dimensional low-temperature (90 °K.) and room-temperature data respectively. The structure of the β modification of *p*-nitrophenol, previously analyzed by Toussaint (*Bull. Soc. Sci. Liège* (1954), **23**, 24), was refined from full three-dimensional room-temperature Geiger-counter data. The average standard deviations in the coordinates of the 'heavy' atoms in the three analyzes are estimated to 0·004, 0·007 and 0·002₅ Å respectively.

The (thermodynamically stable) α form of *p*-nitrophenol changes its colour from yellow to red on irradiation by sunlight. The structure of the polymeric product is unknown, but the first step of the reaction is likely to be the transfer of an oxygen from the nitrogroup to the aromatic ring, in analogy with photochemical reactions of other aromatic nitrocompounds (Splitter & Calvin, *J. Org. Chem.* (1955), **20**, 1086; Hastings & Matsew, *J. Amer. Chem. Soc.* (1948), **70**, 3514). This reaction is evidently dependent upon the packing of the molecules in the α-modification, since the β-form and solutions of *p*-nitrophenol are light stable. Differences in the packing arrangement, in particular in the contacts between the oxygen atoms of the nitrogroup and the CH groups of the aromatic ring, of the two forms, will be analyzed and related to the proposed mechanism of the reaction.

o-Nitrobenzaldehyde rearranges in the solid state (as well as in solution) to *o*-nitrosobenzoic acid, the observed configuration of the reactive centers supports the tentative conclusions drawn from the *p*-nitrophenol structures.

A full account of the present investigation will be submitted to the *J. Chem. Soc.*

6·50. The crystal structure of 1,4-dibromocycl (3,2,2)azine. By A. W. HANSON, *Division of Pure Physics, National Research Council, Ottawa, Canada.*

The crystal is monoclinic, probably $P2_1/n$,

$$a = 16·52, \ b = 4·01, \ c = 14·13 \text{ Å}, \ \beta = 91·2°, \ Z = 4 \ .$$

The structure was determined by heavy-atom methods, and refined with the aid of three-dimensional differential syntheses. The molecule is almost exactly planar, and the

distance between adjacent parallel molecules is 3·46 Å. The analysis was complicated by the considerable anisotropy of thermal motion of the bromine atoms.

It is expected that a complete account will appear in *Acta Cryst.*

6·51. The crystal structure of acepleiadylene. By A. W. HANSON, *Division of Pure Physics, National Research Council, Ottawa, Canada.*

A complete account has been published in *Acta Cryst.* (1960), **13**, 215.

6·52. Die Kristallstruktur des d,l-1,4,7-Trithia-2,5,8-endazacyclononan (d,l-$C_6H_9NS_3$). Von A. PREISINGER & F. HOFER, *Mineralog. Institut Universität, Wien I, Austria.*

d,l-1,4,7-Trithia-2,5,8-endazacyclononan kristallisiert aus Pyridin in Form von Stäbchen, die einen Schmelzpunkt von 144 °C. besitzen.
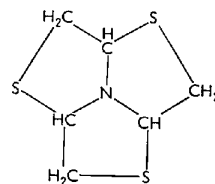
Die kristallographischen Daten ergaben:

$$a = 12{,}250 \pm 0{,}005, \ c = 9{,}265 \pm 0{,}005 \text{ Å}, \ Z = 6,$$

Raumgruppe: $R3c$.

Die Intensitäten wurden mittels der multiplen Filmmethode bestimmt. Die Strukturbestimmung erfolgte mit Hilfe von Patterson- und Fourier-Synthese und deren Verfeinerung. Es wurde eine gute Übereinstimmung der Intensitäten erzielt ($R_{hko} = 0{,}08$). In der z-Richtung liegen abwechselnd Links- und Rechtsmoleküle übereinander. Die Links- bzw. Rechtsmoleküle sind durch schwache Wasserstoffbrücken zwischen S und C räumlich miteinander verbunden. Die intramolekularen Abstände betragen:

N –CH	:	1,486 Å
CH –CH$_2$	:	1,551
CH –S	:	1,812
CH$_2$–S	:	1,811

6·53. Crystal and molecular structure of 2,5-dimethyl-thio-thiophthen. By MARIO MAMMI, RENATO BARDI, CARMINE GARBUGLIO & SILVIO BEZZI, *Centro di Strutturistica Chimica del C.N.R., Padova, Italy.*

By means of X-ray diffraction analysis we have discovered a new type of aromatic system (which we named thio-thiophthen), containing three sulphur atoms on two pentatomic condensed rings (*Nature, Lond.* (1958), **182**, 247; *Gazz. Chim. Ital.* (1958), **88**, 1226).

Such a system may be regarded as the resonance hybrid between four structures, two of them covalent and two polar:

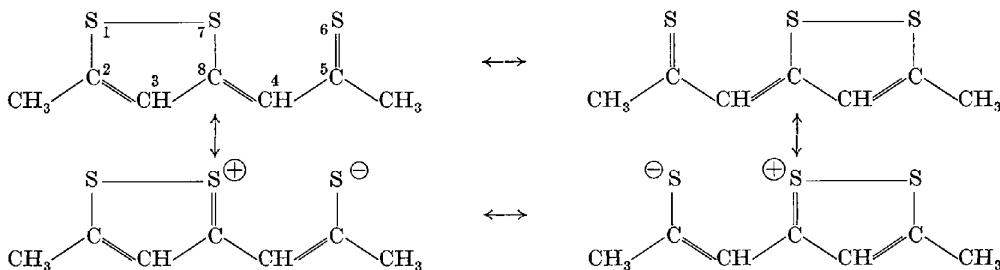
Structure refinement was carried out on (001), (100), and (010) projections by Fourier and difference syntheses, with individual anisotropic temperature factor correction. In the final difference syntheses, all the significant electron-density maxima could be interpreted as hydrogen atoms.

The values of R for the final atomic parameters are 0·12, 0·14, and 0·15 for the reflections of the $hk0$, $0kl$, and $h0l$ types, respectively.

The S–S bond distance observed in this structure is of abnormal length (2·35 Å), and is made up from both fractional σ and π bonds. The central C–S bond (1·74 Å) is longer than the other two (1·65), and the C–C bonds are about the same as in benzene.

These results fully agree with the values predicted by G. Giacometti & G. Rigatti (*J. Chem. Phys.* (1959), **30**, 1633).

The full-length account is likely to be published in *Acta Cryst.*

6·54. The crystal and molecular structure of pyrazole. By H. W. W. EHRLICH, *Chemistry Department, King's Buildings, West Mains Road, Edinburgh 9, Scotland.*

Pyrazole,

The pyrazole structure diagram is shown here.
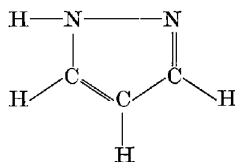
crystallizes in a non-centrosymmetric space group, $P2_1cn$. There are eight molecules in the unit cell, whose dimensions are $8·23 \times 12·84 \times 7·05$ Å, and there are thus two crystallographically independent molecules.

The agreement in bond lengths between the two molecules is very good, but some corresponding bond angles are significantly different.

There is almost a mirror plane at right angles to the plane of the molecule, this symmetry being destroyed by only one hydrogen atom. The position of this hydrogen atom has been fixed by a consideration of the values of $\Sigma[|F_o| - |F_c|]^2$ for the two possibilities.

The results from the analysis show that the bonds with most double bond character exist between the two carbon atoms opposite the NH group, and between the

nitrogen atom of this NH group and its adjacent carbon atom. This would indicate that the betaine form

The betaine form structure diagram is shown here.
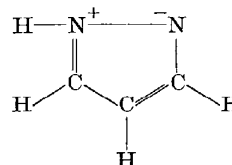
contributes heavily to the resonance hybrid.

Evidence for the existence of charged nitrogen atoms in the ring comes from a consideration of the hydrogen bond lengths, which are 2·93 and 2·86 Å. Bonds of this length have only been reported between $N^+\text{–}H \cdots N$.

This strong hydrogen bond is the foundation of the crystal structure. Long chains of molecules exist, these chains being looped together in an arrangement which bears the same relation to the figure 8 as a helix does to the figure 0. These spirals behave like cylinders, and the crystal consists of a close packed arrangement of these cylinders.

The full account will probably appear in *Acta Cryst.*

6·55. The three-dimensional refinement of positional and anisotropic temperature parameters of β-methyl xyloside, trans-azobenzene, p-azotoluene, hexamethylene diammonium adipate (nylon salt) and catechol. By C. J. BROWN, 53 *Heaton Park Road, Manchester 9, England.*

A group of five organic crystal structures have recently been refined on a Ferranti Pegasus computer using three-dimensional structure amplitude data and anisotropic temperature factors.

β-Methyl xyloside, p-azotoluene and catechol are completely new structure determinations; trans-azobenzene and hexamethylene diammonium adipate (nylon salt) are further refinements of structures already published by other authors but with new intensity data.

The R factor in each case has been reduced to ≈ 6% with corresponding standard deviations of atomic coordinates of < 0·003 Å. The resulting molecular dimensions provide some highly accurate values for inter-atomic bond-lengths and inter-bond angles. In particular, the mean aliphatic carbon–carbon distance in both the xyloside and the nylon salt, where the possibility of resonance seems remote, is ≈ 1·51 Å.

β-Methyl xyloside is the first three-dimensional analysis of a carbohydrate and shows the pyranose ring in the Sachse trans form (chair-shaped). In the asymmetric unit of trans-azobenzene there are two non-equivalent molecules whose dimensions are significantly different. In

the p-azotoluene structure there is disorder in azo link-age, and in the catechol structure there is disorder in the system of hydrogen bonds.

The overall time taken in the determination of the structure of catechol is worthy of mention being ap-proximately three weeks.

It is expected that the structure of β-methyl xyloside will be published in the J. Chem. Soc., and the structures of the other four compounds in Acta Cryst.

6·56. The stereochemistry of molecules containing the C=C=N group. The crystal and molecular structure of N-ethyl-2,2'-dimethylsulphonylvi-nylidineamine. By J. J. DALY, Monsanto Research S. A., Zürich 3/45, Switzerland.

A three dimensional structural analysis of a third compound containing the C=C=N-R group is described. Crystals of N-ethyl-2,2'-dimethylsulphonylvinylidine-amine are orthorhombic $P2_12_12_1$ with

$$a = 12 \cdot 02, \quad b = 5 \cdot 85, \quad c = 14 \cdot 47 \text{ Å}.$$

The bond angle at the nitrogen atom is 144° in sharp contrast to the value of 180° found in two other vinyli-dineamines in which $R = CH_3$. The bond lengths and other bond angles exhibit no unusual features with the ex-ception of the C=N bond which has the length of a normal C≡N bond. It is suggested the linearity of the −N= bond in N-methyl vinylidineamines is due mainly to hyperconjugation.

6·57. The crystal structure of rhodanine, $C_3H_3ONS_2$. By DICK VAN DER HELM, ARTHUR E. LESSOR, Jr. & LYNNE L. MERRITT, Jr., Indiana University, Blooming-ton, Indiana, U.S.A.

The structure of rhodanine,
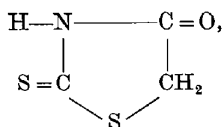
has been determined by three-dimensional Fourier and least-squares methods using an IBM 650 computer. The crystals are monoclinic with

$$a_0 = 10 \cdot 02, \quad b_0 = 7 \cdot 67, \quad c_0 = 7 \cdot 28 \text{ Å}, \quad \beta = 102° 38', \quad Z = 4,$$

space group $P2_1/n$. The molecule is planar. All bonds within the molecule except those adjoining the CH_2 group appear to be involved in resonance structures. The $C(H_2)$–S bond distance is 1·82 Å, in agreement with C–S distances in compounds where no resonance is expected. The $C(=S)$–S bond distance is 1·74, C=S is 1·64, $C(=S)$–N is 1·37, $C(=O)$–N is 1·38, C=O is 1·23 and $C(=O)$–C is 1·51 Å.

The pairs of atoms related by centers of symmetry at the origin and body center of the unit cell are held together by N–H · · · O hydrogen bonds of length 2·85 Å.

The molecules are tightly packed in the unit cell. Chains of atoms, O–S–S—S–S–O, extend along the (211) and the (422) planes, parallel to the [201] line. Such chains are found separated by $\frac{1}{4}a$ and $\frac{1}{2}b$. The origin of the chains shifts $\frac{1}{2}a$, $\frac{1}{2}b$ and $\frac{1}{2}c$. The rest of the molecule fits in the space between these chains.

The sulfur atoms of two molecules approach to within

3·47 Å of each other, indicating a van der Waals radius of 1·72 to 1·73 Å. This is somewhat less than the 1·85 Å given by Pauling but in agreement with other values found in recent investigations.

The final R value, $R = \Sigma ||F_o| - |F_c||/\Sigma |F_o|$ of the deter-mination was 0·14 including all of the nearly 1100 reflec-tions.

To be published in Acta Cryst.

6·58. The crystal structure of 1-methylthymine. By K. HOOGSTEEN, Church Laboratory, California Institute of Technology, California, U.S.A.

As part of a program for the structure determination of compounds related to nucleic acids, the crystal structure of 1-methylthymine
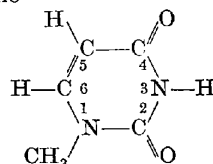
has been determined. The unit-cell parameters and space group were determined from oscillation and Weissenberg photographs;

$$a = 7 \cdot 22, \quad b = 11 \cdot 96, \quad c = 7 \cdot 52 \text{ Å}, \quad \beta = 90° 0',$$

space-group $P2_1/c$ with 4 molecules per unit-cell. Three-dimensional data were collected from Weissenberg photo-graphs along the a- and c-axes using copper radiation. The approximate structure was found by trial and error methods with the help of structure factor graphs. The refinement was carried out by least-squares analyses, initially of the $hk0$- and $0kl$-data, and later of the three-dimensional data. Individual anisotropic temperature factors were introduced and refined for each of the atoms and the positions of the hydrogen atoms were obtained from a three-dimensional difference map. At present the R factor is 0·105.

The plane of the molecule is nearly parallel to (102). The molecules are arranged in pairs, hydrogen-bonded around a center of symmetry. The oxygen atom at C_2 forms a hydrogen-bond with the hydrogen at N_3.

The final results will be submitted for publication to Acta Cryst.

§ 7. Proteins and related compounds

7·1. The structures of ferritin and apoferritin. By PAULINE M. HARRISON, Biochemistry Department, The University, Sheffield 10, England.

Wet apoferritin crystals have a face-centred cubic lattice with $a = 184$ Å and space group $F432$. The mole-cules are composed of identical sub-units, of which there are either 24 (point group symmetry 432) or 12 (point group symmetry 23), in the latter case the molecules being distributed statistically in mutually perpendicular orientations. Chemical evidence is given for excluding a structure with 60 sub-units (532 symmetry). Molecular models having 432 and 23 symmetry are discussed in relation to the X-ray data.

At low resolution (to spacings of about 25 Å) the X-ray data for wet apoferritin crystals of low salt content, can be fitted with the calculated scattering for uniform

spherical shells of external radius about 62 Å and ratio of internal to external radii about 0·6. Signs can therefore be given to structure factors of low index.

Wet ferritin crystallizes in two forms, one of which, ferritin B, is isomorphous with apoferritin. Electron micrographs show that the hydrated iron oxide (which accounts for about 40% of the weight of the ferritin molecule) is at the centre of the molecule and consists of about four particles. With a view to obtaining the structure of the iron-containing part of the molecule, structure factors for the isomorphous ferritin B, apoferritin and apoferritin/ferritin B mixed crystals are compared. The situation is not that of a 'normal' isomorphous replacement by a heavy atom, where the atomic scattering factor of the substituent is known and its position can be found. In this case the scattering factor of the substituent is unknown, although its structure is known to be centred at the centre of the molecule. For certain reflections it can, however, be shown that the signs of the structure factors of the protein and iron oxide fractions are opposite. Using the phases derived for the protein part of the molecule as above, it is then possible to deduce, for certain structure factors, the phases of the iron-containing micelles. These are compared with those derived from the Fourier transforms of models composed of either a single sphere or of 4, 6 or 8 spheres located respectively at the apices of a tetrahedron, octahedron or cube.

Full length account is likely to be submitted to the *J. of Mol. Biol.*

7·2. Studies on the structures of some small spherical viruses. By J. T. Finch & A. Klug, *Birkbeck College, 21, Torrington Sq., London, England.*

(a) Turnip yellow mosaic virus (TYMV)

TYMV is a small approximately spherical virus of diameter 280 Å, consisting of 62% protein and 38% ribonucleic acid. As previously reported (*Biochim. Biophys. Acta* (1957), **25**, 292) precession photographs were obtained from crystals of the virus grown in ammonium sulphate, and from these the space group was determined as $F4_13$ with 16 virus particles per unit cell (lying at the lattice points of a body-centred cubic arrangement). The distribution of the intensities of the X-ray reflections indicated that the virus particles possess the point group symmetry 532, and it was suggested that it was probably the virus protein which was the seat of this symmetry.

Precession photographs have now been obtained from crystals of the nucleic acid free, virus protein particles, which are found accompanying the virus particles in infected plants. These confirm that it is the virus protein which has 532 symmetry and thus consists of 60 asymmetric sub-units.

(b) Poliovirus

The poliovirus particles are about 300 Å diameter and contain about 25% ribonucleic acid. Precession photographs have been obtained from crystals of the virus (Mahoney strain) grown in phosphate–saline solution. The unit cell was found to be orthorhombic with sides 320, 353, and 378 Å (± 6 Å). The space group is of the type $P2_12_12$, but the unique axis has not yet been determined.

The intensity distribution of the X-ray reflections

indicates that this virus also possesses 532 point group symmetry, and that, as in TYMV, this symmetry is associated with the protein component of the virus.

7·3. A section through the basal projection of the tobacco mosaic virus particle. By K. C. Holmes & A. Klug, *Children's Cancer Research Foundation, Boston, 15, Mass., U.S.A.*

Tobacco mosaic virus (TMV) particles are rod-shaped and of length 3000 Å and mean diameter 150 Å. Each particle consists of wedge shaped protein sub-units, of molecular weight, ca. 18,000, arranged on a helix which repeats in three turns, with 49 sub-units in one repeat. Diffraction photographs of well orientated gels of TMV and of an isomorphous mercury derivative of TMV (TMV–Hg) have been obtained by the use of Cu $K\alpha$ radiation, a bent quartz crystal monochrometer, and an evacuated Guinier focussing camera. TMV–Hg contains one heavy atom per protein sub-unit. This derivative has been used to determine phases on the zero layer line and the work is part of a determination of the structure of TMV by means of the method of isomorphous replacement.

The diffraction pattern obtained records a section through the cylindrically averaged square of the structure factor of a single virus particle. The intensity along each layer line is continuous. The zero layer line may be considered in regions demarcated by the order of Bessel function contributing to each. The inner part is given by the term

$$\sum_j f_j J_0 \left(2\pi R r_j\right)$$

(R is the reciprocal space radius, r_j and f_j are the radius and scattering factor of the jth atom), which is real. The Fourier–Bessel transform of the amplitudes calculated from the measured intensities gives the radial density distribution (R. E. Franklin & K. C. Holmes, *Acta Cryst.* (1958), **11**, 213). Farther out the zero layer line comprises largely the term

$$\sum_j f_j J_{49}\left(2\pi R r_j\right) \exp\left(i49\varphi_j\right)$$

(φ_j is the azimuthal co-ordinate of the jth atom), which is complex. The Fourier–Bessel transform of the amplitudes in this region would give the first component of a 49-fold harmonic analysis of the basal projection (which has 49-fold symmetry). An attempt was made to find the amplitudes and phases of the J_{49} term: since only one heavy atom derivative was available only the real part could be determined. From the radial density distribution and the real part alone, a section along a line through the basal projection has been calculated.

7·4. Recent studies of the structure of deoxyribonucleic acid (DNA). By M. H. F. Wilkins, W. Fuller, D. A. Marvin & M. Spencer, *Biophysics Research Unit, King's College, Strand, London, W.C. 2, England.*

DNA can be studied by means of X-ray diffraction, in the form of fibres containing oriented microcrystals. Fairly complete 3-dimensional intensity data (down to 3 Å) has been obtained for 2 different configurations (*A* and *B*) of the molecule. Three-dimensional Fourier synthesis has been made using phases derived from

molecular models. Study of difference syntheses suggests that some of the water molecules in the structure can be located. Recently reflections down to 1·5 Å have been observed in the near-meridional part of the pattern and attempts are being made to use this data in the Fourier synthesis. 2-dimensional diffraction data have been obtained from a semi-crystalline form of DNA in which the molecule is in a third configuration (C). A molecular model for this configuration has been derived.

7·5. Structure de l'acide desoxyribonucleique (ADN), des nucleoprotamines (DNP) et des nucleohistones (DNH) en solution. Par A. NICOLAIEFF & V. LUZZATI, Centre de Recherches sur les Macromolécules, Strasbourg, France.

Nous avons décrit récemment l'organisation des gels aqueux d'ADN, DNP et DNH telle que nous l'avons mise en évidence par l'étude de la diffusion centrale des rayons X (J. Mol. Biol. (1959), 1, 127).

Nous avons examiné ensuite l'action du NaCl concentré (jusqu'à 3 molaire) sur la structure des gels, et nous avons mis en évidence le mécanisme de la dissociation des nucléoprotéines.

Nous avons étudié également des mélanges d'ADN, DNH, DNP et eau, en proportions variables; les résultats obtenus nous ont aidé à interpréter la structure des DNH.

En outre, par l'interprétation de mesures de diffusion centrale absolue par des solutions diluées et isotropes, nous avons déterminé certains paramètres relatifs à la structure des ADN et DNH.

Publication: J. Mol. Biol.

7·6. X-ray diffraction studies of synthetic polynucleotides. By ROBERT LANGRIDGE & ALEXANDER RICH, Department of Biology, Massachusetts Institute of Technology, Cambridge 39, Massachusetts, U.S.A.

Polyribonucleotide chains are able to combine together to form helical complexes. It has been shown by fiber crystallographic methods that polyriboadenylic acid (poly A) will combine with polyribouridylic acid (poly U) to make a two stranded helical complex with screw parameters which are very similar to those seen in deoxyribosenucleic acid (DNA). In a similar fashion, it has been possible to demonstrate that other two stranded helices will form: poly A with polyriboinosinic acid (poly I), as well as poly A with polyribothymidylic acid (poly T). These two stranded complexes will take on an additional polynucleotide strand to form three stranded complexes. Thus we have the combinations poly A + 2 poly U and poly A + 2 poly T. In these cases it is believed that one pyrimidine is hydrogen bonded to adenine in the same manner as adenine is hydrogen bonded to thymine in the Watson–Crick structure for DNA. However, the second chain of poly U or poly T is hydrogen bonded to another side of the adenine base and is connected by two hydrogen bonds through N_7 and the amino group of adenine.

Further crystallographic work has been done on the structure of poly A and poly I. By computing Fourier transforms for a series of models, it has been possible to locate the axis of the molecule and to define limits for the configuration of the ribose–phosphate chains.

In addition, we will discuss stereochemical work on a model of DNA in which the cytosine residue exists in the imino form. The imino cytosine hydrogen bonds to guanine in the same way that the second uracil is linked to poly A in poly A + 2 poly U. This type of bonding has also been found in the mixed crystal of N-methyl thymine and N-methyl adenine by Hoogstein. In this tautomeric form, DNA exists as a two stranded helix with antiparallel chains which are related by a diad axis passing between the adenine–thymine and guanine–cytosine pairs. However, a model of this type introduces some stereochemical difficulties which make it less likely than the Watson–Crick model. Computation techniques will be described which have been developed for the IBM 704 for the calculation of strain energies and Fourier transforms of these structures.

Publication in Biochim. Biophys. Acta.

7·7. La structure du poly-L-glutamate de benzyle en solution. Par M. CESARI & V. LUZZATI, Centre de Recherches sur les Macromolécules, Strasbourg, France.

On a étudié, au moyen de la diffusion centrale des rayons X, des solutions du polypeptide en différents solvants organiques, dans une gamme de concentrations allant des fibres sèches jusqu'aux solutions diluées (1% environ).

A des concentrations relativement élevées on a observé des organisations mésomorphes, dont on a étudié l'évolution avec la concentration. On a pu remarquer d'une part qu'aux concentrations élevées la structure est formée d'un arrangement hexagonal de bâtonnets, dont les dimensions sont celles de l'hélice α, et d'autre part qu'à des concentrations plus faibles l'organisation du système dépend de la nature du solvant. Ces observations ont été mises en rapport avec les phénomènes optiques décrits par Robinson (Trans. Faraday Soc. (1956), 52, 571; Disc. Farad. Soc. (1958), 25, 29).

Par ailleurs, en étudiant les solutions diluées et isotropes au moyen de la diffusion centrale absolue, on a constaté que le polypeptide adopte une configuration en forme de bâtonnet, et que les dimensions des bâtonnets dépendent de la nature du solvant. En particulier on a montré que dans un groupe de solvants, les dimensions du bâtonnet sont en bon accord avec celles de l'hélice α, tandis que dans un autre groupe l'hélice doit être différente. Ces résultats confirment en outre les observations effectuées avec les solutions concentrées.

Publication: J. Mol. Biol.

7·8. Structure of frizzle mutant feather keratin. By S. KRIMM, Harrison M. Randall Laboratory of Physics, The University of Michigan, Ann Arbor, Michigan, U.S.A.

One of the central problems which challenges our understanding of the molecular basis of biological phenomena is the genetic control of protein synthesis and structure. While several cases are known in which a mutation influences the amino acid sequences in a protein, there is relatively little evidence on how the configurational structure of the protein is affected. The Frizzle mutation (in fowl) offers an example of this latter type. X-ray diffraction patterns of the calamus of a homo-

zygous Frizzle chicken were obtained and compared, under comparable conditions, with the diffraction pattern of the calamus of a normal chicken. The patterns differ in two respects: (1) there is less of the crystalline structure manifested in the pattern of the mutant feather, with a comparable increase in the amorphous scattering, and (2) the crystalline part of the pattern that is given by the mutant feather exhibits much poorer orientation than that of a normal feather. The latter effect is also seen in polarized infrared spectra of the two kinds of feathers. Chemical analyses of such feathers indicate that the mutation is also associated with a change in some of the gross amino acid compositions. A tentative hypothesis can be formulated in terms of recent ideas on the structure of feather keratin as to how the mutation is probably influencing the structure. Since the mutation affects primarily the mechanical properties of the feather (thereby leading to poorer feather coverage and increased heat loss, and consequent physiological changes in the animal), this furnishes an example of how changes in protein structure can be correlated with defects in function.

To be published in *J. Mol. Biol.*

7·9. Structure of shark-fin collagen. By N. N. SAHA & S. DAS, *Crystallographic & Solid State Physics Laboratory, Saha Institute of Nuclear Physics, Calcutta University, India.*

The present investigation comprises in its scope the study of collagen (elastoidin) from fin-rays of elasmobranch by X-ray diffraction, chromatographic, electron microscopic and optical methods and the study of the effect of irradiation by 14 Mev. neutrons. This substance, unlike other collagens, does not respond to usual gelatin test. This inertness was attributed by earlier workers to the presence of some cross-linkages not usually met with in other collagens. But, the present study shows that the removal of the outer sheath surrounding the inner fibres eases the gelatinisation and the response to usual gelatin test was immediate. The swelling property of this fibre has been found very significant in our structural study. When kept in water the fibre increases without any tension whatsoever by about 30% in length in addition to its marked increase in diameter.

Birefringence study of the native, contracted, elongated and neutron irradiated fibres has been made and the results obtained were found very useful in elucidating the structural details.

An extensive X-ray study of this substance under various conditions, e.g. native, contracted, elongated and irradiated fibres, has been made. Our findings, which have been discussed in details in the paper, reveals the shortcomings of the existing three-strand coiled coil model for collagen and necessitates its modification. Suggestion in this direction has been put forward.

The amino acid composition of this substance has been found to differ from other collagens in having a high tyrosin content and also in containing an appreciable percentage of cystin. The effect of neutron irradiation in this substance, with special reference to the hydrogen bonds breakage, is being studied by nuclear magnetic resonance method.

7·10. Preliminary X-ray observations on the transverse packing of filaments in muscle. By C. R. WORTHINGTON, *Biophysics Research Unit, Kings College, Strand W.C. 2, England.*

Electron microscopy of striated muscle has shown that the proteins, myosin and actin are in separate longitudinal filaments and pack together in an hexagonal array. The myosin filaments define the primitive lattice and each myosin filament is surrounded by 6 actins. Most striated muscles, e.g. rabbit psoas, frog sartorious have the actins in trigonal positions and this lattice is denoted $L2$, 2 actins per unit cell at $\frac{2}{3}$, $\frac{1}{3}$ and $\frac{1}{3}$, $\frac{2}{3}$. However, electron micrographs of insect flight muscle indicate that the actins are mid-way between the myosins and this lattice is denoted $L3$, 3 actins per unit cell at $\frac{1}{2}$, 0; 0, $\frac{1}{2}$ and $\frac{1}{2}$, $\frac{1}{2}$.

Low angle X-ray patterns were obtained using effective pinhole collimation and, for purposes of comparison, the muscles were extracted in glycerol. Most of the measurements were made on $L3$ using flight muscle from a blowfly and a waterbeetle, although the $L2$ lattice (Huxley, *Proc.Roy.Soc.*, B (1953), **141**, 59) was reaffirmed using rabbit psoas muscle.

The X-ray data is summarized:

$L2$ (10) and (11) reflections of a 440 Å.

$L3$ (10) and (20) reflections of a 560 Å.

The above reflections are equatorials, as expected from a two-dimensional hexagonal lattice. The X-ray data is consistent with the electron micrographs for, with the actins in the above positions, the actin filaments contribute strongly to the (11) and (20) reflections respectively, whereas the myosins contribute mainly to the (10) reflection.

The hydration of each lattice is estimated to be 90% by volume.

(1) Drying. Spacings decrease and the order quickly breaks down. No reflections are observed on air drying the muscle.

(2) Rehydrating. It has been shown for insect flight muscle that an air-dried specimen kept for 3 months will regain its lattice after rewetting.

(3) Swelling. Most fluids in which muscle is immersed increase the lattice. This involves an increase in the myosin–actin distance as the same reflections are observed as in intact muscle.

A previous X-ray study on the axial spacings of striated muscle (Worthington, *J. Mol. Biol.*, (1959), **1**, 398) has described a spacing of about 400 Å. This period has often been seen in electron micrographs associated with 'cross-bridges' between the myosin and actin filaments. In the case of well preserved specimens of insect flight muscle, the 400 Å spacing is a layer line repeat with discrete reflections observable. Consequently, this muscle behaves more like a three-dimensional lattice with a hexagonal unit cell, $C = 400$ Å.

To be published in *J. Mol. Biol.*

7·11. Phase determination in the Fourier synthesis of haemoglobin at 5·5 Å resolution. By A. F. CULLIS, H. MUIRHEAD, M. F. PERUTZ, M. G. ROSSMANN, *Medi-*

cal Research Council Unit for Molecular Biology, Cavendish Laboratory, Cambridge, England and A. C. T. NORTH, *The Royal Institution, 21 Albemarle Street, London W. 1, England.*

Wet crystals of horse met haemoglobin crystallize in space group $C2$ with cell dimensions

$$a = 109 \cdot 2, \quad b = 63 \cdot 2, \quad c = 54 \cdot 7 \text{ Å}, \quad \beta = 110 \cdot 7°.$$

There are two molecules per unit cell, each containing a crystallographic two-fold axis. It was possible to prepare six different isomorphous haemoglobin derivatives by attaching different kinds of mercury compounds at each of two independent sites.

The relative positions of the heavy atom were found by means of a suitable correlation function. The average weight and anisotropic shape parameters were determined by a least-squares procedure (M. G. Rossmann, *Acta Cryst.* (1960), **13**, in press).

The calculated structure factors of the heavy atom contributions in each compound and the corresponding observed structure factors of the heavy atom derivatives were combined, in order to determine the phase of each reflection in the unsubstituted protein. The probability of the phase being 0°, 5°, 10° ... 355° was calculated and then two different procedures were adopted. The first method used the observed structure factors of the native protein as Fourier coefficients and that phase which was found to have the highest probability. In some cases anomalous dispersion could be used to distinguish between phases of almost equal probability. The second alternative method (D. M. Blow & F. H. C. Crick, *Acta Cryst.* (1959), **12**, 794) calculated the center of gravity of all the probabilities plotted around a circle; the displacement of the center of gravity from the origin gave a 'best' phase with a suitable weighting. The second method was found to produce a superior electron-density distribution.

This work will be submitted to *Proc. Roy. Soc.* for publication.

7·12. An evaluation of methods for isomorphous substitution in proteins. By MURRAY VERNON KING, *Orthopedic Research Laboratories, Massachusetts General Hospital, Boston 14, Massachusetts, U.S.A.*

Since bovine pancreatic ribonuclease does not possess amino-acid residues capable of specific chemical reaction with heavy-atom compounds, it has been necessary to apply a diversified trial-and-error approach, relying on unknown steric factors, to the problem of isomorphous substitution in this protein. Some regularities in the ability of substances to bind to ribonuclease have emerged. Substrate analogs containing heavy atoms, e.g., mercurated cytidylic acid, have shown effects indicating binding. However, multiply-charged oxygenated anions are found generally to be substrate analogs in that they bring about competitive inhibition and refolding of urea-denatured ribonuclease. Thus, anionic chelates containing coordinatively-saturated heavy metals have been tried as heavy-atom dyes, in some cases successfully. Some chelates containing coordinatively-unsaturated metals also show evidence of binding, possibly through interaction of the metal with side-groups of the protein. Functional groups found not to lead to specific binding include: $-CO_2H$, $-HgCl$, and positively-charged groups.

The only generally suitable method found for determining specific binding has been the study of changes in X-ray diffraction intensities upon dyeing the crystal. If changes in diffraction intensities are observed, one-dimensional and two-dimensional difference methods are then used as successive steps in screening the crystals to eliminate cases showing diffuse binding or structural changes. The orthorhombic symmetry of ribonuclease I makes possible a check for consistency among the difference Patterson projections along all three axes.

The results of tests for specific heavy-atom dyeing show that the list of successful dyes for ribonuclease differs from those found suitable for other protein crystals. Successful dyes include:

Pt-ssen, Ir-ssen (bis(sulfosalicylal)ethylene-diamine chelates) $Pt(C_2O_4)_2^{-2}$, $Ir(C_2O_4)_3^{-3}$, p-chloromercuribenzenesulfonate, Uranyl complex of Eriochrome Cyanine R.

7·13. Further developments in the structure determination of ribonuclease. By C. H. CARLISLE, *Birkbeck College, Crystallography Laboratory, London, W.C.1, England.*

A study of the fully sharpened three-dimensional Patterson functions of the crystals of ribonuclease and ribonuclease – parachloromercuribenzoate, respectively, has shown that there are two mercury atoms per molecule. These are located at

$$x = 0 \cdot 153, \quad y = 0 \cdot 049, \quad z = 0 \cdot 075,$$

and

$$x = 0 \cdot 806, \quad y = 0 \cdot 951, \quad z = 0 \cdot 175 .$$

The phase contributions of the Hg atoms to the general hkl reflections for spacings greater than 1·7 Å have been calculated and using this information the following partial three-dimensional electron-density maps have been obtained:

(1) Electron-density maps of the crystals with and without the metal using reflections with spacings greater than 6 Å. A comparison of these maps should show the shift of the molecules relative to one another in the presence of the mercury atoms, and also the possible directions and folding of the single polypeptide chain to yield the tertiary structure of the molecule.

(2) An electron-density map of the metal-free crystal using reflections with spacings greater than 3 Å, from which it is hoped to find the positions of the sulphur atoms belonging to the 4 cystine and 4 methionine residues in the molecule and also some information concerning the detailed nature of folding of the polypeptide chain itself.

This work is likely to be published in *Acta Cryst.*

7·14. A comparison of the Fourier transforms of sperm-whale and seal myoglobin molecules. By A. C. T. NORTH, D. C. PHILLIPS & H. SCOULOUDI, *Davy Faraday Research Laboratory, The Royal Institution, London, W. 1, England.*

H. Scouloudi (*Nature* (1959), **183**, 374) has shown that the electron density in a sperm-whale myoglobin molecule (J. C. Kendrew, G. Bodo, H. M. Dintzis, R. G.

Parrish, H. Wyckoff & D. C. Phillips, *Nature, Lond.* (1958), **181**, 662; G. Bodo, H. M. Dintzis, J. C. Kendrew & H. W. Wyckoff, *Proc. Roy. Soc.* (1959), A, **253**, 70) can be projected in such a way that it agrees closely with the electron density in the centrosymmetric *b*-axis projection of seal myoglobin (determined by the method of isomorphous replacement). The comparison has now been extended to a non-centrosymmetric projection of seal myoglobin. Since the electron density in this projection has not been directly determined, the comparison was made in reciprocal space rather than in real space. The electron density in an isolated sperm-whale myoglobin molecule was projected in a direction corresponding to the *a*-axis of seal myoglobin. This projected density was then used to calculate $0kl$ structure factors in the seal myoglobin unit cell and these structure factors were compared with the observed amplitudes. The good agreement obtained confirms the similarity of the two myoglobin molecules previously indicated by the *b*-axis projection.

An assessment of the two methods of comparison, in real and in reciprocal space, will be presented.

Paper likely to be published in *Acta Cryst.* or *J. Mol. Biol.*

7·15. Structural relationship of horse and ox haemoglobins. By A. C. T. NORTH, *Medical Research Council External Staff, Davy Faraday Research Laboratory, The Royal Institution, London, W. 1, England.*

The 3-dimensional electron-density distribution in horse haemoglobin is now known (M. F. Perutz, M. G. Rossmann, A. F. Cullis, H. Muirhead, G. Will & A. C. T. North, *Nature, Lond.* (1960), **185**, 416), but only the centrosymmetric projections of ox haemoglobin are available at present (D. W. Green & A. C. T. North, accompanying paper). H. Scouloudi (*Nature, Lond.* (1959), **183**, 374) showed that there was close agreement between corresponding projections of sperm whale and seal myoglobins. A similar comparison has now been made for ox and horse haemoglobins.

The relative orientations of the two unit cells with respect to the molecule are known with fair accuracy from consideration of molecular packing, protein Pattersons, optical dichroism and the positions of the sulphydryl groups as revealed by heavy atom coordinates.

The Ferranti Mercury computer was used for the calculation. The electron-densities of the horse haemoglobin structure were read into the machine; a linear 8-point interpolation was used to evaluate the density at points on a new grid with axes parallel to the ox haemoglobin axes. The projections were derived by appropriate summations. Calculations were made for several slightly different relative positions of the horse and ox axes.

Structure factors, corresponding to the projections of the horse molecule in the ox unit cell, were calculated, so that a comparison could be made directly with the ox haemoglobin data.

The degree of similarity, both of the projected electron-density maps and of the structure factors, will be discussed with reference to the structural similarities which it implies.

Paper probably to be submitted to: *J. Mol. Biol.*

7·16. Isomorphous replacement in ox haemoglobin. By D. W. GREEN & A. C. T. NORTH, *Medical Research Council External Staff, Davy Faraday Research Laboratory, The Royal Institution, London, W. 1, England.*

Ox haemoglobin has been studied by means of the isomorphous replacement method, as used in horse haemoglobin (D. W. Green, V. M. Ingram & M. F. Perutz, *Proc. Roy. Soc.* (1954), A, **225**, 287). Ox haemoglobin has the advantage of orthorhombic symmetry with three centrosymmetric projections, but the asymmetric unit of structure is a whole molecule.

Isomorphous derivatives containing one or two silver or mercury atoms per half molecule of protein have been prepared, though the satisfactory compounds all have the heavy atom groups at the same two sites, the sulphydryl groups. The resultant intensity changes enable signs to be determined for about two thirds of the reflections of the *a* and *c* projections, neither of which suffers appreciably from overlap of adjacent molecules.

The electron-densities in both projections show a tendency to dyad symmetry about an axis roughly parallel to the *b* axis. Together with the presence of heavy atoms in two sites symmetrically placed about such an axis and the existence of a second, cubic, form of ox haemoglobin in which the molecules lie on dyad axes (A. C. T. North, *Acta Cryst.* (1959), **12**, 512), this suggests that the molecules of orthorhombic ox haemoglobin have axes of two-fold symmetry which are not made use of in the crystal structure.

The features of electron-density are of a similar nature to those found in projections of other proteins.

The position of the molecular boundary was determined from packing considerations, from the appearance of the electron-density maps and from 'salt–water' Fouriers calculated from the intensity changes produced by varying the salt concentration of the crystal mother liquor. The distance between the two heavy atom sites within one molecule is closely equal to the separation of the sulphydryl groups of horse haemoglobin; the similarity of horse and ox haemoglobins is discussed further in a separate paper.

Paper probably to be submitted to: *J. Mol. Biol.*

7·17. Insulin-crystal structure studies of heavy atom derivatives. By BARBARA W. LOW, J. DRENTH, H. C. WATSON, W. TRAUB, J. A. ROSENCRANTZ & C. H. CHEN, *Department of Biochemistry, College of Physicians and Surgeons, Columbia University, New York 32, New York, U.S.A.*

Efforts to prepare heavy atom derivatives of insulin (1) by immersing orthorhombic type *A* insulin sulfate and insulin citrate (B. W. Low & J. E. Berger, in preparation for *Acta Cryst.*) crystals in solutions containing heavy atom salts and (2) by growing crystals from solutions containing these salts have so far yielded three preparations which merited further study. After immersion for several weeks in buffered solutions of either (*a*) barium platinocyanide or (*b*) thallium nitrate the intensity distributions of the three principal zones of reflection for insulin citrate crystals are markedly changed. The two crystal modifications are both isomorphous with the metal-free crystals. Difference Patterson projections have been calculated and the positions of heavy-atom vectors

tentatively identified. The results of these investigations will be presented.

After insulin citrate crystals have been immersed in a buffered solution of potassium platino-iodide for ten days, the unit cell dimensions change by shrinkage from

$$a = 57 \cdot 7, \quad b = 51 \cdot 4, \quad c = 38 \cdot 1 \text{ Å}$$

to

$$a = 59 \cdot 1, \quad b = 50 \cdot 6, \quad c = 29 \cdot 5 \text{ Å},$$

although the space group $P2_12_12_1$ remains unchanged. The X-ray photographs are rather poor with minimum spacings of 4·5–5 Å. The crystals have been studied after three months and nine months immersion. Marked intensity changes have been observed, and time-difference Patterson projections have been calculated. The projections appear to be interpretable in terms of two heavy-atom groups per asymmetric unit. Confirmation is being sought through the calculation of three-dimensional Patterson series. The results of this study will be presented.

This is a report of work in progress rather than of a complete structure determination and so it is not possible to specify with certainty the Journal in which the work is likely to be published—probably *Acta Cryst.*

7·18 Insulin — gross molecular structure. By BARBARA W. LOW, A. S. McGAVIN AND J. R. EINSTEIN, *Department of Biochemistry, College of Physicians and Surgeons, Columbia University, New York 32, New York U.S.A.*

The three principal weighted reciprocal-lattice sections of type A and type B (both wet) and type P (air-dried) orthorhombic insulin sulfate crystals all show some rather remarkably simple features of intensity distribution. Preliminary efforts to account for these features in terms of simple distributions of gross scattering centers in the three structures have been partially successful for projections along the a axis.

During the study of shrinkage in insulin sulfate crystals several new crystal forms were discovered (J. R. Einstein, Ph.D. Thesis, Harvard University, 1958; J. R. Einstein & B. W. Low (in preparation for *Acta Cryst.*)). In one of the intermediate drying stages, type C, the space group of the crystal is $I2_12_12_1$ with eight general equivalent positions. The drying stages proceed through crystal forms of space group $P2_12_12_1$ to $I2_12_12_1$ and finally to an air-dried form space group $P2_12_12_1$. In the normal wet form there are two molecules of molecular weight 5733 in the asymmetric unit. In type C crystals pairs of molecules are related by two-fold rotation axes. From a detailed study of the transformations and from other studies we have concluded that the molecular dimer has basically an invariant structure of point group 2 in all these forms and probably also in solution.

The three basal sections of the weighted reciprocal lattice of type C crystals also show simple features of intensity distribution. By further study, using optical transform techniques and Patterson projections, it has been possible to define a simple arrangement of gross scattering centers which accounts for the principal intensity distributions in the $0kl$ zone of types A, B, C and P crystals (B. W. Low, A. S. McGavin & J. R. Einstein (in preparation for *Acta Cryst.*)).

7·19. X-ray studies on the structure of insulin. By MARJORIE HARDING, DOROTHY HODGKIN, SABINA COLE, ANN KENNEDY, A. O'CONNOR, BERYL RIMMER, J. S. ROLLETT & D. WEITZMAN, *Chemical Crystallography Laboratory, South Parks Rd., Oxford, England.*

We have examined several different crystalline forms of insulin. One of these, crystallized from a citrate buffer containing sodium chloride, is closely related to the already familiar rhombohedral zinc insulin; but it has a higher zinc content, there is an expansion of 4 Å along the threefold axis, and a small rotation of the molecules is suggested by the Patterson projections. The function of the zinc in both forms is important; the new form contains four zinc atoms per unit cell (of molecular weight 36,000), the old form two zinc atoms.

We have searched for heavy metal derivatives isomorphous with either of these forms, almost entirely by soaking techniques rather than crystallization. Uptake of heavy metal has been detected either by the change in intensity in one zone of reflections, or by the increase in density, measured in a density gradient column, or by both methods. The amount of one ion taken up, mercuri-iodide, has been studied by chemical analyses.

Intensities have been measured to a resolution of $2\frac{1}{2}$ to 3 Å, for numerous projections and for four sets of three-dimensional data on the two unsubstituted forms, a uranyl acetate and a mercuri-iodide derivative; then the sharpened Patterson series were calculated. Determination of the heavy atom positions from projections which are non-centrosymmetric, was not possible. A probable mercury position was found from the three-dimensional Patterson series. Using only the data from the mercuri-iodide derivative a Buerger minimum function and a heavy atom phased Fourier series were calculated; both were able to suggest the arrangement of molecules in the lattice and some features within the molecules.

Eventual publication; probably *Proc. Roy. Soc.*

§ 8. Fibrous structures

8·1. Röntgenstrukturuntersuchungen am Polyäthylen. Von R. BONART & R. HOSEMANN, *Fritz-Haber-Institut der Max-Planck-Gesellschaft, Berlin–Dahlem, Deutschland.*

Röntgenkleinwinkel- wie auch Röntgenweitwinkeldiagramme vom Polyäthylen sind seit längerer Zeit bekannt. Dabei rührt das Kleinwinkeldiagramm von der räumlichen Anordnung der sog. 'amorphen' bzw. 'kristallinen' Bereiche, also von der Kolloidstruktur her. Das Weitwinkeldiagramm ist dagegen durch die atomare Struktur in den 'amorphen' und 'kristallinen' Bereichen gegeben.

Während nun die Kristallstruktur des Polyäthylens als gesichert angesehen werden darf, sind die Untersuchungen über die Struktur in den 'amorphen' Bereichen noch in Fluss. Diese Untersuchungen stützen sich auf die Analyse der diffusen Streuung im Weitwinkeldiagramm und auf das Temperaturverhalten der Kleinwinkel- und Weitwinkelstreuung. Die bisher vorliegenden Befunde deuten darauf hin, dass die 'amorphe' Struktur des Polyäthylens parakristallinen Charakter trägt. Auch in den 'amorphen' Anteilen liegt vermutlich eine kristallähnliche Struktur mit definierter Koordinationszahl vor.

Die Kolloidstruktur konnte im vergangenen Jahr durch

die Annahme sog. parakristalliner Schichtgitter bzw. Schichthaufwerke weitgehend analysiert werden. Von Hendus (BASF) mitgeteilte Kleinwinkeldiagramme verschieden stark gereckter Polyäthylenfolien haben zu einer Erweiterung und Präzisierung unserer bisher mitgeteilten Vorstellungen über die Makrostruktur geführt. Lichtoptische Modellversuche (Frauenhofer Diagramme) an zweidimensionalen Modellstrukturen veranschaulichen die gewonnenen Ergebnisse. [K. Hess u. H. Kiessig, *Z. phys. Chem.* **193**, 196 (1944), R. Bonart u. R. Hosemann, *Z. Elektrochem.* **64**, 314 (1960), R. Bonart u. R. Hosemann, *Makromol. Chem.* **39**, 105 (1960), H. Hendus, *Koll. Z.* **165**, 32 (1960)].

Ausführliche Veröffentlichung ist vorgesehen in *Kolloidzschr.*

8·2. The effect of degree of polymerization on crystallite orientation in regenerated cellulose filaments.
By K. C. ELLIS and J. O. WARWICKER, *British Cotton Industry Research Association, Shirley Institute, Didsbury, Manchester, 20, England.*

The azimuthal intensity distributions of the 020 and 101 reflections have been determined by photometer measurements on suitable photographs of bundles of cellulose filaments prepared from fractions of cellulose acetate having a very limited range of degree of polymerization.

The shapes of the measured azimuthal intensity distributions of the 101 and 020 reflections of representative specimens have been compared with those predicted by Kratky's 'Rodlet' Theory and it has been shown that the filaments show no appreciable selective orientation of the (101) planes.

The degree of orientation of the (101) planes has been determined for a total of 24 specimens at 6 different degrees of polymerization by taking the reciprocal of the half-breadth of the azimuthal intensity distribution of the 101 reflection. It was found that at low effective stretches no crystallite orientation occurs but at higher effective stretches the degree of crystallite orientation increases with increasing effective stretch. At constant effective stretch, the crystallite orientation increases with increasing degree of polymerization until a degree of polymerization of about 600 is reached but then tends to assume a constant value.

The results can be explained if it is assumed that when the filament is stretched it is in a state in which the bonding between molecules is very weak so that flow can occur in addition to 'affine' deformation.

To be submitted for publication to *J. Polym. Sci.*

8·3. The measurement of crystallinity in polyethylene terephthalate ('Terylene'): A comparison of X-ray, infra-red and density measurements. By
G. FARROW & I. M. WARD, *Research Department, I.C.I. (Fibres Division), Hookstone Road, Harrogate, Yorkshire, England.*

Crystallinities have been measured in drawn polyethylene terephthalate ('Terylene') yarns by methods based on density, infra-red spectra and X-ray diffraction. The results have been compared and no correlation exists between the three; the values from infra-red are high, those from X-ray low, and those from the density fall roughly between the two.

The crystallinity of a polymer fibre is by definition the relative amount of three-dimensional ordered material present in a sample and this is most directly measured by X-ray diffraction. In the X-ray method the drawn fibres are chopped and pelleted to make a randomised sample suitable for mounting on the circumference of an X-ray focusing camera. A line shaped, strictly monochromatic X-ray beam is used and the X-ray camera is evacuated. This enables the photographic film, which is used to record the X-ray reflections, to be free of 'white' radiation and parasitic X-ray radiation normally termed air scatter. Exposure times are of the order of one hour.

The results reported here show that in polyethylene terephthalate the infra-red measurements are only correlated with configurational changes affecting the order within individual molecules. Using the X-ray measurements to define crystallinity it is found that the density of non-crystalline material increases with orientation so that density measurements based on the concept of constant non-crystalline density (equal to the density of amorphous material) are inevitably in error when applied to oriented samples.

The results also show that highly oriented pin drawn yarns of low draw ratio have no appreciable crystallinity which is in contradiction to the view that the limiting stress built up in the drawing process is caused by the onset of crystallinity. Although the onset of crystallinity may well increase the reinforcement it is clear that it is not essential to it.

Account to be published in *Polymer.*

8·4. Structure de la cellulose IV. Par THÉRÈSE PETIT-PAS & JACQUES MERING, *Institut National de Recherche Chimique Appliquee, Service de Rayons X, Paris (4°), France.*

La cellulose IV est généralement considérée comme une forme orthorhombique, proche de la cellulose I. Le calcul de la distribution radiale horizontale $P(r_0)$ (distribution des projections équatoriales des distances interatomiques) a été effectué en utilisant les données d'une photométrie continue. Cette distribution est en accord avec le modèle structural de Meyer & Misch d'une chaîne *unique*. Mais $P(r_0)$ ne contient aucune indication sur une répétition du motif. On doit ainsi considérer la cellulose IV comme un assemblage de chaînes parallèles, sans ordre latéral. Les maxima équatoriaux du diagramme ne doivent donc pas être considérés comme des réflexions de Bragg. Il faut noter, d'autre part, que la structure de la chaîne apparaît mieux dans $P(r_0)$ de cette forme 'amorphe' que dans celle de la forme 'cristallizée' (cellulose I): en effet dans la cellulose IV la distribution des distances *intramoléculaires* n'est plus brouillée par les distances *intermoléculaires*.

Publication: Note aux *C. R. Acad. Sci., Paris.*

§ 9. Order-disorder phenomena

9·1. Diffusion hors des domaines de Bragg dans la muscovite. Par LUCIEN GATINEAU, *Institut National de Recherches, Chimiques Appliquées, Paris 4°, France.*

La recherche de la répartition des substitutions isomorphes Al–Si n'est possible qu'à cause de la différence d'encombrement de ces ions. Une projection à une dimen-

sion permet de voir qu'ils ne peuvent être cristallo-graphiquement confondus. Leur différence de diamètre entraîne des distorsions dans le plan des atomes d'oxygène qui leur sont liés.

Une exploration continue de l'espace réciproque, par sections sphériques successives, met en évidence des phénomènes complexes de diffusion en dehors des domaines de Bragg. L'étude de ces phénomènes de diffusion permet d'établir les relations d'ordre-désordre qui existent dans ces substitutions Al–Si à l'intérieur d'un feuillet et d'un feuillet à un autre feuillet.

9·2. The structure of the intermediate plagioclase felspars. By HELEN D. MEGAW, *Cavendish Laboratory, Cambridge, England.*

The ideal plagioclase structure has a unit cell made up of 18 albitoid subcells, 16 of which belong to one or other of the four types found in anorthite, and are arranged so as to give extensive blocks of anorthite structure. Sets of stacking faults on several different fault planes occur with probabilities depending on the composition, and have the effect of displacing the systematically-weak intensity maxima ('difference reflections') from their ideal lattice positions, in three dimensions. These results, with a detailed quantitative description of the stacking faults, are deduced directly from the diffraction effects, without the use of *any* hypotheses about atomic arrangement or atomic 'ordering'. With the assumption that faults in annealed material have their origin in site-mistakes which necessarily occur at non-stoichiometric compositions, it is then possible to make some generalisations about the (Si, Al) and (Ca, Na) distributions throughout the series, with the help of the observed resemblances to anorthite. It is shown that the geometrical or 'puckering' effect noticed in anorthite plays a more fundamental part than does the (Si, Al) ordering, though the latter is also important.

The theory provides a complete quantitative explanation of the positions of the intensity maxima and the variation with composition of all three reciprocal-space coordinates; it explains qualitatively their variation of breadth and intensity with composition and with heat treatment; and it shows the relationship of the intermediate plagioclases to high and low albite on the one hand, to low anorthite ('primitive anorthite'), high anorthite and 'body-centred anorthite' on the other. It opens up possibilities for further understanding of the potash felspars in their relation to the soda felspars.

Probably to be submitted for publication in *Proc. Roy. Soc.*

9·3. Short order and X-ray Debye temperature of Ni₃Pt. By V. I. IVERONOVA & A. A. KAZNELSON, *Physical Faculty, Moscow State University, Moscow B–234, U.S.S.R.*

No abstract provided.

9·4. Electron microscope observations on the disorder → order transition in CuAu. By D. W. PASH-LEY & A. E. B. PRESLAND, *T.I. Research Laboratories, Hinxton Hall, Cambridge, England.*

Following the earlier work on the CuAu(I)–CuAu(II)

transition (D. W. Pashley & A. E. B. Presland, *J. Inst. Met.* (1958–59), p. 419), a study of the transition from the disordered state to CuAu(I) and CuAu(II) has been made. This involves a change from f.c.c. to a tetragonal structure with $c/a = 0.92$. The observations have mainly been made on specimens produced by electrochemical thinning of $0.001''$ thick copper-gold foil. The foils were given various heat treatments before the thinning. A few direct observations on the ordering of specimens inside the electron microscope have also been made.

Since the transition occurs by a diffusion process, the formation of the tetragonal structure from a cubic structure leads to very high elastic strains. The long range effect of these strains is partially accommodated by frequent changes in the direction of the $[001]_{ordered}$ axis, from one $\langle 100 \rangle_{disordered}$ direction to another. Each crystal grain is divided into cells within which a lamellar structure is formed. The lamellae result from alternation of the $[001]_{ordered}$ axis between just two of the three possible $\langle 100 \rangle_{disordered}$ directions. The detailed crystallography of the arrangement, as deduced from the correlation between electron micrographs and selected area electron diffraction patterns, will be described.

9·5. On the ordering kinetics of the alloy Cu₃Au. By ELEMÉR NAGY, *Institute for Experimental Physics, R. Eötvös University, Budapest, Hungary.*

Electrical resistivity and absolute thermoelectric power of the alloy Cu₃Au were measured at various temperatures below the Curie-point in dependence on time. The behaviour of these transport properties is entirely different: the thermoelectric power tends to a constant value, while the resistivity decreases continually. The time dependence of the resistivity in the later stage of the anneal can be represented by an exponential with an activation energy of 0.81 e.V. The first phase of the resistivity variation and the time dependence of the thermoelectric power cannot be described by any simple law. It is tentatively assumed, that the exponential dependence is due to the elimination of antiphase domain boundaries by diffusion, while the first stage—which is alone effective in the variation of the thermoelectric power—corresponds to the ordering within a domain. Experiments with two-step anneals (successive heat treatments for definite times at different temperatures) were in full accord with this interpretation.

9·6. Ordering in the βAuCd-βAgCd alloy system. By L. MULDAWER & F. ROTHWARF, *CENG, Institut Fourier, Grenoble, France.*

Residual resistivity measurements of the quasi-binary AuCd–AgCd system shows the expected parabolic behavior near the terminal binary alloys but not near the composition AuAgCd₂. In this region, the resistivity dips markedly below the Nordheim value and indicates ordering of the gold and silver atoms. The minimum is found at the equiatomic solid solution of βAuCd and βAgCd. Electrical resistivity measurements as a function of temperature show a rise greater than that produced thermally over the range from 75 to 225 °C. This is

associated with the gold–silver disordering. Order as a function of temperature is obtained by use of Muto's theory. X-ray studies show that the ordered structure has the space group $Fm3m$ and is identical with the Heusler alloys. This represents a sodium–chloride arrangement of the unit cells of βAuCd and βAgCd. Ordering is found at room temperature to include alloys from 40% to 60% AgCd as expected from the residual resistivity data.

Will probably be submitted to *J. Appl. Phys.*

9·7. The concept of long-range order and the measurement of order parameters. By J. M. COWLEY, *Division of Chemical Physics, C.S.I.R.O., Australia.*

The long-range order parameter, S, defined by Bragg & Williams and subsequently used almost universally, must be rejected as a valid order parameter since its definition involves making an arbitrary assumption in that one particular position in the unit cell is arbitrarily chosen as the 'right' site for one type of atom. The parameter S is multi-valued for any given state of order.

Correspondingly the Bragg & Williams theory of long-range order and all subsequent developments and modifications of it which involve the quantity S contain logical fallacies which falsify the conclusions.

The observable quantities relating to long range order, e.g. diffraction intensities and electrical resistance, are functions of S^2 rather than S, and it seems appropriate to define order parameters accordingly. This can be done by considering the state of order of a system to be specified by its auto-correlation, or Patterson, function. For an ordered alloy in which all atoms can be assumed to have the same size, the Patterson function has a periodic component with peak heights proportional to S^2, and a non-periodic part near the origin where peak height are proportional to α_i, the short-range order parameters (J. M. Cowley, *Phys. Rev.* (1950), **77**, 669). Thus S^2 appears as the limiting value of α_i for large distances from the origin.

Consideration of the Patterson function also allows calculation of configurational entropy and energy and so allows the derivation of equations giving all order parameters as functions of temperature. From these equations it emerges that a single order parameter, S^2, is usually insufficient to specify long range order. For Cu$_3$Au-type lattices, for example, S_1^2, the limiting value of α_i for sites at the corners of unit cells of the periodic Patterson component, differs appreciably from S_2^2, which is given by taking the limiting value of α_i for face-centre sites. This implies that fluctuations in the composition of the alloy must take place in a non-random way, as is the case, for example, when gold-rich or copper rich antiphase domain boundaries are present.

The intensity of superlattice diffraction spots is proportional to $S_1^2 + S_2^2/3$, which gives excellent agreement with the experimental values of D. T. Keating & B. E. Warren (*J. Appl. Phys.* (1951), **22**, 286). In addition there is a small increase in the intensities of the fundamental reflections, proportional to $S_1^2 - S_2^2$.

Probable journal for publication: *Phys. Rev.*

9·8. The effect of temperature on short range order diffuse scattering from Alloys.* By C. B. WALKER, *Institute for the Study of Metals, University of Chicago* and D. T. KEATING, *Brookhaven National Laboratory, U.S.A.*

The theory of the diffuse scattering of X-rays from binary alloys with local order has been extended to include explicitly the effects of thermal vibration. By adopting certain simplifying assumptions about the lattice vibrations it is found that the thermal effects can be simply expressed in the form of appropriate Debye–Waller factors modifying the usual diffuse scattering terms. Experimental measurements verify the predicted general nature and magnitude of this temperature effect. Neglect of this temperature effect appears to be a source of significant error in past determinations of local order in alloys.

To be submitted for publication in *Acta Cryst.*

9·9. X-ray determination of crystallinity and diffuse disorder scattering. By W. RULAND, *European Research Associates s. a., Bruxelles 18, Belgium.*

An X-ray method of crystallinity determination has been developed which takes into account the diffuse disorder scattering, due to thermal vibrations and lattice imperfections in the crystalline part of a substance.

The method uses the ratio of integrated intensities of diffraction peaks to the total coherent scattering and the dependence of this ratio on the scattering angle.

Application of the method to a series of polypropylene samples shows that diffuse disorder scattering is predominantly caused by thermal motions.

The normalization of the scattering curves leads to special absorption corrections for compton scattering and indicates a scattering effect due to the carbon–hydrogen bond orbital.

The paper will be submitted for publication in *Acta Cryst.*

9·10. The structure of pyrographite.† By O. J. GUENTERT & S. CVIKEVICH, *Research Division, Raytheon Company, Waltham, Mass., U.S.A.*

A series of pyrographite samples have been investigated by X-ray diffraction methods. The specimens were obtained by pyrolysis of hydrocarbon gases on a plane graphite surface at temperatures ranging from about 1700 to about 2500 °C. This process yields massive deposits of a thickness up to several millimeters whose density increases with the deposition temperature from about 1·50 g.cm.$^{-3}$ to over 2·20 g.cm.$^{-3}$. The deposits are polycrystalline but exhibit a considerable degree of preferred orientation. The 'crystallites' consist of groups of parallel and approximately equidistant graphite layers with nearly random layer order. These results are in agreement with those reported on pyrolytic graphite by A. R. G. Brown & W. Watt (Conference on Industrial Carbon and Graphite, London (1957)).

In the present study the various structural features such as preferred orientation, particle size, r.m.s. strains, degree of layer order, and layer spacing have been examined for different deposition temperatures. The particle sizes and strains were determined from Fourier analyses of the diffraction peak shapes. The Stokes method was applied in correcting for the instrumental broadening and the Fourier coefficients thus obtained were then separated into particle size and distortion coefficients using the Warren & Averbach method. The degree of layer order is indicated by modulations in the two-dimensional (hk) reflections. Detailed data on the temperature dependence of these structural features will be presented. The results indicate an increase of the preferred orientation, the particle size, and the degree of layer order with increasing deposition temperature and a corresponding reduction of the layer spacing from about 3·45 to nearly 3·35 Å.

Full account to be published in *J. Appl. Phys.*

§ 10. Deformations and imperfections

10·1. Characteristics of the X-ray diffraction method for observing individual dislocations. By A. R. LANG, *H. H. Wills Physics Laboratory, University of Bristol, England.*

Several X-ray diffraction methods of observing individual dislocations have been described. In these the specimen may be used either in reflection or transmission, the incident radiation may be divergent or collimated by crystal reflection, and the radiation may be either strongly or weakly absorbed in the specimen. The author has chosen to use specimens in transmission in order to study conditions in their interiors not observable by other means, to use divergent incident radiation for simplicity, with wavelength and thickness of specimen chosen so that absorption is small. Such conditions give, with nearly perfect crystals, extremely high contrast of dislocation images in section topographs (A. R. Lang, *Acta Met.* (1957), 5, 358) and good contrast in projection topographs (A. R. Lang, *Acta Cryst.* (1959), 12, 249). The apparent size of dislocation images depends upon various factors. Firstly, the geometrical disposition of source, specimen and film, which conditions are easily controlled. Secondly, the lengths of photoelectron tracks in the X-ray film; these are troublesome with penetrating radiation but can be minimized by using dense emulsions. Thirdly the intrinsic form of dislocation images, which varies considerably with orientation of the dislocation line and position in the crystal. Various diffraction effects associated with individual dislocations will be described. Similarities and contrasts to electron microscope images of dislocations will be pointed out. An attempt will be made to interpret such diffraction effects theoretically.

To be published (in part) in *Acta Cryst.*

10·2. A comparison of X-ray diffraction microscopy with etching and decoration techniques. By KATA-RINA KRANJC, *Physical Institute, Faculty of Science, Zagreb, Yugoslavia.*
Withdrawn.

10·3. Observations on imperfections and deformation in beryllium by divergent beam X-ray photography. By J. SAWKILL & D. R. SCHWARZENBERGER, *Tube Investments Research Laboratories, Hinxton Hall, Nr Saffron Walden, Essex, England.*

When a highly divergent beam of X-rays from a point source is transmitted through a crystalline specimen two distinct types of contrast may be recorded: (i) the diffraction pattern of excess and deficiency conics which is normally used to study the perfection and lattice parameters of good single crystals, and (ii) the microradiograph which is formed by absorption contrast arising from variations in thickness and composition of the specimen. There are advantages in considering these two types of information together, particularly for metallurgical specimens of suitable grain size and thickness where both diffraction and absorption contrast are recorded simultaneously on a photographic plate placed in the path of the transmitted beam. These advantages are discussed, and demonstrated by a series of divergent X-ray beam photographs taken on a point projection X-ray microscope (i) at intervals along a zone refined single crystal rod of beryllium, giving information about the variation in perfection and subgrain structure, the variation in lattice parameter, and the distribution of impurities along the rod; (ii) at different stages during the deformation and recrystallization of polycrystalline beryllium, revealing the formation and extension of cracks and the changing perfection of the grains.

To appear in *Brit. J. Appl. Phys.*

10·4. A study of age-hardened Al-3·85% Cu and Al-19·7% Ag alloys by means of the divergent X-ray beam method. By T. IMURA, S. WEISSMANN & J. J. SLADE, JR., *Materials Research Laboratory, College of Engineering, Rutgers, The State University, New Brunswick, New Jersey, U.S.A.*

Single crystal specimens were studied after solution treatment and successive quenching as well as at various stages of age-hardening.

Anisotropic lattice distortions associated with precipitation phenomena were studied by means of the divergent X-ray beam method. Metallographic and microhardness studies were also carried out.

Using more than ten reflections from the back reflection patterns at every stage of aging a complete strain analysis of the specimens was carried out.

The strain distribution could be represented in terms of a strain ellipsoid and could therefore be characterized by three values, λ_1, λ_2 and λ_3, associated with the principal axes of the ellipsoid.

The following results were obtained:

(1) The three principal axes of the strain ellipsoid coincide with the $\langle 100 \rangle$ directions. Since the magnitude of the observed strain for these three principal directions differed, it is concluded that the amount of G.–P. [2] zones and θ' phase formed is different for the three principal $\{100\}$ planes. This suggests that after quenching the quenched-in lattice defects which play a vital rôle in the aggregation of solute atoms and precipitation seem

to be distributed in unequal amounts on the three different sets of {100} planes.

(2) The lattice strain due to the formation of the G.-P. [2] zones is given by $\lambda_1 = \lambda[010] = 0 \cdot 41\%$, $\lambda_2 = \lambda[001] = 0 \cdot 18\%$ and $\lambda_3 = \lambda[100] = -0 \cdot 10\%$ and that due to the formation of θ' is given by $\lambda[010] = 0 \cdot 46\%$, $\lambda[001] = 0 \cdot 15\%$ and $\lambda[100] = -0 \cdot 03\%$.

(3) The matrix, after precipitation of the θ phase, produces sharp reflection lines, but still retains a maximum strain component in a different cube direction identified as the [100] direction.

(4) Line-broadening characteristics were also observed in the Al–Ag system, although the changes of lattice spacings during aging were considerably smaller.

Paper to be submitted to *Acta Cryst.*

10·5. Surface alterations of silver iodide. By GORDON BURLEY, *National Bureau of Standards, Washington, D. C., U.S.A.*

Single crystals of hexagonal (β)AgI, when exposed to light in the presence of water vapor and certain catalysts, develop clouded surfaces. The prism faces are affected first, and the basal plane last.

This deterioration of the surfaces has been detected on polycrystalline samples with X-ray diffraction. The relative intensities of diffracted radiation from certain sets of planes have been found to vary with the length of exposure time to a light source. Initially, the (100), (101) and (102) reflections increase, while all others remain constant. After a period of time, varying with the light intensity and spectral characteristics of the source, these reflections reach a plateau. At the same time, the diffracted intensity from the basal plane begins to increase markedly. At a still later time, the intensities of the (101), (102) and (103) reflections begin to rise again, while the (002) reflection continues to increase at a constant rate.

Qualitative evaluation of these results leads to the conclusion that the increase in diffracted intensities is due to a decrease in extinction. This is caused by a fragmentation of the initially well ordered surface layers. At the same time, there is some loss of iodine leading to a decrease in scattering material.

10·6. The anomalous enhancement of the intensity of X-rays reflection at the boundary of different treatment of a crystal. By E. FUKUSHIMA, *Department of Physics, Faculty of Science, Tokyo Metropolitan University, Tokyo, Japan.*

It is known that the intensity of X-ray diffraction from such crystal as, for instance, a quartz or a lithium fluoride can be greatly increased by grinding the surface. It has been reported moreover (E. Fukushima, *Acta Cryst.* (1954), **7**, 459) that, when a boundary separating the etched and ground regions on one surface and parallel to a net plane is prepared, the intensity of the transmitted diffraction from the net plane through the boundary is found to be anomalously higher even than one through ground region on the surface.

This 'boundary effect' was studied by means of micro-scopic observation. The boundary was prepared on the upper surface of a plate-shaped LiF crystal or quartz, and the lower surface was etched and chemical polished alternatively keeping the upper free from any chemical attack. At the depth of about 100μ from the upper, a sudden increase in the density of etch pits of dislocations was observed which seemed due to be originated in the treatment on the upper surface. Thus it is plausible that the dense distribution of dislocations by grinding caused the increase in the intensity diffracted through the ground region. Anomalous increase in the intensity at the boundary is explained by the gradient of the density of dislocations from a ground to an etched region.

This boundary effect has been also found by Z. Ishii & K. Kohra (private communication) by Borrmann's method.

E. Aerts, S. Amelinckx & W. Dekeyser (*Acta Met.* (1959), **7**, 29) has reported the surface hardening at the boundary between irradiated and unirradiated regions of NaCl crystal. The anomalous intensity at the boundary was much reduced by annealing at about 400 °C.

These phenomena can be interpreted by the behavior of nucleated dislocation by the surface treatment.

The full-length account will be published in *J. Phys. Soc., Japan.*

10·7. Diffraction of nearly monochromatic X-rays by certain types of random structures. By J. J. SLADE, *College of Engineering, Rutgers, The State University, New Brunswick, New Jersey, U.S.A.*

From the electron-density distribution $f_r(x)$ for an atom the distribution of scattering matter

$$f(x) = \Sigma f_r(x - x_r - a_n)$$

corresponding to a defective crystal is constructed. Here x is a vector in physical space, x_r the set of defective unit cell vectors, and a_n the set of translation vectors subject to cumulative errors. The defects in x_r and a_n are characterized by a set of probability density distributions. The functional

$$P(u) = TE(1/X) \int_X f(\lambda)f(x + \lambda)dv_\lambda$$

is the transform of the expected value of the integral, in which X is ordinary space and dv_λ its measure element; u is a vector in reciprocal space.

When the cumulative errors are characterized by a single p.d.d. with characteristic function $\varphi(u) = \exp(-\zeta)$, then

$$P(u) = K \left[\sinh^3 \zeta / \Pi_r \left(\cosh \zeta - \cos a_r u_r \right) \right].$$

If the beam has a distribution $g(\xi)$ of wave lengths about a mean length λ_0, then

$$R(u_0) = \int P[u_0(1 - (\xi/\lambda_0))]g(\xi)d\xi.$$

In the neighborhood of a maximum R may be represented by the rational function

$$R = (M + N\eta)/(m + n\eta + \eta^2),$$

where $\eta = \theta - \theta_B$ and θ_B is the Bragg angle.

A least-squares scheme of computation has been developed which utilizes ordinates of the observed profile near the peak. The Bragg angle and parameters of the p.d.d. are expressed in terms of these arithmetical parameters.

To be submitted to *Acta Cryst.*

10·8. Operational unfolding of composite X-ray diffraction profiles. By J. J. SLADE & L. F. NANNI, *Bureau of Engineering Research, Rutgers, The State University of New Jersey, U.S.A.*

In a recent paper* we have obtained certain operational expressions, suitable for use with the aid of an analogue computer, which permit the abstraction of Cauchy & Gauss elements from multipeak line profiles. Here we consider two problems: the resolution of peaks without regard to an 'unfolding' procedure, and the unfolding of two peaks resulting from a doublet source.

The problem of resolution, other than through the abstraction of simple elements, presents a number of difficulties that may only be partially overcome.

In the doublet problem we consider the wave length distribution, transformed to the angular domain, to be represented by a function $g(\theta) = g_1(\theta) + g_2(\theta - \theta_1)$ which yields the observed line profile $h(\theta)$ through the convolution $h = g * f$ with the profile $f(\theta)$ that would result from a monochromatic beam of suitable chosen wave length. The inverse transform

$$f = T^{-1}G^{-1}H$$

is equivalent to the operational relation

$$f(\theta) = G_{op}^{-1}h(\theta) = G^{-1}i(d/dt)h(\theta) \,,$$

which yields an expression for the monochromatic profile

$$f = \Sigma(-1)^n \psi_{op}^n G_{1op}^{-1} h\,(\theta - n\theta_1)$$

in which

$$\psi_{op} = G_2(i(d/dt))/G_1(i(d/dt)) \,.$$

The operations

$$f_n(\theta) = \psi_{op}^n G_{1op}^{-1} h\,(\theta)$$

may be performed by an analogue computer whilst other means may be more suitable for obtaining the sum

$$f = \Sigma(-1)^n f_n(\theta - n\theta_1) \,.$$

The problems of distortion and 'noise' have been previously discussed.

To be submitted to *Acta Cryst.*

10·9. Electron microscopic observation of dislocations in layer structures. By S. AMELINCKX & P. DELAVIGNETTE, *Centre d'Etudes Nucléaires (C.E.N.), Mol-Donk, Belgium.*

Dislocations in a number of layer lattices (Bi_2Te_3, Sb_2Te_3, muscovite, talc, pyrophyllite, chlorite, graphite) have been observed by means of transmission electron microscopy of thin foils. Layer lattices have the consider-

---

* 'Analysis of Composite X-ray Diffraction Profiles', to be published in Journal of Applied Physics.

able advantage that they have usually a pronounced cleavage plane parallel to a glide plane. In such a case one may expect extensive dislocation arrangements parallel to the plane of the foil. In particular talc turned out to be of special interest, since the dislocations appear as wide ribbons ($\sim$ 0·5 micron) consisting of four partials, separated by stacking faults. Complicated nodes resulting from the interaction of such dislocations have also been observed. These observations provide an explanation for the fact that Grüne as well as Hendricks have been unable to determine unambiguously the stacking of the micalayers in talc and pyrophyllite.

Observations of dislocations in the other structures will be discussed also.

10·10. The observation of dislocations in mica. By E. C. H. SILK & R. S. BARNES, *Atomic Energy Research Establishment, Metallurgy Division, Building 393, Harwell, Nr. Didcot, Berkshire, England.*

Thin cleaved fragments of mica which have been examined in the electron microscope contained dislocations lying in the cleavage planes. These dislocations, which are formed by slip, interact simply to produce either zig-zag dislocations or hexagonal networks when they lie on the same plane. The superposition of loose sheets of the mica produced moiré patterns which revealed those dislocations which were perpendicular to the cleavage plane.

10·11. Deformation mechanisms active during tensile tests of iron whiskers. By E. B. HENSCHKE & H. WEIK, *Electronic Technology and Materials Laboratory, Wright Wir Development Division, Wright–Patterson Air Force Base, Ohio, U.S.A.*

A peculiar transition of a regular hexagonal cross section of an iron whisker into an elongated cross section having two right angles, observed after tensile test, is assumed to be caused by twinning in {112} planes and consecutive flexural glide, which convert the original hexagonal cross section into a cross section having four {100} faces and two {110} faces. Multiple occurrence of the same combined deformation and the appearance of slip lines in the deformed cross section are in agreement with the assumed twinning-flexural glide mechanism. The brittle fracture and the relatively high tensile strength, observed in the same whisker, are considered as a support for the suggested twinning mechanism which is believed to occur with whiskers also at room temperature providing the barrier to slip.

Submitted to *J. Appl. Phys.* for publication.

10·12. Compression textures and the surface reorientation of metals and non-metals by abrasion. By H. WILMAN, *Applied Physical Chemistry of Surfaces Laboratory, Chemical Engineering Department, Imperial College, London, S. W. 7, England.*

Extensive recent results obtained in the *Appl. Phys. Chem.* of Surfaces Lab., Imperial College, are described, extending those reported at the 4th Congress of 1957.

On most metals, unidirectional abrasion, filing or scraping of single- or polycrystalline surfaces leads in the immediate surface region to a one-degree ('fibre-') orientation, with outwardly directed axis tilted back from the surface normal, by an angle $\delta = \tan^{-1} \mu$ for Be, Mg, and graphite, but a smaller value for cubic metals. The orientation is usually (except for Zn and Cd) the same as the compression texture and is evidently due to the compression exerted via the indenting abrasive particles on the metal. For Be, Mg (Scott & Wilman, 1958) and graphite (Porgess & Wilman, 1960) it is [001]; for f.c.c. metals (Pb, Al, Ag, Cu, Ni, Pt, Au) it is $\langle 110 \rangle$ (Goddard, Harker & Wilman, 1960; Avient & Wilman, 1960) with additional {111} twinning rather than complete rotation round $\langle 111 \rangle$ as previously suggested; for In it is also $\langle 110 \rangle$ relative to the tetragonal pseudo-cubic cell (Avient & Wilman, 1960); for Sn it is $\langle 100 \rangle$ relative to the usual cell, or $\langle 110 \rangle$ relative to $a = 8\cdot21$, $c = 3\cdot17$ Å (Avient & Wilman, 1960); and for b.c.c. metals (Fe, Cr, Mo, W, Ta, Nb) it is a mixture of $\langle 100 \rangle$ (mainly) and $\langle 211 \rangle$ (Goddard, Harker & Wilman, 1960). Compression textures of In and Sn do not appear to have been determined previously.

For non-metals there is little published data. We find that at least the softer compounds show well-marked compression texture (by electron- and X-ray diffraction) when powders are compressed at up to 75 t.in.^{2}. The orientation found, and also observed (though oblique) on abraded surfaces, is $\langle 100 \rangle$ for LiF, NaF, NaCl, KCl, KBr, but $\langle 111 \rangle$ for MgO; $\langle 110 \rangle$ for CuCl and CuBr; $\langle 111 \rangle$ for NH$_4$Cl; and $\langle 111 \rangle$ for NaNO$_3$ (rhomboh. axes). On abraded NaCl and NH$_4$Cl there was in addition (also with axis oblique) some azimuthally limited $\langle 110 \rangle$ orientation associated (as for scraped Cu) with the final shear as the abrading particles pass over the compressed metal, causing orientation with the slip plane {110} nearly parallel to the surface, with the slip direction (here $\langle 100 \rangle$) normal to the abrasion direction.

Probably to be published in *Acta Cryst.*

10·13. The preferred orientation of abrasive-crystal fragments embedded in abraded metal surfaces.

By H. WILMAN, *Applied Physical Chemistry of Surfaces Laboratory, Chemical Engineering Department, Imperial College, London, S. W. 7, England.*

Earlier electron diffraction results showed that metals abraded by emery papers contain diaspore fragments oriented with a definite face (mainly (010)) parallel to the specimen surface (Kerr & Wilman, 1955); and that metals polished with commercial metal polishes contain much embedded α-quartz partly in certain preferred orientations (Mutucumarana & Wilman, 1958).

Recent results in collaboration with Dr J. Harvey have much extended these results in the case of metals, principally niobium and tantalum, abraded by various common abrasives, including emery, α- and γ-alumina, quartz, silicon carbide and diamond. The diaspore tended to be in mixed (010), (110) and (001) orientations; α-Al$_2$O$_3$ in (0001); γ-Al$_2$O$_3$ in (111) and (110); SiC (hexagonal, form II) in (110); and diamond in (111) and (110). These orientations correspond to well-marked cleavage or fracture-planes being parallel to the surface, where

such data is previously known. No previous data for fracture of SiC or γ-Al$_2$O$_3$ appear to have been available.

Probably to be published in *Acta Cryst.*

10·14. A discussion concerning the X-ray determination of deformation stacking fault probabilities in face centred cubic metals.

By MANFRED WILKENS, *Max-Planck-Institut für Metallforschung, Stuttgart-N, Deutschland.*

In the past few years several publications based on the theory of M. S. Paterson (*J. Appl. Phys.* (1952), **23**, 805) have been concerned with the determination of stacking fault probabilities in deformed metals. Several authors (e.g. J. W. Christian & J. Spreadborough (*Proc. Phys. Soc.* (1957), B, **70**, 1151) have pointed out that difficulties in interpreting the measured probabilities arise because of the assumptions of the Paterson theory.

The main assumptions are:

(1) The stacking faults are distributed randomly throughout the crystal.

(2) The stacking faults extend laterally through the entire crystal.

The restriction of assumption (1) can be avoided by introducing general distribution functions for the distances between the stacking faults. The relation between the Fourier coefficients of the intensity profiles and the distribution functions are similar to those for the distribution function of particle size as shown by E. F. Bertaut (*Acta Cryst.* (1950), **3**, 14). The shift of the centre of gravity of the intensity profile (but not the shift of the position of maximum intensity) is nearly independent of the form of the distribution functions as long as there is no strong departure from a random distribution. If, contrary to assumption (2), the stacking faults occur as small ribbons (extended dislocations), the distortion of the lattice above and below the ribbons causes a shift of the centre of gravity of the order of magnitude of that due to the stacking fault. The direction of the shift on the θ-scale depends on the relative orientation between the reflecting planes and the ribbons. The main part of these additional shifts cancels out for powder samples and also for single crystals if the assumption is made that the distribution of the ribbons within the (111)-plane concerned has threefold symmetry.

Will be published in *Acta Cryst.*

10·15. Structure and stacking faults of HfFe$_2$.

By ELIZABETH A. WOOD & VERA B. COMPTON, *Bell Telephone Laboratories, Murray Hill, N. J., U.S.A.*

The structure of HfFe$_2$ and its relation to the stacking faults which cause reciprocal lattice rods (*Z. Kristallogr.* (1959), **112**, 97) will be discussed.

Full length account likely to be published in the *Z. Kristallogr.*

10·16. Residual stresses and stacking faults in cold drawn wire. By H. M. OTTE, *RIAS, 7212 Bellona Avenue, Baltimore 12, Maryland, U.S.A.*

A number of FCC metals have been investigated in order to examine more closely X-ray diffraction line displacements due to stacking faults (SFs) and due to residual stresses.

Polycrystalline wires were cold-drawn to various reductions and all Bragg reflexions measured with monochromated Cu $K\alpha_1$ radiation in a Debye–Scherrer arrangement using a G.E. spectrogoniometer modified for the purpose. Lattice parameters were obtained by standard extrapolation techniques even when shifts due to stacking faults were present.

Cold-drawn wires should have at the surface zero radial residual stress which reaches at the center a peak tensile or compressive value depending on the severity of the reduction. Due to the finite penetration of the X-rays, some strain should, however, be observed at the surface.

Commercial purity aluminium wire, found metallographically to recrystallize between 250 and 300 °C., showed no change in lattice parameter after 83% R.A. nor any significant shifts of individual lines due to SFs.

A commercial Cu–6·6 A/O Si (1·1% Mn) alloy yielded upon deformation a marked change in lattice parameter. Individual lines were displaced in accordance with SF-theory, and the displacement increased with increasing amounts of deformation. If only the separation between two diffraction lines had been measured, appreciable line broadening due to SFs would have been observed but in certain cases the lattice parameter decreases would have been such that the expected decrease, say, in separation of the 111 and 200 lines would not have been found.

This effect is probably also responsible to a large extent for discrepancies and inconsistences experienced in attempting to measure residual strains in FCC metals by X-rays. The details of the work to be reported suggest that residual elastic strains in metals may be smaller than is generally considered to be the case.

10·17. Imperfections in crystals of zinc sulfide. By W. L. ROTH, *General Electric Research Laboratory, Schenectady, New York, U.S.A.*

A variety of crystal forms and polymorphs are produced when zinc sulfide is crystallized from the vapor phase. X-ray diffraction and electron microscope studies have been used to elucidate the nature and origin of the imperfections in single crystals. Although most crystals are imperfect and contain large concentrations of stacking faults and dislocations, a few crystals have been found to be essentially perfect in both respects. There is considerable difference in the physical properties of the perfect and imperfect crystals: their strength, resistance to phase transformation upon heat treatment, photoconductivity, and sublimation characteristics. Most of these properties can be explained by the dislocation and fault structures in the crystals.

A quantitative study of the stacking faults in quenched and annealed crystals has been accomplished by measuring the diffuse X-ray scattering in the reciprocal lattice. From these data a probability distribution function is constructed which describes the variation in stacking

sequence of planes perpendicular to the C axis. The measured function is compared with functions computed for models which assume the faults (a) were produced coincidental with the growth process, (b) are the consequence of shearing of the crystal after growth, or (c) are associated with small coherent nuclei of a second phase. It is concluded that the faults originate from shear processes which occur when the crystal is cooled through the phase transition region. In subsequent low temperature anneals, the faults become nuclei for the growth of the low temperature cubic phase and the faulted regions grow into twinned cubic crystals with the (111) planes of the cubic phase parallel to the basal plane of the parent hexagonal crystal.

Direct observation under the microscope shows that the non-perfect crystals usually contain bands parallel to (00·1). The fault model deduced from X-ray measurements is confirmed by electron diffraction which shows that the bands contain faults as a substructure. The faults can be seen directly in transmission electron micrographs, and the magnitude of their separation, as well as their crystallographic orientation, agrees with that deduced from the diffraction experiments.

To be submitted for publication in *Acta Cryst.*

10·18. Formation of ZnS polytype and mixed structures by partial phase transitions. By LESTER W. STROCK, *Sylvania Lighting Products, 60 Boston St., Salem, Mass., U.S.A.*

Withdrawn.

10·19. The stacking-faults and the intensity of the X-ray diffraction lines. By V. I. IVERONOVA, I. I. POPOVA & G. P. REVKEVICH, *Physical Faculty, Moscow State University, Moscow B-234, U.S.S.R.*

No abstract provided.

10·20. On the formation of interstitials in alkali halides*. By R. E. HOWARD, R. SMOLUCHOWSKI & D. A. WIEGAND, *Carnegie Institute of Technology, Pittsburgh, Pennsylvania, U.S.A.*

There is little doubt that ionizing radiation decreases the density of alkali halides and that it leads to the formation of halogen ion vacancies. It is far less certain whether there is a parallel formation of metal ion vacancies, halogen interstitials, or metal interstitials. This is related to our lack of knowledge of the underlying mechanism of defect generation. Some theoretical estimates and extensive measurements of changes of density and of optical properties have been made down to 4 °K. on LiF, KCl and NaCl. While the complete data are not yet available it appears that there is considerable evidence

for the formation of interstitial halogens in LiF at low temperatures by X-ray photons which have a too low energy to produce displaced atoms directly. Changes in configuration of the interstitials account for the observed density changes during annealing. It appears further that the mechanism and kinetics of defect formation depends strongly on temperature and on the nature of the metallic and halogen ions. In particular, the time constant associated with the rate of generation of defects in KCl at room temperature appears to be proportional to the square of intensity, while it is linear in LiF at room temperature and at low temperature. The influence of previous plastic deformation and of heat treatment also differs for the different alkali halides. Possible models and theoretical correlations are suggested.

About one third of this material will appear in *Phys. Rev.* before summer this year. The rest will be submitted to the same journal at a later date.

10·21. Defects in the crystal and magnetic structures of ferrous oxide. By W. L. ROTH, *General Electric Research Laboratory, Schenectady, New York, U.S.A.*

Ferrous oxide (Wüstite) forms NaCl type phases in which the Fe/O ratio is variable. Below the Neel temperature of 198 °K., ferrous oxide is antiferromagnetic and a periodic magnetic structure is superimposed on the atomic structure. The deviation from stoichiometry produces defect regions in the atomic structure, and these in turn produce magnetic defects in the antiferromagnetic structure. Neutron and X-ray diffraction have been used to elucidate the nature of these imperfections in the crystal and magnetic structures.

The deviations from stoichiometry are the result of perturbations to the cation portion of the structure, and the substructure of oxygen anions essentially is intact. Cation vacancies alone do not explain the observations, and it is found that the simplest defect consists of two cation vacancies associated with an iron in an interstitial position. The structure is described formally by distributing vacancies and interstitials among the $16(d)$ and $8(b)$ positions, respectively, of space group $Fd3m$. These defects are further associated in clusters, and consequently the non-stoichiometry produces diffuse scattering effects in addition to alterations in the intensities of the sharp Bragg peaks. The atomic arrangement in the vicinity of the defect is similar to that in magnetite, and the crystal may be regarded as a transition structure intermediate to that of rock salt and spinel.

The iron atoms associated in the vacancy-interstitial defect region form small islands in which the magnetic moments are ferromagnetically coupled. These clusters are so small that their magnetization directions fluctuate with thermal excitation, so the clusters may be regarded as 'super-paramagnets'. At sufficiently low temperature, the magnetic moments in the larger clusters become stabilized with respect to the antiferromagnetic matrix and a ferromagnetic remanence is observed in confirmation of the model deduced from the diffraction experiments.

To be published in *Acta Cryst.*

10·22. Cleavage–surface fracture of NaCl crystal. By TAKEO FUJIWARA, TAKAO KINO & SHUSO NAKAGAWA, *Laboratory of Crystal Physics, Faculty of Science, Hiroshima University, Hiroshima City, Japan.*

The behaviours of the cleavage surface of NaCl crystal formed in NaCl aqueous solution containing Mn^{++} ion were studied through electronmicroscopical observations. The experiment succeeded in getting the figures matching together on both cloven surface, and on the flat cleavage surfaces, protuberances of various shapes, circular-cone or square-cone, or long narrow height, etc., and those presenting torn off fractures were found at the same time. It was seen that both the wide step lines running roughly parallel to the direction of cleavage crack and the steep and zigzag ones running almost at right angle to that direction are generated.

Some large disc-shaped flat eminences were found on the cleavage surface, and on the central flat surfaces of them many small round protuberances could be detected in fairly regular rows. And it was also detected, that small round protuberances, some of their tops shaped like crater either arranged on the low cleavage step line or on the flat surface taking the direction of $\langle 110 \rangle$ or $\langle 100 \rangle$, and that the longish and flat protuberances arrange themselves straight in the direction of $\langle 100 \rangle$.

It is considered that these small protuberances occurred out of the impurities which some kind of vacancies enfolded tightly.

Such view concerning the impurity and vacancy can be also proposed on the basis of our research work on quench hardening of aluminium of two kinds in purity. That is, the process of resoftening of the quenched specimen was remarkable at two stages near of 200 °C. and near of 400 °C. respectively. From the isothermal annealing experiments at each stage, the activation energy of those process were obtained as about 1·4 e.V. and about 3 e.V. respectively. This second stage of resoftening, (the case that the activation energy is 3 e.V.) was found only in the specimen of lower purity.

10·23. Auf prismatische Versetzungen hinweisende ringförmige Spaltstrukturen auf NaCl-Kristallen und deren Abhängigkeit von der Vorbehandlung des Kristallmaterials. Von HEINZ BETHGE, *Arbeitsstelle für Elektronenmikroskopie, Deutsche Akademie der Wissenschaften zu Berlin, Forschungsgemeinschaft, Halle/Saale, Deutschland.*

Durch die Anwendung der Golddekorationsmethode (Bassett) gelingt die elektronenmikroskopische Abbildung von Strukturen mit Stufenhöhen bis herab zu einem Netzebenenabstand. Durch diese Technik konnten auf Spaltflächen von NaCl-Kristallen ringförmige Strukturen aufgefunden und in Abhängigkeit von verschiedenen Vorbehandlungen untersucht werden.

In Abänderung des im Programm angezeigten Inhaltes der Mitteilung wurde auf diese ringförmigen Strukturen, die auf prismatische Versetzungen hinweisen, nur kurz eingegangen. Da nach den erst kürzlich erzielten eigenen Ergebnissen der unter Vakuum durchgeführten Spaltversuche klargestellt werden konnte, dass die Luftfeuchtigkeit der freien Atmosphäre von ausserordentlichem Einfluss auf die 'Spaltstrukturen' ist,

scheint es notwendig, auch die ringförmigen Spaltstrukturen und deren Abhängigkeit unter Vakuumbedingungen zu untersuchen.

Die unter Vakuum erhaltenen Spaltstrukturen sind durch gerade Stufen ausgezeichnet, die aber unter spitzem Winkel ein etwa blitzartiges Muster bilden. Aussagen über die Stufenhöhe sind schwierig, es ist aber wahrscheinlich, dass die Höhe der Stufen des Musters nur einen oder zwei Netzebenenabstände beträgt. Wird eine solche Spaltfläche nur für eine kurze Zeit der freien Atmosphäre ausgesetzt, so sind die echten Spaltstrukturen zerstört; es werden jetzt die in elektronenmikroskopischen Arbeiten der letzten Zeit als 'Spaltstrukturen' beschriebenen bogenförmigen und etwa parallele Anordnungen bildenden Stufen aufgefunden. Eine Erklärung hierfür ist folgende: Der Wasserdampf der freien Atmosphäre löst die Kristalle in einer dünnen Oberflächenschicht. Beim Einbringen der Kristalle ins Vakuum zum Zwecke der Aufdampfung des Abdruckfilms wird das Wasser wieder verdampft, und die zuvor gelösten Kristallbausteine bewirken ein Wachstum auf der Oberfläche. Erstaunlich ist dass dieses Wachstum offenbar genügend langsam erfolgt, so dass dabei sehr gut ausgebildete Wachstumslamellen atomarer Stufenhöhe (monosteps) entstehen, die mit dem Dekorationsverfahren abgebildet werden. Durchstosspunkte von Versetzungen bilden Zentren besonderer Tröpfchenbildung; beim nachfolgenden Wachstum sind oftmals in Form einer Spirale verlaufende Wachstumslamellen um Schraubenversetzungen herum zu beobachten.

Likely to be published in *Z. Naturforsch.*

10·24. Étude des précipités de lithium metallique formés dans les sels de lithium par irradiation.

Par M. LAMBERT, C. MAZIÈRES & A. GUINIER, *La Residence, Orsay (Seine et Oise), France.*

On étudie par rayons X et microanalyse thermique différentielle les précipités de lithium qui apparaissent lorsqu'on bombarde des monocristaux de sels de lithium (fluorure, hydrure) au moyen de neutrons thermiques.

Lorsque la dose de neutrons croît, on constate la formation de plaquettes de lithium d'épaisseur faible (1 ou 2 distances atomiques), puis de globules de lithium métallique en epitaxie dans le réseau des sels de lithium considérés.

Dans le cas du fluorure de lithium, le métal apparaît sous une forme anormale c.f.c. qui, par chauffage, se transforme en donnant la phase stable c.c., sous forme de grains plus gros mais toujours orientés dans le réseau du fluorure. Des mesures quantitatives sont faites de façon à déterminer la teneur en lithium des cristaux irradiés.

10·25. X-ray diffraction studies of fission fragment damage.

By J. ADAM, A. C. FOX, M. D. ROGERS & E. WAIT, *United Kingdom Atomic Energy Authority, Atomic Energy Research Establishment, Harwell, Didcot, Berks., England.*

When fission fragments pass through matter a large number of atoms are knocked out from their positions in the crystal. A problem of determining the number of atoms affected by a fission event has been approached using X-ray diffraction techniques. Uranium carbide and nitride show measurable increases in unit cell size after irradiation in a nuclear reactor. The increase in unit cell size follows $(1 - \exp[-\gamma n])$ law where n is the neutron dose and γ a constant for given material. Assuming that a given crystal can contain only a certain concentration of defects of a given type at least until it becomes very heavily damaged we can deduce a number of atoms affected by one fission. The numbers obtained for uranium carbide and nitride are of the order of 2×10^6 atoms per fission event.

These results were obtained on powders of natural materials irradiated to low neutron dose of the order of 10^{18} thermal neutrons per sq.cm. and examined in a specially designed diffractometer.

Examination of highly enriched minute single crystals ($10–50 \mu$ diameter) of UC confirmed the measurements of cell size changes and showed that the strain broadening of X-ray reflection is readily detectable at a burn up above 50 watt days/g. and above 200 watt days/g. crystal fragmentation is observed.

Paper will be submitted to *Journal of Nuclear Energy.*

10·26. Phase change induced by pile irradiation of UZr₂.

By J. W. HARRISON, *United Kingdom Atomic Energy Research Establishment, Harwell, Didcot, Berkshire, England.*

A specimen of U–70 a/o Zr in the room temperature stable ordered delta phase was irradiated in the Harwell reactor BEPO at a temperature not exceeding 100 °C. X-ray diffraction patterns indicated that the ordered phase was transformed to the metastable disordered gamma phase on irradiation. It was observed that the degree of transformation due to a given neutron dose was given by a single exponential term. From the measurements it was concluded that the number of atoms in the delta phase converted to the gamma phase was of the order of 2×10^6 per fission event in the material.

Full length accounts to be published in the *Journal of Nuclear Energy.*

10·27. Irradiation effects in rochelle salt crystals.

By R. T. QUINN & J. R. CLARK, *United States Naval Postgraduate School, Monterey, California, U.S.A.*

Alterations in the hysteresis loops and the coloring of Rochelle salt crystals by X-rays are discussed. Absorption spectra in the visible and infra red are compared in irradiated and unirradiated crystals. Microscopic examination of irradiated crystals shows a structure of fine lines; apparently decomposition products have coalesced within the crystal.

10·28. Dynamic crystal defects produced during irradiation. By M. W. Thompson & R. S. Nelson, *Metallurgy Division, Building* 393, *A.E.R.E., Harwell, Berks., England.*

Specimens of copper, silver and gold have been bombarded with 0·3 mV. protons and 10 kV. ions of argon and xenon. Atoms were ejected from crystal surfaces with maximum intensity along low index crystal directions. The effects are interpreted as being due to the arrival at the surface of three types of focussed collision sequence. The first travels along $\langle 110 \rangle$ directions, momentum being focussed by the geometrical properties of a close-packed line of spheres. No mass transfer is thought to occur in this type of sequence and experiment shows its range to be roughly 350 Å. The second and third types travel along $\langle 100 \rangle$ and $\langle 111 \rangle$ directions and are thought to consist of successive collisions in which the projectile atom replaces the target; focussing being due to the rings of atoms which encircle the projectile's path. A theoretical study shows these rings to behave with formal similarity to the thin lens in optics, and an upper energy limit for focussing is derived. It is predicted that the maximum ranges in copper are roughly 35 Å for $\langle 100 \rangle$ sequences and 120 Å for $\langle 111 \rangle$ sequences, the corresponding figures in gold being 50 Å and 300 Å respectively. These predictions are shown to be in agreement with experiment.

10·29. Action des ions argon de basse energie (10 KV) sur des surfaces d'uranium. Par P. Haymann & Melle C. Lecomte, *7me du Colonel Moll, Paris XVIIme (Seine), France.*

Le bombardement effectué sur des échantillons d'uranium placés dans une enceinte sous faible pression d'oxygène (10^{-5}) par des ions argon accélérés sous des tensions pouvant varier entre 5.000 et 15.000 V. provoque une croissance de l'oxyde UO_2 orienté qui se produit sélectivement sur les joints de grains, les sous joints de polygonisation, les joints de macles et les lignes de glissement. Le nombre de ces germes dépend de l'orientation cristalline et la dimension des germes du temps de bombardement. Ces conditions sont étudiées plus en détails.

D'autre part ces phénomènes ne peuvent se produire que pour un domaine de densité ionique compris entre I/I_0 et $I \, \mu A./mm.^2/s.$ et peuvent sans doute intervenir dans le cas ou l'on bombarde d'autres métaux oxydables. Ces résultats doivent fournir des renseignements sur l'activation superficielle due aux processus secondaires qui suivent le choc d'un ion.

Publication: *R. C. Acad. Sci. Paris.*

10·30. Atomic displacements produced by low energy bombardment. By D. G. Brandon, *University Dept. of Metallurgy, Cambridge, England.*

(*a*) *Preliminary observations on metals bombarded with ions of the rare gases and hydrogen*

Cathodic sputtering has previously been studied by many different techniques, but it has not so far been investigated on the atomic and near-atomic scale. In the present work an attempt is being made to study the effects produced at the surface and just below the surface of thin metal films bombarded by low energy ions in a beam of small (1·5 e.V.) energy spread.

(*b*) *Some theoretical aspects of low energy ion bombardment*

Previous results indicate that the sputtering process is a function of the masses of the bombarding ion and sputtered atom and of the elastic properties of the target material. By considering the different mechanisms of energy transfer, both by the original ion and by subsequently displaced atoms, it is possible to draw some conclusions as to the threshold energies for the different processes which may occur and the metallographic features to which they may give rise.

10·31. Diffraction patterns of perfect crystals and their slopes. By M. Renninger, *Kristallographisches Institut der Universität, Marburg-Lahn, Deutschland.*

The experimental diffraction patterns of well-grown, nearly perfect crystals (calcite, Ge, Si) measured by the three-crystal-method described by the author agree rather well with those predicted by the dynamical theory in the central regions of the patterns. But the slopes on both sides of the experimental patterns are much less steep than demanded by theory. The slopes are containing two shares, of which only one is given by the dynamical theory: The proper slope of the diffraction pattern is superimposed by another dropping of intensity, that of the 'extra spot' which results from temperature movement of the crystal lattice. Both shares can be observed separated: If the crystal is turned, the proper beam reflected by the ideal crystal lattice is turning with double speed seeming as if optically reflected by the net planes. The other share, however, the (diffuse) beam resulting from the lattice oscillations holds its direction inclined to the primary beam at twice the Bragg-angle nearly without turning if the crystal is turned. The latter is dropping down more rapidly in intensity with deviation of the primary beam from the Bragg angle than the former. Besides its intensity is too small for getting comparable with that of the former at deviations less than half a degre. Therefore it cannot be made responsible for the disagreement in steepnes between theoretical and experimental diffraction patterns. – The real intensity of the extra spot may be disturbed by superimposition of Bragg reflexions from crystal particles slightly disorientated against the main lattice, especially if the crystal face has been treated mechanically, for example if it has been ground.

10·32. Zusammenhänge zwischen den röntgenographischen Merkmalen verschiedener Diamanten. Von M. Renninger, *Kristallographisches Institut der Universität, Marburg-Lahn, Deutschland.*

Systematische Röntgenographische Überprüfung einer grösseren Zahl herausgegriffener Exemplare aus einem dem Verfasser von Dame Kathleen Lonsdale zur Verfügung gestellten Sortiment von kleinen Diamanten ergab folgendes:

(1) Entgegen früher vom Verfasser geäusserter Auffassung konnte in Übereinstimmung mit den Feststellungen aus dem Labor von Dame Kathleen Lonsdale keinerlei Zusammenhang zwischen (röntgenographischer) Wachstumsgüte und dem Auftreten der anomalen Extra-spots ('spikes') gefunden werden. Es befinden sich unter den untersuchten Steinen sowohl extreme Mosaikkristalle mit sehr ausgeprägten und scharfen 'spikes' als auch nahezu ideale Kristalle mit kaum angedeuteten solchen.

(2) Eindeutiger Zusammenhang besteht dagegen durchweg zwischen Wachstumsgüte (charakterisiert durch die Intensitätsverhältnisse der regulären Reflexe) und Umweganregung (double reflexion), beobachtet am (222)-Reflex. Letztere tritt durchweg umso intensiver auf, je geringer die Extinktion.

(3) Unter den untersuchten Steinen war die Häufigkeit von Mosaik-Typen *grösser* als die von röntgenographisch vollkommeneren. Dies steht in gewissem Widerspruch zu den bisherigen anderweitigen Feststellungen, wonach Diamanten des Typ II (Mosaik-Typ) sehr viel seltener sein sollen als solche des Typ I (Ideal-Typ).

10·33. Anomalous transmission of X-rays in highly perfect, stressed, germanium. By H. COLE, G. E. BROCK & F.W. CHAMBERS, *IBM Research Laboratory, Poughkeepsie, New York, U.S.A.*

The predictions of the dynamical diffraction theory, especially with regards to the Borrmann effect, have been the subject of several recent investigations (H. Cole & G. E. Brock, *Phys. Rev.* (1959), **116**, 868; G. Hildebrandt, *Z. Kristallogr.* (1959), **112**, 312). It is now well-known that the energy flow through a perfect crystal during diffraction is along the diffracting planes, even under certain types of deformation. Further studies of the anomalous transmission of X-rays in highly perfect, stressed and unstressed, doped and undoped, bars of germanium and silicon have been carried out in this laboratory, with both Geiger counter and film detection. A summary of the experimental results, and an interpretation in terms of what is presently known about energy flow paths, will be presented.

Would be submitted to *Acta Cryst.*

10·34. Laue studies of extinction in silicon single crystals. By ROBERT H. BRAGG, *Armour Research Foundation, Physics of Solids Section, Chicago 16, Illinois, U.S.A.*

Withdrawn.

10·35. Vérifications quantitatives de la théorie dynamique sur le silicium dans le cas de la transmission et étude photographique des dislocations. Par A. AUTHIER, *Laboratoire de Minéralogie et Cristallographie, Faculté des Sciences de Paris, France.*

On sait que lorsqu'un faisceau incident $T_0^{(a)}$ de rayons X tombe sur un cristal parfait sous l'incidence de Bragg pour une famille de plans réticulaires suffisamment inclinés par rapport à la face d'entrée du cristal, il donne naissance, sur l'autre face du cristal, à deux faisceaux $T_0^{(d)}$ et $T_h^{(d)}$ dirigés, le premier parallèlement au faisceau incident $T_0^{(a)}$ et le second parallèlement à la direction réfléchie. Nous avons étudié la variation des pouvoirs réflecteurs R_0 et R_h de ces deux faisceaux en fonction de l'angle d'incidence sur des cristaux de silicium d'épaisseurs différentes et contenant peu de dislocations. Pour cela, nous avons utilisé un double spectrographe par transmission, les deux cristaux étant de même épaisseur et taillés dans le même échantillon. Les différents faisceaux sont reçus dans une chambre d'ionisation et leurs intensités sont enregistrées en fonction de la position du deuxième cristal. Ce montage nous a permis de vérifier que la largeur de raie, la forme des courbes et les intensités intégrées sont en bon accord avec les valeurs théoriques prévues à l'aide de la théorie dynamique.

Nous avons utilisé, d'autre part, un montage analogue, mais avec un monochromateur par réflexion, ce qui simplifie considérablement les réglages, pour faire une étude photographique des dislocations dans nos cristaux de silicium. Si l'on place une plaque photographique derrière le cristal, parallèlement à la face de sortie, on observe en effet dans les traces des faisceaux $T_0^{(d)}$ et $T_h^{(d)}$ de fines traînées que l'on montre être les images de dislocations. Les dislocations que l'on voit sont proches de la face de sortie du cristal et leur densité est en bon accord avec celle des figures d'attaque obtenues chimiquement. L'étude cristallographique de l'orientation des traînées confirme leur interprétation comme des dislocations. Elles se présentent sous la forme de doubles traits, noirs et blancs, le contraste noir-blanc étant inversé dans les faisceaux $T_0^{(d)}$ et $T_h^{(d)}$ et étant indépendant de la disymétrie du défaut cristallin.

The work described above will be published partly in *Acta Cryst.* and partly in the *Physics and Chemistry of Solids.*

10·36. Théorie dynamique de la réflexion des rayons X par des cristaux courbés elastiquement. Par A. GUINIER & D. TAUPIN, 205 *Rue Marcadet, Paris XVIII°, France.*

Nous avons appliqué les principes de la théorie dynamique de Darwin au cas des cristaux perturbés. La perturbation est supposée régulière et continue et ne dépend que d'une seule coordonnée d'espace, perpendiculaire aux plans réflecteurs et aux surfaces du cristal; (nous nous sommes limités au cas de Bragg symétrique). Nous en avons déduit une équation différentielle, intégrable numériquement, qui donne la forme des raies et la valeur absolue du pouvoir réflecteur.

Nous avons étudié en détail le cas où la perturbation est fonction linéaire de la coordonnée et nous donnons

une méthode de calcul pratique du pouvoir réflecteur dans le cas général où le déplacement est fonction quadratique des trois coordonnées de l'espace. Nous avons étudié numériquement le cas du silicium.

Nous avons étudié expérimentalement la *réflexion 400* du silicium avec la radiation du molybdène (mesures absolues de pouvoirs réflecteurs), pour des courbures élastiques variables. L'accord est satisfaisant et les écarts semblent dus aux défauts de l'échantillon.

The account is likely to be published in *Acta Cryst.*

§ 11. Liquids, liquid crystals, amorphous materials, glasses

11·1. La structure des colloides d'association. Par V. LUZZATI, A. SKOULIOS, F. HUSSON & J. SPEGT, *Centre de Recherches sur les Macromolécules, Strasbourg, France.*

Après avoir déterminé la structure des phases mésomorphes des systèmes amphiphile–eau (*Acta Cryst.*, sous presse) et des savons de sodium purs, à température élevée (*Nature, Lond.* (1959), **183**, 1310) nous avons étudié un système ternaire savon–eau–solvant non polaire et nous avons entrepris la détermination de la structure des micelles de savon dans l'eau.

Dans le système ternaire nous avons rencontré plusieurs phases mésomorphes dont la structure dérive de celles des systèmes savon–eau. Nous avons analysé la variation de la surface disponible pour chaque groupe hydrophile et nous avons mis en évidence le rôle de la polarité du solvant.

Dans l'étude des phases micellaires, c'est la technique de la diffusion centrale absolue qui nous a permis d'obtenir des résultats nouveaux et assez inattendus. Nous avons montré, en effet, que la forme des micelles dépend de la nature de l'amphiphile et de la concentration: dans certains cas il semble exister une transition entre la forme sphérique et la forme de bâtonnet. Nous avons pu déterminer les dimensions et la masse des micelles.

11·2. Molecular arrangements in completely disordered coherent states and their application to the theory of liquids. By J. D. BERNAL, *Birkbeck College, London, W.C. 1, England.*

An extended homogeneous arrangement of molecules of finite dimensions is defined by the statistical constancy of the particle density over volumes large compared with the molecular dimensions. The arrangement is called disordered if no two molecules are identically surrounded by others. Coherence is defined by the impossibility of drawing extended surfaces through the medium without touching a molecule.

For spherical molecules the type of coherent arrangement is specified when the overall density is given. This density can in general not be less than one third of the close packed density.

The variations of neighbour arrangements, the radial distribution function and the number, size and shape of holes between molecules for intermediate densities can be explained in terms of groups of quasi equidistant molecules formed by tetrahedra sharing faces in a variety of ways, called pseudo-nuclei. These are in general non-crystallographic in character, in particular possessing pentagonal and helical symmetries. With diminution of density, the size and, ultimately, the number of pseudo-nuclei diminish.

These concepts can be extended to cover non-spherical molecules where the pseudo-nuclei will in general be more stable and may even be more so than regular arrangements of such molecules.

These geometrical considerations are used to explain on a statistical basis the transport and thermodynamic properties of liquids.

11·3. The structure of liquid alloys of iron and aluminium. By P. J. BLACK & J. A. CUNDALL, *Physics Department, The University, Birmingham 15, Great Britain.*

Aluminium-rich compounds of transition metals form complicated structures which seem to be based on polyhedra in which nine or ten aluminium atoms closely surround a central transition metal atom. If the bonds within the polyhedra are much stronger than the bonds which link the polyhedra to each other, then only these latter bonds will be disordered on melting so that the polyhedral units will still exist in the liquid alloys. Certain density anomalies in liquid aluminium–iron alloys seem to support this hypothesis. To investigate it further, an X-ray diffraction camera has been built in which the specimen is the free horizontal surface of a liquid alloy contained in a vacuum furnace. Bragg–Brentano focussing is maintained by moving both the X-ray tube and the detector in a vertical plane about an axis which lies in the surface. The detector is a curved monochromator crystal which focusses characteristic radiation onto a Geiger counter. Amongst the corrections applied to the measured intensities are new correction factors which have been evaluated to allow for the combined effects of specimen absorption and departures from ideal Bragg–Brentano conditions.

Measurements of the scattering from iron–aluminium alloys are compared with scattering curves which are predicted for different structural models of the liquid alloy; computer programmes have been prepared which calculate the scattering both for a random mixture of iron and aluminium atoms and for a mixture composed of iron–aluminium polyhedra in liquid aluminium.

The full-length account of this work will probably be published in *Acta Cryst.*

11·4. Die Koordination in den geschmolzenen intermetallischen Verbindungen NaHg, KHg und KHg₂. Von H. SCHUHMANN, *Institut für physikalische Chemie der Universität, Halle (S), D.D.R.*

Withdrawn.

11·5. The experimental determination of order phenomena in liquids by X-rays. By H. Mendel, *Koninklijke-Shell-Laboratorium, Amsterdam. The Netherlands.*

Order phenomena in liquids show up in the distribution curves, which are a function of the deviation of the actual electron density from an average one. A reliable interpretation of these curves is only possible if they are the outcome of careful experiments and calculations. A criterion for the reliability of distribution curves obtained from X-ray measurements is their slope near the origin; which must conform to the slope calculated from the mean volume per atom and the average electron density of the sample. A method has been developed for obtaining distribution curves that closely meet this criterion of reliability up to distances of the order of an atomic radius. This has been effected by using non-sharpened intensities, while the use of recently calculated atomic scattering curves proved to be essential for a correct calculation of the background. The distribution curves thus obtained did not show any spurious ripples at small distances.

The method stood a check on amorphous quartz, where for Si it gave the expected distance to O and the expected coordination number. It has already proved valuable in the study of water, giving distances of H to O, intra- and intermolecular.

A recent study of 1,3 di-(trimethyltin)-propane is described in which the distribution of the intramolecular Sn–Sn distances was determined experimentally. The results are interpreted in terms of a model consisting of the trans- and one gauche configuration.

To be published in *Acta Cryst.*

11·6. Bestimmung der Polydispersität kolloider Systeme. Von F. Motzkus & R. Hosemann, *Fritz-Haber-Institut der Max-Planck-Gesellschaft, Berlin-Dahlem, Deutschland.*

Withdrawn.

11·7. Über die Nahordnung im flüssigen Germanium. Von H. Krebs & Cl. Winkler, *Chemisches Institut der Universität Bonn, Bonn-Rhein, Deutschland.*

The abstract can not be submitted yet because the experimental investigations are still in progress.

The paper will be published in *Z. anorg. Chem.*

§ 12 Phase transformation, martensitic transitions, ferroelectrics, λ-point transitions

12·1. Ferroelectricity and normal modes of vibration in barium titanate. By W. Cochran, *Crystallographic Laboratory, Cavendish Laboratory, Cambridge, England.*

The atomic parameters which determine the lattice vibrations of a cubic ionic crystal may be chosen in such a way that the crystal will exhibit ferroelectric or antiferroelectric properties. The transition to a phase of lower symmetry is to be regarded as the result of an instability of the crystal against a certain normal mode of vibration —a transverse optic mode having wavenumber zero, in the case of a ferroelectric transition. An outline of the calculation for a diatomic crystal has been published (*Phys. Rev. Lett.* (1959), **3**, 412).

Application of the method to $BaTiO_3$ leads to the conclusion that the three successive transitions, the dielectric properties and the relative movements of the atoms, can be accounted for numerically using atomic parameters which are physically reasonable. Devonshire's expression for the free energy as a power series in the polarization is derivable in terms of these atomic parameters. The more important physical assumptions involved are as follows:

(i) Atoms may be polarized not only in an electric field, but also as a direct result of short-range interaction between them. This fact (for which there is direct experimental evidence from crystals of simple structure such as germanium) does not affect the principle of the method, but results in the replacement of ionic charges and short-range interatomic force constants by 'effective' values, which are the atomic parameters already referred to.

(ii) The oxygen atoms are linked by bonds having comparatively large force constants. This assumption is necessary to account for the experimental fact that the oxygen octahedron is very little distorted at the first transition.

(iii) The short-range force between titanium and the oxygens depends on powers of their relative displacement higher than the first. Only a small anharmonic component is required, there is no question of a double-minimum potential.

The theory relates the lowest dielectric dispersion frequency v_2 to the static dielectric constant, the spontaneous polarization and the displacements of the atoms at the first transition. v_2 should vary with temperature as $(T - T_c)^{\frac{1}{2}}$ in the cubic phase, reaching a minimum value of about 3.5×10^{11} c.p.s. Diffuse scattering of X-rays near reciprocal lattice points (in addition to the usual thermal diffuse scattering by acoustic modes of vibration) is also predicted, with an intensity approximately proportional to the product of dielectric constant and absolute temperature.

12·2. Studies on the phase transformations of NH_4NO_3, $NaNO_3$ and $NaNO_2$*. By J. L. Amorós, M. L. Canut, P. Alonso, E. Riaño, R. L. Banerjee, M. Moreno, F. Arrese & C. Abasolo, *Departamento de Cristalografía, C.S.I.C., Madrid, Spain.*

We first found disorder diffuse scattering in NH_4NO_3, II phase (55–83 °C.) and interpreted in terms of packing disorder of the NO_3 groups. The mechanism of this metastable IV–II transition has now been studied by

refinement of the IV and II phases by Fourier methods. This transition occurs by development of packing disorder of the NO_3 groups in two extreme centrosymmetric A and B positions along the polar axis. The structure of the II phase is formed by the sum of about 75% and 20% of the A and B positions respectively, as well as a residue of the room temperature phase. This residue depends upon the experimental conditions and the hysteresis of the phenomenon.

The NH_4NO_3 transition IV–V (at -18 °C.) occurs with superlattice formation. The low temperature phase is tetragonal, $P4_2/ncm$, $Z = 8$ and $a = 7.90$, $c = 9.79$ Å. The NH_4 are located at a and e positions; the NO_3 groups on the mirror planes. The crystal structure analysis is in progress.

The phase transition of $NaNO_3$ has been studied via diffuse scattering and dilatometric techniques. Thermal diffuse scattering of the room temperature phase has been recorded and also the diffuse scattering versus temperature through the transition point in some specific reciprocal positions by Geiger counter and monocromatized $CuK\alpha$ radiation.

The diffuse scattering of both the ferroelectric and non-ferroelectric phases of $NaNO_2$ has been recorded at 20 °C. and at 220 °C. respectively and plotted in $[100]_0$ and $[100]_1$. The diffuse scattering of the ferroelectric phase is associated to reciprocal lattice points with F_0 strong. The non-ferroelectric phase shows the same diffuse scattering pattern as the ferroelectric phase but stronger. The X-ray diffuse scattering versus temperature near the transition point (159 °C.) has been studied by Geiger counter and monocromatized Cu $K\alpha$ radiation near 040, 002 and 022. The anomalies found will be discussed.

Probably to be published in *P. Dep. Crist. Min.*

12.3. X-ray studies of absolute configurations of ferroelectric crystals.* By R. Pepinsky, Y. Okaya & F. Unterleitner, *Crystal Research Laboratory, The Pennsylvania State University, University Park, Pa., U.S.A.*

In determining the structural mechanism for ferroelectric behavior, it is necessary to know not only the atomic displacements which occur with polarization, but also their directions with respect to the polarization direction.

Ferroelectrics can be divided into two classes: one, those with centrosymmetric pseudo-symmetry, such as (glycine)$_3$. H_2SO_4 (TGS), the perovskites, the alums, (glycine)$_2$.HNO_3, glycine.$AgNO_3$, NH_4HSO_4, and probably also $(NH_4)_2SO_4$ and lithium hydrazinium sulfate; and two, those with non-centric pseudo-symmetry, such as the tartrates (Rochelle salt, LiH tartrate.H_2O), guanidinium aluminum sulfate hexahydrate, KH_2PO_4(KDP), ammonium monochloracetate, di-calcium strontium hexapropionate, (glycine)$_2$.$MnCl_2$.2 H_2O, etc.

In class one, X-ray anomalous dispersion observations

are necessary to establish the directions as well as magnitudes of small atomic displacements with respect to the electric field; in class two, the absolute configuration of the pseudo-symmetric non-centric phases must be established, then the magnitudes of small displacements in the ferroelectric phase determined, and finally the *directions* of these ascertained with respect to the field direction. In the case of the ferroelectric tartrates, the absolute configuration of the d-tartrate ion is already known (J. M. Bijvoet, *Proc. K. Ned. Akad. Wet.* (1949), **52**, 313; A. F. Peerdeman, A. J. van Bommel & J. M. Bijvoet, *Proc. Roy. Soc. Amst.* (1951), B, **54**, 16), but the directions of O and H displacements with the field is unknown.

In class two, *if* the absolute configuration of a pseudo-symmetric (paraelectric) phase is *known* (as in *RS*), then the ferroelectric atomic displacements can in principle be determined without anomalous dispersion if all domains are polarized in one direction by a field. Thus neutrons could be used to determine the displacement directions of atoms in ferroelectric *RS*. This is not true for class one crystals.

Anomalous dispersion measurements of

$$|F_h|^2 - |F_{\bar{h}}|^2 = \Delta F_h^2$$

values, for determination of the small atomic displacements in crystal of either class, can be made extremely accurately on a counter diffractometer, since field reversal alters h to $-h$ values along the ferroelectric axis essentially without disturbing angular positions of the reflections.

Using the $P_s(u)$ function (R. Pepinsky & Y. Okaya, *Proc. Nat. Acad. Sci., Wash.* (1956), **42**, 286), it has been possible to determine the entire structure and absolute configuration (as a function of field direction) of TGS. Cu $K\alpha$ was used to excite the imaginary component of S. The planar glycinium ion nearly in the pseudo-mirror plane tilts in the direction of the field.

In tetragonal $BaTiO_3$, measurements using Co $K\alpha$ establish that Ti ions move in the field direction.

In the KDP group (class two), KH_2AsO_4 was examined with Mo $K\alpha$. $P_s(u)$ immediately revealed the absolute configuration of the paraelectric phase; and both field-reversal X-ray measurements and deductions from piezoelectric observations showed that arsenic (with charge $\sim +4.5\varepsilon$) moves in the field direction, while K^+ moves *oppositely*. This is confirmed with KH_2PO_4 also, using Cu $K\alpha$. This is contrary to the conclusions of G. E. Bacon & R. S. Pease (*Proc. Roy. Soc.* (1955), **230**, 359), who assigned -3ε as charge to P.

Similar measurements are in progress on other ferroelectrics of both classes. The field-reversal method plus application of $P_s(u)$ is the best route to structure analyses of many ferroelectrics, particularly those in class one. Most accurate results are obtainable using the stroboscopic diffraction method with a periodically-pulsed X-ray tube (K. Drenck & R. Pepinsky, *Rev. Sci. Instrum.* (1951), **22**, 539), since this entirely eliminates effects of primary beam intensity fluctuations. Stroboscopic studies of ferroelectric reversals were previously applied by P. B. Braun (private communication, 1958), using a dc-operated tube with gated counter amplifier.

Paper in full to be submitted to *Phys. Rev.*

12·4. Phase transitions and crystal structures of the alkali iodates as studied by nuclear quadrupole resonance, X-ray diffraction and dielectric measurements. By F. HERLACH, H. GRÄNICHER, D. ITSCHNER & P. KESSELRING, Physikalisches Institut der ETH, Zürich, Switzerland.

The pure quadrupole resonances of I^{127} in the alkali iodates have been studied in the temperature range from liquid helium up to several hundred degrees centigrade. The resonance frequencies at 0 °C. (in Mc./sec.) and their temperature coefficients $\partial\nu/\partial T$ (in kc./sec. °C.) are: $LiIO_3$ 151·5 − 8; $NaIO_3\cdot H_2O$ (a) 149·6 − 15; (b) 162·8 − 30; KIO_3 (a) 144·6 − 27; (b) 145·1 − 27; (c) 145·6 − 27; (d) 146·1 − 27; $RbIO_3$ very weak resonance at 145; $CsIO_3$ 144·2 − 14; NH_4IO_3 147·9 − 14.

From these results and from the behaviour of the resonances as a function of temperature the following conclusions can be drawn:

(1) The iodine atoms are not in centrosymmetrical positions (in contradiction to the published structure data). In KIO_3 there exist 4 different iodine lattice sites. The different temperature coefficients of the two resonances in $NaIO_3\cdot H_2O$ indicate different modes of thermal motion at the two sites.

(2) The surrounding of the iodine atoms is similar in all alkali iodates although they have different structures.

(3) Several phase transitions have been observed in the alkali iodates. KIO_3 undergoes four phase transitions at −190, −10, 75 and 220 °C. At the upper transition, the pseudocubic symmetry changes from trigonal to triclinic with falling temperature, and there is a change in the mode of thermal vibration. The 75 °C transition shows almost no changes in the X-ray diagrams, but the number of iodine sites increases from 1 to 4. Resonance (a) derives from the high-temperature resonance whose intensity decreases at the transition while (b), (c), (d) appear. This might indicate the coexistence of two phases at room temperature.

The structures of the alkali iodates have also been reinvestigated by Debye–Scherrer photographs from liquid air temperature up to several hundred degrees centigrade. Unfortunately, the growth of single crystals has proved to be rather difficult, so that only preliminary dielectric measurements have been performed. These investigations are still in progress.

A paper with the complete and more recent results, including the discovery of ferroelectricity in KIO_3, will be published in Helv. Phys. Acta.

12·5. Two structures in the system (Na,K)NbO₃. By M. WELLS & H. D. MEGAW, Cavendish Laboratory, Cambridge, England.

$NaNbO_3$ and $(Na_{0.975}K_{0.025})NbO_3$, the latter to be referred to as phase II, are two distinct phases at the sodium rich end of the system (Na,K)NbO₃. At high (> 600 °C.) temperatures, when the structure is that of an ideal perovskite, with one formula unit per cubic unit cell, there is a complete range of solid solution. It has been established optically that at room temperature only two

phases appear between $NaNbO_3$ and $(Na_{0.7}K_{0.3})NbO_3$ which coexist over a narrow (0·3%) range near the boundary at $(Na_{0.99}K_{0.01})NbO_3$. The room temperature structures investigated are distortions of the ideal perovskite structure, the distortions leading to the formation of multiple unit cells.

$NaNbO_3$, space group Pbma, is antiferroelectric at room temperature; the orthorhombic unit cell contains eight formula units, the a and c axes being face diagonals of the original cubic unit cell and the length of the b axis being four times that of the cubic cell edge.

Phase II, space group $P2_1ma$, is ferroelectric at room temperature; the orthorhombic cell has a b axis which is twice that of the cubic unit cell and is thought to be one half of that of $NaNbO_3$. It is probable that phase II is identical with the 'forced ferroelectric' structure found when large fields are applied to $NaNbO_3$.

Detailed analyses of both these structures have been carried out using three-dimensional data and Fourier synthesis techniques.

To be published in Acta Cryst.

12·6. Structure and non-stoichiometry of ferroelectric PbNb₂O₆-type compounds. By E. C. SUBBARAO & G. SHIRANE, Westinghouse Research Laboratories, Pittsburgh, Pennsylvania, U.S.A.

The crystal structure of tetragonal $PbNb_2O_6$ is related to that of some alkali tungsten bronzes (e.g., $K_{0.57}WO_3$) and consists of a three-dimensional framework of NbO_6 octahedra linked through corners to form four- and five-membered rings. The Pb^{2+} ions occupy 5 out of 6 interstitial sites formed by the octahedra. The possibility of variable occupancy of Pb^{2+} sites has been investigated by preparing several single-phase, non-stoichiometric compounds with $PbNb_2O_6$-type structure. The non-stoichiometry was achieved, for example, by replacing one Pb^{2+} ion by two monovalent ions (Li, Na, K, Rb or Cs) or by two-thirds trivalent ions (Y, La, or Sm). The resulting family of compounds may be represented by $A_{1+x}B_2O_6$ where A and B may consist of two kinds of atoms of different valency and x has values between −0·08 and 0·15. The observed changes in lattice parameters can be explained in terms of the size of ions replacing Pb^{2+} and the variable occupancy of Pb^{2+} sites. X-ray intensity data are consistent with the assumption that the additional ions introduced occupy the same sites as Pb^{2+} ions.

$PbNb_2O_6$ has orthorhombic symmetry at room temperature and is ferroelectric. It undergoes an orthorhombic-tetragonal phase change at the Curie temperature, 570 °C. Besides ionic size and other factors, non-stoichiometry has been investigated as a parameter in changing the Curie temperature. For compositions with $x > 0$ in $A_{1+x}B_2O_6$, the Curie temperature is not very sensitive to composition, changing by ± 30 °C. in the investigated systems. As the number of unfilled interstitial sites increase ($x < 0$), the transition temperature decreases sharply (by several hundred degrees).

To be published in J. Chem. Phys.

12·7. On crystal chemistry of perovskite-type compounds possessing special dielectric properties.
By Yu. N. Venevzev, G. S. Zhdanov, S. P. Soloviev, H. V. Bezus, V. V. Ivanova, S. A. Fedulov, A. G. Kapishev, *Institute for Phys.-Chem. Research, Moskow, USSR.*

The experimental and theoretical studies of the crystal chemistry of the ABO_3 perovskite-type compounds possessing special dielectric properties are carried out with the purpose of finding out the origin of the unusual properties of these compounds.

Experimental

(1) The anomalous changes of the lattice parameters, dielectric and piezoelectric properties have been found in $(BaPb)TiO_3$ solid solutions. Some of these anomalies are due to the different ions responsible for the ferroelectric activity of $BaTiO_3$ and $PbTiO_3$ (ions $B = Ti$ and $A = Pb$ respectively).

(2) The discrepancy between the X-ray and the optical data concerning the symmetry of the high-temperature phases of $NaNbO_3$ has been eliminated. Using the X-ray method it was in particular proved by us that within 360–430 °C. the distortion of the sub-cell of $NaNbO_3$ is monoclinic (the true symmetry–orthorhombic) the lattice parameters being $a = b = c$, $\beta > 90°$.

(3) The $BaTiO_3$-type solid solutions obtained as a result of a simultaneous substitution of Ba and Ti ions by A' and B' ions respectively (where $A' =$ Ca, Sr, Bi and $B' =$ Sn, Zr, Al, Cr) have been studied.

The combined data obtained and the known data on solid solutions in which Ba and Ti ions are substituted by $A' =$ Ba, Sr, Ca and $B' =$ Ti, Sn, Zr ions permit to analyse the influence of different factors on the Curie temperature.

(4) It has been shown that the dielectric properties of some ferro- and non-ferroelectric materials can be essentially improved by varying their compositions.

Theoretical

(1) A general method for the calculation of the internal fields has been developed for the crystal structures of any possible dipole configuration.

(2) The method has been applied to the real orthorhombic structure of $CaTiO_3$. In this case the internal electric field acting upon the Ti ions comes to nought contrary to the case of the ABO_3-type ferroelectrics.

The results of the above mentioned studies will be published in *Kristallographija, the Bulletin of the Academy of Sciences of the USSR (Izvestija Academii Nauk USSR)* and the *Solid State Physics* (Fizika Tverdogo Tela).

12·8. X-ray and neutron analyses of ferroelectric and piezoelectric-ferromagnetic crystals.* By Y. Okaya, R. Pepinsky, I. Shibuya, I. Krstanovic,

K. Vedam, S. Hoshino, T. Mitsui, B. Singh, M. Kay & B. C. Fraser, *Crystal Research Laboratory, The Pennsylvania State University, University Park, Pa. and Brookhaven National Laboratory, Upton, New York, U.S.A.*

The recent development of automatic high-speed least-squares refinement methods (V. Vand & R. Pepinsky, *Z. Kristallogr.* (1958), **111**, 46; cf. IBM 704 programs PS XR3 and PS XR4) has prompted re-examination of a number of ferroelectric structures, in order that the structural mechanisms of their polarizations can be better understood.

The structures of the three phases of Rochelle salt (at 32, 20 and −50 °C.) have been accurately determined in three dimensions from X-ray data. Significant departures have been found from the Beevers–Hughes structure (C. A. Beevers & W. Hughes, *Proc. Roy. Soc.* (1941), A, **177**, 251), and from the Frazer–Pepinsky two-dimensional neutron determination (B. C. Frazer, M. McKeown & R. Pepinsky, *Phys. Rev.* (1954), **94**, 1435; details to be published). Two- and three-dimensional difference maps reveal the positions of all hydrogens. No anisotropy of K-ion vibrations appear in any phase, nor are these ions displaced from their special positions. The tartrate ion alters in configuration in the ferroelectric phase, due to a transfer of charge $(\sim \frac{1}{4}\varepsilon)$ from one carboxyl to the other in the same ion. The two orientations of the H atom on O_5 and water W_8 are confirmed (B. C. Frazer, M. McKeown & R. Pepinsky, *Phys. Rev.* (1954), **94**, 1435; details to be published). The infamous O_1–W_{10} H bond (C. A. Beevers & W. Hughes, *Proc. Roy. Soc.* (1941), A, **177**, 251) plays no apparent role in the polarization.

All H coordinates in $(glycine)_3 . H_2SO_4$ have been established from *b*- and *c*-axis projections, using neutron data. The structure and polarization mechanism from a three-dimensional X-ray study (S. Hoshino, Y. Okaya & R. Pepinsky, *Phys. Rev.* (1959), **115**, 323) are confirmed. Experimental and theoretical results of critical X-ray scattering and thermal measurements near the Curie point establish that the transition is of order–disorder type (S. Hoshino, T. Mitsui, F. Jona & R. Pepinsky, *Phys. Rev.* (1957), **107**, 1255; I. Shibuya, T. Mitsui, Y. Okaya & R. Pepinsky. Paper A–4, Program and Abstracts, Amer. Cryst. Assoc., Washington, Jan. 24 (1960)). Changes in Bragg intensities are related to the spontaneous polarization, and critical scattering to the dielectric constant. A pair-correlation function is evaluated from the critical scattering.

Structural features based on extensive X-ray and neutron studies of the various phases of $(NH_4)_2SO_4$ and $(NH_4)_2BeF_4$ (S. Hoshino, K. Vedam, Y. Okaya & R. Pepinsky, *Phys. Rev.* (1958), **112**, 405) are reported, and polarization mechanisms explained in terms of these. Complete X-ray analyses of ferroelectric phases of $LiH_3(SeO_3)_2$ and paraelectric $NaH_3(SeO_3)_2$ are described, as are X-ray studies of

$$RbHSO_4, \ Li(N_2H_5)SO_4, \ (glycine)_2 . MnCl_2 . 2 \ H_2O \ ,$$
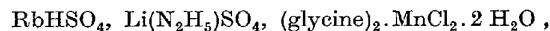
and $(glycine)_2 . HNO_3$.

The structure of $GaFeO_3$, a piezoelectric-ferromagnetic, has been determined with Mo $K\alpha$ radiation. The structure is a new type, composed of highly-distorted AO_3 and BO_3 octahedra and ABO_3 cubes.

This paper involves X-ray and neutron determinations

of 15 structures, diffuse X-ray studies of two phases of (glycine)$_3$.H$_2$SO$_4$, and several theoretical studies.

Proposed publications: *Phys. Rev.*, *Z. Kristallogr.*, and *J. Physics and Chemistry of Solids*.

12·9. Quantitative study of low frequency hysteresis loops of polarized polycrystalline barium titanate.

By GRAHAM W. MARKS & DEAN A. HANNA, *Solid State Physics Section, Code 2646, Acoustics Division, U.S. Navy Electronics Laboratory, San Diego 52, California, U.S.A.*

Quantitative studies at 25 °C. were made of the 60 c.p.s. hysteresis loops of polarized barium titanate ceramics which contained the following additives respectively: 0%, 2%, 4%, PbTiO$_3$, and 12% PbTiO$_3$ plus 8% CaTiO$_3$. Polarization versus time and field strength versus time curves were analyzed by the Fourier method. The latter curves do not depart greatly from a sine wave. It was found that the energy loss represented by the area enclosed by a ferroelectric hysteresis loop varies as the square of the maximum applied field over a range from an initial value on the field axis up to saturation. Differential permittivities were deduced from measured angles of slope at points on the hysteresis loops. Maxima are found in all curves when the applied field is opposite to the direction of polarization, and the value is constant or nearly so when the applied field is in the polarized direction. The normal permittivity also was deduced from the hysteresis loops. By replacing the mica condenser in series with the polarized ceramic with a non-inductive resistor in the display circuit, current density versus field strength diagrams were obtained. From such diagrams the differential complex conductivity was determined. A small anomalous loop was observed in these diagrams at high field strengths. A partial explanation for this occurrence is given.

Probably appear in *Trans. Amer. Inst. Elect. Engrs.*

12·10. The structural transformations of a single crystal of potassium cyanide at a temperature of about −106 °C.

By G. S. PARRY, *Department of Chemical Engineering, Imperial College of Science and Technology, London, S.W. 7, England.*

The behaviour of a single crystal of the cubic high temperature form (C) of potassium cyanide when it transforms into domains of the orthorhombic low temperature form (R), has been discussed by Cimino, Parry & Ubbelohde (*Proc. Roy. Soc.* (1959), A, **252**, 445). It was shown that if a crystal was immediately recooled after a transformation cycle C → R → C, it transformed into domains of a third structure I which was apparently stable with time and which transformed into the normal low temperature form R at a temperature several degrees lower than that at which the form R appeared in the straight transformation C → R.

The detailed appearance of oscillation photographs of this new form I has now been interpreted in terms of a monoclinic cell with dimensions

$$a = 9·2, \ b = 4·5, \ c = 7·6 \text{ Å}, \ \beta = 124°$$

whose orientation relative to the high temperature form are [001]$_C$ || [102]$_I$, (111)$_C$ || (011)$_I$. The unit cell contains four formula units KCN and the systematic absences are consistent with the space groups Aa, $A2$ or $A2/a$. Of these, the space group Aa is preferred. At the time of writing this abstract, no detailed structure of this form has been proposed but consideration of the intensities of the superlattice reflexions suggests that the y parameters of the potassium ions are small although significant. An attempt is being made to estimate this unknown parameter in the hope that a knowledge of the potassium ion lattice in the three structures C, I and R will throw some light on the complex problem of domain coexistence in these crystals.

A detailed account of this work will be submitted for publication in *Acta Cryst.*

12·11. Phase transitions in potassium thiocyanate KSCN and ammonium thiocyanate NH$_4$SCN.

By M. SAKIYAMA, Y. YAMADA, H. SUGA, S. SEKI, T. WATANABÉ & I. NITTA, *Department of Chemistry, Faculty of Science, Osaka University, Nakanoshima, Osaka, Japan.*

The polymorphic phase transitions in ammonium compounds containing anions of spherical shape have been investigated extensively by many workers with application of various kinds of physical and chemical methods. As one of the typical ammonium compounds involving rod-shape anion we have investigated here NH$_4$SCN by use of various kinds of experimental methods. Potassium thiocyanate was taken for study as the comparative material to the ammonium compound and its crystal structure above the transition point (142 °C.) was determined by the X-ray methods. By use of the methods of differential thermal analysis, volume dilatometry and specific heats measurement, the lower transition of NH$_4$SCN at 90·2 °C. was found to be of the first-order type accompanied with large volume contraction, whereas the higher transition at 119·8 °C. and the transition in KSCN at 142 °C. was recognized as the typical higher-order transition. Volume expansion coefficient, amount of volume change and also the heats and entropies of transition were determined. The expansion coefficients, along three crystallographic axes of KSCN crystal below and above the transition point were determined by the X-ray methods and their results together with the data mentioned above led us to conclude that the abnormal behavior found recently by Plester, Rogers & Ubbelohde (1959) could not be detected in our case. With the polarized light the infra-red spectra of the temperature variation of the anisotropy of the bending vibration (ν_{2a}, ν_{2b}) of SCN$^-$ ion in KSCN and the combination band ($\nu_4 + \nu_6$) of NH$_4^+$ radical in NH$_4$SCN were studied below and above the transition points. Finally, the explanation of the mechanism on these phase transitions was given

on the basis of the results obtained by these structural, thermal and optical measurements.

The part of the X-ray crystal analysis of KSCN will be published by T. Watanabé & Y. Yamada in *J. Phys. Soc., Japan* and the other part will be published by M. Sakiyama, H. Suga, S. Seki & I. Nitta in *Bull. Chem. Soc., Japan.*

12·12. A structural study of transformations in metastable body-centered cubic alloys*. By H. L. YAKEL, *Metallurgy Division, Oak Ridge National Laboratory, Oak Ridge, Tennessee, U.S.A.*

Recent investigations have shown that several body-centered cubic (β) alloys of titanium or zirconium with other $3d$ or $4d$ transition metals may be retained in a metastable condition at room temperature by quenching from high-temperature regions of β stability. Further studies have demonstrated that transitions from the metastable β state may proceed through another metastable phase—'omega' phase.

The metastable or transitory nature of the 'omega' phase in such systems as Ti–V, Ti–Cr, and Zr–Nb may be contrasted to the occurrence of a stable intermetallic phase with a partially ordered 'omega' structure in the zirconium–uranium system.

This paper presents results of a search for the formation of metastable 'omega' phases in binary alloys of titanium, zirconium, and uranium with $4d$ and $5d$ transition metals. In these alloys, the X-ray scattering powers of the components are sufficiently different to show possible ordering of the 'omega' structure. Single-crystal X-ray diffraction techniques were employed to enhance the sensitivity of the measurements and to fix lattice relationships of the phases formed.

Paper will probably be submitted to *Acta Met.*

12·13. Studies of dimensional changes at and below the 'diffusionless non-martensitic', transformation in MnAs: examination of ternary alloys. By R. O. KORNELSEN & W. B. PEARSON, *National Research Council, Division of Pure Physics, Low Temperature and Solid State Physics, Sussex Drive, Ottawa, Ontario, Canada.*

Manganese arsenide undergoes a first order transition at about 313 °K. with a loss of ferromagnetism on heating, but without change in its NiAs type of structure. At the transformation which shows hysteresis, a and U decrease discontinuously on heating but there is little change in c. The change is diffusionless, but rather than occurring by the normal martensitic mechanism it occurs with a 'brute-force-bust' process, since the strain energy of the transformation is reduced by the grains fracturing along [001] to form a stack of slightly misoriented pencil-like subgrains whose axes lie along the c direction (Basinski & Pearson).

* Operated for the U.S. Atomic Energy Commission by the Union Carbide Corporation.

The unusual nature of the transformation makes it interesting to examine the change of lattice spacings above and below it in greater detail than hithertofore (cf. Guillaud, Willis & Rooksby) and therefore lattice spacings and magnetic properties of MnAs and ternary alloys with Mn partially replaced by Co, Fe or Cr have been measured. Addition of Co or Fe lowers the transformation temperature. The alloy 2 at.% Co, 48% Mn does not become ferromagnetic down to 173 °K., whereas that with 1% Co becomes ferromagnetic at 265 °K. on cooling. The 2% Co alloy does, however, transform at about 250 °K. and both high and low temperature phases *could coexist* in this alloy.

Below the transformation a increases while c and c/a decrease with decreasing temperature. In pure MnAs a increases rapidly from 313 to about 275 °K. and then less rapidly down to at least 185 °K. The net effect of these dimensional changes is a *negative* volume expansion coefficient between 313 and 275 °K. where it changes rapidly being positive below this temperature. Similar effects are, for instance, found in ternary alloys with $\frac{1}{4}, \frac{1}{2}, 1$ and 2 at.% Co, the maximum in the atomic volume-temperature curve moving to lower temperatures with increasing cobalt content. (The discontinuous change of U at the transformation also increases in size with the cobalt content of these alloys.) The rapid change of volume expansion coefficient in MnAs at about 275 °K. appears to be discontinuous suggesting a further—second order—transformation at this temperature. The origins of this and the negative expansion coefficient are at present unknown.

Publication Journal: Undecided—publication will not occur for some time.

§ 13. Crystal growth, morphology, twinning

13·1. A method for observing the solid-liquid interface in melt grown halides. By WILLIAM ZIMMERMAN, III & WILLIAM H. VAUGHAN, *U.S. Naval Research Laboratory, Washington 25, D.C., U.S.A.*

In an attempt to observe solid-liquid interface in melt grown alkali halides, we have been able to freeze bubbles inserted during the actual growth into the solid crystal. Briefly, the technique involves the insertion of a bubble of gas below the surface of the melt; controlling the size of the bubble; making contact with the interface in such a way that the bubble adheres without motion at the growth interface; and finally growing the bubble into the crystal. After cleavage to expose the surface of the bubble, it may be examined for growth features by microscopic and interferometric means. Various observed growth features will be discussed.

To be published in *J. Appl. Phys.*

13·2. Growth features on surface dendrites of tin. By K. E. PUTTICK, *Davy Faraday Laboratory, The Royal Institution, London, W. 1, England.*

When the surface of liquid Chempur tin is rapidly cooled, for instance by sudden contact with an ingot wall,

flat leaf-shaped dendrites form. Examination of these shows a number of features which throw some light on their growth:

(a) A system of impurity sub-boundaries originating at the central axis of the dendrite. The pattern of these suggests that the tip of the dendrite grows by *thermal* supercooling (i.e. heat conduction into the liquid) while the redistribution of heat and impurity produced by the growing tip results in conditions of *constitutional* supercooling along the dendrite edge.

(b) On surfaces which nearly coincide with a (100) plane, a system of steps develops bounding (100) plateaux. These steps (previously noted on steadily grown crystals by Chalmers *et al.*) pile up along the impurity boundaries.

(c) On basal and near-basal surfaces, very low growth mounds possessing 4-fold symmetry in the shape of Maltese crosses are observed. These appear to be centred on lattice singularities which can move, and therefore may represent growth on screw dislocations.

To be submitted to *Acta Met.*

13·3. The crystallisation, conversion and melting mechanisms of the II forms of suphur, grown from thin films of undercooled melts. By G. MUELLER, *University of Concepción, Chile.*

The most interesting results obtained through direct observations under appropriate conditions of mounted thin melts are summarized below:

(1) New modifications

5 known and 6 new forms were identified through optic properties, S.G., M.P., X-ray data, etc. These are symbolised with greek letters, in order of stability beneath 97 °C., and they further subdivide, with more or less gradual transitions into high and low temperature varieties, habit-types, and all reveal one or more quasi-constant orientations to the plane of the film.

(2) Growth history

The temperature ranges of the II forms overlap, thus at 20 °C., α, η, ι, $\varkappa$ and ωS are spontaneously seeded from randomly distributed points. The growth rates reach a maximum some 15 °C. below the M.P., they decrease with the thickness and age of the melt and when two crystals approach within 0·005 mm. The time gaps of commencement of spontaneous seeding, and the subsequent rates, can be respectively decreased and increased, through the addition of minute quantities of crystalline powders, friction, ultrasonics, surface tension along bubbles, etc. No simple relations exist between growth and nucleation rates and stabilities.

(3) The definition of 'families'

The independent α-S and two families with most stable members of β and ι-S respectively can be defined thus:

(A) *Continuous growth.* The growth front of a given modifications may convert to another member of the same family, quasi-reversibly with T., either through a series of ever diminishing twin lamellae, leading to a homogeneous phase, or through spontaneous, random and often co-orientated seeding of a faster growing form.

(B) *Spontaneous Conversions.* (See below), are restricted to within families except very close to M.P.

(4) Post-crystallization processes

Protracted crystallization consists of gradual increase of birefringence of a given form, on heating, illumination or ageing, without any morphological change. An L.T. variety of a given form may undergo *partial spontaneous conversion* to the H.T. one, through the formation (particularly on rapid heating) of a generation of discrete and often co-orientated H.T. grains, which cease to grow due to progressive protracted crystallization of the remaining original phase, whereas the '*full spontaneous conversion*' between members of the same family, results in 100% recrystallization. *Contact conversions* proceed from interfaces between all the forms, and they often reveal a more or less stable transitional phase, which may even randomly nucleate. Partial conversions are sluggish, those towards the family β speed up rapidly between 50 and 70 °C.; they all depend on pre-crystallizations thermal history of the melt, relative orientations of the two phases, etc., except of the conversion α–β all are irreversible at I atm.

(5) Ageing effects

The rate of conversions ω–τ and ω–α, drastically increase, within minutes and days, respectively, with the age of the original form, whereas that of ε–α slows to a standstill in 10 sec.

(6) Dissolution and melting

Solution in $CHBr_3$ of freed films results in residues, which differ in colour, etc. from form to form. The M.P.–s with characteristic melting patterns range from 95 to 120 °C., increasing, on the whole, with stabilities over 97 °C. After brief heating a few degrees over the M.P., a given melt preferentially nucleates the original modifications.

The present work attempts to illustrate the full exploration of potentialities of 'direct observation methods' in problems of crystallization and is being extended to other substances, including silicate melts.

13·4. A new theory of melting. By T. A. HOFFMANN, *Central Research Laboratory for Physics and Research Institute for Telecommunication, Budapest, II, Hungary.*

The author shows theoretically that the energy-mixing-entropy curve of a crystal containing vacancies has two inflexion points if the block contains a definite number of atoms. The existence of two inflexion points includes the existence of a temperature at which one state with a higher entropy and one with a lower one can coexist. This is the melting temperature. The theory predicts very small intrinsic crystallite blocks in the solid state, containing about 2–10,000 atoms only. The numerical results for the melting point agree with the experimental values within 6% for alkali metals and for noble metals. The theory is supported also by some numerical results concerning the anomalous behaviour of specific heat near the melting point and by a general relation between the melting entropy and crystal structure.

To be published in *Acta Phys. Hung.*

13·5. A new theory of grain formation. By T. A. HOFFMANN, *Central Research Laboratory for Physics and Research Institute for Telecommunication, Budapest, II, Hungary.*

Based on his theory of melting the author shows that in a simple melt there may exist grains even over the melting point. However there exists a definite melting point for each grain-size, a smaller grain having a higher melting point. At a fixed temperature higher than the melting point of the solid there exist therefore only grains smaller than that which has its melting point at this temperature. At the real melting point the final grains are formed the sizes of which are about containing 2–10,000 atoms. Conclusions are drawn relating to the circumstances at which an even growth of the crystal may be efforted.

To be published in *Festkörperphysik Tagung Balatonfüred*, 1959.

13·6. Thèses de la communication 'La formation de cristaux'. Par A. V. SHUBNIKOV, *Institute of Crystallography, Academy of Sciences of the USSR, Moscow, B-17, USSR.*

L'auteur veut montrer un film à propos de plusieurs phénomènes de la cristallisation, les plus intéressants et les moins étudiés, entre eux quelques nouveaux phénomènes et ceux, qui jusqu'aujourd'hui ne sont pas adoptés par l'écran. La démonstration du film sera suivi d'une explication.

(1) La cristallisation de la chlorure d'ammonium, dissoute dans l'eau. Les dendrites se forment seulement à la périphérie de la goutte. Les cristaux ne naissent jamais dans le milieu de la goutte.

(2) La naissance de cristaux sous l'influence du champ électrique. Le commencement de la cristallisation est le même. Quand on approche un corps chargé (par exemple un peigne frotté aux cheveux) on peut voir une grande quantité de petits cristaux en forme de croix ou de petites étoiles.

(3) La cristallisation de salol fondu et légèrement surrefroidi. Les cristaux ont la forme d'un rhombe.

(4) La formation de cristaux du salol dans la fusion fortement surrefroidie (vingt degrés). Ces cristaux ont la forme d'un petit bateau. Dans le stade dernier de la cristallisation les bateaux monocristallins se transforment en rhombes.

(5) La formation de sphérolites de menthol. Il existe trois modifications cristallines de cette substance.

(6) La cristallisation de tymole. Les marches du cristal se mouvent d'une façon tangentielle.

(7) La croissance rythmique de cristaux de tymole.

(8) La régénération de cristaux de thiosulfate de sodium.

(9) La croissance rythmique de sphérolites de triphenylmethane. Un phénomène neuf, mal étudié. La cristallisation est accompagnée de la formation des ondes dans la fusion visqueuse, où se trouve un peu de colophane.

(10) Les cristaux nageants de pentaerythrite. Le phénomène, décrit par Renninger & Krause. Les cristaux ne se touchent pas. Ils sont chargés négativement. Le peigne, chargé aussi négativement, les repousse. Les plus grands cristaux éxigent pour soi un espace plus vaste. Parfois le champ électrique favorise l'apparition d'une grande quantité de cristaux.

(11) La formation d'anneaux de Liesegang.

(12) La cristallisation de sodium nitrate sur la surface de calcite. Les cristaux apparaissent sur les marches de la surface.

(13) La texture de salol, ayant la forme d'une enveloppe. La cristallisation s'expance de quatre cotés du couvreverre. Dans la lumière polarisée la préparation s'éteint quatre fois, quand on la fait tourner autour de sa normale.

(14) L'engloutissement de bulles d'air par les cristaux de salol croissants. Par la forme de bulles englouties on peut déterminer la direction de la croissance de cristaux.

(15) La formation de bifeuilles de diphenylamine. La bifeuille prend naissance d'un petit cristal, ayant la forme d'un baton ou d'une aiguille, par l'embranchement de deux bouts.

(16) La cristallisation rythmique de salol. On étale une petite quantité de salol fondu sur la surface d'un verre dépoli. La cristallisation commence, quand on touche le liquide par une aiguille, infectée par le salol cristallisé. On trace sur un verre dépoli avec un tire-ligne, rempli du salol fondu, deux lignes croisées et on excite la cristallisation au bout d'une de cettes lignes. Le front des ondes prend la disposition normale à chaque branche de la croix. La ligne de salol a maintenant la forme d'un cercle. Les ondes n'ont pas assez de temps pour se mettre normalement à la ligne.

(17) La formation de sphérolites de cholesterylacetate de la phase cristalline liquide.

(18) La formation de bifeuilles de benzoïne. L'embranchement de cristaux, qui ont la forme d'un baton.

(19) La croissance spirale de cristaux de paratoluidine de la vapeur par la méthode de Prof. Laemmlein. La goutte liquide de cette substance se mouve irrégulièrement près du centre de la dislocation. La goutte nourrit le cristal, mais ne change pas sa dimension.

13·7. The growth of cadmium crystals from the vapour. By P. B. PRICE, *Research Laboratory for the Physics & Chemistry of Solids, Cavendish Laboratory, Cambridge, England.*

A cell for the growth of crystals of cadmium from the vapour in an atmosphere of argon was designed so that the temperature, T, could be measured and the supersaturation, σ, calculated at every point. The crystals were grown on a thin quartz fibre which could be moved into various regions of σ and T in the cell. Crystal habits and growth rates were studied as a function of σ and T. A critical σ of $\sim 40\%$ for nucleation was observed below which no crystals grew and above which the density of crystals increased with σ. Once nucleated, crystals were observed to grow when σ was as low as 12%. At low supersaturations ($\sigma \lesssim 2$) the crystal habit appeared to be determined at a very early stage in growth and was independent of σ and T, consisting mainly of whiskers and thin platelets. For $\sigma \gtrsim 2$ the frequency of two-dimensional nucleation was so great that whiskers and thin platelets thickened and grew into each other, leaving as the stable growth forms mainly thick hexagonal plates. The average plate dimensions decreased as the density increased, because of increased competition for the vapour. At very high supersaturations ($\sigma \gtrsim 10^2$) crystals with dendritic habits grew to large dimensions from the deposit, the most frequent and interesting type being a

twinned leaf-like dendrite with a [12̄30] twin axis and a (0001) composition plane.

Axial growth rates of whiskers were measured as a function of σ and whisker radius and found to give fair agreement with rates derived assuming growth to be controlled by the diffusion of cadmium vapour through argon. Evidence for both tip growth and non-tip growth of whiskers was obtained.

To be published in *Phil. Mag.*

13·8. Beobachtungen zum Kristallwachstum von ZnS aus der Dampfphase. Von H. HARTMANN, *Deutsche Akademie der Wissenschaften zu Berlin, Physikalisch-Technisches Institut, Bereich Lumineszenzforschung, Liebenwalde, Deutschland.*

Bekanntlich ist Zinksulfid ein wichtiger Luminophor. Um eine gute Grundlagenforschung betreiben zu können, wurde die Einkristallzüchtung des ZnS durchgeführt. Die geeignetesten Bedingungen für die Züchtung der ZnS-Einkristalle aus der Dampfphase sind experimentell ermittelt worden. Die erhaltenen Kristalle wurden kristallographisch unter besonderer Berücksichtigung des Kristallwachstums und der Morphologie untersucht und die Frage der Abhängigkeit des Wachstums von den verschiedensten Kristallisationsbedingungen, wie Ausgangsmaterialien, Gasatmosphäre, Temperatur, Druck u. a., näher betrachtet. So wurde z. B. das Verhältnis von HCl-Gasstrom: H₂S-Gasstrom geändert und die Beeinflussung von Kristalltracht und -habitus beobachtet. Es wurden ausserdem noch einige interessante Ergebnisse mikroskopischer und röntgenographischer Untersuchungen erhalten. Auch die Lumineszenzerscheinungen der Kristalle werden durch die schon oben erwähnten Kristallisationsbedingungen beeinflusst.

13·9. Continuous observation by electron microscopy of the growth of evaporated metal films. By G. A. BASSETT, *Tube Investments Research Laboratories, Hinxton Hall, Hinxton, Nr. Saffron Walden, Essex, England.*

The microstructure of certain single crystal evaporated metal films has been extensively studied in the past. Characteristic features of such films are for example, the occurrence of a relatively high dislocation content, about 10¹⁰/cm.² is typical, the presence of stacking faults, and various types of boundaries. Speculation about the origin of these structural features during growth and subsequent rearrangement when the film is removed from its substrate has lacked experimental support.

In the present investigation an attempt has been made to elucidate the origin of some of these structural features by preparing the film inside the electron microscope enabling the growth mechanism to be followed in considerable detail. A hot specimen stage eliminates side effects due to specimen contamination and enables a specimen temperature to be maintained, sufficient for epitaxial growth to occur on suitable substrates.

In the case of the growth of a polycrystalline silver film on an amorphous carbon substrate, it has been found that after the initial production of nuclei, growth proceeds by addition of new material to these nuclei, and new ones are but rarely formed. Although adjacent nuclei have no fixed orientational relation on co-alescence a visible boundary does not always form. Some nuclei join more in the manner of liquid drops and at the moment of touching a rapid movement of material occurs. Occasionally isolated nuclei completely vanish leaving no visible trace.

As an example of the growth of a single crystal film, the growth of silver on a cleavage face of molybdenite (MoS₂) has been studied. Silver grows in (111) orientation and in this situation a moiré pattern with a periodicity of 17 Å is formed between deposit and substrate. The moiré pattern is highly sensitive to the angular misorientation of nuclei observed in the early stages of growth. As growth proceeds misorientation between adjacent nuclei is not always accommodated by building a dislocation into the structure. If the misorientation is sufficiently small the moiré pattern in the nuclei is observed to rotate to become parallel. Possible mechanisms whereby this may occur will be discussed.

13·10. The epitaxy of copper bromide on copper. By KENNETH R. LAWLESS & ROBERT H. KEAN, *Cobb Chemical Laboratory, University of Virginia, Charlottesville, Virginia, U.S.A.*

Single crystals of copper were exposed at room temperature to a known vapor pressure of bromine and the reaction product was examined by electron diffraction and electron microscope techniques. The reaction product was γ-CuBr and was epitaxially oriented on the copper substrate with apparent twinning of the bromide. Carbon replicas of the surface were examined in the electron microscope and showed the surface to consist of small facets. The relative rates of formation of the bromide film were different for different crystal faces, but the magnitude of the differences was apparently small.

Journal: Most likely *Acta Cryst.*

13·11. Growth of trioxane crystals. By JOHN H. ROBERTSON, *School of Chemistry, The University, Leeds, 2, England.*

Single crystal whisker-like filaments of s-trioxane grow very readily when this substance sublimes at room temperatures in a closed space, and the growing crystal-filaments can be demonstrated to bend elastically towards one another of their own accord within the vessel.

Physical properties of these crystals are discussed in the light of their known crystal structure (found by Moerman, 1937). Attention is directed to the pronounced strength along the needle axis, and the electrical charge developed by growing or evaporating crystals which is responsible for their mutual attraction, bending and curvature during growth. These properties may be explained by the dipolar nature of the trioxane molecule, together with the polar symmetry of the crystal space group.

13·12. Sucrose crystallisation studies. By H. E. C. POWERS, *Tate & Lyle Limited, Thames Refinery, Silvertown, E. 16, England.*

The study of sucrose crystallisation in thin films offers increased facility for:

(1) Observation and photo-micrographic recording of crystallisation phenomena.

(2) More rapid control, or deliberate change of temperature, hence degree of supersaturation.

(3) More rapid change of concentration by diffusion of solvent from the film to the vapour phase, or vice versa, if one face is open to the surrounding atmosphere.

(4) Operating at higher degrees of supersaturation, before spontaneous nucleation sets in, on account of the very small volumes so used.

(5) Producing either continuous films, or a dispersion of droplets of widely varying size, by manipulation of surface tensions.

(6) Ensuring immediate vegetative growth by using sucrose cleavage face as supporting medium, or delayed spontaneous nucleation by using glass or plastic for this purpose, in each case starting with the solution slightly sub-saturated to ensure freedom from pre-existing nuclei.

By taking advantage of the above facilities it has been possible to investigate and record some remarkable new sucrose crystal forms. An effort has been made to put forward a more specific nomenclature for the various dendritic and multi-crystal forms. Many illustrations will be exhibited.

Evidence is accumulating indicating that not only do sucrose crystals *grow* by a complex and varied layer mechanism, but that, under suitable conditions, this action appears to be reversible. The surface of a crystal covered by a saturated solution is in dynamic rather than static equilibrium. If the solution becomes supersaturated, immediately the layer growth advances, building up the crystal mass. If the solution becomes very slightly sub-saturated, the layers recede as the crystal mass dissolves. A crystal freshly immersed in the latter solution first develops faint etching, then receding layers develop and proceed continuously as the crystal dissolves away. These receding layers have been recorded upon several faces of a dissolving sucrose crystal.

13·13. Observations on impurity distributions in alkali halides. By PAUL L. SMITH, WILLIAM H. VAUGHAN & LEWIS R. JOHNSON, *U.S. Naval Research Laboratory, Washington, 25, D.C., U.S.A.*

Several methods which have proved useful in the study of macroscopic impurity distributions in alkali halides (regions of 0·1 mm. and larger) will be described. These include (*a*) a differential bleaching rate of color centers formed by high intensity low energy *x*-irradiation, (*b*) precipitation at low temperature (~ 300 °C.) and (*c*) strain birefringence. Although these methods alone do not provide information on the type of impurity and only qualitatively on the amount, they do clearly distinguish regions which can then be studied by other means such as optical absorption (ultra violet and infrared) chemical analysis and X-ray techniques for measuring misorientation.

An even more sensitive technique for detecting small amounts of impurities in the as-grown crystal, is by ultra microscopic illumination. After a suitable heat treatment impurities cluster on dislocation, grain boundaries and at isolated random spots. This method of collecting impurities at grain boundaries by heat treatment to make them visible, has made it possible to easily view impurities at the lowest concentrations.

These methods will be illustrated by examples of both melt- and solution-grown NaCl and KCl with and without added impurities.

To be published in *J. Appl. Phys.*

13·14. Growth textures in solution grown alkali halides. By LEWIS R. JOHNSON & PAUL L. SMITH, *U.S. Naval Research Laboratory, Washington 25, D.C., U.S.A.*

The techniques described by Smith, Vaughan & Johnson[*] in combination with standard X-ray methods were used to study growth textures in alkali halide crystals grown from solution on melt grown seeds. The term 'texture' as used here refers to regions of macroscopic size (0·1 mm. and larger).

The textures observed were studied as functions of growth temperature, growth rate, concentration of impurity, degree of agitation, and index of the seed surface.

It was possible to distinguish textures of growth formed on 100, 110, and surfaces of positive and negative curvature. Regions parallel to the growth front, marking successive stages of growth are distinguished as well as distinctly defined individual crystallites. Growth on a concave surface was found to be more rapid than growth on a convex surface. The texture formed appears independent of degree of agitation, temperature of growth, and to some extent independent of overall growth rate.

Correlation of surface features observed during growth with final texture is considered in relation to theories of crystal growth.

To be published in *J. Appl. Phys.*

13·15. Études sur la croissance et les imperfections des cristaux d'halogénures d'argent. Par CLAUDE SELLA, *Laboratoire de Microscopie et Diffraction Electroniques de la Faculté des Sciences de Paris, France.*

L'étude en microscopie, diffraction et microdiffraction électroniques de la structure et de la morphologie des cristaux d'halogénures d'argent, à différents stades de leur croissance, et en particulier après maturation physique, permet d'analyser les mécanismes de cristallisation et en particulier les phénomènes et croissance secondaire résultant de l'agglomération et l'accolement épitaxique des cristallites primaires.

La croissance ultérieure et le réarrangement interne de ces cristaux secondaires sont contrôlés par un mécanisme de dislocations. Ces cristaux présentent alors, suivant les conditions de sursaturation, des faciès géométriques très variés (polyèdres, filaments, dendrites, etc.).

Une attaque chimique spéciale permet de révéler d'une façon particulièrement nette les détails de leur structure interne, dislocations, joints de flexion, plans de glissements, mâcles, etc. La diffraction et la microdiffraction électronique permettent également une analyse fine de la structure et des sous structures de ces cristaux.

---

* *Impurity Distributions in Alkali Halides*, Paul L. Smith, William H. Vaughan & Lewis R. Johnson, paper submitted to International Union of Crystallography, 5th General Assembly, Cambridge, England, 1960.

13·16. The effect of impurities on graphite ←→ diamond transitions. By H. JUDITH MILLEDGE & ERIC NAVE, *Department of Chemistry, University College London, London W.C. 1, England.*

A resume will be given of the results of X-ray studies of synthetic diamonds formed with different catalysts. The effect of impurities on the transition diamond → graphite at high temperatures is reported for pressures ranging from zero to 75,000 atmospheres for both natural and synthetic diamonds. The relationship between the products of these experiments (which included the graphitisation of irradiated diamonds) and various graphite ←→ diamond phases found in meteorites and in certain diamond mines will be discussed.

To be published in *Phil. Trans. Roy. Soc.*

13·17. Über Wachstum und Absorption von manganaktivierten Korunden. Von W. KLEBER, *Mineralogisch-Petrographisches Institut der Humboldt-Universität, Berlin N 4, Deutschland.*

Bei der Züchtung von Korund-Einkristallen nach dem Verneuil-Verfahren mit Zusätzen von Manganverbindungen wird Mangan nur zum geringen Teil als diadocher Ersatz des Aluminiums in das Korundgitter eingebaut. Aus kristallchemischen Gründen kann angenommen werden, dass beim Wachstum manganaktivierter Korunde Adsorptionsmischkristalle ('anomale' Mischkristalle) zwischen α-Al_2O_3 und kubischem Mn_2O_3 gebildet werden.

Auch die Absorptionskurven der manganhaltigen Korund-Einkristalle stützen weitgehend diese Annahme: Die gemessene Rotverschiebung der Absorptionskante mit zunehmendem Mangangehalt kann mit einer Einlagerung von Mn_2O_3-Schichten in das Korundgitter zwanglos erklärt werden. Der Verlauf der Kantenverschiebung als Funktion des Mangangehaltes stimmt recht gut mit der theoretischen Kurve überein.

Im übrigen können die Absorptionsbanden, deren Intensitäten mit wachsender Mangan-Konzentration linear zunehmen, auf Grund der Theorie der Termaufspaltung im Kristallfeld (Bethe, Hartman, Hellwege u. a.) gedeutet werden, wobei das eingebaute Manganion als dreiwertig angenommen werden muss. Eine geringe Verschiebung der Hauptbande nach kürzeren Wellen mit zunehmender Mangankonzentration kann auf Änderungen des Kristallfeldes zurückgeführt werden.

Bei Röntgenbestrahlung der manganaktivierten Korund-Einkristalle erscheint in unmittelbarer Nähe der Mn^{3+}-Bande eine weitere Absorptionsbande, die wahrscheinlich mit der Bildung von F-Zentren zusammenhängt. Weitere Veränderungen des Absorptionsverhaltens können auf tiefer greifende Störungen des Korundgitters durch die Röntgenbestrahlung zurückgeführt werden.

13·18. Observations on the reduction of the spontaneous detonations probability of lead azide crystals during crystal growth. By MARYLAND D. KEMP, *U.S. Army Engineer Research & Development Laboratories, Basic Research Group, Fort Belvoir, Virginia, U.S.A.*

There are at least two crystalline modifications of lead azide, an alpha form that is orthorhombic and a beta form

that is monoclinic. Both forms are explosive and are generally grown from solutions. The alpha form may be obtained by slowly cooling saturated solutions. The beta form is obtained utilizing the diffusion techniques of Miles. During crystal growth of both forms from purely aqueous solutions spontaneous detonations frequently occur. In general, prior to exploding, the crystals exhibit, when observed visually, very desirable optical properties. The probability of explosion for the alpha form during growth for long periods of time approaches 1, while that for the beta form is considerably less, about 0·3. As part of the effort to obtain reasonably sized crystals, a study was conducted to reduce the explosion probability of the growing crystals.

It is generally known that once the crystals are obtained free of the mother liquor, they may be stored on the shelf for indefinite periods. They are still sensitive to thermal or impact initiations. Theoretical considerations led to the use of additives to the growing media and it was found that the use of ethylene glycol as an additive considerably reduced the explosion probability. For the beta form, glycol concentrations of 50%, or more, completely eliminated the spontaneous detonations. For the alpha form, similar results were obtained. Observations were made on the thermal and physical properties of the two forms as obtained from purely aqueous media and from the glycolcontaining media. It was found that insignificant changes occur in the crystal habit and none in the chemical and physical properties.

An explanation for these observations will be suggested in terms of solvent parameters.

To be published in *Faraday Soc.*

13·19. Investigations of tactoid-forming microcrystals of β-FEOOH from slowly hydrolyzing iron chloride solutions. By JOHN H. L. WATSON & JONATHAN PARSONS, *Physics Dept., Edsel B. Ford Institute for Medical Research, Detroit 2, Michigan, U.S.A.* and WILFRIED HELLER & TODD SCHUSTER, *Chemistry Dept., Wayne State University, Detroit 2, Michigan, U.S.A.*

Results are reported for experiments concerning the properties of microcrystals which occur in the sediments of a series of concentration-controlled, hydrolyzing iron chloride solutions (W. Heller, O. Kratky & H. Nowotny. *C. R. Acad. Sci., Paris* (1936), **202**, 1171; H. Zocher, & W. Heller, *Z. Anorg. Chem.* (1930), **186**, 73). From particle size studies all samples showed quite monodisperse, single distributions, with standard deviations of the order of 10%. The distributions were negatively skewed in all cases with crystal lengths ranging from 330 to 480 mμ, and axial ratios from 5·1 to 7·3. The influence of original concentration upon crystal dimensions will be discussed. The influence is stronger at lower concentrations. The rate of schiller layer formation increased with decreasing original $FeCl_3$ concentration, as was found previously by, W. Heller, O. Kratky & H. Nowotny (*C. R. Acad. Sci. Paris* (1936), **202**, 1171). Preliminary observations indicate that the rate of schiller layer formation is dependent upon more than original solution concentration alone.

X-ray diffraction powder analysis has been carried out on these specimens. The d-values obtained here have agreed closely with values given for β-FeOOH earlier by

H. B. Weiser & W. O. Milligan (*J. Amer. Chem. Soc.* (1935), **57**, 258), and O. Kratky & H. Nowotny (*Z. Kristallogr.* (1938), **100**, 356), but a much more complete table of reflections has been obtained. Because of the purity of the preparations and the experimental care exercised in the work, it is felt that particularly useful identification data for β-FeOOH has been obtained. These data will be given.

Likely to be published in *J. Phys. Chem.*

13·20. Kristallogenetische Experimente zu einer Matrizentheorie der Silikose. Von H. SEIFERT & G. LABROT, *Mineralog.-Petrologisches Institut der Universität, Münster/Westf., Deutschland.*

On the base of general principles of surface activity of solids and of the structure bound and structure controlled molecular processes of lung dust particles, R. Jäger & H. Seifert, in 1949 and further on, developed a template theory of silicosis. Especially quartz was thus considered to be a false template, instead of, for example, nucleic acids, for the biological production of transformed proteins. Although the adsorption of proteins upon quartz was verified and it was shown, in the meantime, that adsorbed protein has changed enzymatic properties, the crystallographer should give experimental facts in support of the thesis above. During the last years, proofs were given in many series of experiments, stepwise pushed on, about strictly selected oriented overgrowths of aminoacids upon quartz and other silicates which are considered to be analogous effects of the postulated primary adsorption processes of the effective particles in the lung. Biogenetic consequences were discussed elsewhere.

It is considered as important that, further on, the selective epitaxial tests were also successful with oligopeptides. A statistical discussion about nearly twenty such substances is given. Structural and epitaxial details are considered for two of these, because of their interesting morphological properties, i.e. glycyl-tyrosine and diglycylglycine.

With a high probability, we were also successful in the production of epitaxial growth of minute rods of albuminoid proteins under the condition of crystallization of such proteins after the information in biochemical literature. Because of the difficulties of their identification, we tried to get an epitaxial effect with more simple globuline proteins, the pepsine etc. The effects are hitherto still somewhat doubtful. The investigations are continued. The epitaxial effect would be of great importance for the mechanism of the processes of folding and unfolding of the molecules connected with nucleation and crystallization. — Some interesting and partly positive results with saccharides upon quartz are also discussed in the light of the theory.

Probably published in *Kolloidzschr.* or *Beiträge zur Silikoseforschung.*

13·21. Elektronenmikroskopische Untersuchungen zum Kristallabbau durch Verdampfung im Hochvakuum. Von H. BETHGE & W. KELLER, *Halle/Saale, Deutschland.*

Gelegentlich früherer Untersuchungen zur Temperaturbehandlung von Ionenkristallen im Hochvakuum wurden auf NaCl-Spaltflächen bei Temperaturen um 500 °C. sehr feine ausgebildete Abdampfstrukturen beobachtet, die elektronenmikroskopisch sehr viel mehr Einzelheiten zeigten als die bei Temperaturen dicht unter dem Schmelzpunkt in freier Atmosphäre erzielten. Diese Strukturen wurden inzwischen näher untersucht. Als Präparationsverfahren eignete sich vorzüglich die von Bassett angegebene Methode der Golddekoration. Dieses Verfahren erlaubt die Abbildung des Verlaufes von Stufen auf der Kristalloberfläche, die nur einen Netzebenenabstand hoch sind.

Die Abdampfung im Hochvakuum bei Temperaturen von 400–500 °C. erfolgt hinreichend langsam, so dass die entstehenden Abdampfstrukturen Gleichgewichtsbedingungen entsprechen.

Besonderes Interesse beanspruchen die um Durchstoffpunkte von Versetzungen herum ausgebildete Strukturen. Sowohl für Schrauben- als auch für Stufenversetzungen sind die entsprechenden Abdampfstrukturen eindeutig zu beschreiben. Die Ergebnisse entsprechen den von Frank u. a. gegebenen Vorstellungen über das Kristallwachstum auf der Oberfläche von Realkristallen. Für den Fall der Schraubenversetzungen lassen sich aus den Einzelheiten der in Form einer Spirale ausgebildeten Abdampflamellen Voraussagen zur Grösse des Burgersvektors gewinnen. Aussagen zur Stufenhöhe der Abdampflamellen lassen sich aus der Wechselwirkung der von verschiedenen Versetzungen herrührenden Lamellensysteme gewinnen.

Mit geringerer Häufigkeit aufzufindende pyramidenförmig begrenzte Gruben mit wesentlich höheren Lamellenkanten sind wahrscheinlich verunreinigte Versetzungen zuzuordnen.

Die Wechselwirkung der von einzelnen dicht benachbarten Versetzungen ausgelösten Abdampfstrukturen und die in Entfernung von einigen μ vom Zentrum entstehenden, jetzt die einzelnen Versetzungen gemeinsam umfassenden Abdampfstrukturen zeigen, dass genaue Angaben über Versetzungsdichten nur aus dem elektronenmikroskopischen Bild zu gewinnen sind.

Infolge der um Schrauben- und Stufenversetzungen verschiedenen Mechanismen zur Entstehung der Lamellensysteme ist deren jeweilige Ausbildung von der Temperatur abhängig. Auch hierzu wird entsprechendes Bildmaterial vorgelegt.

In press: *Z. Naturforsch.*

13·22. Twinning, stacking, and polytypism in aluminum borides and potassium cobalticyanide. By J. A. KOHN, W. D. TOWNES & D. W. ECKART, *U.S. Army Signal Research and Development Laboratory, Fort Monmouth, New Jersey, U.S.A.*

Twinning is commonly regarded as a specific form of defect structure, defined by one of several twin laws. It is of greater significance to consider twinning as the application of an operator (or operators) to (a) a structure (i.e., twinning in its more physical sense) or (b) a unit cell (i.e., repetitive twinning in its more geometrical sense). Thus T. Ito (*X-ray Studies on Polymorphism*, Maruzen Co., Ltd., Tokyo (1950)) differentiates 'structure twinning' and 'cell twinning'. The usefulness of treating twinning in this larger sense is aptly demonstrated by α-, β-, and γ-AlB$_{12}$ and by the polytypes of K$_3$Co(CN)$_6$.

Orthorhombic, pseudotetragonal β-AlB$_{12}$ shows ex-

tremely fine ($\sim$ 2000 Å), regular, polysynthetic 'structure twinning' on both (110) and (1$\bar{1}$0). Single-crystal X-ray diffraction patterns show quadruply multiple reflections. Tetragonal, pseudocubic α-AlB$_{12}$ is observed as a simple, macroscopic 'structure twin' on (101) (=pseudocubic (111)) after the spinel law. The α phase can also be 'cell twinned' on (101) after a singly repetitive scheme (i.e., a 1·1 stacking sequence) to generate orthorhombic γ-AlB$_{12}$. The α and γ phases, most often syntaxically intergrown, thus represent end members of a potential polytypic series. The K$_3$Co(CN)$_6$ polytypic series has five known members: 1-, 3-, 7-, and 8-layer monoclinic (1M, 3M, 7M, 8M) and 2-layer orthorhombic (2 Or.). 1M shows simple, macroscopic, (100) 'structure twinning', diffraction effects being additive. 'Cell twinning' of 1M on (100) after 1·1 and 2·1 stacking sequences gives 2 Or. and 3M unit cells, respectively. More complex sequences are required for 7M and 8M, the latter probably being 2·1·1·2·1·1 or 3·1·3·1. 2 Or. can be derived from 1M using either of two 'cell twinning operators' (stacking mechanisms). Only one gives the observed space group, permitting unambiguous designation of the correct stacking geometry.

Intended for *Z. Kristallogr.*

13·23. Twinning in leucite. By M. KOREKAWA, *Max-Planck-Institut für Silikatforschung, Würzburg, Deutschland.*

The twin structure of leucite (from Albano mountains near Rome) has been determined by means of precession photographs. At room temperature leucite has the lattice constants:

$$a_0 = 13 \cdot 10, \quad c_0 = 13 \cdot 78 \text{ Å}, \quad c_0/a_0 = 1 \cdot 052$$

and a preliminary space group $I4_1/a$. The twin structure consisting of four individuals is shown in reciprocal space in Fig. 1. When the (101) direction in the crystal space of leucite (low-temperature modification) is fixed, then two possibilities for the lattice direction exist (Fig. 2). In the case where $c_0/a_0 = 1 \cdot 052$ the calculated value for α in Fig. 2 is 2° 52'. In considering the mechanism of twinning
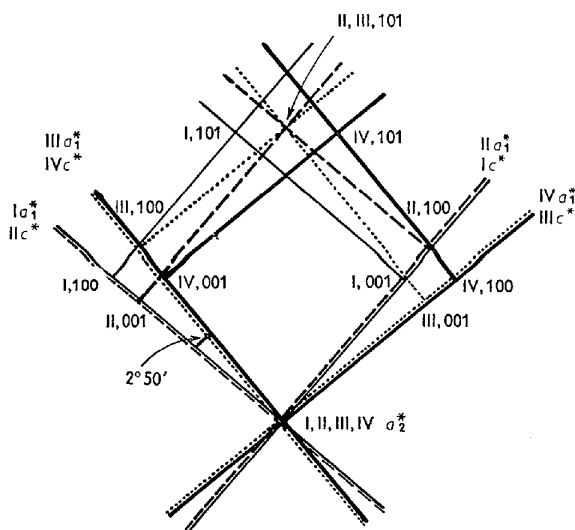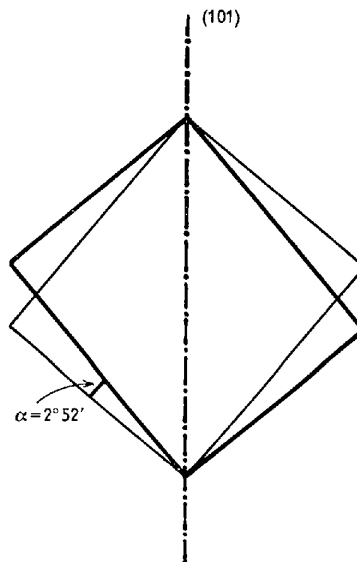

Fig. 1.

Fig. 2.

it is noteworthy that the calculated and observed values for α are equal.

13·24. A simple method to deduce the morphology of a crystal from its structure. By P. HARTMAN, *Geologisch en Mineralogisch Instituut, Garenmarkt 1 b, Leiden, The Netherlands.*

The periodic bond chain theory of crystal morphology (cf. P. Hartman & W. G. Perdok, *Acta Cryst.* (1955), 8, 49) enables one to classify the crystal faces into three classes: flat, stepped and kinked faces. To this end all possible periodic bond chains in the structure have to be found and their combinations to form flat faces are to be studied. This procedure is rather tedious.

A far more simple method consists in the use of projections. First, a projection is made on the plane perpendicular to the shortest lattice translation. The periodic bond chains parallel to this lattice row are drawn; each of them should have the same composition as the crystal and its projection should be centrosymmetrical. Only in certain directions are these chains connected to each other by strong bonds, so as to form slices parallel to the flat faces in the zone under consideration. Other periodic bond chains must be responsible for these connections and projections are made parallel to each of these chains. In each projection the chains again form slices, so that eventually new flat faces and new chains are found. In practice a few projections are sufficient to find all flat faces.

Moreover this method gives some indications on the possible types of growth features to be expected on the various faces.

Publication: will probably be submitted to *Acta Cryst.*

13·25. An extended theory of crystal forms and the morphology of twins. By I. SHAFRANOVSKI, *Institute of Mines, Vasilievsky Ostrov, Leningrad, USSR.*

Forty-seven simple crystallographic forms in fact per-

mit to characterize exactly only the convex crystal poly-hedrons. Skeleton crystals, twins, inductive surfaces, zones and pyramids of growth, sculptural complications on the faces require other geometrical models for their exact description.

This necessitated the introduction of a series of new conceptions in the modern morphology of crystals. It has proved expedient to put forward the conception of simple peak and edge forms—the aggregates of corners and edges of a crystal interconnected by its symmetry elements. It became also necessary to extend the limits of the theory of simple face forms of crystals by introducing into it the varieties of reentrant angles.

At present the definition of all these geometric varieties of crystallographic forms is completed. The varieties of face forms with reentrant angles are particularly important for the exact morphologic description of skeleton forms and twins.

H. Curien & Le Corre suggested that bichromatic symmetry using the Shubnikov elements of antisymmetry be applied for the characteristics of twins. H. Curien & J. D. H. Donnay use the conception of chromatic symmetry to define the complete symmetry of twins. However these methods concern only the general symmetry of the twin and give no conception about its form. Here the varieties of simple face forms, frequently displaying themselves on twins, may be successfully applied.

Using in the description of twins the conception of summarized simple forms, with reentrant angles or without them, we must consider all these forms as bichromatic figures; so, for instance, a penetration twin of two tetrahedrons of a tetrahedrite gives a summarized simple bichromatic form corresponding to the variety of an octahedron with reentrant angles. The penetration twin of two pentagon—dodecahedrons of pyrite corresponds to a summarized simple bichromatic form—a variety of a tetrahexahedron with reentrant angles.

The addition of a list of bichromatic simple forms to the formulas of general symmetry gives an exhaustive conception of twins.

§ 14. Symmetry, including extensions of space-group theory

14·1. Antisymmetrical arrangements in the plane, and regular three-dimensional bodies as sources of inspiration to an artist. By M. C. ESCHER, *Van Heemstralaan* 28, *Baarn, The Netherlands.*

The division of a plane into identical and/or similar figures in such a way that no 'empty' space is left, is a problem which has fascinated me as an artist for over thirty years. However, I wish to indulge in this jig-saw puzzle mania only by using figures which have a 'meaning', which are recognized as such by an observer. Animal shapes are the most suitable for this purpose, plants to a lesser degree, and objects only rarely.

From the beginning of my investigations, the use of contrasting colours or shades was both self-evident and necessary in order to distinguish visually between neighbouring figures. I was therefore surprised to learn that the notion of antisymmetry has only recently been introduced into and accepted by crystallography. My own applications are unthinkable without the use of colour contrast.

A series of sets of two pictures each, projected simultaneously, will be shown, to the left, a fragment of an infinite planar array of identical interlocking figures, and to the right, a drawing in which the 'motif' shown on the left has been used to build up a closed composition. In these compositions chiefly three different ideas have been visualised.

(1) If the antisymmetry is restricted to two shades, say, black and white, then the white figures can serve as a background to the black ones, and vice versa. This may lead to the conception of a polar duality, such as day-and-night, or sky-and-water.

(2) A transition from flat to spatial, from inanimate to living, from rigid to moving, can be suggested.

(3) The figures can gradually change their shape; also, though remaining similar, they can gradually expand or contrast. This may lead to the notion of infinity, which can be approached in various ways.

After these imaginations which all pertain to planar antisymmetry, there will be shown and discussed some reproductions the subject of which are suggestions of space, my inspiration here has been the sense of beauty I experience when looking at regular polyhedra or spherical bodies.

14·2. Early contributions to the theory of symmetry groups. By J. D. H. DONNAY, *Johns Hopkins University, Baltimore* 18, *Maryland, U.S.A.*

The historical development of t-translational d-dimensional symmetry groups G_d^t (A. Niggli's notation) is marked by the following milestones.—The 32 G_3^0: Hessel (1830), Bravais (1849), who also enumerated the non-crystallographic cases, Gadolin (1871), and Minnigerode (1887).—The 230 G_3^3: Jordan (1867) and Sohncke (1879), for the 65 groups of movements only; for the remaining 165 groups Fedorov (1891)–Schoenflies (1891), followed by Barlow (1894), who missed a few possibilities.—The 17 G_2^2: Fedorov (1891); followed by Fricke & Klein (1897), Polya (1924), who considered them as G_3^2 groups of movements, P. Niggli (1924), and Günzburg (1929), followed by Shubnikov (1940).—The 75 crystallographic G_3^1: C. Hermann (1928); the non-crystallographic G_3^1: C. Herman (1928) and E. Alexander & K. Hermann (1928).—The 80 G_3^2: C. Hermann (1928), Weber (1929), E. Alexander & K. Hermann (1929), Heesch (1929), followed by Shubnikov (1940, 1946). Motzok (1930) found $2n+1$ generalized symmetry operations in G_n; Hurley (1951) gives 222 crystallographic G_4^0. On the faith of $G_{n+1}^n = 2\ G_n^n + (G_n^n)$, where G stands for the *number* of groups G, we get 1651 G_4^3.—As to the (black-white, neither colorless nor grey) antisymmetry groups $(G_d^t)'$, the 58 $(G_3^0)'$ are due to Heesch (1930), who also began the study of the $(G_3^t)'$ and lists the 7 triclinic and the 91 monoclinic $(G_3^3)'$. The complete enumeration of the 1191 $(G_3^3)'$ came 25 years later: Zamorzaev (1953–54), Belov, Neronova & Smirnova (1955–57).—Recent developments deal with degenerate symmetry, including color groups, and superpositions of groups (see next abstract).

14·3. Later contributions to the theory of symmetry groups. By A. L. MACKAY, 21, *Torrington Square, London, W.C. 1, England.*

(See paper by J. D. H. Donnay). The development of symmetry group theory since about 1950 is reviewed and an attempt is made to relate individual advances to each other. Most contributions are concerned with describing the systematic ordering of elements which have more properties than mere position. Many of these properties can be identified with physical features (spin or dipole moments, etc.). Types of disordering have also been systematised theoretically as a result of observing certain of them experimentally. Various non-crystallographic groups have been encountered (cylindrical lattices, helical and surface packings, etc.). Progress has also been made in treating theoretical aspects.

14·4. Cryptosymmetry and tensors. By A. NIGGLI, *Institut für Kristallographie, Eidg. Techn. Hochschule, Zürich, Switzerland.*

The cryptosymmetry concept, covering antisymmetry, color symmetry and more complex degenerate kinds of symmetry, has been introduced as a generalization of the point symmetry concept (A. Niggli & H. Wondratschek, *Z. Kristallogr.* (1960), in the press). It is now applied to space-group symmetries as well.

Furthermore, the combined effect of inherent and imposed symmetries on a tensor describing any physical property will be characterized in terms of crypto-symmetries.

The inherent cryptosymmetry describes the proper symmetry of the tensor, caused by additional general conditions intrinsic to the physical property.

The imposed cryptosymmetry describes the modification (or annihilation) of the tensor, caused by the behaviour of the tensor (e.g., invariance) under external symmetry conditions.

The inherent cryptosymmetries and the imposed ones do not operate in the same way.

14·5. Symmetry in Fourier space. By A. BIENENSTOCK, *Division of Engineering and Applied Physics, Harvard University, Cambridge 38, Mass., U.S.A.* and P. P. EWALD, *19 Fordyce Road, New Milford, Conn., U.S.A.*

Since the symmetry properties represented in crystal space by the array of symmetry elements, or the coordinates of equivalent points, are equally contained in the expressions of the geometrical structure factor, it should be possible to derive the symmetry of the latter directly in Fourier space, without any reference to crystal space. This program involves the distribution of complex weights on the lattice points of the reciprocal lattice. The relative phases of the weights at symmetry-related points can be determined by considerations of uniqueness. This leads to the Fourier space equivalent of complex symmetry groups in crystal space (including black/white and colored groups). In order thence to arrive at the 230 Fourier transforms of the Schoenflies–Fedorov groups a restriction has to be placed on the phase relations which corresponds to the exclusion of complex and anti-symmetry elements in crystal space.

To be submitted to *Acta Cryst.*

14·6. Theory of OD-groupoids—an extension of space group theory. By K. DORNBERGER-SCHIFF, *Deutsche Akademie der Wissenschaften zu Berlin, Institut für Strukturforschung, Berlin-Adlershof, Deutschland.*

As is well known, space groups are not applicable to structures showing one- or two-dimensional disorder. An extension of space-group theory is therefore necessary, in order to obtain the adequate tools for such structures (see K. Dornberger-Schiff (1956) and submitted). In an other session a report will be given on two examples of such applications.

The elements of the Brandt groupoids which correspond to the space groups are partial operations which will bring part of the structure into coincidence with part of the structure, without necessarily transforming the whole structure into itself.

The principles of a groupoid theory of OD-structures i.e. of structures which have essential properties (namely a certain kind of short range order) in common with ordered structures, will be given and shown, how the groupoid family may be deduced from the distribution of sharp points and diffuse rods in reciprocal space, from the symmetry of this distribution and from systematic absences. From the groupoid family general expressions for the coordinates of atoms are obtained, which may serve as a basis for structure factor calculations and certain modified Patterson- and Fourier-projections. On the other hand, twinning of such a kind, that the twin-individuals have a layer—the boundary layer—in common (see e.g. W. T. Holser (1958), K. Dornberger-Schiff (1959)) may also be described as special cases of OD-structures.

14·7. The interpretation and nomenclature of coloured space groups. By C. HERMANN, *Kristallographisches Institut der Universität, Marburg, Deutschland.*

Coloured space groups admit of several interpretations. E.g.: (1) Different colours may mark different atoms. Any crystal, in which different atoms occupy equal lattice complexes, may be described by two space groups: an 'upper group' that considers all points equivalent and a 'lower group' (necessarily a subgroup of the former) that transforms only one set of one colour into itself. The index of the lower group in the upper group gives the number of colours required. If it is a prime number, the subgroup must be either class equivalent or cell equivalent. In these cases it is sufficient to describe, respectively, the upper group by its translation symbol only, or the lower group by its symmetry elements only. Examples:

NaCl, $P_2m3m:Fm3m$ or $P_2:Fm3m$; CsCl, $Im3m:Pm3m$ or $I:Pm3m$; Zinc blende, $Fd3m:F\bar{4}3m$ or $Fd3m:\bar{4}3m$; Wurtzite, $C6/mmc:C6mc$ or $C6/mmc:6mc$; FeSi, $Pa3:P2_13$ or $Pa3:2_13$. If, before the distribution of colours, the symmetry of the upper group is reduced, the maximum group may be prefixed between parentheses. Examples:

CuAu, $(Fm3m)F:C4/mmm$; cubic PtCu, $(I_2)P_2:Fd3m$. If the lower group is a self-conjugate subgroup of the upper group (as is always the case for bicoloured groups), the lower group transforms not only one but each set of atoms into itself and is the conventional space group. If it is a general subgroup, and all colours represent different atoms, the group of the total structure is only the

largest self-conjugate subgroup of the upper group contained in the lower group. Thus, the 4-coloured group $F:Pm3m$ will describe structures of symmetry $Pmmm$ only. No symmetry is lost, however, when one kind of atoms is assigned to black points, and another to points of all other colours, as in Cu_3Au, space group $Pm3m$. Likewise $MoSi_2$ would have $I_C:I4/mmm$, with space group $I4/mmm$ (instead of $I4mm$, if the two sets of Si were different).

(2) Colours may symbolize additional dimensions. No full n-dimensional crystallography will be derived in this way, as space dimensions are never transformed into colour dimensions. E.g. bicoloured groups based on the 17 plane groups lead, depending on the z-coordinates assigned to the two colours, either to 46 of the 80 net groups or to 46 hemimorphic space groups with only two alternating layers in the z-direction. If more than 2 colours occur, the number of additional dimensions must be determined by group theory: Mark all colour permutations that accompany any translation or symmetry operation of the upper group and find the minimum number of dimensions needed to represent their group by transformations. If this group consists only of real transformations there is no need to introduce translations in the colour dimensions. If complex factors $\exp(2\pi i/n)$ are admitted, some of the colour dimensions may be spared, but we shall have operations with glide components in colour directions creating additional translations in colour space.

14·8. The application of magnetic symmetry to neutron diffraction data. By J. S. KASPER, *General Electric Research Laboratory, Schenectady, N.Y., U.S.A.*

An elegant procedure (G. Donnay, L. M. Corliss, J. D. H· Donnay, N. Elliott & J. H. Hastings, *Phys. Rev.* (1958), **112**, 1917–1923), utilizing considerations of symmetry and antisymmetry, has been proposed for the determination of magnetic structures from neutron diffraction data. Since the materials often are available only in polycrystalline form, a unique magnetic space group determination frequently cannot be made. In such circumstances, the procedure is still useful in providing systematically a variety of possible models; it may even allow a greater certainty in the assignment of magnitudes of magnetic moments since these may be found to be the same in all possible space groups. On the other hand, caution is advisable regarding the choice of the highest symmetry group as defining the spin direction. It is desirable to utilize information on magnetic anisotropy or in the lack of it to give due consideration to models, possibly of lower symmetry, which may be physically more acceptable.

The main examples to be considered are (1) NiMn— an antiferromagnet of simple crystal structure; (2) α-Mn —an antiferromagnet of complex crystal structure; and (3) Mn_3O_4 a ferrimagnet of complex magnetic structure.

Probably to be published in *J. Phys. Chem. Solids.*

14·9. Tables of magnetic space groups. A joint project. By N. V. BELOV & N. N. NERONOVA, *U.S.S.R.* and J. D. H. DONNAY & G. DONNAY, *U.S.A.*

The recently proposed tables of magnetic space groups

(J. D. H. Donnay & G. Donnay, *Fedorovskaya Sassiya po Kristallografii, Tezisy Dokladov*, 45–46, Leningrad, May 21–27, 1959; *C. R. Acad. Sci., Paris*, **248**, 3317–19, June 8, 1959), in which the magnetic moment, considered a dipole, is represented by an axial vector, are now being constructed independently in Moscow and in Baltimore. The presentation of the results for all general positions lends itself to great simplification; in any one crystal system a one-or-two-page table suffices to answer the following question: letting $[uvw]$ be the moment on site xyz, what is the moment on all the remaining sites of the general position (in any colorless or black-white space group)? At least a one-page table is required for the special positions of a colorless space group and its related black-white groups with colorless lattice (cp. the list given by N. Belov, N. N. Neronova & T. S. Smirnova, *Kristallografiya* (1957), **2**, 315–325); groups with black-white lattices require special treatment. Various modes of presenting the results are being considered.

Publication. It is expected that these tables will be published as a special volume, possibly in the series of *International Tables.*

14·10. Further studies of three-dimensional networks. By A. F. WELLS, *Research Department, I.C.I. Ltd., Dyestuffs Division, Hexagon House, Manchester, 9, England.*

In earlier papers a number of three-dimensional networks were derived and illustrated, in particular networks in which either three or four links meet at each point. Some entirely new families of three-dimensional networks can now be described. They will be illustrated by models and stereoscopic photographs.

To be submitted to *Acta Cryst.*

14·11. A modular algebra for the description and classification of crystal structures. By A. L. LOEB, *Department of Electrical Engineering, M.I.T., Cambridge, Mass., U.S.A.*

Algorithms have been presented (A. L. Loeb, *Acta Cryst.* (1958), **11**, 469; *Acta Cryst.* (1960), in print) for the location of cubically and hexagonally close-packed arrays and their interstices. The distribution of ions over these interstices is given by a binary distribution function. The purpose of these algorithms is three-fold: (1) To describe directly the symmetry of fields surrounding any given ion rather than the symmetry of a unit cell; (2) to provide a description of crystal structures suitable for storage in a computer memory, and (3) to classify, unify and correlate a wide variety of different structures. Building blocks have been designed to demonstrate the algorithms and use them to build a variety of different crystal structures. Structures analyzed since the latest publication (*Acta Cryst.* (1960)) include cuprite, cadmium iodide and corundum. The method has also been extended to include structures containing no close-packed arrays, such as caesium chloride and rutile.

Results likely to be published in *Acta Cryst.*

14·12. Classical number theory and linear relations between lattice sums. By P. NAOR, *Technion-Israel Institute of Technology, Haifa, Israel.*

The following problem is posed: It is desired to find the number of relations between lattice sums (i.e. crystalline potentials made up of elementary atomic or ionic potentials each of which is isotropic with respect to its source) at the points p_1/q, p_2/q, ..., p_l/q, ..., p_ν/q, where q is some fixed natural integer, p_l an integer between 0 and $q-1$, and ν the dimensionality of the lattice. A solution is presented for the following cases:

(a) $\nu = 1$. It is shown that the number of relations between lattice sums can be obtained from Euler's number-theoretic function $\varphi(q)$.

(b) $\nu = 2$. (Square lattice and hexagonal lattice). It is shown that the solution may be obtained from a generalisation of Euler's number-theoretic function.

(c) $\nu = 3$. (Cubic lattice). It is shown that the three-dimensional case differs radically from the first two cases and that the solution is connected with the (so-called) optical equation in number-theory.

This study is a continuation of the author's 'Linear Dependence of Lattice Sums' (*Z. Kristallogr.* (1958), **110**, 112) and will be submitted to the same journal.

§ 15. Neutron diffraction

15b·1. The effect of crystal imperfections in ferromagnetic materials on the depolarization of cold neutron. By ALFRED SEEGER & HELMUT KRONMÜLLER, *Max-Planck-Institut für Metallforschung, Stuttgart, Deutschland.*

Hughes, Wallace & Holtzman showed experimentally that small deviations from the uniform magnetization of a ferromagnetic material give rise to a measurable depolarization of a neutron beam transmitted through the magnetized material. We have investigated theoretically the effect of the deviations from uniform magnetization due to lattice imperfections, in particular dislocations. The measurement of the depolarization of the transmitted beam provides the same information on the number and arrangement of dislocations as direct susceptibility measurement in the saturation range do. However, considerable additional information can be obtained if the depolarization of the scattered neutrons is measured as a function of scattering angle. We shall present detailed theoretical results relating the degree of depolarization to the dislocation distribution.

The full account of the work may be submitted to *J. Phys. Chem. Solids.*

15·2. The use of nuclear null-matrix in neutron diffraction studies of crystal structures and magnetic structures. By S. S. SIDHU, LEROY HEATON & M. H. MUELLER, *Argonne National Laboratory, Lemont, Illinois, U.S.A.*

Crystal structure studies of systems containing light atoms such as hydrogen, carbon, nitrogen, etc., among heavy atoms, and studies of magnetic moment align-

ments in magnetic structures have been made by means of 'nuclear null-matrices'. A null-matrix consists of two types of nuclei. One type scatters thermal neutrons 180° out of phase with the other. The atomic percentages and the amplitudes of randomly distributed atoms in a matrix are such that the structure factor:

$$F_{hkl} = \sum_n (p_A b_A + p_B b_B) \exp 2\pi i(hu_n + kv_n + lw_n) = 0 .$$

Since $p_A b_A + p_B b_B = 0$.

Here p_A and p_B are the fractions of all sites occupied by A and B type atoms respectively and b_A and b_B are the amplitudes. From the known amplitudes* of various nuclei the following null-matrices were prepared: (1) $M_{Ti-Zr} = 62$ at.% Ti and 38 at.% Zr; (2) $M_{Ti-W} = 55$ at.% Ti and 45 at.% W; (3) $M_{Mn-Co} = 43$ at.% Mn and 47 at.% Co; and (4) $M_{Mn-Cu} = 69$ at.% Mn and 31 at.% Cu.

Each matrix was employed for a specific investigation. M_{Ti-Zr} was deuterated to $M_{Ti-Zr}D_{1\cdot99}$, which was studied by neutron diffraction to determine the positions of deuterium atoms with respect to one another and to the metal atoms; M_{Ti-W} was made into $M_{Ti-W}C$ to study the positions of carbon atoms; $Mn_{1\cdot88}Co_{2\cdot12}C$ was prepared from M_{Mn-Co} to study atomic ordering of Mn, Co and C, and magnetic moment ordering of Mn and Co, and M_{Mn-Cu} was studied for magnetic moment alignments of Mn atoms.

When the atoms of the null matrix remain random in a compound formed by the null-matrix with another element, the intensities of the diffraction peaks in a neutron diffraction pattern result from the coherent scattering by the compounding atoms only. Where additional neutron scattering takes place due to ordering of magnetic moments, these intensities superimpose in the case of ferrimagnetic and the ferromagnetic materials, but give additional diffraction peaks for the antiferromagnetic materials. These results then may determine uniquely the positions of light atoms among heavy atoms, and the magnetic moment alignments in the unit-cell.

If, however, the atoms of the null-matrix take ordered positions in the compound, then the intensities of the peaks result from scattering both by the null-matrix elements and the compounding atoms. This has been found to be the case in $M_{Ti-Zr}D_{1\cdot2}$ and $Mn_{1\cdot88}Co_{2\cdot12}C$.

15·3. Anomalous neutron scattering in α cadmium sulfide. By S. W. PETERSON & H. G. SMITH, *Chemistry Division, Oak Ridge National Laboratory, Oak Ridge, Tennessee, U.S.A.*

Breit–Wigner dispersion theory implies that the neutron scattering amplitude is complex, thus that there is a component of scattering, from an isotope in a resonance state of the compound nucleus, which is 90° out of phase with normal scattering. While the Breit–Wigner formulation has been tested in total cross section measurements, no explicit demonstration of the 90° out of phase scattering or measurement of the magnitude of the imaginary component has previously been given.

---

* $b_{Ti} = -0\cdot38 \times 10^{-12}$ cm.; $b_{Zr} = 0\cdot62 \times 10^{-12}$ cm.; $b_W = 0\cdot466 \times 10^{-12}$ cm.; $b_{Mn} = -0\cdot36 \times 10^{-12}$ cm.; $b_{Co} = 0\cdot28 \times 10^{-12}$ cm.; $b_{Cu} = 0\cdot75 \times 10^{-12}$ cm.

The present experiments on the coherent neutron scattering of α-CdS give clear indication of anomalous scattering which is in excellent agreement with theory. The measurements consist of integrated intensities of the (hkl), $(\bar{h}\bar{k}\bar{l})$ mates of a series of reflections from single CdS crystals at several wave lengths. Values for the scattering amplitude of cadmium and its real and imaginary components as a function of wave length have been obtained. Comparisons have been made of the anomalous scattering of both X-rays and neutrons from the same crystal establishing that the direction of the phase shift is the same for X-rays and neutrons in accord with expectation.

Neutron measurements can, in principle, be used then to establish absolute configuration; in the present case the direction of the polar axis in CdS. A number of isotopes with resonances close to thermal energies exist, making similar measurements possible in a number of potentially interesting cases.

Expected to be published in the *Phys. Rev.*

15·4. Pyroniobates et pyrotantalates de métaux de transition bivalents composés antiferromagnétiques. Par E. F. BERTAUT, F. FORRAT, *Centre d'Etudes Nucléaires, Grenoble, France*, et L. M. CORLISS, *Brookhaven National Laboratories, Upton, U.S.A.*

On a préparé les composés $Nb_2M_4O_9$ et $Ta_2M_4O_9$ où M = Mn, Fe, Co, Ni et Mg. Les composés de Ni sont orthorhombiques. Tous les autres pyroniobates et pyrotantalates sont hexagonaux. Leur structure dérive simplement de la structure rhomboédrique de Al_2O_3. Si l'on désigne par $(0, 0, 0)$, $(\frac{1}{3}, \frac{2}{3}, \frac{1}{3})$ et $(\frac{2}{3}, \frac{1}{3}, \frac{2}{3})$ les 3 sous-réseaux rhomboédriques de Al_2O_3, dans les pyro-niobates et tantalates, Nb respectivement Ta occupent le sous-réseau $(0, 0, 0)$ tandis que les cations M occupent les sous-réseaux $(\frac{1}{3}, \frac{2}{3}, \frac{1}{3})$ et $(\frac{2}{3}, \frac{1}{3}, \frac{2}{3})$.

Les structures cristallines et magnétiques obtenues aux rayons X et aux neutrons seront données avec plus de détail.

Publications planned in *Phys. Chem. Solids*.

15·5. Neutron diffraction studies of the hexahydrates of some transition metal fluosilicates.* By WALTER C. HAMILTON, *Chemistry Department, Brookhaven National Laboratory, Upton, L. I., New York, U.S.A.*

The compounds $M^{+2}SiF_6$, where M is a divalent transition metal, crystallize as hexahydrates, the metal ion being surrounded by a nearly regular octahedron of water molecules. As these ions are thought to be similarly coordinated in aqueous solution, it is of great interest to determine the detailed configuration of the water molecules, as well as the vibrational parameters. The study of these crystals was undertaken as the first part of a neutron diffraction program to obtain similar information about a variety of crystalline hydrates. Although all the fluosilicates have been assumed to be isomorphous to $NiSnCl_6 . 6 H_2O$, which crystallizes in space group $R\bar{3}$ with

Sn at the origin, Ni at the body center, and the oxygen and halogen atoms in general positions, X-ray and neutron diffraction data agree in indicating that the iron, nickel, and cobalt fluosilicates have structures which belong to space group $R\bar{3}m$. This apparent symmetry is due to disorder in the packing of the octahedral ions. The neutron data for $FeSiF_6 . 6 H_2O$ are being refined to obtain very accurate values for the structural and thermal parameters. The $Fe(H_2O)_6$ octahedron is quite regular with an Fe–O distance of 2·15 Å. The O–H distance and the H–O–H angles are normal, and the two-fold axis of the water molecule is directed directly toward the metal ion, within the estimated errors at the present stage of refinement; the Fe–H distances are 2·79 and 2·68 Å, both with a standard deviation of 0·07 Å. The SiF_6 octahedron is also regular.

To be published in *Acta Cryst.*

15·6. Neutron diffraction study of orthorombic lead monoxide. By JANUSZ LECIEJEWICZ, *Institute of Nuclear Research, Warszawa 9, ul. Dorodna 18, Poland.*

The oxygen positions in the elementary cell of orthorhombic modification of lead monoxide were determined using powder neutron diffraction data. In the proposed structure model each Pb atom coordinates two oxygen atoms at a distance of 2·19 Å forming an infinite chain along the a axis. The chains are packed to form a layer lying in the ac plane with the Pb–O distance of 2·48 Å between atoms belonging to separate chains. The bond distances indicate a polarized covalent bond within the chains, and weaker most probably of van der Waals type between the chains and between the layers.

Submitted for publication to *Acta Cryst.*

15·7. A neutron diffraction investigation of the structure of CaNH. By M. I. KAY* & A. F. ANDRESEN, *Institutt for Atomenergi, Kjeller, Norway.*

The alkaline earth imides were originally prepared and characterized by H. Hartmann, H. J. Fröhlich & F. Ebert (*Z. Anorg. Chem.* (1934), **218**, 181). They reported them to be face centered cubic. The present investigation has confirmed the appearance of a face centered cubic powder pattern corresponding to the lattice constant 5·13 Å for the calcium imide.

X-ray and neutron diffraction data show the nitrogen and calcium atoms to be placed in the corner and body-centered positions respectively $(N = 4)$. For the hydrogen atoms, the neutron data at room temperature indicate a spherical distribution around the nitrogen atoms. The possibility of a statistical distribution can, however, not be excluded.

Such a rotation or disorder suggests the possibility of a phase transition at low temperature. The results of an investigation at liquid nitrogen temperature will be discussed.

Proposed publisher: *Acta Cryst.*

15·8. Three-dimensional neutron diffraction study of ferrocene. By B. T. M. WILLIS, *Atomic Energy Research Establishment, Harwell, Didcot, Berks., England.*

Ferrocene has been examined in order to determine the hydrogen atom positions and to investigate the suggestion of J. W. Edwards, G. L. Kington & R. Mason, *Trans. Faraday Soc.* (1960), to be published), based on thermodynamic grounds, that the cyclopentadienyl rings are rotationally disordered at room temperature. A number of attempts were made to solve the structure by a least-squares analysis of two-dimensional F_{h0l} and F_{hk0} data; these proved only partially successful, because the ratio of the number of measured F values to the number of unknown parameters was too small. The spectrometer was accordingly modified to allow collection of full three-dimensional F_{hkl} data.

The modification consists of the addition of a two-circle device to the spectrometer table, which acts as the third circle. By mounting the crystal on the innermost circle and rotating the three circles through appropriate angles, each (hkl) plane of the crystal can be brought into the Bragg reflecting position, with the reflected neutron beam entering the counter moving in the horizontal plane. The choice of these three angles is not unique, but for one set the normal to the (hkl) plane lies in the plane of the vertical circle. The advantage of this method of setting is that three-dimensional data can be obtained from a pillar-shaped crystal with approximately the same accuracy (with respect to absorption and extinction) as two-dimensional data, obtained with a conventional (one-circle) spectrometer by rotating the crystal about its long axis.

The analysis of the three-dimensional data indicated that the hydrogen atoms were in the planes of the rings and that the rings were rotationally disordered.

Probably to be published in *Acta Cryst.*

15·9. A mechanism for ferromagnetic ordering in crystals, with structural applications. By R. E. RUNDLE, *Department of Chemistry, Iowa State University, Ames, Iowa, U.S.A.*

In a rather large group of transition metal halides, the cations are symmetrically bridged together by halide ions, with M–Cl–M very nearly 90°. In these circumstances a molecular orbital treatment of the compound reveals that the unpaired, magnetic electrons are usually in antibonding molecular orbital with some halide contribution. Moreover, the molecular orbitals contributing to the magnetic electron density at the halide ion from different metal centers are, in many cases, orthogonal. In this case the largest term in the interaction of unpaired electrons from different metal sites is a Hund's Rule type of interaction at the halide, which leads to ferromagnetic ordering. The magnitude of the interaction depends upon the square of the electron density at the halide, and can be relatively large.

Such an interaction must be responsible for ferromagnetic ordering in the layered structures of the MX_2 and many of the MX_3 chlorides, bromides and iodides of the first transition group. It is expected to lead to ordering in Cu X_2 (chloride and bromide) chains, and in a wide variety of other compounds.

Limitations on the mechanism will be discussed, along with neutron diffraction, magnetic and thermal data bearing on these compounds, as well as the relation of this mechanism to the general theory of the magnetic ordering by P. Anderson *(Phys. Rev.* (1959), **115**, 2).

15·10. The crystal and magnetic structures of lithium cupric chloride dihydrate and of ludlamite at the temperature of liquid helium. By S. C. ABRAHAMS,* *Bell Telephone Laboratories, Murray Hill, N. J., U.S.A.*

Lithium cupric chloride dihydrate, $LiCuCl_3 . 2 H_2O$, has been studied below its Neel point of 5·2 °K. by the neutron diffraction method, using techniques previously published (E. Prince & S. C. Abrahams, *Rev. Sci. Instrum.* (1959), **30**, 581; S. C. Abrahams, *Rev. Sci. Instrum.* (1960), **31**, 174). Two dimensional Fourier series and least-squares refinement give the position of the lithium and hydrogen atoms, in addition to those of the remaining atoms previously determined by Vossos & Rundle (Iowa State College, Communication No. 1074, 1958). Reflections forbidden by the nuclear space group are shown to be magnetic in origin, on the basis of a temperature dependence which follows a Brillouin function. The magnetic scattering indicates an orientation of the 'magnetic' electrons parallel with the 011 plane. The variation of the paramagnetic diffuse scattering at small angles is consistent with a ferromagnetic interaction between the copper atoms in the Cu_2Cl_6 'dimer'.

Ludlamite, $Fe_3(PO_4)_2 . 4 H_2O$, becomes ferrimagnetic below 16 °K. The neutron diffraction pattern at 4·2 °K. contains a large number of reflections: in one zone, over 150 independent nuclear and over 40 independent magnetic reflections have been measured. The positions of all the atoms are being refined, based upon the iron, phosphorus and oxygen parameters reported by T. Ito & H. Mori *(Acta Cryst.* (1951), **4**, 412). The vibrational amplitudes will also be given. Analysis of the magnetic scattering gives the spin orientation and distribution of the unpaired electrons on the two magnetic sublattices.

This paper will probably be submitted to *Acta Cryst.*

15·11. Antiferromagnetism in CrVO₄ type structures.† By B. C. FRAZER, *Brookhaven National Laboratory, Upton, New York, U.S.A.*

$CrVO_4$ is a typical member of a series of orthorhombic crystals belonging to the space group $Cmcm(D_{17}^{2h})$ (K. Brandt, *Ark. Kemi, Min. Geol.* (1943), A, **17**, 1). Recently it has been shown by neutron diffraction that this crystal transforms to an antiferromagnetic phase at about 50 °K. $NiSO_4$ and $FeSO_4$ also exhibit antiferromagnetic behavior at low temperatures. The neutron data in the case of $CrVO_4$ agree with a model involving alternating ferromagnetic Cr^{+3} sheets on the (002) planes. These compounds are of interest not only because they belong to a new antiferromagnetic class of crystals, but also there are some structural similarities to the extensively investigated spinel system.

Proposed journal: *J. Phys. Chem. Solids.*

15·12. A neutron diffraction refinement of the tetragonal structure of BaTiO₃.* By H. R. DANNER, C.B.N., Mol-Donk, Belgium and B. C. FRAZER, Brookhaven National Laboratory, Upton, New York, U.S.A. and R. PEPINSKY, Pennsylvania State University, University Park, Pennsylvania, U.S.A.

The results of a single neutron diffraction study of the ferroelectric tetragonal phase of $BaTiO_3$ were reported several years ago (B. C. Fraser, H. R. Danner & R. Pepinsky, Phys. Rev. (1955), **100**, 745). While excellent agreement between calculated and observed data was obtained, the atomic temperature parameters appeared to be somewhat unreasonable. Also, possible effects of thermal anisotropy were not investigated. This problem has now been re-examined using additional data collected at higher Bragg angles. The atomic coordinates found by least-squares refinement are very close to those found earlier, but substantial changes were found for the temperature parameters. In every case these parameters are larger than the previously reported values. While a high degree of vibrational anisotropy was not found for any of the atoms, it may be significant in the cases of Ti and O_{II}.

Proposed journal: J. Phys. Chem. Solids.

15·13. A neutron diffraction study of the high temperature modification of NaNO₂.† By B. C. FRAZER, RYUZO UEDA,‡ & M. I. KAY,§ Brookhaven National Laboratory, Upton, New York, U.S.A.

The transformation of $NaNO_2$ at 158 °C. from the ferroelectric phase to the high temperature paraelectric phase is marked by the gain of a mirror plane perpendicular to the b axis. The crystal remains orthorhombic, but the space group changes from Im2m to Immm. The disorder necessary for this change could arise either from thermal motions (rotations about c̄, or anomalously large oscillations parallel to b), or from positional disorder. In an earlier X-ray study (B. Strijk & C. H. MacGillavry, Rec. Trav. Chim. Pays-Bas (1943), **62**, 705) the evidence was slightly in favor of the positionally disordered model. Neutron diffraction provides a somewhat more favorable tool for investigating this problem. The angular independence of the atomic scattering lengths provides considerable advantage in the determination of accurate thermal vibration parameters. Also, some advantage is gained from the relative increase in nitrogen scattering for neutrons as compared to the X-ray case. A preliminary study with single crystal neutron data shows agreement with the positionally disordered model, although the evidence is not regarded as conclusive at this writing. The results of an analysis with a more accurate and more extensive set of data will be presented. This work will be compared with a recently completed neutron refinement of the ferroelectric phase (M. I. Kay & B. C. Frazer, Acta Cryst. (1960), in press).

Proposed journal: J. Phys. Chem. Solids.

15·14. Spin polarization, crystalline field effects and magnetic form factors for the transition elements. By A. J. FREEMAN, Materials Research Laboratory, Ordnance Materials Research Office, Watertown, Massachusetts and Solid State and Molecular Theory Group, M.I.T., Cambridge, Massachusetts, U.S.A. and R. E. WATSON,* Solid State and Molecular Theory Group, M.I.T., Cambridge, Massachusetts, U.S.A.

The relation between measured neutron form factors and theoretical charge densities has been investigated for some iron group transition elements in ionic compounds. Unlike the case for X-ray scattering (see the report at this Congress by D. R. Chipman, J. J. DeMarco & B. W. Batterman), magnetic form factors based on free atom charge densities do not give agreement with experiment. Our studies consider the effects of crystalline fields and spin polarization on the 3d charge densities and magnetic form factors in order to understand and explain these differences. The effects of the crystalline environment are discussed using the results of Hartree–Fock self-consistent field calculations which were carried out for some ions in both free ion and external cubic field potentials (see for example, the calculation reported by R. E. Watson, Phys. Rev. Feb. 1960). Furthermore, in order to determine the effect of spin (or exchange) polarization on the form factor, several 'unrestricted' Hartree–Fock calculations (for an example of the unrestricted Hartree–Fock formalism (applied to atomic lithium) see R. K. Nesbet & R. E. Watson, Annals of Physics, Feb. 1960) were also carried out (for Mn⁺⁺ and Ni⁺⁺). Since, for an ion with a net spin greater than zero, there are more electrons with spin up (i.e. the majority spin) than with spin down, the greater exchange interaction causes the spin up electrons to be more contracted than the spin down electrons. The effect of the spin polarization is to give rise to different radial charge densities for electrons in the same shell but differing in spin. (The Hartree–Fock calculations are called 'unrestricted' because of this relaxation of the conventional restriction on having a single radial charge density per shell). The spin polarization results in a net 3d charge density (for Ni⁺⁺) which is more contracted than the restricted Hartree–Fock free atom 3d charge density and hence in a magnetic form factor which is larger than the free atom 3d form factor. Comparisons between the results of these theoretical considerations and experiment are made and differences discussed in the light of current theory and the information available from optical absorption data.

Part of this work has been submitted for publication in the Phys. Rev.; the remainder will also be submitted to this journal.

15·15. The magnetic structure of high-purity chromium. By G. E. BACON, A.E.R.E., Harwell, England.

A neutron diffraction study has been made of high purity chromium in both polycrystalline and single-crystal form. Particular attention is paid to the temperature dependence of the antiferromagnetic reflection in the neighbourhood of 40 °C. (which corresponds to the point

---

of anomaly for many physical properties) and at low temperatures.

Probable publication: *Acta Cryst.*

15·16. Le système Fe—Rh. Par F. DE BERGEVIN, *Laboratoire d'Electrostatique et de Physique du Métal, Institut Fourier, Place du Doyen Gosse, Grenoble, France.*
Withdrawn.

15·17. Atomic magnetic moments in FeV by neutron diffraction.* By RONALD CHANDROSS & DAVID P. SHOEMAKER, *Department of Chemistry, Massachusetts Institute of Technology, Cambridge, Massachusetts, U.S.A.*

Iron–vanadium alloy (1:1 atomic composition), quenched from 1250 °C. and heat treated at 600 °C. for several hours, is largely ordered with the CsCl structure (T. V. Philip & P. A. Beck, *J. Metals* (1957), **9**, 1269). This has been verified in our neutron powder diffraction work (specimen kindly furnished by Prof. P. A. Beck, University of Illinois), which indicates about 75% order before correction for magnetic scattering. The alloy is ferromagnetic at room temperature. Additional specimens have been prepared and are being studied. Results will be presented from neutron powder diffraction work at various temperatures, and in the presence of a saturating magnetic field.

§ 16. Electron diffraction

16·1. Bestimmung von Strukturfaktoren aus der Aufspaltung der Elektronenbeugungsreflexe bei der Durchstrahlung von Kristallkanten. Von G. LEHMPFUHL & K. MOLIÈRE, *Fritz-Haber-Institut der Max-Planck-Gesellschaft, Berlin-Dahlem, Deutschland.*

Die Aufspaltungen der Elektronenbeugungsreflexe bei der Durchstrahlung keilförmiger Kristallbereiche (Interferenzbrechung) war bisher nur an submikroskopischen Kristallen (meist MgO) studiert worden. Dabei wurde der ganze Kristall (oder ein polykristallines Präparat) der von einer nahezu punktförmigen Quelle ausgehenden Strahlung ausgesetzt. Aus der Geometrie der Feinstrukturen konnten Strukturfaktoren ohne Intensitätsmessungen bestimmt werden. Einer allgemeinen Anwendung dieser Methode steht der Umstand im Wege, dass sich nur aus wenigen Substanzen gut ausgebildete, submikroskopische Kristalle von kubischer oder parallelepipedischer Gestalt herstellen lassen. Nur für diese Form ist eine einfache Auswertung der Feinstrukturen möglich.

Wir haben die Aufspaltung der Beugungsreflexe untersucht, die bei der Durchstrahlung makroskopischer, keilförmiger Kristallbereiche entsteht, welche z. B. durch Spalten hergestellt sind. Es wurde ein Feinstrahlkondensor verwendet, mit dem auf der Photoplatte ein Fokus von 11 μ Durchmesser bei einer Bestrahlungsapertur von 1,3 . 10⁻⁵ erzeugt werden kann. Die von den beiden Spaltflächen gebildete Kante wurde nur wenig in den Strahl hineingetaucht; der Hauptteil des Primärstrahls ging am

Kristall vorbei. Aufladungen wurden durch einen Decharger beseitigt. Die Beugungsreflexe konnten durch eine transversale elektrische Wechselspannung zu Strichen auseinandergezogen werden. Die gegenseitigen Abstände der Feinstrukturkomponenten des Nullstrahls und der Interferenzstrahlen liessen sich so photometrisch mit guter Genauigkeit bestimmen. Die Kristallorientierung wurde aus dem Kikuchidiagramm ermittelt, das bei Fokussierung im Kristall entsteht. Durch Beobachtung dieses Diagramms konnte die Kristallorientierung so reguliert werden, dass im wesentlichen nur Beugung an einer Netzebenenschar auftrat ('Einfachanregung').

Die Aufspaltung des 000- und des hkl-Reflexes bei exakter Erfüllung der Lauebedingung betrug z. B. für die 220-Interferenz von MgO etwa 80 μ (Elektronenenergie 50 kV., Beugungslänge 405 mm.). Aus dem Abstand der beiden Dublettkomponenten des hkl- oder 000-Reflexes konnte der Strukturfaktor, aus dem mittleren Abstand des 000-Dubletts vom Primärfleck das mittlere, innere Potential bestimmt werden. Die stärkeren Strukturfaktoren liessen sich mit einer Genauigkeit von 3% ermitteln.

16·2. Measurements of dynamical effects on electron diffraction intensities. By M. HORSTMANN & G. MEYER, *Hamburg 36, Jungiusstr. 11, Deutschland.*

By means of a retarding field apparatus direct intensity measurements in electron scattering distributions have been made with an accuracy of some percent in order to check the kinematical theory in the energy range from 20 to 50 kV. Previous experiments with polycrystalline aluminium foils (*Z. Phys.* (1959), **154**, 633) have shown marked deviations of the ring intensities from the kinematical values, when the crystal size exceeds 100 Å. The deviations can be interpreted as dynamical effects.

The apparatus used for these investigations in principle consists of a Faraday cage which can be moved on circular arcs around the scattering foil. The cage current is measured by a d.c. amplifier. The potential of the Faraday cage can be varied in order to filter off the inelastically scattered electrons or to measure (integral) energy distributions.

In order to investigate more closely the dynamical effects, the mean crystal size of a polycrystalline aluminium foil (thickness 200 Å) was increased by annealing in several steps from 30 to 200 Å and at each step unfiltered and filtered scattering diagrams were taken at different accelerating voltages. From these diagrams the dependence of the ring intensities on crystal size and energy of the incident electrons was determined.

By comparison of unfiltered and filtered diagrams the portion of inelastically scattered electrons in the rings and in the continuous background was determined at constant foil thickness and at various crystal sizes and electron energies. Moreover by this comparison the broadening of the Debye–Scherrer-rings by the inelastic scattering processes could be investigated.

To be published in *Z. Phys.*

16·3. Electron diffraction intensities from polycrystalline material containing heavy atoms. By J. M. COWLEY & SHIGEYA KUWABARA, *Division of Chemical Physics, C.S.I.R.O., Melbourne, Australia.*

The two beam approximation to the dynamic theory of electron diffraction does not give an adequate description of intensities from small crystals because, especially when heavy atoms are present, appreciable deviations from kinematic scattering can occur while the crystals are so thin that many diffracted beams appear simultaneously. A more realistic estimation of the deviations from kinematic scattering in the case of very thin crystals containing heavy atoms is obtained by using the first approximation proposed by J. M. Cowley & A. F. Moodie (*Acta Cryst.* (1959), **12**, 360) in which the diffraction pattern from a thin crystal is taken as the Fourier transform of the projection of the lattice considered as a phase grating. For polycrystalline materials the intensity of a ring or arc is given by the average Fourier coefficient of the projections for the corresponding range of orientations, or, what is not very different if special orientations are ignored, the Fourier coefficient of the average of the projections.

It follows that in 'oblique texture' patterns obtained from oriented polycrystalline material the relative intensities of the arcs will vary with the angle between the axis of orientation and the beam direction. This prediction has been tested by careful measurements of the relative intensities of the $hk0$ arcs given by very thin crystals, of the order of 10 unit cells thick, of BiOCl, oriented with the c-axis perpendicular to a supporting carbon film. With an angular spread of about 5° in the orientation of the crystal axis, the relative intensities of the stronger reflections were found to vary by up to 40% for tilting angles of 0 to 25° in excellent agreement with calculations made from the above model.

It is expected that for more accurately aligned crystals and for thicker crystals the intensity variations will be greater and also more difficult to calculate. For thicker crystals especially, it may be necessary to make use of the second approximation of J. M. Cowley & A. F. Moodie in which some account is taken of Fresnel diffraction within the crystal i.e. of the finite curvature of the Ewald sphere.

Probable journal for publication: *Acta Cryst.*

16·4. A dynamical theory of wave diffraction in crystals. By N. KATO*, *Division of Engineering and Applied Physics, Harvard University, Cambridge 38, Massachusetts, U.S.A.*

The layer crystal approach of dynamical theory (C. G. Darwin, *Phil. Mag.* (1914), **27**, 315, 675, (1922), **43**, 800; J. M. Cowley & A. F. Moodie, *Acta Cryst.* (1957), **10**, 609; L. Sturkey, *Acta Cryst.* (1957), **10**, 858) is reformulated by using the Fourier transform method for optical problems (e.g. J. A. Ratcliffe, Report on Progress in *Physics* (1956), **19**, 188). Certain assumptions made by J. M. Cowley & A. F. Moodie, such as smallness of the Bragg angle, paraboloidal form of wave front, and the symmetrical Laue case are shown to be unnecessary and can be eliminated. This opens the way for application of the theory also to X-rays. Perfect and deformed crystals are considered in the two beam case. Matrix methods are used throughout the treatment. In perfect crystals com-

* Now at: H. H. Wills Physics Laboratory, University of Bristol, England.

plete equivalence between the present approach and the Laue–Bethe approach can be demonstrated. Pendellösung patterns in X-ray cases (N. Kato & A. R. Lang, *Acta Cryst.* (1959), **12**, 787) are interpreted by the present approach as due to multiple reflection in reciprocal space, whereas they are interpreted as an interference between two wave bundles corresponding to conjugate points on the dispersion surface by the Laue–Bethe approach (N. Kato; in preparation).

The theory can be extended to deformed crystals under certain conditions, which are satisfied in most cases of electron micrographs. In particular, if the distortion is expressed by a relative displacement between crystal slices the results are the same, in the kinematical limit, as those of M. J. Whelan (*J. Inst. Met.* (1959), **4**, 392).

To be published in part in *Acta Cryst.*

16·5. Théorie dynamique rigoureuse de la diffraction des électrons suivant un nombre quelconque de faisceaux à travers une lamelle cristalline absorbante. Par M. TOURNARIE, 40, *rue Mangeon, Massy, (S. et O.), France.*

Pour décrire la propagation des électrons à travers des cristaux non infinis, la souci de rigueur interdit l'emploi des zones de Brillouin et de la théorie des bandes (établies seulement pour des cristaux infinis), de la décomposition en ondes de Bloch (applicable seulement aux électrons restant dans un cristal infini ou à parois réfléchissantes), de la théorie des rayons X (où ne se réfléchissent jamais plus de deux faisceaux), du développement de Born pour des raisons de convergence lente ou incertaine, de l'approximation Wentzel, Kramers, Brillouin, Rayleigh par suite du déphasage négligé entre les faisceaux, et exige la conservation de la continuité de la fonction d'onde et de sa dérivée dans tout l'espace.

L'auteur a donc repris la théorie dynamique à partir de l'équation de Schrödinger. Pour une lamelle cristalline absorbante, l'équation de propagation se résout sans approximation grâce à une représentation matricielle dans un 'espace mixte' (direct dans la direction normale à la face d'entrée et réciproque dans les deux autres directions).

La forme de la solution montre que les conditions aux limites doivent être rigoureusement exprimées dans un milieu absorbant pour que le résultat soit représentatif du phénomène vrai.

On retrouve dans le cas à un faisceau les pouvoirs de réflexion et de transmission du mur de potentiel, à deux faisceaux la solution pendulaire et l'effet Bormann. On peut traiter le cas fréquent d'un très grand nombre de faisceaux.

Ainsi formulée, la théorie dynamique devient un outil encore lourd à manier, mais déjà susceptible de permettre la comparaisons entre différentes théories, de préciser des domaines de validité et de calculer certains diagrammes.

Probably will be published in *Acta Cryst.*

16·6. Intensity of forbidden reflections from germanium. By SATIO TAKAGI, FUMINORI FUJIMOTO, MIEKO TAKAGI & SETSU MORIMOTO, *Institute of Phycics, College of General Education, University of Tokyo, Komaba, Meguro-ku, Tokyo, Japan.*

The intensity of reflections in electron diffraction deviates markedly from the kinematical value owing to the dynamical effect. One of the most prominent example is the appearance of forbidden reflections such as 222-reflection from diamond type crystals. Hoerni has calculated the intensity of 222-reflection from diamond type crystals, assuming the systematic interactions among hhh-reflections.

We have calculated the intensity of forbidden reflections from germanium by the method developed by one of us (F. Fujimoto, *J. Phys. Soc., Japan* (1959), **14**, 1558), making use of the expansion of the scattering matrix in power series. The intensity of 222-reflection is calculated assuming the systematic interaction, and the intensity of 200-reflection is calculated assuming the accidental interaction between 111- and $1\bar{1}\bar{1}$-reflections. It is found that the ratio of the integrated intensities I_{222}/I_{400} varies as $(\lambda D)^2$ and I_{200}/I_{222} as $1/D$ for small λD (λ = wave length, D = crystal thickness).

The intensity of reflections from evaporated germanium films is measured by the photographic method, using the high voltage diffraction camera. The ratio I_{222}/I_{400} is obtained as the function of λD, which agrees with the theoretical predictions.

The full-length account will be published in *J. Phys. Soc., Japan*.

16·7. Anomalous electron absorption effects in metal foils. By H. HASHIMOTO, *Metallurgy Dept., Cambridge University* and P. B. HIRSCH, A. HOWIE & M. J. WHELAN, *Cavendish Laboratory, Cambridge, England*.

Transmission electron micrographs of metal foils show certain interesting contrast effects in the form of dark bands in thicker regions (greater than about 0.1μ in thickness), which can be explained in terms of an anomalous absorption effect similar to the well-known Borrmann effect observed with X-rays. The bands appear dark and show poor resolution, suggesting strong absorption, whereas regions just outside the bands show very good electron transmission and resolution. Selected area diffraction experiments have shown that a dark band with its light borders is associated with Bragg reflexions (hkl) and $(\bar{h}\bar{k}\bar{l})$, where (hkl) is usually a low index reflection. In thin regions of the foil the bands merge into bend extinction contours showing principal and subsidiary maxima.

The observations can be explained phenomenologically by application of the dynamical theory of electron diffraction to a crystal with complex lattice potential. The imaginary part of the lattice potential gives rise to absorption. Theory shows that the intensity profile of the bright field image of a bend extinction contour is asymmetrical about the centre of the Bragg reflection, the effective absorption coefficient being increased on one side of the Bragg reflexion and reduced on the other. The ratio of the intensities transmitted on either side of the Bragg reflection increases with increasing crystal thickness, while the visibility of subsidiary fringes decreases. The intensity profile of the dark field and bright field images are similar, in contrast to the case of a thin crystal where they are complementary.

The theory accounts for the high electron transmission of thick foils orientated close to the reflecting position.

The nature of the imaginary part of the scattering potential is not known at present.

Will be published in *Phil. Mag.*

16·8. The solution of the dynamical equations of electron diffraction for two strong reflexions. By M. J. WHELAN & A. HOWIE, *Cavendish Laboratory, Cambridge, England*.

The fundamental secular equation of the dynamical theory of electron diffraction has been solved using a high speed digital computor for the case where two strong 'systematic' lowest order reflexions (hkl) and $(\bar{h}\bar{k}\bar{l})$ occur. The form of the dispersion surface, and the variations of wave amplitudes and effective absorption coefficients on the various branches of the dispersion surface have been investigated and compared with the results of the theory for one strong reflection. The results are particularly relevant to the detailed interpretation of extinction contours due to buckling of thin foils examined by transmission electron microscopy.

Will be published in *Phil. Mag.*

16·9. The effect of absorption of electron waves on the appearance of interference fringes observed at stacking faults by transmission microscopy. By H. HASHIMOTO, *Metallurgy Department, Cambridge University. Department of Physics, Kyoto Technical University, Japan* and A. HOWIE & M. J. WHELAN, *Cavendish Laboratory, Cambridge, England*.

The profile of the fringes observed at a stacking fault inclined to the crystal surface has been studied taking account of absorption of electron waves. The phenomenological theory of absorption (assuming only one strong diffracted beam) shows that the intensity profile of the interference fringes across the stacking fault is complicated and depends on the deviation from the reflecting position and on certain absorption parameters determined by Fourier coefficients of the imaginary part of the lattice potential and by the crystal thickness. At the reflecting position (for small absorption parameters) the depth periodicity of the fringes is approximately half the extinction distance for the Bragg reflexion, as in the case of zero absorption. The fringes may show alternating intensity of either fringe maxima or minima depending on crystal thickness particularly near the edges of the fault. For large absorption parameters the depth periodicity of the fringes near the edges of the fault is approximately equal to the extinction distance. The average transmitted intensity and the visibility of the fringes decreases towards the centre of the fault. The intensity profile of the fringes is symmetrical about the centre of the fault in the bright field image whereas it is asymmetrical for the dark field image. Observations of the predicted effects will be described.

To be published in *Phil. Mag.*

16·10. Dynamical theory of diffraction contrast from dislocations. By A. HOWIE & M. J. WHELAN, *Cavendish Laboratory, University of Cambridge, England*.

Dynamical equations of diffraction in the form of

simultaneous differential equations for the direct and diffracted waves in a deformed crystal have been derived for the case when the angle of diffraction is small. These equations make it possible to investigate the image contrast due to the strain field round imperfections in thin metal foils examined by transmission electron microscopy. A high speed digital computer has been used to study in detail the contrast from dislocations in various configurations. Many of the predictions of a simple kinematical theory previously derived have been confirmed. The effects of absorption can also be included in the equations.

Paper probably will be published in *Phil. Mag.*

16·11. Study on anti-phase domains of the ordered Cu₃Pd alloy by electron diffraction and electron microscopy. By Shiro Ogawa & Denjiro Watanabe, *The Research Institute for Iron, Steel and Other Metals, Tohoku University, Sendai, Japan.*

The anti-phase domain structure of the ordered Cu_3Pd alloy was previously studied by electron diffraction (D. Watanabe & S. Ogawa, *J. Phys. Soc., Japan* (1956), **11**, 226), using thin films, and the domain structure was concluded to be two-dimensional, unlike the one-dimensional structure in Cu_3Au or $CuAu(II)$.

In the present study anti-phase domains in well oriented, evaporated films of sufficiently ordered Cu_3Pd have directly been observed by transmission electron microscopy. The electron diffraction pattern has shown the splits of superlattice reflections characteristic of the domain structure as previously concluded. The size of a domain has been estimated from these splits to be 20·7 Å along the a axis and 14·4 Å along the c axis, respectively. The dark field technique has been adopted in transmission electron microscopy, that is, the $(110)_{cub.}$ splits or the $(100)_{cub.}$ splits of superlattice reflections have been brought into the position of the direct spot by inclining the electron gun, and electron micrographs have been taken, utilizing these split reflections. Corresponding to the $(110)_{cub.}$ splits, four sets of parallel lines have separately been observed on the micrographs, two sets of them being orthogonal to the other two. The parallel lines have the two spacings 20 ∼ 22 Å and 14 ∼ 14·5 Å, which nearly coincide with the said domain lengths along the two directions. The moiré patterns due to the overlapping of domains of different sets have also been observed. Corresponding to the $(100)_{cub.}$ splits, two sets of parallel lines, with the spacings 20∼22 Å and 14∼14·5 Å, have separately been observed along one direction. Another set of crossing parallel lines has been observed, the two spacings of this cross grid having also the said values. These crossing lines best reveal the two-dimensional domains.

The above observations support the domain structure previously concluded only by electron diffraction, in the size as well as in the distribution of the domains. The two-dimensional antiphase domain structure in the present alloy has thus been confirmed by electron microscopy.

The full-length account of the present paper will be published in *J. Phys. Soc., Japan* or in *Acta Cryst.*

16·12. Contrast of anti-phase boundaries in electron micrographs of ordered AuCu₃. By R. M. Fisher, *Department of Metallurgy, University of Cambridge, England* and M. J. Marcinkowski, *U.S. Steel Res. Center, Monroeville, Pa., U.S.A.*

The anti-phase boundaries in $AuCu_3$ show different types of contrast in electron micrographs depending on the thickness and orientation of the ordered crystal. The boundaries may appear lighter or darker than the background and frequently are outlined by darker lines. All of these types of contrast can be explained by introducing the appropriate phase angle across the boundary and extinction distance in the crystal into the dynamical theory of Whelan & Hirsch for the contrast of stacking faults. The phase angle is 0 or 2π when the crystal is oriented for diffraction contrast by one of the principle reflections and the boundares are not visiible. The phase angle is 0 or π for super-lattice reflections and for the latter case the boundaries are visible in the microscope. From knowledge of the exact indices of the super-lattice reflections which cause the anti-phase boundaries to appear and or disappear it is possible to distinguish between type I and type II. For super-lattice reflections the structure factor is very small and the corresponding extinction distances are quite long, e.g. for (110) $t_0 = 1100$ Å as compared to (111) $t_0 = 225$ Å for 100 kV. electrons. Since the thickness of the foil specimens is usually less than the super-lattice extinction distance, multiple sets of interference fringes do not occur. The long extinction distance also causes the contrast of the boundaries to decrease more rapidly with increasing deviation from the reflecting position as compared to the case for stacking faults and the boundaries are not visible if the crystal is tilted more than one degree away from a reflecting position. Application of these considerations to other ordering systems suggests that the domain structure will not be visible unless the components are separated by more than five places in the periodic chart of the elements.

To be published in *Phil. Mag.*

16·13. Electron diffraction and moiré-patterns of the waved superlattice of antigorite. By G. Kunze, *Institut für Metallkunde der Bergakademie Clausthal, Clausthal-Zellerfeld, Deutschland.*

The X-ray analysis of antigorite showed that the single layers $O_3-Si_2-O_2OH-Mg_3-(OH)_3$ of this mineral are sinusoidally waved (satisfactory representation of the shape of the atomic networks by 3 Fourier-components). Structure-theoretically it could be predicted that not only *one* antigorite with a single superperiod (= layer wavelength) but a whole antigorite series with different, but discretely differentiated superperiods should be existent (non discrete superperiod intervals being caused by fluctuations of chemical parameters, lattice distortions, vacancies, ...). Electron optical examinations confirmed this supposition. Near the primary beam of electron diffraction patterns no satellite-reflections ($H00$) appear, or at best only the first order of these (100), which, however, is overlapped by the primary beam. The paucity of (000)-satellites results from the wave-shape of the antigorite layers; this is compatible with X-ray observations. Consequently the appearence of the superlattice in the form of electron optical fringes has to be thought

of as caused only by the zero order and first order beam (angle between the two beams 0·05° for spacing $A \sim 43$ Å and $\lambda \sim 0{\cdot}04$ Å). This fact restricts the information about the waved antigorite layers to that of the superperiod. Because of the long superperiod, electron optical fringes can also occur in relatively thick crystals (up to $\sim 2{.}10^3$ Å), for which the 3rd *Laue* condition is practically fulfilled. It is only in thin antigorite platelets that the higher order reflections possibly take part in producing the electron optical fringesystems, though the next reflection of the (H00)-clusters occurs only when $H \sim 16$. Electron optical moiré-patterns disclose in this mineral, too, lattice distortions in the form of dislocations, but of low density. These dislocations possibly contribute to the thermal dissolution of the antigorite superlattice during electron bombardment, which can be observed in the diffraction patterns. Simultaneously the remaining reflections increase in width pointing stresses and deformation in the lattice prior to the subsequent phase change.

Probably will be published in *Fortschritte der Mineralogie*.

16·14. An attempt to determine structure parameters of condensed ring hydrocarbons using the electron-diffraction method on gas molecules. By A. Almenningen, O. Bastiansen & F. Dyvik, *Institutt for teoretisk kjemi, Norges tekniske Høgskole, Trondheim, Norway*.

Both theoreticians and experimentalists have shown great interest in studying bond distances in condensed ring hydrocarbons. J. M. Robertson's and D. W. J. Cruickshank's pioneering work using X-ray crystallography has inspired us to study the potentiality of the electron-diffraction gas method for such molecules.

In spite of the promising results obtained for benzene using the electron-diffraction method, electron diffractionists have hesitated to apply the method to large aromatic molecules. This is connected to the fact that the intensity values as well as the radial distribution curve, as studied in electron-diffraction gas work, represent one-dimensional descriptions. For benzene this does not introduce particular difficulties, as all the three C–C distances in benzene show up as three well resolved peaks in the radial distribution curve. In molecules like naphthalene, anthracene, and coronene practically all the peaks of the radial distribution curve are composed of contributions from two or more distances of slightly different values. The peaks of the radial distribution curves cannot be resolved. The structure parameter determination has to be based upon least-squares calculations.

For naphthalene one unambiguous result was obtained. For anthracene no single set of parameters was found. For coronene one set of parameters was obtained, but the standard deviations were too large to admit unambiguous conclusions to be drawn.

Our attempt leaves us with a moderate optimism as to the potentiality of the electron-diffraction method on this kind of molecules. Further work has to be carried out to give definite conclusions as to the best possible accuracy obtainable.

Likely to be published in *Acta Cryst*.

16·15. Electron diffraction patterns from molecules in the process of excitation. By J. Karle, *U.S. Naval Research Laboratory, Washington 25, D.C., U.S.A.*

A new technique has been developed in our laboratory for studying energy levels and diffraction patterns from molecules being excited by the incident electron beam. In the usual scattering experiments electrons suffer inelastic collisions which raise molecules to quantized excited states with a consequent loss of energy. The total inelastic scattering falls off monotonically with scattering angle. If a specific quantum loss is considered, the scattering curve will not, in general, be monotonically decreasing, but rather will contain maxima and minima arising from interatomic interactions. We have demonstrated this experimentally by use of a velocity analyzer of the Mollenstedt type.

It is of considerable interest therefore to derive a theory of scattering for the individual levels of energy loss, corresponding to the eigenstates of the system. This may be done by use of scattering theory, the Franck–Condon principle and the application of group theory to form correct linear combinations of atomic orbitals. As in spectroscopy this is another example of the power of group theory to predict valuable results about the nature of a physical process without the necessity of producing explicit functions for the eigenstates. By the use of tables similar to character tables, the form of the electron scattering for any type of molecular symmetry and any possible eigenstate within that symmetry can be readily found. The electron scattering theory to be used in conjunction with the tables has been worked out. We thus have a theory for predicting the possible forms for the incoherent scattering of any molecule.

To be published in *J. Chem. Phys.*

16·16. Measurement of intensity in electron diffraction by the electron-bombardment induced current in a CdS single crystal. By Satio Takagi & Fuminori Fujimoto, *Institut of Physics, College of General Education, University of Tokyo, Komaba, Meguro-Ku, Tokyo, Japan*.

One of us reported the possibility of the intensity measurement in electron diffraction by the electron-bombardment induced current (EBIC) in a CdS single crystal (S. Takagi & T. Suzuki, *Acta Cryst*. (1955), 8, 441). The method has been developed and now is used for the intensity measurement work in our laboratory with satisfactory results.

The crystal used are made by the Frerichs' method, no impurity being added. They have sticklike shape and are $0{\cdot}5 \sim 1$ mm. in diameter and $3 \sim 5$ mm. in length. Indium metal is evaporated onto the surface with a gap of 0·03 mm. width which serves as electrodes and at the same time as a slit of the detector, the effective area of the detector being about $0{\cdot}03 \times 0{\cdot}7$ mm.^{2}. The electron beam intensity suitable for the measurement is about $1 \times 10^{-14} \sim 2 \times 10^{-12}$ A.mm.$^{-2}$ which gives EBIC of about $1{\cdot}5 \times 10^{-8} \sim 3 \times 10^{-6}$ A. in a good CdS crystal with the applied voltage gradient of 50 V.mm.$^{-1}$. The relation between the electron current I_e and the EBIC I is approximately expressed as

$$I = \text{const. } I_e^p$$

with $p = 0.9 \sim 1.0$. The response time of EBIC is sufficiently short, and the reproducibility is satisfactory.

The CdS crystal is set on a insultating base and can be moved perpendicular to the incident beam by a screw driven by a synchronous motor. EBIC is measured directly with an automatic recording millivoltmeter. Time of total run covering the half of a diffraction pattern is about 8 min. The intensity of the incident electron can be kept constant sufficiently by suitable precautions i.e. (1) self biasing the Wehnelt cylinder, (2) the automatic stabilization of the accelerating voltage and (3) the high vacuum (8×10^{-5} mm.Hg) in the diffraction apparatus.

Examples of measurement with Ag and CuCl will be given.

The full-length account will be published in the *J. Phys. Soc., Japan.*

16·17. Precision lattice constant determination of TlCl by electron diffraction. By K. MEYERHOFF, *Institut für Angewandte Physik der Universität Hamburg, Hamburg 36, Deutschland.*

Withdrawn.

16·18. Structural transformations in the iron oxide-hydroxide system. By A. L. MACKAY, 21, *Torrington Square, London, W.C. 1, England.*

A combination of electron diffraction, electron microscopic and X-ray diffraction methods has been used to study the transformations, chiefly those occurring on heating, of the less common phases of the iron oxide-hydroxide system. The materials particularly studied were β-FeOOH, δ-FeOOH and the 'green rusts', the hydrated ferrous-ferric oxysalts which decompose to lepidocrocite (γ-FeOOH) or to spinel phases. These substances have previously only appeared as powders to X-ray techniques and much more information is provided when single crystal patterns can be obtained by selected area diffraction techniques from individual crystals of mass about 10^{-14} g. An EM–6 microscope with an optional diffraction specimen holder has been employed for this micro-mineralogical study.

16·19. A new focussing aid, applied to the investigation of gamma MnO₂. By F. H. PLOMP, J. B. le POOLE & P. M. de WOLFF, *Adr. Pauwstraat 67, Delft, The Netherlands.*

In our electron diffraction camera, two magnetic lenses situated between the electron source and the specimen produce a central spot of about 5 micron diameter. This spot is focussed as follows: A Pt-target is mounted on the shutter, slightly above the film. Secondary radiation from this target projects the shadow image of a fine grid on a fluorescent screen with a high magnification.

The sharpness of this image, therefore, affords a sharp criterion for the quality of focusing.

With this camera, we succeeded in obtaining transmission diffraction patterns of a small number of gamma-MnO_2 crystals. The shifts and the diffuse streaks predicted earlier from X-ray powder patterns for reflections with $k =$ odd, (De Wolff, *Acta Cryst.* (1959), **12**, 341) have now been confirmed in a much more direct way.

A detailed account is to be published in *App. Sci. Res.*

16·20. Electron diffraction studies of stacking modifications in the calcium silicates. By J. A. GARD, *Department of Chemistry, University of Aberdeen, Old Aberdeen, Scotland.*

Single-crystal electron diffraction was used to determine the positions of weak reflections with k-odd in the reciprocal lattices for natural and synthetic specimens of β-CaSiO₃, foshagite, xonotlite, and tobermorite. These positions indicate that, even in disordered specimens, certain stacking modifications occur while others do not.

β-CaSiO₃ and foshagite both give streaks parallel to a^*, which have maxima indicating the predominant modifications. c is always equal in both the true and pseudo-cells of β-CaSiO₃, but c is doubled in the true cell of foshagite, which is either A-centred or F-centred. The occurrence of the modifications which give these reflections, and the exclusion of others, are explained in terms of the coordination to calcium atoms of the oxygen atoms and hydroxyl ions (*Acta Cryst*, in the press). The reciprocal lattice of xonotlite is more complex. The streaks have no distinct maxima, but are continuous in the a^*-direction; they pass close to the centre of the $0a^*b^*$ face, as with foshagite, but each streak appears to be split in two lengthwise. This recalls the reciprocal lattice of tobermorite from Loch Eynort, which has similarly doubled streaks parallel to c^* (*Miner. Mag.* (1957), **31**, 361). The implications of the resemblance between the two reciprocal lattices are discussed.

16·21. Preparation and behaviour of metal crystals of a spherical surface non contacted by any physical or chemical treatment. By E. MENZEL, CHR. MENZEL-KOPP, M. OTTER, W. STÖSSEL, *Phys. Inst., Tech. Hochschule, Darmstadt, Deutschland.*

A piece of metal is degassed by melting it on an electrically heated tungsten ribbon in a vacuum of better than 10^{-6} mm. Hg. Metals which form an alloy with tungsten are kept separated from the ribbon by a thin layer of sintered BeO or Al_2O_3. The metal drop is placed on the ribbon asymmetrically in order to initiate crystallization at one point only, when the current is diminished. In this way single crystals were prepared, their surfaces are very smooth, they are not contacted by any physical or chemical preparation.

Electron diffraction experiments show a very clear Kikuchi diagramm of great contrast. No point patterns due to surface contaminations are present on crystals of Ag, Cu or Ni. If a crystal is heated, the contrast of the

diffraction diagram decreases; this is evidence for a correlation of the temperature and the amplitude of the thermal vibrations in the surface. The optical behaviour of Cu spheres, prepared in this way, were measured by analysis of the ellipticity of the reflected light. On crystal spheres of Cu, Ag and Ni, the epitaxy of the metal oxide, grown at elevated temperature was investigated by X-ray and electron diffraction. Using the method of crystal spheres described, the epitaxy on all possible crystal planes may be observed with one preparation only. If the oxygen pressure is small enough, the oxidation of Cu and Ag does not produce coherent films but isolated crystallites of the oxide spread over the sphere; their forms depend characteristically on the position with respect to the crystal lattice inside the sphere. On Ag spheres sulphur vapour produces isolated crystallites of Ag_2S.

To be published in *Acta Cryst.*

16·22. A superlattice compound in the epitaxy of NaF on NaCl. By H. WILMAN, *Applied Physical Chemistry of Surfaces Laboratory, Chemical Engineering Department, Imperial College, Prince Consort Road, London, S.W. 7, England.*

Electron diffraction results are outlined, obtained in collaboration with Dr M. Levy, on the epitaxial orientation of NaF deposits condensed in vacuo on NaCl faces. In particular, a compound between NaF and NaCl was observed on two occasions, though repeated attempts to determine the conditions of its formation have not so far been successful. It appears to represent a segregated state of the nature of a superlattice having a cubic cell (not necessarily a cubic structure) with a about twice that to be expected from a roughly 50% solid solution of the two materials. The diffraction-spot intensities are compatible with a f.c. cubic lattice of Na ions of the usual size, with F and Cl ions shared equally between the usual anion sites of the NaCl-type structure. In the suggested structure, each (001) plane has alternate Na–F and Na–Cl rows parallel to one cube edge, and if this cube axis (a) of the cell is an Na–Cl row, then in the vertical plane (010) through it (and the origin) the next three such rows are all Na–F. No such compound formation in binary alkali–halide systems appears to have been reported previously.

Probably to be published in *Acta Cryst.*

§ 17. Physical techniques (other than diffraction)

17·1. Etude des mouvements des cations et des molécules d'eau dans la Chabasie par relaxation diélectrique et résonance magnétique nucléaire. Par P. DUCROS, *Laboratoire de Minéralogie et Cristallographie, Faculté des Sciences de Paris, France.*

La résonance magnétique nucléaire des protons permet de mettre en évidence deux raies identiques et fines (0,1 G.) dont l'écartement varie comme

$$H = 0,7(3 \cos^2 \theta - 1) \text{ G.} ,$$

θ étant l'angle de l'axe ternaire avec le champ magné-

tique H_0. Cet effet est interprété par l'existence d'une diffusion facile des molécules d'eau (temps de corrélation 10^{-7} sec.) et par l'influence du champ cristallin possedant la symétrie rhomboèdrique.

Des mesures de la constante diélectrique et des pertes diélectriques ont été réalisées à diverses fréquences (entre 100 C. et 100 Kc.), diverses températures (20 à 80 °C.) et pour diverses valeurs du rapport Ca/Na (modifié par échange d'ion). Les domaines de relaxation mis en évidence sont attribués à l'existence d'une mobilité des cations Ca et Na (temps de relaxation respectivement de 10^{-2} et 10^{-7} sec.). On montre que la teneur en eau influe notablement sur le temps de relaxation. Cet effet est attribué à l'influence electrostatique de la molécule d'eau assimilée à un dipôle.

The work described above will be published in *Bull. Soc. Franç. Minér. Crist.*

17·2. N.M.R. Study of the boron sites in inderite and lesserite. By H. E. PETCH & K. PENNINGTON, *Departments of Physics and Metallurgy, Hamilton College, McMaster University, Hamilton, Ontario, Canada.*

N.m.r. techniques have been used to study single crystals from the Kramer district, Cal., U.S.A., of inderite and lesserite which are believed to be triclinic and monoclinic polymorphs, respectively, of $Mg_2B_6O_{11}.15 H_2O$. The quadrupolar splittings of the B^{11} n.m.r. signals were investigated as the crystal was rotated in turn about three mutually perpendicular axes held normal to the magnetic field. The complex B^{11} spectra can be explained in detail if one assumes that in both cases the asymmetric unit contains three boron sites and that the electrostatic interactions at two of the sites are weak, whereas the interaction at the third site is strong. The electric quadrupole coupling constant, the asymmetry parameter, and the directions of the principal axes of the electric field gradient tensor will be given for each boron site in the asymmetric units of inderite and lesserite. The results will be interpreted in terms of boron coordinations.

17·3. Propriétés cristallographiques et magnétiques de FeAsS. Par MICHELINE WINTENBERGER, *Laboratoire de Minéralogie et Cristallographie, Faculté des Sciences de Paris, France.*

Utilisant une méthode appropriée à l'étude des minéraux naturels, on a mesuré la magnétorésistance d'échantillons de mispickel de diverses origines. On met ainsi en évidence des phénomènes d'hystérésis qui pourraient s'expliquer par une structure magnétique particulière. Diverses méthodes physiques ont été mises en œuvre pour obtenir une confirmation de cette hypothèse.

A paraître dans *Bull. Soc. Franç. Minér. Crist.*

17·4. A technique for the rapid accurate and strain free machining of metal single crystals. By M. COLE, I. A. BUCKLOW & C.W.B. GRIGSON, *Metals Research Ltd.,* 91, *King Street, Cambridge, England.*

Spark planing, a new spark erosion method for the production of flat smooth metal surfaces, is described and its application to single metal crystals and to metallographic preparation is illustrated. The use of conventional

spark erosion methods for crystal cutting and forming is also described.

The spark planing technique is far more rapid and accurate than chemical or electrochemical machining and it causes very much less damage to the surface than the most careful grinding operation.

Spark planed surfaces have been examined by X-ray diffraction, reflection electron microscopy and a Talysurf tracer; these results are presented and the nature and extent of surface damage to various metals is discussed.

§ 18. Crystal Data

18·1. Crystallographic data. By J. D. BERNAL, *Birkbeck College, Malet Street, London, W.C. 1, England.*

The nature of crystallographic investigations requires a most thoroughgoing system of data collection and preservation. The problem is a cumulative one and may become unmanageable if not dealt with systematically now. Data need not only be collected but kept up-to-date and be readily accessible within a short time after publication. The Union, however, could furnish through appropriate national bodies, the means to carry out this task, while the use of modern methods of storage and reference can provide the technical means.

18·2. The organisation and some results of crystallographic documentation. By O. KENNARD, *National Institute for Medical Research, Mill Hill, London, N.W.7, England.*

No abstract provided.

18·3. Report on 'crystal data'. By J. D. H. DONNAY, *Department of Geology, The Johns Hopkins University, Baltimore, Md., U.S.A.*

No abstract provided.

18·4. Documentation in the U.S.S.R. By G. B. BOKII, *Ministry of Higher Education, Moscow State University, Faculty of Geology, Moscow, U.S.S.R.*

No abstract provided.

18·5. The work of the Japanese National Commission on crystallographic data and structure reports. By R. SADANAGA, *Mineralogical Institute, Science Department, University of Tokyo, Hongo, Tokyo, Japan.*

No abstract provided.

18·6. Crystallographic information retrieval methods in the Groth Institute.* By R. PEPINSKY & V. VAND, *Physics Department, Pennsylvania State University, Pa., U.S.A.*

In the *Groth Institute,* all data on the physical and chemical properties of crystalline solids are being extracted from the literature and transferred to IBM punched cards. Each card contains: a card number; a 3-character operator symbol to indicate the character of following information; a Peek-a-Boo card number; the information (in a limited number of formats); perti-

---

* Supported by Air Force Office of Scientific Research, ARDC; IBM 704 computations supported by U.S. Atomic Energy Commission.

nent remarks; and codes which completely identify primary and secondary references.

Information is coded in Publication (P) language, with upper and lower case (plus subscript) control symbols for Cardatype printouts; and in Sort (S) language, which is upper case only for printouts by fast tabulators.

The following classes of Reports are issued:

L = *Literature Image,* including not more than 500 crystalline species.

S = *Property Sort,* with information from a given L-report sorted according to properties.

PKB = Peek-a-Boo cards, corresponding to a given S-report, for rapid manual or machine retrieval.

C = Concordance, for each L-report.

RMS = Reference Merged Sort, for a complete single secondary source.

CML = Compound Merge Image, including all data for one species and from all sources—arranged chemically.

CMS = Property Sort of information from all sources.

Concordances of RMS, CML and CMS Reports.

Critical Monographs.

Request Reports—answering various search questions.

MD = Missing Data Reports.

Second and third-stage Peek-a-Boo cards, for retrieval of Report Numbers in mega-item files.

All classes of Reports subsequent to L-reports, with exception of Critical Monographs, are machine-preparable using simple programs.

Data amenable to computation are so arranged that calculations are automatically made on signals to the machine.

Information retrieval methods are divisible into two classes: those using small-scale punched-card and paper-tape machines (IBM Cardatype and associated arithmetic unit, 407 tabulator, sorter, reproducing punch, collator, etc., Flexowriter); and those using large-scale processing machines with magnetic tape and core storage (IBM 704, etc.). Coding of input data on punched cards is designed for processing by either class of processing equipment.

Large advances have been made in the applicability of small-scale machines for preparations of concordances and indices, and for retrieval of data in mega-item card files. Peek-a-Boo cards, one for each property and with a maximum of 500 species on a card, are automatically prepared on Cardatype and 407 machines. To permit sorting on any word (of any variable size) in a sentence, the word order in the sentence is automatically *rotated* by a Cardatype-407 program, and a concordance of words is prepared by machine sorting. Automatically-prepared *second-stage* Peek-a-Boo cards indicate in which Report of 500 items crystals showing a given property may be found. This is equivalent to preparation of an index of indices of 500 volumes. Higher-stage retrieval is equally feasible. Thus mega-item files may be searched very rapidly, to identify materials with any given property or collection of properties.

To facilitate machine calculations and rapid print-outs of answers to any search question, information is transferred from cards to magnetic tapes. All the above small-scale machine processes are also programmed for fast tape machines with core storage. Search speeds are two or more orders of magnitude faster than with cards; very fast tabulation of answers to search questions is provided;

and computations are available automatically on demand. Files, concordances and indices are kept up-to-date, automatically.

Paper in full to be submitted to *Scientific American*. Abstract exceeds 300 words because it covers about 80 man-years of work.

18·7. Zur numerischen Behandlung der Systeme von Eigenschaftsdaten bei Kristallen. Von F. E. BURESCH & H. V. PHILIPSBORN, *Mineralogisches Institut, Poppelsdorfer Schloss, Bonn-Rhein, Deutschland.*

Zur Untersuchung der Abhängigkeit mehrerer Eigenschaftsdaten von Kristallen von vorgegebenen Bedingungen wird üblicherweise die graphische Darstellung benutzt. 3 Veränderliche werden z. B. in einem Dreieck dargestellt. Für die Untersuchung der Abhängigkeit 4 Variabler werden Tetraeder benutzt, während für 5 die Ineinanderstellung mehrerer Tetraeder vorgeschlagen worden ist. Die Schwierigkeiten, die sich bei diesen graphischen Methoden bei der Interpolation ergeben sind bekannt. Zur numerischen Behandlung wurden lineare Beziehungen aufgestellt.

Hier wurde versucht den Funktionsverlauf durch ganze rationale Funktionen mehrerer Veränderlichen n nach der Methode der kleinsten Quadrate anzunähern. Geometrisch sind dies Hyperflächen $m$ten Grades in einem n-dimensionalen Raum. Sie werden als Matritzenfunktionen dargestellt, deren Elemente quadratische Formen sind. Das lineare Gleichungssystem, das sich bei der Minimalisierung ergibt, hat z. B. bei einer Funktion 5 Veränderlicher 3. Grades 56 Unbekannte. Programme für die Lösung linearer Gleichungssysteme liegen bei jeder Rechenmaschine vor.

Die Hyperflächen n-Veränderlicher schneiden sich in solchen $(n-1)$-Veränderlicher deren Gleichungen sich durch Transformationen ergeben. Dadurch sind die Randwerte eines Gebietes festgelegt, die somit experimentell nicht ermittelt werden müssen bzw. durch gezielte Versuche bestimmt werden können. Beliebige Schnitte durch die Hyperflächen erlauben den Verlauf einer abhängig Veränderlichen für vorgegebene Verhältnisse der Variablen zu ermitteln.

Das Verfahren eignet sich besonders auch für das Studium des Gleichgewichtes polynärer Systeme von 4, 5 und mehr Stoffen.

Part of the dissertation of Mr F. E. Buresch at the University of Bonn, 1960.

18·8. Revision of the crystallographic section in the handbook of chemistry and physics. By G. DONNAY, *Department of Geology, The Johns Hopkins University, Baltimore, Md., U.S.A.*

No abstract provided.

18·9. Current and future operations of the X-ray Powder Data File. By J. V. SMITH, *Department of Mineralogy, Pennsylvania State University, Pa., U.S.A.*

Current and future operations of the XRPDF are described to provide a basis for constructive criticism by users of the file. Future plans include the following: annual publication of a new set of cards, each to include data for at least 1,000 substances; preparation of a larger proportion of data by the File organization and its

affiliates; revision of the index volumes to permit faster use of the index; systematic preparation of data to fill in especially useful regions; utilization of modern data processing and retrieval methods; publicity to disseminate information on X-ray powder diffraction methods, and to, encourage the preparation of data by individual scientists; and cooperation with other data-collection agencies.

May be published in *ASTM Bulletin*.

18·10. Standard X-ray powder patterns at the National Bureau of Standards. By H. F. McMURDIE & H. E. SWANSON, *National Bureau of Standards, Washington 25, D.C., U.S.A.*

The National Bureau of Standards, in cooperation with the Joint Committee Fellowship, prepares X-ray powder patterns of materials of known high purity for inclusion as starred patterns in the Powder Data File. Counter diffractometer methods are used with special precaution taken to prevent errors resulting from lack of random orientation or from lack of proper fineness. The patterns are indexed and the cell dimensions refined using an IBM 704 calculator. Problems in the source of suitable samples will be discussed. A design of a back reflection camera for precision measurement of unit-cell size has been made.

18·11. Some aspects of the Cardiff work for the A.S.T.M. X-ray powder data file. By B. W. DELF, J. W. HUGHES, I. E. LEWIS & A. J. C. WILSON, *University College, Cardiff, England.*

The preparation of specimens, choice of radiation and relative advantages of camera and diffractometer methods for obtaining data for the *A.S.T.M. X-ray Powder Data File* are discussed. A simple procedure for the determination of the specimen-surface displacement in a diffractometer by direct measurements is described. An account is given of the choice of substances for investigation and the indexing of the patterns obtained from them.

18·12. Precision requirements for automatic handling of powder data. By P. M. DE WOLFF, *Laboratorium voor Technische Fysica der Technische Hogeschool, Delft, The Netherlands.*

Whereas automatic sorting methods are often applied to powder data for identification purposes, little use has so far been made of computers for the physical interpretation of these data. Such applications could be useful primarily for (*a*) indexing of patterns with unknown unit-cell; (*b*) precise determination of lattice parameters when the unit cell is approximately known; (*c*) calculation, from these parameters, of 'ideal' *d*- or *Q*-values which in several cases would increase the selectivity of identifications.

Some examples of such calculations will be given, with special emphasis on the influence of the precision of the experimental data on the results.

18·13. A recommended practice for the X-ray counter diffractometry of polycrystalline specimens. By W. PARRISH, *Philips Laboratories, Irvington on Hudson, New York, U.S.A.*

The selection of a specific set of optimum experimental conditions requires a knowledge of certain characteristics

of the specimen and of the precision required for the intensities and reflection angles. Varying the conditions may cause large variations in the quality of the data. It is not possible to set up specific experimental conditions that are optimum for all types of analyses. An outline will be presented to show the effects of many of the instrumental and specimen factors. The information will enable one to select and apply the methods best suited for the particular analysis. Interpretation and comparison of data obtained at different laboratories will then be facilitated and the limits of precision can be better evaluated.

Most of the factors contributing to the quality of the data are now well known. These will be described in several major categories. (1) *X-ray spectra*: stability, selection of targets, beta filters, spectral purity; (2) *Diffractometer geometry*: X-ray optical system, tube focus, apertures in focussing and axial planes, 2:1 setting, receiving slit; (3) *Alignment and angular calibration*; (4) *Specimen factors*: preparation, homogeneity, surface displacement, transparency, preferred orientation, strain and plastic deformation, crystallite sizes; (5) *X-ray counters*: electronic circuits, linearity, quantum counting efficiency, pulse amplitude distribution, electronic discrimination and its effect on peak-to-background ratio, non-X-ray background; (6) *Counting statistics*; (7) *General considerations*: comparison of diffractometer and camera data, peaks versus centroids and other angular measures, peak versus integrated intensities, absolute intensities, lower limits of intensities to be listed, d-spacing range.

18·14. Identification of organic compounds from X-ray powder Patterns. By B. JERSLEV, *Organic Chemistry Dept., Royal Danish School of Pharmacy, Universitetsparken 2, Copenhagen Ø, Denmark.*

No abstract provided.

§ 19. Miscellaneous

19·1. Low-angle X-ray scattering by crystalline polyethylene. By B. G. RÅNBY & H. BRUMBERGER, *Department of Chemistry, Syracuse University, Syracuse 10, New York, U.S.A.*

Rånby, Morehead & Walter have recently shown (in press) that the folding length d^* of polyethylene chains arranged perpendicularly to the top and bottom surfaces of single-crystal platelets is linearly dependent on the crystallization temperature t_c, as predicted, and that d^* tends to increase when material crystallized from dilute solutions (0·5 g./100 ml.) at low t_c is recrystallized at a higher temperature.

This work is continued, with the intention of finding out whether d^* is thermodynamically or kinetically determined. If d^* is an equilibrium value at t_c, it should decrease when polyethylene crystallized at higher temperatures is recrystallized at lower ones.

The low-angle X-ray scattering of crystalline, pressed polyethylene flakes oriented parallel to the X-ray beam was recorded on film, using Cu $K\alpha$ radiation and a Kratky–Skala camera. One to three orders of diffraction were observed, as well as the intense, diffuse scattering shown by all samples.

The linear dependence of d^* on t_c is confirmed; d^* increases from 115 to 164 Å as t_c increases from 50 to 110 °C. These d^* values are uniformly higher than earlier ones, but with the same slope. Recrystallization of 78 °C.-samples at 90 and 100 °C. caused d^* to increase from 141 to 152 Å, the latter value being predicted for $t_c = 95°$ from the d^*–t_c curve. Samples crystallized at high t_c and allowed to recrystallize at lower temperatures for periods up to 24 hr. showed a very high barrier to changes in d^*, no significant changes being observed except in one case, where d^* decreased very slightly.

The diffuse scattering yielded exponential Debye correlation functions for all samples, with correlation distances of 30–50 Å, indicating a random arrangement of the amorphous portion of the polymer.

On the basis of these results, no conclusion can yet be reached concerning the thermodynamic or nucleation-controlled growth of the crystals. Further experiments are in progress, particularly with samples recrystallized over much longer periods, and will be reported at the meeting.

19·2. Small angle X-ray scattering from prisms.* By PAUL W. SCHMIDT & AKELEY MILLER, *Dept. of Physics, University of Missouri, Columbia, Mo., U.S.A.*

The techniques previously developed (P. W. Schmidt & R. Hight, Jr., *J. Appl. Phys.* (1959), **30**, 866) for calculating the intensity of small angle X-ray scattering at the larger angles of the small angle region have been applied to a study of the scattered intensity from prismatic solids. Also, an expression for the characteristic function (A review of the characteristic function and its properties is given in Chapter II of *Small Angle Scattering of X-Rays*, by A. Guinier *et al.* (1955). New York: Wiley) of a prism has been developed. This expression gives the characteristic function for the solid in terms of an integral over the two-dimensional characteristic function of the cross section of the prism. The scattered intensity for rectangular parallelepipeds has been evaluated. A study has been made of the case of very long, rod-like prisms. The relation of the resulting expressions for the scattering intensity to the calculations of A. R. Stokes (*Proc. Phys. Soc.* (1957), B, **70**, 379) is discussed.

Probable place of publication: *J. Appl. Phys.*

19·3. Small angle X-ray scattering from clay suspensions.† By PAUL W. SCHMIDT & R. HIGHT, JR., *Dept. of Physics, University of Missouri, Columbia, Mo., U.S.A.*

A study has been made of the small angle X-ray scattering from montmorillonite clay suspensions. After collimation corrections were made, the scattered intensity was found to be proportional to the inverse square of the scattering angle, except at the largest angles, for which the intensity decreased more rapidly. The shape of the scattering curve did not depend on the concentration or upon the average particle size, as determined by centrifugation. The intensity was proportional to the concen-

---

tration and at a given concentration was independent of the average particle size.

These results can be explained if one considers the suspensions to consist of thin, non-interacting platelets. From the angle at which the scattering begins to fall off more rapidly than with the inverse square of the scattering angle, the thickness of the platelets was estimated to be 9 Å. Using the method outlined by P. W. Schmidt & R. Hight, Jr. (*J. Appl. Phys.* (1959), **30**, 866), an independent thickness determination was made by measuring the absolute intensity of scattering in the inverse square region. The results were found to be in essential agreement with the above value of the thickness. From the fact that the inverse square angular dependence persists at the smallest angles measured, a lower limit of about 500 Å can be established for the large dimension of the platelets.

Probable place of publication: *J. Chem. Phys.*

19·4. Low angle scattering from wheat proteins and lipo-proteins. By J. C. GROSSKREUTZ, *Midwest Research Institute, Kansas City, Missouri, U.S.A.*

Low angle scattering curves from stretched, freeze dried crude glutens extracted from a pure strain flour dough show marked orientation and can be interpreted in terms of parallel sheets of gluten platelets whose thickness does not exceed ~ 70 Å. Electron micrographs taken of surface replicas of the stretched glutens confirm the sheet structure. Moist, relaxed glutens, while not exhibiting the orientation into sheets still give the characteristic platelet scattering. Scattering from dilute dispersions of gluten in acetic acid give a radius of gyration of 31·5 Å for the platelet.

Low angle scattering curves were also obtained from the gluten components, gliadin and glutenin, as well as the water soluble proteins extracted from the parent flour. Scattering from dry powdered samples did not differ markedly from the gluten scattering.

Several small angle diffraction peaks observable in both dry and moist glutens, in glutenin and in evaporated films of gliadin can be traced to bound phospholipids which are extractable with water saturated *n*-butanol. These peaks correspond to *d*-spacings in the range 40–60 Å, and are characteristic of the bimolecular leaflet structure of many phospholipids. Removal of the lipids from Gluten does not materially change the lipid scattering pattern but does destroy the ability of the remaining gluten to form into continuous sheets. Based on the available data a lipo-protein complex is postulated for crude gluten consisting of protein chains adsorbed onto the hydrophillic ends of phospholipid bimolecular leaflets. Such lipo-protein sheets should be of the order of 60 Å thick in agreement with the X-ray data.

A major portion of this work will appear in *Biochim. et Biophys. Acta*, (1960), **38**, 400. It is planned that only the later, unpublished interpretive work be presented at the Congress.

19·5. Sur l'emploi de la diffusion centrale des rayons X mesuree à l'echelle absolue: technique et resultats. Par V. LUZZATI, *Centre de Recherches sur les Macromolécules, Strasbourg, France.*

Cette technique est basée sur la comparaison directe de l'intensité des faisceaux incidents et diffusés. Le problème expérimental est assez délicat: nous l'avons résolu en employant un générateur de rayons X à débit stabilisé, un faisceau monochromatique focalisé, un détecteur à compteur de Geiger et un jeu de filtres étalonnés.

Un certain nombre de paramètres deviennent accessibles à l'expérience grâce à cette technique. Dans le cas des solutions de particules globulaires, on peut déterminer leur masse et leur degré de solvatation: nous avons étudié plusieurs protéines. Dans le cas des particules en forme de bâtonnet on mesure leur masse spécifique linéaire ainsi que le rayon de giration des particules autour de leur axe: nous avons examiné l'acide désoxyribonucléique, le poly-L-glutamate de benzyle. Dans tous ces exemples nous avons fait des observations nouvelles.

A paraître dans *Acta Cryst.*

19·6. Mesure des surfaces spécifiques par la diffusion centrale des rayons X. Par R. BARO & V. LUZZATI, *Centre de Recherches sur les Macromolécules, Strasbourg, France.*

On sait depuis Porod qu'il est possible de déterminer la surface spécifique d'un échantillon hétérogène en étudiant le comportement asymptotique de la diffusion centrale des rayons X obtenue avec une préparation de faible épaisseur. Par ailleurs, en analysant le phénomène de la diffusion multiple, nous avons montré récemment que, lorsque l'épaisseur de l'échantillon est grande, l'allure de la courbe des intensités diffusées au centre ne dépend que de la surface spécifique.

Nous avons utilisé cette méthode nouvelle pour déterminer la surface spécifique d'un grand nombre de substances que nous avons étudiées également selon la méthode de Porod, et dont les surfaces spécifiques mesurées par le microscope électronique et par les isothermes d'adsorption (BET) étaient connues.

La comparaison de tous ces résultats nous a permis de confirmer la validité de la technique basée sur la diffusion multiple, et de préciser les domaines d'application et les limitations inhérentes aux différentes techniques.

A paraître dans *Acta Cryst.*

19·7. Absolute configuration and optical rotatory power of $NaClO_3$ and $NaBrO_3$ crystals. By J. M. BIJVOET, *Laboratorium voor Kristalchemie, Utrecht, The Netherlands.*

$NaBrO_3$ and $NaClO_3$ crystals of same sign of optical rotatory power are proved, by the anomalous scattering technique, to be of inverse configuration.

Reflexions hkl and $hk\bar{l}$ ($\equiv \bar{h}\bar{k}\bar{l}$) have been registered simultaneously and measured photometrically on oscillation diagrams. With Cr $K\alpha$ rays

$$(\Delta f''(Br) = 2 \cdot 7, \ \Delta f''(Cl) = 1 \cdot 3)$$

the calculated ratios $I_{hkl}/I_{\bar{h}\bar{k}\bar{l}}$ of 4 reflections in the case of $NaBrO_3$ and 6 reflections in that of $NaClO_3$ give significant anomalous effect. In all these reflections measured and calculated ratio are in good agreement and consistent as to configuration.

The view has been expressed in the literature that in

the presence of more than one scattering atom per cell, the anomalous scattering factor should not be calculable taking into account the anomalous scattering effect for each atom independently. This conclusion has been proved to be in error.

The remarkable result mentioned in the first paragraph finds some affirmation in the fact that whilst a crystal of $NaBrO_3$ or $NaClO_3$ brought into its supersaturated solution continues growing with the same sign of optical rotation, a crystal of $NaBrO_3$ in the supersaturated solution of $NaClO_3$ grows with *opposite* rotation sign. In both cases it is the configuration which is preserved in the growth.

The crystals of $NaClO_3$ and especially those of $NaBrO_3$ occasionally exhibit deviations from cubic symmetry. It is hard to see how this could influence the above finding. It is under investigation whether a refinement of the calculation of the rotatory power can bring out the unexpected difference in optical behaviour.

Will be published in *Acta Cryst*.

19·8. The statistics of superexchange interaction and ionic distribution in substituted ferrimagnetic rare earth iron garnets.

By S. GELLER, *Bell Telephone Laboratories, Incorporated, Murray Hill, New Jersey, U.S.A.*

Ideas on the statistics of superexchange interaction developed and applied to substituted yttrium–iron garnet by M. A. Gilleo (*J. Phys. Chem. Solids* (1960) in press) are extended and applied to substituted rare earth iron garnets. It is shown by means of structural considerations that only four interactions per c site ion with d site ions are important in determining the contribution of the c site ions to the 0 °K. saturation magnetization. The statistical theory accounts especially well for the behavior of $n_B(0$ °K.) versus $x(=y+z)$ of the system

$$\{Gd_3\}[Al_yFe_{2-y}](Al_zFe_{3-z})O_{12}$$
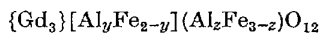
(G. Villers, R. Pauthenet & J. Loriers, *J. Phys. et Radium* (1959), **20**, 382) and for

$$\{Gd_{2\cdot 4}Ca_{0\cdot 6}\}[Al_yFe_{2-y}](Al_{z-0\cdot 6}Si_{0\cdot 6}Fe_{3-z})O_{12}$$
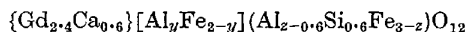
(R. M. Bozorth & S. Geller, *J. Phys. Chem. Solids* (1960), **11**, 263) corrects the previously obtained ionic distribution which had been considered anomalous. Other systems are also considered.

Crystal chemical aspects of some of the results, compensation points and some minor limitations of the treatment are discussed.

Manuscript submitted to *J. Phys. Chem. Solids*.

19·9. Decomposition of azides under the influence of X-rays.

By BRIGITTE H. KRAUSE & FRANKLIN E. WAWNER, JR., *Engineer Research and Development Labs., Fort Belvoir, Virginia, U.S.A.*

A serious difficulty encountered in determining the structure of α- and β-lead azide, thus far not taken into consideration by investigators, is the slow decomposition of the crystals while under the influence of X-ray irradiation. This decomposition produces lattice constant changes, intensity changes, and changes of the shapes of the reflections (differing for different crystallographic directions).

While NaN_3, as investigated by Krasner & Keating (*Picatinny Arsenal Tech. Report* 2489 (May, 1958), undergoes under the influence of irradiation a lattice contraction due to induced stacking faults, various other azides with layer structures experience a lattice expansion. These expansions are investigated along different crystallographic directions at different stages of decomposition. The results are correlated with the crystal structures. Furthermore, the results of experimental investigation of the measurement of nitrogen escape, line profile analysis on powder reflections and shape of single crystal reflections are discussed in terms of structural damages.

19·10. Structure and therapeutic properties of mangostein scales.

By N. N. SAHA, *Crystallographic & Solid State Physics Laboratory, Saha Institute of Nuclear Physics, Calcutta University, India.*

Mangostein scales are locally used in Burma as a quack remedy for dysentry. These are administered orally both in the form of paste as well as water-extract. Both the forms have curative effect, but the latter, as they claim, is more effective. No experimental data or reliable statistics were available. An investigation employing X-ray diffraction and chemical analysis was, therefore, undertaken by the author.

On chemical analysis, the pounded air dried scales was found to contain 12·86% moisture, 3·5% proteins, 2·48% ash (soluble), 23·63% fibrous matter, 4·5% tannin, 4·5% nontannin astringents and the rest pithy material. The analysis of water-extract and acetone-extract reveals that the major constituents of both are tannin and nontannin astringents, constituting about 90%.

X-ray diffraction patterns of all these samples mainly consist of diffuse haloes. The pattern due to pounded scales contains some additional reflections characteristic of cellulose and that due to acetone-extract contain some due to resinous substances. Comparison photographs of these samples and some vegetable tannins show that there is an overall correspondence between the patterns due to water-extract and that of a particular vegetable tannin, Goran.

As the removal of components other than tannin and non-tannin astringents does not seem to affect the curative property and also that it is not a characteristic property of all tannins, the structure appears to be the decisive factor. An attempt to get the oriented patterns has been made by taking X-ray photographs of the samples in the form of films with the X-ray beam parallel and perpendicular to the film surface. A detailed discussion of our findings has been incorporated in the paper.

19·11. The temperature dependence of the interlayer spacing in carbons of differing graphitic perfection.

By E. G. STEWARD, B. P. COOK & E. A. KELLETT, *Research Laboratories of The General Electric Co. Ltd., Wembley, Middlesex, England.*

A recent literature survey (*Nature, Lond.* (1960), **185**, 78) of the temperature variation of the interlayer spacing in graphitic carbons revealed some important incon-

sistancies and gaps in our knowledge. Preliminary experiments to resolve these, were reported.

Measurements at low temperatures (down to -180 °C.) have now been made with graphites of widely different degrees of graphitization: the effect of structural disorder (turbostratic layer-stacking etc.) on the ultimate close approach of the adjacent aromatic layer-planes, is considered.

Measurements and technique to obtain data at temperatures well in excess of 2000 °C. are also described. This part of the investigation is resolving the past uncertainty as to the temperature dependence of the interlayer expansion coefficient.

Journal for publication uncertain: possibly *J. Chim. Phys.*

19·12. Some considerations on X-ray protection in X-ray crystallography. By S. A. WYTZES, N. V. Philips Gloeilampenfabrieken, Scientific Equipment P.I.T., Eindhoven, The Netherlands.

No abstract provided.

Symposium 1: Thermal motion in crystals and molecules

S1·1. Introductory lecture. The interaction of mechanical and electromagnetic waves in crystals. By J. C. SLATER, Massachusetts Institute of Technology, Cambridge, Mass., U.S.A.

As shown by Huang (K. Huang, *Nature, Lond.* (1951), **167**, 779; M. Born & K. Huang, *Dynamical Theory of Crystal Lattices* (1954). Oxford: University Press), and earlier by Lyddane and others (R. H. Lyddane & K. F. Herzfeld, *Phys. Rev.* (1939), **54**, 846; R. H. Lyddane, R. G. Sachs & E. Teller, *Phys. Rev.* (1941), **59**, 673; H. Fröhlich & N. F. Mott, *Proc. Roy. Soc.* (1939), A, **171**, 496), a transverse electromagnetic wave in an ionic crystal such as an alkali halide interacts with the transverse optical mode of the crystal, producing the phenomenon of anomalous dispersion around the Reststrahlen frequency. This can be indicated by plotting the angular frequency ω of the wave as a function of k, the propagation constant. We can derive the relation easily. The dielectric constant is given by

$$1 + \frac{4\pi Ne^2/m}{-\omega^2 + \omega_0^2 - 4\pi Ne^2/3m}$$

in which N is the number of displacable ions per unit volume, e their charge and m their mass, ω_0 their resonant natural frequency in the absence of a local field, and in which we have assumed the presence of the Lorentz field, equal to $4\pi/3$ times the polarization. For simplicity we neglect electronic polarizability. The dielectric constant is the square of the index of refraction, or equals $(kc/\omega)^2$. If we equate this to the value above, we have a relation between k and ω.

This relation is plotted in the figure. There are two branches to the curve, each corresponding to two trans-

verse oscillations at right angles to each other; the introduction of the electromagnetic oscillations has introduced a new type of mode in addition to the ordinary acoustic and optical modes of mechanical vibration. If
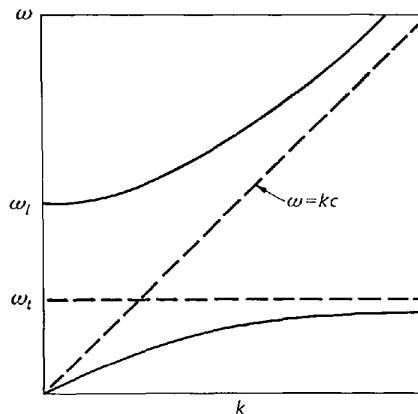
it were not for the interaction, the electromagnetic mode would follow the curve $\omega = kc$, and the mechanical vibration the curve $\omega = \omega_t$, the angular frequency of transverse oscillation. The interaction has pushed the two branches of the curve apart. The lower branch consists largely of a transverse mechanical oscillation, the upper one largely of an electromagnetic oscillation, except near the crossover, where they are mixed together. One can show that the frequency marked ω_l is also the frequency of the longitudinal optical oscillation, which does not interact with the electromagnetic wave. All of the phenomena shown take place at very small values of k, corresponding to long waves, equal in wave length to electromagnetic waves of infrared frequency.

The transverse mechanical frequency ω_t can be found easily. It is determined by the condition that k be infinite, or the dielectric constant be infinite, leading to $\omega_t^2 = \omega_0 - 4\pi Ne^2/3m$. It is known that we can obtain a simplified model of a ferroelectric by assuming that $4\pi Ne^2/3m$ is large enough so that it equals ω_0^2; the theories of Devonshire and of the author (A. F. Devonshire, *Phil. Mag.* (1949), **40**, 1040; (1951), **42**, 1065; J. C. Slater, *Phys. Rev.* (1950), **78**, 748) for the ferroelectricity of barium titanate are refinements of this simple theory. In such a case, as Cochran (W. Cochran, *Phys. Rev. Letters* (1959), **3**, 412) has pointed out, ω_t will go to zero, so that the dielectric constant becomes infinite at zero frequency, instead of at a higher frequency ω_t. This simple model, then, reproduces this behavior discussed by Cochran.

The model shows, however, that probably the phenomenon is not as simple as it seems at first sight, namely an observable lowfrequency resonance of the crystal as we approach the ferroelectric behavior. For in the interval of frequencies between ω_t and ω_l in the figure, k^2 is negative, k imaginary, or we have damping. In the ordinary case of Reststrahlen, this absorption is associated with the high reflectivity of the crystal for the Reststrahlen frequency. But in the ferroelectric case, it seems likely that this absorption would extend over the whole spectrum from low frequency up to the infrared. Hence this absorption, rather than any sharp resonance, would be observed experimentally.

S1·2. Invited paper. The determination of atomic vibration amplitudes in crystals by X-rays and their interpretation. By D. W. J. CRUICKSHANK, *School of Chemistry, The University, Leeds 2, England.*

The determination of atomic vibration amplitudes in crystals by X-rays will be surveyed. Particular attention will be paid to molecular crystals, in which the vibrations are necessarily anistropic. In the harmonic approximation a mean square vibration tensor with six independent components can be found for each atom. The methods of analyzing these tensors in terms of the rigid body and internal vibrations of the molecules will be considered; no complete solution is possible from X-ray data only. For relatively rigid molecules at room temperature the internal vibrations are small compared with the external vibrations, and the latter can generally be analyzed into translational and rotational components. Examples will show that appreciable angular oscillations can be expected when a molecule has an axis of low inertia. As the temperature decreases the relative contribution of the internal vibrations to the total atomic vibrations increases. Among the different kinds of internal vibration, twisting vibrations (as in hindered rotors) are particularly important and can produce effects comparable with the rigid body angular oscillations. To assist an analysis in terms of external and internal vibrations it is important to use available spectroscopic and other data.

It is hoped to discuss the X-ray diffuse scattering from crystals containing molecules in angular oscillation.

The paper in this form is unlikely to be published.

S1·3. Thermal motion in crystals and molecules. Studies at University College, London. (Collected work). By KATHLEEN LONSDALE, RONALD MASON, H. JUDITH MILLEDGE & JACK FORRESTER and others, *University College, London W.C. 1, England.*

Studies at University College, London, have been directed mainly along two lines:

I. Investigations of thermal vibrations in small molecular crystals of two types: (a) those of high symmetry, in which the principal directions of rigid-body vibrations are identical with those of intra-molecular vibrations; (b) those of low symmetry, where the directions are different. Examples: (a) hexamine, urea; (b) naphthalene, anthracene.

Experiments at various temperatures lead to independent sets of data from which to estimate the magnitude and temperature-dependence of rigid-body and non-rigid-body vibrations and their influence on thermal expansion coefficients. Problems of bond anisotropy and zero-point energy will be considered.

II. Methods of obtaining and correcting data accurately enough for the above analyses.

To be published in *Acta Cryst., Proc. Roy. Soc., J. Chem. Soc.* etc.

S1·4. Electron scattering and internal rotation. By J. KARLE, *U.S. Naval Research Laboratory, Washington 25, D.C., U.S.A.*

In order to facilitate the interpretation of the Fourier transform of the molecular intensity, theoretical functions have been derived for the probability distributions describing the interatomic vibrations. We are here concerned with the probability distributions associated with restricted internal rotation. In addition to the torsional oscillation, it is necessary to include the over-all vibration of the molecular frame. Probability distributions for distances whose equilibrium positions occur anywhere on the circle of rotation have been derived.

The theory has been applied to the study of 1,2-dichloroethane, hexachloroethane, hexafluoroethane, and hexachlorodisilane. The nature of the results obtained will be described.

S1·5. Thermal effects in crystals. By BEN POST, *Polytechnic Institute of Brooklyn, New York, U.S.A.*

The thermal motions of atoms in a number of organic and inorganic compounds have been analyzed on the basis of measurements of diffraction intensities at room temperature and at several temperature intervals down to -160 °C. The substances include:

(a)	Graphite and diamond.	(e)	Calcium carbonate
(b)	Alpha quartz.		(calcite).
(c)	Titanium diboride.	(f)	Urea.
(d)	Zinc sulfide (cubic).	(g)	Fumaronitrile.

Diffraction intensities were recorded with proportional and scintillation counters. Filtered Mo K radiation was used.

The experimental data have been analyzed by least-squares and difference Fourier methods for the determination of anisotropic temperature motions of individual atoms as well as for the variation with temperature of peak electron densities, central curvatures and positional parameters of the atoms. Coefficients of thermal expansion have also been determined.

The experimentally determined amplitudes of thermal motion of carbon atoms in graphite have been compared with amplitudes computed on the basis of a theoretical model proposed by J. Krumhansl & H. Brooks (*J. Chem. Physics* (1953), **21**, 1663).

The above work was supported by the Office of Scientific Research of the U.S. Air Force and by the Office of Naval Research.

Papers based on above will be published in *Acta Cryst.*

S1·6. The collection of X-ray diffraction data from single crystals at liquid hydrogen temperature. By J. D. FORRESTER, *Chemistry Department, University College, London W.C. 1, England.*

A liquefier–cryostat is used to produce the liquid hydrogen and the crystal is cooled in situ to liquid hydrogen temperature.

This method introduces problems involving crystal cooling, crystal mounting, the rotation of the crystal and the provision of X-ray transparent windows in the cryostat walls. These are discussed together with some preliminary results obtained with the apparatus.

To be published in *J. Sci. Instrum.* or *Acta Cryst.*

S1·7. The atomic and molecular thermal vibrations in chrysene crystals. By D. M. BURNS & J. IBALL, *Queen's College, Dundee, Scotland.*

In the course of the three-dimensional refinement of the structure of chrysene a detailed analysis has been

made of the atomic and molecular thermal motions. There were 1034 observed structure factors and the thermal parameters of the carbon atoms were determined by three-dimensional least-squares refinement using only those structure factors for reflections with $\sin \theta > 0.65$. This was at a late stage in the refinement when the positional parameters were known quite accurately. The final value of $R = \Sigma||F_o| - |F_c||/\Sigma|F_o|$ is 7.5%. Adopting the method of D. W. J. Cruickshank (Acta Cryst. (1956), 9, 754) the molecule was regarded as a rigid body and from the individual atomic parameters, the two symmetric tensors (T) giving the translational vibrations of the mass centre and (ω) the angular oscillations about axes through the centre were calculated. The values were as follows:

$$T = \begin{pmatrix} 5.07 & -0.05 & 0.29 \\ & 4.61 & -0.42 \\ & & 3.55 \end{pmatrix}; \quad \sigma(T) = \begin{pmatrix} 0.06 & 0.06 & 0.07 \\ & 0.09 & 0.09 \\ & & 0.14 \end{pmatrix}$$

$$\omega = \begin{pmatrix} 17.43 & -1.54 & -0.76 \\ & 5.68 & 0.39 \\ & & 6.11 \end{pmatrix}; \quad \sigma(\omega) = \begin{pmatrix} 1.61 & 0.39 & 0.66 \\ & 0.33 & 0.30 \\ & & 0.26 \end{pmatrix}$$
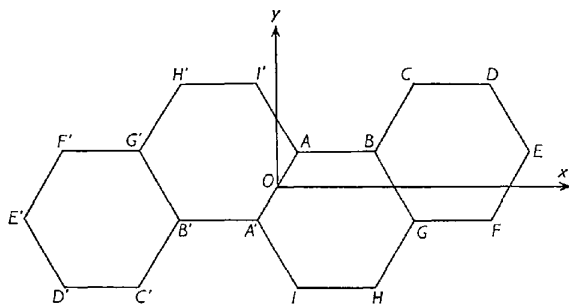

Fig. 1. Chrysene ($C_{18}H_{12}$).

These refer to molecular axes OX (parallel to bond GF, see Fig. 1), OY (perpendicular to OX and in the same plane), OZ (perpendicular to OX and OY) which are related to the rectangular crystal axes $x'(\bar{a})$, $y'(\bar{b})$, $z'(\bar{c}^*)$ by the equation:

$$\begin{matrix} X = \\ Y = \\ Z = \end{matrix} \begin{pmatrix} -0.2122 & -0.0361 & 0.9766 \\ 0.4815 & -0.8735 & 0.0724 \\ 0.85036 & 0.4856 & 0.2027 \end{pmatrix} \begin{pmatrix} x' \\ y' \\ z' \end{pmatrix}$$

From the above tensors it was now possible to compute the U tensors for each atom and to compare these 'calculated' values with those obtained from the least-squares refinement directly. The r.m.s. difference between U_{ij}(obs.) and U_{ij}(calc.) was 0.0017 Å^{-2}. It is therefore reasonable to regard the thermal motions of the atoms in chrysene as being due to the motion of the molecule vibrating as a rigid framework.

It is hoped that a full account of this work will be published in Proc. Roy. Soc., London.

S1·8. Thermal motions in polytetrafluoroethylene.

By E. S. CLARK & L. T. MUUS,* Polychemicals Department, E. I. du Pont de Nemours & Company, Du Pont Experimental Station, Wilmington, Delaware, U.S.A.

_____

* Present Address: Physical Chemistry Department, Aarhus University, Aarhus, Denmark.

The X-ray diffraction patterns of the highly crystalline polymer, polytetrafluoroethylene, lend themselves readily to interpretation in terms of the physical nature of the thermal motions of long chain molecules. X-ray diffraction studies as well as published information from specific heat, specific volume, nuclear magnetic resonance and dynamic mechanical experiments suggest that the polymer chains undergo both torsional oscillation and an untwisting of the helical conformation.

The diffraction patterns are interpreted using the helical structure approach originated by W. Cochran, F. H. Crick & V. Vand (Acta Cryst. (1952), 5, 581) extended to include the effect of specific types of disorder about the axes of the helices in the polytetrafluoroethylene crystal lattice. Below the crystalline transitions taking place close to room temperature, the polymer molecules are arranged in an orderly fashion into a triclinic lattice. As the temperature is increased to the first crystalline transition (about 19 °C.), the chain molecules untwist from a 13_6 symmetry (a 180° twist of the zig-zag molecule per 13 CF_2 groups) to a 15_7 symmetry (a 180° twist per 15 CF_2 groups) and pack into a hexagonal lattice. At the same time, the chain molecules exhibit a torsional oscillation with a long distance between nodes. This particular torsional oscillation affects the diffraction pattern in the same way as small angle librations of chain segments which take place about a preferred direction perpendicular to the helix axis. Between the first and second crystalline transition, approximately in the temperature range from 19 to 30 °C., no additional untwisting takes place but the chain segments retain the 15_7 conformation. The 15_7 conformation is accommodated by the hexagonal lattice with the space group $P3_1$. Packing of the chain molecules into this lattice apparently imposes a restraint on the untwisting.

At the second crystalline transition, the chain molecules are subject to further untwisting and lose their preferred orientation relative to their neighbors. The distance between the nodes in the torsional oscillation is decreased and the torsional oscillation now gives rise to segmental libration with a random angular distribution of chain segments.

Data from specific heat, specific volume, nuclear magnetic resonance and dynamic mechanical experiments are consistent with the thermal motions suggested by the X-ray diffraction work.

Full length account is likely to be published in J. Chem. Phys.

S1·9. The temperature variation of the lattice vibrations of hexamethylenetetramine.

By L. N. BECKA & D. W. J. CRUICKSHANK, School of Chemistry, The University, Leeds, 2, England.

On account of its cubic symmetry with one molecule in the primitive cell hexamine is a key substance in the study of the lattice vibrations of molecular crystals. On the simplest theory the external vibrations in hexamine can be separated into translational and librational modes, respectively obeying Debye & Einstein approximations. The published two-dimensional X-ray (Brill et al., 1939) and three-dimensional neutron data (Andresen, 1957) at room temperature have been refined ($R = 7.9\%$ and 2.2%) and analyzed in terms of mean molecular vibrations with 0.17 Å r.m.s. translational and

7° r.m.s. angular amplitudes. The latter causes a correction of 0·02 Å to the CN bond length and raises it to 1·48 Å in agreement with the gaseous electron diffraction value (Schomaker & Shaffer, 1947). The angular oscillation corresponds to a lattice frequency of about 40 cm.$^{-1}$ and confirms Couture-Mathieu's (1951) assignment in the Raman spectrum. The translational amplitude implies a Θ_D close to that derived from the elastic data.

New three-dimensional single crystal data have been measured photographically with X-rays at $\sim$ 295 °K., $\sim$ 130 °K. and $\sim$ 40 °K. At the time of writing $R = 6\%$ for both the 295 °K. and 40 °K. data. The results of the refinements show a great reduction at the lower temperature of both the translational and angular oscillations. Their measured temperature variation will be discussed in terms of the simple theory. Specific heat measurements (with T. P. Melia), which we hope to extend down to 30 °K., have been made between 100 °K. and 300 °K., and agree to 1% with those calculated theoretically.

The material of this paper will probably be submitted to *Acta Cryst.* in due course.

$S1·10$. Theory of thermal diffuse scattering by a molecular crystal. By W. Cochran, *Crystallographic Laboratory, Cavendish Laboratory, Cambridge, England.*

The theory of lattice dynamics can be used to calculate the scattering of X-rays by a molecular crystal. In many cases the main features of the scattering will be correctly given when the internal degrees of freedom of the molecule are neglected and only first order (one phonon) scattering is considered, (W. Hoppe, *Z. Kristallogr.* (1956), **107**, 406). In this approximation, the diffuse intensity can be calculated rather simply by the method of W. Cochran & G. Kartha (*Acta Cryst.* (1956), **9**, 941). It is found that, for a primitive unit cell containing one kind of molecule, the amplitude of the diffusely scattered radiation in general involves a sum of two terms, only one of which depends on the molecular Fourier transform. In the case of a symmetrical molecule, only this latter term is involved for certain directions of the scattering vector, whatever the details of the molecular interactions. In general the same term will dominate to the extent that displacements due to translational components are greater than those due to rotational components in all normal modes of vibration which contribute to the scattering. (The concept of separate translational and rotational modes having different frequencies is shown to have very limited validity.) These and other conclusions will be illustrated by numerical calculations made for a simple model of a molecular crystal in which forces act between adjacent molecules only.

$S1·11$. The theory of diffuse X-ray scattering on elastic waves in molecular crystals. By W. Hoppe, *Abteilung für Röntgenstrukturforschung am Max-Planck-Institut für Eiweiss- und Lederforschung, München 2, Deutschland.*

We have extended the Faxén–Waller–Laval theory of diffuse scattering to molecular crystals (W. Hoppe, *Z. Kristallogr.* (1956), **107**, 406; W. Hoppe, *Acta Cryst.*

(1956), **9**, 770; W. Hoppe, *Z. Elektrochem.* (1959), in print) (taking also into account the optical branches of the elastic spectrum), and we have shown that the scattering consists of 2 factors, i.e.

(*a*) A factor that describes the enhancement of diffuse scattering in the neighbourhood of reciprocal lattice points (depending on the elastic constants of the crystal) and that describes the overall increase of the diffuse scattering with the reciprocal space vector **H**.

(*b*) A structural factor, which consists of a phase-dependant superposition of the Fourier transforms of the rigid groups in the unit cell.

The theory differs from the elder theory of diffuse electron diffraction from A. Charlesby, G. I. Finch & H. Wilman (*Proc. Phys. Soc., London* (1939), **51**, 479), which was recently used by J. L. Amorós *et al.* (J. L. Amorós, M. L. Canut, S. Annaka & A. de Acha, *Publicaciones del Departemento de Cristalografia y Mineralogia,* 1958) for the explanation of diffuse X-ray scattering as well—that it takes into account the strong coupling of the movement of the rigid groups in the crystal. The results of the two theories differ mainly in the following details:

(1) Our theory explains the enhancement of diffuse scattering in the neighbourhood of reciprocal lattice points, whereas the Finch–Charlesby theory does not reveal it.

(2) In the theory of Charles–Finch the Fourier transforms superpose without phases, in our theory they superpose with the phase differences of the vibrating rigid groups in the unit cell.

In order to find relations for these phase differences, we have developed the 'pseudoacoustic approximation' (W. Hoppe, *Z. Kristallogr.* (1956), **107**, 406) for the normal type of molecular crystals (similar masses, inertia moments and force constants of the molecules in the crystal). It can be shown (W. Hoppe, *Z. Elektrochem.* (1959), in print) that the phase-dependent superposition of the different components of diffuse scattering simulates a phase-independent superposition in special planes of the reciprocal space (p.e. in the interlayer lines). Our experiments and the experiments of J. L. Amorós *et al.* (J. L. Amorós, M. L. Canut, S. Annaka & A. de Acha, *Publicaciones del Departemento de Cristalografia y Mineralogia,* 1958) have shown a diffuse scattering of this type in several organic molecular crystals. J. L. Amorós *et al.* (J. L. Amorós, M. L. Canut, S. Annaka & A. de Acha, *Publicaciones del Departemento de Cristalografia y Mineralogia,* 1958), have pointed out that the 'phase-independent' superposition of the Fourier transforms between the reciprocal lattice points demonstrates independent vibrations of the molecules in the optic branches. Our results show that such arguments—which would hardly be physically understandable—are not necessary in the explanation of the diffuse scattering in molecular crystals and that a diffraction theory based on the Born lattice dynamics accounts for all details of the experiments.

$S1·12$. The determination of structures by diffuse X-ray scattering on elastic waves in molecular crystals. By W. Hoppe, G. Will, R. Rauch & K. Anzenhofer, *Abteilung für Röntgenstrukturforschung*

am Max-Planck-Institut für Eiweiss- und Lederfor-schung, München 2, Deutschland.

Our theory (preceding lecture) shows that the study of the diffuse X-ray scattering in crystals has made it possible to study the structure of rigid groups; experiments on known structures have proved these conclusions (W. Hoppe, *Naturwis.* (1955), **42**, 484; W. Hoppe, *Z. Kristallogr.* (1956), **107**, 434).

The diffuse scattering of molecular crystals consists of two factors, the second of which contains the structural information. When doing quantitative interpretations, first the elasticity will have to be determined (at least approximately). This is possible by measuring the diffuse scattering near strong reciprocal lattice points; then the distribution of the first factor can be calculated and can be used for the reduction of the diffuse scattering to the second (structural) factor.

For semi-quantitative interpretations it is frequently sufficient to identify position and form of the diffuse regions only and to compare them with the maxima of the square of the Fourier transform.

The diffuse scattering shows an overall increase depending on the vector in the reciprocal space $|H|$ (see the formulas in our theoretical paper (W. Hoppe, *Z. Kristallogr.* (1956), **107**, 406). This increase can also be deduced from the Charlesby–Finch theory (A. Charlesby, G. I. Finch & H. Wilman (*Proc. Phys. Soc., London* (1959), **51**, 479). It can be incorporated into the Fourier transform of the rigid groups ('Difference Fourier Transform' (J. L. Amorós, M. L. Canut, S. Annaka & A. de Acha, *Publicaciones del Departemento de Cristalografia y Mineralogia,* 1958) and leads to a better representation of the intensities of the diffuse domains for qualitative interpretations.

But it should be pointed out that this reduction is not essential; the function used $(1 - \exp(-B.|H|))$ is monotonously rising and does not alter the number and the distribution of the Fourier transform maxima (apart from the elimination of the zero-maximum). In connection with such a reduction it is advantageous to correct the calculated distribution by the Lorentz and the polarization factor as well.

Examples showing the application of the method in several organic structure determinations will be given. Compared with the Fourier transform method, the elimination of the influence of the translational parameters of the rigid groups is of special interest. This will be demonstrated on experimental results of diffuse scattering of biflorin.

This method must not be confused with the method of the determination of orientation in chain and layer structures using diffuse stratifications caused by the pronounced elastic anisotropy in such structures (K. Lonsdale, J. M. Robertson & I. Woodward, *Proc. Roy. Soc.* (1941), A, **178**, 43).

S1·13. Thermal motion in molecular crystals.* By M. L. CANUT & J. L. AMORÓS, *Departamento de Cristalografia, C.S.I.C., Madrid, Spain.*

The theoretical isodiffusion contours derived by using a simple model of molecular crystal whose 'rigid-body'

molecules undergo independent molecular motion gives account for the observed extended regions of X-ray diffuse scattering. As the above model neglects interactions between molecules, good agreement is achived only when weak van der Waals forces held the molecules in the lattice. A new function, the Difference Fourier Transform (of the molecules at rest and at motion respectively) can be used when translational motion contribution is considered. The isodiffusion lines can also be computed by taking into account the librational molecular movement.

The experimental results obtained with several crystals of different molecular shape and structural type (dicarboxylic acids, hexamine, pentaerythritol, naphthalene, acridine) have shown that the shape and location of the extended diffuse domains are correlated with the shape and orientation of the individual molecules. The agreement obtained when theoretical isodiffusion contours are compared with the observed values shows that these diffuse regions arise from independent (out of phase) molecular motion with vibrational frequencies of the optical type, being this kind of diffuse scattering a function of $(1 - \exp[-2B \sin^2 \theta/\lambda^2])$ as was first predicted by Debye, and it has the same nature as the electron diffuse scattering bands found in anthracene by Charlesby, Finch & Wilman.

The whole X-ray diffuse pattern (extended regions and sharp spots) of the $[001]_0$ reciprocal space of hexamine has been recorded by diffractometer technique with Geiger counter and monochromatized Cu $K\alpha$ radiation. Three effects have been taken into account in the computation of the diffuse intensity distribution: translational and anisotropic librational independent molecular motion and thermal elastic waves (computed in the neighbourhood of non forbidden reciprocal lattice points in terms of the elastic constants given by Haussühl). The good agreement achieved when compared experimental and theoretical isodiffusion lines is shown.

S1·14. Extended thermal diffuse scattering of X-rays from molecular single crystals. By E. SÁNDOR & W. A. WOOSTER, *Cavendish Laboratory, Cambridge, England.*

In addition to the thermal diffuse scattering restricted to the immediate neighbourhood of the reciprocal lattice points the diffraction pattern of molecular single crystals shows extended diffuse areas covering several reciprocal lattice points. The intensity distribution in these areas can be approximated by an expression of the type $\sum_i \{F_i^2(O) - F_i^2(T)\}$, where $F_i(O)$ is the Fourier transform of the ith molecule at rest, $F_i(T)$ the same at the temperature of observation and the summation is to be taken over all molecules in the unit cell.

The above expression is strictly valid according to the theory only for molecules carrying out independent translational vibrations. The departures of the observed diffuse patterns from the above expression (e.g. the parallel fringe system passing through the diffuse pattern of anthracene) indicates that the actual thermal motion of molecules is more complex than is assumed in the derivation of the above expression.

Nevertheless the approximation is good enough to be useful for structural analysis in two ways. One possible

use is the determination of the orientation of a molecule, whose approximate shape is known. If the molecule is planar, the procedure is quite simple and straightforward and can be carried out with an accuracy of 2–3°.

The other possible use is the determination of the molecular structure by calculating a molecular Patterson function from the intensity distribution of the extended diffuse areas. Again the method is most effective in the case of planar molecules, where it reduces to a two-dimensional problem. But even in three dimensions it offers two advantages over conventional Patterson methods, namely, the possibility of measuring intensities on a finer mesh than that of the reciprocal lattice, and also the possibility of separating the contributions of the molecules within a unit cell.

Similar extended diffuse areas were first observed in electron diffraction patterns. X-ray diffraction has the distinct advantage that by using an appropriate technique the extended diffuse areas can be studied in sections, which are practically free from disturbing Laue spots and the strong diffuse regions surrounding them.

To be published in *Acta Cryst.*

S1·15. La densité électronique du milieu cristallin et la diffusion des rayons X par l'agitation thermique des atomes. Par JEAN LAVAL, *Collège de France, Paris, France.*

L'agitation thermique des atomes fait fluctuer la densité électronique du milieu cristallin. Cette densité ne reste périodique qu'en moyenne dans le temps. Néanmoins, on peut en effectuer l'analyse harmonique au moyen de l'intégrale de Fourier. Outre des composantes stationnaires qui donnent lieu aux réflexions sélectives de Bragg, on trouve des trains d'ondes progressives planes, produits par l'agitation thermique des atomes. Comme les strates cristallines, ces trains d'ondes de densité électronique réfléchissent sélectivement les rayons X. Leur pouvoir diffusant global $\bar{\omega}$ (par angle solide unitaire et par électron du cristal) peut être exprimé par une série:

$$\bar{\omega} = \bar{\omega}_1 + \bar{\omega}_2 + \ldots$$

dont le terme $\bar{\omega}_n$, mesure l'intensité des rayons X qui sont rejetés par les réflexions sélectives sur les ondes de densité électronique formées par n oscillations harmoniques des atomes. Si la fréquence, la forme et l'amplitude des oscillations thermiques sont connues, on peut déduire du pouvoir $\bar{\omega}$ les modules de facteurs de structure qui, semblables aux facteurs de structure associés aux réflexions sélectives de Bragg, sont déterminés par la densité électronique du milieu cristallin. Les modules de ces facteurs livrent de nouvelles données sur la densité électronique, ils permettent de la définir avec une précision accrue.

S1·16. Fréquences des oscillations optiques dans la sylvine à 140 °K. Par M. N. BOCCARA, *Collège de France, Paris, France.*

Par la photométrie des rayons X diffusés par un cristal de sylvine maintenu à 140 °K., nous avons déterminé les fréquences des oscillations 'optiques' ou 'rapides'.

Cette étude a montré que, pour un vecteur d'onde dirigé suivant un axe de symétrie ternaire, les fréquences des oscillations optiques longitudinales sont supérieures à celles des oscillations optiques transversales.

Pour les très grandes longueurs d'onde le rapport des fréquences des oscillations longitudinales et transversales est sensiblement égal à 1,1.

Pour interpréter ces résultats expérimentaux, nous avons décomposé le champ de force qui règne dans le cristal en deux parties:

(1) Un champ de force représenté par des tenseurs assujettis à la symétrie du milieu cristallin rendant compte des interactions à courte distance.

(2) Un champ de force coulombien produit par la polarisation électrique développée par une onde d'agitation thermique.

Ce champ de force est défini à partir des constantes élastiques, de la fréquence d'absorption infra-rouge et de la charge effective des ions supposés rigides et non polarisables.

La charge effective ajustée aux résultats expérimentaux doit être prise égale à 0,3 fois celle d'un électron.

S1·17. The effect of thermal vibration of gaseous molecules in electron diffraction studies. By YO-NEZO MORINO, *Department of Chemistry, Faculty of Science, The University of Tokyo, Tokyo, Japan.*

A general formula for analyzing the electron diffraction halos by gaseous molecules is presented by taking into account the thermal motion of atoms in molecules. The exact meaning of the quantities obtained by electron diffraction, i.e., the atomic distances and their mean square amplitudes, is discussed based on the thermal vibration of polyatomic molecules.

The atomic distances revealed by electron diffraction depend upon the parallel and perpendicular amplitudes as well as the anharmonicity terms in the potential function. Prof. Bastiansen and his co-workers found the interesting relation that the atomic distances between carbon atoms in molecules such as allene, butatriene, and dimethyldiacetylene were shorter than the sum of the individual bond lengths. It can be shown that these differences are mainly due to the perpendicular displacements of the atom pair. The influence of the anharmonicity factors which have the *first-order effect* on the atomic distances is cancelled out by the procedure of taking the difference stated above.

On the other hand the mean square amplitudes obtained can be compared with the values computed by the use of spectroscopically obtained normal modes because the anharmonicity of the potential function of the molecular field gives only a second-order effect on the mean square amplitudes. The agreement between the observed and the calculated values were found to be good. It suggests that the mean square amplitudes will offer additional information for determining the potential field of the molecule. A few examples are presented along this line.

The paper is to be published in *J. Chem. Phys.* or in *Bull. Chem. Soc. Jap.*

S1·18. The influence of thermal motion on structure determination of linear molecules using the electron-diffraction method. By O. BASTIANSEN & M. TRÆTTEBERG, *Institutt for teoretisk kjemi, Norges tekniske Høgskole, Trondheim, Norway*.

In the study of dimethyldiacetylene it was discovered that the observed non-bonded C–C distances were shorter than that calculated summing up the observed bond distances. Though the effect was small it appeared to be real, and it was attributed to out-of-linearity vibrations. It was found worth while to study this effect in other molecules with linear equilibrium conformation. The effect has been observed in allene and butatriene, and for these molecules quantitative data for the effect were obtained. If the effect is neglected, linear molecules appear bent. The out-of-linearity vibrations will complicate structure determinations of linear molecules using a spectroscopic method based upon measurements of moments of inertia. The average moment of inertia about an axis perpendicular to the molecule will be a trifle smaller than for the presumed stiff model.

The effect might obscure electron-diffraction determination of slightly bent molecules, as these are difficult to distinguish from linear molecules with a large out-of-linearity amplitude of vibration. One case that was supposed to be on the limits of the two alternatives is presented by the molecule of disilylether studied by V. Ewing. It can be shown that this molecule is most likely bent also in the equilibrium conformation.

Likely to be published in *Acta Chem. Scand.*

S1·19. Structure anomalies and molecular vibrations in carbon suboxide. By H. BREED, O. BASTIANSEN & A. ALMENNINGEN, *Institutt for teoretisk kjemi, Norges tekniske Høgskole, Trondheim, Norway*.

The sector method of electron diffraction has been used to reinvestigate the molecular structure of carbon suboxide throughout the range of s from 2 to 65 Å^{-1} (where $s = (4\pi/\lambda)\sin\theta$). Fourier transformation of this data shows the $C=C$ distance well resolved from the $C=O$ distance. The overall length of the molecule, and the distances from first to third, and first to fourth atoms are distinctly less than the sum of the individual component $C=O$ and $C=C$ distances. The effect is reproduceable and more than an order of magnitude larger than the uncertainties in the experiment. In carbon suboxide the effect is larger than that observed in allene, butatriene, and dimethyldiacetylene. Carbon suboxide seems to represent a case where it is difficult to distinguish between a linear molecule with a large out-of-linearity amplitude of vibration, and a molecule with bent equilibrium configuration.

Likely to be published in *J. Chem. Phys.*

S1·20. The effect of temperature on the mean square amplitudes of vibration of PCl₃. By KENNETH HEDBERG & MACHIO IWASAKI, *Department of Chemistry, Oregon State College, Corvallis, Oregon, U.S.A.*

Although one expects an increased temperature to increase the mean square amplitudes of vibration of molecules, the effect is too small to have been evident

from electron diffraction data in the past. Recent improvements in experimental techniques, however, yield accurate intensity data over a much larger scattering angle, and it seemed worthwhile to investigate the effect of temperature anew.

Our data were taken at 27 and 232 °C. in the Norwegian apparatus from gaseous PCl₃, a molecule of well-known structure and thoroughly studied vibrational spectrum, and with atoms of atomic numbers so close as to make the effect of phase shift negligible. The data were reduced in the usual way and radial distribution curves calculated from the resulting intensity curves.

We find PCl₃ to have the same structure, within experimental error, at the two temperatures ($r_{P-Cl} = 2\cdot039$ and $2\cdot044$ Å, and $r_{Cl\cdots Cl} = 3\cdot131$ and $3\cdot138$ Å at 27 and 232 °C., respectively (in good agreement with the corresponding ground state microwave values $2\cdot043$ and $3\cdot134$ Å); however, there is a considerable difference in the root mean square amplitudes of vibration for both the P–Cl and Cl$\cdots$Cl distances: at 27 °C. the preliminary values are respectively 0·050 and 0·081 Å, and at 232 °C. 0·059 and 0·111 Å. These results are in fairly good agreement with prediction from spectroscopic data.

Probable publication: *J. Chem. Phys.*

S1·21. Determination of potential constants for PCl₃ from gaseous electron diffraction data and normal vibration frequencies. By MACHIO IWASAKI & KENNETH HEDBERG, *Department of Chemistry, Oregon State College, Corvallis, Oregon, U.S.A.*

Vibrational potential constants are usually determined from the frequencies of normal vibrations. Most often these are not sufficient to determine constants for a general quadratic potential function, so that either a simplified field must be assumed or data must be obtained for isotropic species.

The recent developments in gas phase electron diffraction techniques have made it possible to determine mean square amplitudes of vibration with high accuracy and it has been shown that these are in generally good agreement with those calculated from assumed potential functions. But it seems especially attractive to combine the mean amplitudes of vibration from electron diffraction with the vibrational frequencies and to attempt to determine potential constants directly.

PCl₃ was chosen for this study because (1) the complicating phase shift is negligible (see preceeding abstract), (2) the geometry is quite favorable, i.e., the chlorine atoms are far enough apart so that steric effects, which might be reflected in distorted radial distribution curve peak shapes, would be small and (3) the four well-known vibrational frequencies and the two mean square amplitudes permit evaluation of the six constants in the general quadratic potential function. The procedure was to calculate the values of the root mean square displacements for each distance with the four fundamental frequencies by methods similar to those described by Morino, Kuchitsu & Shimanouchi (*J. Chem. Phys.* (1952), **20**, 726) or Cyvin (private communication). Contours corresponding to these values were plotted as a function of two convenient potential constant parameters for comparison with the observed values. We find that our preliminary observed values of 0·050 and 0·081 Å for

P–Cl and Cl · · · Cl at 27 °C. lead to imaginary potential constants, but only very small changes which may lie well within the standard errors, are necessary to obtain real potential constants. For example, root mean square displacements of 0·0515 and 0·0812 Å correspond to the reasonable values $f_r = 2\cdot842$, $f_{rr'} = 0\cdot637$, $f_{r\theta} = 0\cdot350$, $f_{r\theta'} = 0\cdot050$, $f_\theta = 0\cdot304$, $f_{\theta\theta'} = 0\cdot047$, all in units of 10^5 dyn.cm.$^{-1}$.

Probable publication: *J. Chem. Phys.*

S1·22. The temperature diffuse scattering of electrons from the surface of a single crystal. By SATIO TAKAGI & MIEKO TAKAGI, *Institute of Physics, College of General Education, University of Tokyo, Komaba, Meguro-ku, Tokyo, Japan.*

The perturbation theory of the temperature diffuse scattering of electrons developed by one of the authors (S. Takagi, *J. Phys. Soc. Japan* (1958), **13**, 278, 287) is applied to the case of reflection from a crystal surface. It is shown that diffuse spots due to temperature scattering appear separately from the spots due to ordinary diffraction, and that strong diffuse spots can be observed when the incident beam satisfies closely the Bragg condition concerning a set of lattice planes and resulting Bragg reflection makes a small angle with the surface. These results are in accordance with the observed features of diffuse spots in the electron diffraction pattern from the surface of single crystals; e.g. zincblende, germanium and diamond.

The intensity of diffuse spots from the surface of diamond crystals is measured. It has previously been confirmed with X-rays that they do not give 'diffraction spikes' which are believed to be due to imperfections. The intensities of the 444- and 555-diffuse spots at the room temperature and at 400 °C. are plotted against the distance ζ in the reciprocal space between the Ewald sphere and the 444- or the 555-points. It is shown that the intensity is inversely proportional to the square of ζ and proportional to T.

The profiles of diffuse spots are also obtained which show that the intensity region due to temperature scattering around the 444-reciprocal lattice point is not spherically symmetrical. Though these experimental results are not fully explained yet, this method may be used for the elucidation of the surface mode of thermal vibration in crystals, since the penetration depth of electrons is very small in the reflection case.

The full-length account will be given in *Acta Cryst.*

S1·23. Studies of lattice dynamics by neutron spectroscopy at Chalk River. By B. N. BROCKHOUSE, W. COCHRAN, A. D. B. WOODS, T. ARASE, G. CAGLIOTI, M. SAKAMOTO & R. N. SINCLAIR, *Atomic Energy of Canada, Chalk River, Ontario, Canada.*

For nearly six years experiments have been underway at Chalk River Laboratories to study atomic motions in crystals (and in liquids) by measurement of energy distributions of scattered neutrons. [See *Phys. Rev.* (1958), **111**, 747]. This abstract outlines work (by various authors in the group) not yet published. An extensive series of measurements has been made on lead single crystals,

in which the frequency/wave vector [$\nu(\mathbf{q})$] dispersion relation has been measured for several directions at temperatures from 100 °K. to 570 °K. [*Bull. Amer. Phys. Soc.* (1960), **5**, 39, 199]. Within the limits of error ($\sim 2\%$) all dispersion curves can be fitted by Fourier series with few terms. The number of terms and their interrelationship indicate that long range forces are involved. The range of the forces seems to decrease on the whole with increasing temperature. At the higher temperatures the neutron groups are notably energy broadened, suggesting that phonons in lead have very short lifetimes. If the full width at half maximum (W) of the broadened neutron group is related to the phonon lifetime (τ) through the uncertainty relation $W\tau = h/2\pi$, the lifetimes near the melting point are found to be roughly equal to the periods of the vibrations!

A phenomenological theory of phonon lifetimes has been constructed by adding to the equations of motion of the Born–von Kármán theory dissipative terms proportional to the relative velocities of the ions. For symmetry directions, [100] and [111], and dissipative forces between first neighbors only, the damping rate constant and therefore the energy width turns out to have the form

$$W = \Gamma\{1 - \cos{(q/q_{\text{max.}})}\},$$

where Γ is proportional to a linear combination of the dissipative constants, depending on the branch and direction. For experimental reasons it is difficult to get accurate widths, but results so far are consistent with the phenomenological theory.

Extensive measurements have been made on the alkali halides, potassium bromide and sodium iodide [*Bull. Amer. Phys. Soc.* (1959), **4**, 246, and *Phys. Rev.* to be published]. For both materials dispersion relations in the symmetric [1, 0, 0], [1, 1, 0], and [1, 1, 1] directions are fitted reasonably well by curves calculated on a simple version of the 'shell' model [see *Proc. Roy. Soc.* (1959), A, **253**, 260] in which the negative ion only is polarizable. Measurements on KBr at 95 °K. verify the well known relation $\nu_{LO}/\nu_{TO} = (\varepsilon_0/\varepsilon_\infty)^{\frac{1}{2}}$ between the longitudinal and transverse optical modes at $\mathbf{q} = 0$, and the low and high frequency dielectric constants. The LO modes of fairly long wavelength are noticeably energy broadened even at 95 °K. Other modes are much less broadened, even at higher temperatures.

The experiments on Pb and KBr were greatly facilitated by apparatus which permits energy distributions to be taken at constant neutron wave vector change, and thus at constant $\mathbf{q}$.

The distribution of optical modes in LiH has been studied by a new method in which neutrons of variable incoming energy are scattered into a beryllium shielded detector sensitive only to neutrons of energy $< 0\cdot005$ e.V. The distribution, which extends from 0·070 e.V. to 0·145 e.V., has a strong maximum at 0·097 e.V. and a weaker maximum at 0·128 e.V.

S1·24. Effect of thermal vibrations on estimation of interatomic distance. By HENRI A. LEVY & W. R. BUSING, *Oak Ridge National Laboratory, Post Office Box X, Oak Ridge, Tennessee, U.S.A.*

Crystal structure parameters refined by least-squares from Bragg diffraction intensities generally define the

centroids of the atomic positions under the perturbing influence of thermal vibrations. The rigorous estimation of interatomic distances from crystal parameters requires knowledge of the joint distribution of pairs of atoms under thermal displacement, knowledge not directly obtainable from Bragg diffraction data. Under suitable assumptions, useful estimations can however be made. A general formalism for the problem will be presented and several special cases discussed with applications.

Probable publication: *Acta Cryst.*

S1·25. Thermal motions in cupric fluoride dihydrate at 298 °K and at 4·2 °K. By S. C. ABRAHAMS,* *Bell Telephone Laboratories, Murray Hill, N.J., U.S.A.*

The 0kl, hk0 and hkh reflections of $CuF_2.2H_2O$ have been measured by the neutron diffraction method, both at room temperature and at liquid helium temperature. These measurements were made using the Single Crystal Automatic Neutron Diffractometer (Prince & S. C. Abrahams, *Rev. Sci. Instrum.* (1959), **30**, 581) and also a new goniometer-mounted cryostat (S. C. Abrahams, *Rev. Sci. Instrum.* (1960), **31**, 174). The hydrogen atom positions were determined by standard means, starting from the 'heavy' atom positions reported by Geller & Bond (*J. Chem. Phys.* (1958), **29**, 925) using X-rays. A least-squares analysis of the complete set of structure factors was made, in which all the (six) positional and (seventeen) thermal parameters were varied, in addition to an overall scale factor. The calculations were performed on an IBM 704 using the Busing & Levy program. The anisotropy in vibrational amplitudes present at room temperature does not disappear at 4·2 °K., nor do these displacements become vanishingly small. In the case of the hydrogen atoms, the motions (ca. 0·25 Å r.m.s.) are virtually identical at the two temperatures.

The bond lengths and angles in $CuF_2.2H_2O$ at 298 °K. and at 4·2 °K. have also been measured, using an extrapolation of Barbieri, Bond & Cooper's (private communication, 1959) precision lattice constants determined at 298, 273, 196 and 80 °K. The Cu–O and one pair of Cu–F distances remain the same at 298 and 4·2 °K.: the O–H distance is significantly shortened and the H–O–H angle decreased at the lower temperature. Another significant change is the reduction in the long Cu–F octahedral contact.

The structure of the antiferromagnetic electron array has also been determined. The 'magnetic' electron at the origin is antiparallel to that at the body center, and both are approximately parallel to the c-axis direction.

This paper will probably be submitted to *Acta Cryst.*

S1·26. Neutron scattering investigation on a few metal hydrides. By J. BERGSMA, *Instituut for Atomenergi, Kjeller, Norway.*

A study of the dynamical behaviour of hydrogen atoms in a number of metal lattices has been made using neutron diffraction techniques for elastic and inelastic scattering.

* Guest Scientist, Brookhaven National Laboratory, Upton, N.Y.

Due to the favourable energy momentum relation the phonons of atomic oscillators are comparable in size to the energy of thermal neutrons.

Single crystal neutron diffraction data obtained from two zones of $PdH_{0·63}$ confirm the occupation of the octahedral positions in the palladium lattice by the hydrogen atoms as has been reported by Worsham *et al.* (*J. Phys. Chem. Solids* (1957), **3**, 303).

The vibrational amplitudes derived from the decrease of this coherent scattering intensity could be correlated with inelastic scattering experiments.

Fermi gave a derivation of the neutron cross section of hydrogen chemically bound as a harmonic oscillator. Basically this function shows a number of sharp dips at energies equal to multiples of the fundamental vibrational energy quantum. The cross section variation was measured by means of a crystal spectrometer, the results of which were found to be in substantial agreement with the decrease in the Bragg scattering.

Using the cold neutron scattering technique, the exchange of energy with the lattice vibrations gave more direct information concerning the acoustical and optical vibration branches. The results from these inelastic scattering measurements and the elastic diffraction data could be correlated with the activation energy for diffusion of hydrogen in palladium. The various data may be collected in a diagram showing the potential energy of the proton as it is displaced in the [111]-direction and are in good agreement with each other.

A Debye temperature obtained from the mean square displacement of the palladium atoms and compared with the interaction of the cold neutrons with the acoustic branch turns out to be lower than the one for pure metal, which suggests a somewhat weaker binding between the palladium atoms.

Besides the experiments on palladium hydride work has been done on copper hydride and the hydride of the intermetallic alloy $AlTh_2$. The hydrogen atoms in these systems occupy the centres of tetrahedra, formed by the metal atoms.

The paper is likely to be published in *J. Phys. Chem. Solids.*

S1·27. Determination of Debye-Waller factors in Li H by X-ray and neutron scattering. By R. S. CALDER & W. COCHRAN, *Cryst. Lab., Cavendish Laboratory, Cambridge, England* and D. GRIFFITHS & R. D. LOWDE, *Atomic Energy Research Establishment, Harwell, England.*

The values of B_H and B_{Li} in the expression

$$f = f_0 \exp(-B \sin^2 \theta / \lambda^2)$$

have been determined by two independent methods in each case. B_L was obtained by X-ray diffraction and neutron diffraction using single crystals, B_H by the latter method and also by measuring the intensity of neutrons scattered *incoherently* from powdered material. The results are in good agreement with one another, and support earlier conclusions about the electron distribution in LiH. (*Rev. Mod. Phys.* (1958), **30**, 47.) At room temperature $B_{Li} = 1·0_0$ Å^2, $B_H = 1·8_5$ Å^2.

S1·28. On the zero point vibrations in crystals and their relation to diffraction experiments. By I. WALLER, *Institutionen för teoretisk fysik, Uppsala, Sweden.*

An analysis will be given of the influence of the zero point vibrations in crystals for those cases where these vibrations are of essential importance. The accuracy of the approximations which have been used in calculating the zero point vibrational amplitudes and energies will be discussed and also the importance of the anharmonicity of the residual vibrations at low temperatures. The possibilities to get further insight into the zero point vibrations by crystal diffraction experiments will be discussed in some detail.

S1·29. Nullpunktunruhe und Fluktuationsterm. Von R. HOSEMANN, *Fritz-Haber-Institut der Max-Planck-Gesellschaft, Berlin-Dahlem, Deutschland.*

Die quantitative und direkte Auswertung der Röntgeninterferenzen von Kristallen liefern nicht nur Informationen über die mittlere Elektronendichteverteilung in einem Atom, sondern auch über die statistische Schwankung der Dichteverteilung um diesen Mittelwert. Die Auswertung der Röntgeninterferenzen von Kochsalz (Messung von Schoknecht & Renninger) mittels Faltungsintegralen und Gauss-Analyse beweisen, dass die Dichteverteilungen nicht starr mit dem Schwerpunkt der Ionen mitschwingen. Der Fluktuationsterm wirkt sich im diffusen Untergrund aus und gibt die Erklärung für die von Harvey 1933 bei Sylvin gefundenen Anomalien. Berücksichtigt man diese Fluktuation, so ist es nicht mehr nötig aptierte Temperaturfaktoren einzuführen. Die direkte Auswertung der Röntgeninterferenzen an Diamant (Messungen von Brill bei 290 °K.) mittels Faltungsintegralen und Gauss-Analyse beweist die Existenz der Nullpunktunruhe mit einer Genauigkeit von wenigen Prozent. Die äusseren Schalenelektronen sind allerdings auch hier durch die Nachbaratome beeinflusst. Es wird der Schluss gezogen, dass der Fluktuationsterm so lange vernachlässigbar ist, als die Temperatur genügend weit unterhalb der charakteristischen Temperatur liegt. [R. Hosemann u. G. Schoknecht, *Z. Nat. Forsch.* **12a**, 932 (1957). G. Schoknecht, *Z. Nat. Forsch.* **12a**, 983 (1957). R. Hosemann u. G. Voigtlaender-Tetzner, *Z. Elektrochem.* **63**, 902 (1959)].

Ausführliche Veröffentlichung ist vorgesehen in *Z. Elektrochem.*

S1·30. Thermal motion in crystals and molecules as revealed by nuclear magnetic resonance. By E. R. ANDREW, *Department of Physics, University College of North Wales, Bangor, Caernarvonshire, Wales.*

Thermal motions in crystals generally reduce the static magnetic dipolar interaction between the atomic nuclei, and as a consequence the observed nuclear magnetic resonance spectrum is narrower than it would be if the motion were absent. There is a marked reduction in spectral width only if the nuclear displacements are comparable with the inter-molecular spacing. Vibration about fixed sites therefore produces only small effects. On the other hand the method readily reveals the rotation of molecules, molecular ions and groups (whether free or hindered), the rotational oscillation of molecules, and the diffusion of molecules and ions. The method is sensitive since rates of 10^4 c./s. generally suffice to cause spectral narrowing. Unlike the dielectric method the nuclear magnetic resonance method can be applied not only to polar but also to non-polar molecules which are often of interest since, having greater symmetry, they are usually more mobile.

Although the method can be applied to any nucleus having a magnetic moment, most work has concerned protons. Examples will be given of applications to motion in ionic and molecular crystals, metals and polymers. A quantitative examination of the spectrum enables the nature of the motion to be determined. Furthermore a study of the nuclear spin lattice relaxation time frequently yields the rate of motion; from its temperature dependence an activation energy can, in suitable cases, be determined. Some of the effects can be readily demonstrated by the macroscopic rotation of crystals.

S1·31. Molecular motion in some simple amides. By J. W. EMSLEY & J. A. S. SMITH, *School of Chemistry, The University, Leeds, 2, England.*

The proton magnetic resonance spectra of single crystals of urea, thiourea, and formamide have been recorded over a range of temperature. From a careful study of the angular dependence of the spectra, it is shown that the changes observed in thiourea between 220 to 260 °K. and urea between 300 to 370 °K. are produced by essentially the same type of molecular motion, despite the differences in crystal structure. Both molecules undergo hindered rotation about the C=O (or C=S) bond, that is the molecule flips between the two planar, or near-planar, equilibrium configurations related by the mirror plane perpendicular to the plane of the heavy atoms and passing through the carbon and oxygen (or sulphur) atoms. The energy barriers hindering reorientation are approximately 9 Kcal./mole for urea and 4 Kcal./mole for thiourea, possibly indicating differences in the strength of hydrogen bonding between the two crystals. The existence of this motion is in agreement with the large X-ray temperature factors of the nitrogen atoms in a direction perpendicular to the molecular plane. In contrast to the results of other investigators, the spectra of formamide are found to undergo no significant change from 138 °K. up to the melting-point; there are no changes that can be attributed to reorientation of the NH_2 group about the C–N bond in agreement with recent high-resolution studies of the liquid.

To be submitted for publication in *Trans. Faraday Soc.*

S1·32. Calcul des constantes élastiques par la méthode de la déformation homogène. Par Y. LE CORRE, *Collège de France, Paris, France.*

Contrairement à l'avis de M. Born & K. Huang, on montre qu'il est possible de calculer les constantes élastiques d'un cristal par la méthode de la déformation homogène. Il est important pour y parvenir de dénombrer les variables indépendantes.

Le résultat est le même que celui qui est obtenu par la méthode des ondes longues.

Si on suppose que l'énergie de cohésion du cristal libre ne dépend que des distances relatives des noyaux (condition qui permet de retrouver la théorie classique de l'élasticité), on trouve que l'invariance par rotation rigide donne certaines relations dans les interactions entre proches voisins; exemple, pour les cristaux du type diamant:

73*

Matrice d'interaction entre premiers voisins:

$$\begin{pmatrix} a & b & b \\ b & a & b \\ b & b & a \end{pmatrix}.$$

Matrice d'interaction entre deuxièmes voisins:

$$\begin{pmatrix} c & d & d \\ -d & e & f \\ -d & f & e \end{pmatrix}.$$

On trouve la relation:

$$d = f - c - e + \tfrac{1}{4}(b - a) + \ldots .$$

En particulier, dans l'approximation dite des 'premiers voisins',

$$d = \tfrac{1}{4}(b - a) .$$

Il est, en effet, nécessaire de tenir compte des variations distances entre deuxièmes voisins pour transcrire l'écartement des liaisons tétraédriques.

Doit être publié dans *J. Phys. Radium*.

S1·33. Thermal motion in cubic metal crystals. By T. Ll. RICHARDS, *College of Advanced Technology, Birmingham, England.*

It can be shown that for cubic metal crystals the major part (in many cases nearly the whole) of the elastic energy associated with an externally applied stress corresponds to the energy of the mean longitudinal displacement of the atoms in the direction of the stress. When the applied stress is near a $\langle 100 \rangle$ direction practically all the energy is associated with the displacement along $\langle 100 \rangle$. This may signify that elastic distortion of metal crystals occurs in domains analogous to those of magnetism.

The elastic moduli of crystals are proportional to the net attractive forces between atoms, and, since also at room temperature nearly all the heat energy is due to the thermal motion of the atoms then it is possible to equate the energy $J\,h\,T$ associated with a small temperature rise T to the work done against the attractive forces given by $C_{11}\,T2(S_{11} + S_{12})/S_{11}$ where the constants have the usual significance. This leads to a relation for J which is similar to that of Gruneisen except that C_{11} is used in place of the compressibility modulus. Using the new relation, values of J derived for nine cubic metals, for which all the necessary data are available, are as follows:

Mechanical equivalent of heat J ($\times 10^7$ ergs./cal.)

Copper	Aluminium	Iron	Gold	Lead
4·06	5·67	4·10	4·32	4·38

Molybdenum	Nickel	Silver	Tungsten
5·55	4·25	4·40	5·00

The agreement with the standard value (4·18) is reasonable for six of the metals but appreciably in error for the remaining three. These latter are known to be different from the others in their degree of elastic anisotropy.

The general agreement of the new relation may be of significance in connection with the theory of metallic cohesion and an attempt is made in another contribution

to extend the concept and thereby predict the ultimate strength of metals.

To be published in *Acta Metallurg.*

S1·34. Comparison of the Debye temperatures of some cubic crystals measured by different experimental methods. By F. H. HERBSTEIN, *National Physical Research Laboratory, South African Council for Scientific and Industrial Research, Pretoria, South Africa.*

A number of different experimental methods are used for determining the Debye temperatures of cubic crystals. These include the derivation of Θ from specific heats, thermal entropies, thermal-expansion coefficients, elastic constants and neutron, X-ray or electron-diffraction measurements at a single temperature or over a range of temperatures. Comparison of Debye temperatures determined by different experimental methods is complicated by theoretical differences due to the different methods of averaging over longitudinal and transverse vibrational modes, and by the differing contributions of various regions of the frequency spectrum to the quantity measured experimentally.

A survey of available results shows that, in general, the various values of Θ for cubic metals and alloys at 300 °K. do not differ by more than 5–10%. It seems likely that some larger discrepancies reported between X-ray values, on the one hand, and specific-heat or elastic-constant values of Θ on the other, are due to experimental errors in the application of the X-ray methods. Accurate values of Θ (X-ray) at 300 °K. are available for Cu, Ag, Al, Pb, and α-Fe and these are all slightly lower than the elastic-constant values. X-ray measurements at very low temperatures are not available for direct comparison with elastic-constant or specific-heat values, which have recently been shown to be in excellent agreement in the vicinity of 0 °K. (G. A. Alers & J. R. Neighbours, *Rev. Mod. Phys.* (1959), **31**, 675). However extrapolation of the meagre results published does suggest that Θ (X-ray) may also be systematically lower than the other values at very low temperatures. At high temperatures the variation of Θ_M with T is in reasonable agreement with the Zener–Bilinsky–Paskin theory of the volume-dependence of Θ_M for some crystals (e.g. Ag) but not for others (e.g. Al, Pb).

This material will probably be submitted for publication to *Rev. Mod. Phys.*

Symposium 2: Lattice defects and the mechanical properties of solids

S2·1. Introductory lecture. Lattice defects and the mechanical properties of solids. By N. F. MOTT, *Cavendish Laboratory, Cambridge, England.*

The mechanical properties of crystalline solids are determined by the distribution and properties of crystal defects such as dislocations, vacancies, etc. In recent years experimental methods have been developed for direct observation of dislocations, stacking faults, small precipitates and clusters of point defects. The theory of dislocations has now a firm experimental foundation, and many of the predicted properties of these defects

have been confirmed. Whereas previously phenomena such as work-hardening had to be interpreted assuming what appeared to be likely distributions of dislocations, direct correlation is now possible between the particular mechanical property of interest and the actual observed distributions. However, although the arrangement of defects may be known, there still remain the difficult problem of quantitative interpretation of bulk properties in terms of the complex structures observed and also the processes by which these structures are formed. Recent advances made in this field will be reviewed and some of the outstanding problems indicated.

S2·2. The yield strengths of crystals. By JOHN J. GILMAN, General Electric Research Laboratory Schenectady, N.Y., U.S.A.

Direct experimental measurements now provide abundant evidence that the stress required for plastic flow in crystals is primarily determined by the mobility of screw dislocations. The sharp dependence of this mobility on the applied stress is what causes plastic 'yielding' in a narrow range of stress. Since dislocations multiply in number as they move through a crystal, the yielding process is further sharpened, and becomes catastrophic under some conditions. Many factors influence dislocation mobilities and thereby change the yield stress of a crystal. Some of these are: dislocation type, glide plane, elastic modulus, temperature, impurities, radiation damage, and strain-hardening. These effects have not only been measured in ionic crystals (LiF), but also in metal crystals (iron–silicon).

S2·3. The deformation of germanium. By R. L. BELL & W. BONFIELD, Metallurgy Dept., Royal School of Mines, London, S.W. 7, England.

Germanium single crystals oriented for single slip were deformed in tension at 570 °C. A large yield-point drop was observed both in materials that had been doped with indium or gallium impurity, and in the purest (50 ohm.cm.) material. The restoration of the yield point by annealing did not occur unless the treatment were sufficient to reduce the dislocation density to values approaching that in the starting material. From studies of the postyield flow stress and its variation with strain rate, it is concluded that the major portion of the yield drop is associated with the velocity-stress dependence of the dislocations.

S2·4. Effects of doped impurities on the strength of germanium crystals. By TAIRA SUZUKI, The Institute for Solid State Physics, Tokyo University, Tokyo and HIDEO KAYANO & JIRO WATANABE, The Research Institute for Iron, Steel and Other Metals, Tohoku University, Sendai, Japan.

Effects of doped impurities of both n- and p-types on fracture strength and plastic yield stress of germanium crystals grown from the melt were examined by bending tests in a controlled atmosphere. The concentration of doped impurities ranged from 10^{13} to 5×10^{19} cm.$^{-3}$. Dislocations were found to be of the order of 10^4 cm.$^{-2}$ for each sample. Increasing concentration of impurities decreased the fracture stress from 40 to 8 kg.mm.$^{-2}$ and

also shifted the brittle-ductile transition point from 380 to about 400 °C.

Upper yield stress for plastic flow could be expressed as $\sigma_u = \Delta\sigma + \sigma_f$, where $\Delta\sigma$ is the difference between upper and lower yield stresses and σ_f is the lower yield or flow stress. $\Delta\sigma$ tends to disappear with the increase of doped impurity for the case of phosphorus owing to a rapid increasing rate of σ_f overwhelming that of σ_u. In this case, $\Delta\sigma = 0$ occurs at about 10^{19} cm.$^{-3}$, above which the yield stress increases in a different manner probably by precipitation hardening. In general, however, the temperature dependence of σ_f was found to be similar to silicon crystals measured by Pearson et al., whereas the variation of σ_u with temperature was slightly slower.

It is quite important to remark that p-type samples loose the feature of characteristic yielding and it becomes $\sigma_u = \sigma_f$ above 600 °C., while n-type crystals persist the feature even at 800 °C. The pinning energies thus estimated are 1·4 e.V. for p-type and 1·8 e.V. for n-type. These are certainly based on an electronic origin. Any positive evidence of the nucleation of dislocations in a perfect region of the lattice responsible for plastic yielding was not found here.

To be published in J. Phys. Soc., Japan.

S2·5. The temperature dependence of the yield stress of NaCl crystals. By C. W. A. NEWEY & P. L. PRATT, Department of Metallurgy, Imperial College, Kensington, London, S.W. 7, England.

The yield stress of single crystals of NaCl, of high purity and also containing known concentrations of Cd^{++} and Ca^{++}, has been measured in compression over the temperature range -196 to 550 °C. After annealing at 650 °C. and slowly cooling, the yield stress of the pure crystals was found to decrease rapidly as the temperature was increased from -196 to 0 °C., (450 g.mm.$^{-2}$ to 60 g.mm.^{2}), and then more gradually at higher temperatures. A 0·1 proof stress varied in a similar way except that a wide peak occurred between 200 and 400 °C. Crystals containing 0·05 at.% Cd^{++} were translucent after a slow cool from 650 °C., and electrolytic conductivity and density measurements showed that some of the Cd^{++} was in precipitate form. These crystals had increased yield stresses at all testing temperatures, (e.g. 750 g.mm.$^{-2}$ at room temperature), and a maximum of 1300 g.mm.$^{-2}$ was observed at 265 °C. After an air-cool from 300 °C., the crystals were transparent and their yield stress was increased further, by about 500 g.mm.$^{-2}$, at temperatures below 300 °C.; a maximum of 1700 g.mm.$^{-2}$ occurred at 240 °C. A similar addition of Ca^{++} produced no obvious precipitation; the room temperature yield stress of both slowly-cooled and air-cooled crystals was about 4000 g.mm.$^{-2}$ and a peak at higher temperatures was not observed.

Possible Journal: Phil. Mag.

S2·6. Introductory lecture. Work-hardening, from the point of view of the long range stresses-theory. By A. SEEGER, Max-Planck-Institut für Metallforschung, Stuttgart, Deutschland.

The basic explanation of the three stages of the work-hardening curve of f.c.c. single crystals and of the work-

hardening and recovery characteristics of hexagonal metal single crystals such as Zn or Cd will be reviewed. Quantitative formulations of the theory which account well for the experimental facts are now available for the work-hardening of hexagonal metals at low temperatures, for the work-hardening in the easy glide region and in stage II of the stress strain curve of f.c.c. crystals, and for the beginning of stage III. The striking differences in the work-hardening rates in the hexagonal metals and in the easy glide region on one hand and in stage II on the other hand are attributed to different ways in which gliding dislocations feel the stress-fields of piled up dislocation groups. Roughly speaking, in stage II a piled-up group acts as a giant dislocation, whereas in stage I the stress fields of the dislocations in a piled-up group (which are separated by rather large distances) have to be considered individually. The irreversible temperature dependence of work-hardening is either due to climbing of dislocations (hexagonal metals, and f.c.c. metals at high temperatures) or to cross slip of screw dislocations (f.c.c. metals at low or moderate temperatures). The relation of these 'primary' processes of glide, work-hardening and softening to the 'secondary' features like kink-bands, bands of secondary slip and development of a cell structure will be briefly discussed.

Recent evidence supporting this picture will be presented: (1) Measurements of the temperature variation of the flow-stress as a function of strain, showing that in stage I and II of f.c.c. metals the Cottrell–Stokes law is not valid. The variation is such as to correspond with the theory. (2) Detailed electronmicroscopic studies of slip lines showing that the same sizes of piled-up groups are obtained from cross slip data and from slip line heights. (3) Measurements of the approach to saturation in ferromagnetic metals and alloys which give directly the long range stress-fields of the dislocations without any uncertainties due to the averaging procedure. They confirm quantitatively the description of stage I and II given above. (4) A calculation of the fractional stored energy, giving 7–8% in stage II. This seems to agree with the existing experimental data, if they are taken at sufficiently small strains.

S2·7. Invited paper. Flow stress and workhardening of face-centred cubic metals. By P. B. HIRSCH, Crystallographic Laboratory, Cavendish Laboratory, Cambridge, England.

Recent results on the strain rate and temperature dependence of the flow stress have led to a reinterpretation of the flow stress. The forest intersection mechanism and the role of jogs are discussed and a model of the flow stress proposed, based on these considerations.

Transmission electron micrographs of single crystals of Cu deformed at room temperature show that the dislocations are arranged in dense irregular networks; pile-ups are not observed. A theory of work-hardening is proposed which accounts for the observed work-hardening rate without involving the presence of long range elastic stresses.

Paper to be published in *Phil. Mag.*

S2·8. Observations of dislocation distributions as a function of strain in single crystals of various f.c.c. metals and alloys of different stacking fault energy. By A. HOWIE, Cavendish Laboratory, University of Cambridge, England.

Single crystals in the form of long strips 0·02″ in thickness were prepared (by strain anneal methods in the case of Al and by cooling from the melt in the case of Cu and some CuAl alloys in the solid solution range). The crystals were then strained to various points on the stress strain curve and the resulting dislocation distribution examined by the transmission electron microscopy technique.

In the easy glide region most of the dislocations were found to lie on the principal slip plane and few interactions were observed. No signs of piled up groups of dislocations were found in aluminium or copper.

In stage II in copper an increasing number of interactions were seen leading to the formation of a ragged dislocation network with a rough cell structure. The cell structure was less clearly defined in the CuAl alloys of stacking fault energy $\gamma \simeq 20$ ergs/cm.[2]. Piled up groups of dislocations were not observed in either the pure copper or in this alloy but they were seen in an alloy of very low stacking fault energy $\gamma \simeq 3$ ergs/cm.[2].

In stage III of the stress strain curve the cell structure observed in Al and Cu became increasingly well defined. The cell walls in Al were very sharp. In the alloy with $\gamma \simeq 20$ ergs/cm.[2] a more uniform extremely dense dislocation distribution with regions of heavy misorientation was seen. Observations of the low stacking fault energy alloy and also of one with a stacking fault energy $\gamma \simeq 10$ ergs/cm.[2] are in progress.

Paper will probably be published in *Phil. Mag.*

S2·9. Deformation of close packed metals at low temperatures. By Z. S. BASINSKI, Division of Pure Physics, National Research Council, Ottawa, Canada.

The results of measurements of strain rate dependence of the flow stress in close packed metals at sub atmospheric temperatures will be presented. Special emphasis will be laid on the causes of deviations from the Cottrell–Stokes Law. Correlation will be made between the results from tensile tests and electron microscope observations.

S2·10. Flow stress measurements in metals and alloys. By J. W. CHRISTIAN, B. C. MASTERS, A. MITCHELL & F. W. J. PARGETER, Department of Metallurgy, Oxford, England.

Reversible changes of flow stress with temperature and strain rate have been measured in single and polycrystalline specimens of the hexagonal metals cadmium and cobalt, the b.c.c. metals niobium and vanadium, and the f.c.c. α-phase copper–aluminium alloys. For the pure metals, two general types of behaviour may be distinguished:

(1) Cottrell–Stokes law. Here the change in stress $\Delta\sigma$ produced by a given temperature or strain rate change is proportional to the stress level σ at which the change is made. The constancy of the Cottrell–Stokes ratio is one starting point for the current 'forest theory' of work

hardening in f.c.c. metals. In the hexagonal metals in which the basal plane is the usual slip plane, the law is found to be valid for polycrystalline specimens, but for single crystals it only applies after extensive twinning. The Cottrell–Stokes law does not apply to the copper–aluminium alloys of low stacking fault energy.

(2) Change of stress independent of stress. Here $\Delta\sigma$ is a constant for any given change, irrespective of the stage in the stress-strain curve at which the change is made. This implies that the density of obstacles which dislocations overcome with the aid of thermal agitation does not increase with strain. The change in stress is approximately constant in the easy glide region of single crystal stress-strain curves, and in the basal slip deformation of hexagonal single crystals. This law is also valid for b.c.c. metals in polycrystalline form, and for iron it has been interpreted in terms of the Peierls–Nabarro force. The applicability of this interpretation to other b.c.c. metals will be considered.

The flow stress measurements have been supplemented by metallographic and X-ray investigations. The results include observations on mechanical twinning in copper–aluminium alloys, the temperature and strain rate dependence of the transition from linear to parabolic hardening in these alloys, and the effects of zone purification of the b.c.c. metals.

This work may be submitted to *Phil. Mag.* or *Acta Met.* when complete.

S2·11. Interaction of dislocations and creation of point defects in workhardening. By G. SAADA, *Faculté des Sciences d'Orsay (Groupe II), Service de Physique des Solides, B.P. N° 11, Orsay (Seine et Oise), France.*

The elastic interactions of a gliding dislocation with a 'forest' due to a three dimensional network of dislocations are studied in some detail. The parts of the hardening which depend or not on temperature are shown to be mainly related to the crossing of repulsive or attractive trees respectively. A mechanism for creating point defects after crossing attractive trees is described. Average numerical values are given, in the FCC structure, for the hardening and the rate of creating point defects. They are compared with known observations.

S2·12. The strength of attractive dislocation intersections in metals. By J. D. BAIRD & B. GALE, *National Physical Laboratory, Teddington, Middlesex, England.*

Dislocations of certain Burgers vectors combine when they intersect to form a length of a new junction dislocation. During cold work these intersections must be made and broken. The stress required to reach the breakaway configuration is derived by following the movement of the equilibrium positions of the nodes as the dislocations bow out under stress. The main variables are the dislocation spacing R, the angles of intersection of the dislocations, the type of junction dislocation formed, and the applied stress system. The general equation is solved for a number of different combinations of these variables to give an estimate of the flow stress due to this type of barrier.

In f.c.c. metals most attractive junctions are found to break down by inward movement of the nodes at shear stresses in the range 0 to $2Gb/R$. This includes the cases where the junction dislocations are Lomer–Cottrell sessiles, so that in practice almost all long Lomer–Cottrell barriers will collapse in this way at quite small stresses. The mean flow stresses are estimated to be about Gb/R for f.c.c. and $Gb/2R$ for b.c.c. metals, where R is approximately the maximum spacing of dislocations which give intersections of this type. These figures lead to reasonable estimates for the total flow stresses.

Calculations of the positions of the nodes at junctions as a function of the applied stress show that in some cases the maximum stress is reached before the nodes coincide (the breakaway point). In some of these cases the intersection jog energy will be supplied automatically so that intersection will not be temperature sensitive.

Only in very rare cases does a loop bow out to a semicircle before it breaks free, so that Frank–Read sources are infrequent.

Probable publication: *Acta Metallurg.*

S2·13. The dislocation distribution, flow stress and stored energy in cold-worked polycrystalline silver. By J. E. BAILEY & P. B. HIRSCH, *Cavendish Laboratory, Cambridge, England.*

Distribution and densities of dislocations, determined by electron transmission microscopy, flow stress and stored energy measurements (by microcalorimetry) on cold worked polycrystalline silver are correlated with each other. The dislocations are arranged in dense networks forming the boundaries of an otherwise relatively dislocation free cell structure. The flow stress is explained quantitatively in terms of the forest intersection mechanism at the boundaries. The stored energy after recovery is of the same order as the total self energy of the dislocation arrangement, so that the long range stresses must be largely relaxed. The considerable energy release during the recovery stage produces no observable change in dislocation distribution. This recovery stage is thought to be due to the relief of long range stresses or to the removal of point defects.

While the values of flow stress and stored energy can be accounted for in terms of the observed non-uniform distribution of dislocations (cell structure), they are not compatible with each other on a model based on a uniform distribution of pile-ups; nor are pile-ups observed on the electron micrographs.

To be published in *Phil. Mag.*

S2·14. The theoretical strength of metals. By T. LL. RICHARDS, *College of Advanced Technology, Birmingham, England.*

So far all theories of the strength of metals have yielded values many times greater than those actually observed, and as M. Born & R. Fürth (*Proc. Camb. Phil. Soc.* (1940), **36**, (4), 454) suggested this is probably because the effect of thermal motion of the atoms has been neglected. In an analysis (T. Ll. Richards, *Rheologica Acta* (in the press)) of the tensile deformation of copper strip in cube-texture orientation the author has shown

that yielding is determined by a shear energy criterion. In common with other theories, the total elastic energy of the specimens at maximum loading was only about 1/700th of the stacking fault energy. If it is assumed, however, that stress fields associated with stacking faults are triggered-off by thermal waves then an estimate can be made of the real technical strength of metals.

Two approaches are possible, one from the energy of thermal waves and the other by consideration of the dynamics of atom movement from one lattice site to another. As indicated below, both approaches yield reasonably accurate results in some cases. The possible significance of the relatively high theoretical strength of aluminium and lead will be discussed.

Ultimate tensile strength (t./sq.in.)	Observed	Theoretical	Wave energy approach	Atom dynamics approach
Aluminium	3·8	7·6	7·23	—
Nickel	20·5	27·7	18·2	—
Copper	14·0	14·0	14·0*	—
Silver	9·0	7·5	8·4	—
Gold	7·9	5·9	7·16	—
Lead	1·28	1·56	4·12	—

* This value fitted for copper to derive the strengths of the other metals by the atom dynamics approach.

To be published in *Acta Metallurg.*

S2·15. Cross-slip, work-hardening, and the ductility of ionic crystals. By P. L. PRATT, *Dept. of Metallurgy, Imperial College, London, England.*

Ionic crystals normally slip on (110) in [1$\bar{1}$0]. In addition there is experimental evidence for slip on (100) in [1$\bar{1}$0] at room temperature, and theoretical arguments suggest that this is a more difficult process than the normal (110) slip. Cross-slip on (100) planes however is an important feature of the deformation of ionic crystals since it provides a mechanism for the broadening of glide bands observed by etch pit studies. From the temperature dependence of the flow stress for slip on (100), and the shape of crossing screw dislocations, estimates are made of the degree of broadening at different temperatures. In addition, cross-slip is the easiest way in which dislocations can by-pass barriers in the lattice. The relation between the onset of wavy slip in ionic crystals with increase of temperature, and the simultaneous reduction in the rate of work-hardening and the enhancement of ductility, is discussed in some detail.

To be published in *J. Appl. Phys.*

S2·16. Creep of sodium chloride. By C. E. SILVERSTONE & P. L. PRATT, *Dept. of Metallurgy, Imperial College, London S.W. 7, England.*

The creep behaviour of relatively pure and of cadmium doped NaCl has been measured in compression at applied stresses between 150–1500 g.mm.$^{-2}$ in the range -196 to 400 °C. The logarithmic law of creep is obeyed by the relatively pure material at all temperatures and stresses within these ranges. The creep strain occurring between one and ten minutes after the application of the full load, a, varies anomalously with temperature. After increasing linearly from -196 to -80 °C., a sharply decreases, and

from -40 °C. to a critical temperature, dependent on the applied stress, it remains constant at about five times less than at -80 °C. At temperatures above the critical value, a increases very rapidly.

The cadmium doped material creeps in a similar way to the purer NaCl except at temperatures higher than 200 °C., where linear creep predominates.

To be published in *Phil. Mag.*

S2·17. The effects of surface coatings on the mechanical properties of lithium fluoride crystals. By A. R. C. WESTWOOD, *Research Institute for Advanced Studies, Baltimore* 12, *Maryland, U.S.A.*

A study has been made of the mechanical behavior of coated and uncoated lithium fluoride crystals. Coatings were produced by vacuum-deposition, by chemical reaction with pure magnesium oxide powder at 600–700 °C. and by adsorption from solution.

Extremely thin vacuum-deposited coatings of chromium increased the yield stress by some ten percent but had no significant effect on the critical resolved shear stress. 'Thin' reacted-coatings ($\ngtr$ 10μ thick) increased the yield stress of as-cleaved crystals by more than fifty percent but had little effect on the yield stress of previously chemically-polished specimens. Thinly coated as-cleaved specimens also exhibited a 'catastrophic' stress-drop at the critical resolved shear stress and the subsequent rate of work-hardening was less than that of uncoated as-cleaved crystals. Thicker reacted coatings ($\ngtr$ 50μ thick) increased both the yield stress and the critical resolved shear stress by sixty percent but stress drops were not observed. However, the stress and strain to fracture was reduced to half that of uncoated crystals. Failure occurred by the formation of Stroh-type cracks at intersecting bands of edge dislocations.

The adsorption of stearic acid molecules from a hexadecane solution resulted in large decreases in mechanical properties with maximum effects (up to sixty percent) occurring at concentrations of order 10^{-4}.N. At higher concentrations positive effects were observed.

An explanation of these and other results will be offered based on considerations of the effects of surface films, cleaving and chemical polishing on the distribution and operation of dislocation sources, possible mechanisms of work-hardening in lithium fluoride and the piling-up of dislocations at intersecting slip bands and beneath surface films. Metallographic evidence for such pile-ups will be presented.

A note entitled 'Evidence for the piling-up of dislocations beneath a surface film' has been submitted to *Nature*. A full-length account of this work will be submitted to *Trans. A.I.M.E.*

S2·18. Précipitation du cuivre dans le silicium; microdureté du germanium. Par BERNARD, BERTH, BURGEAT, DEVAUX, Mme SOULA & TSOUCARIS, *Centre National d'Etudes des Telecommunications, Issy-les-Moulineaux, Seine, France.*

Le cuivre introduit dans les monocristaux de silicium par diffusion à haute température forme des précipités

que l'on a observés par microscopie infrarouge et par microscopie électronique; ces précipités présentent des aspects différents selon les conditions expérimentales: vitesse de refroidissement, présence ou absence de dislocations naturelles ou introduites par déformation plastique. Ces precipités peuvent conduire à un marquage très fin des dislocations, comme W. C. Dash l'avait réalisé, ou indépendamment des dislocations, atteindre une taille considérable (200 microns); dans ce cas on montre que les précipités sont formés de 12 lamelles issues d'un centre de nucléation et parallèles aux directions 110 du réseau de silicium. On a examiné l'influence de ces propriétés sur les diagrammes de rayons X (pouvoir réflecteur et domaine angulaire de réflexion).

On a étudié d'autre part la microdureté du germanium: on a montré qu'à température ambiante et jusqu'à 160 °C. la microdureté est indépendante de la température, de l'orientation de la face étudiée (100, $\bar{1}$10 ou 111), de la densité des dislocations et de la concentration des impuretés substitutionnelles. Au contraire, des essais de microdureté à chaud (250, 350 et 450 °C.) ont montré que l'impact produit un réseau de dislocations dont la densité décroit en fonction de la distance du point d'impact; on discute l'interprétation théorique de ces résultats.

S2·19. Decomposition of dislocations in body-centered iron. By C. CRUSSARD, IRSID, 185, rue Président Roosevelt, Saint Germain en Laye (S. et O.), France.

Possible models of decomposition of dislocations in α iron are examined, in (110), (112) or other planes. Some rules are presented in order to select the probable mechanism between the many possible stacking faults. Influence on mechanical properties is studied, and compared with observed facts.

Full text likely to be published in C. R. Acad. Sci., Paris.

S2·20. Work-hardening and recovery in iron. By K. F. HALE & D. McLEAN, National Physical Laboratory, Teddington, Middlesex, England.

The arrangements of the dislocations had been studied in iron in various conditions, namely annealed, coldworked, recovered and after creep by thin foil electron microscopy. In all conditions the dislocation network is characterized by attractive intersections where two dislocations join to make one dislocation.

Cold-worked specimens have been examined after various strains between 3% and 85% and it was seen that the dislocation density increased and a cell structure made up of dislocations developed with increasing strain. A mechanism of dislocation multiplication is proposed. Observations on the dislocations in the cell interior have been correlated with experimental determinations of the flow stress. Agreement over a range of strains between a simple theory of the effect of attractive junctions on the flow stress and the observed flow stress lend support to the idea that attractive junctions are important. There are also repulsive intersections but they are considered to be weaker obstacles to flow than the attractive junctions. Considerable numbers of dislocation rings probably formed from collapsed vacancy clusters have been observed after cold-work but their contribution to flow stress is not yet clear.

Observations have also been made on the recovery of the cold-worked structure in iron after annealing at temperatures between 450 and 600 °C. During recovery the dislocations making up the cell walls resolve themselves into simple sub-boundary networks made up of twist-tilt boundaries on random planes whilst the interior of the sub-grains become relatively dislocation free. Some 50 of these networks have been analyzed by the methods of Frank and there is convincing evidence that the junctions of many of these networks consist of two $\frac{1}{2}a\langle111\rangle$ dislocations joining up to make one $a\langle100\rangle$ dislocation.

Probable publication: A physical journal.

S2·21. A correlation of the substructure produced during high temperature deformation with the mechanical properties of metals. By D. H. WARRINGTON & P. B. HIRSCH, Cavendish Laboratory, Cambridge, England.

The work has been concerned mainly with the metals aluminium and copper though observations on iron and the low melting point hexagonal metals are also discussed. The techniques used included:

(a) Optical observation of subgrain boundary migration and the interaction of the boundaries with slip lines at room temperature.
(b) X-ray microbeam–microfocus observations of subgrain size and boundary misorientation.
(c) Transmission and diffraction electron microscope observations on the sub-structure introduced during deformation.

In copper observations show many sub-boundaries are parallel to the crystallographic planes (100), (110) and (111), indicating a predominance of slip on two systems. In no metal investigated was any indication of remaining slip band structure observed in the interior of the metal.

In all metals investigated a temperature range has been found where the sub-grain life begins to increase rapidly and the cell walls become clean; this temperature being in the region where appreciable grain boundary migration and sliding (observed by electron microscopy and optically) occurs. Throughout this range the ratio of flow stress to that at 0 °C. decreases appreciably. That this decrease is not fundamentally due to grain boundary migration is shown by the fact that it also occurs in single crystals.

Activation energy studies from the flow stress ratio curves are in support of the hypothesis that diffusion is a controlling factor in determining the type of substructure observed. The physical significance of this and its consequent effect upon work hardening theories applicable to elevated temperatures is discussed.

S2·22. Direct measurements of stacking fault energies in some alloy systems. By A. HOWIE, Cavendish Laboratory, University of Cambridge, England and P. R. SWANN, Metallurgy Department, University of Cambridge, England.

Thin foils of various alloys with compositions in the solid solution range of the systems Cu–Zn and Cu–Al have been highly deformed and examined by transmission

electron microscopy. By measuring the radius of curvature of three-point dislocation nodes a direct determination of the stacking fault energy γ can be made. There appears to be a steady fall in γ with increasing electron/atom ratio to a value of ~ 5 ergs/cm.[2] for the Cu–Zn alloys and ~ 1.5 ergs/cm.[2] for the Cu–Al alloys at the phase boundary (electron/atom ratio ~ 1.34). These results can be qualitatively understood in terms of interactions of the conduction electrons with the Brillouin zones. They are of considerable interest for the theory of work hardening and also in theories of the stability of crystal structures. Although the difference between the results for the Cu–Zn alloys and the Cu–Al alloys could perhaps be explained by segregation of solute atoms at the stacking faults no direct evidence of segregation has been found.

S2·23. Stacking faults at dislocation nodes. By B. A. BILBY, A. GRINBERG* & K. H. SWINDEN, *Metallurgy Department, University of Sheffield, England.*

When suitable dislocation lines fall across one another in the face centred cubic lattice small regions of stacking fault appear at the resultant dislocation node. These curvilinear triangles of stacking fault are observed in electron microscope pictures of thin metal films, and an estimate of the stacking fault energy may be obtained by measuring their size and geometry. In this paper the equilibrium position of such an arrangement of partial dislocations is determined by minimizing the contributions due to the stacking fault, and the elastic self energy and interaction energy of the dislocation lines. The calculations are carried out assuming isotropic elasticity and a symmetrical dislocation arrangement. An equilibrium configuration is determined for various values of the stacking fault energy and the elastic constants, and the results are compared with more approximate treatments.

This paper will probably be submitted to *Phil. Mag.*

S2·24. The rôle of dislocations and stacking faults in the deformation of evaporated silver films. By V. A. PHILLIPS, *General Electric Research Laboratory, Schenectady, New York, U.S.A.*

Single crystal {100} silver films have been grown on cleaved rocksalt crystals. The nature of the defects present has been studied by transmission electron microscopy. The major defects are stacking faults and line dislocations running from surface to surface of the film. The minor defects are dislocation loops, tetrahedral stacking faults, triangular defects probably Frank sessile dislocations, and 'point' defects believed to be unresolved loops or vacancy clusters.

In fresh areas of film the stacking faults are mainly 'simple' faults, that is, faults confined to a single plane, and are mostly relatively narrow (0.2–0.5μ). Stressing in the electron beam produces glide of partials in the fault plane resulting in widening of the faults and interaction to form 'complex' faults extended on two or more different {111} planes. Faults act as barriers to dislocation

movement. Continued stressing causes further widening. Fault widths of several microns are commonly observed. Hole edges act as sources of new faults. Holes also act as barriers to dissociation and as pinning points for faults. A ciné film has been made to illustrate the effect of stressing.

Annealing at 300 °C. decreases the number of stacking faults by a factor of 2–3 and gives mostly short simple faults. The remarkable stability of these is attributed partly to the low stacking fault energy and partly to a marked reduction in the energy of the partial dislocations when they lie in $\langle 110 \rangle$ directions.

The minor defects are thought to form by a vacancy collapse mechanism. The major defects are ascribed to dissociation of dislocations, the low line energy in $\langle 110 \rangle$ directions playing a major rôle in determining the fault shapes.

It is believed that the stacking faults play a major rôle in determining the mechanical properties, such as the yield strength, of evaporated silver films.

Full-length account is likely to be published in *Phil. Mag.*

S2·25. The deformation of thin single crystal films produced by evaporation. By D. W. PASHLEY & A. E. B. PRESLAND, *T.I. Research Laboratories, Hinxton Hall, Cambridge, England.*

The paper describes studies made on single crystal films of f.c.c. metals produced by evaporation, and consists of the following parts. (1) The deformation of the films by controlled application of tension inside the electron microscope; (2) the observation of dislocation movement induced by the use of an intense localised electron beam in the electron microscope; (3) attempts at correlation of the mechanical behaviour with the observed microstructure of the films.

The earlier work (D. W. Pashley, *Proc. Roy. Soc.* A, 1960, in press) on (111) gold films has been extended to include films in (100) orientation, and also films of silver. In particular, the effect of holes in the films has been studied.

S2·26. Kinking in cadmium single crystals deformed in tension. By K. C. A. BLASDALE, R. KING & K. E. PUTTICK, *Davy Faraday Research Laboratory, The Royal Institution, London, W. 1, England.*

Kinking has been observed to occur profusely throughout the length of single crystals of cadmium of certain high purities, tested in tension under normal conditions, when crystals of other degrees of purity show no evidence of kinking, apart from occasional kinks near the grips. The tendency to form kinks has been found to be sensitive to both temperature and rate of strain. Taking as a criterion the number of kinks formed in a specimen of standard length extended by a standard amount, the intensity of kinking is for a rate of strain of 10% per min., a maximum around room temperature, falling at higher and lower temperatures to as little as 10% of the room temperature value. Increasing the rate of deformation raises the temperature at which the maximum occurs. The kinking appears to be dependent upon specific impurities, as the intensity differs between batches of cadmium of the same nominal overall purity.

---

* A. G. is a member of the Facultad de Ciencias Exactas, Universidad de Buenos Aires, Argentina.

A dependence upon crystallographic orientation of the specimen has been observed but no simple relation yet established. Metallographic examination has revealed several interesting features. The detailed structure of the kinked region is complex, there being, in general, a number of subsidiary kink walls besides the major boundaries across which changes of orientation estimated to be as high as 45° have been observed to occur. The structure differs significantly from that previously postulated for kink bands.

Paper to be submitted to *Acta Metallurg*.

S2·27. Twinning. By J. W. CHRISTIAN, *Dept. of Metallurgy, Parks Rd., Oxford, England*.

Current ideas on mechanical twinning will be discussed under the following headings:

(1) *Crystallography*

Consideration of the actual atomic movements at the interface has recently led to a better understanding of the factors determining the operative twinning modes in many single and double lattice structures. The work of Crocker & Bilby indicates that in order of importance these factors are (*a*) the magnitude of the lattice shear, (*b*) the 'shuffle' mechanism, (*c*) the magnitude of the shuffles, and (*d*) the direction of the shuffles.

(2) *Nucleation*

Experiments suggest that twin nuclei are either present initially, or are formed in regions of high local stress. Twins may be able to form from monolayer nuclei (stacking faults) in b.c.c. metals, but not in other structures. A suggestion that twin boundaries may result from high concentrations of edge dislocations of one sign does not usually seem to fit the observed crystallography.

(3) *Growth*

In a type *I* twin, displacement of the rational K_1 interface apparently requires either the two-dimensional nucleation of successive twin layers or the presence of indestructible steps (twinning dislocations) in the interface. Indestructible steps, as in the Cottrell–Bilby theory, seem essential if the twinning shear is large. In tetragonal or orthorhombic crystals, the shear may be small, and twins are mobile under very small stresses; deformation by twin boundary displacements may be 'rubber-like' at low temperatures.

(4) *Twinning and slip*

Twinning, as opposed to slip, is generally more probable at low temperatures. Other effects are not so consistent; e.g. twinning is reported to be favoured by decreasing purity in iron, but by increasing purity in tantalum. The present information on mechanical twinning in f.c.c. metals and alloys will be summarized.

(5) *Twinning and fracture*

Several workers have shown that cracks in brittle b.c.c. and h.c.p. single crystals may be nucleated at twins or twin intersections. Current theories of brittle fracture attribute cracks to coalescence of dislocations on single or intersecting slip planes. It is not yet clear whether cracks in polycrystalline material are usually initiated by slip or twinning.

S2·28. Mechanical twinning in face centred cubic metals. By J. A. VENABLES, *Crystallographic Laboratory, Cavendish Laboratory, Cambridge, England*.

A model will be proposed for the initiation of mechanical twinning in workhardened and neutron-irradiated face centred cubic metals. The dissociation of dislocations (long jogs in the case of workhardened metals and dislocation loops in the case of neutron-irradiated metals) which are not in their glide plane has been considered, and their rôle as twin sources discussed semi-quantitatively. The predictions on this model of the orientations of the tensile axis required for twinning to occur and of the possible twin systems are in agreement with the published observations on copper, silver and gold. The relationship between discontinuous slip and twinning has been considered in some detail for workhardened materials, and an upper limit to the stacking fault energy for which twinning can occur calculated. This calculation is in agreement with published observations on aluminium.

S2·29. Interaction of twins and dislocations in alpha-iron. By A. W. SLEESWYK, *Koninklijke/Shell-Laboratorium, Amsterdam, The Netherlands*.

Armco iron specimens were strained in tension at room temperature and subsequently broken at lower temperatures down to 35 °K. In the interpretation of the results it is assumed that microcracks, once they are created, deform in conformity with the bulk of the material. The experiments show that at room temperature microcracks are created exclusively during the propagation of Lüders bands, but that below 85 °K. during the apparently elastic loading of the prestrained specimens new cracks may be formed. This is presumably due to the interaction of dislocations and twins created during the application of the load.

It is shown that a dislocation with a $\langle 111 \rangle$ Burgers vector which is incorporated in a $\langle 111 \rangle \{211\}$ twin band may be transformed, depending on the relative orientation, into either a similar $\langle 111 \rangle$ dislocation in the new lattice orientation, or a $\langle 100 \rangle$ dislocation. In the latter case the incorporation of the dislocation in the twin band requires extra energy; thus arrays of such dislocations may act as barriers against the propagation of twins. Furthermore it was realized that $\langle 100 \rangle$ dislocations in the b.c.c. lattice are not stable as such, but must be regarded as nuclei of microcracks.

From a micrographic investigation of high-purity iron deformed in liquid oxygen it is evident that slip planes act as barriers against the propagation of twin bands, and furthermore that twins, created either in tension or in compression often contain many microcracks.

Abstract of a lecture based on two papers to be offered for publication in *Acta Metallurg*.: 'Strain-hardening and crystalline fracture in polycrystalline iron' by A. W. Sleeswyk, and 'Cracks through twin-bands in alpha-iron' by A. W. Sleeswyk & J. N. Helle.

S2·30. Initiation of slip at the tip of a deformation twin in silicon-iron. By D. HULL, *Department of Metallurgy, University of Liverpool, England.*

Evidence will be presented to show that slip on (011) [111] systems can be initiated at the tip of a twin, which is held up, either at the free surface or inside single crystals of 3% silicon iron. The slip results from a dislocation reaction involving the $a/6$ [111] twinning dislocations, and not from the operation of dislocation sources in the matrix material by the stress field ahead of the twin. The details of the dislocation reaction will be considered and also the importance of this effect on brittle fracture.

S2·31. Deformation twinning in nearly perfect zinc crystals. By P. B. PRICE, *Research Laboratory for the Physics & Chemistry of Solids, Cavendish Laboratory, Cambridge, England.*

The deformation of nearly perfect zinc crystals was studied by transmission electron microscopy. Vapour-grown whiskers and platelets with {0001} faces, less than $\frac{1}{2}$ micron thick and initially completely free of dislocations, were deformed in tension inside a Siemens Elmiskop 1. In some cases crystals were deformed in a high sensitivity microtensile testing machine and examined in the electron microscope at various stages in the deformation. Since the axis of tension was in the basal plane, only twinning and non-basal glide could occur. It was observed that plastic deformation always began by the nucleation of a narrow lenticular twin at a large growth step at the edge of a crystal, where the stress was highest ($\sim \frac{1}{100}\,\mu$ to $\frac{1}{50}\,\mu$). Further deformation occurred at a lower stress ($\sim 10^{-3}\,\mu$) by growth of the twin and by the production of dislocations at the twin boundary and at surface steps. The interactions of dislocations on various observed glide systems in the matrix and in the twin are discussed, and the results of moving a twin boundary through dislocations with various possible Burgers vectors are considered. A mechanism for the propagation of a twin boundary is proposed and compared with experimental observations.

To be published in *Phil. Mag.*

S2·32. The growth of twins in tin single crystals as observed by transmission electron microscopy. By J. T. FOURIE, F. WEINBERG & F. W. C. BOSWELL, *Physical Metallurgy Division, Mines Branch, Department of Mines and Technical Surveys, Ottawa, Ontario, Canada.*

During examination of thinned tin single crystals in the electron microscope, the formation and growth of deformation twins due to stresses set up in the foil in the microscope were observed. It was verified by selected area electron diffraction that the observed structures were twins associated with the usual (301), [$\bar{1}$03] twinning system. The twins nucleated primarily near the edge of the foil and also at etch pits, other twin boundaries and at unidentified defects within the foil. In general nucleation occurred in areas relatively free from dislocations. It is concluded from the observations that a twin nucleus in the foil is formed as a whole by a local homogeneous shear of the lattice in a time interval of less than 1/35 sec.,

rather than by a Cottrell–Bilby dislocation mechanism. In many cases twins were observed to grow in length at a rate of about 10^{-6} cm. per sec. Widening was also observed which probably occurred by the stress-induced creation of additional twinning dislocations. In some cases several parallel twins were observed to grow in width until they merged to form a relatively large twinned area.

A Ciné film will be shown which illustrates the arrangements and growth characteristics of the twins. This film was made by photographing the fluorescent screen of the electron microscope.

A complete account of this work will probably appear in *Acta Metallurg.*

S2·33. Deformation twinning in thin evaporated gold films. By AVERY CATLIN, WALTER P. WALKER & KENNETH R. LAWLESS, *Cobb Chemical Laboratory, University of Virginia, Charlottesville, Virginia, U.S.A.*

Single crystal gold films of 1000 to 5000 Å thickness with a [001] orientation were grown by vacuum evaporation onto heated (375 °C.) sodium chloride substrates. The films were continuous and free of holes. The mechanical properties were determined both by stressing the films using the 'bulge' technique, a small hole having been drilled through the substrate with a water jet, and by dissolving away the substrate and subjecting the films to uniaxial tensile stress in the [110] direction. Apparent deformation twinning was observed with the optical microscope at resolved shear stresses of approximately 5×10^8 dynes per square centimeter. Electron microscope observations of the gold films showed both small and large lenticular bands having a different orientation from that of the original unstressed gold film. X-ray diffraction studies showed these bands to have a twin relationship to the original material.

To be published in *Acta Metallurg.*

S2·34. Fracture. By A. H. COTTRELL, *Department of Metallurgy, Cambridge, England.*

The brittle or semi-brittle fracture of many crystalline solids at applied stresses considerably below the theoretical value is attributed to the formation of small cracks. Many such fractures in ionic crystals are caused by surface defects. These defects can be removed by careful treatment of the surface but cracks are often formed as soon as the material is allowed to deform plastically, especially at places where slip bands intersect. High strength and fair ductility can be produced in some crystals, normally considered weak and brittle, by proper control of such sources of cracks. Cleavage fracture in steel often occurs at the instant of plastic yielding by slip or twinning and cracks nucleated by intersecting twins have been observed. A striking feature of cleavage cracks in steel is that they are often nucleated more easily than they are grown; non-propagating microcracks are thus produced. The recognition of this fact has enabled the dislocation theory of brittle fracture in steel to take in effects of hydrostatic stress and of various kinds of hardening, including irradiation hardening.

The role of lattice defects in other types of fracture is less clear. Many aspects of ductile fracture can be

accounted for in terms of plastic instability without referring explicitly to lattice defects. Vacancies are probably important in fractures under creep and fatigue conditions.

S2·35. Effect of slip distribution on the cleavage fracture of magnesium oxide single crystals. By R. J. STOKES, T. L. JOHNSTON & C. H. LI, *Honeywell Research Center, Hopkins, Minnesota, U.S.A.*

The extent to which chemically polished magnesium oxide crystals deform in tension has been correlated with the distribution of slip manifested at the *onset* of plastic flow. If the dislocation sources generate two slip bands on orthogonal (110) planes which intersect to nucleate a crack [by the mechanism of Stokes *et al.*, *Phil. Mag.* (1959), **4**, 920] before other slip bands are produced, then the crystal will be brittle. This is because there are no adjacent bands to stabilize the crack. If a single slip band is generated which expands laterally to fill the entire gauge length, then the crystal will be ductile because conditions necessary to nucleate a crack are not satisfied within the gauge length. Between these two extremes of behavior, cracks can become stabilized by adjacent slip bands and the ductility depends upon the number and spacing of slip bands.

Thus, the critical conditions for crack nucleation and propagation are strongly influenced by slip band width, inter-slip band spacing and the number of operative systems. A 16 mm. motion picture taken with polarized light illustrates these important aspects of the cleavage fracture of magnesium oxide.

For polished crystals, slip distribution and therefore mechanical behavior cannot be predetermined. However, it is possible to *ensure ductility* by first injecting dislocation sources into the crystal surface by sprinkling with carborundum. When such a crystal is deformed, slip is distributed uniformly on a very fine scale throughout.

In crystals deformed by bending, the above surface treatment produces a profound change in fracture behavior. Instead of cleaving simply in two, they shatter. The fracture surface is very rough and the component pieces contain many secondary cracks. Fracture originates from a nucleus formed *parallel to the tension direction* by a mechanism which is not fully understood.

To be submitted to *Phil. Mag.*

S2·36. The Joffe effect. By R. J. STOKES, T. L. JOHNSTON & C. H. LI, *Honeywell Research Center, Hopkins, Minnesota, U.S.A.*

It will be shown that the Joffe effect in sodium chloride may be interpreted quite simply in terms of the removal of surface microcracks.

Although it is well appreciated that ionic solids of the rock salt structure are brittle in the presence of a notch, insufficient attention has been paid to the experimental techniques necessary for the *complete* elimination of surface flaws. Microcracks may be introduced easily by conventional cleavage and handling techniques; such damaged crystals are brittle. Removal of surface flaws by immersion in water leads to an enhancement of ductility which is retained indefinitely in dry air providing:

(a) Microcracks are not reintroduced by mishandling the gauge length.

(b) The crystal is dried without leaving a surface precipitate.

We have found that the crystal must be thoroughly rinsed on removal from the water otherwise, when it is dried, crystallites precipitate onto the surface. Plastic deformation then leads to the formation of microcracks at the interface between the crystal and the surface deposit and it is re-embrittled. Evidence will be presented which indicates that these cracks originate by the pile up of edge dislocations at the surface deposit.

With special care a perfect surface can be prepared in which case single crystals of sodium chloride may be elongated in tension by as much as 40% before cleavage fracture. This ductility is retained indefinitely providing the crystal is stored in dry air, storage in a damp atmosphere results in the formation of surface deposits and consequent embrittlement. This is considered to be the explanation of the aging effects described by recent authors.

Submitted to *Trans. A.I.M.E.*

S2·37. An investigation of the fracturing of silicon-iron by the etch-pit technique. By F. B. CUFF, *IRSID, 185, rue Président Roosevelt, Saint Germain en Laye (S. et O.), France.*

This paper describes certain observations on the fracturing and the associated deformation in silicon–iron. The standard etch-pit technique was used for determining dislocation distributions in the vicinity of the fracture.

Three different types of tests were employed to cause fracture:

(1) low-temperature cleavage tests of single crystals,

(2) high-temperature, high velocity compression tests and

(3) high-temperature, high velocity torsion tests.

The various phenomena related to fracture are reported upon and certain conclusions are drawn.

S2·38. Der Einfluss von Kolloiden als Inhomogenitäten auf die Struktur von Spalt- und Reissflächen. Von HEINZ BETHGE & VOLKER SCHMIDT, *Arbeitsstelle für Elektronenmikroskopie, Deutsche Akademie der Wissenschaften zu Berlin, Halle, Saale, D.D.R.*

Zum Studium des Einflusses von Inhomogenitäten auf die Ausbildung von Bruchflächen eignet sich in ausgezeichneter Weise der NaCl-Kristall. Durch Anwendung besonderer Präparationsverfahren gelingt die elektronenmikroskopische Abbildung feinster Oberflächenstrukturen, und durch die gut reproduzierbare Erzeugung von Kolloiden sind die gewünschten Inhomogenitäten herzustellen. Es wurde zunächst die Einwirkung von Kolloiden auf die Spaltstrukturen untersucht. Die Erzeugung der Kolloide erfolgte durch Verfärbung von NaCl-Kristallen im Goldchloriddampf. In bestimmter Tiefe von der Oberfläche sind Goldkolloide aufzufinden, die als Würfel von etwa 0,1 μ Kantenlänge vorliegen. Das elektronenmikroskopische Bild von Spaltflächen in entsprechenden

Ebenen zeigt typische durch das Kolloid hervorgerufene Spaltstrukturen. An genügend voneinander entfernt liegenden Kolloiden sind Strukturen zu beschreiben, die von der allgemeinen Spaltstruktur unabhängig sind und nur vom Kolloid herrühren. Die aus dem elektronen-mikroskopischen Bild folgende wahrscheinliche Mitwirkung der an den Kolloiden ausgelösten Versetzungen wird diskutiert.

Ein anderes Bild ergeben die im natürlichen blauen Steinsalz vorliegenden Kolloide. Hier wirken die Kolloide als Ausgangszentren zahlreicher neuer Spaltstufen. Die gesamte Spaltstruktur wird in diesem Fall wesentlich von den Kolloiden bestimmt.

In Ergänzung zu den Ergebnissen auf Spaltflächen wurden auch Reissflächen untersucht, die bei verschiedenen Belastungsgeschwindigkeiten erhalten wurden.

Wahrscheinlich veröffentlicht in *Z. Naturforsch.*

S2·39. Fracture of the aluminium thin foils. By TAKEO FUJIWARA & SHO YOSHIDA, *The Laboratory of Crystal Physics, Hiroshima University, Japan.*

The process of fracture caused by the stretching of an aluminium foil was studied under an electron microscope by using the specially designed stretching apparatus and the cine camera attached to the electron microscope.

The aluminium thin foils to be examined, were prepared from the cold-rolled aluminium plates (99·993% Al, 0·01 mm. in thickness) by the treatment of so-called electrolytical polishing.

The specimen of such thin foils was stretched gradually with the stretching apparatus in the electron microscope, and the process of its fracture was continuously observed. Moreover, the behaviour of dislocations and habit of thin foils show during fracturing were taken on a 35 mm. cine film with the special camera under the following conditions. The cine film was directly exposed to an electron beam in the electron microscope with the camera speed of 2–3 frames per sec., and the accelerating voltage of the electron microscope was 80 kV. and electronic magnifications were from 60,000 to 100,000.

The cine film thus taken were reprinted to the 16 mm. cine film and will be presented, in which the movement of the dislocations behaves during stretching of the thin foil and etc., could be seen.

S2·40. Deformation and rupture of thin metal foils. By R. M. FISHER, & J. NUTTING, *Department of Metallurgy, Univ. of Cambridge, England.*

Observations have been made of the deformation of thin metal foils in the electron microscope using a specimen straining device. Most frequently dislocations are generated at the edges or at holes in the foil but occasionally a Frank–Read type of source has been observed in operation. Much higher local stress concentrations can occur in such foils compared to bulk materials and up to

1000 dislocations have been found to originate from one point. Similarly very dense pile-ups of as many as 500 dislocations against a grain boundary or other obstacle have been seen. The surface offset resulting from the movement of large numbers of screw dislocations in the foil occasionally is sufficient to cause the crystal to separate completely along the slip plane. In other cases the presence of fine precipitates or intersection slip systems results in the formation of a jagged fracture crack.

To be published in *Trans. A.I.M.E.*

S2·41. Fracture in zinc. By J. T. BARNBY & P. L. PRATT, *Fulmer Research Institute, Stoke Poges, Bucks, England.*

Variation of ductility and flow-stress with temperature were measured for polycrystalline zinc. A plot of fracture stress versus $d^{-1/2}$, d being the average grain diameter, gave a slope, k, of 0·23 tn.in.$^{-3/2}$ agreeing with that measured by Petch & Zein, but not with $k = 0·46$ tn.in$^{-3/2}$ obtained by Greenwood & Quarrell. The latter authors found $\sigma_i = 0$, whereas Petch & Zein and the present work found values of 0·5 tn.in.$^{-2}$ and 1·0 tn.in.$^{-2}$ respectively for σ_i, the stress ordinate intercept.

No increase in ductility was observed in testing zone-refined zinc specimens. Thus either the starting material is typical of pure zinc, or the dislocation locking element was not removed.

Kenneford reported high ductility in a 1·0% aluminium in zinc alloy containing a fine, globular precipitate. It seemed possible that precipitates acted as barriers to dislocations, effectively reducing grain size. Fracture testing of different grain sizes of this alloy showed a higher k and σ_i than for zinc. As expected from Cottrell's analysis of fracture the alloy was more brittle than zinc.

Addition of 0·01% cadmium to zinc gave an increase in k, but no further increase occurred with more cadmium. This is evidence that 0·01% cadmium is sufficient to saturate dislocations in zinc. Cadmium produced no change in σ_i.

Locking forces deduced from measurements of k are higher than expected. An explanation is sought in terms of deformation modes in zinc, and models of crack nuclei.

Cottrell's analysis of fracture is successful in explaining the low k for cadmium relative to zinc, in predicting a reasonable surface energy for zinc from the grain-size fracture-transition condition, and in explaining stable micro-cracks observed at -196 °C. in zinc.

To be submitted to *J. Inst. Met.*

S2·42. The possible rôle of embrittlement in stress-corrosion cracking. By A. J. FORTY, *H. H. Wills Physics Laboratory, University of Bristol, England.*
Withdrawn.

S2·43. The origin of the surface cracks responsible for brittle fracture in glass. By S. A. F. Murrell, Mining Department, The University of Sheffield, Sheffield, 1, England.

Recent observations by light and electron microscopy have confirmed the existence of the surface microcracks originally postulated by Griffith to explain the brittle fracture of glass. However, the origin of these cracks is still unexplained.

The problem is to explain how local stresses of the order of magnitude of the theoretical strength can arise in glass. It has been necessary to invoke the conception of crystallographically oriented dislocations in the crystal structure to explain the discrepancy between the theoretical and observed strength of crystalline solids, and it might therefore be expected that glassy (non-crystalline) solids should be extremely strong, in which case the existence of cracks in glass is difficult to explain.

It is shown in the paper that surface devitrification on quite a fine scale could give rise to the observed cracks and would thus remove the apparent anomaly. The stresses due to devitrification could cause groups of dislocations in the crystallites to pile up against the crystal-glass interface, which would produce the stress concentrations necessary for crack formation.

The stresses in and around a spherical devitrified region have been calculated and using Stroh's equation for the stress required to produce a crack by dislocation pile-up it is found that crystallites of diameter $\simeq 0.1$ micron are required in vitreous silica. The length of the crack produced is also about 0.1 micron on this hypothesis, which is the right order of magnitude.

S2·44. Fatigue. By N. Thompson, H. H. Wills Physics Laboratory, Royal Fort, Bristol, 8, England.

An attempt is made to survey recent work relating to the production of vacant lattice sites, and other point defects, by the action of an alternating stress on a metal. The relevance of such defects to the process of fatigue fracture is discussed. Phenomena more directly attributable to dislocations are also considered in a similar way.

S2·45. The dislocation distribution in fatigued face-centred-cubic metals. By P. G. Partridge & R. L. Segall, Crystallographic Laboratory, Cavendish Laboratory, Cambridge, England.

Transmission electron microscope observations have been carried out on fatigued polycrystalline copper, nickel and gold. Some experiments have also been done on copper single crystals. The dislocation arrangement found in these metals can be compared with that found in previous experiments on aluminium and austenitic stainless steel (18/8 type).

The dislocation arrangement in fatigued copper, nickel and gold is quite unlike that found after unidirectional deformation. There is no tendency to form sub-grains after fatigue. The dislocations are arranged in regions of

very high density ($\sim 10^{10}$ to 10^{11} cm.$^{-2}$) surrounded by less dense regions ($\sim 10^8$ cm.$^{-2}$). There are many small dislocation loops, up to about 200 Å in diameter. In addition there are many large elongated dislocation loops. Experiments on copper single crystals have shown that the elongated loops have their long axis normal to the operative Burgers vector and in the slip plane. It is suggested that these loops are formed from multiple jogs on screw dislocations.

The differences between aluminium, where the dislocations after fatigue are arranged in a random network, and copper, nickel and gold are discussed in terms of the relative ease of cross slip and vacancy migration. The annealing kinetics and tensile properties of fatigue-hardened metals are considered in relation to the observed dislocation distribution.

S2·46. Cross-slip as a significant mechanism in the fatigue of metals. By T. Broom, Department of Industrial Metallurgy, University of Birmingham, Birmingham 15, England.

An essential condition for fatigue failure is continuing reversed slip in local regions. The common manifestation of this is the production of slip 'striations'.

The fatigue softening of work-hardened copper single crystals is shown to be dependent on the production of striations. The chief criterion for their formation is that the fatigue stress should exceed a value which is close to that necessary for cross-slip as indicated by the end of stage II in tensile tests.

Striations are prolific in aluminium single crystals because of the ease of cross-slip and their suppression in dilute aluminium–magnesium alloy crystals can be associated with increasing difficulty of cross-slip.

Based on papers to be submitted as follows:

R. K. Ham & T. Broom, Phil. Mag.
T. Broom & G. J. Waldron, Acta Met. or Phil. Mag.

S2·47. The temperature dependence of fatigue life. By P. B. Hirsch & R. L. Segall, Crystallographic Laboratory, Cavendish Laboratory, Cambridge, England.

The temperature dependence of the fatigue life of aluminium single crystals has been studied in the temperature range 4·2 to 293 °K. The specimens were fatigued in push-pull and the stress necessary to cause failure in 10^6 cycles was determined. The results are interpreted in terms of a process of thermally activated cross slip.

S2·48. Dislocation theory of the extrusion, intrusion and fatigue crack. By Francisco Eiichi Fujita, Japan Atomic Energy Research Institute, Tokai, Ibaraki, Japan.

The most interesting and important outcome of recent works concerning fatigue phenomena may be the observation of extrusion and intrusion in slip bands. However,

whether or not they play the main rôle in fatigue is not certain at present. The theory first treats a dislocation mechanism of extrusion and intrusion: The proposed mechanism is somewhat similar to those by Cottrell & Hull & Thompson, in such point that a latent slip system causes the disturbance of the main slip system, but more general one. In the second, the theory treats the oxidation process which would take place in active slip bands during fatigue: By to-and-fro motion of dislocations in a slip band during stress cycles of period of the order of 10^{-3} sec., a step with new metallic surface appears in every first half cycle and disappears in the second half cycle. Applying the theory of the initial rapid oxidation developed by Mott et al., the rate of oxidation of such surface can be estimated. The result shows that oxygen atoms may be supplied at this step, be transported or diffuse into the slip band, and finally form oxide layers or inclusions at the depth of several microns from the crystal surface, which would become the strong obstacles for dislocations to generate a fatigue crack even in absence of intrusions. Such oxidation mechanism can explain not only microscopic observations such that the incipient crack does not always occur in the region where extrusions and intrusions are frequently observed, but also the effects of temperature, stress, atmosphere and speed of testing on fatigue life. Oxidation may take place at the inner surface of intrusions too, and would cause the crack generation there especially at higher temperatures.

To be published in the J. Phys. Soc. Jap.

S2·49. The mechanism of fatigue crack propagation in aluminum single crystals. By J. C. Grosskreutz, Midwest Research Institute, Kansas City, Missouri, U.S.A.

Aluminum single crystals grown by strain-anneal have been stressed at ~ 400 c.p.s. in pulsating tension and the initiation and propagation of fatigue cracks observed continuously under $300 \times$ magnification. Motion photomicrographs have been taken under controlled conditions of illumination and exposure. Playback of the film at accelerated speeds allows the surface mechanism of crack initiation and propagation to be studied at leisure. In all cases cracks were observed to initiate in surface slip bands; three or more neighboring bands may develop simultaneously and independently and later join by cross-slip to form the main failure crack. Propagation occurs strictly along crystallographic slip systems, usually {111}. The direction of propagation is as nearly perpendicular to the tensile axis as is possible with the available slip systems. Even while maintaining a steady course, the crack frequently jumps from one parallel slip band to another by means of cross-slip. The primary mechanism of propagation appears to be a series of re-initiations in persistent slip bands at the tip of the advancing crack. Large grain (~ 5 mm.) samples were grown to study the effect of grain boundaries. The effect depends in large measure on the relative orientation of the two grains. Examples are shown and discussed. Taper sections and sections cut transverse to the crack have shown that the crack always propagates from the surface into the volume of the sample. The path taken is again strictly crystallographic and roughly perpendicular to the tensile axis.

Average dislocation densities in polycrystalline aluminum samples were measured at various stages of fatigue by back reflection X-ray methods. Saturation at about 2×10^8 lines/cm.^{2} occurs after about the first 1% of fatigue life. A further increase by a factor of 10 occurs near the vicinity of the crack as failure occurs. A model for crack propagation is proposed based on these observations and the evidence obtained from the motion photomicrographs.

To be submitted to J. Appl. Phys.

S2·50. Resistivity recovery of cold-worked dilute copper alloys. By C. Pritchard & P. L. Pratt, Dept. of Metallurgy, Imperial College, Kensington, London S.W. 7, England.

The effect of impurities on resistivity recovery was studied by carrying out experiments on a series of polycrystalline dilute copper alloys. These alloys contained up to 1 at.% of beryllium, arsenic, cadmium or silver. After extending by 15% at -196 °C., the temperature of Stage III recovery (that occurring near room temperature) and also the activation energy with which it occurred were found to depend both on the alloy content, and on its concentration. The lifetime of the migrating defects remained the same, and, except for those containing arsenic, the amount of recovery attributable to point defects was the same in each alloy.

During deformation the concentration of point defects was found, from resistivity measurements, to increase as the square of the applied strain, after allowing for the dislocation contribution to the resistivity. This is in good agreement with van Bueren's prediction based on the production of vacancies by jogged screw dislocations during multiple slip. Prestrain experiments indicated that defect production is normally balanced by a simultaneous sweep-up process which goes on during the deformation itself.

The recovery of the arsenical alloys differed from the others, and the results were interpreted in terms of the diffusion of arsenic atoms to form atmospheres around dislocations.

To be published in Phil. Mag. or Acta Met.

S2·51. Irradiation effects in cold-worked and lightly-doped copper. By A. Sosin, Atomics International, Canoga Park, California, U.S.A.

An extensive study has been made of the low temperature, high energy electron irradiation and residual resistivity recovery characteristics of pure copper which has been previously subjected to varying degrees of plastic deformation at room temperature. The following characteristics have been observed.

(1) In specimens irradiated below 10 °K., the recovery characteristics below 33 °K. (Stage I_A, I_B and I_C) are only slightly altered by previous deformation.

(2) In specimens irradiated below 10 °K., the recovery characteristics between 33 °K. and 65 °K. (Stages I_D and I_E) are appreciably altered by previous deformation. In particular,

(a) the initial rates of isothermal and isochronal recovery are enhanced by cold work; however,

(b) the fractional amount of damage in cold-worked specimens remaining above 65 °K. is greater than in annealed specimens. The amount of damage retained increases with the amount of deformation but appears to reach a limiting value even for extreme amounts of deformation.

(3) In specimens irradiated near 90 °K., the initial damage rate (resistivity increase per unit integrated flux) is enhanced by previous deformation. This increase is compatible with the reduced recovery in Stages I_D and I_E.

(4) The 90 °K. damage rate is not constant but decreases and approaches the damage rate characteristic of annealed specimens.

(5) The recovery kinetics in Stage III ($\sim$ 0 °C.) are no longer bimolecular, as is characteristic of annealed copper, but, for intermediate amount of plastic deformation, may be fitted to a model based upon mutual annihilation at sinks introduced by deformation.

(6) Under proper pre-irradiation treatment, the residual resistivity value obtained after Stage III recovery is less than the pre-irradiation value.

The effects of suitable solute atoms appear to exceed those of dislocations. For example, Stage I_D and I_E are more thoroughly suppressed by 0·1 at.% of silver than by large amounts of plastic deformation. Irradiations at 10 and 90 °K. and subsequent recovery in a series of lightly-doped copper specimens is in progress.

S2·52. Lattice defects in molybdenum and niobium.
By A. A. Johnson, D. E. Peacock & A. Wronski, *Physical Metallurgy Dept., Imperial College of Science and Technology, London, S.W. 7, England.*

The yield stress, σ_Y, of molybdenum was measured as a function of grain diameter, l, at room temperature. The results can be fitted to Petch's relation

$$\sigma_Y = \sigma_I + k_Y l^{-1/2}$$

with $\sigma_I = 11·0$ kg.mm.$^{-2}$ and $k_Y = 1·7 \times 10^8$ dyn.cm.$^{-3/2}$. The yield stress of niobium was found to be independent of grain size at 20, 76, 195 °K., and room temperature. Interpreted in terms of current theories of deformation these results mean that the dislocations in niobium are not appreciably locked by Cottrell atmospheres of impurity atoms but that in molybdenum the locking is particularly strong.

The effect of irradiating molybdenum to an integrated flux of 2×10^{19} n.v.t. cannot be described in terms of changes in σ_I and k_Y. It is suggested that the complex effects actually observed were the result of the dislocation structure of the metal being modified by climb processes caused by the point defects created during irradiation.

The recovery of both irradiated and plastically deformed niobium and molybdenum was studied by making electrical resistivity measurements on wire specimens. A species of point defect was found to anneal out of both types of niobium specimen in the temperature range 80–120 °C. with an activation energy of about 1·0 e.V., and a similar defect to anneal out of molybdenum specimen in the temperature range 130–170 °C. with an

activation energy of about 1·3 e.V. The defects in both metals are tentatively identified as lattice vacancies.

To be published in *Phil. Mag.* and *Acta Metallurg.*

S2·53. Low temperature recovery in titanium and zirconium.
By E. Smith & M. S. Stagg, *Associated Electrical Industries Limited, Research Laboratory, Aldermaston Court, Aldermaston, Berkshire, England.*

Results of tensile experiments on polycrystalline samples of the hexagonal metals titanium and zirconium at room temperature and below, suggested that point defects were mobile at sub-zero temperatures in these metals, which have melting points in excess of 1500 °C. In order to study the mobility of these defects, wires of titanium and zirconium were strained in tension at -195 °C. and the extra resistivity introduced by the plastic strain was measured at -195 °C. as a function of this strain. The wires were then annealed for 15 min. at progressively higher temperatures and the resistivities re-measured at -195 °C. after each anneal. The amount of deformation induced resistivity recovered after a room temperature anneal was about 50% for titanium and 30% for zirconium. These resistivity results confirmed that point defect migration was occurring at sub-zero temperatures. Moreover, it was observed that in titanium, the resistivity was recovering at -195 °C. Accordingly, deformation experiments have been conducted at much lower temperatures, wires being strained at -253 °C., and then annealed at -195 °C. and higher temperatures. It was observed that both in titanium and zirconium, approximately 30% of the resistivity induced by the -253 °C. deformation was recovered after 15 min. annealing at -195 °C. This recovery, at temperatures below -195 °C., of resistivity induced by plastic deformation in the hexagonal metals titanium and zirconium, is in marked contrast to the behaviours of face-centred-cubic metals in which there is essentially no resistivity recovery after plastic deformation at such temperatures. In this latter group of metals, resistivity recovery below -195 °C. is only observed after irradiation. The various ideas proposed for such recovery are:

(a) Free migration of interstitials to vacant lattice sites.
(b) Recombination of close pairs of interstitials and vacancies.
(c) Atomic re-arrangements in displacement spikes formed by irradiation.

These proposals are considered in explaining our results.

The journal in which this paper will be published has not been decided.

S2·54. Some observations of etch pits in alkali halide crystals. By R. W. Davidge, R. W. Whitworth & P. L. Pratt, *Dept. Metallurgy, Imperial College, London S.W. 7, England.*

Certain etching reagents produce several types of etch pits in NaCl and LiF. For example, in lightly deformed NaCl etched with acetic acid plus methyl alcohol shallow rather indistinct pits are sometimes formed on $\langle 110 \rangle$ slip bands, together with the normal pyramidal pits which are believed to be formed at dislocations. These shallower pits are not formed in crystals which have been either

annealed at 250 °C. or X-irradiated subsequent to deformation, and thus the total density of pits formed along slip bands is smaller after these treatments. These observations suggest that some defects other than normal dislocation lines are present on slip planes after deformation.

Accepted for publication in *Phil. Mag.*

S2·55. Effect of pressure and plastic deformation on point defects. By D. Lazarus, *Department of Physics, University of Illinois, Urbana, Illinois, U.S.A.*

Studies have been made of the effects of hydrostatic pressures to 10,000 atmospheres and of small torsional plastic strain on the generation and mobility of point defects in solids. A variety of experimental techniques have been used, including anelastic relaxation methods for substitutional and interstitial solid solutions, quenched resistivity measurements for pure gold, and electrical conductivity methods for alkali halides. Pure hydrostatic pressure causes a decrease in the rate of production of vacancies and in the rate of motion of vacancies and small interstitials, the effect varying exponentially with pressure. Small amounts of plastic deformation cause a considerable enhancement in the rate of diffusion-limited relaxation at low temperatures, possibly demonstrating the generation of mobile vacancies by moving dislocations, although the effect may involve more complex mechanisms.

To be published (as several papers) in *Phys. Rev.*

S2·56. Internal friction of cold-worked gold and copper at low temperatures. By Ryukiti R. Hasiguti, *Department of Metallurgy, University of Tokyo* and Sigeo Okuda, *Institute of Physical and Chemical Research, Tokyo, Japan.*

The aim of this paper is to find the behaviours of dislocations and point defects which give rise to internal friction peaks and changes of dynamic modulus of gold and copper. The measurements were performed at temperatures from about 100 to 360 °K. Lattice defects were introduced by cold-working at liquid nitrogen temperature or at room temperature.

Three new peaks of low frequency (~ 1 c.p.s.) internal friction, P_1 (~ 130 °K. in Au), P_2 (~ 190 °K. in Au) and P_3 (~ 210 °K. in Au), were found between liquid nitrogen temperature and room temperature. These peaks all disappear by the room temperature annealing.

P_2 is observed in the specimen which is cold-worked at liquid nitrogen temperature. P_1 and P_3 are found in the specimen which is cold-worked at liquid nitrogen temperature and then annealed at higher temperatures below room temperature, or in the specimen immediately after the room temperature cold-working.

A new theory was proposed to explain the above experimental results. The dislocations produced by cold-working are pinned down by the point defects which are produced during the cold-working and migrate to the dislocations during and after the cold-working. A dislocation segment which contain a pinning point has a certain probability to be torn off from the pinning point by the help of thermal energy. When the frequency of the tearing off process coincides with the external

vibrational frequency of the specimen, there appears an internal friction peak as a relaxation process. It is considered that vacancies, interstitials and divacancies may be the pinning point defects.

The activation energies obtained from the peak shifts correspond to the interaction energies between a dislocation and respective point defects, and the activation energies of the growth processes of peaks are those for the migrations of respective point defects to dislocations.

The authors intend to submit the manuscript of full paper to *Phil. Mag.* in near future. The preliminary short-note was published in *Proc. Jap. Acad.* (1959), **35**, 284.

S2·57. Interaction of dislocations and point defects in silver chloride.* By L. Slifkin, M. Kabler & H. Layer, *University of North Carolina, Chapel Hill, North Carolina, U.S.A.*

Single crystals of silver chloride subjected to successive tensile tests exhibit strain-aging near room temperature. The magnitude of the effect in nominally 'pure' crystals increases monotonically with impurity content, as gauged by the room-temperature ionic conductivity. Whereas after brief aging both upper and lower yield points are observed, prolonged aging so strongly anchors the dislocations that the lower yield point disappears. The kinetics of the increase in flow stress during aging have been studied as a function of aging temperature, giving an activation energy of 0·4 e.V., a value very close to that for vacancy migration. Since at these temperatures the crystals are in the extrinsic, or impurity, conductivity range, this result is consistent with the migration of either the impurity atoms or the vacancies themselves to the dislocations. The two possibilities are distinguished, however, by the fact that the time required for substantially complete hardening (a few hours at room temperature with a vacancy concentration of 10^{-5}) is too long for vacancy migration times, but is consistent with the diffusion rate of impurities. This is in contrast to the situation in alkali halides, where it appears that impurity hardening is primarily due to the interaction of vacancies with dislocations, rather than the impurities themselves.

The ionic conductivity of silver chloride has been studied *during* a pulse of plastic deformation. After an elongation of 10 or 20%, a further extension of 3% in 5 milliseconds produces a transient conductivity increase which at room temperature builds up and decays with a relaxation time of 2 milliseconds. It is believed that this effect is due to the production of excess interstitial silver ions by dislocation intersection. The very small magnitude of the effect (a maximum transient increase of $1·5 \times 10^{-10}$ mho/cm.) indicates a production rate of defects at room temperature far below the often-quoted value of 10^{-4}/unit strain. Large voltages (of the order of tenths of a volt) also appear across the faces of the crystal during extension, especially when the deformation is very inhomogeneous.

Probable publication medium: *J. Phys. Chem. Solids.*

*S*2·58. Influence des déformations mécaniques sur la conductibilité électrique et la polarisation de monocristaux de fluorure de lithium. Par H. CURIEN & Z. MIHAILOVIC, *Laboratoire de Minéralogie de la Faculté des Sciences, Paris, France.*

Dans un cristal de fluorure de lithium soumis à une différence de potentiel continue fixe, le courant évolue en fonction du temps depuis une valeur I_0 jusqu'à une valeur plus faible I_∞. Le temps d'évolution est de l'ordre de l'heure. Seule, la valeur I_0 obéit à la loi d'Ohm. Le taux de polarisation repéré par le rapport $S = (I_0 - I_\infty)/I_0$ varie avec la température, l'intensité du champ électrique, les traitements mécaniques subis par le cristal.

L'allure des courbes de dépolarisation permet de distinguer les parts respectives dues au phénomène parasite provenant de la modification chimique des électrodes et au phénomène de polarisation dans le cristal.

A 400 °C., un écrouissage faible dans le sens des lignes de courant (taux de variation de la longueur dans le sens de la compression de 1,2%) provoque une légère diminution de I_0 et une augmentation de S; d'autre part l'évolution de la polarisation est beaucoup plus rapide. Un écrouissage plus important (de l'ordre de 5%) provoque une forte diminution de I_0 et une diminution de S. Le même échantillon, recuit après écrouissage à 5%, présente une conductibilité plus faible encore, et un taux de polarisation pratiquement nul. On peut rendre compte de ces diverses observations en faisant intervenir les interactions entre les dislocations et les lacunes d'ions positifs qui constituent les porteurs de charges.

To be published in *Journal des Recherches de C.N.R.S.*

*S*2·59. Erzeugung elektrischer Ladungen bei plastischer Deformation von NaCl-Einkristallen. Von H. BETHGE & F. FRÖLICH, *Institut für experimentelle Physik, Halle, Saale, D.D.R.*

Im Anschluss an vor einiger Zeit bekannt gemachte Experimente (J. E. Caffyn & T. L. Goodfellow, *Nature, Lond.* (1955), **176**, 878; D. B. Fischbach & A. S. Nowick, *J. Phys. Chem. Solids* (1957), **2**, 226; (1958), **4/5**, 302) wurden die bei plastischer Deformation von NaCl-Einkristallen ohne angelegtes äusseres Feld kurzzeitig auftretenden elektrischen Ströme untersucht. Die plastische Deformation der Kristallproben erfolgte in zeitlich aufeinanderfolgenden Stufen zwischen zwei Stempeln verschieden grosser Druckflächen, die gleichzeitig als Elektroden für die elektrischen Messungen dienten. Die bei der Deformation gebildeten Versetzungen liessen sich durch geeignete Ätzverfahren auf der Oberfläche der Proben und durch spannungsoptische Beobachtungen nachweisen und gestatteten Rückschlüsse auf den Gleitmechanismus bei den verschiedenen Belastungsstufen.

Bei der Deformation entstanden in der Umbegung der kleineren Druckelektrode bei den ersten Belastungen nur positive, nach weiteren Belastungsstufen jedoch negative Ladungen. Vorzeichen und Betrag der erzeugten Ladung hängen neben der Gesamtbelastung weiter von der Form der Proben und in hohem Masse von der Vorbehandlung des verwendeten Kristallmaterials ab. Insbesondere wurde untersucht der Einfluss einer vorhergehenden Röntgenbestrahlung, einer nachfolgenden Bleichung und einer Dotierung der Kristalle mit Kalziumionen.

Ferner wurde gezeigt, dass in röntgenverfärbten Kristallen eine Einstrahlung von Licht aus der *F*-Bande ebenfalls zeitlich schnell abklingende Stromimpulse hervorruft, falls die Kristalle vorher im Dunkeln plastisch deformiert werden.

Mögliche Deutungen für die gefundenen Ergebnisse werden diskutiert.

Veröffentlichung erfolgt voraussichtlich in *Z. Phys.*

*S*2·60. The kinetics of impurity migration to dislocations. By R. BULLOUGH & R. C. NEWMAN, *A.E.I. Research Laboratory, Aldermaston, Berks, England.*

Previous theoretical treatments of this problem may be criticized for the neglect of either diffusion flow (A. H. Cottrell & B. A. Bilby, *Proc. Phys. Soc. Lond.* (1949), **62**, 49) or drift flow (B. A. Bilby, *J. Phys. Soc. Japan* (1955), **10**, (8), 673) or the imposition of an inflexible boundary condition at the dislocation core (F. S. Ham, *Appl. Phys.* (1959), **30**, 915).

In the present treatment we shall investigate: (*a*) the kinetics of formation of a true Maxwellian atmosphere (R. Bullough & R. C. Newman, *Proc. Roy. Soc.* (1959), A, **249**, 427) round a dislocation in the absence of any precipitation, (*b*) the kinetics of migration to such a dislocation when precipitation of a second phase takes place at discrete sites along the dislocation; allowance is made for a finite dislocation density in both cases. In the model adopted for (*b*) we assume that the core of the dislocation acts as a channel of high mobility for the impurities and that there is a finite rate limitation controlling the incorporation of the impurities into the prenucleated precipitate particles.

Both problems have been solved analytically, regarding the drift flow as a small perturbation on the diffusion flow and where the form of the interaction potential is assumed to be:

$$\varphi = -Ar^{-1}, \ r \geq r_0 \ \Big\}$$
$$= -Ar_0^{-1}, \ r \leq r_0 \ \Big\}$$

For larger, more physically realistic drift flows, relevant solutions of the governing partial differential equation have been obtained by direct numerical methods. For this work a more sophisticated interaction potential appropriate to a non-Hookian dislocation.

$$\varphi = -A[r^2 + r_0^2]^{-\frac{1}{2}} \quad \text{all } r$$

has been used. The latter results are compared both with the former analytic treatment and with the available experimental results for quench and strain aging in some steels.

*S*2·61. The contribution of thermal lattice defects to the structural energy and expansion in pure metals. By H. U. ÅSTRÖM, *Department of Physics, Institute of Technology, Stockholm 70, Sweden.*

The development of thermal lattice defects has been studied by means of isothermal calorimetry for silver (H. U. Åström, *Ark. Fys.* (1959), **14**, 263) and for aluminium, gold and molybdenum (H. U. Åström, *Ark. Fys.* (in print)). All metals were of high purity. The specimens, enclosed in argon-filled Pyrex containers, were heated

74*

from room-temperature to various temperatures in the range 160 to 480 °C. The energy absorbed in order to obtain equilibrium at the new temperature had an exponential tail, with a time-constant of a few hours. Increasing temperature leads to an isothermal absorption of heat which becomes larger with increasing grain size and purity of the metal. In (H. U. Åström, *Ark. Fys.* (in print)) the thermal expansion in gold has been studied with an isothermal method. With the same pre-annealings as in the calorimetric case a small exponential expansion was observed which took place with about the same velocity as the energy absorption. The temperature dependence of the energy and volume increase corresponded to an energy of formation of 0·11–0·27 e.V. The time-constants of the experimental curves changed, however, very little with temperature. As impurities, vacancies and/or dislocations cannot explain more than a smaller part of the observed effects, it has been supposed that they may be caused by an unidentified type of thermal defect discussed by G. Borelius (*Ark. Fys.* (1959), **15**, 65; **16**, 119).

S2·62. Introductory talk. Quench hardening. By R. MADDIN, *School of Metallurgical Engineering, University of Pennsylvania, Philadelphia 4, U.S.A.*

The effect of quenching and ageing on properties (mainly mechanical) of solids will be reviewed. Recent data concerned with the temperature dependence of the yield strength, with the resoftening of the quench hardened state and the results of recent experiments on quenching effects in body centered cubic metals will be reported. The observations will be considered in light of results from transmission electron microscopy of quenched metals and theories of the interaction of point defects with dislocations.

S2·63. Vacancy trapping in quenched aluminium alloys. By K. H. WESTMACOTT, R. S. BARNES, R. E. SMALLMAN & D. HULL, *Atomic Energy Research Establishment, Metallurgy Division, Building 393, Harwell, Berkshire, England.*

Foils of some aluminium alloys have been given various quenching treatments and the density and distribution of the vacancy clusters observed in an electron microscope. It is concluded that the solute atoms trap the vacancies and that their binding energies determine both the scale of the clusters and the number of vacancies they contain.

S2·64. The interaction of solute atoms and dislocations in aluminium alloys. By R. B. NICHOLSON, *Department of Metallurgy, University of Cambridge, Cambridge, England.*

Transmission electron microscopy has been used to study the interaction of solute atoms and dislocations

in supersaturated Al–Cu, Al–Ag, Al–Mg, Al–Si, and Al–Zn alloys. Some solute atoms lower the stacking fault energy of aluminium and this phenomenon influences the structure of the quenched alloy and the early stages of precipitation on dislocations. The structure near grain boundaries may also be affected but here the attraction between solute atoms and vacancies is usually the deciding factor.

To be published in *Acta Metallurg.*

S2·65. The part of vacancies in the ageing of quenched aluminium and aluminium alloys. By G. BORELIUS & L. E. LARSSON, *Tekniska Högskolan, Stockholm 70, Sweden.*

Withdrawn.

S2·66. The influence of quenched-in vacancies on the rate of clustering in aluminium-zinc alloys. By VOLKMAR GEROLD & WERNER SCHWEIZER, *Max-Planck-Institut für Metallforschung, Stuttgart N, Deutschland.*

The change in small angle X-ray scattering from Al–Zn alloys has been measured using counter techniques. The scattered intensity is due to the formation and growth of zinc-rich clusters in the quenched alloys (6, 9 and 12 at.% Zn). The intensity has been measured at a constant scattering angle for different quenching temperatures ($T_s = 250$ to 550 °C.) at a constant ageing temperature ($T_a = 20$ °C.). After times of 20 min. to several hrs. (depending on T_s) the intensity reaches a final maximum value. The time, t_h, required for the necessary intensity to reach half its value was taken as a measure of the rate of clustering. A plot of log t_h versus $1/T_s$ gives straight lines in the range from 300 to 500 °C., indicating an activation energy of $Q_1 \approx 20$ kcal. or 0·86 e.V. With higher quenching temperatures (550 °C.) the rate is lowered instead of increased.

If it is assumed that the rate is proportional to the concentration, c_v, of quenched-in vacancies, which is

$$c_v \sim \exp(-U_v/kT_s),$$

the activation energy Q_1 may be identified with the energy U_v of vacancy formation. At higher quenching temperatures (550 °C.) the vacancies form clusters and hence are less effective in diffusion processes. As a result the diffusion rate of Zn atoms is lowered in agreement with our observations.

The migration energy of vacancies has been determined from the clustering rate at two different ageing temperatures ($T_a = 20$ and 50 °C.). A value of $Q_2 \approx 10$ kcal. or 0·43 e.V. was found. The activation energy for the diffusion of zinc atoms is then given by $Q_1 + Q_2 \approx 30$ kcal., which is in agreement with high temperature measurements.

The influence of plastic deformation on the clustering rate has also been studied. Deformation immediately after quenching gives (1) an increase of the clustering rate and (2) leads to a more rapid attainment of the final value, which is lower than in the undeformed state. Both effects

may be explained by (1) an increase of vacancy concentration due to plastic deformation and (2) a higher concentration of vacancy sinks as dislocations in the deformed foils.

This paper will be published in *Z. Metallk.*

S2·67. An investigation on the effect of quenching on the internal friction of Al. By D. GELLI & T. FEDERIGHI, *Istituto Sperimentale Metalli Leggeri, Novara, Italy.*

The effect of quenching on the internal friction (i.f.) of samples of high purity aluminium (99·995%) have been investigated at very low strain amplitude ($\sim 10^{-7} - 10^{-8}$) by the electrostatic (Bordoni type) method of excitation. Some observations on the variation of the resonance frequencies are also included.

Measurements have been carried out at room temperature after furnace cooling and after quenching from several temperatures, on specimens of different size and at various resonance frequencies; polycrystalline samples and also single crystals have been employed; finally the effect of quenching rate has been investigated.

Although the i.f. of well annealed specimens is amplitude-dependent even at the very low strain amplitude employed, the results obtained after quenching are very complex and are depending on many factors as size, rate of quenching, quenching temperature, time of aging after quenching and so on. Generally speaking however the effect of quenching is to eliminate the amplitude-dependence, to increase the i.f. (when the evaluation is made at the lowest vibration amplitude) and also to decrease slightly the frequency of resonance. Many of these results are in agrement with the results obtained previously by Levy & Metzger.

Preliminary results of annealing after quenching show that the effects of quenching are practically but not completely eliminated in the range 150 to 200 °C., while the well annealed state is obtained only after annealing at higher temperatures.

An attempt of interpretation of the results on the basis of internal strains produced by the quenching and on the pinning of dislocations by point defects and dislocation loops is made.

To be submitted to *Nuovo Cimento.*

S2·68. Introductory talk on climb and creep. By J. FRIEDEL, *Physique des Solides, Faculté des Sciences, Orsay (S et O), France.*

The elementary processes and kinetics of dislocation climb are briefly discussed. Applications to the growth of loops and helices, to polygonization and creep are reviewed.

S2·69. Direct observations of climb in deformed zinc crystals. By P. B. PRICE, *Research Laboratory for the Physics and Chemistry of Solids, Cavendish Laboratory, Cambridge, England.*

The climb of dislocations in zinc crystals at room temperature was studied by transmission electron microscopy. Vapour-grown whiskers and platelets, less than $\frac{1}{2}$ micron thick and initially completely free of dislocations, were deformed in tension, parallel to the {0001} faces, inside a Siemens Elmiskop 1. Climb occurred in the following instances: (1) During the deformation $\langle 11\bar{2}0 \rangle$ type dislocations were observed to glide rapidly along the directions of their Burgers vectors and to climb slowly in other directions in order to avoid obstacles. (2) In regions where pyramidal glide on the system $(\bar{1}\bar{1}22)/[11\bar{2}3]$ took place, circular prismatic dislocation loops up to 1000 Å in radius were produced, which appeared to lie on basal planes and which shrank in size and disappeared in a few minutes at room temperature. The measured rates of decrease of loop radii were consistent with rates predicted assuming that climb by vacancy diffusion was taking place. A mechanism for the production of loops during pyramidal glide is proposed. (3) After glide occurred on non-basal planes in a twinned region, the dislocations remaining in the twin arranged themselves, by a combination of glide and climb, into low-angle boundaries perpendicular to the basal plane in the twin. The rate of polygonization was comparable to the rate of disappearance of prismatic loops.

To be published in *Phil. Mag.*

S2·70. On the mechanism of formation of helical dislocations in silicon.* By W. C. DASH, *General Electric Research Laboratory, Schenectady, New York, U.S.A.*

Screw dislocations climb to form helices when gold is diffused into silicon crystals at about 1200 °C. (W. C. Dash, *Phys. Rev. Letters* (1958), 1, 400). The following experiments have been performed to elucidate the mechanism of formation of the helices. From localized surface damage, a small number of dislocation loops are moved into an otherwise dislocation-free crystal by an applied stress at 900 °C. The geometry of deformation is such that the screw portions of the loops are left-handed. Upon diffusion of gold only right-handed helices are formed. This leads to the conclusion that in effect a vacancy deficiency produces the climb. The present investigation has shown that only those screw dislocations which are substantially free from impurities climb to form helices. In other cases either distorted helices form, or there may be no climb of the screw dislocations. In such specimens randomly distributed prismatic loops are frequently found.

Will be submitted to *J. Appl. Phys.*

S2·71. The interaction of point defects with dislocations in silicon.† By R. C. NEWMAN, J. WAKEFIELD, J. B. WILLIS & R. BULLOUGH, *A.E.I. Research Laboratory, Aldermaston, Berks, England.*

The phenomenon of strain aging (G. L. Pearson, W. T.

Read & W. L. Feldmann, *Acta Met.* (1957), 5, 181) has been demonstrated in silicon crystals known to contain oxygen and probably carbon. By the use of infra-red spectrographic techniques it has also been shown that oxygen precipitates on annealing at a temperature of 1000 °C. and there is indirect evidence of interaction with dislocations (S. Lederhandler & J. R. Patel, *Phys. Rev.* (1957), 108, 239).

The present work (R. Bullough, R. C. Newman, J. Wakefield & J. B. Willis, *J. Appl. Phys.*, to be published (April, 1960)) is concerned with a direct observation of these precipitation phenomena, in single crystals containing controlled grown-in dislocation densities from zero up to 10^5 cm.$^{-2}$, together with some isolated crystal boundaries; the effect of plastic deformation has also been studied. The location of any precipitated oxygen after annealing is revealed by a novel method using crystals which contain accurately predetermined concentrations of aluminium and phosphorus, the aluminium being slightly in excess so that initially the crystal is wholly *p*-type. It is shown thermodynamically that the aluminium will undergo an exchange reaction with the 'precipitated' silicon–oxygen complex, similar to that observed in chromium steels. In the vicinity of the oxygen precipitates the aluminium concentration is therefore reduced and the crystal becomes locally *n*-type. From the nature of the resulting $p - n$ junctions, which are delineated by etching, the type of nucleating site, random, dislocations or boundaries can be readily ascertained. The actual precipitates can be revealed by transmission optical microscopy and correlated with the former surface features. Observations have been made over the temperature range 950 to 1350 °C.; the mode of precipitation is dependent both on this temperature and on the oxygen concentration. Electron diffraction observations indicate that carbon is also involved in the precipitation process.

S2·72. Radiation hardness in copper. By T. H. BLE-WITT, R. R. COLTMAN, R. E. JAMISON,* & J. K. RED-MAN, *Solid State Division, Oak Ridge National Labora-tory,*† *U.S.A.*

The effect of nuclear radiation on the mechanical properties of copper has been studied. It has been found that the yield stress, which is substantially increased by the radiation, increases as the cube root of the flux. A strong temperature dependence of the yield stress of irradiated copper is observed with the yield stress being given by a function similar to $\sigma = A - BT^{\frac{1}{2}}$ above 40 °K. A Luders band with slip lines of very large step height is associated with the enhanced yield stress at small strains. At large strains the phenomena of overshoot is observed.

The annealing kinetics of the radiation hardness have also been studied in the temperature range from 25 to 700 °K. Little or no annealing is observed in the region below 80 °K. In the region from 80 to 300 °K. approximately 20% of the yield stress is recovered with the remainder annealing in the range from 600 to 700 °K.

---

* Now with the Research Department of Carrier Corporation, Syracuse, New York.

† Oak Ridge National Laboratory is operated by Union Carbide Corporation for the United States Atomic Energy Commission.

These results have been discussed in terms of the possible mechanisms by which the hardening can occur. While by no means conclusive, these data support a dislocation locking mechanism. On the other hand a very close analogy to radiation hardening and the hardening which arises from the addition of impurities exists, e.g., the hardening in α brass. The correlation between work hardening and radiation hardening appears to be quite small.

Submitted to *Journal of Nuclear Materials*.

S2·73. Radiation damage in face-centred cubic metals. By J. SILCOX, *Crystallographic Laboratory, Cavendish Laboratory, Cambridge, England.*

The transmission electron microscopy technique was applied to the study of the dislocation distribution in thin foils of face-centred cubic metals prepared by electro-polishing from neutron-irradiated bulk material. The bulk specimens were neutron-irradiated in the A.E.R.E. Harwell atomic piles BEPO and DIDO at temperature of ~ 35 °C. and 60–100 °C. to doses of $6 \cdot 7 \times 10^{17}$ n.cm.$^{-2}$, $5 \cdot 6 \times 10^{18}$ n.cm.$^{-2}$ and $1 \cdot 4 \times 10^{20}$ n.cm.$^{-2}$ of fast neutrons (Energy > 1 MeV.). In copper and gold at low doses the observations show the existence of small regions of strain (~ 50 Å in diameter at densities ~ 10^{16} c.c.$^{-1}$) some of which at high magnifications can be resolved as small dislocation loops. At higher irradiation the loops grow in size and density and in copper at the highest dose many large (~ 300 Å in diameter) loops are detected. Other dislocations thought to be present in the material prior to irradiation are observed to be 'joggy'. This is thought to be due to the absorption of point defects produced during irradiation.

The stability of the loops and the behaviour on annealing (in copper) are as expected from prismatic dislocation loops and can be interpreted in terms of any displacement spike mechanism which produces separated vacancies and interstitials. The loops are considered to nucleate as a result of the collapse of discs of vacancies produced by vacancy clustering in the central region of a displacement spike, and to grow by migration of vacancies or vacancy clusters.

Radiation hardening is interpreted in terms of the large density of dislocations in loops. In copper, radiation hardening anneals out at the same temperature at which the loops are observed to disappear by climb.

A full-length account of the work on copper will be published in *Phil. Mag.*

S2·74. The mechanism of irradiation hardening in copper. By M. J. MAKIN, A. D. WHAPHAM & F. J. MIN-TER, *Atomic Energy Research Establishment, Metallurgy Division, Building 393, Harwell, Nr. Didcot, Berkshire, England.*

The mechanism of irradiation hardening in copper is being studied both by detailed mechanical property measurements and by thin film transmission electron microscopy. The lattice and dislocation components of irradiation hardening have been measured as a function of testing temperature and neutron dose and the results compared with Seeger's theory of lattice hardening,

which is based on dislocations cutting through a forest of obstacles under both stress and thermal activation. The observed temperature dependence is in excellent agreement with the theory in the as-irradiated condition but mild annealing treatments greatly reduce the temperature sensitivity, indicating that lattice hardening is due to obstacles of various activation energies.

The hypothesis that these obstacles are the dislocation loops observed in thin film electron microscopy of irradiated copper is being investigated and it has been shown that the density of loops increases rapidly with dose to a saturation value of about $5 \cdot 6 \times 10^{15}$ cm.$^{-3}$ and that the average size of the loops increase steadily with dose. Experiments are also in progress on the formation of loops during irradiation at -195 °C., where the full lattice hardening is observed, and on the effect of the recovery stage at 0 °C., where a reduction in dislocation hardening takes place. In addition the correlation between the loop size and density and the great reduction in the temperature sensitivity of the lattice hardening on annealing is being studied and will be presented at the Conference.

Expected to be published in *Phil. Mag.*

S2·75. Study of work-hardening and slip-line patterns of neutron-irradiated copper single crystals.
By ALFRED SEEGER, SIEGFRIED MADER & UWE ESS-MANN, *Max-Planck-Insitut für Metallforschung, Stuttgart, und Institut für theoretische und angewandte Physik der Technischen Hochschule, Stuttgart, Deutschland.*

The work-hardening and the surface phenomena of copper single crystals deformed in tension at 90, 293 and 513 °K. after a neutron bombardment of $nvt \approx 6 \times 10^{17}$ fast neutron/cm.^{2} were investigated and compared to the behaviour of unirradiated crystals. The similarity between irradiated and unirradiated crystals was largest at high strains, i.e. in stage III of the stress-strain curve. The irradiated crystals show qualitatively the same temperature dependence of the work-hardening rate, slip bands, and cross slip between slip band fragments as unirradiated crystals. Stage III is preceded by a stage of constant and temperature independent rate of work-hardening, the reciprocal length of active slip lines varying linearly with stress or strain. Both the work-hardening rate and the length of the slip lines are smaller than in stage II of the unirradiated crystals, although the general appearance of the slip pattern in the electron microscope resembles the structurized fine slip of the unirradiated crystals.

The largest differences between irradiated and un-irradiated crystals are found at small deformations. We confirmed the result of previous authors that the critical shear stress τ_0 increases strongly with decreasing temperature, and that it is followed by a region of jerky flow without an increase in the average flow stress. This region is the more pronounced the lower the temperature. The deformation occurs by the migration of two Lüders bands starting from the grips. The Lüders strain increases markedly with decreasing temperature. The front between the strained and the unstrained portions of the crystals is less sharp at lower temperatures, where it may even appear that the crystal is gradually filled with clusters of slip lines, each cluster containing about 50

lines. Slip in the cross slip system similar to that in the Lüders bands of α-brass is found with a frequency increasing with temperature.

From the temperature dependence and the recovery characteristics of τ_0 it is concluded that the radiation hardening is mainly due to extended defects generated by the neutron bombardment and not due to point defects. The work-hardening and slip line characteristics have to be interpreted in terms of the gradual reduction of the radiation hardening by the deformation and the build-up of internal stresses due to the normal work-hardening process.

S2·76. The interaction between dislocations and irradiation-induced defects in metals.
By A. SOSIN, *Atomics International, Canoga Park, California, U.S.A.*

Since irradiation is an excellent method of introducing known concentrations of various point defects, irradiation studies should be valuable in the study of the interaction between dislocations and point defects in metals. Although a relatively large amount of attention has been directed toward an establishment of the possible mechanisms of radiation damage and recovery, only a small amount of this work is useful in advancing our understanding of dislocation-point defect interaction. Most of the pertinent data in this area comes from measurements of internal friction, elastic moduli, and critical shear stress. The large amount of resistivity data serves mainly to complement the above measurements.

A review is made here of the available information in this area. Account is also made of other, non-irradiation experiments which bear 'on the subject. The following general statements are inferred.

(1) All types of point defects are capable of pinning dislocations.

(2) The strength of the pinning interaction is dependent on the type of dislocation. Both dislocation orientation and extension are probably important.

(3) The importance of point defects in pinning dislocations is limited to low stresses.

(4) The hardening of metals produced by neutron irradiation is not primarily due to point defects. Displacement spikes or zones are the most probable cause of neutron-hardening.

(5) Dislocations act both as sinks and traps for point defects.

S2·77. The nature of radiation induced dislocation loops in copper.
By R. S. BARNES & D. J. MAZEY, *Atomic Energy Research Establishment, Metallurgy Division, Building 393, Harwell, Berkshire, England.*

Dislocation loops formed by the clustering of point defects have been studied in copper foils which have been bombarded with 38 MeV. alpha-particles. The foils through which the alpha-particles have passed contained clusters which annealed differently from those contained in the foil in which the alpha-particles came to rest. The helium atoms contained in this latter foil take vacancies from the clusters during heating and form helium bubbles in the metal permitting the nature of the irradiation induced clusters to be inferred.

S2·78. Radiation damage by nuclear fission in uranium steel. By A. J. BAKER & J. NUTTING, *Department of Metallurgy, Cambridge University, Cambridge, England.*

In order to study the effect of radiation damage in steel a small quantity of enriched uranium has been alloyed with a low carbon steel and the alloy irradiated in a fast neutron flux. This method enables large amounts of damage to be produced in the material by fission fragments after relatively short irradiation times.

The damage has been observed directly by transmission electron microscopy of thin foils of the irradiated material. From these observations it is possible to draw some conclusions on the influence of radiation damage on the physical properties of steel and to contrast the effects of damage due to neutrons alone and a combination of neutrons and fission fragments.

S2·79. Studies of radiation damage in graphite. By G. K. WILLIAMSON,* *Berkeley Nuclear Laboratories* and C. BAKER, *Department of Metallurgy, Cambridge University, Cambridge, England.*

Irradiation damage produces a spectacular rise in the elastic moduli of polycrystalline graphite. Studies are in progress, using transmission electron microscopy and mechanical testing of single crystals, which will test whether these effects are due to the pinning of the dislocations by point imperfections. These results, and possible interpretations, will be given in the paper.

S2·80. Observation of lattice defects and irradiation effects in graphite. By FRANCISCO EIICHI FUJITA & KAZUHIKO IZUI, *Japan Atomic Energy Research Institute, Tokai-mura, Ibaraki, Japan.*

By using the electron microscope with resolution of about 10 Å, lattice defects inherent and irradiation induced in graphite crystals were directly observed. Dislocations are created, move and form subboundaries or networks as those observed in metal crystals. Especially, from the analysis of disturbances in moiré patterns due to the dislocations lying in basal planes, their Burgers vectors can be determined. The analysis predicts the existence of half dislocations, which are actually observed as paired partials. Although extra terminating half lines in moiré patterns are sometimes observed, most of them are the so-called ghosts. Nevertheless, there are a few examples which seem to indicate the real existence of edge dislocations lying in the c-direction in graphite crystal which are very difficult to consider in the weakly interacting layer structure of graphite. Moiré pattern is also very useful to see the irradiation effects in graphite. The crystals irradiated by fission fragments from U^{235} exhibit small localized disturbances in moiré patterns which may be the highly imperfect areas or possibly be the temperature spiked regions. It is possible as well to see the traces of fission fragments in the crystals as the straight lines with contrast different from that of the matrix and sometimes apparently as the straight narrow recrystallized regions. Moiré patterns are found even in artificial graphite of reactor grade. But, they are very

rare and highly disturbed, corresponding to the fact that artificial graphite is far from the complete graphitization or is very imperfect. Neutron irradiation to the total flux of 10^{20} *nvt* thoroughly extinguishes the moiré patterns.

To be published in *J. Phys. Soc. Jap.*

S2·81. The yield strength of alloys. By A. KELLY, *Department of Metallurgy, University of Cambridge, Cambridge, England.*

Many ideas have been proposed to account for the values of the stress at which alloy crystals yield in a tensile test. These are such things as segregation of solute atoms at a dislocation, long and short range order, variation of lattice parameter in solute enriched regions, internal stresses etc. They can be conveniently classified into those interacting with dislocations over long distances in the crystals and interaction of a short range nature. The problem is to decide on the particular effects of importance in any given alloy system. Measurements of the temperature dependences of the flow stress can in some cases be used to separate the various effects in much the same way as short and long range interactions between dislocations are distinguished during work-hardening of pure metals.

In many precipitation hardening systems the dislocations are known to pass through precipitates and in some cases the short range effects can be calculated. The same is true of alloys showing short range order in which short range order coefficients have been obtained from X-ray measurements. Aluminium base precipitation hardening alloys have been extensively studied and in these a fairly clear picture can be obtained of the relative importance of the various effects.

S2·82. The interaction between dislocations and the ordered lattice in CuAu. By D. W. PASHLEY & A. E. B. PRESLAND, *T.I. Research Laboratories, Hinxton Hall, Cambridge, England.*

The movement of dislocations in a crystal grain of ordered CuAu is influenced by the following factors which are specific to the ordered lattice: (1) two-thirds of the grown-in dislocations are joined together in pairs by ribbons of anti-phase boundary, which will be extended when one of the terminating dislocations moves; (2) all moving dislocations must repeatedly cut through existing anti-phase boundaries, often producing jogs in them; (3) the ordered structure is tetragonal, and the direction of the $[001]_{ordered}$ axis changes frequently from one $\langle 100 \rangle_{disordered}$ direction to another, to form a lamellar structure. This gives rise, at the interface between the lamellae, to lattice strain and discontinuities in the slip planes.

The effect of these on the mechanical behaviour of the alloy is being investigated by studying CuAu foil deformed in tension. The foil is thinned electrochemically and examined by transmission electron microscopy. In addition, suitable thin specimens are deformed inside the electron microscope, and the resulting dislocation motion observed directly.

The results of these experiments will be described and discussed in relation to the mechanical properties of CuAu.

---

* At present at Department of Metallurgy, Cambridge University, Cambridge, England.

S2·83. Dislocation arrays in ordered alloys. By M. J. MARCINKOWSKI, U.S. Steel Research Center, Monroeville, Pa., U.S.A., N. BROWN, Ford Scientific Laboratory, Detroit, Michingan, U.S.A. and R. M. FISHER, Department of Metallurgy, Univ. of Cambridge, Cambridge, England.

Single dislocations moving through an ordered lattice would leave a strip of disordered material in an antiphase boundary in their wake. The large amount of energy required for this process is greatly reduced if the dislocations move as coupled pairs rather than as individuals. The equilibrium separation between the pairs has been analyzed theoretically for ordered $AuCu_3$ ($L1_2$ structure) and predicted to be 111 Å for pure edge ($0°$) dislocations and 179 Å for near screw ($60°$) dislocations. The mutual attraction due to the strip of antiphase boundary between the two extended dislocations tends to compress the stacking faults. In the disordered alloy, the stacking fault ribbon widths are 10·6 Å and 20·5 Å for the $0°$ and $60°$ orientations, whereas in ordered $AuCu_3$ they are reduced to 9 Å and 11 Å. Electron microscopic observations on deformed samples of ordered alloys of $AuCu_3$ and Ni_3Mn show that the dislocations do occur as pairs and that the spacing is in good agreement with the predicted values. The dislocations remain grouped as pairs in low density pile-ups and when severely jogged by intersections with other dislocations during deformation.

To be published in Acta Metallurg.

S2·84. Order and precipitation hardening in an austenitic steel. By M. J. BLACKBURN & J. NUTTING, Department of Metallurgy, Cambridge University, Cambridge, England.

A steel containing 24% Ni, 15% Cr, and 3·5% Al has been solution treated and then aged. Changes in hardness occur and these are found to be associated with an initial ordering within the matrix followed by the formation of a precipitate. The ordered structure and precipitated phases have been examined by transmission electron microscopy, electron diffraction and X-ray diffraction.

S2·85. Dislocation generation by precipitates and their significance on the creep resistance of austenitic alloys steels. By J. M. ARROWSMITH & J. NUTTING, Department of Metallurgy, Cambridge University, Cambridge, England.

Thermal contraction stresses around large niobium carbide particles are considered to be responsible for the generation of dislocations in an alloy steel on cooling it from below the solidus temperature. During subsequent ageing, these dislocations are the only sites in the matrix for precipitation. This mode of precipitation is considered to be largely responsible for the high creep resistance of austenitic alloys containing niobium.

To be published in J. Iron Steel Inst.

S2·86. Martensitic transformations and lattice defects. By T. A. READ, Department of Mining and Metallurgical Engineering, University of Illinois, Urbana, Illinois, U.S.A.

Lattice defects are of interest in connection with martensitic transformations in two ways. First, they are presumably responsible for the initiation of martensite formation at certain preferred sites in the lattice. Second, lattice defects are generated or multiplied during martensitic transformation; the product lattice is always less perfect than the parent lattice unless some annealing process is allowed to intervene. Recent results bearing on these two aspects of the rôle of lattice defects in transformations will be surveyed.

S2·87. Plasticity of metals undergoing polymorphic transformations. By T. A. READ, Department of Mining and Metallurgical Engineering, University of Illinois, Urbana, Illinois, U.S.A.

It has long been known that iron and certain iron alloys exhibit a lower resistance to deformation in the temperature range of the alpha–gamma transformation than they do at lower or higher temperatures. This effect was dramatically illustrated by Sauveur, who twisted iron bars of square cross-section held in a temperature gradient. Some authors have suggested that this behavior may be associated with polymorphic transformations in general. The necessity of considering the crystallographic features of a particular transformation will be pointed out. The essential distinction is between (a) those transformations for which the crystallographic symmetry of the product phase differs from that of the parent phase only by the disappearance of some of the symmetry elements of the latter and (b) transformations for which disappearance of symmetry elements is coupled with the appearance of other new symmetry elements. An example of type (a) is the cubic-tetragonal transformation in indium-thallium alloys. Examples of (b) are the f.c.c.–b.c.c. transformation, as in iron, and the b.c.c.–h.c.p. transformations. The effects of an applied shear stress on a complete cycle of transformation will be discussed for each type.

S2·88. The generalized theory of the martensitic cubic to orthorhombic phase transformation. By M. S. WECHSLER, Solid State Division, Oak Ridge National Laboratory,* Oak Ridge, Tennessee, U.S.A. and H. M. OTTE, RIAS, 7212 Bellona Avenue, Baltimore 12, Maryland, U.S.A.

The crystallographic theory of the martensitic cubic-orthorhombic phase transformation is described in terms of a generalized lattice invariant shear, G. The complexity of the analysis depends chiefly upon k_g, the direction mutually perpendicular to the shear direction, i_g, and the shear plane normal, j_g. When k_g coincides with one of the axes of the pure lattice distortion, T, considerable simplification occurs and the normal to the undistorted planes may be expressed as explicit functions of the lattice parameters and an isotropic dilatation, $δ$. The expressions obtained are more general than those derived

---

* Oak Ridge National Laboratory is operated by Union Carbide Corporation for the U. S. Atomic Energy Commission.

by Christian (1955) and include his solutions as special cases.

For a given set of i_g, j_g, and k_g, there are, in general, four distinct (non-crystallographically-equivalent) solutions. Two types of degeneracy, K-degeneracy and g-degeneracy, may occur to reduce the number of distinct solutions to two or one. The conditions for these degeneracies are discussed. K-degeneracy pertains when k_g coincides with one of the axes of T and is a two-fold or four-fold axis of symmetry in the cubic system. When the shear elements are rational, g-degeneracy results when either i_g of j_g coincides with one of the axes of T and is a direction of two-fold or four-fold symmetry in the cubic system.

The conditions for the existence of a solution are analyzed for the case where k_g coincides with one of the axes (the r-axis) of T. A necessary condition for the existence of a solution is that the pure distortions, ξ_c, ξ_s, ξ_t be such that $(\xi_r^2 - 1)$ and $(\xi_s^2 \xi^2 - 1)$ do not have the same sign. Thus, one of the three factors $(\xi_i^2 - 1)$, $i = r, s, t$, must differ in sign from the other two. When $(\xi_r^2 - 1)$ bears the unique sign, the above condition is sufficient. But, when $(\xi_r^2 - 1)$ does not bear the unique sign, a second condition is derived, which must be satisfied in order that there be a solution.

Submitted to *Acta Metallurg*.

S2·89. The hardness of martensite. By P. M. KELLY, *Department of Metallurgy, University of Cambridge, Cambridge, England*.

Thin foils of martensitic steels have been prepared from bulk material and examined by transmission electron microscopy. In high carbon steels and iron–nickel alloys the martensite was found to consist of plate-like grains internally twinned on a fine scale (the average twin spacing was about 100 Å) while no evidence of twinning was found in the needles of martensite in low carbon steels. This fine internal structure has been considered as responsible, at least in part, for the high hardness of martensite, while an explanation of the variation of the hardness of quenched steels with carbon content has been based on the change of morphology of martensite from the low carbon needles to the internally twinned plates found at high carbon contents.

S2·90. Some experimental evidence regarding dislocations and the martensitic transformation in 18Cr–8Ni steel. By R. P. REED & R. L. GREESON, *Cryogenic Engineering Laboratory, National Bureau of Standards, Boulder, Colorado, U.S.A.*

A dislocation etch pit technique has been developed for austenitic stainless steels (18 Cr–8 Ni). At low temperatures (below approximately 150 °K.) these steels partially transform to a martensitic structure.

Some investigators have predicted that the martensitic transformation must proceed by a dislocation mechanism. Therefore, the etch pit technique was used to examine dislocation positions in the austenite prior to the trans-

formation and to examine dislocation positions in the austenite resulting from the martensitic transformation. This paper will present these result.

Probably to be published in *Acta Metallurg*.

S2·91. The martensite transformation in stainless steel. By J. A. VENABLES, *Crystallographic Laboratory, Cavendish Laboratory, Cambridge, England*.

Thin foils of an austenitic stainless steel (18% Cr, 8% Ni) have been observed by transmission electron microscopy. Specimens strained up to 5% in tension at 77 °K. contained platelets of the ε (h.c.p.) phase, the thickness of the platelets depending on strain. Above a certain thickness all such platelets had the α' (b.c.t.) structure, with both {111} and {522} habit planes. Further experiments on straining at low temperatures followed by annealing in the range 300–500 °C. also suggested that the reaction takes place in the sequence

$$\gamma \quad \to \quad \varepsilon \quad \to \quad \alpha'$$
$$\text{f. c. c.} \qquad \text{h. c. p.} \qquad \text{b. c. t.}$$
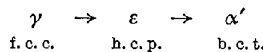
and that the reaction $\varepsilon \to \alpha'$ is thermally activated.

S2·92. Recovery and recrystallization. By K. LÜCKE, *Technische Hochschule, Aachen, Deutschland*.

Withdrawn.

S2·93. Recovery and recrystallisation in polycrystalline silver. By J. E. BAILEY, *Crystallographic Laboratory, Cavendish Laboratory, Cambridge, England*.

The annealing processes occurring in cold worked polycrystalline silver have been investigated using the transmission electron microscopy technique.

Stored energy measurements show that two annealing stages occur in silver deformed 25% in tension, a recovery stage followed by recrystallization. During the recovery stage there is no observable change in dislocation distribution but there is a possiblity of small scale re-arrangement within the cell boundaries. Recrystallization occurs by the migration of the grain boundaries present in the metal and this process is discussed in some detail.

Observations on heavily rolled silver foil (95% reduction) show that subgrains form prior to recrystallization. Although recrystallization occurs by the migration of high angle boundaries, it is not clear whether the moving boundaries formed part of the original grain boundaries or of subgrain boundaries produced during the deformation or during annealing. The distinction between these two mechanisms may be trivial, since in the heavily rolled silver the misorientations across subgrain boundaries are large.

Observations on heavily rolled silver (95% reduction) using a heating stage in the electron microscope showed

that thin foils (~ 1000 Å) behaved differently to the bulk material. The foils did not recrystallize at the same temperature as the bulk material; instead subgrain formation and some growth was observed over a wide range of temperatures.

To be published in *Phil. Mag.*

S2·94. Recrystallization and grain growth in a titanium 10% molybdenum. By T. H. Schofield & A. E. Bacon, *National Physical Laboratory, Teddington, Middlesex, England.*

The distribution of dislocations in a titanium 10% molybdenum alloy after cold deformation and annealing has been studied using a decoration technique to reveal the dislocation sites. The technique has been previously described (*Acta Met.* (1959), **7**, 403) and depends on heating the alloy in the β phase field followed by cooling at a fairly critical rate.

Specimens have been deformed at various degrees of strain by cold rolling between 4 and 80% reduction and subsequently reheating for increasing periods in the β phase field followed by cooling at the critical rate.

In lightly deformed material recrystallization begins at the comparatively few points of high strain that occur at the intersection of deformation bands. At the same time sub-grains are formed in the lesser strained regions; the size of the sub-grains also seems to depend on the degree of strain and is smaller for higher strains. The new crystals grow preferentially along the deformation bands but also gradually absorb the surrounding sub-grains; islands of sub-grains may remain however even after prolonged annealing if the initial strain is slight. As growth proceeds dislocations appear to segregate into closely spaced arrays at some of the advancing boundaries.

After high degrees of deformation and very short heating periods the microstructure shows a partly ordered network (mesh size $\sim 0·3\mu$) that probably indicates the recovery stage. Further slight heating results in the nucleation of numerous new crystals scattered at many points. The new crystals grow rapidly and consume the surrounding network and the remaining dislocations are again accommodated in arrays at the boundaries.

Continued heating results in further growth and it appears that during this process some dislocations are removed by interaction of the arrays at intersecting boundaries. Even after prolonged heating however some arrays remain.

The phenomena in general resemble those occurring during the reheating of deformed iron as revealed by electron microscopy.

Probable publication: *Acta Metallurg.*

S2·95. Growth processes and substructure in the recrystallization of pure and impure aluminum. By S. Weissmann, T. Imura & Y. Nakayama, *Materials*

Research Laboratory, College of Engineering, Rutgers. The State University, New Brunswick, New Jersey, U.S.A.

Using the combined techniques of light and X-ray reflection microscopy, as well as diffraction analysis based on the double-crystal diffractometer method, it was observed that the recrystallized grains of pure and impure aluminum incur lattice defects during the growth process.

The lattice defects were studied as a function of prior cold-working. Comparing grains of the same size, the grains of the weakly deformed pure aluminum specimens (2% and 6%) exhibited single-peaked rocking curves with halfwidth values of the order of $1·5'–3'$ of arc, whereas the grains of the strongly deformed specimens (81% deformation) often exhibited multi-peaked intensity distribution curves indicative of extensive substructure. The disorientation angles of adjacent macroscopic subgrains in the latter specimens sometimes reached values of the order of $\frac{1}{2}°$ and the lattice misalignment within these subgrains expressed in terms of their rocking curve halfwidth was of the order of $10'$ of arc.

The formation of lattice defects during the growth process resulting from grain impingement and adaptation in orientation could be qualitatively shown by X-ray reflection micrography through extinction contrast and quantitatively expressed by the increased halfwidths of the rocking curves.

Paper to be submitted to the *Trans. Amer. Soc. Met.*

S2·96. The roll textures of the aluminium single crystal plates and the recrystallization. By Takeo Fujiwara & Yasumasa Takano, *Laboratory of Crystal Physics, Faculty of Science, Hiroshima University, Hiroshima City, Japan.*

The roll textures of micro-crystals produced in the single crystal plates through rolling done them always along the lengthwise direction, were examined by means of X-rays about the eight kinds of specimens having the particular crystallographic orientation. And the recrystallization of these rolled plates at various stages of rolling was also studied by means of X-rays and microscopical observation.

It can be pointed out that the single crystal, as its rolling proceeds, is destroyed into aggregates of microcrystals, and they are respectively arranged symmetrically around three different directions (axes) which are crossed almost perpendicularly to each other, but have changed the manner of their arrangements accordingly to each direction, and are also related to the main plate axes of the original single crystal. Concerning the manners of destruction and settlement of the roll texture and the relation between the main plate axes of the original single crystal and the axes of the new created fibre texture each original crystallographic orientation of the specimen has its own characteristic variation.

In particular, it has been found that in each case of single crystal plates [001]–(110), [1$\bar{1}$0]–(110) and [$\bar{1}$12]–(110), as to the fibre axes of the roll texture, they remain the same with those of the original plate axes in spite

of the rolling; and that concerning the distribution range of the orientation of micro-crystals, they make the largest variation in both the specimens [001]–(110) and [1$\bar{1}$0]–(110), and it is least in the specimen [112]–(110).

The manners of recrystallization, are differed according to the original crystallographic orientation of the single crystal plate.

S2·97. The rôle of grain boundary motion in the last stage of sintering. By J. HORNSTRA & H. G. VAN BUEREN, *Philips Research Laboratories, Eindhoven, The Netherlands.*

In many technically important metallurgical processes, such as sintering, recrystallization and grain growth, diffusion of vacancies to grain boundaries (G.B.) takes place. The vacancies, being absorbed at the boundaries, provide a driving force for the motion of the latter, as will be shown for the case of the disappearance of isolated pores in the last stages of sintering. Here the driving force of the diffusion is the surface energy of the pores. If the grains cannot slide along the G.B., the rate of precipitation has to be uniform over the entire area of the G.B., otherwise elastic stresses normal to the G.B. will be formed, and these will cause the rate of precipitation to become uniform (H. G. van Bueren & J. Hornstra, 4th International Symposium on the Reactivity of Solids, Amsterdam 1960). Diffusion of vacancies along the G.B. is not fast enough to eliminate these stresses. If the G.B. (e.g. an asymmetric tilt-boundary) allows sliding of the grains along it and is able to migrate side-ways, it will change its form in such a way as to allow a non-uniform rate of precipitation. In the latter case the vacancies have to diffuse a shorter distance and hence sintering is faster than in the former case.

This sliding may be caused by an external shear stress but also by the stresses that arise from the non-uniform rate of precipitation. The mechanism of these processes will be discussed and different types of G.B. will be considered. Use will be made of the dislocation model of a G.B. because it has been shown that in certain lattices dislocation models may be constructed even for large-angle grain-boundaries (J. Hornstra, *Physica* (1959), **25**, 409).

The paper will probably be published in *Physica.*

Abstracts of Supplementary Papers

This supplement contains: (a) Abstracts of contributed papers (included in the published Congress Programme) received too late for printing in the Collected Abstracts issued to members. (b) Abstracts of contributed papers received too late for inclusion in the published Congress Programme.

Supplementary Abstracts (a)

9·3. The short-range order and the Debye temperature of the alloy Ni_3Pt. By V. I. IVERONOVA & A. A. KAZNELSON.

1. The short-range order of the hardened alloy Ni_3Pt was measured by means of diffuse X-ray scattering. It was shown that independently of the temperature of hardening the parameter of short-range order of the first shell (α_1)-negative and of the second shell (α_2)-positive. This fact means the augmentation of the number of different-signed pairs in comparison with the statistic disordered distribution.

2. The temperature dependence of the parameters of short-range order has been studied. It was shown that in the range of temperature 700–1050 °C. the absolute value of the parameter α_1 is decreasing and the absolute value of the parameter α_2 is increasing. As a result the exceeding number of Ni atoms (comparing with the disordered state) on the first two shells surrounding the atom of Pt quickly decreases approaching zero at $t = 1050$ °C. whereas the parameter α_1 essentially differs from zero ($\alpha_1 = -0·130$). This means that the dimensions of the concentrated unhomogenities decrease with the temperature more rapidly than the number of the nearest neighbours of the type AB.

3. The kinetic of establishment of the short-range order during the annealing by $t = 700$ °C. in previously strained samples has been studied. It was shown that in this case the rate of approach to the equilibrium of the parameters α_1 and α_2 essentially differs one from another. Hence the number of Ni atoms on both first shells surrounding Pt atom passes through the maximum. The parameters of short-range order of the samples hardened at $t = 1050$ °C. and annealed at $t = 700$ °C. slowly approach the data α_1 and α_2 obtained on the samples previously plastically strained and then annealed at $t = 700$ °C. The surplus of atoms Ni on the first two shells change monotonously without passing through a maximum.

4. Together with the measurements of the parameters of the short-range order on the same samples were carried out X-ray measurements of the Debye temperature Θ. The coincidence between the change of number of exceeding Ni atoms on both first shells and the change of the Debye temperature of heat treated samples is shown. The Debye temperature as well as the number of Ni atoms on both first shells pass through the maximum for short-term annealed (1 hr. at $t = 700$ °C.) and previously strained samples.

Such changes of parameters of short-range order and the Debye-temperature may be explained by the specifically concentrated micro-unhomogenities occurring during the annealing of alloy saturated with dislocations.

10·19. The influence of the stacking-faults on the intensity of the Debye-Scherrer lines. By V. I. IVERONOVA, I. I. POPOVA & G. P. REVKEVITCH.

1. A. J. C. Wilson & B. E. Warren showed in their investigations that the integral intensity of the selective reflections does not change in the presence of the stacking faults. Their calculations are carried out by integrating all the energy scattered, i.e. the background intensity is added to intensities of the lines. However, experimentally the line intensities are measured over certain level of background. If this is taken into consideration, it is obvious, that the presence of stacking faults should lead to the decrease of the measurable integral line intensities.

2. We experimentally confirmed the decrease of line intensities and the increase of background intensity for the samples of metal filings (for Cu, α-brass (f.c.c.) and β-brass (b.c.c.)). The intensity of the most broadening lines is the weakest. It is for these lines that the structure factor has changed the most of all.

3. The probability of stacking faults distribution obtained from intensity measurements was compared with that obtained from the line broadening measurements. This was done for β-brass specimens.

Supplementary Abstracts (b)

1(i)·X·1. Chambre de poudre à très haute température. PAR F. FOURNIER & A. RIMSKY, 8 *bis rue des Jardies Meudon-Set O, France.*

L'appareil consiste essentiellement en une enceinte sphérique où règne un vide élevé dont un grand cercle est constitué par une fenêtre cylindrique en béryllium destinée au passage des rayons X.

Au centre de la Sphère est disposé un support qui peut entraîner la préparation d'un mouvement de rotation continu. Cet ensemble est entouré d'un miroir réflecteur sphérique, qui l'isole thermiquement.

Sous la préparation est disposé un canon électronique qui bombarde cette dernière et permet de la porter à haute température. Il est possible, ainsi, de monter à 3000 °C. en moins de 15 sec.

A l'extérieur un cylindre enveloppe l'enceinte et porte le film qui enregistre les diffractions sélectives.

Ce film peut se déplacer corrélativement à un programme de chauffe défini.

1(ii)·X·1. X-ray determination of electron distribution and physical properties of some crystals of diamond, zincblende-types and its change by phase transformation. By N. N. SIROTA, *Institute of Solid State and Semiconductors Ac, Sci. BSSR USSR, Minsk, Podlesnaja 25.*

No abstract provided.

2·X·1. Some quantitative evaluations for the Patterson function. By S. V. BORISOV & V. V. ILJUKHIN, *Institute of Inorganic Chemistry, Sovietskaja street, 20, Novosibirsk, USSR.*

The method of computing of the integral characteristics which was developed for the electron-density function has been used for evaluation of the magnitudes and shapes of Patterson peaks and also for determination of the

influence of the atomic thermal vibrations in crystals. The Patterson function

$$P(\mathbf{r}) = (1/V)\Sigma\Sigma\Sigma F_{\mathbf{H}}F_{\mathbf{H}}^{*} \cos 2\pi(\mathbf{r}.\mathbf{H})$$

is being interpreted as the electron-density function of the structure with structure amplitudes:

$$\Phi_{\mathbf{H}} = F_{\mathbf{H}}\cdot F_{\mathbf{H}}^{*} = \sum_{k=1}^{N} f_k^2 + \sum_{k \neq j} f_k f_j \exp 2\pi i(\mathbf{H}., \mathbf{r}_k - \mathbf{r}_j) .$$

The heighth of the three-dimensional Patterson peak due to the pair of atoms k and j may be found from

$$P_{kj}(0) = \frac{1}{2\pi^2}\int_0^{\infty} f_k(S)f_j(S)S^2 dS \approx \frac{1}{2\pi^2}\sum_{n=0}^{n_{max}} f_k(S_n)f_j(S_n)S_n^2 \Delta S_n .$$

In the process of the peak shape's determination the following integral is approximately computed for the range of values near the maximum.

$$P_{kj}(r) = \frac{1}{2\pi^2}\int_0^{\infty} f_k(S)f_j(S)S^2 \frac{\sin (Sr)}{(Sr)} dS$$

$$\approx \frac{1}{2\pi^2}\sum_{n=0}^{n_{max}} f_k(S_n)f_j(S_n)S_n^2 \frac{\sin (S_n r)}{(S_n r)} \Delta S_n .$$

In the same way it is possible to determine the height and the shape of the two-dimensional Patterson peaks. The fairly good agreement between calculated and observed values (the discrepancy less than 10%) obtained for the three-dimensional Patterson function of Zr-silicate-lovozezite is illustrated in a number of corresponding graphs. The influence of thermal vibration and the methods of introducing corresponding corrections are discussed.

2·X·2. ПРОЕКЦИИ ВЗВЕШЕННОЙ ЭЛЕКТРОННОЙ ПЛОТНОСТИ В СТРУКТУРНОМ АНАЛИЗЕ КРИСТАЛЛОВ. *И. М. Руманова. Institute of Crystallography, Academy of Sciences of USSR, Pyzhevskii per 3, Moscow, USSR.*

Предложены проекции взвешенной электронной плотности

$$\int_0^c \varrho(x, y, z)f(z)dz = \sum_h \sum_k \sum_l^{\infty} \left[A'_{hkl} \cos 2\pi \left(\frac{hx}{a} + \frac{ky}{b}\right) \right.$$
$$\left. + B'_{hkl} \sin 2\pi \left(\frac{hx}{a} + \frac{ky}{b}\right) \right],$$

для которых коэфициенты разложения Фурье быстро убывают с увеличением индекса l. Для их построения требуется значительно меньший объем эксперимента и вычислений, чем для синтеза трехмерного распределения электронной плотности и обычных поясных проекций Фурье.

Обычные взвешенные проекции электронной плотности

$$\sigma_l(x, y) = \int_0^c \varrho(x, y, z) \exp \frac{2\pi i l z}{c} dz$$

служат »кирпичами«, из которых затем »собираются« более сложные проекции. В связи с этим для практической работы рассмотрена и протабулирована симметрия обычных взвешенных проекций электронной плотности для пространственных групп симметрии.

Выведены формулы разложения Фурье для каждой плоской группы симметрии взвешенных проекций и указаны коэфициенты разложения для всех возможных проекций.

3·X·1. The crystal structure of brandisit. By S. C, Mamedov, *Institute of Chemistry, Tolstoj street, 142, Baku, USSR.*

No abstract provided.

3·X·2. The electron diffraction refinement of the structure of muscovite. By B. B. Zvjagin.

No abstract provided.

5·X·1. The crystal chemistry of complex compounds of metals of group VIII. By G. B. Bokii & M. A. Poraj-Koshits, *Academy of Sciences, USSR.*

1. The central position of elements of group VIII of the Periodic Table in the chemistry of complex compounds. Main properties (parameters) characterizing the elements of group VIII: atomic and ionic radii; main valency typical of complex compounds; electronic state of free and chemically bonded atoms; magnetic state (spin-bonded and spin-free complex compounds).

2. General features of octahedral compound structures. Analogy in the structures of compounds of elements of group VIII having different valencies but identical electron composition. Changes in structural types resulting from changes in the metric relations between outer-spheric and complex ions.

Peculiarities in the structures of metals of the first triad. Differences in the structures of high-spin complex compounds of cobalt and nickel. Chain structures of the composition MeA_2X_2.

3. The crystal chemistry and stereochemistry of complex compounds of square and distorted octahedral coordinations. Structure, properties and typical addenda of compounds of planar coordination (Pt, Pd, Ni). The rôle of isomorphism as the qualitative criterion of coordination. Dimeric Pd and Pt compounds. The effect of trans-influence in crystals. Complex Pd and Pt compounds with three-centered bonds. Distorted octahedral coordination of Cu atoms. Distorted octahedral complexes in diamagnetic compounds of Ni, Pd and Pt.

4. Structure, properties and typical addenda of complex compounds of tetrahedral coordination. The special position of divalent cobalt, and isomerism of Co compounds of the composition CoA_2X_2.

5. The crystal chemistry of complex compounds with multiple bonds.

General features of complex compounds with multiple bonds. Their differences from ordinary complex compounds. Ruthenium compounds containing NO-group as an addendum. Osmium compounds containing oxygen and nitrogen atoms as addenda. Carbonyl compounds of metals.

Conclusion.

The full-length account of the paper is likely to be published in *Kristallografija*.

5·X·2. Crystal structures of two heteropoly salts: potassium 12-tungstocobaltiate, $K_5[CoW_{12}O_{40}]$. 20 H_2O and sodium 6 - tungstonickelate, $Na_4[NiW_6O_{24}H_6]$.16 H_2O. By KLAAS ERIKS, NICHOLAS F. YANNONI, UMESH C. AGARWALA, VIOLET E. SIMMONS & LOUIS C. W. BAKER, Boston University, Chemistry Department, Boston, Mass. USA.

The crystal structure of potassium 12-tungstocobaltiate, first prepared by L. C. W. Baker & T. P. McCutcheon (J. Amer. Chem. Soc. (1956), 78, 4503), has been determined. Bright yellow, well-formed hexagonal prisms were grown from aqueous solution for this work.

The unit cell is hexagonal with $a = b = 19\cdot11 \pm 0\cdot06$ and $c = 12\cdot56 \pm 0\cdot08$ Å, $Z = 3$, giving an X-ray density of 4·33 g.cm.$^{-3}$ as compared with 4·401 g.cm.$^{-3}$ determined pycnometrically. The space group is $P6_222$.

The structure of the anion resembles that of the 12-tungstophosphate anion described by J. F. Keggin (Proc. Roy. Soc. (1934), A, 144, 75). The twelve tungsten atoms in the anion are located at the corners of a slightly distorted cube-octahedron with the cobaltic ion at its center.

The most significant feature of the oxygen arrangement in the anion is that the cobaltic ion is surrounded by four oxygens at the vertices of a nearly regular tetrahedron. This is the first cobaltic compound to be reported in which the cobalt is located in a tetrahedral site.

The structure of the anion in 6-tungstonickelate was determined from the light blue crystals obtained from aqueous solution.

The unit cell in this case is triclinic with

$$a = 10\cdot55, \ b = 12\cdot14, \ c = 8\cdot00 \ \text{Å},$$
$$\alpha = 105°\ 4', \ \beta = 96°\ 23', \ \gamma = 107°\ 21'.$$

There is one molecule per cell, $d_c = 3\cdot54$ g.cm.$^{-3}$, $d_o = 3\cdot66$ g.cm.$^{-3}$. The space group is $P\bar{1}$.

The anion structure is identical to that of the molybdotellurate anion $[TeMo_6O_{24}]^{-6}$ determined by H. T. Evans (J. Amer. Chem. Soc. (1948), 70, 1291).

The interesting result of this determination is that three molecules of structural water are incorporated in the anion, a feature not previously observed in heteropoly compounds.

5·X·3. Structural studies on $Me_{6-4}^+ Me_{2-0}^{++} UO_2(CO_3)_3$ nH_2O compounds I. The crystal structure of $NaK_3UO_3(CO_3)_3$. By FIORENZO MAZZI & FRANCESCO RINALDI, Istituto di Mineralogia Università, Piazza S. Marco 4, Firenze (Italy).

$NaK_3UO_2(CO_3)_3$ crystals were obtained from aqueous solutions of UO_2-nitrate mixed with K- and Na-carbonates. The crystals are yellow in color with hexagonal prismatic habit.

The lattice constants are as follows: $a_0 = 9\cdot29$; $c_0 = 8\cdot26$ Å; the unit cell contains two formula units. The space group is $P\bar{6}2c$ from structural determinations. The X-ray studies were carried out by means of Weissenberg pictures along the c- and a-axes. The radiation was the filtered Cu $K\alpha$. The intensities were visually estimated, then corrected for the absorption according to the Grdenić formulas.

The electron-density projection along the [0001] axis is enough to obtain the x- and y-parameters of all the atoms. The z-parameters of almost all the atoms are

determined by the space group $(z = 0, \frac{1}{4}, \frac{1}{2}, \frac{3}{4})$; only the UO_2-oxygen atoms have different z-parameters.

According to the space group $P\bar{6}2c$, the atoms lie on the following positions:

2 U	c	$\bar{6}$		4 O(UO$_2$)	e	3
2 Na	d	$\bar{6}$		6 O	h	m
6 K	g	2		6 O	h	m
6 C	h	m		6 O	h	m

The uranium and sodium atoms have a ditrigonal dipyramidal coordination, whereas potassium has a trigonal prismatic coordination. Carbon atoms have an almost regular triangular coordination.

The full-length account will likely be published in Atti della Accademia Nazionale dei Lincei, Roma (Italy).

5·X·4. Die Kristallstruktur von Kupferacetat $Cu_2(CH_3COO)_4$.2 C_5H_5N. VON F. HANIC, D. ŠTEMPELOVÁ & K. HANICOVÁ, UNTER MITARBEIT VON T. VESELSKÁ, Institut für anorganische Chemie der Slovakischen Akademie der Wissenschaften in Bratislava, Lehrstuhl für anorganische und physikalische Chemie der Naturwissenschaftlichen Fakultät an der Komensky-Universität in Bratislava, Tschechoslovakei.

Kupferacetat $Cu_2(CH_3COO)_4$. 2 C_5H_5N kristallisiert rhombisch mit den Gitterkonstanten:

$$a = 13,21, \ b = 8,67, \ c = 19,77 \ \text{Å}$$

und mit einem Zellinhalt von 4 $Cu_2(CH_3COO)_4$.2 C_5H_5N. Die Raumgruppe ist $Pbca$. Die Struktur ist von den zweikernigen Komplexmolekülen $Cu_2(CH_3COO)_4$.2C_5H_5N aufgebaut, wobei für jede von diesen Molekülen eine Cu-Cu Bindung typisch ist. Ein Vergleich mit der Struktur von Kupferacetat–Hydrat (J. N. van Niekerk & F. R. L. Schoening, Acta Cryst. (1953), 6, 227) wird angegeben. Es wird über den Einfluss von Pyridinmolekülen auf die Struktur der Bindungsorbitale von Cu(II) diskutiert.

5·X·5. Crystal structure of baotite. By V. I. SIMONOV, Institute of Crystallography, Academy of Sciences of the USSR, 3 Pyzhevsky per Moscow 13–17, USSR.

Crystal structure of baotite (space group $I4_1/a$, dimensions of the unit cell: $a = 19\cdot68$, $c = 5\cdot88$ Å) has been established by the method of minimalization of Patterson projections. The final atomic coordinations resulted from several computing signs of reflexions alternating with Fourier syntheses. Baotite is a new example of ring silicate with a tetragonal radical $[Si_4O_{12}]$. The detailed formula of baotite is $Ba_4(Ti, Nb)_8ClO_{16}[Si_4O_{12}]$. The ring radicals $[Si_4O_{12}]$ are on the 4-fold inversion axes, and (Ti, Nb)-octahedra are around 4-fold screw axes in columns analogous to those in the structure of rutile.

Кристаллическая структура баотита (пространственная группа $I4_1/a$, параметры элементарной ячейки $a = 19,68$ Å, $c = 5,88$ Å) определена методом минимализации проекций функции Патерсона. Уточнение структуры проведено последовательным расчётом знаков структурных амплитуд и проекций электронной плотности. Баотит оказался кольчатым силикатом с кремнекислородным радикалом $[Si_4O_{12}]$. Развёрнутую химическую формулу баотита следует писать $Ba_4(Ti, Nb)_8ClO_{16}[Si_4O_{12}]$. Ради-

калы $[Si_4O_{12}]$ в баотите нанизаны на четверные инверсионные оси, а (Ti, Nb)-октаэдры расположены вокруг винтовых осей четвёртого порядка таким же образом, как Ti-октаэдры в структуре рутила.

6·X·1. The crystal structure of diphenyliodonium fluoroborate. By Ju. T. Struchkov & T. L. Khotsyanova, Institute of Organo-Element Compounds, Leninsky prosp. 31, Moscow, USSR.

The X-ray study was carried out by employing the procedure of oscillation and taking reciprocal lattice photographs (K Cu and K Mo radiation).

The coordinates of the atoms were determined by calculating two approximations of the triple series of the electron density (the total number of non-zero reflections being 1·509). The precision of determination of bond length is not worse than $\pm 0·03$ Å, that of valency angles $\pm 2°$.

The purely ionic structure of diphenyliodonium fluoroborate consists of sets of four ions (two cations $[(C_6H_5)_2I]^+$ and two anions BF_4^-), situated at the centres of symmetry $\frac{1}{2}, 0, 0$. Such sets are superimposed by translation a to form endless columns elongated along axis a, each column being surrounded by six other columns, with no ionic interaction between the columns. The packing coefficient of the structure $k = 0·66$. Cation $[(C_6H_5)_2I]^+$ has an angular configuration: $I–C = 2·02$, $C–C = 1·40$ Å; $\angle\ C_1–I–C_1' = 94°$. The angle between the plane C_1IC_1' and the plane of the benzene nucleus 1 is 92°, that between the plane C_1IC_1' and the plane of the benzene nucleus 2 being 30·5°. The increase in the valency angle C_1IC_1' as compared to the theoretical one (90°) as well as the mutual turning of benzene nuclei is accounted for by steric hindrances. Anion BF_4^- has an essentially non-distorted tetrahedral configuration: $B–F = 1·43$, $F–F = 2·34$ Å, $\angle\ F–B–F = 109·5°$. The van der Waals radii determined from the structure are as follows: C $-1·70$, H $-1·10$, F $-1·39$, I $-2·11$ Å.

The distances $I \cdots F$ 2·94, 2·96, 3·01, and 3·40 Å correspond to electrostatic attraction. The present work is one in the series of investigations that we are undertaking to study the crystals of diphenyl-halogen onium compounds of true ionic character.

6·X·2. On the theory of solid solutions of organic compounds.* By A. I. Kitaygorodsky & R. M. Myasnikova, Inst. of Organo-Element Compounds, Leninsky prosp. 31, Moscow, USSR.

In the middle 50's we started our systematic experimental and theoretical investigation of the solubility and structure of organic substances in solid state to obtain information on the interaction of molecules and thereby enlarge our knowledge of organic crystallization phenomena.

1. Solubility conditions

The geometrical conditions formulated previously for the mutual solubility of two organic substances can be convincingly expressed in terms of thermodynamics by stating the conditions of solubility as

---

$$T.\,|\Delta S_{conf.}| > \Delta U_{str.} + \Delta F_{vibr.}^{cryst.} + x(F_A^{cryst.} - F_B^{cryst.}) + x.\Delta E$$

that is, the configurational mixing effect must exceed the sum of the four terms such as (1) the strain energy, (2) the change in the free energy at the expense of the change of the vibrational spectrum of the crystal lattice, (3) the additive change in the crystal part of the free energy, and (4) the change in the energy of the conformation of the foreign molecule. These four factors determine the conditions of solubility. For the solubility conditions to be checked experimentally one must estimate (1) the strain energy—in terms of the change of the crystal cell volume and by means of the energy interaction curve of the non-bonded atoms, (2) the change of the vibrational molecular energy—by means of X-ray determination of the characteristic temperature, and (3) the difference in the free energies of components—by measuring the heat of sublimation.

The preliminary calculations have shown the suggested simple thermodynamic scheme to be in agreement with the experimental data.

2. The effective region of the foreign molecule

The foreign molecules by entering the cells of the solvent cause some distortion of the volume of the surrounding cells. One may logically assume this distortion to decrease from the 'centre' of perturbation in symmetrical spheres in terms of the distance r following the exponential law $\Delta V = \Delta V_m.e^{-\alpha r}$, with ΔV_m being the change in the volume of the cell that has incorporated a foreign molecule. For sufficiently low concentrations, when the mean distance between the foreign molecules 2ϱ exceeds the range of the action of a single molecule ($\varrho > r$) one can determine the mean value of the cell volume:

$$V_3 = V_0 + \frac{\Delta V_m}{\frac{4}{3}\pi\varrho^3} \int_0^\varrho \exp[-\alpha r].4\pi r^2 dr\,.$$

The value of α, referring to the rate with which the distortion decreases, is estimated from the experimental data and evidence obtained from the geometrical analysis of the acridine phase in the acridine–anthracene system. The calculations show that the action range of a foreign molecule $r \simeq 25$ Å, there being about 200 molecules (over 20 cells) in this effective region.

3. True and interblock solid solutions

The results of the precision determination of parameters of unit cells of monocrystals in solid solutions enable to distinguish in binary organic systems between two types of solid solutions: (1) true solid solutions, whose elementary cells considerably increase in volume, V_3, as the concentration of the admixtures (dibenzylstilbene, acridine–anthracene, para-di-chloro-benzene, para-di-bromo-benzene) is increased (2) interblock solid solutions, whose V_3 undergoes almost no change with the increase in the concentration.

As these solid solutions, being investigated as monocrystals, belong to one-phase system we are to assume that the foreign molecules should be situated at the block boundaries in some oriented way, such being the case with solid solutions of β-Cl-naphthalene in naphthalene and 1,8-di-nitro-naphthalene in 1,5-di-nitro-naphthalene.

6·X·3. Structure du cristal mixte NH₄Cl, C[NH₂]₂.

6·X·3. Structure du cristal mixte NH_4Cl, $C[NH_2]_2$. Par A. Rimsky.

Ce cristal, obtenu par l'évaporation d'une solution aqueuse saturée d'urée et de chlorure d'ammonium, appartient à l'holoédrie du système orthorhombique.

Les caractères cristallographiques, sont:

classe: m·m·m.-groupe: *Pcnm*, avec

$$a = 8{,}03, \quad b = 17{,}08, \quad c = 7{,}81 \text{ Å} .$$

8 molécules par maille de composition $[NH_4Cl, C(NH_2)_2]$. Densité $= 1{\cdot}40$ g.cm.$^{-3}$. Cristal biaxe positif.

La structure a été déduite de l'étude de 1200 réflexions sélectives indépendantes.

Il s'agit d'une structure ion dipôle, comportant deux chaînes ioniques $Cl \cdots NH_4$ indépendantes, et maintenues en place, par des molécules d'urée fortement polarisée.

L'ion ammonium est tétra coordonné.

Cette structure rappelle, les répartitions atomiques à la fois de l'urée et du chlorure d'ammonium.

6·X·4. The crystal structure of quaterrylene. By N. H. Shrivastava & J. S. Speakman, *Chemistry Department, The University, Glasgow, W. 2, England.*

The crystal structure of perylene (I) was reported from this department in 1953. The interesting feature of this structure was the two long peri-bonds (1·50 Å)

(I)   (II)
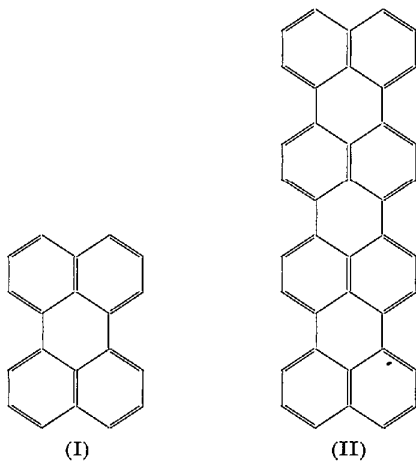
linking the two naphthalenic residues in this molecule. In quaterrylene (II) there are six such peri-bonds and a greater statistical significance would attach to the length obtainable from it. We have now completed the structure analysis of this compound by 2D X-ray methods. Although, difficulties similar to those encountered in perylene beset this analysis, we have been able to carry it to a stage of refinement further than that of perylene. The length we find (1·53 ± 0·01 Å) is greater than that currently accepted for this type of bond in this class of compounds. Possible explanations are considered.

A full account of this work will be published in *Proc. Roy.Soc.*

6·X·5. Possibilite d'existence d'une liaison hydrogene dans les chlorhydrates et bromhydrates

d'amines et d'aminoxydes. Par G. Tsoucaris, *Laboratoire de Cristallographie du C.N.R.S., Bellevue, France.*

Par analyse radiocristallographique et par spectrographie infrarouge, nous avons étudié les liaisons $N \cdots H \cdots Cl$ et $O \cdots H \cdots Cl$ dans les sels d'amines primaires $[RNH_3]^+X^-$, secondaires $[R_2NH_2]^+X^-$, tertiaires $[R_3NH]^+X^-$, ainsi que dans les sels d'aminoxydes $[R_3NOH]^+X^-$; les principaux résultats sont les suivants:

(a) La coordinence du chlore est égale au nombre d'hydrogènes mobiles.

(b) La distance N–Cl diminue régulièrement avec la coordinence; elle est de 3,35 Å pour le NH_4Cl (coordinence 8) et de 3,12 Å pour une amine secondaire (coordinence 2).

(c) Les spectres infrarouges des sels d'amines présentent des bandes d'absorption dans la région de 2000–3400 cm.$^{-1}$ qui sont absentes dans les spectres des amines, et dont les fréquences diminuent avec la coordinence.

Les résultats expérimentaux permettent d'envisager l'existence d'une liaison hydrogène pour les raisons suivantes:

(1) Les directions des vecteurs N–Cl et O–Cl observées coïncident approximativement avec celles qu'on peut prévoir pour les directions N–H et O–H:. Les groupes $N \cdots H \cdots Cl$ et $O \cdots H \cdots Cl$ sont pratiquement linéaires dans toutes les structures connues.

(2) Les distances N–Cl et O–Cl sont plus petites que la somme des rayons de van der Waals (de l'ordre de 3,3 Å et de 3,2 Å respectivement).

(3) Plusieurs faits indiquent que les bandes d'absorption larges ou multiples dans la région de 2000–3000 cm.$^{-1}$ peuvent être attribuées à une liaison hydrogène:

— La forme très élargie de certaines bandes.

— Le fait que les fréquences varient peu lorsque l'on remplace le Cl par un autre halogène.

— La constance relative de ces fréquences pour une série d'amines de formules chimiques voisines.

(4) On constate une corrélation entre la distance N–Cl et O–Cl et la fréquence correspondante.

Ainsi pour le triméthylaminoxyde $(CH_3)_3NO$ et le pyridinoxyde C_5H_5NO les distances O–Cl sont respectivement égales à 2,94 et à 2,84 Å et les fréquences à 2650 cm.$^{-1}$ et à 2000 cm.$^{-1}$.

7·X·1. Some diffractional principles of fibrous proteins structure classification. By N. S. Andreeva & V. I. Iveronova.

On the ground of recent chemical investigations it is possible to establish some new principles of fibrous proteins structural classification. This classification may also be found on their diffractional features. All fibrous proteins can be divided into two groups. One may include the proteins with chain configuration and packing mainly independent from sequence of amino acid residues along the chains. It may include all proteins with statistical or approximate statistical arrangement of various residues. To another group may belong those proteins which chain packing and configuration in crystalline parts is the consequence of the special arrangement of residues. It may be possible if some residues or more or less regular sequence of simple combination of several residues concentrate in certain parts of chains. The diffractional basis for such classification is the following:

1. Statistical arrangement of different side chains in proteins of the first group prevent regular azimuthal orientation and displacement (along fibre axis) of neighbouring chains, as well as regular displacement of layers in their β-modifications. Intensity distribution in reciprocal space for three schemes was calculated. As our calculations show such distortions of lattices predetermine the difference of intensity distribution for zero and non-zero layer lines (three-dimensional Laue function for zero layer line and two or unidimensional Laue function for non-zero layer lines).

2. Rather regular sequence of simple combination of residues in proteins of second group permit more regular packing of chains. The main feature of their wide angle X-ray pattern is the appearance of Laue maxima on non-zero layer lines.

To the first class belong all α-proteins. To the second fibroin silk and collagen. In crystalline parts of these proteins more or less regular sequence of simple combination of residues was found (gly-ala)n-fibroin silk Bombyx mori, (ala)n-silk Tussah, (gly-pro-hypro)n-collagen.

8·X·1. X-ray diffraction by systems of long molecules and one-dimensional X-ray diffraction of cellulose.* BY A. I. KITAYGORODSKY & D. YA. TSVANKIN, *The Institute of Organo-Element Compounds of the USSR Academy of Sciences, Moscow, USSR.*

The report deals with methods of calculating the intensity of scattering by groups of parallel macro molecules packed with a different degree of order.

I

1. Equations were deduced to calculate the diffraction intensity by a system of parallel macromolecules or packages forming the textures.

All packages were taken as equal and built up of chain molecules with axes parallel to that of the texture. Three alternative distributions of the macromolecules inside the packages were considered: (a) with a complete tri-dimensional order within each package, (b) with random azimuthal rotations of the chains about their axis, the shifts of the chains along the texture axis remaining regular, (c) with random shifts of the chains along the texture axis.

The second and third alternatives assume the chain centres in the equatorial plane as forming a regular two dimensional lattice.

For the first alternative the scattering intensity is represented as a series in terms of Bessel functions of different orders, in the second and third alternatives only the zero order Bessel functions being effective.

To make use of the formulas deduced it is necessary to have at one's disposal a set of all inter atomic distances in a cell of the chain, inter-chain distances in the equatorial plane, and the magnitudes of the relative shifts along the axis. Therefore, the calculations in terms of these formulas are tiresome and mostly useful with packages containing few chains.

2. If the distribution of the intensity in the case of the texture is known, it is easy to deduce the formulas for the scattering intensity by the isotropic system of the macro-

*Translated by A. L. Pumpiansky, Moscow.

molecular packages. The passing to the isotropic system is accompanied by the averaging of the intensity, this interval for averaging broadening with the decreasing chain length and increasing the number of the layer line. With a longer chain one must allow for the angle factor of a new type.

3. With the diffraction by a system of parallel chains, in some cases the intensity is distributed continuously along the layer lines of a small width. When measuring the X-ray pattern the measuring slit will be wider than the layer line, but along the layer line the intensity across the slit may be taken to be constant. Therefore, to be compared with the experimental data, the theoretical distribution of intensity should be integrated in one direction that is, across the layer line. This has been done and resulted in formulas of integral intensity for different X-ray photography procedures.

4. To check the intensity formulas obtained the diffraction has been calculated by a system of package containing 10, 25, and 60 chains $(CH_2)_n$. The results were compared with values of the structural factors F_{hkl}^2. The calculations were carried out for packages with a three dimensional order and for random azimuthal rotations.

The calculations show that the maxima on the intensity curves fairly well denote the position and relative intensity of structural factors. With the three dimensional order, good agreement is achieved by means of a curve build up from two members of the series consisting of zero- and second order Bessel functions or even solely from the first member of the series.

The calculations also show that in the case of azimuthal randomness of the chain system $(CH_2)_n$, the X-ray texture pattern must reveal simultaneously two types of interference, the usual three dimensional reflections on the zero layer line and the scattering by individual chains or one-dimensional diffraction on the first layer line.

II

Applying monochromatic radiation, X-ray diffraction patterns of various cellulose- and hydrated cellulose fibers were obtained.

A peculiar characteristic of the X-ray texture patterns of highly oriented fibers (Rami, Fortisan) is the one-dimensional diffraction on the zero- and non-zero layer lines. As the intensity of this diffraction is low and continuously distributed along the layer lines, the distortion of orientation leads to the one-dimensional diffraction merging with the general background of the pattern. On the X-ray pattern of an imperfectly oriented viscose it will therefore be seen only on the second layer line. This also accounts for the absence of one-dimensional diffraction on the X-ray pattern of cotton.

One-dimensional diffraction can appear as a result of diffraction by separate chains or a group of chains situated in the short range order or due to statistical deviations of chains from their ideal position corresponding to the three-dimensional order. It has been shown that the latter case results in one-dimensional diffraction such as:

$$\varphi_0 [1 - \exp(-0\cdot5\pi^2 S_r^2 \overline{\varDelta\varrho_c^2} - 4\pi^2\xi^2 \overline{\varDelta\eta_c^2})],$$

where φ_0 is the scattering by a single chain, $\sqrt{(\overline{\varDelta\varrho_c^2})}$—the square mean deviation of chain centres in the equatorial plane, $\sqrt{(\overline{\varDelta\eta_c^2})}$—the square mean deviation of the

relative shift of the chains along the axis, S_r—the projection of $S (S = 4\pi \sin \theta/\lambda)$ on the equatorial plane, ξ—the number of layer lines.

The distribution of the intensity of the one-dimensional diffraction on the zero layer line has been calculated for three possible alternatives. The curves obtained were compared with the experimental one. Comparison showed that one-dimensional diffraction is due to statistical scatterings of chains about the sites corresponding to the three-dimensional order.

Using the experimental intensity relations of one-dimensional diffraction in different layer lines it is possible to estimate the values of $\sqrt{(\overline{\Delta\varrho_c^2})}$ and of $\sqrt{(\overline{\Delta\eta_c^2})}$. It was found to be $\sqrt{(\overline{\Delta\varrho_c^2})} = 0\cdot6\text{–}0\cdot9$ Å and $b.\sqrt{(\overline{\Delta\eta_c^2})} = 0\cdot7\text{–}1\cdot4$ Å ($b = 10\cdot35$ Å).

As the intensity of the one-dimensional diffraction is proportional to the number of chains in one region—n, and that of three-dimensional reflections is proportional to h^2, the comparison of intensities permits to estimate one region as containing about 170 to 300 chains.

Thus, the structure of cellulose displays considerable displacement of chains from their ideal position.

Besides, the continuous part of the scattering, that is often segregated from X-ray patterns of isotropic samples to determine the percentage of crystallinity consists essentially of one-dimensional diffraction. The determination of crystallinity percentage for cellulose seems therefore meaningless.

9·X·1. Diffuse scattering of X-rays by aluminum brass.
By A. S. KAGAN, V. A. SOMENKOV & J. S. UMANSKY, *Steel Institute, Leninsky Prospekt 6, Moscow, USSR.*

Measurements of the diffuse scattering of X-rays by aluminum brass containing 18 at.% Al is carried out in an evacuated camera by means of a Geiger counter.

Cu $K\alpha$ radiation used in the investigation was monochromatised through the diffraction from a germanium crystal cut parallel the plane (111); the advantage of such Ge monochromator being the absence of (222) reflection.

The scattered intensities were converted to absolute scale by comparison with the scattering by melted silica. The contribution of Compton scattering, temperature diffuse scattering and double Bragg scattering was estimated and eliminated. A correction for anomalous dispersion was included into calculations of Laue scattering.

The diffuse scattering by quenched from 700 °C. samples was measured in the range from 8° to 43° in Bragg angles. The calculation of the short range order coefficients carried out for six coordination shells in the assumption that coefficients of the size effect β_i are equal to zero gave following figures:

$$\alpha_1 = -0\cdot43 \pm 0\cdot10, \quad \alpha_2 = +0\cdot12 \pm 0\cdot05, \quad \alpha_3 = -0\cdot32 \pm 0\cdot05,$$
$$\alpha_4 = +0\cdot28 \pm 0\cdot10, \quad \alpha_5 = -0\cdot27 \pm 0\cdot05, \quad \alpha_6 = -0\cdot77 \pm 0\cdot10.$$

The diffuse scattering curve plotted on the basis of the short range coefficients given above agrees reasonably with the experimental curve, thus supporting the assumption $\beta_i = 0$ made previously. This assumption is supported also by measurements of static displacements estimated from the intensities of structure lines.

The annealing reduces the short range order, the amount of reduction increasing with the annealing temperature. The short range order is considerably destructed by cold working. The best short range order was discovered after a low-temperature annealing (260 °C.) of cold worked sample.

These data explain the anomaly of the behavoir of aluminum brass after cold working and annealing.

As the coefficients of the short range order for the first coordination shell were considerably higher than they should be for the superstructure Cu_3Au it was assumed that the atomic scattering functions of alloy components differ from atomic scattering functions of pure elements. This assumption was confirmed by an analysis of the intensities scattered by an intermetallic compound NiAl.

10·X·1. Modifications de la structure cristalline de quelques mineraux par broyage.
PAR CHARLES LEGRAND, 11, *rue Lagarde, Paris V°, France.*

On a vérifié que le broyage effectué en présence d'eau ou d'un liquide non polaire était sans effet appréciable sur la structure cristalline.

Dans le cas de ce broyage à sec, les effets sont très variables selon le mode de broyage. Ainsi, avec un broyeur à Boulets les kaolinites montrent de faibles perturbations liées au développement d'un réseau bidimensionnel; par contre, l'emploi d'un vibrobroyeur oscillant conduit à des modifications beaucoup plus profondes qui vont jusqu'à la disparition de toute structure cristalline.

Le mica montre une extinction rapide des réflexions basales avec la durée de broyage tandis que l'intensité des autres réflexions diminue moins vite pour s'annuler ensuite brusquement.

La fluorine manifeste un élargissement des raies qui doit être relié à la déformation du réseau et non à la taille des particules.

Le mode de broyage a une influence spécifique sur les altérations structurales obtenues et par conséquent sur les propriétés physico-chimiques des produits obtenus.

10·X·2. X-ray study of distortions in steel structure due to wear and tear.
By I. TERMINOSOV & W. SERGEEVA, *Institute of Economic Engineers, Marot Street 27, Leningrad, USSR.*

No abstract provided.

10·X·3. X-ray investigation of fatigue in metals.
By I. TERMINOSOV & W. BUYKO, *Institute of Economic Engineers, Marot Street 27, Leningrad, USSR.*

No abstract provided.

12·X·1. On the nature of omega-phase in quenched titanium alloys.
By YU. A. BAGARYATSKII, G. I. NOSOVA & T. V. TAGUNOVA, *Central Scientific Research Institute for Ferrous Metallurgy, Radio Street, 23, Moscow, USSR.*

Withdrawn.

12·X·2. О КИНЕТИКЕ ФАЗОВЫХ ПРЕВРАЩЕНИЙ В НЕКОТОРЫХ ДВУХКОМПАНЕНТНЫХ СПЛАВАХ. К докладу В. В. Санадзе.

Были изучены твердые растворы в системах никель-золото, платина-золото и серебро-медь.

Исследование проводилось методом последовательных закалок с последующим изменением микротвердости, электропроводности, фонда и ширины рентгеновских линий.

Показано, что в твердых растворах системы никель-золото имеет место двухфазный распад. Этот двухфазный распад последовательно проходит через ряд упорядочен-ных состояний: Au_3Ni, $AuNi$ и Ni_3Au. Упорядоченые структуры получаются в результате перераспределения атомов золота межлу твердыми растворами на основе никеля и золота.

При распаде твердых растворов системы платина-золото появляется промежуточная фаза с параметром значительно уменьшенным по сравнению с параметрами чистых компонентов.

Двухфазный распад в твердых растворах системы серебро-медь был наблюден и ранее. Однако рассмо-трение кинетики распада этих сплавов вышеупомянутым методом показало, что образование упорядоченных фаз происходит с той же последовательностью, что и в случае сплавов никель-золото.

12·X·3. Investigation of the matrix structure during the ageing process in high manganese steel and aluminium zinc alloys. By M. I. ZACHAROVA & VAN CHYA-FOY, Moscov State University, Faculty of Physics, Moscow, USSR.

X-ray analyses of stationary single crystals of steel with 12 wt.% Mn and 1·2% C quenched and aged at 750 °C. show, that the transformation $\gamma \to \gamma$ + carbide produced the appearance of extra maxima and arcs near maximum γ solide solution.

Similar diffraction picture is observed in Al–4% Zn alloy quenched and aged at 100 and 150 °C. The analyse of geometry of diffraction picture has shown, that the appearence of extra maximums and arcs are produced desorientation of blocs of some volume matrix around the precipitate.

With the grow of the precipitate desorientation of blocs increase up to several degrees, then it decrease again. In aluminium = 20 wt.% zinc alloy such diffraction effects not appear. The explanation local elastic desorientation of blocs for about several degrees is given.

13·X·1. Epitaxie et adsorption reciproque de l'uree et du chlorure d'ammonium. PAR A. RIMSKY.

Withdrawn.

14·X·1. I. О ПРАВИЛЬНЫХ РАЗБИЕНИЯХ ПРО-СТРАНСТВА. Б. Делоне, Н. Сандакова.

Как показывает рассмотрение правильных разбиений плоскости, вопрос этот в основном топологический, а поэтому также по существу топологический и вопрос о 2-мерных кристаллографических группах. Для $N \geq 3$ такого топологического решения вопроса пока найти не удается. Авторами для любого n дано полное решение вопроса, если рассматривать не любые, а только правиль-ные разбиения Дирихле, т. е. такие, которые получаются, если рассматривать области Дирихле точек правильной системы точек Ag, где A любая зафиксированная точка, а G пространственная кристаллографическая группа.

14·X·2. Zur Reduktionstheorie. VON B. DELAUNAY, Institute of Mathematics, I Academicheski proezd 8, Moscow, USSR.

Ich gebe in diesem Aufsatz den vollständigen Beweis derjenigen Reduktionsbeginnungen welche Voronoi ohne Beweis in seiner Arbeit über die perfekten Formen ange-führt hat. Ich erforsche nachher diejenigen Bereiche des 5-dimensionalen (ähnliche Gittern werden nicht als ver-schieden betrachtet) reduzierten Raumes von Voronoi welche verschiedenen meinen 24 Sorten entsprechen. Die monoklinen Sorten erfüllen 9 ganz bestimmte 3-dimen-sionale Tetraedern und die Sorten von höheren Symmetrie ganz bestimmte Dreiecke, Segmente und Punkte in diesen Tetraedern.

14·X·3. Antisymmetry of Fourier transforms of figures with a particular point. BY B. K. VAINSH-TEIN, Institute of Crystallography, Academy of Sciences of the USSR, Pyjewsky, 3, Moscow, B-17, USSR.

It is advisable to use the idea of 'black–white', i.e. 'anti'-symmetry for describing symmetry of continuous or discrete distributions of complex values. The anti-symmetry of Fourier transforms of the function of real variable, with particular point is considered. This trans-formation gives mutual (one to one) connection between the point group of symmetry of initial function and the point-group of antisymmetry of its Fourier transforms, and gives also the connection with Laue symmetry. In the special case of 32 crystallographical point groups 11 centrosymmetrical ones are in connection with 11 grey centrosymmetrical point groups of antisymmetry, and 21 non-centrosymmetrical—with 21 point groups of anti-symmetry possessing the centre of antisymmetry.

Для описания симметрии распределений комплексных величин, как непрерывных, так и дискретных целесо-образно использовать понятие »черно-белой« симметрии— т. е. антисимметрии. Рассмотрена антисимметрия преоб разования Фурье функции действительного перемен-ного, обладающей особой точкой. Это преобразование устанавливает взаимно-однозначную связь между точеч-

ной симметрией исходной функции, и антисимметрией ее трансформанты Фурье, а также дает связь с лауэвской симметрией. В частном случае 32 кристаллографических точечных групп 11-ти центросимметричным группам соответствуют 11 центросимметричных серых групп антисимметрии, и 21-й без центра—21 группа антисимметрии с центром антисимметрии.

16·X·1. РАЗРАБОТКА ПРЕЦИЗИОННОЙ МЕТОДИКИ ЭЛЕКТРОНОГРАФИЧЕСКОГО СТРУКТУРНОГО АНАЛИЗА. З. Г. Пинскер.

1. Большая часть выполненных до сих пор электронографических структурных работ основана на использовании кинематической теории рассеяния электронов, причем хорошее соответствие электронографических и рентгеновских структурных данных для многих веществ указывает на обоснованность использования кинематических формул.

2. В работах советских, а также японских авторов, выполненных с 1957-го года, с успехом используется динамическая поправка (на первичную экстинкцию), предложенная в свое время М. Блекмэном. Для нормировки экспериментальных $(\Phi)^2$ можно рекомендовать метод Вильсона.

3. Важные для вычисления динамической поправки данные о размерах рассеивающих кристалликов могут быть получены различными методами: из (интегральной) полуширины отражений, из значений величин $\mathcal{D}(A)$-динамической поправки или в результате Фурье анализа формы линий. Этот последний метод позволяет вычислить также кривую распределения кристалликов по величине.

4. Оценки и расчеты средних значений величин рассеивающих кристалликов, выполненные различными методами в ряде работ, указывают с несомненностью на то, что теоретические оценки границ применимости кинематической теории фактически не подтверждаются.

Повидимому, важнейшей причиной того обстоятельства, что кинематическая теория применима к кристалликам, линейные размеры которых превышают теоретические пограничные значения, является несовершенство рассеивающих кристалликов в исследуемых пленках, несмотря на малые размеры этих кристалликов. Прямым указанием такого рода является результаты Фурье-анализа формы линий, проведенной для электронограмм-от WN, а также данные по исследованию электрических свойств тонких слоев Ge.

Очевидно, что в зависимости от условий образования кристалликов в тонких слоях и степени их совершенства можно ожидать все типы рассеяния: кинематическое, промежуточное, при котором используется поправка на экстинкцию, и чисто динамическое.

5. Для более широкого и глубокого применения электронографического анализа необходимо развивать Фурье-синтез в электронографии. Используя Фурье-ряды потенциала, вычисленные на основе достаточно большого числа экспериментальных структурных амплитуд, можно решать важные задачи кристаллографии, физики твердого тела и кристаллохимии. Существенным является получение точных значений интенсивности (фотографическим или электрометрическим методами) и правильный переход от значений интенсивности к исправленным экспериментальным амплитудам. Необходимо обратить внимание на получение данных по абсолютным значениям распределения потенциала в решетке.

6. Анализ данных по распределению потенциала может быть использован как для нахождения координат атомов, так и для уточнения природы химической связи, характера тепловых колебаний атомов в решетке, дефектности и разупорядочения структур и других параметров идеальной и реальной структуры. Обсуждаются на конкретных примерах указанные применения электронографического анализа.

16·X·2. ИССЛЕДОВАНИЯ СТРУКТУР И ПРОЦЕССОВ УПОРЯДОЧЕНИЯ В ИНТЕРМЕТАЛЛИЧЕСКИХ И ПОЛУПРОВОДНИКОВЫХ ФАЗАХ. З. Г. Пинскер, С. А. Семилетов, В. И. Хитрова, Г. Г. Дворянкина. Institute of Crystallography, Acad. Sci. USSR. 3 Pyzhevsky per., Moscow B-17, USSR.

За последние годы в электронографических лабораториях Института кристаллографии и отчасти Горьковского Университета (Иссл. Физ. Ин-та) были получены новые данные, относящиеся к структурам неупорядоченных фаз к процессам упорядочения, значительно расширяющие наши представления о типах упорядочения. Имея в виду упорядочение тепловое и концентрационное, можно предложить следующую классификацию неупорядоченных или частично упорядоченных фаз и фазовых переходов порядок-беспорядок:

I. Неупорядоченные фазы

А: Атомы различных компонентов занимают упорядоченно или неупорядоченно различные, т. е. кристаллографически неэквивалентные положения в структуре.

В: Атомы различных компонентов занимают одинаковые положения в структуре.

Более детальная классификация, включающая примеры соответствующих типов (и подтипов):

A^1—Атомы одних компонентов неупорядочены, атомы других компонентов образуют вполне упорядоченный, жесткий каркас решетки. Примеры: I. Переходные фазы в системах Ni–Sb, Ni–Te в области концентраций Ni: 50%-33%.

2. Гексагональные нитриды железа в области концентраций до 30% азота.

3. Фазы приближенного состава: Cu_2Se, Cu_2Te, Ag_2S, Ag_2Se.

4. Некоторые фазы состава Ga_2Se_3, In_2Te_3. и др.

5. Кубический нитрид W.

A^2—Атомы одних компонентов занимают одни положения в структуре упорядоченно, другие положения неупорядоченно, создавая дефектную решетку. Атомы других компонентов могут быть упорядочены или неупорядочены.

Примеры:

1. Кубический нитрид MO.

2. Один из гексагональных нитридов W.

A^3—Повидимому возможен общий случай, когда атомы каждого из компонентов занимают неупорядоченно свои, особые положения в структуре.

В. Примеры:

1. Фазы в системе Cu–Au.

2. Фазы в системе Fe–Al.

3. Фазы в системе Ag–Cd.

4. β'–Cu_3Ti.

II. Типы фазовых переходов порядок-беспорядок

1. Упорядочение в некоторых фазах A^1, причем жесткий

каркас решетки проходит без изменения через точку (при тепловом упорядочении) или область (при концентрационном переходе) превращения.

Примеры:

1. Тепловое упорядочение в $A^1 3$.

Концентрационное упорядочение в $A^1 1$ и $A^1 2$.

2. Упорядочение в некоторых фазах A^1 и A^2, сопровождающееся изменением жесткой или частично-упорядоченной структуры, образованной атомами одного компонента.

Примеры: Тепловое упорядочение в $TlBiSe_2$, вероятно в $TlSbSe_2$.

Концентрационное упорядочение в системах W–N и Mo–N.

3. Примеры теплового (Au–Cu) или концентрационного (Fe–Al)(Ag–Cd) упорядочения в B^1, B^2, B^3, B^4.

Далее рассматривается структурная характеристика упорядочения в указанных системах, экспериментальные данные сопоставляются с теорией упорядочения и теорией химической связи в кристаллах.

16-X-3. Electron diffraction investigation of thiourea at 20 °C. and —140 °C. By B. K. VAINSHTEIN & V. F. DVORJANKIN.

1. Review of X-ray and other data on the crystal structure of thiourea at room temperature.

2. Electron diffraction investigation of the high-temperature phase of $CS(NH_2)_2$. The influence of dynamical correction Q on peak's co-ordinates. The structure of thiourea molecule and hydrogen atom's positions from electron diffraction data.

3. Crystal chemistry of high-temperature phase of thiourea and related compounds. The hydrogen bonds. The packing of molecules.

4. X-ray and other data on low-temperature phases of $CS(NH_2)_2$. The low-temperature electron diffraction technique. Electron diffraction investigation of thiourea at —140 °C. The structure of low-temperature phase and hydrogen atoms positions.

5. The discussion of mechanism of phase transition of thiourea from paraelectric to ferroelectric phase.

1. Обзор рентгенографических и других данных о структуре высокотемпературной фазы тиомочевины.

2. Электронографическое исследование высокотемпературной фазы $CS(NH_2)_2$. Влияние динамической поправки Q на координаты атомов. Структура молекулы тиомочевины и положение водорода согласно электронографическим данным.

3. Кристаллохимическое рассмотрение структуры высокотемпературной фазы тиомочевины и родственных ей соединений. Вопрос о водородных связях в данной структуре. Упаковка молекул.

4. Рентгенографические и другие данные по низкотемпературным фазам $CS(NH_2)_2$. Аппаратура для электронографических исследований при низких температурах. Электронографическое исследование $CS(NH_2)_2$ при —140 °C. Структура низкотемпературной фазы тиомочевины согласно электронографическим данным. Положение атомов водорода в данной фазе.

5. Обсуждение механизма фазового перехода тиомочевины из параэлектрической фазы, существующей при комнатной температуре, в сегнетоэлектрическую, стабильную ниже —140·8 °C.

17-X-1. Radiofrequency absorbtion of imperfections in natural and synthetic alumosilicates. By V. JOFFÉ, Institute of Silicates Chemistry, Nab Makarowa 2, Leningrad B-164, USSR.

No abstract provided.

17-X-2. Nuclear quadrupole resonance investigation of radiation damage in cristalline p-dichlorobenzene. By A. I. KITAIGORODSKII & E. I. FEDIN. Inst. of Elem.-Organic Compounds, Moscow.

Nuclear quadrupole resonance [1] (NQR) seemed to be a fine method for investigation of real crystal. The NQR frequency depends upon value of intracrystalline electric field gradient q, in which nucleus is, a width of resonance line defining by spreading of q from one nucleus to another. That is why crystalline lattice imperfections influences directly and strongly on NQR signal. For example instiling of 1–2% of impurity into lattice of investigated crystal decreases the intensity of NQR signal in 10 or more times [2].

We have used NQR as indicator of radiation damage of polycrystalline samples of p-dichlorobenzene, being irradiated by different electron radiation doses, energy being 750 kV. Frequency modulated spectrometer with lock-in detector and recording millivoltmeter was used [3, 4]. The circuit voltage have been measured continuously during the experiment. NQR lines from each sample was recorded many times with following averaging of all amplitudes, error being not more than 5%. Equal weight samples (4·1 g.) were used.

The results of experiment: (1) There is a saturation, when an increasing of satur radiation dose does not effect on NQR amplitude. (2) This saturation realizes, NQR amplitude decreasing unexpectedly little. If A_0 is a NQR amplitude in unradiated sample and A—an amplitude after achieving of saturation, then $A/A_0 = 0.75$ in our experiments. An essential decreasing of signal (till $A/A_0 = 0.3$) managed to watch in a sample, being not enough cooled during irradiation forming melting centers. An overheated irradiated sample has lost both an external similarity with unradiated crystals and melting point, NQR frequency being the same.

Similar saturation of radiation damage being registered by NQR, was noticed in report [5], where Co^{60}-radiation was used. This fenomenon was not explained there.

It can be simply explained suggesting chemical convertions resulting in NQR frequency shift under γ- and β-radiation may be unreversibly realized in that places of crystal, where packing density is decreased in comparison with ideal lattice (cracks between the blocks and similar regularity disturbances). In places with normal package an arrangement of molecular fragments, formed by β-radiation, remains rigidly fixed and chemical bond is instantly reproduced. With that point of view chemical convertions may take place only on the surface of crystalline block where free space is for placing of molecular fragments. It is clear that molecular fragments will be packed in interblock free space with less density than molecules in a crystalline lattice. Volume of these fragments as performed calculations show for probable ways of chemical convertions of p-dichlorobenzene, coincides with that of initial molecules (with error not exceeding 2–3%). Thus splitting of molecules on the block surface ceases, when molecular fragments packed with co-

efficient K will fill the whole volume formed after destroying of the block surfaces. The height of layer on the block surface, which will be destroyed till further chemical convertions ceases, depends upon interblock spacing. There is simple equation between those values:

$$b = 2na_0(K_0/K - 1) , \qquad (1)$$

where b is the interblock spacing, a_0 the average molecular dimension, n is the number of destroyed monomolecular layers, is the packing coefficient of molecules in the ideal lattice. For organic crystals $K_0/K \leq 1 \cdot 25$.

According to suggesting model a relative decreasing of NQR amplitude must be equal to ratio of number of molecules being on the block surface to whole number of molecules in the block:

$$(A_0 - A)/A = N_1/N . \qquad (2)$$

One may correlate the ratio N_1/N with block dimensions. If V is an average block volume and V_1 is the volume of its surface layer being destroyed by radiation, then $N_1/N = V_1/V$. Let us assigne that Δa is height of surface layer and a is linear block dimension. Simply speaking block has a cubic form. Then $V_1 = 6a^2 . \Delta a$, $V = a^3$ and taking into consideration (2) we have

$$\Delta a/a = \tfrac{1}{6} . (A_0 - A)/A_0 . \qquad (3)$$

We shall receive a minimal estimation of block dimensions suggesting $\Delta a = a_0$. Substituting a molecular dimensions of p-dichlorobenzene and its unit cell volume one may calculate that such block contains $4 . 10^4$ molecules. If $\Delta a = 3a_0$, then block contains $\sim 10^6$ molecules. Thus, estimation of block dimensions on the basis of developing suggestion gives sensible results. It is interesting to note that combined consideration of equations (1) and (3) results in a conclusion that crack volume occupy $\sim 4\%$ of whole crystal volume well coinciding with X-ray data. One may conclude that thoroughly grown single crystal in which lattice is near to ideal one, must have more resistance to γ- and β-radiation than polycrystalline one. It is interesting to test this conclusion experimentally.

References

1. T. P. Das & E. L. Hahn (1958). *Nuclear Quadrupole Resonance Spectroscopy*. N.Y.
2. A. Monfils & A. Grosjean (1956). *Physica*, XXII, No. 6, 541.
3. Э. И. Федин, Ю. С. Константинов. *Приборы п техн. эксп.*, Д2, 27–30, (1959).
4. А. И. Китайгородский, Э. П. Федин. *ДАН*, **130**, 1005 (1960).
5. J. Depireux, J. Duchesne & A. Van-de-Vorst (1958). *Bull. Acad. roy. Belgique*, **44**, 693.

*S*1·X·1. **Date on thermal motion obtained by X-ray spectral method.** By I. B. Borovsky, *Moscow 17 rcn, Leninsky Prospect, 49, A. A. Baikov Institute of Metallurgy of Academy of Sciences, USSR.*

No abstract provided.

*S*1·X·2. **X-ray measurement of thermal motion in some crystals with diamond, zincblende, wurzite and spinel-type structures.** By N. N. Sirota.

No abstract provided.

*S*2·X·1. **Translational slip and lattice reorientation.**
By M. V. Klassen-Nekludova, *Institute of Crystallography, Academy of Sciences of the USSR, Pyzhevskii per. 3, Moscow, USSR.*

Different variants of lattice reorientation resulting from non-uniform distribution of gliding within a deformed crystal were discussed by many authors beginning with N. A. Brilliantov & I. V. Obreimov. Some of the proposed schemes of the lattice reorientation process have been included into different handbooks though their validity has not yet been experimentally tested. The test proves difficult, as a rule, due to insufficient resolution obtainable with usual methods applied to studying space and time intervals. The first problem can be solved by using modern techniques of revealing individual dislocations, the resolution of the second problem requires the application of high-speed filming.

The parallel investigations with X-ray, interferometric and optical-polarization methods as well as by selective etching has revealed that in the NaCl type crystals the formation of desoriented regions previously called 'irrational twins' is caused by the fact that in certain crystal areas the slip occurs along different glide systems. The boundaries of these areas are determined by conditions of deformation compatibility (equality of tangential displacement on both sides of the boundary). If the boundary deviates from the correct position macroscopic stresses appear on both of its sides.

To study the process of kink formation high-speed filming has been used at the speed of 5,000 frames/sec. To synchronize the deformation and the moment of shooting a compressive impact load has been employed. Applying polarized light permitted to observe stress rearrangement (in CsI crystals) and lattice reorientation (in naphthalene crystals) during the compression process. Specimen orientation has ensured the slip along only one of the possible glide systems; plastic deformation prior to kink formation as well as the process of kink formation itself occurring along the same glide system.

Kink formation is immediately preceded by sharp stress rearrangement. Slip in the initial kink band always occurs in the direction opposite to that of the previous plastic deformation. Then reoriented wedge-shaped regions are being formed, in each series of successively formed wedges the slip occurring in the opposite directions. If the formation of the first kink lamella is followed by the formation of a second lamella the slip in this second lamella will spread in the opposite direction.

Each reversal of slip direction is connected with the change of sign of the shear stress in the direction of glide on the glide plane.

This is due to: *a* deflection of loading axis from specimen axis as a result of plastic distortion of specimen butts, *b* relative displacement of specimen parts separated by kink band due to slip localization in this hand, *c* lagging of kink boundary tilt in relation to plastic deformation run in the kink band.

The phenomena investigated show the determinant role of stress rearrangement in the process of lattice reorientation.

*S*2·*X*·2. О РАСПРЕДЕЛЕНИИ НАПРЯЖЕНИЙ И ЗАРОЖДЕНИИ ДИСЛОКАЦИЙ ПРИ РАСПРОСТРАНЕНИИ ТРЕЩИН В ИОННЫХ КРИСТАЛЛАХ.

М. П. Шаскольская, доцент, кандидат физико-математических наук (кафедра физики Московского Института Стали им. И. В. Сталина). (The Moscow Steel Institute, Leninsky prospect, 6, Moscow, USSR.

Изучаются трещины спайности, создаваемые искусственно в кристаллах NaCl, KCl и LiF путем введения лезвия ножа. При постепенном увеличении нагрузки на лезвие трещина продвигается скачками. Методом фотоупругости показано, что на конце трещины возникает крестообразная область локальной концентрации напряжений. После достижения некоторого предельного значения напряжений в этой области, трещина скачком продвигается дальше, концентрация напряжений у ее конца резко ослабевает, и возникает новая область такой же локальной концентрации напряжений. На пути распространяющейся трещины сохраняются локальные области остаточных напряжений.

Методом избирательного травления показано, что в этих областях возникают также и локальные сосредоточения дислокаций, геометрия расположения которых отвечает геометрии распределения напряжений. На продолжении трещины образуется ряд дислокаций в плоскости (100). Предполагается, что это сидячие дислокации, образовавшиеся при частичном слиянии трещины при полном восстановлении целостности кристалла.Такое же слияние трещины с восстановлением целостности кристалла и с рядом дислокаций на месте, где проходила трещина, можно получить и искусственно. Место залечивания трещины обладает повышенной прочностью.

S2·X·2. The distribution of stresses and the generation of dislocations caused by cleavage cracks in ionic crystals. By M. Shaskolskaya, *Chair of Physics, Moscow Steel Institute, USSR.*

Cleavage cracks artificially produced in crystals of NaCl, KCl and LiF by inserting a razor blade are investigated. A gradually increasing load on the blade causes the crack to proceed by jumps. By means of the photoelasticity method it is shown that at the end of the crack there arises a cross-shaped region of local stress concentration. When the stresses in this region have reached a certain limit value, the crack jumps further; the concentration of stresses at its former end decreases abruptly, while further on there arises a new region of local stress concentration. Along the advancing crack remains a succession of local regions of residual stresses.

It is shown by etching that these regions coincide with those of local concentration of dislocations, the arrangement of the latter corresponding to the distribution of stresses. As a continuation of the cracks appears a row of dislocations in the (100) plane. These are supposed to be sessile dislocations, formed by a partial closing up of the retreating crack, while the perfection of the crystal is wholly restored. The same phenomenon may be caused artificially.

The region of the former crack is characterized by increased strength.

S2·X·3. СТРОЕНИЕ ГРАНИЦ ЗЕРЕН ФЕРРИТА.
(Тезисы доклада на V Международном конгрессе кристаллографов). (On the nature of grain boundaries in α-iron). *Скаков Ю. А., доцент кафедры рентгенографии и физики металлов Московского ин-та стали. The Moscow Steel Institute, Leninsky prospect, 6, Moscow, USSR.*

Обсуждается строение границ зерен в обычных поликристаллических материалах (техническое железо, трансформаторная сталь). При электронномикроскопическом исследовании методом отпечатков получены свидетельства упорядоченной структуры границ при значительных разориентациях зерен. Впервые выявлены и подробно исследованы »многостеночные« границы, т.е. границы, состоящие из двух и более параллельных стенок с разрешаемой в электронном микроскопе дислокационной структурой (дислокации выявлялись по точкам травления в местах сегрегаций).

Установлено, что многостеночной границей осуществляется связь между кристаллитами с весьма большой разориентировкой (больше 20°). Рассматривается вопрос об устойчивости границ данного типа и о роли аллотропического превращения в возникновении многостеночных границ.